Kidney Cell Electrophoresis

Comprehensive Final Progress Report

Contract NAS 9-15584

Paul Todd

403 Althouse Laboratory

The Pennsylvania State University

University Park, Pennsylvania 16802

January 1985

CHAPTER 1

INTRODUCTORY SYNOPSIS OF PROGRESS

The tasks that were assigned easily divide themselves into five general categoreis, and this final report is organized around them. Chapters 1 and 2 deal with various aspects of the tesk dascription and summary of results. Chapter 2, which is a collection of Task Description contributions to the annual Materials Processing in Space inventory book, tends to highlight the activities of each year.

2. Electrophoresis technology

Resarch on ground based electrophoresis technology was performed in support of the ground-based methods used in calibrating, testing, and analysing methods and materials used or to be used in space and in support of fundamental electrophroesis reserach in cell biolgoy and on candidate human kidney ceil lots. Chapters 3 - 8 summarize progress in electrophoresis technology.

3. Cell culture technology

Highlights of this aspect of the project tasks were the evaluation of a new antimycotic, a relatively crucial item in space electrophoresis, as it turns out, and the evaluation of medium used in freezing and electrophoresis of cells. Only two chapters, 9 and 10, were prepared for final reporting.

4. Electrophoresis of cells

This activity was by far the major activity of the project, and substantial progress is being reported in understanding the electrophoresis process as it applies to cells. Chapters 11 - 19 detail assessemenbts of buffers and the role of cell parameters in density greadient, free flow, and microgravity electrphoresis.

5. Urokinase assay research

One of the major objectives of this research was the development of a single-cell method of UK positive cells. Several udnergraduate student projects were associated with this activity. Substantial parts of chapters 20, 21, and 22 have been written by undergraduate students. At the time of closing, this problem was on the verge of being solved by flow cytometery.

6. Zero-g electrophoresis

Research was conducted in support of analysis, cell selection, basic principles of electrophoresis, and testing of materials and methods used or to be used in microgravity experiments. Chapters 23-29 detail the results of pre-flight and post flight research and analyses, and a number of scientific articles have been, or are about to be published. As many of these were included among these chapters as was reasonable. Others have ben written mainly by coauthors at JSC and MSFC and are therefore not included.

7. Flow cytometry investigations

This task was added part way through the 6-year project and was not among the original tasks. This powerful method turned out to strongly support the microgravity electrophoresis effort (Chapter 31), and light scattering measurements as a sorting tool for live kidney cells holds very great promise (Chapter 30). Chapters 30-32 represent many of the findings to date, but more were being discovered at the close of the contract period. It can be stated in general that kidney cells do appear to have a light scattering signature relted to their function.

CONCLUSIONS

The above 7 tasks have were undertaken in support of two objectives: to carry out electrophoresis experiments on cells in microgravity and to assess the feasibility of using purified kidney cells from embryonic kidney cultures as a source of important cell products. Although both of these questions still remain somewhat open, a great deal has been learned about the electrophoretic subpopulations of embryonic kidney cells, and there has been considerable progress in the development of a coapbility in microgravity cell electrophoresis.

Chapter 2.

Task Descriptions for the Catalog of Tasks for the Materials Processing in Space Program.

THE PENNSYLVANIA STATE UNIVERSITY
PAUL M. ALTHOUSE LABORATORY
UNIVERSITY PARK, PENNSYLVANIA 16802

College of Science
Department of Microbiology, Cell Biology,
Biochemistry and Biophysics

Area Code 814
865-5497

January 8, 1982

Dr. Robert Naumann
ES-71
Marshall Space Flight Center
Huntsville, AL 35812

Dear Bob,

In response to your letter of December 31, 1981, concerning our page in the 1982 Catalog of Tasks for the Materials Processing in Space program, I would like to suggest the following changes:

1. Funding level: I think this is now about twice the amount shown in the 1981 catalog, but the project is funded in irregular increments so I do not know how to report an annual dollar amount. Maybe it is best to check with JSC.

2. Paragraph 2, item (4) change to: (4) development of standard cells, standard cell culture methods, and standard urokinase assay procedures.

3. The entire final paragraph can be updated as follows:

Cells from cultures obtained from 26 commercially-prepared explants have been studied with respect to electrophoretic mobility distribution, growth in culture, and urokinase production. The testing of various electrophoresis buffers, which also must be used as a medium for freezing viable cells, has indicated that the low ionic strength required for effective electrophoresis in microgravity experiments compromises the viability of the cells. A buffer designated "D-1", which contains DMSO and EDTA, is phosphate buffered, and is made isotonic with sucrose has been chosen for use in microgravity experiments. Optimum culturing conditions for urokinase production by cells in monolayer have been established. In close collaboration with Johnson Space Center a human kidney cell explant designated "HEK-8514" has been chosen for microgravity experiments. In close collaboration with Michael Reese Research Foundation in Chicago, procedures have been established for urokinase assay of cultures derived from cells separated in microgravity experiments, which will take place on Shuttle OFT-3 mission.

Bibliography: P. Todd, W. C. Hymer, L. D. Plank, G. M. Marks, M. E. Kunze, V. Giranda and J. N. Mehrishi,. Separation of functioning mammalian cells by density-gradient electrophoresis. In Electrophoresis '81, Ed. R. C. Allen and P. Arnaud, W. DeGruyter Co., NY, 1981.

By the way, as a result of USRA activities I was asked to write a short letter to headquarters concerning what I could find out about the selection of macromolecular candidate materials for NASA-sponsored experiments using the MDAC electrophoretic separator aboard Shuttle. A copy is enclosed for you.

Finally, could you please send us two copies of Jacob Savage's report, Preparation of Guinea Pig Macrophages for Electrophoretic Experiments in Space, NASA CR-158777 (N79-27814/NSP). Many thanks.

If there are any problems with the catalog entry, please let me know.

Sincerely,

Paul Todd
Professor of Biophysics

PT:th

Enclosure

Task Description for the 1983 catalog of tasks for
the Materials Processing in Space Program

Edited by

Elizabeth Pentecost
ES71
George C. Marshall Space Flight Center
Marshall Space Flight Center, Alabama 35812

January, 1983

Kidney Cell Electrophoresis

Pennsylvania State University
Dr. Paul Todd
NAS9-15584 $60K/year
Continuing task

The objective of this investigation is to repeat the MA-011 experiment under conditions which are optimum for the viability of human kidney cells and most favorable for the best possible electrophoretic separation of those few (about 5%) cells which produce urokinase or human granulocyte conditioning factor (HGCF), and erythropoietin.

This study effort will perform the gound-based research necessary to establish all of the optimum experimental conditions required to accomplish the best possible electrophoretic separation of human kidney cell fractions which produce urokinase, granulocyte stimulating factor, or erythropoietin. This overall effort will include: (1) development of optimum buffer systems, (2) viability tests, (3) ground-based research on electrophoretic mobilities, (4) development of standard cells, standard cell culture methods, and standard urokinase assay procedures, (5) acquisition of the ground control data to be compared with results using cells returned from the electrophoretic separations carried out in microgravity, and (6) ground-based research on the electrophoretic mobilities of suspended pituitary cells (last task added in 1982).

Cells from cultures obtained from 32 commercially-prepared explants have been studied with respect to electrophoretic mobility distribution, growth in culture, and urokinase production. The testing of various electrophoresis buffers, which were also used as the medium for freezing viable cells in Shuttle flight STS-3, indicated that their low ionic strength compromised cell viability somewhat, and the buffer "D-1", which contains EDTA and DMSO, was used in the microgravity experiments involving electrophoresis of human kidney cells and test particles (fixed human and rabbit red blood cells). Ground-based electrophoretic characterization of human kidney cell line "HEK-8514" was accomplished prior to the STS-3 flight, as was the characterization of the test particles. Procedures for post-flight analysis had been established and evaluated prior to the flight. These were not implemented, owing to the well-known post-flight accidental loss of the samples.

Post-flight analysis of the test-particle electrophoresis data recorded on film during the STS-3 flight has been accomplished. A time-sequence photograph (Figure 1) shows the progression of the human red blood cell band along the column during electrophoresis in flight. Optical density scans of the negatives of these photographs, provided by Johnson Space Center, were analysed by computer, and ground-based laboratory studies were carried out to simulate the conditions of flight. These studies indicated that the migration rate of cells in space is predictable on the basis of temperature and ionic strength of the "D-1" buffer that was used.

Collaborations with Johnson Space Center and Michael Reese Research Foundation in Chicago continue. Their purpose is the preparation of human kidney cell electrophoresis experiments that will utilize the McDonnell-Douglas continuous-flow electrophoretic separator (CFES) aboard future STS flights under the MDAC-NASA Joint Endeavor Agreement. Media and buffers suitable for this purpose are under investigation, and a very-low-ionic-strength triethanolamine electrophoresis buffer is being evaluated as is a serum-free or low-serum medium in which cells can both multiply and produce urokinase. Media are being screened by the fibrin-plate assay method, in which, as Figure 2 shows, urokinase activates the dissolution of a blue-stained fibrin clot resulting in a clear "lysis zone", the area of which is related to urokinase activity. In collaboration with Dr. W. C. Hymer of The Pennsylvania State University a task to perform ground-based electrophoretic studies on suspended rat pituitary cells has begun, and results to date indicate a unimodal electrophoretic mobility distribution of this cell population, which is otherwise very heterogeneous. Separations of this cell type in microgravity using CFES are anticipated.

PUBLICATIONS

M. E. Kunze and P. Todd. Evaluation of Econazole as an antifungal agent in quantitative cell culture experiments. In Vitro (in press, 1983).

P. Todd, W. D. Hymer, L. D. Plank, G. M. Marks, M. E. Kunze, V. Giranda, and J. M. Mehrishi. Separation of functioning mammalian cells by density-gradient electrophoresis. In "Electrophoresis '81" (Ed. R. C. Allen and P. Arnaud), Walter De Gruyter Co., Berlin, 1981, pp. 871-882.

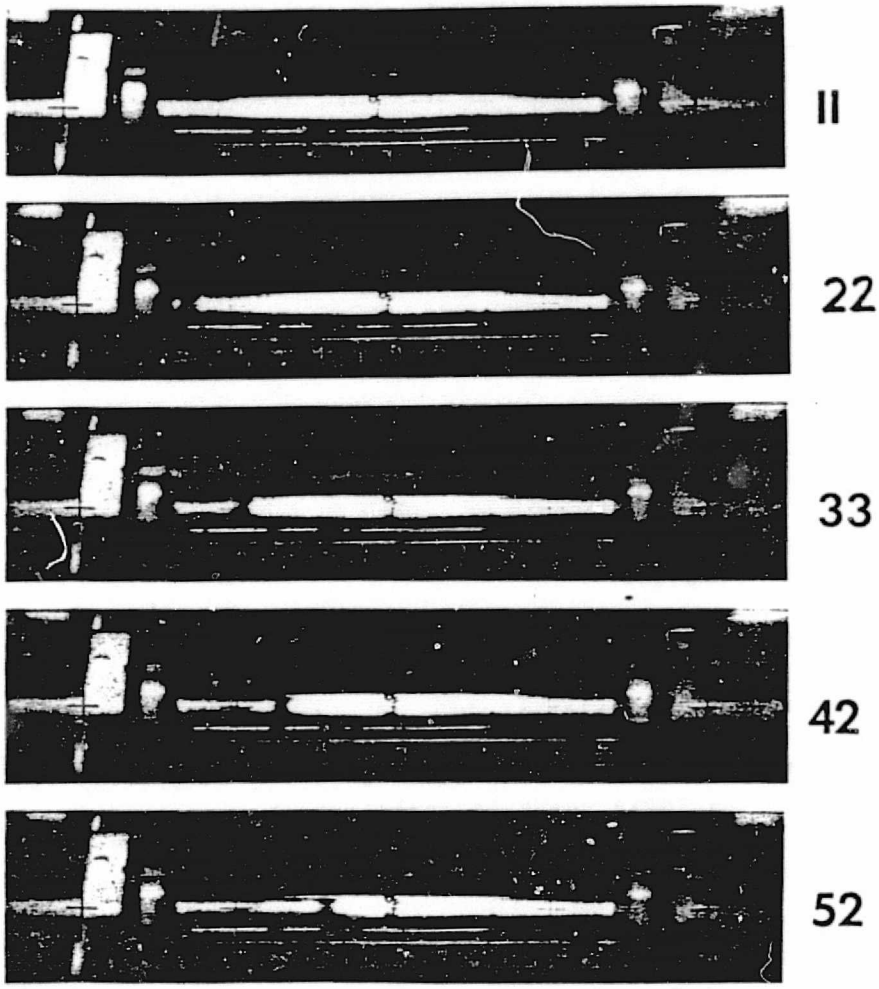

Figure 1. Sequence of photographs taken at 11 minute intervals on Shuttle flight STS-3 during electrophoresis of fixed human and rabbit red blood cells as test particles. The band of human red cells can be seen moving from left to right as time progresses.

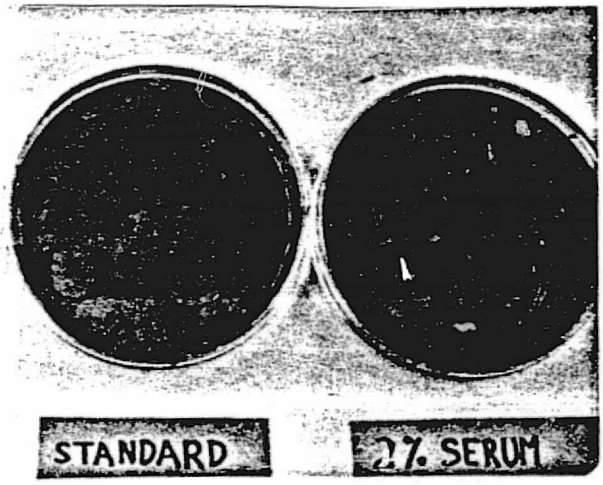

Figure 2. Lysis zones in blue-stained fibrin clots as a means of demonstrating urokinase activity in the medium of urokinase-producing cultured human kidney cells.

2-6

THE PENNSYLVANIA STATE UNIVERSITY

PAUL M. ALTHOUSE LABORATORY
UNIVERSITY PARK, PENNSYLVANIA 16802

College of Science
Biochemistry, Microbiology,
Molecular and Cell Biology

Area Code 814
865-5497

27 July, 1983

Mr. Salvatore J. Grisaffe
EN-1
National Aeronautics and Space Administration
Washington, D. C. 20546

Dear Mr. Grisaffe:

In reply to your letter of July 19, 1983, I enclose a "capsule" summary of our project "Kidney Cell Electrophoresis". I did not receive your letter sent in early June requesting a reply by June 14. I understand that a headquarters briefing involving these "capsule" summaries has already occurred but that you are still receiving the summaries. I hope that ours will still be useful to you.

I hope that sometime during the next few months it will be possible to discuss this work, and other MPS projects as well, with Mr. Halpern. Workers in the field are appreciative of efforts of this type on the part of Headquarters leadership. If there is any additional information that you need please contact me at 814-865-0242.

Sincerely yours,

Paul Todd

Paul Todd

Area: Living cell purification by electrophoresis

- Objectives: Characterization and optimization of electrophoretic separation of human kidney cells and pituitary cells at zero-g and in the laboratory.

Major Gaps in Technology Major Scientific Questions	Major Benefits if Fill Gaps and Answer Questions
Can zero-gravity electrophoresis of living cells produce greater quantities of a purer product than other means of purifying living cells that cannot be cloned for the indefinite production of differentiated progeny?	Production of purified cell types for *in vitro* mass production of biologicals (urokinase from human kidney cells, for example) or implantation *in vivo* (growth hormone from pituitary cells, for example.

- New Understanding/Technology Expected from Overall Effort

Understanding of the role of gravity in electrophoretic cell purifications and the relative merits of electrophoresis in comparison to other cell purification methods.

- Approach*‡ In collaboration with Johnson Space Center and W. C. Hymer: Cultured human kidney cells and freshly-suspended rat pituitary cells are studied with respect to electrophoretic mobility distributions and viability under conditions of 1-g and zero-g electrophoresis. Effects of buffer composition, ionic strength, temperature, storage conditions, suspending method, and starting material are under investigation. The materials were chosen for study because they produce some of the world's most demanded cell products. Model materials in electrophoresis experiments are fixed human and rabbit erythrocytes, chosen because they have been extensively characterized electrokinetically.

*List of other current related efforts (Government or commercially supported) and brief description of approach attached.

‡Why did you choose your model material or real material?

FOR THIS PROJECT

- Key Progress/Impact Made to Date: Preflight experimentation and post-flight (Model/Data/Predictions/Properties/Etc.)
  laboratory analysis was completed for the EEVT experiments on Shuttle flight STS-3 (kidney cells and fixed erythrocytes). Preflight experimentation is nearly complete for the CFES experiments on Shuttle flight STS-8 (kidney and pituitary cells).

- Other Outputs: Papers/Presentations/Patents/Awards (list attached)

- Program Now in Category: I II III IV

- Funding History, $K

	FY 78	FY 79	FY 80	FY 81	FY 82	FY 83	FY
Start	49.98	15.21	59.59	62.25	87.76	64.17	
Cumulative			124.78	187.02	274.78		

Future Flight Hardware or Facility Needs/$K	Estimated Flight/ Facility Schedule	Prob. of Success
Continued use of MDAC CFES or similar equipment. Cell culture incubators and centrifuges for on-board processing of starting material and separated fractions. (Additional costs unknown).	At least 2 more flights utilizing CFES in collaboration with JSC, using specific cell-compatible electrophoresis and storage buffers.	

- Projected Commercial Benefits: Far-term goals are pure cells for producing urokinase and other kidney products and implantable growth-hormone secreting cells for treating abnormal pituitary conditions, possibly including weightlessness.

- Recommendations: Continue/Discontinue. Necessary Revisions -

ATTACHED LIST

Todd, P., W. C. Hymer, L. D. Plank, G. M. Marks, M. Hershey, V. Giranda, M. E. Kunze and J. R. Mehrishi. 1981. Separation of functioning mammalian cells by density-gradient electrophoresis. In: Electrophoresis '81 (eds. R. C. Allen and P. Arnaud) W. DeGreuter Press, NY pp. 871-882.

Kunze, M. E. and P. Todd. 1983. An evaluation of Econazole, an antifungal agent, for use in quantitative cell culture experiments. In Vitro 19, 175-178.

Plank, L. D., W. C. Hymer, M. E. Kunze, G. M. Marks, J. W. Lanham and P. Todd. A study of cell electrophoresis as a means of purifying growth-hormone secreting cells. J. Biochem. Biophys. Meth. (in press).

Sarnoff, B. E., M. E. Kunze and P. Todd. Electrophoretic purification of cells in space: Evaluation of results from STS-3. In Proceedings of 6th Princeton Conference on Space Manufacturing, (ed. G. K. O'Neill) (in press).

Plank, L. D., P. Todd, M. E. Kunze and R. A. Gaines. 1981. Electrophoretic mobility of cells in a vertical Ficoll gradient. Electrophoresis '81 Book of Submitted Abstracts for Papers and Posters, p. 125.

Plank, L. D., M. E. Kunze, C. Goolsby and P. Todd. 1982. Density gradient electrophoretic separation of living mammalian cells: Effect of position in the cell cycle. Biophys. 37, 78a.

Presentations:

P. Todd. 1 June 1983. Electrophoretic separation of living cells from human kidney cultures and rat and human anterior pituitary. Seminarium, Biomedical Center, University of Uppsala, Sweden.

P. Todd. 30 June 1983. Präparative elektrophoretische Trennung von Zellen, mit Berichte über einige Experimente hierzu in der Raumfähre "Columbia." Wilhelm-Pieck University, Rostock, DDR.

Kidney Cell Electrophoresis

The Pennsylvania State University
Dr. Paul Todd
NA59 - 15584 $65K/year
June 1980 - continuing task

The objective of this project is to evaluate materials and procedures for microgravity electrophoresis of living human embryonic kidney cells, to provide ground support in the form of analytical cell electrophoresis and flow cytometry and to analyse cells returned from space flight.

In collaboration with D. R. Morrison, principal investigator, and M. L. Lewis of Johnson Space Center and G. H. Barlow, co-investigator, of Michael Reese Research Foundation, pre-flight culture media, electrophoresis buffer, fraction collection media, temperature profiles, and urokinase assay procedures were tested prior to flight. Electrophoretic mobility distributions of aliquots of the cell population to be fractionated in flight were obtained. The following protocol was established and utilized:

Cells were prepared in suspension prior to flight in electrophoresis buffer and 10% calf serum. Electrophoretic separation proceeded in electrophoresis buffer without serum in the McDonnell-Douglas Continuous Flow Electrophoretic Separator, and fractions were collected into sample bags containing culture medium and concentrated serum. Two separations were performed, and subsequent culturing and biochemical measurements were conducted at Johnson Space Center. Fractions that yielded enough progeny cells were analysed at The Pennsylvania State University for morphology and electrophoretic mobility distributions. The mobility distributions of progeny cells cultured from four electrophoretic fractions are shown in Figure 1, where it can be seen that the lowest-mobility fraction studied produced higher-mobility progeny while the other fractions produced progeny cells with mobilities related to the fractions from which they were collected.

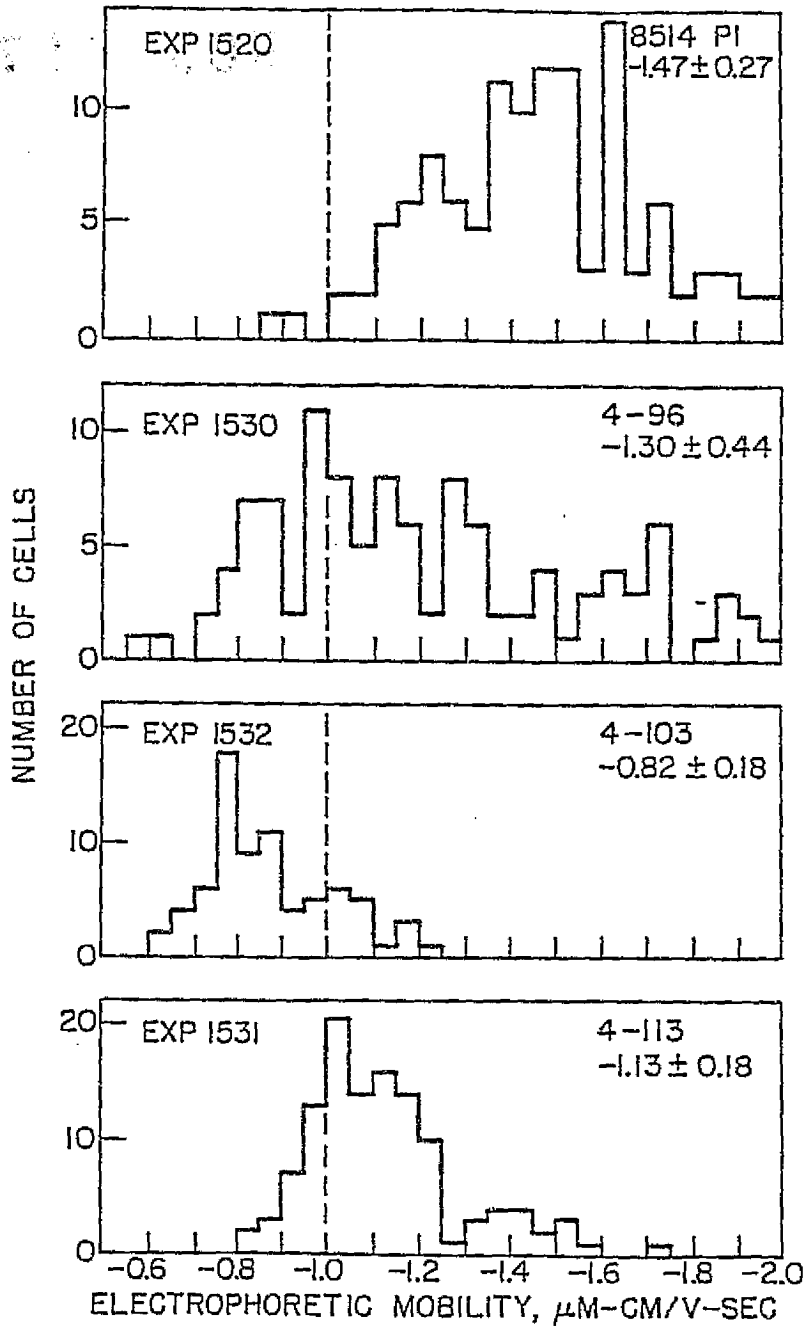

Figure 1. Electrophoretic mobility (EPM) distributions of starting mixture and 4 fractions of human embryonic kidney cells (strain HEK-8514) separated by Continuous Flow Electrophoresis in microgravity and subsequently grown in cell culture. EPM is linearly related to fraction number. Low-EPM fractions differentiated into higher-EPM cells.

PART III

ELECTROPHORESIS TECHNOLOGY

Chapter 3.

Electrophoresis Studies on Methylcellulose Chamber Coating.

EFFECTS OF COATING RECTANGULAR MICROSCOPIC ELECTROPHORESIS CHAMBER WITH METHYLCELLULOSE

L. D. Plank

INTRODUCTION

Although precision in analytical cell electrophoresis is usually fairly high, one of the biggest problems in obtaining high accuracy in microscopic electrophoresis is the parabolic flow of liquid in the chamber due to electroosmotic backflow during application of the electric field. In chambers with glass walls the source of polarization leading to electroosmosis is the negative charge of the silicate and other ions that form the wall structure. It was found by Hjertén, who used a rotating 3.0 mm capillary tube for free-zone electrophoresis, that precisely neutralizing this charge was extremely difficult, but if a neutral polymer matrix (formaldehyde-fixed methylcellulose) was formed over the glass (quartz) wall the double layer was displaced and the viscosity at the shear plane increased so that electroosmotic flow could be eliminated. This principle was applied to rectangular and cylindrical microscopic electrophoresis chambers by Van Oss and Fike, who used agarose coating and agarose plugs to eliminate electroosmotic flow. The reduction of parabolic flow in the chamber was verified by depth-mobility profile determinations. Electrophoresis of cells in suspension in microgravity was found to produce severe electroosmotic backflow problems, and these were managed by glow-discharge cleaning of the cylindrical glass tubes and coating them with pure methylcellulose after treatment with a silylating compound, Dow "Z-6040".

Experiments were designed to determine the reliability with which methylcellulose coating of the Zeiss Cytopherometer chamber reduced electroosmotic backflow and the effect of coating on the accuracy of cell electrophoretic mobility (EPM) determinations.

MATERIALS AND METHODS

Fixed rat erythrocytes (RBC) were used as test particles. Electrophoretic tests were performed using 0.145 M NaCl, 10^{-4} M $NaHCO_3$, pH 7.2 as electrophoresis buffer. The batch of Dow Methocell used in this research was obtained from Dr. Hjertén's laboratory, Biochemical Institute, The Biomedical Centre, University of Uppsala. EPM was determined at various depths in the rectangular chamber by recording the position of the microscope objective and making the optical correction, using the front and back chamber surfaces as landmarks. Each cell was timed for at least three sec in each direction by reversing polarity, and the velocity parabolas were analyzed by the method described in Chapter 4, using the BASIC program with a subroutine for coated chambers.

Coating Procedure

The method of Hjertén as modified by Catsimpoolas was used to coat the rectangular microelectrophoresis chamber. The coating solution was prepared as follows:

a) 0.52 g methylcellulose (Dow Methocel MC) was dispersed in 30 ml boiling water and stirrec until dissolved;

b) 70 ml cold (4° C) water was added, and stirring was resumed in the cold room until the solution appeared clear;

c) formic acid (7 ml) and the formaldehyde (35 ml) were added, with stirring;

d) the final solution was clarified by filtration.

The chamber to be coated was rinsed thoroughly with a detergent solution, hot and cold tap water, distilled water, and air dried. The methylcellulose solution was drawn into the chamber, held vertically, by suction and after five min was allowed to run out slowly, leaving a film of uniform thickness on the chamber walls. After draining for five min the chamber was dried at 120° C for forty min. The coating and drying procedures were then repeated once more. Care was taken to ensure that no air bubbles adhered to the chamber walls during the procedure.

RESULTS

Figure 1 shows a typical mobility parabolas that is obtained when fixed rat RBC's are subjected to electrophoresis in an uncoated rectangular chamber. When the chamber is coated according to Hjertén's procedure, the parabolic shape of the depth-mobility profile disappears, as shown in Figure 2. When EPM distributions are derived from the depth-mobility profiles with and without coating the chamber, there is reasonable agreement, although standard deviation is somewhat higher, as Figure 3 indicates.

Although the above results are encouraging, it can be noted in Figure 2 that the data are clustered near the center of the chamber. The methyl-cellulose coat was apparently not very thin compared to the chamber dimensions, so there were no cells near the chamber walls due to the thickness of the methylcellulose coat. Although this shortcoming should not seriously interfere with EPM determinations, it was also found that the effect of coating the

chamber was not fully reproducible, and Figure 4 is a depth-mobility profile obtained when the chamber was coated a second time after cleaning the first coat. The profile is not flat.

DISCUSSION

Although methylcellulose coating of the Zeiss Chamber did have the effect of eliminating electroosmotic backflow, it did not do so in a consistent, reproducible manner. It was therefore decided to make experimental mobility measurements with a clean chamber and to obtain mobility distributions by the analysis of asymmetric parabolic flow profiles, as discussed thoroughly in Chapter 4.

REFERENCES

Allen, R. E., P. H. Rhodes, R. S. Snyder, G. H. Barlow, M. Bier, P. E. Bigazzi, C. J. Van Oss, R. J. Knox, G. V. F. Seaman, F. J. Micale, and J. W. Vanderhoff. Column electrophoresis on the Apollo-Soyuz test project, Sep. and Purif. Meth. 6, 1-28, 1977.

Catsimpoolas, N., A. L. Griffith, J. M. Williams, A. Chrambach, and D. Rodbard. Electrophoresis with continuous scanning densitometry: Separation of cells in a density gradient, Anal. Biochem. 69, 372-384, 1975.

Hjertén, S. Freezone electrophoresis (Ph.D. thesis) Almquist and Wiksells Boktryckeri AB, Uppsala, 1967.

Hjertén, S. Free zone electrophoresis, Chromatogr. Rev. 9, 122-219, 1967.

Snyder, R. S., M. Bier, R. N. Griffin, A. J. Johnson, H. Leidheiser, Jr., F. J. Micale, J. W. Vanderhoff, S. Ross, and C. J. van Oss. Free fluid particle electrophoresis on Apollo 16, Sep. Purif. Meth. 2, 259-282, 1973.

Van Oss, C. J., R. M. Fike, R. J. Good, and J. M. Reinig. Cell microelectrophoresis simplified by the reduction and uniformization of the electroosmotic backflow, Anal. Biochem. 60, 242-251, 1974.

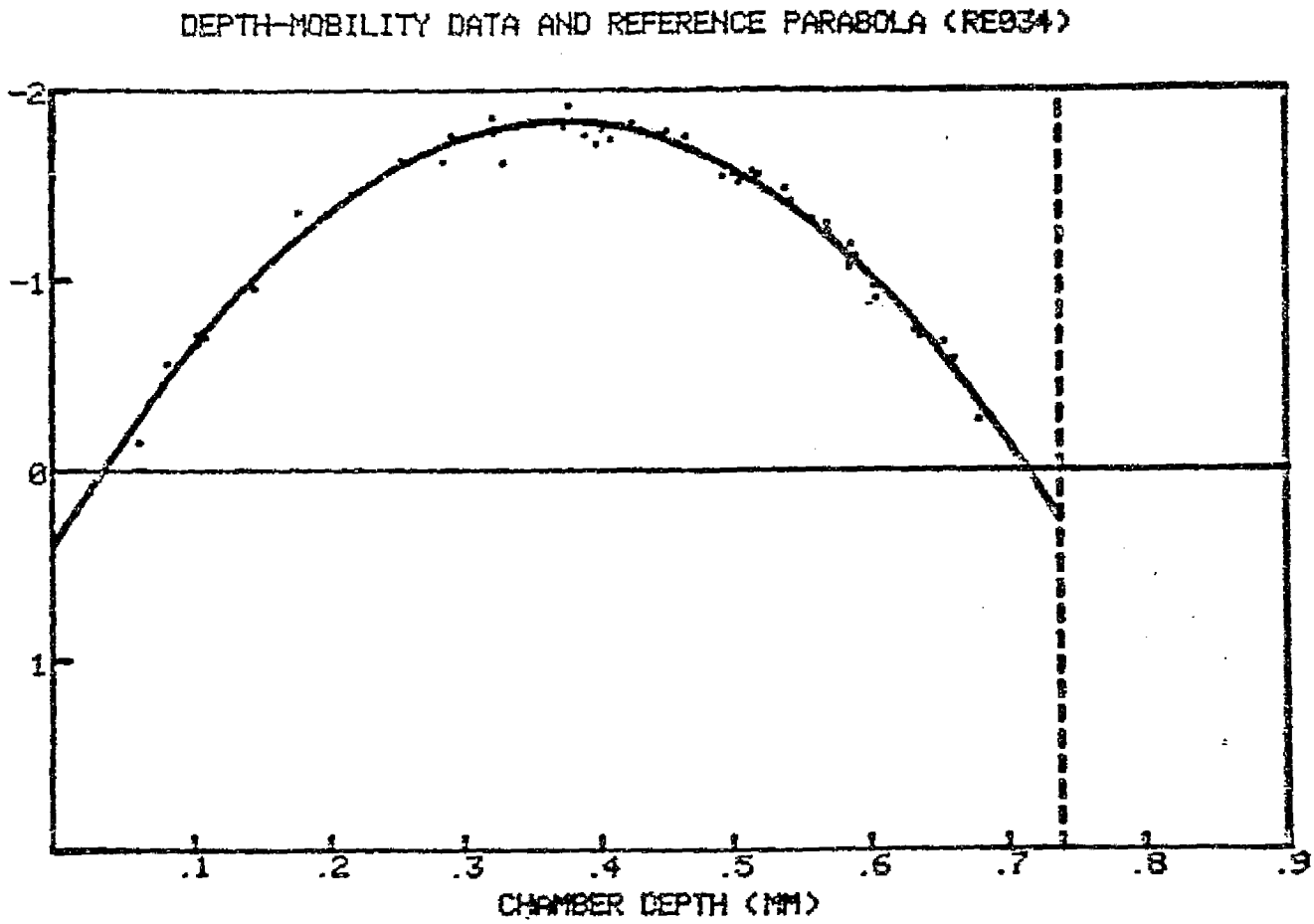

Figure 1. Typical electroosmotic flow parabola obtained by measuring cell velocities at different depths in the Zeiss Cytopherometer chamber with uncoated walls, cleaned as specified in Chapter 5.

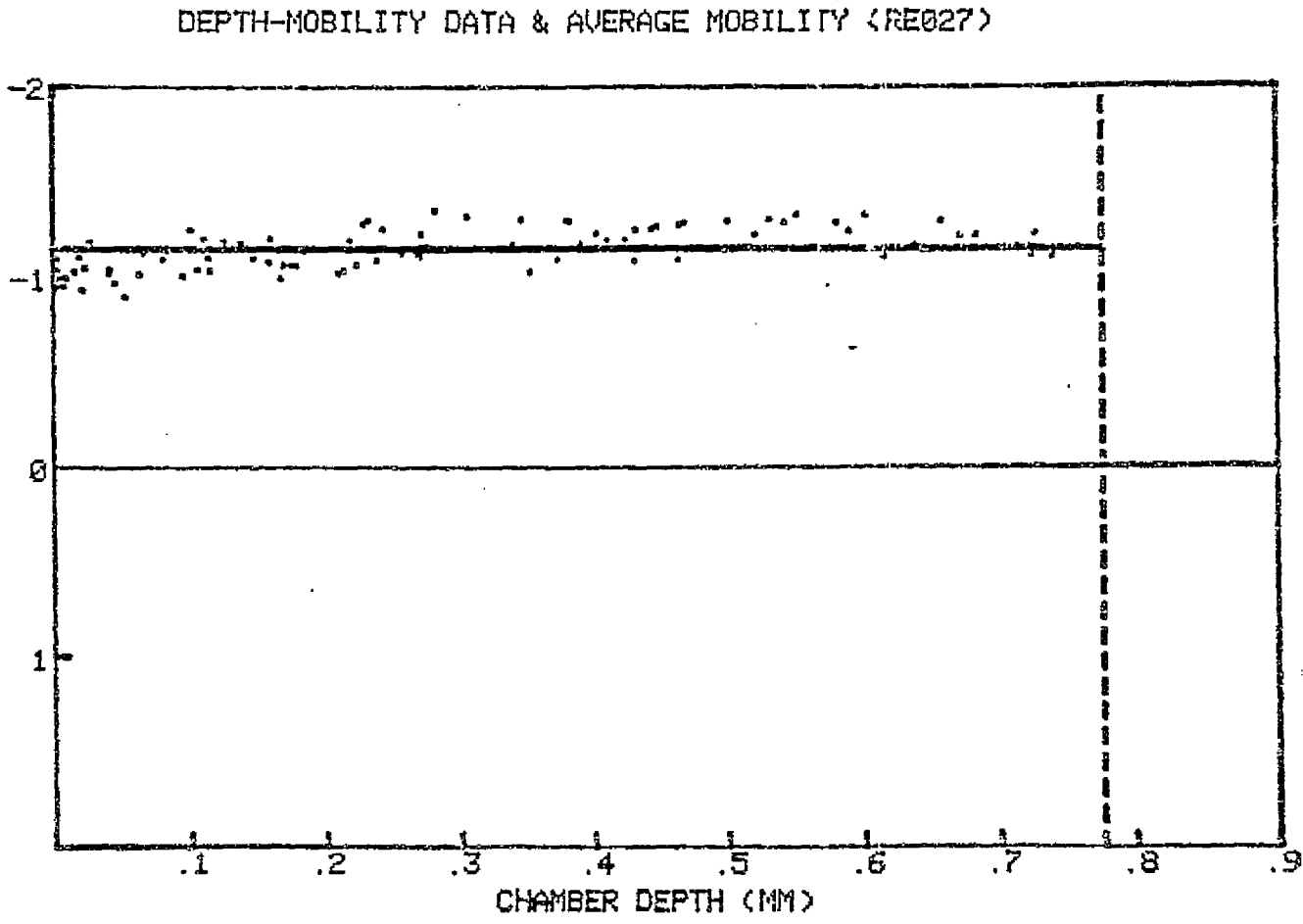

Figure 2. Depth-mobility profile, determined as in Figure 1, for fixed rat erythrocytes in 0.145 M NaCl in methylcellulose coated chamber.

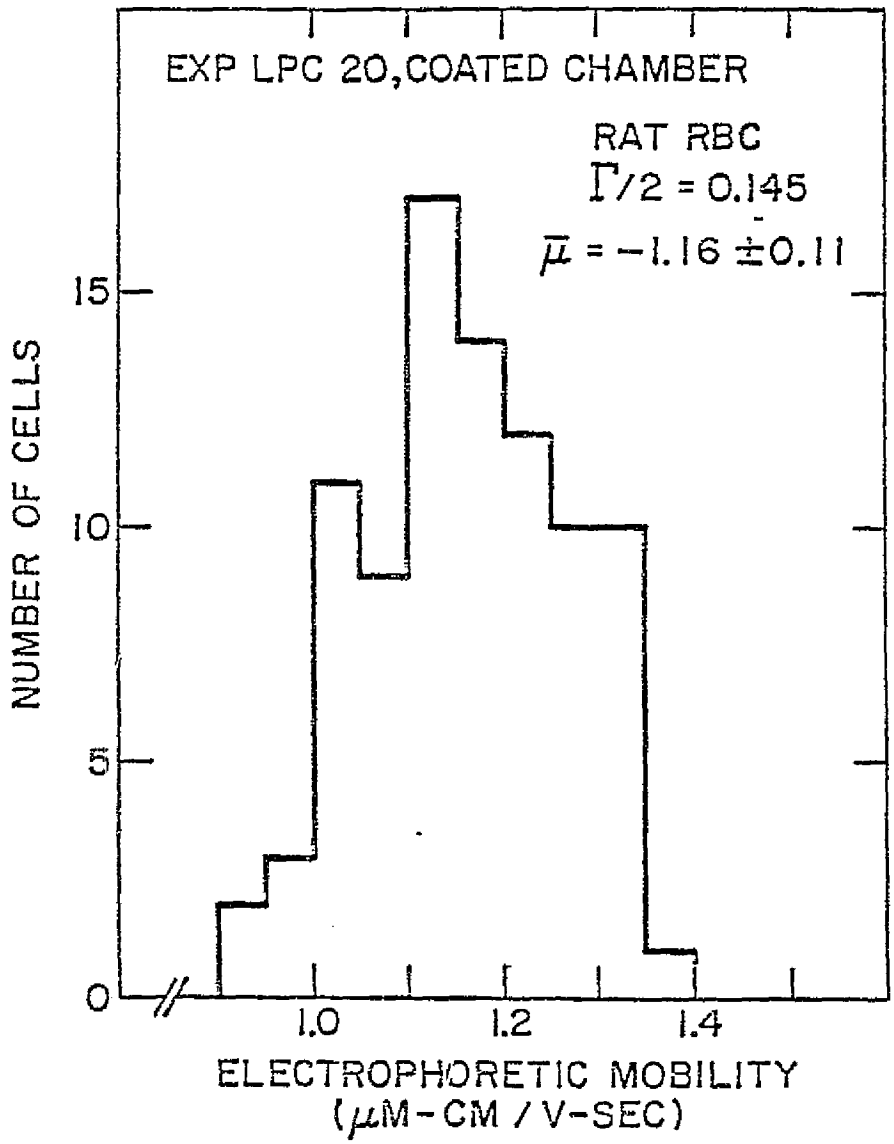

Figure 3. Histogram of cell electrophoretic mobilities obtained from the data of Figure 2, giving mean mobility and standard deviation.

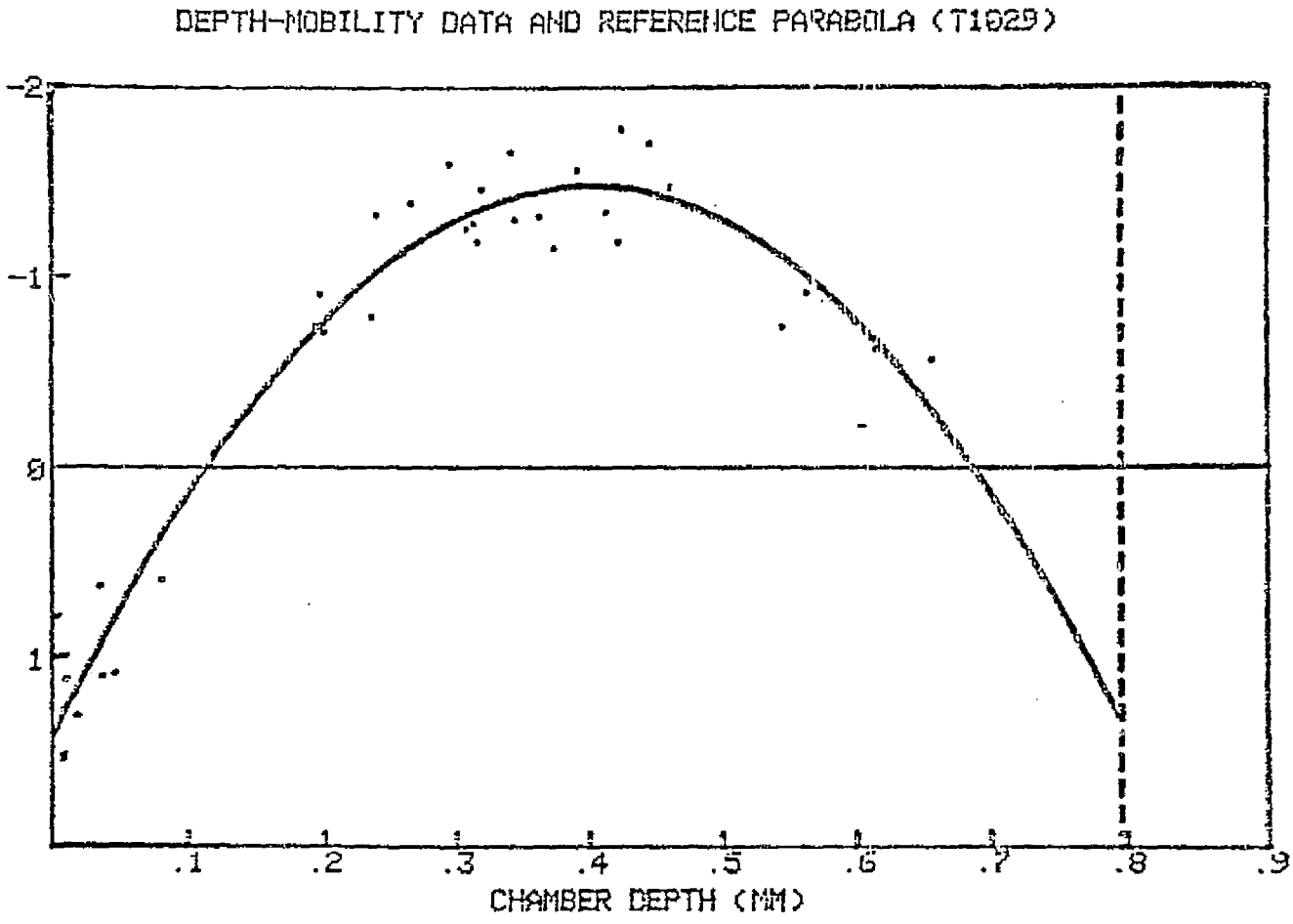

Figure 4. Same as Figure 2, but chamber was cleaned and coated a second time.

Chapter 4.

A New Method of Analysing Microelectrophoretic Data.

CHAPTER 4

A NEW METHOD OF ANALYZING MICROELECTROPHORETIC DATA

Asymmetric Electroosmotic Flow and Mobility Measurements at Nonstationary Positions in the Rectangular Chamber

Introduction

The electrophoretic mobility of a cell in solution is defined by its velocity divided by the electric field strength it experiences. An obvious way to measure the mobility of cells is to apply a constant electric field to a suspension of cells in a glass chamber and clock the velocities of individual cells through a microscope. Although more sophisticated methods have recently been developed (187), this microscope method is the classic technique in cell electrophoresis and it has been used for the bulk of research in this field (25). Two aspects of the microscope method can critically affect the accuracy and consistency of its cell mobility measurements: the electroosmotic fluctuations in the chamber from measurement to measurement (25), and the number of cells which can be practically measured for statistically meaningful results. A new method of analyzing microelectrophoretic data which addresses both of these aspects has been developed.

The Assumption of Symmetric Electroosmotic Flow

The ease and accuracy of measuring cell mobility has always been hampered by the electroosmotic flow of buffer in the chamber. A thin layer of water against the glass walls of the chamber is polarized by the fixed negative charges of the glass. If an electric potential is

applied across ends of the chamber, this polarized water layer will be dragged along the four side walls toward the cathode and then forced back through the center of the chamber toward the anode because the system is sealed at both ends. This situation creates laminar, parabolic flow of buffer across the two dimensions of the chamber perpendicular to the electric field (160) (see Figure 10). The observed velocity of a cell in this chamber is the vector sum of its electrophoretic velocity and the velocity of the buffer at the cell position. Any contribution to the observed cell velocity due to a net drift of fluid through the chamber is eliminated by routinely reversing the field polarity and averaging left and right transit times for each cell. One can only observe true electrophoretic cell velocities if the microscope is focused at positions in the chamber where the fluid velocity is zero. In the thin, rectangular chambers required for high resolution microscopy, these positions form two planes, called stationary planes or stationary levels. These stationary positions could be determined experimentally by observing chamber positions at which particles having a net charge of zero in solution do not move during application of a field. However, no suitable particle has been found and experimenters resort to using theoretical predictions for stationary positions based on work by Smoluchowski (160) and Komagata (91). Their theoretical, hydrodynamic treatment, which predicts stationary positions solely on the basis of chamber geometry, is based on the assumption that the fluid velocity is always symmetric; that is, that the electroosmotic velocities along all four side walls of the chamber are forever equal. The error in mobility measurements introduced by this assumption is examined and corrected.

Limits to the Number of Observations

There are limitations to the number of cells which can be accurately measured by the microscope method during a single experiment. This number is crucial to the statistical significance of the results. There is a natural time limit to the consistent behavior of the cells, the chamber and the experimenter. The condition of the cell surface can change with time by active metabolism and transport of surface macromolecules, or by degeneration, particularly at extremes of pH (152). The surface charge densities of the chamber walls, which determine the shape of the internal electroosmotic flow, can change with time by direct chemical modification or by adsorption of material from the cell suspension. Also the level of concentration demanded of the experimenter will drop after a certain length of time. Given an interval of time defined by these limits, the method of taking data determines the number of cells which can be accurately measured.

Present Techniques

In the literature, most microscope mobility measurements are made by first focusing at a theoretical stationary position and then recording the velocities of only those cells in good focus; these data are then used to construct a mobility histogram (25). There are certain drawbacks to this method. It does not consider the possibility of asymmetric electroosmotic flow and the resulting shifts in stationary positions during mobility measurements. Furthermore, few cells will be readily found in a single focal plane (typically 10-20 cells are measured) and the high concentration of cells required to facilitate these measurements may sometimes be difficult to obtain. Cells which

are slightly out of focus and measured will not be in the predicted stationary position. Although these errors may be minimized by averaging data, they are usually neglected in the calculation of mobilities.

A second method measures cells throughout the chamber depth and plots their velocities against the square of their chamber position, using the chamber center as an origin (54). The best straight line is drawn through these points and the ordinate of this line at the square of the theoretical stationary position is taken as the average electrophoretic velocity of the cell population. There are drawbacks to this method as well. Again, this method ignores possible shifts in the stationary positions due to asymmetric electroosmotic fluid flow. Using this plotting technique, cell data will fall along a straight line only during symmetric electroosmotic flow. Although the average mobility estimate is based on a relatively large number of cells (20-80), the natural dispersion of mobilities about this average value is ignored. This technique is therefore only appropriate for homogeneous cell populations and waives the possibility of detecting mobility subpopulations.

A new method of analyzing microelectrophoretic data using a computer program has been developed which combines the most useful features of each method discussed, and resolves their inherent problems. It makes possible the mobility measurements of individual cells as positions throughout the rectangular chamber depth during asymmetric electroosmotic flow.

Materials and Methods

Rat, chicken and rabbit erythrocytes, fixed with 2.5% glutaraldehyde (167), were washed and resuspended as pure or mixed populations

in Furchgott and Ponder buffer, FPB (52), or phosphate buffer with or without sucrose (PB or PSB; see Table 1) at 1.2×10^6 cells/ml. Mobilities of these cells were measured at a constant current of 1.0 mA, at constant temperatures between 1°-37°C using a rectangular chamber of dimensions $0.7 \times 14.0 \times 60.0$ mm^3. Cell mobilities were normalized for various viscosities to that of water at 25°C, 0.8937 ceitipoise. Cell velocities were recorded with their positions throughout the depth of the chamber; 40-80 cells were timed. These data were punched into computer cards and fed to a Fortran IV program whose function is outlined as follows:

a. The 'apparent mobility', $\mu_a(x)$, is calculated for each cell by dividing its observed velocity, $v_o(x)$, by the electric field strength, E, and correcting for viscosity. This value includes an electroosmotic component. The next four steps serve to subtract out this component.

b. Using least squares analysis, a 'reference parabola' is fitted to the entire set of apparent cell mobilities and their positions. The shape of this parabola reflects the shape of the electroosmotic fluid velocity across the chamber during the experiment: at any position x in the chamber, the average observed velocity of the cell population, $\bar{v}_o(x)$, differs from the fluid velocity, $v_f(x)$, by a constant. This constant is the average electrophoretic velocity of the cell population, $\bar{v}_e$. That is,

$$\bar{v}_o(x) = \bar{v}_e + v_f(x) \qquad (3.1)$$

See Figure 5.

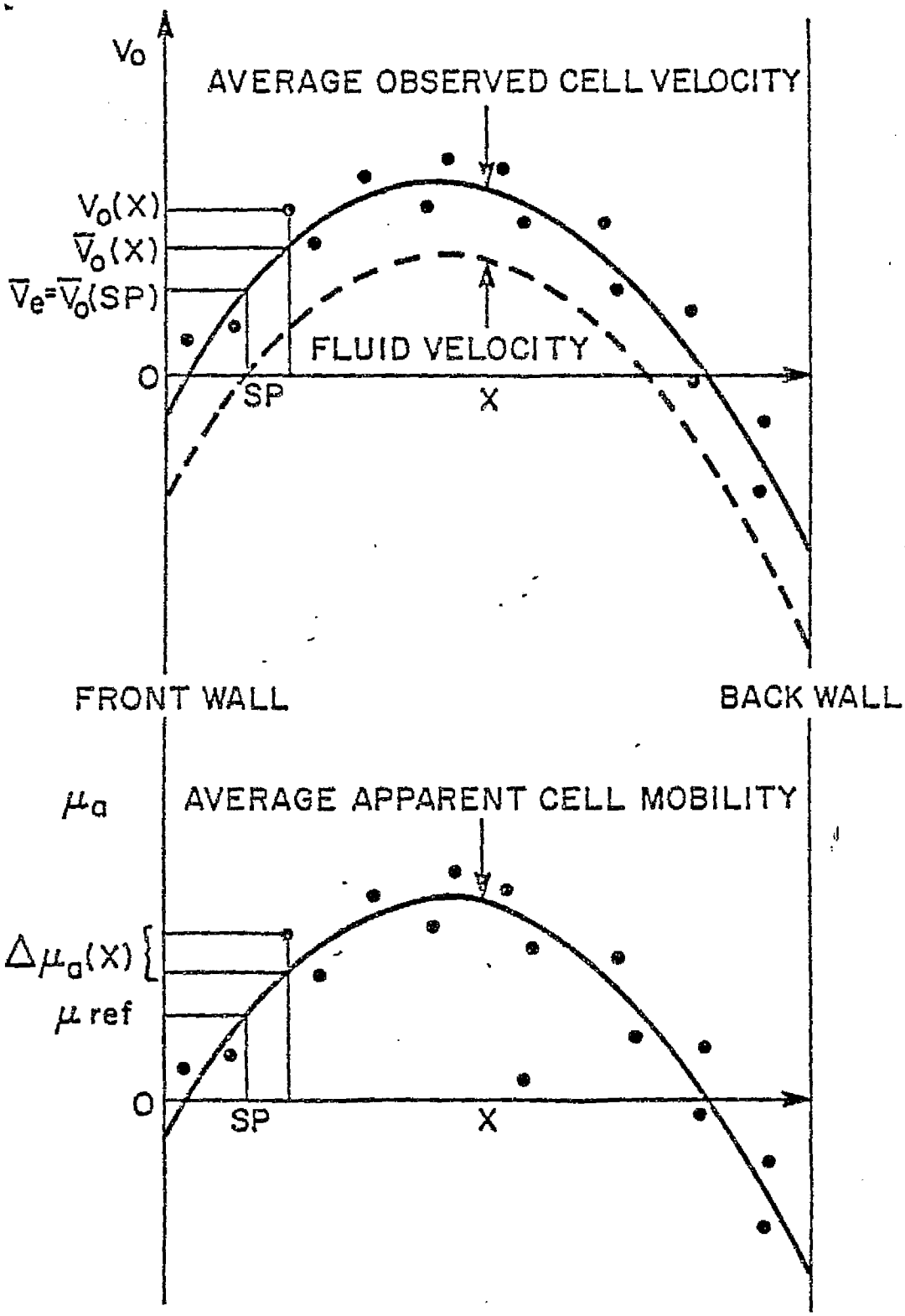

Figure 5. Geometry of cell and buffer flow in the microscopic electrophoresis chamber.

c. The reference parabola equation obtained by regression analysis is used to predict the locations of the stationary positions in the chamber during asymmetric fluid flow by applying the results of the hydrodynamic treatment described in Part B, Chapter III.

d. The reference parabola is assigned its ordinate mobility value, μ_{ref}, on the regression curve at the calculated stationary points. This curve now serves as a reference from which all apparent cell mobilities are recalculated as true mobilities for cells measured throughout the chamber, not simply those at the stationary positions.

e. The true mobilities are obtained by simply adding the vertical displacement between the apparent mobility of each cell and the reference curve, $\Delta\mu_a(x)$, to the reference mobility, μ_{ref}. The derivation of this approach is as follows:

The observed velocity of a cell is the sum of its electrophoretic velocity and the fluid velocity at the cell position x,

$$v_o(x) = v_e + v_f(x) \tag{3.2}$$

This relationship also holds for the average observed velocity of a cell population measured at any position x,

$$\bar{v}_o(x) = \bar{v}_e + v_f(x) = \bar{v}_o(sp) + v_f(x) \tag{3.3}$$

where sp is a stationary position. From Eqs. (3.2) and (3.3) it follows that, for any cell

$$v_e = \bar{v}_o(sp) + (v_o(x) - \bar{v}_o(x))$$

and by dividing by the electric field strength, E, one obtains:

$$\mu(x,v_o) = \mu_{ref} + \Delta\mu_a(x) \qquad (3.4)$$

where $\mu(x,v_o)$ is the true mobility of an individual cell observed at depth x with a velocity v_o (see Figure 5).

Apparent mobility points from cells sharing the reference curve mobility will fall directly on the reference curve. Those data points from a population with a different mobility will fall on a parallel 'iso-mobility' curve which is vertically displaced from the reference by the mobility difference.

f. The program output displays cell mobility data in multiple histogram form, using class widths specified by the user.

This program performs a two-step analysis of data from a maximum of eight experiments. It is compiled under G level Fortran, requires 35K bytes of core, and averages 0.3 seconds execution time per experiment on the IBM 370-168.

Evidence for Asymmetric Flow

The regression curves from three sequential experiments with pure populations of glutaraldehyde-fixed rat, chicken and rabbit erythrocytes, plotted in Figure 6, demonstrate the parallel nature of iso-mobility curves in the chamber. Furthermore, the slope of these curves indicates that the electroosmotic flow was asymmetric during all three experiments. Of 28 experiments with fixed erythrocytes and

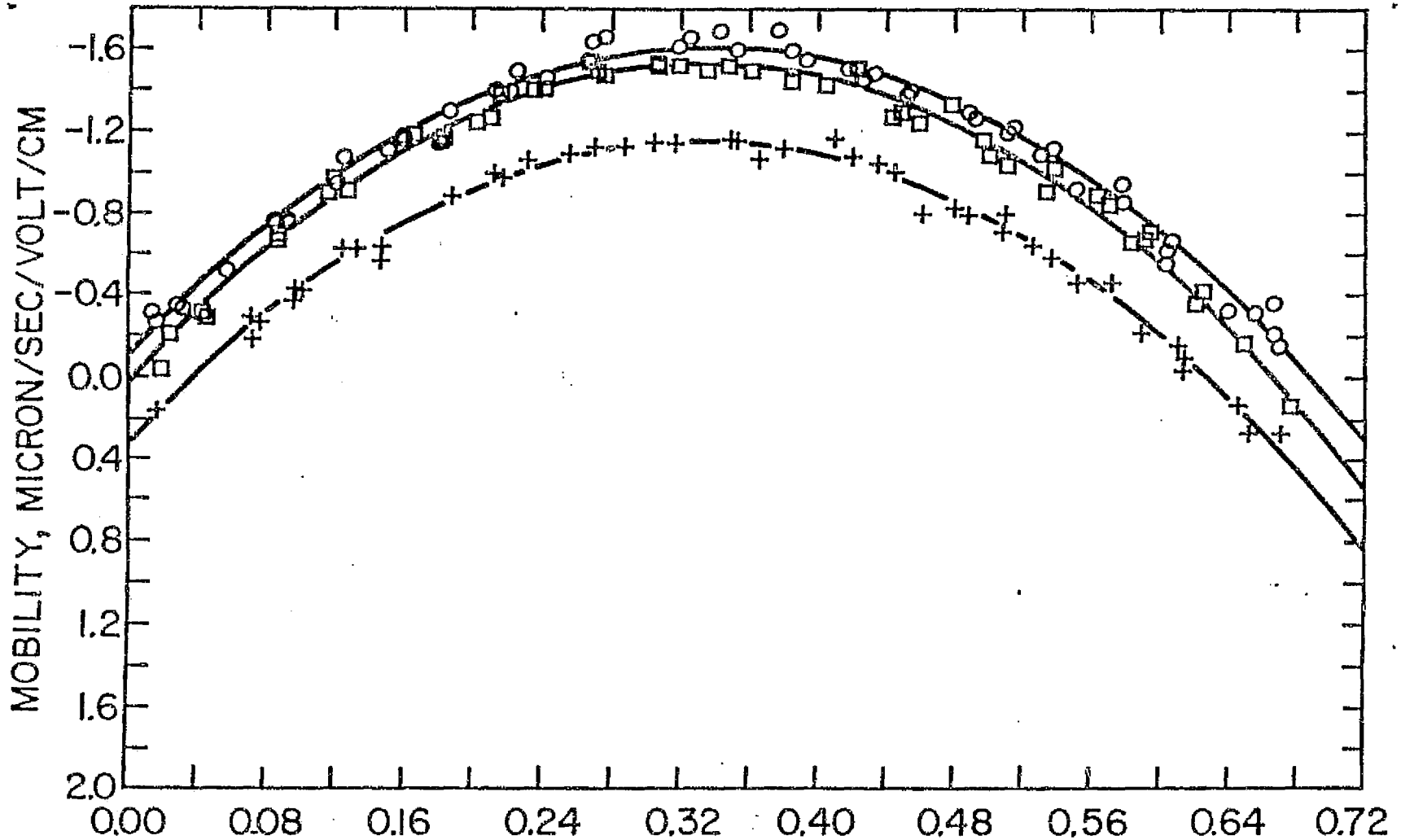

Figure 6. Electrophoretic flow parabolas for sequential measurements on fixed rat, chicken and rabbit erythrocytes.

303 with tissue-cultured cells using this technique (172), all but 26 or 8% were clearly asymmetric to varying degrees. The predicted stationary levels will shift by an amount proportional to the degree of asymmetry.

Asymmetric flow may be caused by an inherent difference in surface charge density on the front and back glass walls of the chamber (25) or by the difference in orientation of reference scratches on these walls. It may also be due to nonuniform heating or heat transfer across the chamber depth in response to electric current or light from the microscope illuminator (25). These explanations seem unlikely in view of the lack of consistency in the degree of asymmetry observed. More likely, asymmetric flow is caused by changes in the surface charge density of the glass walls due to the adsorption of ions from cleaning agents (such as chromic acid: CrO_3/H_2SO_4 or CrO_3/HNO_3), buffer solutes or cells. This includes the accumulation of sedimenting cells on the bottom of the chamber.

The possibility of asymmetric flow in the cylindrical chamber certainly exists, but was not explored.

Evidence for Parallel Iso-mobility Parabolas

Measuring the mobility of a cell at any depth in the chamber, using the computer program previously described, requires two conditions: that the velocity of cells with the same mobility fall on a single velocity-depth parabola during a given experiment; and secondly, that the set of these parabolas from cells with different mobilities will be parallel during a given experiment; that is, each parabola will be vertically displaced from any other by a constant (these two

conditions equally apply to apparent mobility parabolas because they differ vertically from their velocity-depth curves by a constant: the viscosity correlation divided by the electric field strength.

The results of electrophoresis using a mixture of glutaraldehyde-fixed rabbit and chicken erythrocytes, easily distinguishable under the microscope, in PSB at 1°C are plotted in Figure 7 and demonstrate that both of the above conditions are fulfilled. The upper solid curve is the least squares parabola fitted to the apparent mobilities of the chicken erythrocytes, the lower solid curve is that of the rabbit erythrocytes. The mobility spectrum of each cell type falls around its respective mobility parabola, and both curves are closely parallel.

Correction of Mobility Measurements due to Asymmetric Flow

Table 2 contains mobility corrections due to asymmetric flow for 13 experiments. For 28 experiments, the average correction in the front stationary position was 2% of the chamber width, more than double the Komagata correction of 0.9% for our chamber which has a height/width ratio of 20. These shifts in stationary positions resulted in an average correction in mobility calculations of 0.13 μm/sec/volt/cm or 15% of the average mobility value. Calculated shifts in stationary positions exceeding 3% of the chamber depth were recorded between experiments conducted within a three-hour period.

A good approximation of average mobility during asymmetric flow is the average of mobilities measured at the uncorrected stationary positions predicted by Komagata's formula, Equation (3.21). Using this approach, the average mobilities for each of the above 28 experiments were recalculated. The average asymmetric correction required

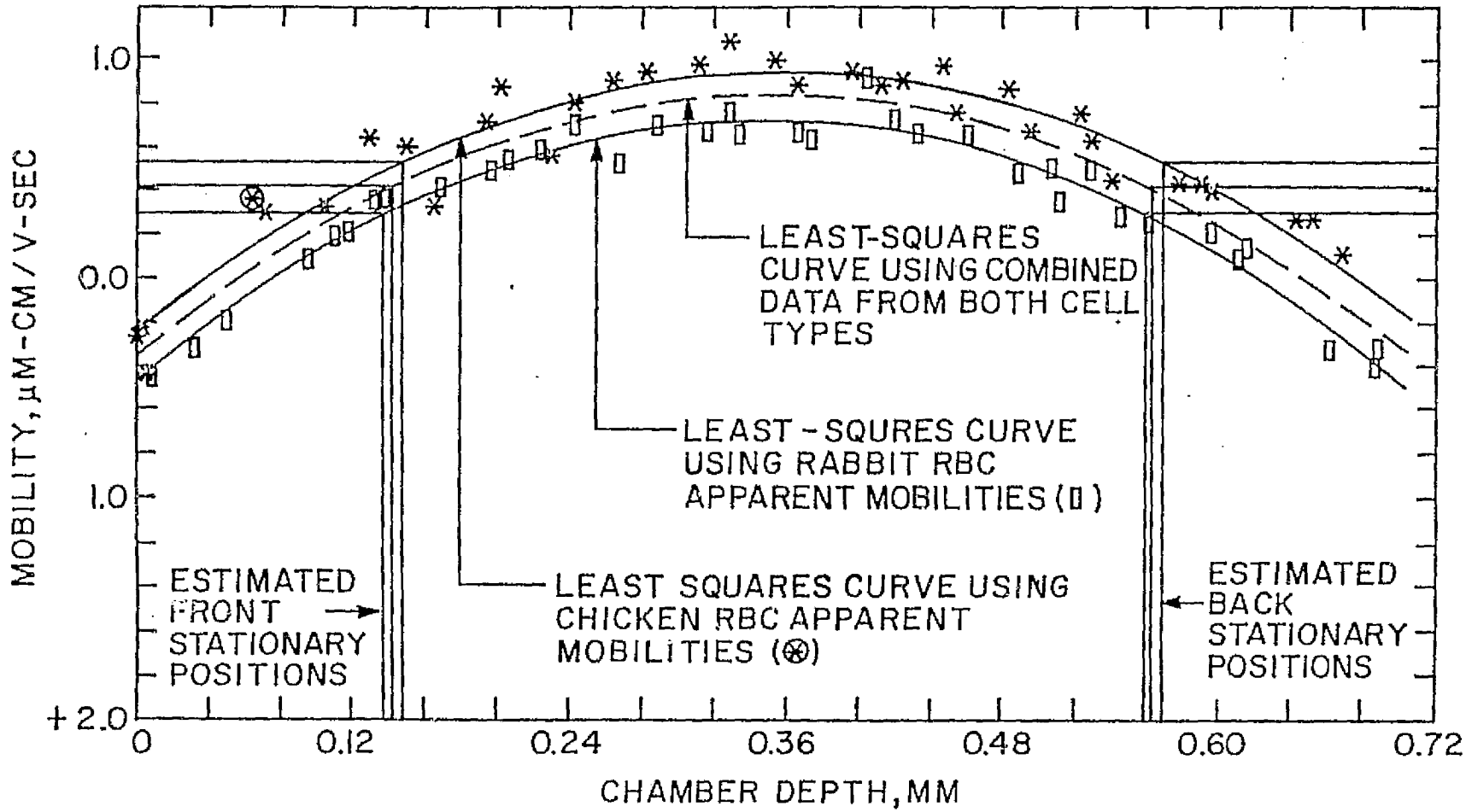

Figure 7. Apparent mobility vs. chamber depth curves for a mixture of rabbit and chicken fixed erythrocytes.

Table 2. Typical Corrections to Cell Mobility Measurements due to Asymmetric Electroosmotic Flow (sp = stationary plane).

Fixed Erythrocyte	Electrophoresis Buffer	Temp. ^{o}C	Front Stationary Position Correction, % Chamber Width	Average Mobility at uncorrected front SP μm/sec/V/cm	Average Mobility at corrected front SP μm/sec/V/cm	Mobility Correction μm/sec/V/cm
Rat	PSB	2.6	3.3	1.262	1.128	-.134
Chicken	PSB	2.6	3.9	1.164	0.997	-.167
Rabbit	PSB	2.6	4.1	0.788	0.617	-.171
Rat	PB	4.0	2.7	1.403	1.225	-.178
Chicken	PB	4.0	2.7	1.231	1.054	-.177
Rabbit	PB	4.0	3.1	0.892	0.679	-.213
Rat	FPB	25.0	1.0	1.198	1.113	-.085
Chicken	FPB	25.0	1.0	0.919	0.882	-.037
Rabbit	FPB	25.0	0.4	0.278	0.301	+.023
Chicken	PSB	20.0	2.7	1.249	1.011	-.238
Rabbit	PSB	20.0	0.7	0.784	0.734	-.050
Chicken	PSB	37.0	1.0	1.913	1.779	-.134
Rabbit	PSB	37.0	1.1	1.059	0.892	-.167

for these new values was only 0.002 μm/sec/volt/cm, or 0.2% of the average mobility value. The mathematical correctness of this approach was not derived rigorously.

The error in mobility measurements contributed by ignoring a shift in stationary position depends directly on the electroosmotic velocity gradient through the true stationary point. This gradient may be reduced by minimizing the electroosmotic velocity. This can be accomplished by modifying the charges on the chamber walls (182) or by increasing the chamber width. An increase in width, however, may result in increased temperature and viscosity gradients in that dimension which would also cause a shift in stationary positions.

Detection of Mobility Subpopulations with Improved Statistics

By focusing throughout the chamber depth, the mobilities of more cells can be measured more accurately than by using the conventional stationary plane technique, for a given time interval and cell concentration. At 1.2×10^6 cells/ml, 70 cells per hour were routinely timed and their data recorded.

The mobility histogram of 72 cells obtained by this computerized analysis on velocity-depth data from a mixture of fixed chicken and rabbit erythrocytes, plotted in Figure 8, clearly indicates the presence of both cell types and demonstrates the ability of this method to detect mobility subpopulations. It represents a statistical improvement over histograms generated from stationary plane measurements. The difference between the average mobilities of the two cell types was 0.2 μm/sec/volt/cm. The histogram in Figure 9, generated from the combined experimental data plotted in Figure 6, presents a slight

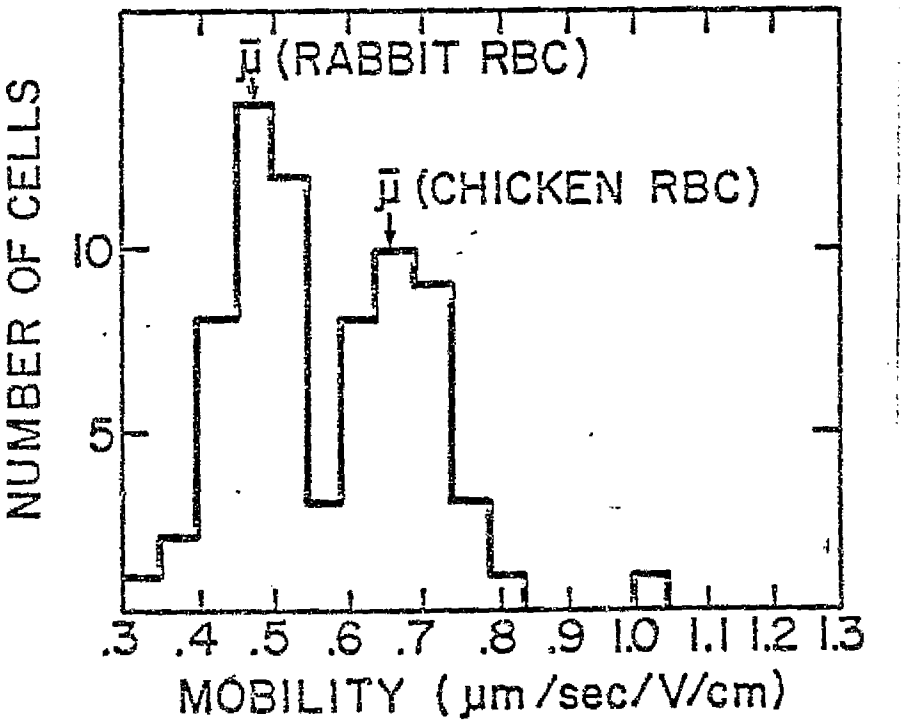

Figure 8. Mobility histogram obtained by computer analysis of micro-electrophoretic data from a mixture of rabbit and chicken fixed erythrocytes.

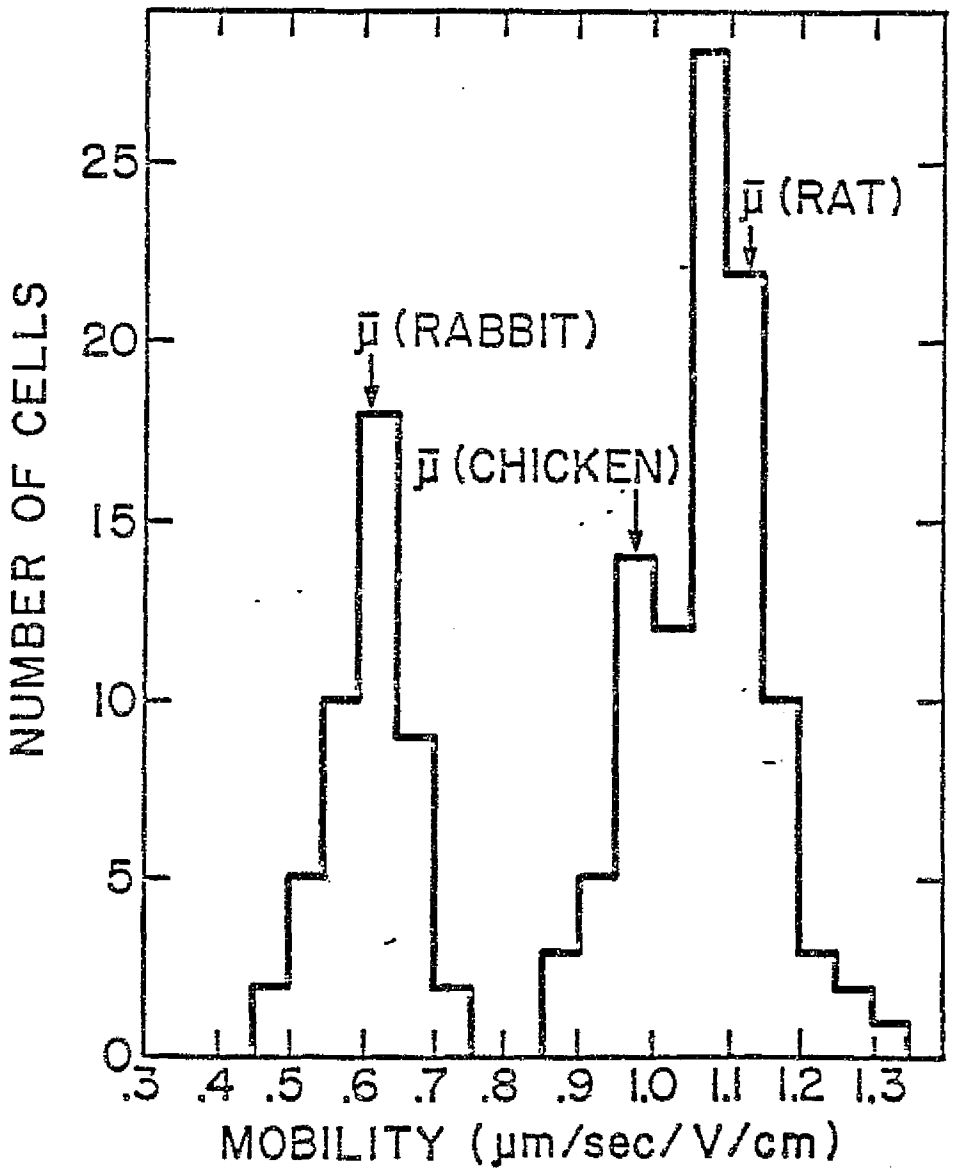

Figure 9. Mobility histogram obtained by computer analysis of combined microelectrophoretic data from rat, chicken and rabbit fixed erythrocytes.

indication of both rat and chicken erythrocyte populations, representing a difference in average mobility of 0.1 μm/sec/volt/cm and possibly defines the limit of resolution of this technique since separation was not improved when smaller histogram class widths were chosen.

Summary

The consideration of time-dependent asymmetric electroosmotic flow is not only important to accurate interpretation of classical microscope mobility measurements, but also to the development and calibration of automated methods in cell electrophoresis which depend on stationary position determinations. It is our experience that electroosmotic flow in a small glass chamber is generally asymmetric to varying degrees and that the resulting corrections to cell mobility measurements are significant. A computerized analysis is presented which determines the electrophoretic mobility of cells clocked at any depth in the rectangular chamber during asymmetric electroosmotic flow.

Theoretical Prediction of Stationary Positions in the Rectangular Chamber during Asymmetric Electroosmotic Flow

Introduction

Most microscopic cell electrophoretic work depends on the theoretical prediction of stationary positions by Smoluchowski (160) and Komagata (91). Their theoretical solutions are based on the assumption that the electroosmotic flow in a chamber is symmetric. Because our experiences with the rectangular chamber indicate that symmetric flow occurs during less than 8% of our experiments, the existing theory for stationary position determination is expanded to include the more general case of asymmetric flow.

Asymmetric Solution for Rectangular Chambers of Height/Width Ratio Greater than 40

Smoluchowski obtained the following equation for symmetric electroosmotic flow in a rectangular chamber having a width much smaller than its height or length:

$$v_f(x) = \tfrac{1}{2}v_f(\pm a)(3x^2/a^2 - 1) \qquad (3.5)$$

where x is the depth in the chamber measuring from the midpoint, a is the distance from the midpoint to either wall and $v_f(x)$ is the electroosmotic velocity of a fluid plane through x (see Figure 10(a)). Solving for x at which $v_f(x)$ is zero (that is, at the stationary positions) yields,

$$x = \pm a/\sqrt{3} \qquad (3.6)$$

This solution predicts a zero fluid velocity at 0.21 and 0.79 of the chamber width and it is used to approximate stationary positions in rectangular chambers with height/width ratios greater than 40 (25). The following derivation uses Smoluchowski's approach in solving the analogous problem with asymmetric flow.

Assume a rectangular chamber of dimensions l x h x w, such that w is very small compared to l and h. Let w = 2a (see Figure 10(a)). Given the electroosmotic flow of a thin water layer against each wall in response to an applied voltage between the two end walls, two forces establish the laminar parabolic flow in the chamber. One is the viscous pull each layer of fluid experiences from its neighbor.

$$F = \eta A \frac{dv_f(x)}{dx}$$

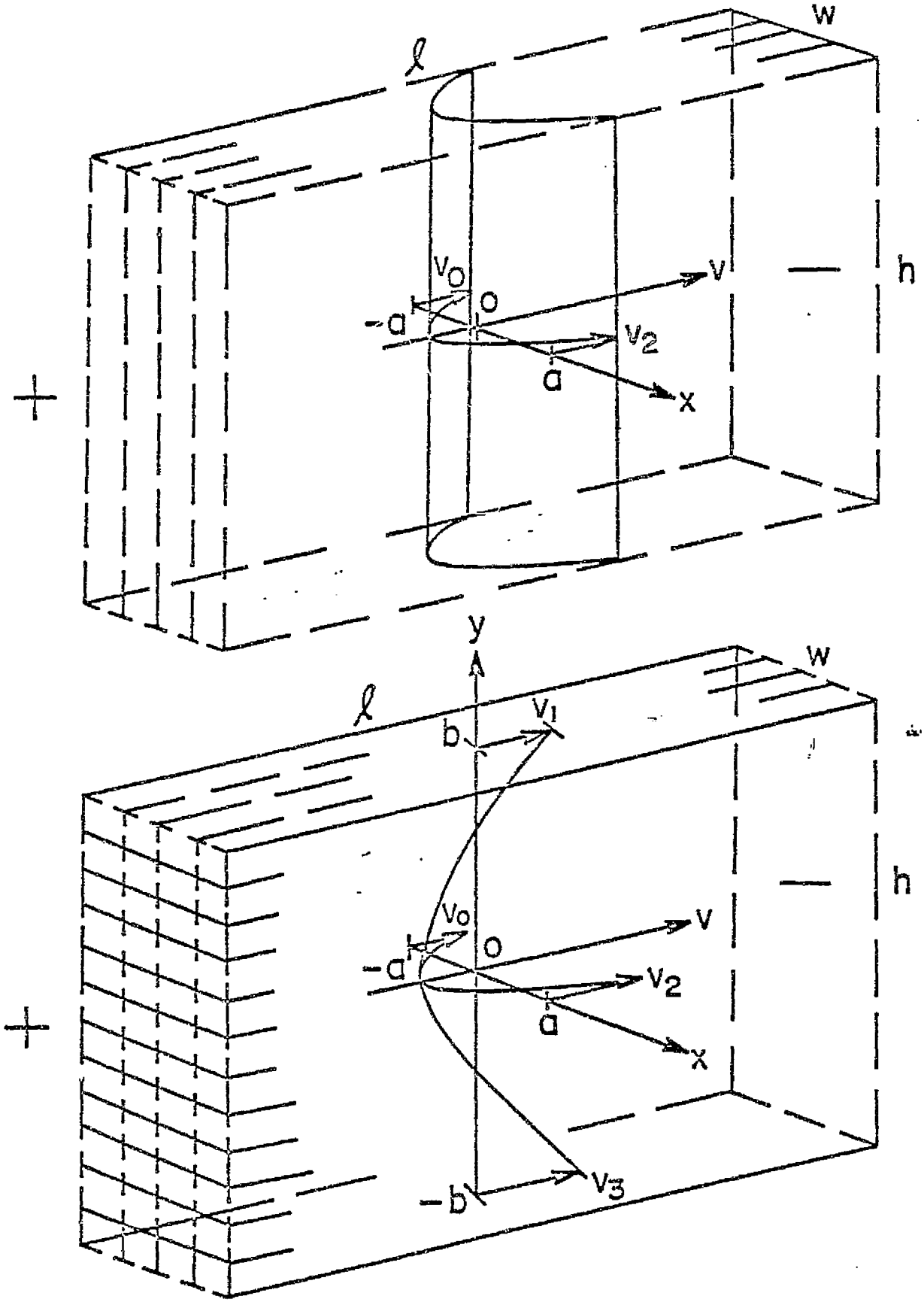

Figure 10. Coordinate system for analyzing electroosmosis in a rectangular chamber.

where η is the fluid viscosity, A = l x h is the area of each fluid layer, and $\frac{dv_f(x)}{dx}$ is the electroosmotic fluid velocity gradient between the neighboring fluid layers at x. Each fluid layer also encounters an equal and opposite force at the end wall of the chamber toward which it is constantly moving. This force is the pressure, P, exerted by this wall over the cross sectional area of the layer against the wall, hdx, and is given by,

$$F = Phdx$$

These two forces are equated as follows:

$$F = \eta A \frac{dv_f(x)}{dx} = Phdx$$

or,

$$\eta(lh) \frac{d}{dx}\left(\frac{dv_f(x)}{dx}\right) dx = Phdx$$

and,

$$\frac{d^2 v_f(x)}{dx^2} = \frac{P}{\eta l} \tag{3.7}$$

Solving Eq. (3.7) for vf(x) by indefinite integration yields,

$$vf(x) = \frac{Px^2}{2\eta l} + A'x + B' \tag{3.8}$$

The fluid velocities at the front and back walls, vf(-a) and vf(a), are boundry conditions which determine the constants of integration, A' and B', as follows:

$$vf(a) = \frac{Pa^2}{2\eta l} + A'A + B' \tag{3.9}$$

and

$$v_f(-a) = \frac{Pa^2}{2\eta l} - A'a + B' \tag{3.10}$$

Subtracting Eq. (3.9) from Eq. (3.10) yields,

$$A' = \frac{v_f(a) - v_f(-a)}{2a}$$

Adding Eq. (3.9) to Eq. (3.10) yields,

$$B' = \frac{v_f(a) + v_f(-a)}{2} - \frac{Pa^2}{2\eta l}.$$

A' is the asymmetric component of the electroosmotic flow parabola and is zero only during symmetric flow. The equation for electrosmotic velocity can now be written from Eq. (3.8),

$$vf(x) = \frac{Px^2}{2\eta l} + (v_f(a) - v_f(-a))\frac{x}{2a} + \frac{v_f(a) + v_f(-a)}{2} - \frac{Pa^2}{2\eta l} \tag{3.11}$$

Because the chamber is sealed in a closed system, the net flux of fluid across its width must be zero,

$$\int_{-a}^{a} v_f(x)dx = 0$$

Therefore,

$$\int_{-a}^{a} \frac{Px^2}{2\eta l}\,dx + \int_{-a}^{a} (v_f(a) - v_f(-a))\frac{x}{2a}\,dx + \int_{-a}^{a} \frac{v_f(a) + v_f(-a)}{2}dx - \int_{-a}^{a} \frac{Pa^2}{2\eta l}\,dx = 0$$

or

$$\frac{Pa^3}{3\eta l} + (v_f(a) + v_f(-a))a - \frac{Pa^3}{\eta l} = 0$$

and

$$P = \frac{3\eta l}{2a^2}(v_f(a) + v_f(-a)) \tag{3.12}$$

Substituting Eq. (3.12) for P in Eq. (3.11) yields.

$$v_f(x) = \frac{3}{4a^2}(v_f(a)-v_f(-a))\ x^2 + (v_f(a)-v_f(-a))\ \frac{x}{2a} - \frac{v_f(a)+v_f(-a)}{4} \quad (3.13)$$

Solving this quadratic for the stationary positions, x, such that $v_f(x) = 0$, yields

$$x = \frac{a}{3}\left[-\left(\frac{v_f(a) - v_f(-a)}{v_f(a) + v_f(-a)}\right) \pm \sqrt{\left(\frac{v_f(a) - v_f(-a)}{v_f(a) + v_f(-a)}\right)^2 + 3}\ \right] . \quad (3.14)$$

Define the quantity

$$\frac{v_f(a) - v_f(-a)}{v_f(a) + v_f(-a)} = F$$

where F is the asymmetric flow factor. Note that F will be zero for symmetric electroosmotic flow and increases in absolute value with increasing degree of asymmetry to a maximum of 1. F is solved by using the following clever technique introduced by Milito (115).

Each fluid velocity parabola exhibits a maximum velocity at its apex, occurring at a chamber position defined as x_m. Taking the first derivative of the equation for fluid velocity, Eq. (3.13), one obtains

$$\frac{dv_f(x)}{dx} = (v_f(a) + v_f(-a))\ \frac{3x}{2a^2} + (v_f(a) - v_f(-a))\ \frac{1}{2a} . \quad (3.15)$$

This first derivative will be zero at x_m,

$$\frac{dv_f(x_m)}{dx} = 0 . \quad (3.16)$$

Therefore from Eq. (3.15),

$$F = \frac{v_f(a) - v_f(-a)}{v_f(a) + v_f(-a)} = -\frac{3}{a}\ x_m$$

Although the chamber position of maximum fluid velocity, x_m, is not directly measured by this method, it will coincide with the position of maximum for the average observed cell velocity, which can be directly measured. Let

$$\bar{v}_o(x') = A + Bx' + C(x')^2 \tag{3.17}$$

represent the least squares parabola fitted to a given set of observed cell velocities obtained by microelectrophoresis, where A, B and C are coefficients determined by computerized regression analysis and x' is the chamber depth measured from the front wall. Transforming Eq. (3.17) from this front wall origin which is more practical for data collection, to the midpoint origin used in this theoretical treatment using the relationship,

$$x' = x + a$$

yields,

$$\bar{v}_o(x) = A + B(x + a) + C(x + a)^2$$

This equation represents the average observed cell velocity at any position x in the chamber. Its first derivative yields,

$$\frac{d\bar{v}_o(x)}{dx} = B + 2C(x + a)$$

This first derivative will be zero at x_m, the position of maximum fluid velocity,

$$\frac{d\bar{v}_o(x_m)}{dx} = B + 2C(x_m + a) = 0$$

Therefore,

$$x_m = \frac{-B}{2C} - a \tag{3.18}$$

and from Eq. (3.16),

$$F = 3\left(1 + \frac{B}{2aC}\right)$$

The solution is now complete. From Eqs. (3.14), (3.16), and (3.18), the stationary positions x, measured from the midpoint, in a rectangular chamber of height/width ratio greater than 40, during asymmetric flow are described by,

$$x = \frac{a}{3}\left(-F \pm \sqrt{F^2 + 3}\right) \tag{3.19}$$

where

$$F = 3\left(1 + \frac{B}{2aC}\right),$$

a is the chamber half width, and B and C are, respectively, the x' and $(x')^2$ coefficients determined by regression analysis on a given observed cell velocity data set obtained using the front wall as $x' = 0$.

Because it is convenient for the experimenter to estimate the stationary positions as fractions of the chamber width (xmax or 2a), Eq. (3.19) is rewritten using the front wall as an origin instead of the midpoint, as follows:

$$x' = x + a = x + \frac{xmax}{2}$$

So, at the stationary positions given by Eq. (3.19),

$$x' = \frac{xmax}{6}\left(-F \pm \sqrt{F^2 + 3}\right) + \frac{xmax}{2}$$

or

$$x' = xmax \left[\frac{1}{2} + \frac{1}{6}\left(-F \pm \sqrt{F^2 + 3}\right)\right] \qquad (3.20)$$

If the electroosmotic flow is symmetric, $a = \frac{-B}{2C}$, $F = 0$ and Eqs. (3.19) and (3.20) reduce to the Smoluchowski result, Eq. (3.6).

Asymmetric Solution for Rectangular Chambers of Any Height/Width Ratio

By ingoring the perturbation of electroosmotic flow due to two side walls and the two end walls of the chamber, Smoluchowski could solve the stationary position problem in one dimension, x. The practical application of his solution however, is limited to rectangular chambers whose height/width ratios are greater than 40 (25).

Komagata later solved the problem in two dimensions, x and y, by considering all four side walls of the chamber and assuming the chamber was long enough to neglect fluid flow perturbations from the end walls at the chamber center where cell measurements are taken. He derived the following equation for electroosmotic velocity at position (x,y) in a rectangular chamber of width 2a, height 2b, and length l such that l is much greater than a and b:

$$vf(x,y) = v_o + \frac{P}{2\eta}(a^2 - x^2) + \sum_{n=0}^{\infty}(-1)^{n+1}\left(\frac{16Pa^2}{\eta\pi^3(2n+1)^3} + \frac{4(v_o - v_1)}{\eta\pi(2n+1)}\right)\frac{\cosh(my)\cos(mx)}{\cosh(mb)}$$

where n is the variable integer from 0 to ∞, $m = \frac{(2n+1)\pi}{2a}$, v_o is the fluid velocity along the front and back walls and v_1 is the fluid velocity along the top and bottom walls. Solving for the stationary positions along the central axis of the chamber used for cell measurements, (x,0), at which $v_f(x,0)$ is zero, yields,

$$x = \pm a\sqrt{\frac{1}{3} + \frac{128}{\pi^5 K}} \tag{3.21}$$

where K is the height/width ratio of the chamber, b/a. Substituting chamber width, xmax, for 2a and moving the x origin from the chamber midpoint to the front wall results in,

$$x' = xmax\ (\frac{1}{2} \pm \sqrt{\frac{1}{12} + \frac{32}{\pi^5 K}}) \tag{3.22}$$

Both Eqs. (3.21) and (3.22) assume symmetric electroosmotic flow in the chamber and reduce to the Smoluchowski result when $K = \infty$.

The following derivation by Elaine Milito (114) adopts Komagata's approach in solving the analogous problem with asymmetric flow.

Assume a rectangular chamber of height h = 2b, width w = 2a, and length l which is great compared to h or w (see Figure 10(b)). Also assume a constant fluid velocity along each side wall, equal at all points on that wall, and that this constant velocity can be unique for each of the four side walls. That is, $v_o = v_f(-a),y)$, $v_1 = v_f(x,b)$, $v_2 = v_f(a,y)$ and $v_3 = v_f(x,-b)$ where v_o, v_1, v_2 and v_3 are constants which can differ from each other. By again equating the laminar force on a fluid volume element dx x dy x l,

$$F = \eta\ (ldx)\frac{dv_f}{dy} + (ldy)\frac{dv_f}{dx}$$

with the force exerted by pressure P on the cross sectional end of this fluid element, dxdy, from the end wall of the chamber toward which this fluid element is constantly moving,

$$F = Pdxdy$$

one obtains,

$$\eta(l dx \frac{d^2 v_f}{dy^2} dy + l dy \frac{d^2 v_f}{dx^2} dx) = P dx dy$$

or

$$\frac{d^2 v_f}{dx^2} + \frac{d^2 v_f}{dy^2} = \frac{P}{\eta l} \tag{3.23}$$

Eq. (3.23) is a second order differential equation which is solved using a separation of variables technique (91). Let

$$v_f(x,y) = \chi(x,y) + \frac{P}{2\eta l}(a^2 - x^2)$$

where the variable χ satisfies the relationship,

$$\frac{d^2 \chi}{dx^2} + \frac{d^2 \chi}{dy^2} = 0$$

Then

$$\chi(x,y) = v_f(x,y) - \frac{P}{2\eta l}(a^2 - x^2) \tag{3.24}$$

Eq. (3.24) is satisfied using,

$$\chi(x,y) = \frac{v_2 + v_o}{2} + \frac{v_2 - v_o}{2a} + \sum_{n=0}^{\infty} \tau_n(y) \cos(mx) \tag{3.25}$$

where v_o and v_2 are the fluid velocities along the front and back chamber walls, respectively,

$$m = \frac{(2n + 1)\pi}{2a}$$

and

$$\tau_n(y) = A_n \cosh(my) + B_n \sinh(mx) \tag{3.26}$$

The following boundary conditions are applied to solve for the unknown constants, A_n and B_n:

$$\chi(o,b) = v_1 - \frac{Pa^2}{2\eta l} \tag{3.27}$$

$$\chi(o,-b) = v_3 - \frac{Pa^2}{2\eta l} \tag{3.28}$$

$$\chi(a,y) = v_2 \tag{3.29}$$

$$\chi(-a,y) = v_o \tag{3.30}$$

where v_1 and v_3 are the fluid velocities along the top and bottom chamber walls, respectively. From Eq. (3.27),

$$\chi(o,b) = v_1 - \frac{Pa^2}{2\eta l} = \frac{v_2 + v_o}{2} - \left(\frac{v_2 + v_o}{2} - v_1 + \frac{Pa^2}{2\eta l}\right)$$

and from Eq. (3.25),

$$\chi(o,b) = \frac{v_2 + v_o}{2} + \sum_{n=0}^{\infty} \tau_n(b)$$

Therefore,

$$\sum_{n=0}^{\infty}\tau_n(b) = -\left(\frac{v_2 + v_o}{2} - v_1 + \frac{Pa^2}{2\eta l}\right)$$

Let

$$F(x) = \frac{Px^2}{2\eta l} - \left(\frac{v_2 + v_o}{2} - v_1 + \frac{Pa^2}{2\eta l}\right)$$

At $x = 0$,

$$F(o) = -\left(\frac{v_2 + v_o}{2} - v_1 + \frac{Pa^2}{2\eta l}\right) = \sum_{n=0}^{\infty}\tau_n(b) \tag{3.31}$$

By the Fourier expansion used by Komagata, F(x) can be expressed as:

$$F(x) = \sum_{n=0}^{\infty}(-1)^{n+1}\left[\frac{16Pa^2}{\eta l\pi^3(2n+1)^3} + \frac{4}{\pi(2n+1)}\left(\frac{v_2 + v_o}{2} - v_1\right)\right]\cos(mx)$$

and at x = 0,

$$F(o) = \sum_{n=o}^{\infty}(-1)^{n+1}\left[\frac{16Pa^2}{\eta_1\pi^3(2n+1)^3} + \frac{4}{\pi(2n+1)}\left(\frac{v_2 + v_o}{2} - v_1\right)\right] \quad (3.32)$$

For F(o) then, the summation term, $\tau_n(b)$, and the Fourier summation term must be equal:

$$\tau_n(b) = (-1)^{n+1}\left[\frac{16Pa^2}{\eta_1\pi^3(2n+1)^3} + \frac{2(v_o + v_2 - 2v_1)}{\pi(2n+1)}\right] \quad (3.33)$$

Using this technique for boundary condition (3.28), one obtains,

$$\tau_n(-b) = (-1)^{n+1}\left[\frac{16Pa^2}{\eta_1\pi^3(2n+1)^3} + \frac{2(v_o + v_2 - 2v_3)}{\pi(2n+1)}\right]$$

By Eqs. (3.26) and (3.33),

$$\tau_n(b) = A_n\cosh(mb) + B_n\sinh(mb) = (-1)^{n+1}\left[\frac{16Pa^2}{\eta_1\pi^3(2n+1)^3} + \frac{2(v_o + v_2 - 2v_1)}{\pi(2n+1)}\right] \quad (3.34)$$

Similarly,

$$\tau_n(-b) = A_n\cosh(mb) - B_n\sinh(mb) = (-1)^{n+1}\left[\frac{16Pa^2}{\eta_1\pi^3(2n+1)^3} + \frac{2(v_o + v_2 - 2v_3)}{\pi(2n+1)}\right] \quad (3.35)$$

The unknown constants, A_n and B_n, can now be obtained using the simultaneous equations (3.34) and (3.35),

$$A_n = \frac{(-1)^{n+1}}{\cosh(mb)}\left[\frac{16Pa^2}{\eta_1\pi^3(2n+1)^3} + \frac{2(v_o + v_2 - v_1 - v_3)}{\pi(2n+1)}\right] \quad (3.36)$$

$$B_n = \frac{(-1)^{n+1}}{\sinh(mb)}\frac{(v_3 - v_1)}{\pi(2n+1)}$$

From Eqs. (3.24), (3.25) and (3.26), the electroosmotic velocity now becomes,

$$v_f(x,y) = \frac{v_2 + v_o}{2} + (v_2 - v_o)\frac{x}{2a} + \frac{P(a^2-x^2)}{2\eta l} + \sum_{n=0}^{\infty}\left[A_n\cosh(my) + B_n\sinh(my)\right]\cos(mx) \qquad (3.37)$$

To solve for the remaining unknown, P, the condition of zero net fluid flux across the chamber is applied:

$$\int_{-b}^{b}\int_{-a}^{a} v_f\,dx\,dy = 0$$

Therefore,

$$\int_{-b}^{b}\left[\int_{-a}^{a}\left(\frac{v_2 + v_o}{2} + \frac{v_2 - v_o}{2}x\right)dx + \frac{P}{2\eta l}\int_{-a}^{a}(a^2 - x^2)\,dx + \sum_{n=0}^{\infty}\int_{-a}^{a}(A_n\cosh(my) + B_n\sinh(mx))\cos(mx)\,dx\right]dy = 0$$

Performing the definite integration with respect to x yields,

$$\int_{-b}^{b}\left[\frac{2Pa^3}{3\eta l} + (v_2 + v_o)a + 2\sum_{n=0}^{\infty}\frac{(-1)^n}{m}(A_n\cosh(my) + B_n\sinh(my))\right]dy = 0$$

Definite integration with respect to y yields,

$$2ab(v_2 + v_o) + \frac{4Pa^3b}{3\eta l} + 2\sum_{n=0}^{\infty}\frac{(-1)^n}{m}\frac{2A_n}{m}\sinh(mb) = 0$$

Substituting Eq. (3.36) for A_n produces,

$$2ab(v_2 + v_o) + \frac{4Pa^3b}{3\eta l} + 4\sum_{n=0}^{\infty}\frac{(-1)^n(-1)^n}{m^2}\left[\frac{16Pa^2}{\eta l\pi^3(2n+1)^3} + \frac{2(v_o + v_2 - v_1 - v_3)}{\pi(2n+1)}\right]$$

$$\frac{\sinh(mb)}{\cosh(mb)} = 0$$

Expanding the above, and substituting $\frac{\pi}{2a}(2n+1)$ for m results in,

$$2ab(v_2 + v_o) + \frac{4Pa^3b}{3\eta l} - \frac{256Pa^4}{\eta l \pi^5} \sum_{n=0}^{\infty} \frac{\tanh\left(\frac{\pi b(2n+1)}{2a}\right)}{(2n+1)^5}$$

$$- \frac{32a^2}{\pi^3} (v_o + v_2 - v_1 - v_3) \sum_{n=0}^{\infty} \frac{\tanh\left(\frac{\pi b(2n+1)}{2a}\right)}{(2n+1)^3} = 0$$

Let

$$S_1 = \sum_{n=0}^{\infty} \frac{\tanh\left(\frac{\pi b(2n+1)}{2a}\right)}{(2n+1)^5} \tag{3.38}$$

and

$$S_2 = \sum_{n=0}^{\infty} \frac{\tanh\left(\frac{\pi b(2n+1)}{2a}\right)}{(2n+1)^3} \tag{3.39}$$

Then,

$$2ab(v_2 + v_o) + \frac{4Pa^3b}{3\eta l} - \frac{256Pa^4 S_1}{\eta l \pi^5} - \frac{32a^2}{\pi^3} (v_o + v_2 - v_1 - v_3) S_2 = 0$$

and

$$P = \eta l \frac{(-2ab(v_2 + v_o) + \frac{32a^2}{\pi^3} S_2(v_o + v_2 + v_1 - v_3))}{\frac{4}{3} a^3 b - \frac{256a^4 S_1}{\pi^5}} \tag{3.40}$$

The solution to electroosmotic flow in two dimensions in the rectangular chamber is now complete. Substituting Eq. (3.40) for P in Eq. (3.37) yields,

$$vf(x,y) = \frac{v_2 - v_o}{2} + (v_2 - v_o)\frac{x}{2a} + \frac{\frac{16a^2 S_2}{\pi^3}(v_o + v_2 - v_1 - v_3) - ab(v_2 + v_o)}{\frac{4}{3} a^3 b - \frac{256a^4 S_1}{\pi^5}}(a^2 - x^2)$$

$$+ \sum_{n=0}^{\infty} \left[A_n \cosh(my) + B_n \sinh(my)\right] \cos(mx)$$

The equation of flow at y=0 is desired because mobility measurements are taken through the center of the chamber; that is, at (x,o),

$$vf(x,o) = \frac{v_2 + v_o}{2} + (v_2 - v_o)\frac{x}{2a} + \frac{\frac{16a^2 S_2}{\pi^3}(v_o + v_2 - v_1 - v_3) - ab(v_2 + v_o)}{\frac{4}{3}a^3 b - \frac{256a^4 S_1}{\pi^5}}(a^2 - x^2)$$

$$+ \sum_{n=0}^{\infty} A_n \cos(mx) \qquad (3.41)$$

Because cos(mx) does not change sign here and its absolute value does not exceed unity,

$$\left| \sum_{n=0}^{\infty} A_n \cos(mx) \right| \leq \left| \sum_{n=0}^{\infty} A_n \right| \qquad (3.42)$$

From Eq. (3.36),

$$\sum_{n=0}^{\infty} A_n = \sum_{n=0}^{\infty} \frac{(-1)^{n+1}}{\cosh(mb)} \left[\frac{16Pa^2}{\eta l \pi^3 (2n+1)^3} + \frac{2(v_o + v_2 - v_1 - v_3)}{\pi(2n+1)} \right]$$

Because cosh(mb) does not change sign in this summation, $\sum_{n=0}^{\infty}$ is a sequence of terms decreasing in absolute value and alternating in sign. Therefore,

$$\left| \sum_{n=0}^{\infty} A_n \right| < |A_o| \qquad (3.43)$$

From Eqs. (3.42) and (3.43), the summation $\sum_{n=0}^{\infty} A_n \cos(mx)$ is bounded by A_o. A_o is much smaller than the first three terms of Eq. (3.41) because of the constant $\frac{1}{\cosh(mb)}$. For a height/width ratio of 20, for example, this constant is smaller than 10^{-4} for all values of n. Therefore we assume that the contribution to the fluid velocity by the summation $\sum_{n=0}^{\infty} A_n \cos(mx)$ can be neglected; that is,

$$\sum_{n=0}^{\infty} A_n \cos(mx) << v\ (x,o)$$

and,

$$v_f(x,o) \cong \frac{v_2 + v_o}{2} + (v_2 - v_o)\frac{x}{2a} + \frac{\frac{16a^2 S_2}{\pi^3}(v_o + v_2 - v_1 - v_3) - ab(v_o - v_2)}{\frac{4}{3}a^3 b - \frac{256a^4 S_1}{\pi^5}}(a^2 - x^2)$$

Solving this quadratic equation for the stationary positions x, such that $v_f(x,o) = 0$, yields,

$$x = a\left[\frac{-\frac{(v_2 - v_o)}{2} \pm \sqrt{\left(\frac{v_2 - v_o}{2}\right)^2 + 4A\left(A + \frac{v_2 + v_o}{2}\right)}}{-2A}\right] \qquad (3.44)$$

where

$$A = \frac{\frac{16S_2}{\pi^3 K}(v_o + v_2 - v_1 - v_3) - (v_o + v_2)}{\frac{4}{3} - \frac{256S_1}{\pi^5 K}} \qquad (3.45)$$

and $K = \frac{b}{a}$, the height/width ratio.

Elaine Milito's solution for stationary positions in the rectangular chamber during asymmetric flow, Eq. (3.44), requires an estimate of the fluid velocity at each of the four side walls of the chamber. Although this is possible using a technique covered in a following section, optical measurements must be taken through both the x and y axes of the chamber. Because the apparatus used for microelectrophoresis prohibits observation through the long axis of the rectangular chamber, the derivation in the next section becomes useful.

Stationary Position Estimates during Asymmetric Flow in a Rectangular Chamber of Height/Width Ratio ≥ 20

To calculate the stationary positions using Eq. (3.44), the value of A, defined by Eq. (3.45), is determined for $K \geq 20$. The summations S_1 and S_2, given by Eqs. (3.38) and (3.39) are first determined.

If $K \geq 20$, $\tanh\left[(2n+1)\frac{\pi b}{2a}\right] \cong 1$ for all values of n. Therefore,

$$S_1 = \sum_{n=0}^{\infty} \frac{\tanh\left[(2n+1)\frac{\pi b}{2a}\right]}{(2n+1)^5} \cong \sum_{n=0}^{\infty} \frac{1}{(2n+1)^5}$$

Similarly,

$$S_2 \cong \sum_{n=0}^{\infty} \frac{1}{(2n+1)^3}$$

S_1 and S_2 converge by the integration test (170) and the following summation estimates, S_1' and S_2', were calculated,

$$S_1' = \sum_{n=0}^{10} \frac{1}{(2n+1)^5} = 1.005$$

$$S_2' = \sum_{n=0}^{30} \frac{1}{(2n+1)^3} = 1.052$$

The remainder of S_1' is bounded by

$$\int_{11}^{\infty} \frac{dn}{(2n+1)^5} = 4 \times 10^{-7}$$

and the remainder of S_2' is bounded by

$$\int_{30}^{\infty} \frac{dn}{(2n+1)^3} = -6 \times 10^{-5}$$

indicating that $S_1' = 1.005$ and $S_2' = 1.052$ are accurate summation estimates for S_1 and S_2 respectively (170).

Using S_2', we can calculate the quantity,

$$\frac{16S_2}{\pi^3 K} \leq 0.027$$

for $K \geq 20$. If we make the reasonable assumption that the fluid velocities at the four side walls (v_o, v_1, v_2, v_3) are of the same sign and order of magnitude, the following approximation can be made,

$$\frac{16S_2}{\pi^3 K}(v_o + v_2 - v_1 - v_3) - (v_o + v_2) \cong -(v_o + v_2) \tag{3.46}$$

for $K \geq 20$. From Eq. (3.45),

$$A = \frac{\frac{16S_2}{\pi^3 K}(v_o + v_2 - v_1 - v_3) - (v_o + v_2)}{\frac{4}{3} - \frac{256S_1}{\pi^5 K}} \cong \frac{-(v_o - v_2)}{\frac{4}{3} - \frac{256S_1}{\pi^5 K}}$$

The possible error introduced by assumption (3.46) was examined by Ronald Milito (116) and by this author in a following section.

For $K \geq 20$, Eq. (3.44) now becomes,

$$x = a \frac{\left[-\frac{(v_2 - v_o)}{2} \pm \sqrt{\left(\frac{v_2 - v_o}{2}\right)^2 - \frac{4(v_o + v_2)}{\frac{4}{3} - \frac{256S_1}{\pi^5 K}} \quad \frac{-(v_o + v_2)}{\frac{4}{3} - \frac{256S_1}{\pi^5 K}} + \frac{v_o + v_2}{2}} \right]}{\frac{2(v_o + v_2)}{\frac{4}{3} - \frac{256S_1}{\pi^5 K}}}$$

which reduces to

$$x = a\left(\frac{1}{3} - \frac{64S_1}{\pi^5 K}\right)\left[-\left(\frac{v_2 - v_o}{v_2 + v_o}\right) \pm \sqrt{\left(\frac{v_2 - v_o}{v_2 + v_o}\right) + \frac{1}{\frac{1}{3} - \frac{64S_1}{\pi^5 K}}\left(\frac{1}{\frac{1}{3} - \frac{64S_1}{\pi^5 K}} - 2\right)} \right] \tag{3.47}$$

We now define the asymmetric factor,

$$F = \frac{v_2 - v_o}{v_2 + v_o}$$

and the chamber constant,

$$H = \frac{1}{\frac{1}{3} - \frac{64S_1}{\pi^5 K}}$$

Milito's technique (Eq. 3.18) is used to solve for F. The position in the chamber of maximum electroosmotic flow, x_m, coincides with the position of maximum observed cell velocity. From Eq. (3.18), the maximum in observed cell velocity occurs at,

$$x_m = \frac{-B}{2C} - a$$

where a is the chamber half width and B and C are respectively, the x' and $(x')^2$ coefficients obtained by regression analysis on a given observed cell velocity data set obtained using the front wall as an x' origin. The position of maximum electroosmotic flow is determined by setting the first derivative of the fluid velocity equation to zero and solving for x. By assumption (3.46), the equation for electroosmotic velocity, Eq. (3.41), becomes,

$$v_f(x,o) = \frac{v_2 + v_o}{2} + (v_2 - v_o)\frac{x}{2a} - \frac{ab(v_o + v_2)}{\frac{4}{3}a^3 b - \frac{256a^4 S_1}{\pi^5}}(a^2 - x^2)$$

and,

$$\frac{dv_f(x,o)}{dx} = \frac{v_2 - v_o}{2a} + \frac{2ab(v_o + v_2)\,x}{\frac{4}{3}a^3 b - \frac{256a^4 S_1}{\pi^5}} \qquad (3.48)$$

$$\text{At } x = x_m, \quad \frac{dv_f(x_m, 0)}{dx} = 0$$

Therefore, rearranging Eq. (3.48) and substituting Eq. (3.18) for x_m, yields,

$$F = \frac{v_2 - v_o}{v_2 + v_o} = \frac{-x_m}{\frac{a}{3} - \frac{64a^2 S_1}{\pi^5 b}} = \frac{(a + \frac{B}{2C})}{\frac{a}{3} - \frac{64a^2 S_1}{\pi^5 b}}$$

which reduces to,

$$F = \frac{v_2 - v_o}{v_2 + v_o} = \frac{(1 + \frac{B}{2aC})}{\frac{1}{3} - \frac{64 S_1}{\pi^5 K}} = H(1 + \frac{B}{2aC}) \tag{3.49}$$

Substituting Eq. (3.49) for F in Eq. (3.47) completes the solution; the stationary positions, x, measured from the midpoint in a rectangular chamber with a height/width ratio, K, of 20 or greater, during asymmetric flow are described by,

$$x = \frac{a}{H}\left[-F \pm \sqrt{F^2 + H(H-2)}\right] \tag{3.50}$$

where H is the chamber constant,

$$H = \frac{1}{\frac{1}{3} - \frac{64 S_1}{\pi^5 K}} \simeq \frac{1}{\frac{1}{3} - \frac{64}{\pi^5 K}}$$

F is the asymmetric factor,

$$F = H(1 + \frac{B}{2aC})$$

a is the chamber half width and B and C are the coefficients previously defined. Transforming Eq. (3.50) to a system of axes with its origin

at the front wall of the chamber using the relationship, $x' = x + a$ and substituting the chamber width, xmax, for 2a, yields

$$x' = \frac{xmax}{2H}\left[-F \pm \sqrt{F^2 + H(H-2)}\right] + \frac{xmax}{2}$$

or,

$$x' = xmax\left[\frac{1}{2} + \frac{1}{2H}\left(-F \pm \sqrt{F^2 + H(H-2)}\right)\right] \qquad (3.51)$$

If $K = \infty$, $H = 3$ and Eqs. (3.50) and (3.51) reduce to the previous asymmetric solutions for chambers with height/width ratios 40 or greater, Eqs. (3.19) and (3.20). If the electroosmotic flow is symmetric, $F = 0$ and Eqs. (3.50) and (3.51) reduce to the Komagata results, Eqs. (3.21) and (3.22).

For a chamber with $K = 20$, $S_1 = 1.005$, $H = 3.098$ and from Eq. (3.51), the stationary positions are given by,

$$x = xmax\left[\frac{1}{2} + 0.1614\ (-F \pm \sqrt{F^2 + 3.4})\right] \qquad (3.52)$$

Examination of Assumption (3.46)

To check the possible error in the determination of stationary positions using Eq. (3.52), and in the subsequent average mobility measurement at these positions, introduced by assumption (3.46),

$$\frac{16S_2}{\pi^3 K}(v_o + v_2 - v_1 - v_3) << (v_o + v_2)$$

the following calculation was done:

Let $v_o = 1.6$, $v_2 = 1.0$, $v_1 = 0.6$, and $v_3 = 0.2$, where v_o, v_1, v_2 and v_3 are the fluid velocities along the chamber side walls as diagrammed in Figure 10(b). These values are chosen to reflect the maximum

asymmetry rarely observed across the chambers width (due to a calculated 40% extreme difference between front and back wall fluid velocities) and to maximize the error introduced by assumption (3.46). Under these conditions of flow, Eq. (3.44), which does not use the assumption, predicts the front stationary position at 0.2475 of the chamber width; Eq. (3.52) predicts this position at 0.2374 of the chamber width, a 1% error. By using these positions to calculate the average cell mobility on a typical regression equation for a chamber with 0.7 mm width,

$$x = -0.14 - 9.2\,x' + 13.5(x')^2$$

a 2.3% error in average mobility calculation results. Therefore, even under the extreme and unlikely conditions assumed for this test, that is that the fluid velocity along one wall of the chamber will be eight times that of another, the 2.3% error in average mobility calculation using Eq. (3.52) as a stationary position estimate in this example remains six times smaller than the average error of 15% in the average mobility calculations using Komagata's equation for the prediction of stationary positions, Eq. (3.22), for the 13 experiments described in Chapter III, Part A.

Experimental Support for the Theory

Support for the theoretical prediction of stationary positions using Eq. (3.52) is given by three types of experimental evidence. A comparison was made of average cell mobilities measured at the estimated front and back stationary positions. For the 13 experiments with fixed erythrocytes described at the beginning of this chapter, the average mobilities measured at the corrected front and back stationary positions given by Eq. (3.52) were within 0.01% of each other. This

contrasts to the average difference of 22% in average mobilities measured at the front and back stationary positions determined by Komagata's equation (3.22) for the same experiments.

A set of experiments was designed to test the uniqueness of the stationary positions predicted by Eq. (3.52). They entailed microscope measurements on mixtures of two cell types having distinguishable morphologies. Using Eq. (3.52), the stationary positions for each experiment were calculated independently from three sets of data: data from cell type 1, data from cell type 2, and the combined data from both cell types. Because all three data sets were obtained under the same electroosmotic conditions for each experiment, all three stationary position estimates should be identical. The results of such an experiment using a mixture of fixed chicken and rabbit erythrocytes are plotted in Figure 7. The upper solid line is the least squares mobility parabola for chicken erythrocytes, the lower solid line is that for rabbit erythrocytes, and the central, dotted curve is that for the combined data. The stationary positions determined for each curve are also indicated. The results of 7 such experiments are compiled in Table 3. The average difference in these three estimates of the front stationary position for the 7 experiments was 0.47% of the chamber width. These reliable estimates depend on at least 30 observations for each cell type distributed evenly throughout the chamber depth.

The average mobilities of rat, chicken, and rabbit gluteraldehyde fixed erythrocytes, measured at the stationary positions estimated by Eq. (3.52) in a standard phosphate buffer (52) at 25°C, were compared to literature values. The mean mobilities of fixed rat and chicken erythrocytes were measured at -1.13 and -0.88 μm/sec/v/cm respectively,

Table 3. Front Stationary Position Estimates Using Suspensions of Mixed Chicken and Rabbit Fixed Erythrocytes.

Electrophoresis Buffer	Temperature, °C	Chamber Width, mm	Front Stationary Position Estimate using mobility-depth data from Chicken RBC, mm	Front Stationary Position Estimate using mobility-depth data from Rabbit RBC, mm	Front Stationary Position Estimate using mobility -depth data from Rabbit and Chicken RBC, mm
PSB	1	0.711	0.147	0.137	0.141
PSB + 5% Acoll	1	0.711	0.128	0.132	0.129
PSB + 10% Acoll	1	0.711	0.137	0.141	0.139
PSB	1	0.711	0.139	0.137	0.138
PSB	4	0.718	0.132	0.128	0.131
PSB	20	0.730	0.129	0.143	0.135
PSB	37	0.740	0.143	0.142	0.143

by this technique. These compare to -1.10 for rat erythrocytes, identically fixed, by Tenforde (167), and -0.82 for chicken erythrocytes measured by vanOss. The average measured mobility of fixed rabbit erythrocytes was -0.30, consistently below the literature values for unfixed cells, -0.48 to -0.55 (2,25).

A Computer Program for Determining the Electrophoretic Mobility of Cells in a Rectangular Chamber during Asymmetric Electroosmotic Flow

Introduction

In the field of cell electrophoresis, computer programs have been used for the estimation of zeta potential and surface charge density of specific charged chemical species from electrophoretic mobility data (106). Computers are also used in laser Doppler spectroscopy electrophoresis to resolve the Doppler shifted frequency spectrum of laser light scattered from a cell suspension under influence of an electric field (187).

The union of computer and microscope cell electrophoresis work in this laboratory has yielded several satisfying results. This approach reduces one tedious man-hour required to analyze the 200 data collected during a typical microelectrophoresis experiment to a few minutes. The method organizes and error-checks these data and stores them on permanent file for future reference or reanalysis. The computer also affords a more accurate mobility measurement of cells observed in the chamber through the application of regression analysis and the asymmetric electroosmotic flow evaluation discussed earlier in this chapter. This computer analysis, accomplished in two steps by two main programs and a major subroutine, provides a quick, useful and realistic presentation

of mobility data in histogram form, and is appropriate for any micro-electrophoretic work using rectangular chambers. Flow charts of these programs are diagrammed in Figures 11 and 12. Appendix A contains a computer listing.

Program 1

Description

Program 1 is the first step of two in the analysis of mobility data. Its purpose is three-fold: (1) to read in and display raw mobility data for verification; (2) to determine the chamber depth and apparent mobility for each cell (the apparent mobility of a cell is defined as its observed velocity divided by the electric field strength and normalized for viscosity to that of water at 25°C); and (3) to punch these calculated data on cards for regression analysis by Program 2.

Program 1 Input

Electrophoretic data from each experiment are punched into standard IBM cards, forming a data pack. Each data pack consists of one header information card followed by a variable number of cell data cards. The header card data, format, and fields are as follows:

	Field	Format	Data
card column	1-2	I2	experiment number, must be equal to '1' for the first data pack
	4-8	F5.2	micrometer reading for chamber thickness
	10-13	F4.2	number of reticule squares between scratches on the front chamber wall, to nearest tenth
	15-18	F4.2	number of reticule squares between scratches on the back chamber wall, to nearest tenth

	Field	Format	Data
card column	19-24	F6.5	current (amperes)
	25-30	F6.5	conductivity of buffer at experimental temperature (mho/cm)
	31-36	F6.4	viscosity of buffer at experimental temperature (cp)
	38-43	F6.4	viscosity of water at 25°C, 0.8937 cp
	45-80	9A4	description of experiment

Each cell data card which follows the header card contains data from four different cells with the possible exception of the last card in each data pack which may contain data from less than four cells. The data description, format and fields for the cell data cards are as follows:

	Field	Format	Data
card columns	1-5	F5.3	micrometer reading of cell position
	7-8	I2	number of reticule squares along which cell was clocked (reversals near the chamber walls will cause the cell to move toward the cathode and are noted by making this number of squares negative)
	10-13	F4.1	cell traverse time to left (seconds, to nearest tenth)
	15-18	F4.1	cell traverse time to right (seconds, to nearest tenth)
	20-24	F5.8	cell position
	26-27	I2	reticule squares
	29-32	F4.1	time left
	34-37	F4.1	time right
	39-43	F5.3	cell position

	Field	Format	Data
card columns	45-46	I2	reticule squares
	48-51	F4.1	time left
	53-56	F4.1	time right
	58-62	F5.3	cell position
	64-65	I2	reticule squares
	67-70	F4.1	time left
	72-75	F4.1	time right
	79	I1	blank unless last card of last data pack, then a negative sign
	80	I1	blank unless last card of any given data pack, then equal to the number of cells from which data are recorded on this last card (1-4)

A data pack from a typical experiment with, say, 38 cell observations would then consist of one header card followed by 10 cell data cards, the last card containing data from just two cells as indicated by the number '2' in card column 80. Program 1 can process a maximum of eight stacked data packs from eight experiments at a time. One hundred forty K bytes of core, 750 output records and 8 seconds actual time are adequate for the compilation and execution of such a job by Program 1 on the IBM 370-168 under Glevel Fortran.

Program 1 Function

Figure 11 provides a descriptive flow chart for Program 1 and Appendix A contains its computer listing complete with comment cards which describe the program algorithms. However, there are four critical steps which deserve further explanation.

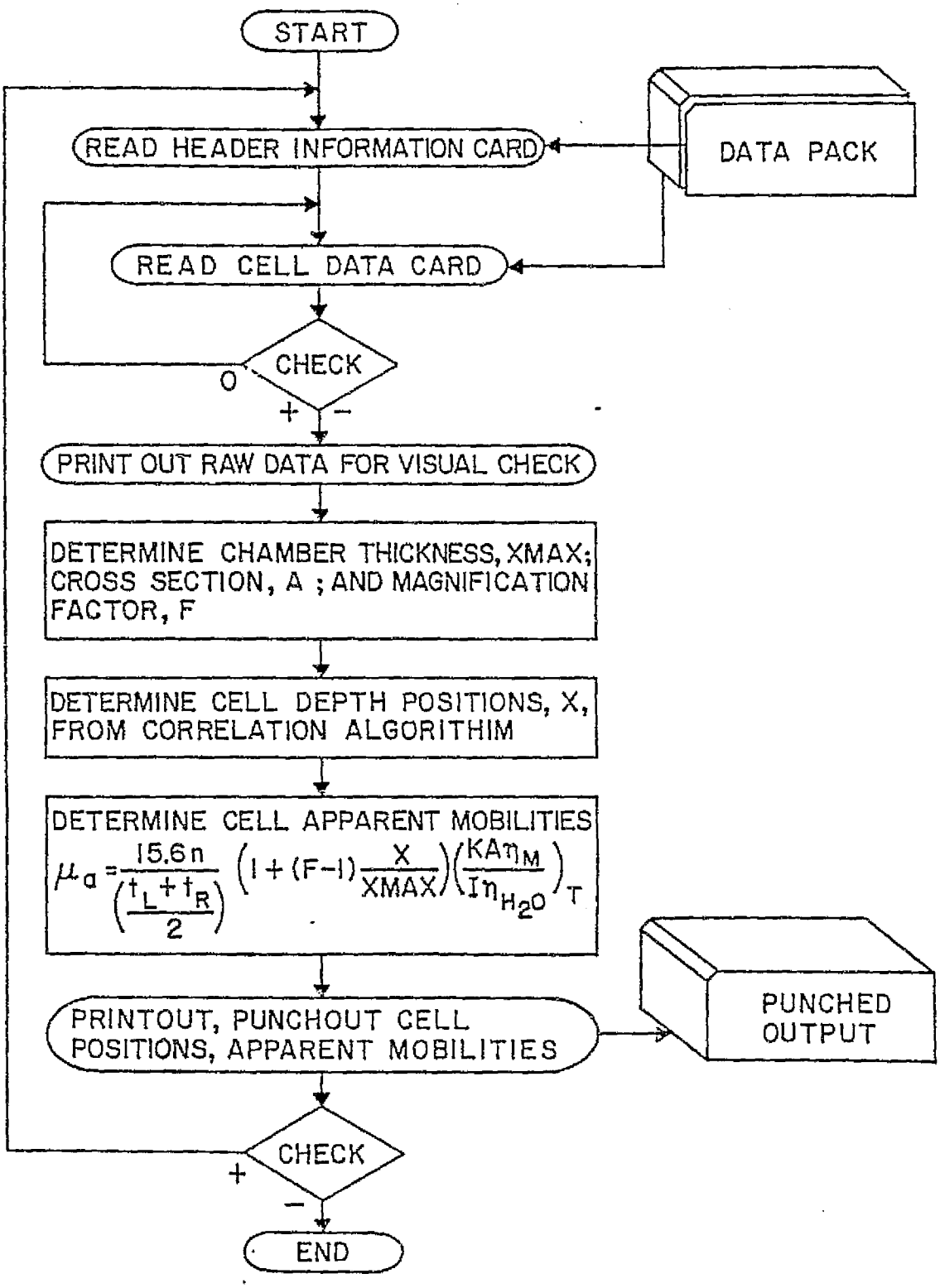

Figure 11. Program 1 flow chart.

Calculation of Cell Depth in the Chamber

The position of a cell in the electrophoresis chamber is conventionally obtained in two steps. First the micrometer reading on the microscope fine-focus knob is recorded when the cell is in good focus. Then this reading is converted to the actual distance in millimeters from the inside surface of the front chamber wall to the cell by using a nonlinear correlation curve which is graphed in the instrument manual (202). To automate this second step, four linear segments were fitted to the correlation curve. These linear segments are plotted in Figure 12, which overlays the original curve in the manual very closely. The algorithm for calculating cell depth determines which linear segment contains the micrometer reading ordinate, and then interpolates on that segment at that position for the chamber depth in millimeters.

Calculation of Chamber Cross Section

By Eq. (2.2), the determination of electric field strength on the cell suspension requires an accurate measurement of the cross sectional area of the chamber. For rectangular chambers, this area was observed to increase by more than 16% through the temperature range 1^{o}-37^{o}C. Assuming the coefficient of expansion is equal along both the height and width of the chamber, the cross section, A, in cm^2 for a rectangular chamber with a height/width ratio of 20 is accurately given by

$$A = \left(\frac{xmax}{10}\right)^2 20 = \frac{xmax^2}{5} \qquad (3.53)$$

where xmax is the inside width of the chamber in mm at the experimental temperature, determined using the depth correlation algorithm just described.

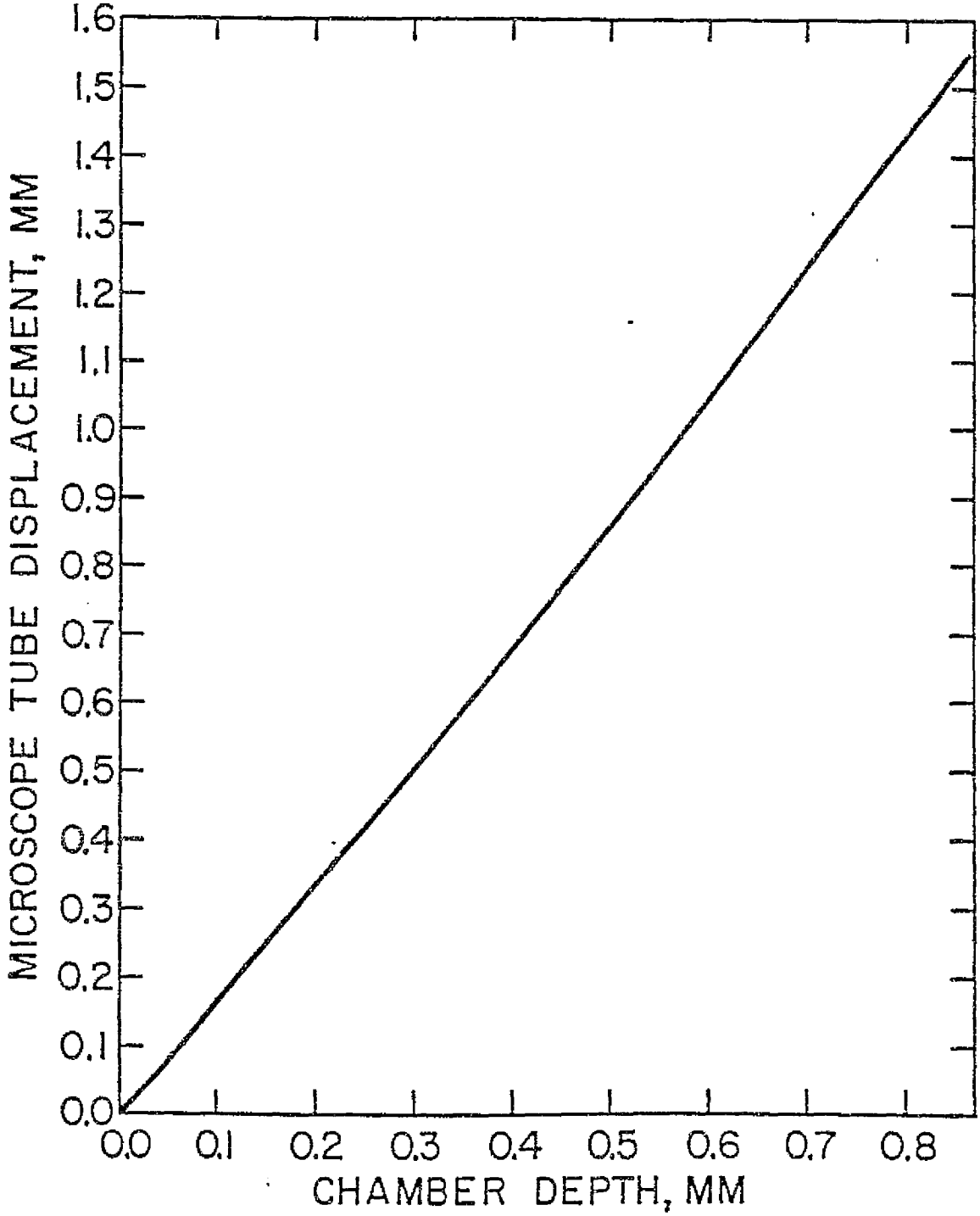

Figure 12. Hicrometer-chamber depth correlation curve.

Calculation of the Magnification Correction Factor

The microscope magnification of the cytopherometer increases linearly with focal length. Therefore the greater the depth at which a cell is observed, the faster it appears to move. This error is compensated for using a correction factor which linearly decreases with depth

$$(1 + (F - 1) \frac{x}{xmax})$$

where xmax is the inside chamber thickness, x is the distance from the inside front wall to the cell, and F is the ratio of magnification at the front wall to that at the back wall (202). The experimental procedure for determining F is covered in Chapter II.

Calculation of Apparent Cell Mobility

The apparent mobility of a cell is defined as its observed velocity, v_o, divided by the electric field strength it experiences, E, and normalized for viscous drag to that of water at 25°C. The observed velocity is determined by clocking the cell along the squares of a reticule in the microscope eyepiece, each square representing a corrected magnified distance of 15.6 microns. The data entry for the program requires clocking the cell along the same number of reticule squares for both its left and right measurement. Using Eq. (2.2), the apparent mobility, μ_a, in μm/sec/V/cm, is given by,

$$\mu_a = \frac{v_o}{E} \frac{\eta_{m,T}}{\eta H_2O,\ 25^oC} = \frac{v_o AK_T}{I} \frac{\eta_{m,T}}{0.8937}$$

or

$$\mu_a = \frac{15.6n}{\frac{(t_L + t_r)}{2}} (1 + (F-1) \frac{x}{xmax}) \frac{xmax^2 K_T}{I5} \frac{\eta_{m,T}}{0.8937} \qquad (3.54)$$

where n is the number of reticule squares the cell was clocked along (equal for both left and right measurements), t_L and t_r are, respectively, the cell migration times in seconds to the left and right, F is the magnification ratio, x and xmax are, respectively, the cell position and the chamber width in mm, I is the current through the chamber in amperes, and K_T and $\eta_{m,T}$ are, respectively, the specific conductivity in mho/cm and the viscosity in centipoise of the cell suspension at the experimental temperature, T.

Program 1 Output

All the raw electrophoretic data fed to Program 1 are printed out to provide a visual check for obvious errors before proceeding to the regression and asymmetric flow analysis in Program 2. Common errors include missing or misplaced decimal points, nonarithmetic characters and incorrect data fields. If an error is found, the data card is repunched and Program 1 is run again. The following is an example of a verification printout of a single experiment by Program 1:

DATA FOR RUN 1: FIXED CHICK RBC, PSB, 1 DEG
MAGNIFICATION FACTOR = 0.926 CHAMBER THICKNESS = 0.711 MM
FRONT STATIONARY PLANE = 0.144 M BACK STATIONARY PLANE = 0.567 MM
MEDIUM VISCOSITY = 2.1830 CENTIPOISE WATER VISCOSITY = 0.8937 CENTIPOISE
MEDIUM CONDUCTIVITY = .00083 MHO-CM CURRENT = .00084 AMPS
NUMBER OF DATA POINTS = 36

X	RET	SECL	SECR
0.041	-1	7.2	5.5
0.229	2	4.8	7.6
0.253	2	3.9	5.4
0.299	2	3.6	4.5
.	.	.	.
.	.	.	.
.	.	.	.

'X', 'RET', 'SECL', and 'SECR' are the tabulations, respectively, of the micrometer readings for each cell, the number of reticules the cell was clocked along (equal for both left and right measurements, negative to indicate reversals), and migration times to the left and right. The stationary positions indicated are the Komagata predictions and are not corrected for asymmetric flow.

In addition, for each cell measured Program 1 prints out its calculated chamber position in millimeters (in the order of increasing depth) and its apparent mobility by Eq. (3.54) in μm/sec/V/cm:

CHAMBER DEPTH	CELL MOBILITY
0.0125	0.393
0.1392	-0.625
0.1545	-0.832
.	.
.	.
.	.

These data are also punched into card output by Program 1, one data pair per card in (10X, 2F10.6) format along with proper control cards as specified by the POLY2 regression analysis routine used in Program 2 and discussed in the next section.

Program 2

General Description

Program 2 consists of the main program, POLY2, which fits a least squares parabola to the apparent mobility data generated by Program 1, and the subroutine EXTRA which determines actual cell mobilities using the regression curve equation. About 180 K bytes of core, 1200 output records, and 15 seconds actual time are adequate for the G level Fortran IV compilation and execution of Program 2 on the IBM 370-168 using data from a typical electrophoresis experiment.

POLY2 Input, Function, and Output

POLY2 is a library routine for polynomial derivation at The Pennsylvania State University Computation Center (PSUCC). The center provides documentation on the control cards which invoke POLY2 and specify the polynomial degree and output format desired by the user.

For each experiment, the input for POLY2 simply consists of the punched card output from Program 1: five POLY2 control cards ('PARAMETER', 'FORMAT', 'OUTPUT', 'TRANSFER', and 'END'), the cell positions and the apparent cell mobilities, one data pair per card in standard (10X, 2F10.6) format. POLY2 accepts such data from one to eight experiments at a time.

The function of POLY2 is to calculate the coefficients of the second degree polynomial which provides the least squares fit to the apparent mobility versus chamber depth data obtained from a single microelectrophoretic experiment. POLY2 also calculates the ordinate errors by this fit.

POLY2 prints the results of its least squares analysis as shown in the following example:

LEAST SQUARES POLYNOMIAL FIT

RBC SEPARATION

DEGREE = 2 POINTS FITTED = 36

POLYNOMIAL

Y = +1.934289D - 01 -6.749936D00*X**1 + 9.4439366D00*X**2

SUM OF ERRORS = 2.3092639D - 14

SUM OF ABSOLUTE ERRORS = 3.1295342D00

SUM OF SQUARES OF ERRORS = 4.8081803D - 01

The two digits and their arithmetic sign following each 'D' constitute the base 10 exponent of the eight digit mantissa which prefaces that 'D'. A single asterisk represents a multiplication; a double asterisk, an exponential.

Input, Function and Output of Subroutine EXTRA

Subroutine EXTRA completes the analysis of mobility data by providing routines for determining stationary positions in the chamber during asymmetric flow, for calculating the average cell mobility and its statistical confidence intervals, and for generating mobility histograms and optimal mobility parabola graphics for each experiment.

There are two sources of input to subroutine EXTRA: two punched cards generated by Program 1 containing the experiment description, desired histogram characters, and symbols and axes labeling for the plotting routines; and data in COMMON with the POLY2 program which include apparent mobilities, cells positions, regression coefficients, and least squares errors.

The function of EXTRA is outlined by Figure 13, a descriptive flow chart, and by Appendix B, a computer listing complete with comment cards which describe the subroutine algorithms. The subroutine contains four major routines which are described here in more detail with their output format.

Plot Routine

As a user option, EXTRA can plot the apparent mobility versus depth parabola for each experiment. EXTRA contains three routines, PLOTIT, SAMEP, and EPLOT, which use the Quick Draw Graphics System (QDGS) subroutines to generate punched card output for graphics. All three plotting routines are contributed library programs complete with user documentation at PSUCC. Their graphical output (punched card) is fed to a dedicated IBM 1401 computer under the execution of the PSUCC plotting program, DRIVEQ, to initiate plotting commands to a Calcomp (California Computer Products, Inc.) drum plotter, model 564. Plotter output is produced on 18-inch paper and typical mobility curves are shown in Figure 6. Apparent cell mobilities, the regression curves and the stationary positions for each experiment are indicated on the plot. These plotting routines, opted for by setting the sense switch 'PLOT' in EXTRA to 1.0, provide a convenient verification of the parabola fit to the mobility data and a visual representation of stationary positions and the asymmetric profile of electroosmotic flow across the chamber depth.

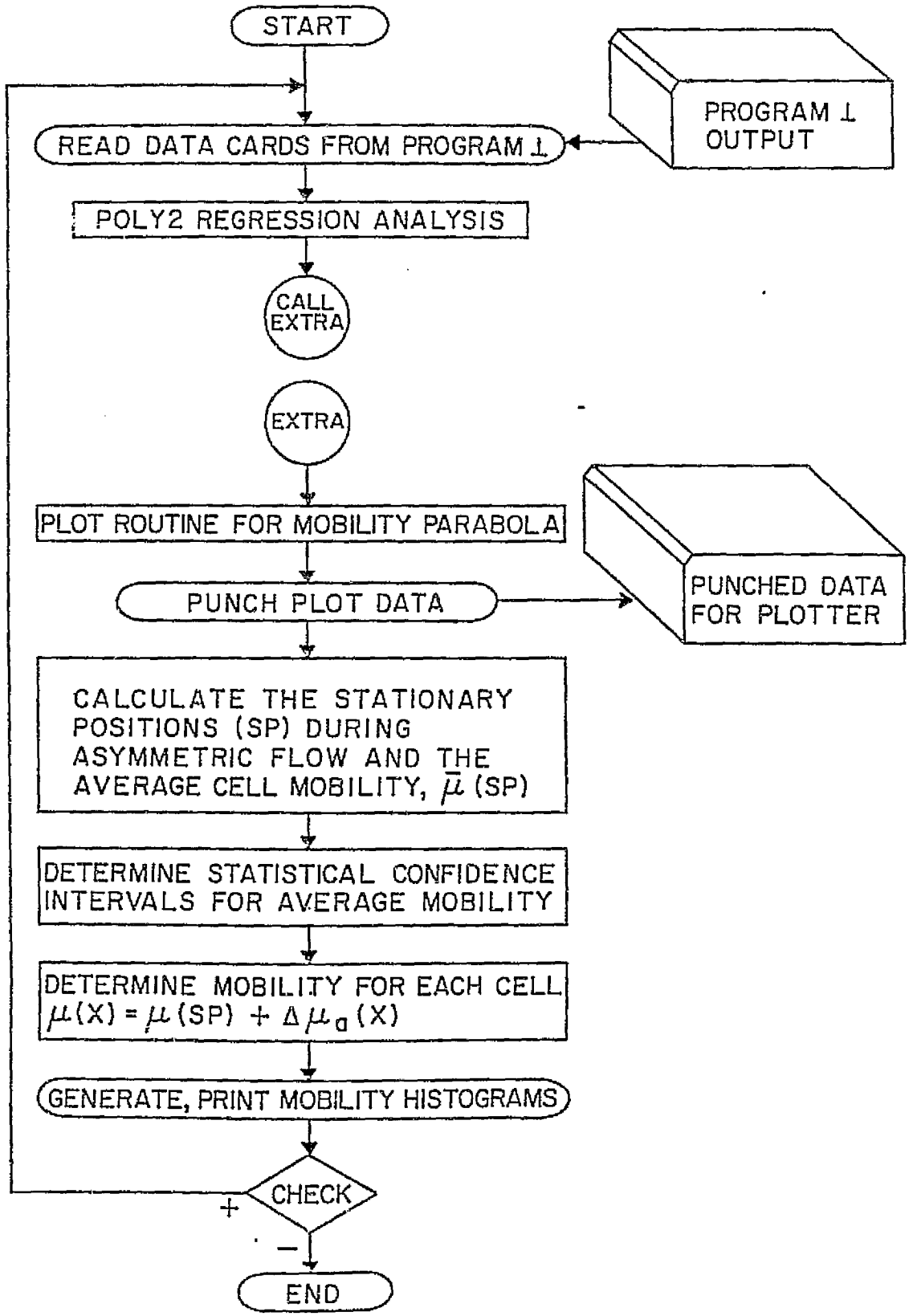

Figure 13. Program 2 flow chart.

Stationary Position Estimates with Asymmetric Flow Correction

Stationary positions in the chamber are calculated by EXTRA using Eq. (3.52), derived earlier in Chapter III. For a rectangular chamber with a height/width ratio of 20, the stationary positions are given by

$$x = xmax\ (.5 + .1614\ (F \pm \sqrt{F^2 + 3.4}))$$

where $F = 3.098\ (1 + \frac{B}{2aC})$, xmax = 2a is the chamber width, and B and C are regression coefficients described in the previous section of this chapter. The value of the mobility parabola at these corrected stationary position estimates is taken as the average mobility of the cell sample. For each experiment, EXTRA prints out the uncorrected Komagata stationary positions, the stationary positions corrected for asymmetric flow, the average cell mobility measured at each of these positions, and the errors introduced by the assumption of symmetric electroosmotic flow as shown in the following example:

RUN 5: FIXED CHICK RBC, PSB, 20 DEG

PLOT SYMBOL +

**********ASYMMETRIC FLOW ANALYSIS**********

	STATIONARY POSITIONS (MM)		AVERAGE MOBILITY OF POPULATION, MEASURED AT:	
	FRONT	BACK	FRONT	BACK
UNCORRECTED FOR ASYMMETRIC FLOW	0.148	0.583	-1.404204	-0.859257
CORRECTED FOR ASYMMETRIC FLOW	0.129	0.565	-1.135999	-1.136017
UNCORRECTED ERROR	-2.6	-2.5	-.268	0.277
	(% OF CHAMBER WIDTH)		(μm/sec/V/cm)	

ASYMMETRIC INDEX = 0.152

The asymmetric index given is the value of the asymmetric factor, F, for the particular experiment as previously described.

The Determination of Statistical Confidence Intervals about the Calculated Average Cell Mobility

The confidence interval, $\Delta\mu$, about the average cell mobility, $\bar{\mu}(sp)$, is determined using the equation

$$\Delta\mu = \pm t(n-3,\ \alpha/2 \quad \frac{\Sigma(\mu-\bar{\mu})^2}{n-2} \quad 1 + \frac{1}{n} + \frac{n(sp-\bar{x})^2}{n(\Sigma x^2) - (\Sigma x)^2} \qquad (3.55)$$

where t is the two-tailed critical value corresponding to a given probability of error, α, sp is the stationary position, and n is the number of measurements of mobility, μ, at chamber depth x (78). Intervals about the average cell mobility are generated for 90, 95, 98 and 99% confidence as shown in the following example:

**********CONFIDENCE INTERVAL ESTIMATE**********

FSP	MOB(FSP)	INTERVAL	% CONFIDENCE
0.129	-1.135999	0.482485	90
		0.573133	95
		0.652085	98
		0.754431	99

The average mobility, 'MOB', and its confidence intervals are calculated in μm/sec/V/cm at both the front stationary position (FSP) and the back stationary position (BSP).

The Calculation of Cell Mobilities for Mobility Histograms

The mobility of an individual cell observed at a depth x in the chamber, moving at the observed velocity, v_o, is given by Eq. (3.4), derived previously in Chapter III,

$$\mu(x,v_o) = \mu_{ref} + \Delta\mu_a(x)$$

where μ_{ref} is the mobility of the reference parabola at the stationary positions and $\Delta\mu_a(x)$ is the ordinate displacement between the observed apparent mobility of a cell and the reference curve at x. EXTRA repeats this calculation for each cell clocked and generates mobility histograms of specified class width by determining the number of these cells having mobilities within each class and printing them out in the following format:

****MOBILITY HISTOGRAM**********

RANGE	N	FREQUENCY
-0.75- -0.80	1	*
-0.80- -0.85	1	*
-0.85- -0.90-	1	*
-0.90- -0.95	3	* * *
-0.95- -1.00	2	* *
-1.00- -1.05	2	
-1.05- -1.10	1	*
-1.10- -1.15	3	* * *
-1.15- -1.20	4	* * * *
-1.20- -1.25	3	* * *
-1.25- -1.30	4	* * * *
-1.30- -1.35	3	* * *
-1.35- -1.40	1	*
-1.40- -1.45	2	* *
-1.45- -1.50	1	*
-1.50- -1.55	0	
-1.55- -1.60	1	*

Histogram class widths are expressed in μm/sec/V/cm. For each experiment EXTRA can produce a set of histograms, each with a different, user-specified class width. This is elected for by setting the sense switch HIST to the number of histograms desired and entering the class width values into the array RES.

A Review for Using the Programs

The first step in the computer analysis microelectrophoretic data is to use the cytopherometer worksheet to record data during experiments. This serves as a guide for an even distribution of observations across the chamber depth and as a reminder for other measurements required by the programs. These data are then punched into cards following the format specified by 'Program 1 Input', and fed to Program 1. Data packs from a maximum of eight experiments can be stacked and run at a time. The printed output from Program 1 is reviewed for data errors. If any are found, they are corrected and the data is again fed to Program 1. The punched card output from Program 1 is submitted with Program 2 after selecting the sense switches for the desired output format. Generally the plot routines are expensive and not elected. All punched card data are stored for future reference or reanalysis.

REFERENCES

25. Brinton, C. C., Jr. and M. A. Lauffer. The electrophoresis of viruses, bacteria, and cells and the microscope method of electrophoresis. In: Electrophoresis, M. Bier (ed.), Academic Press, New York, 427-492, 1959.

52. Furchgott, R. F. and E. Ponder. Electrophoretic studies on human red blood cells, J. Gen. Physiol. 24, 447-457, 1941.

91. Komagata, S. Researches of the Electrochemical Laboratory, No. 348, Electrochemical Laboratory, Ministry of Communications, Tokyo, Japan, June 1933.

106. Mehrishi, J. N. Molecular aspects of the mammalian cell surface, Prog. Biophys. Mol. Biol. 25, 1-20, 1972.

116. Milito, R. P. An analysis of electroosmotic flow in a rectangular microscopic electrophoresis chamber and its application to the study of cultured rat tumor cells, D.Ed. Thesis, The Pennsylvania State University, University Park, PA, 1977.

160. Smoluchowski, M. von. In: Handbuch der Elektrizitat und des Magnetismus. Vol. II, B. Graetz (ed.), Leipzig, 366, 1914.

202. Zeiss Cytopherometer Operational Manual, Carl Zeiss Inc., New York.

APPENDIX 4A. Fortran program for microscopic electrophoresis data analysis.

```
C
C
C      THIS PROGRAM CONVERTS RAW DATA FROM THE CYTOPHEROMETER TO PUNCHED
C     DATA FOR A CURVE FITTING PROGRAM WHICH CALCULATES CELL MOBILITY
C
C
C     DEFINITION OF VARIABLES
C
C     A=ARRAY CONTAINING EXPERIMENTAL DESCRIPTION (LITERAL)
C     AMPS=CURRENT THROUGH CHAMBER (AMPERES)
C     BKRET=NUMBER OF RETICULES BETWEEN REFERENCE SCRATCHES ON BACK WALL
C     BSP=UNCORRECTED BACK STATIONARY POSITION
C     CHECK=NUMBER OF DATA POINTS ON LAST CARD OF EACH EXPERIMENT
C           (NEGATIVE IF LAST EXPERIMENT IN DATA PACK)
C     ERROR=ERROR FLAG FOR INAPPROPRIATE DATA
C     F=MAGNIFICATION FACTOR
C     FRTRET=NUMBER OF RETICULES BETWEEN REFERENCE SCRATCHES ON FRONT
C            CHAMBER WALL
C     FSP=UNCORRECTED FRONT STATIONARY POSITION
C     K=CONDUCTIVITY OF BUFFER(MHO-CM)
C     MOB=ARRAY CONTAINING APPARENT CELL MOBILITIES
C     NUMPTS=NUMBER OF CELLS MEASURED FOR GIVEN EXPERIMENT
C     NUMRET=NUMBER OF RETICULES CELL WAS CLOCKED FOR
C     RUN=EXPERIMENT NUMBER
C     SUMX=SUM OF CHAMBER DEPTH POSITIONS
C     SUMXSQ=SUM OF SQUARES OF DEPTH POSITIONS
C     TIMEL=TRAVERSE TIME, MOVING LEFT (SEC)
C     TIMER=TRAVERSE TIME, MOVING RIGHT (SEC)
C     VISCSM=VISCOSITY OF BUFFER MEDIUM AT EXPERIMENTAL TEMP. (CP)
C     VISCSW=VISCOSITY OF WATER AT EXPERIMENTAL TEMP. (CP)
C     X=MICROMETER READING (MM)
C     XMAX=CHAMBER THICKNESS (MM)
C
      DIMENSION X(200),NUMRET(200),TIMEL(200),TIMER(200),A(9)
      REAL K,MOB(200)
      INTEGER RUN,CHECK
C
C     PUNCH FORMAT CARDS FOR CURVE FITTING PROGRAM, POLY2
C
   10 WRITE(7,17)
   17 FORMAT('PARAMETER RBC SEPARATION',14X,'02',8X,'02',8X,'01',9X,'1'/
     1'STANDARD FORMAT'/'OUTPUT 2')
      SUMX=0.0
      SUMXSQ=0.0
      L=0
      ERROR=0.0
C
C     READ HEADER INFORMATION CARD FOR NEXT EXPERIMENT
C
      READ(5,20)RUN,XMAX,FRTRET,BKRET,AMPS,K,VISCSM,VISCSW,(A(I),I=1,9)
   20 FORMAT(I2,1X,F5.3,1X,F4.2,1X,F4.2,F6.5,F6.5,          F6.4,1X,F6.4,
     11X,9A4)
   30 J=L+1
```

```
      L=J+3
C
C     READ NEXT DATA CARD
C
      READ(5,40)(X(I),NUMRET(I),TIMEL(I),TIMER(I),I=J,L),CHECK
   40 FORMAT(F5.3,1X,I2,1X,F4.1,1X,F4.1,1X,F5.3,1X,I2,1X,F4.1,1X,F4.1,1X
     1,F5.3,1X,I2,1X,F4.1,1X,F4.1,1X,F5.3,1X,I2,1X,F4.1,1X,F4.1,3X,I2)
C
C     CHECK FOR REMAINING DATA CARDS FOR GIVEN EXPERIMENT
C
      IF(CHECK)50,30,50
   50 NUMPTS=L+IABS(CHECK)-4
C
C     CONVERT MICROMETER READING TO ACTUAL CHAMBER DEPTH BY
C     INTERPOLATION ON CORRELATION FUNCTION
C
      XMAX=.633+(XMAX-1.10)/.45*.233
      FSP=XMAX*.2024
      BSP=XMAX*.7976
C
C     DETERMINE CHAMBER CROSS SECTION , CONSIDERING THERMAL EXPANSION
C     AND CONTRACTION, BY CONVERTING XMAX FROM MM TO CM, SQUARING, AND
C     MULTIPLYING BY THE HEIGHT/WIDTH RATIO OF 20.
C
      AREA=XMAX**2/5.
      CONST=15.6*2.0*K*AREA/AMPS*VISCSM/VISCSW
C
C     CALCULATE THE MAGNIFICATION FACTOR
C
      F=FRTRET/BKRET
C
C     PRINT OUT FOR DATA VERIFICATION
C
      WRITE(6,60)RUN,(A(I),I=1,9),F,XMAX,FSP,BSP,VISCSM,VISCSW,K,AMPS,
     1NUMPTS
   60 FORMAT(/'1DATA FOR RUN ',I2,' : ',9A4,     /' MAGNIFICATION FACTOR
     1 = ',F5.3,4X,'CHAMBER THICKNESS =',F5.3,'MM',4X,'FRONT STATIONARY
     2PLANE =',F5.3,'MM',4X,'BACK STATIONARY PLANE =',F5.3,'MM'/' MEDIUM
     3 VISCOSITY=',F6.4,' CENTIPOISE',3X,'WATER VISCOSITY=',F5.3,' CENTI
     4POISE',4X,     'MEDIUM CONDUCTIVITY =',F6.5,'MHO-CM',4X,'CURRENT =
     5',F6.5,' AMPS'     /' NUMBER OF DATA POINTS =',I3/'0',4(' X   RET
     6SECL SECR',10X))
C
C     DETERMINE MATRIX PARAMETERS FOR DATA PRINT OUT
C
      LEFT=MOD(NUMPTS,4)
      IROW=NUMPTS/4
      IF(LEFT.NE.0) IROW=IROW+1
      LIMIT1=IROW-4+LEFT
      LIMIT2=LIMIT1+1
      INC1=3*IROW
      INC2=2*IROW
      IF(LEFT.EQ.0) INC2=INC1
```

```
      DO 62 J=1,LIMIT1
      N=J+INC1
C
C     PRINT OUT FOR DATA VERIFICATION
C
   62 WRITE(6,63)(X(I),NUMRET(I),TIMEL(I),TIMER(I),I=J,N,IROW)
   63 FORMAT(' ',4(F5.3,1X,I2,1X,F4.1,1X,F4.1,11X))
      DO 64 J=LIMIT2,IROW
      N=J+INC2
   64 WRITE(6,63)(X(I),NUMRET(I),TIMEL(I),TIMER(I),I=J,N,IROW)
C
C     CONVERT MICROMETER READINGS TO ACTUAL CHAMBER DEPTH BY
C     INTERPOLATION ON A 4-SEGMENT CORRELATION FUNCTION
C
   68 DO 170 I=1,NUMPTS
      IF(X(I)-.16)70,80,80
   70 X(I)=X(I)/.16*.1
      GO TO 160
   80 IF(X(I)-.65) 90,100,100
   90 X(I)=.1+(X(I)-.16)/.49*.287
      GO TO 160
  100 IF(X(I)-1.10)110,120,120
  110 X(I)=.387+(X(I)-.65)/.45*.246
      GO TO 160
  120 IF(X(I)-1.55)130,140,140
  130 X(I)=.633+(X(I)-1.10)/.45*.233
      GO TO 160
C
C     DATA ERROR DIAGNOSTIC
C
  140 WRITE(6,150)I,X(I)
  150 FORMAT(' RECHECK DATA POINT ',I3,' =',F10.3)
      ERROR=1.0
C
C     CALCULATE APPARENT MOBILITY
C
  160 MOB(I)=-CONST*NUMRET(I)*(1.+(F-1.)*X(I)/XMAX)/(TIMEL(I)+TIMER(I))
      SUMX=SUMX+X(I)
  170 SUMXSQ=SUMXSQ+X(I)**2
C
C     RESEQUENCE DATA ARRAYS BY INCREASING CHAMBER DEPTH FOR EFFICIENT
C     PLOTTING
C
      DO 180 I=1,NUMPTS
      L=I
      XMIN=X(I)
      DO 172 J=I,NUMPTS
      IF(X(J)-XMIN)171,172,172
  171 L=J
      XMIN=X(J)
  172 CONTINUE
      STORE=MOB(L)
      MOB(L)=MOB(I)
```

```
      X(L)=X(I)
      MOB(I)=STORE
      X(I)=XMIN
  180 CONTINUE
C
C     PRINT OUT MOBILITIES FOR VERIFICATION
C
      WRITE(6,185)
  185 FORMAT(////' ',4(' CHAMBER     CELL',12X)/' ',4(' DEPTH    MOBILIT
     1Y',11X))
      DO 190 J=1,LIMIT1
      N=J+INC1
  190 WRITE(6,193)(X(I),MOB(I),I=J,N,IROW)
  193 FORMAT(' ',4(F6.4,5X,F6.3,12X))
      DO 195 J=LIMIT2,IROW
      N=J+INC2
  195 WRITE(6,193)(X(I),MOB(I),I=J,N,IROW)
  200 IF(ERROR.NE.0.0) GO TO 225
C
C     PUNCH CHAMBER POSITIONS, APPARENT MOBILITIES FOR CURVE FITTING
C     PROGRAM
C
  210 WRITE(7,220)(X(I),MOB(I),I=1,NUMPTS)
  220 FORMAT(10X,2F10.6)
C
C     CHECK FOR REMAINING EXPERIMENTS
C
  225 IF(CHECK) 250,230,230
C
C     PUNCH FORMAT CARDS, AXES LABELING AND SYMBOLS FOR PLOT, HISTOGRAM
C     CHARACTERS, AND EXPERIMENTAL DESCRIPTION FOR CURVE FITTING PROGRAM
C
  230 WRITE(7,240) RUN,XMAX,FSP,BSP,(A(I),I=1,9),CHECK,SUMX,SUMXSQ
  240 FORMAT('TRANSFER'/12X,'CHAMBER DEPTH, MM',17X,'MOBILITY MICRON/SEC
     1/VOLT/CM'/'*0+-,123 ************************************************
     2***'/I2,3F5.3,9A4,I2,2F10.4)
      GO TO 10
  250 WRITE(7,260) RUN,XMAX,FSP,BSP,(A(I),I=1,9),CHECK,SUMX,SUMXSQ
  260 FORMAT(     'END'/12X,'CHAMBER DEPTH, MM',17X,'MOBILITY MICRON/SEC
     1/VOLT/CM'/'*0+-,123 ************************************************
     2***'/I2,3F5.3,9A4,I2,2F10.4)
      END
```

```
      SUBROUTINE EXTRA
C
C     THIS SUBROUTINE IS CALLED BY A CURVE FITTING PROGRAM,POLY2, WHICH
C     GENERATES A REFERENCE PARABOLA FROM MOBILITY DATA. THIS SUBROUTINE
C     DETERMINES STATIONARY POSITIONS, CELL MOBILITY, DATA PLOTS,
C     CONFIDENCE INTERVALS, AND MOBILITY HISTOGRAMS FOR EACH EXPERIMENT.
C
C
C     DEFINITION OF VARIABLES
C
C     A=ARRAY CONTAINING LITERAL DESCRIPTION OF EXPERIMENT
C     B=ARRAY OF HISTOGRAM SYMBOLS
C     BSP=BACK STATIONARY POSITION
C     C=ARRAY OF % CONFIDENCE FOR T-INTERVAL
C     CHECK=FLAG FOR LAST EXPERIMENT
C     CIEBSP=MOBILITY CONFIDENCE INTERVAL AT BACK STATIONARY POSITION
C     CIEFSP=MOBILITY CONFIDENCE INTERVAL AT FRONT STATIONARY POSITION
C     COEFN=ARRAY CONTAINING REGRESSION COEFFICIENTS
C     DX=X INCREMENT FOR REGRESSION CURVE PLOT
C     FACTOR=ASYMMETRIC FACTOR
C     FSP=FRONT STATIONARY POSITION
C     HIST=SWITCH FOR HISTOGRAM ROUTINE, 0=NO HISTOGRAM,
C     1=.05 MICRON/SEC/V/CM CLASS WIDTH HISTOGRAM, 2=.05,.02 CLASS
C     WIDTH HISTOGRAMS, 3=.05, .02, .01 CLASS WIDTH HISTOGRAMS
C     LABEL=ARRAY CONTAINING AXES LABELS FOR PLOT
C     MOBBSP=MOBILITY AT BACK STATIONARY POSITION
C     MOBFSP=MOBILITY AT FRONT STATIONARY POSITION
C     NBRPTS=NUMBER OF POINTS CONNECTED BY PLOTTER TO REPRESENT
C           REGRESSION CURVE
C     OBS=NUMBER OF OBSERVATIONS (CELLS) FOR EXPERIMENT
C     PLOT=SWITCH FOR PLOT ROUTINE, 0.0=NO, 1.0=YES
C     RES=ARRAY CONTAINING HISTOGRAM CLASS WIDTHS (MICRON/SEC/V/CM)
C     RUN=EXPERIMENT NUMBER
C     STAT=SWITCH FOR STATISTICAL ROUTINE, 0.0=NO, 1.0=YES
C     SYM=ARRAY OF PLOT SYMBOLS
C     T=T-INTERVAL VALUES
C     X,Y=ARRAYS OF CHAMBER POSITIONS, APPARENT MOBILITIES
C     XMIN=X ORIGIN FOR PLOTTER
C     XPLOT, YPLOT=ARRAYS OF X,Y POINTS TO BE PLOTTED
C
C
      REAL*4 PI
      REAL*8 COEFN,X,Y,ERRSUM,ERRSAB,ERRSSQ,YPRED,DIFNT,RES
      COMMON COEFN(41),X(2000),Y(2000),ERRSUM,ERRSAB,ERRSSQ,YPRED,
     1DIFNT,PI(5),K,I
      INTEGER*2 A1(500),A2(500),A3(500)
      LOGICAL*1 SYM(8),LABEL(40,2)
      DIMENSION B(50),RES(3)
      REAL R1(6,500)
      REAL XPLOT(2000),YPLOT(2000),MOBFSP,MOBBSP,MOBFTW,MOBBKW,A(9),T(4)
     1,CIEFSP(4),CIEBSP(4)
      INTEGER RUN,CHECK,C(4),HIST
      DATA T(1),T(2),T(3),T(4)/1.65,1.96,2.23,2.58/,C(1),C(2),C(3),C(4)/
```

```
     190,95,98,99/,RES(1),RES(2),RES(3)/.05,.02,.01/
      NBRPTS=400
      XMIN=0.0
      OBS=I
C
C     SET OUTPUT SWITCHES
C
      PLOT=1.0
      PLOT=0.0
      STAT=0.0
      STAT=1.0
      HIST=0
      HIST=2
      HIST=3
      HIST=1
C
C     READ PLOT AXES LABELS, PLOT SYMBOLS, HISTOGRAM SYMBOLS,
C     EXPERIMENTAL DESCRIPTION
C
      READ(5,40)((LABEL(I,J),I=1,40),J=1,2)
      READ(5,40) (SYM(I),I=1,8),(B(I),I=1,50)
   40 FORMAT(80A1)
      READ(5,50) RUN,XMAX,FSP,BSP,(A(J),J=1,9),CHECK,SUMX,SUMXSQ
   50 FORMAT(I2,3F5.3,9A4,I2,2F10.4)
C
C     PLOT ROUTINE
C
      IF(PLOT.EQ.0.0) GO TO 250
      I=OBS
      DO 100 J=1,I
      XPLOT(J)=X(J)
  100 YPLOT(J)=Y(J)
      IF(RUN.NE.1) GO TO 150
      CALL INITQ(A1,A2,A3,R1,500)
C
C     PLOT AXES, LABELS, AND DATA FROM FIRST EXPERIMENT
C
      CALL PLOTIT(YPLOT,I,0,0,8.,5.4,0.,.04,18,2.0,-.2,20,LABEL,0.,.72,
     12.,-2.1,XPLOT,SYM(1),1,.060,2,1,.125)
      XPLOT(1)=.72
      YPLOT(1)=-2.0
      YPLOT(2)=2.0
      XPLOT(2)=.72
C
C     COMPLETE AXES PLOT
C
      CALL SAMEP(YPLOT,2,XPLOT,SYM,0)
      GO TO 160
C
C     PLOT DATA FROM NEXT EXPERIMENT ON SAME PLOT
C
  150 CALL SAMEP(YPLOT,I,XPLOT,SYM(RUN),1)
  160 DX=(XMAX-XMIN)/NBRPTS
```

```
      DO 200 J=1,NBRPTS
      RI=J-1
      XPLOT(J)=XMIN+RI*DX
  200 YPLOT(J)=COEFN(1)+COEFN(2)*XPLOT(J)+COEFN(3)*XPLOT(J)**2
C
C     PLOT REGRESSION CURVE
C
      CALL SAMEP(YPLOT,NBRPTS,XPLOT,SYM,0)
  250 WRITE(6,300) RUN,(A(J),J=1,9),SYM(RUN)
  300 FORMAT('-','RUN',I2,' : ',9A4/' ','PLOT SYMBOL ',A1///'0',
C
C     ROUTINE FOR STATIONARY POSITION DETERMINATION
C
     1'************************ASYMMETRIC FLOW ANALYSIS******************
     2*****'//' ',11X,'STATIONARY POSITIONS (MM)    AV. MOBILITY(MICRON/
     3SEC/V/CM)'/' ',40X,'OF POPULATION, MEASURED AT:'/' ',19X,'FRONT',
     43X,'BACK',16X,'FRONT',8X,'BACK')
C
C     CALCULATE AVERAGE MOBILITY AT UNCORRECTED STATIONARY POSITIONS
C
      MOBFSP=COEFN(1)+COEFN(2)*FSP+COEFN(3)*FSP**2
      MOBBSP=COEFN(1)+COEFN(2)*BSP+COEFN(3)*BSP**2
      WRITE(6,360) FSP,BSP,MOBFSP,MOBBSP
  360 FORMAT(/' ','UNCORRECTED',8X,F5.3,2X,F5.3,13X,F10.6,2X,F10.6/' ',
     2'FOR ASYM. FLOW')
      STORE1=FSP
      STORE2=BSP
      STORE3=MOBFSP
      STORE4=MOBBSP
      FACTOR=3.098*(1.0+COEFN(2)/(COEFN(3)*XMAX))
      X2=XMAX*(.5+.1614*(-FACTOR-SQRT(FACTOR**2+3.4)))
      X1=XMAX*(.5+.1614*(-FACTOR+SQRT(FACTOR**2+3.4)))
      FSP=AMIN1(X1,X2)
      BSP=AMAX1(X1,X2)
C
C     CALCULATE AVERAGE MOBILITY AT PREDICTED STATIONARY POSITIONS
C
  350 MOBFSP=COEFN(1)+COEFN(2)*FSP+COEFN(3)*FSP**2
      MOBBSP=COEFN(1)+COEFN(2)*BSP+COEFN(3)*BSP**2
      WRITE(6,370) FSP,BSP,MOBFSP,MOBBSP
  370 FORMAT(/' ',1X,'CORRECTED', 9X,F5.3,2X,F5.3,13X,F10.6,2X,F10.6/' '
     1,'FOR ASYM. FLOW')
      STORE1=(FSP-STORE1)/XMAX*100.
      STORE2=(BSP-STORE2)/XMAX*100.
      STORE3=STORE3-MOBFSP
      STORE4=STORE4-MOBBSP
      WRITE(6,380) STORE1,STORE2,STORE3,STORE4
  380 FORMAT(/' ','UNCORRECTED',8X,F5.1,2X,F5.1,17X,F5.3,7X,F5.3/' ',
     13X,'ERROR',7X,'(% OF CHAMBER WIDTH)',12X,'(MICRONS/SEC/V/CM)')
      WRITE(6,403) FACTOR
  403 FORMAT(/' ',22X,'ASYMMETRIC INDEX = ', F6.3)
C
C     STATISTICAL ROUTINE - GENERATES CONFIDENCE INTERVALS FOR AVERAGE
```

```
C     MOBILITY
C
      IF(STAT.EQ.0.0) GO TO 415
      S=SQRT(SNGL(ERRSSQ)/(OBS-2.))
      XMEAN=SUMX/OBS
      CONST1=S*SQRT(1.+1./OBS+OBS*(FSP-XMEAN)**2/ABS(OBS*SUMXSQ-SUMX**2)
     1)
      CONST2=S*SQRT(1.+1./OBS+OBS*(BSP-XMEAN)**2/ABS(OBS*SUMXSQ-SUMX**2)
     1)
      DO 405 J=1,4
      CIEFSP(J)=T(J)*CONST1
  405 CIEBSP(J)=T(J)*CONST2
      WRITE(6,410) FSP,MOBFSP,CIEFSP(1),C(1),BSP,MOBBSP,CIEBSP(1),C(1),
     1(CIEFSP(I),C(I),CIEBSP(I),C(I),I=2,4)
  410 FORMAT('-','**********************************CONFIDENCE INTERVAL
     1ESTIMATE**********************************'/' ',1X,'FSP',5X,  'MOB
     1(FSP)',5X,'INTERVAL',5X,'%CONFIDENCE',5X,'BSP',5X,'MOB(BSP)',5X,'I
     2NTERVAL',5X,'%CONFIDENCE'/' ',F5.3,3X,F10.6,3X,F10.6,8X,I2,9X,F5.3
     3,3X,F10.6,3X,F10.6,8X,I2,3(/' ',21X,F10.6,8X,I2,30X,F10.6,8X,I2))
  415 CONTINUE
C
C     PLOT FRONT AND BACK STATIONARY POSITIONS AND AVERAGE MOBILITY
C
      IF (PLOT.EQ.0.0) GO TO 420
      XPLOT(1)=FSP
      YPLOT(1)=2.0
      XPLOT(2)=FSP
      YPLOT(2)=MOBFSP
      XPLOT(3)=XMIN
      YPLOT(3)=MOBFSP
      CALL SAMEP(YPLOT,3,XPLOT,SYM,0)
      XPLOT(1)=BSP
      YPLOT(1)=2.
      XPLOT(2)=BSP
      YPLOT(2)=MOBBSP
      XPLOT(3)=.72
      YPLOT(3)=MOBBSP
      CALL SAMEP(YPLOT,3,XPLOT,SYM,0)
      IF(CHECK.LT.0) CALL EPLOT
  420 CONTINUE
      I=OBS
C
C     HISTOGRAM ROUTINE
C
      IF(HIST.EQ.0) GO TO 520
C
C     DETERMINE THE ACTUAL MOBILITY OF EACH CELL FROM REFERENCE CURVE
C
      DO 425 J=1,I
  425 Y(J)=MOBFSP+(Y(J)-(COEFN(1)+COEFN(2)*X(J)+COEFN(3)*X(J)**2))
C
C     ORDER MOBILITY ARRAY WITH INCREASING NEGATIVE VALUES
C
```

```
      DO 450 J=1,I
      L=J
      YMAX=Y(J)
      DO 440 K=J,I
      IF(Y(K)-YMAX) 440,440,430
  430 L=K
      YMAX=Y(K)
  440 CONTINUE
      Y(L)=Y(J)
      Y(J)=YMAX
  450 CONTINUE
C
C     GENERATE 1-3 HISTOGRAMS AT 1-3 RESOLUTIONS
C
      DO 515 L=1,HIST
  458 WRITE(6,455)
  455 FORMAT(//'1','****MOBILITY HISTOGRAM**************************'//
     1' ',4X,'RANGE',6X,'N',1X,'FREQUENCY'/' ','-------------- -- ',
     2'----------')
C
C     DETERMINE UPPER MOBILITY LIMIT WHICH IS AN EVEN MULTIPLE OF
C     HISTOGRAM CLASS WIDTH
C
      RA=Y(1)-DMOD(Y(1),RES(L))
      R2=RA-RES(L)
C
C     GENERATE FREQUENCIES FOR EACH BAR OF THE HISTOGRAM
C
      J=1
  460 N=0
  470 IF(Y(J)-R2) 490,490,480
  480 N=N+1
      J=J+1
      IF(J-I) 470,490,490
  490 N1=N+1
C
C     WRITE OUT HISTOGRAM
C
      WRITE(6,510) RA,R2,N,(B(K),K=1,N1)
      RA=R2
      R2=R2-RES(L)
      IF(J-I) 460,460,500
  500 CONTINUE
  510 FORMAT(' ',F6.2,'-',F6.2,1X,I2,50(A1,1X))
  515 CONTINUE
  520 CONTINUE
      RETURN
      END
```

APPENDIX 4B. CYTOLP, a program in BASIC for microscopic electrophoresis data analysis.

This program is an adaptation of the Fortran program described in Appendix 4A. It is used interactively with the following hardware configuration: PDP 11/10 minicomputer, Tektronix 4010 terminal, DECwriter terminal, and Tektronix 4610 hard-copy unit. The program includes a subroutine for fitting a straight line to depth-mobility data from a coated chamber. Lines 9000-9310 describe a graphics routine for a special operating system, and are probably not applicable to typical computing hardware and monitor configurations.

```
10 REM  CONVERTS RAW CYTOPHEROMETER DATA TO DEPTH-MOBILITY
15 REM  COORDINATES FOR A CURVE-FITTING ROUTINE WHICH
17 REM  CALCULATES CELL MOBILITY
20 REM  E=ERROR FLAG FOR INAPPROPRIATE DATA
25 REM  F=MAGNIFICATION FACTOR
30 REM  B2=UNCORRECTED BACK STATIONARY POSITION
35 REM  F2=UNCORRECTED FRONT STATIONARY POSITION
40 REM  M(I)=ARRAY CONTAINING APPARENT CELL MOBILITIES
45 REM  R(I)=NUMBER OF RETICULES CELL WAS CLOCKED FOR
50 REM  Y(I)=MICROMETER READING (MM)
55 REM  S1=SUM OF CHAMBER DEPTH POSITIONS
60 REM  S2=SUM OF SQUARES OF DEPTH POSITIONS
65 REM  T1=TRAVERSE TIME, MOVING LEFT (SEC)
70 REM  T2=TRAVERSE TIME, MOVING RIGHT (SEC)
100 PRINT "CURRENT THROUGH CHAMBER (AMPS)";\INPUT A1
105 PRINT "NUMBER OF RETICULES BETWEEN REFERENCE"
106 PRINT "SCRATCHES ON BACK WALL";\INPUT B1
110 PRINT "NUMBER OF RETICULES BETWEEN REFERENCE"
111 PRINT "SCRATCHES ON FRONT WALL";\INPUT F1
115 PRINT "CONDUCTIVITY OF BUFFER (MHO/CM)";\INPUT K1
117 PRINT "CHAMBER THICKNESS (MICROMETER READING, MM)";
118 INPUT X1
120 PRINT "VISCOSITY OF BUFFER AT EXPERIMENTAL TEMP. (CP)",
121 INPUT V1
125 PRINT "VISCOSITY OF WATER AT EXPERIMENTAL TEMP. (CP)";
126 INPUT V2
130 PRINT "NO. OF CELLS MEASURED FOR GIVEN EXPT.";\INPUT N
200 DIM Y(400),X(400),R(400),T1(400),T2(400),M(400)
201 DIM A(3),T(4),C6(4),R5(4),R6(4)
```

```
202 DIM H(3),M1(400)
205 REM  INPUT RAW DATA
210 PRINT "DATA FILENAME ";\INPUT D$
212 OPEN D$ FOR INPUT AS FILE #F1(1000)
215 FOR I=1 TO N\I4=4*I
220 LET Y(I)=VF1(I4-3)
221 LET R(I)=VF1(I4-2)
222 LET T1(I)=VF1(I4-1)
223 LET T2(I)=VF1(I4)
225 NEXT I
230 CLOSE #F1
232 READ H(1),H(2),H(3)\REM HISTOGRAM CLASS WIDTHS
233 DATA .05,.02,.01
235 READ T(1),T(2),T(3),T(4)\REM T-INTERVALS
236 DATA 1.65,1.96,2.33,2.58
238 READ C6(1),C6(2),C6(3),C6(4)\REM %-CONFIDENCES
239 DATA 90,95,98,99
240 REM  CONVERT MICROMETER READING TO ACTUAL CHAMBER DEPTH
241 REM  BY INTERPOLATION ON CORRELATION FUNCTION
245 X1=.633+(X1-1.1)/.45*.233
250 F2=X1*.2024
251 B2=X1*.7976
255 REM  DETERMINE CHAMBER CROSS-SECTION, CONSIDERING THERMAL
256 REM  EXPANSION, BY CONVERTING X1 FROM MM TO CM, SQUARING,
257 REM  AND MULTIPLYING BY THE HEIGHT/WIDTH RATIO OF 20.
260 A=X1^2/5
265 C=15.6*2*K1*(A/A1)*(V1/V2)
270 REM  CALCULATE MAGNIFICATION FACTOR
275 F=F1/B1
280 REM  PRINT OUT FOR DATA VERIFICATION
281 PRINT "TYPE HEADING ON DECWRITER (E.G. DATE, EXPTAL. CONDS.)"
282 PRINT "OUTPUT RAW DATA FOR VERIFICATION \SWITCH TO "
283 PRINT "LOCAL, HIT <CR> ON DECWRITER)";\INPUT A$
285 PRINT "MAGNIFICATION FACTOR = ";F
286 PRINT "CHAMBER THICKNESS = ";X1;"MM"
287 PRINT "FRONT STATIONARY PLANE = ";F2;"MM"
288 PRINT "BACK STATIONARY PLANE = ";B2;"MM"
289 PRINT "MEDIUM VISCOSITY = ";V1;"CP"
290 PRINT "WATER VISCOSITY = ";V2;"CP"
291 PRINT "MEDIUM CONDUCTIVITY = ";K1;"MHO/CM"
292 PRINT "CURRENT = ";A1;" AMPS"
293 PRINT "NUMBER OF DATA POINTS = ";N
295 PRINT \PRINT " DATA FILE IS ";D$
296 PRINT

300 PRINT "  Y              RET            DECL           ERROR"
310 FOR I=1 TO N
315 PRINT Y(I),R(I),T1(I),T2(I)
320 NEXT I
330 REM  CONVERT MICROMETER READINGS TO ACTUAL CHAMBER DEPTHS
331 REM  BY INTERPOLATION ON A 4-SEGMENT CORRELATION FUNCTION
```

```
323 S1=0
324 S2=0
325 FOR I=1 TO N
340 IF Y(I)>=.16 THEN 355
345 X(I)=Y(I)/.16*.1\GO TO 420
355 IF Y(I)>=.65 THEN 370
360 X(I)=.1+(Y(I)-.16)/.49*.287\GO TO 420
370 IF Y(I)>=1.1 THEN 385
375 X(I)=.387+(Y(I)-.65)/.45*.246\GO TO 420
385 IF Y(I)>=1.55 THEN 400
390 X(I)=.633+(Y(I)-1.1)/.45*.253\GO TO 420
400 PRINT I,Y(I)
405 PRINT "RECHECK DATA POINT"
410 E=1
415 REM  CALCULATE APPARENT MOBILITY
420 M(I)=-D*K(I)*(2*F-1)*X(I)/X1/(T1(I)+T2(I))
425 S1=S1+X(I)
430 S2=S2+X(I)*X(I)
435 NEXT I
439 REM  RESEQUENCE DATA ARRAYS BY INCREASING CHAMBER DEPTH
440 REM  FOR EFFICIENT PLOTTING
445 FOR I=1 TO N\L=I\X2=X(I)
460 FOR J=I TO N\IF X(J)>=X2 THEN 480 \L=J
475 X2=X(J)
480 NEXT J\S=M(L)\M(L)=M(I)\R=Y(L)\Y(L)=Y(I)\X(L)=X(I)
500 M(I)=S\Y(I)=R\X(I)=X2
501 NEXT I
515 REM  PRINT OUT MOBILITIES FOR VERIFICATION
519 PRINT
520 PRINT "MICROMETER      CHAMBER        APPARENT"
521 PRINT " READING         DEPTH         MOBILITY"
525 FOR J=1 TO N
530 PRINT Y(J),X(J),M(J)
535 NEXT J\IF E=1GO TO 32767
540 PRINT
800 PRINT "CONTINUE WITH CURVE-FITTING (Y=1,N=0)";\INPUT G
810 IF G=0 THEN 32767
820 PRINT "METHYLCELLULOSE COATED CHAMBER? (Y=1,N=0)";\INPUT G1

825 IF G1=1 THEN 10020
830 GO TO 1000
990 PRINT "TRY A PARABOLIC FIT? (Y=1,N=0)";\INPUT G2
991 G1=0

995 IF G2=0 THEN 1920

1000 REM  ROUTINE GENERATES A REFERENCE PARABOLA FROM

1001 REM  MOBILITY DATA BY LEAST-SQUARES CURVE-FITTING

1005 DIM X4(4),C4(2),B(3),C(3,3),D(3,3)
```

```
1020 REM  FORM SUMS OF POWERS OF X(I)
1025 FOR K=1 TO 4\X4(K)=0
1030 FOR I=1 TO N\LET X4(K)=X4(K)+X(I)^K\NEXT I
1045 NEXT K
1050 REM  FORM SUM OF M(I)
1055 M4=0\FOR I=1 TO N\LET M4=M4+M(I)\NEXT I
1065 REM  FORM SUMS OF PRODUCTS OF M(I)*X(I)^K
1070 FOR K=1 TO 2\C4(K)=0\FOR I=1 TO N
1080 LET C4(K)=C4(K)+M(I)*X(I)^K\NEXT I\NEXT K
1090 REM  GENERATE NORMAL MATRIX C USING SUMS OF POWERS OF X(I)
1095 FOR I=1 TO 3\FOR J=1 TO 3\K=I+J-2
1110 IF K<>0 GO TO 1120 \C(1,1)=N\GO TO 1125
1120 C(I,J)=X4(K)
1125 NEXT J\NEXT I
1135 REM  GENERATE R.H.S. MATRIX B
1140 B(1)=M4\FOR I=2 TO 3\B(I)=C4(I-1)\NEXT I
1150 REM  INVERT NORMAL MATRIX C
1165 GOSUB 8000
1170 REM  MATRIX D IS INVERSE OF NORMAL MATRIX
1175 REM  FORM MATRIX PRODUCTS OF INVERSE AND R.H.S. MATRIX
1185 FOR I=1 TO 3\A(I)=0\FOR J=1 TO 3
1200 A(I)=A(I)+D(I,J)*B(J)\NEXT J\NEXT I
1201 E1=0\E2=0\E3=0
1202 FOR I=1 TO N
1203 LET V6=A(1)+A(2)*X(I)+A(3)*X(I)^2
1204 LET V6=V6-M(I)
1205 LET E1=E1+V6
1206 LET E2=E2+ABS(V6)
1207 LET E3=E3+V6^2\LET S5=SQR(E3/(N-4))
1208 NEXT I
1212 GOSUB 9000
1213 PRINT "OUTPUT LEAST SQUARES FIT ANALYSIS (Y=1,N=0)";\INPUT Q
1214 IF Q=0 THEN 1220
1215 PRINT \PRINT "              LEAST SQUARES PARABOLIC FIT"
1220 PRINT \PRINT " POINTS FITTED = ";N
1225 PRINT "  COEFFICIENT OF X^2 = ";A(3)
1230 PRINT "  COEFFICIENT OF X   = ";A(2)
1235 PRINT "  CONSTANT TERM      = ";A(1)
1236 PRINT
1237 PRINT "        SUM OF ERRORS              = ";E1
1240 PRINT "        SUM OF ABSOLUTE ERRORS     = ";E2
1245 PRINT "        SUM OF SQUARES OF ERRORS   = ";E3
1246 PRINT "        STANDARD DEVIATION         = ";S5
1251 PRINT
1300 REM  ROUTINE FOR STATIONARY POSITION DETERMINATION
1305 PRINT "*********ASYMMETRIC FLOW ANALYSIS*********"
1310 PRINT
1311 PRINT TAB(16);"STATIONARY POSITIONS";TAB(40);"MOBILITY";
1312 PRINT TAB(52);"(MICRONS/SEC/V/CM)"
1315 PRINT TAB(41);"OF POPULATION, MEASURED AT:"
1317 PRINT TAB(19);"FRONT";TAB(30);"BACK";TAB(45);"FRONT";TAB(59);"BACK"
```

```
1320 REM  CALCULATE AVERAGE MOBILITY AT UNCORRECTED STATIONARY
1321 REM  POSITIONS
1325 M5=A(1)+A(2)*F2+A(3)*F2^2
1330 M6=A(1)+A(2)*B2+A(3)*B2^2
1335 PRINT "UNCORRECTED",TAB(13);F2,B2,M5,M6
1340 PRINT "FOR ASYM. FLOW"
1345 PRINT \F6=3.398*(1+A(2)/(A(3)*X1))
1355 F7=X1*(.5+.1614*(-F6-SQR(F6^2+3.4)))
1360 B7=X1*(.5-.1614*(-F6+SQR(F6^2+3.4)))
1365 REM  CALCULATE AVERAGE MOBILITY AT PREDICTED STATIONARY
1367 REM  POSITIONS
1375 M7=A(1)+A(2)*F7+A(3)*F7^2
1380 M8=A(1)+A(2)*B7+A(3)*B7^2
1385 PRINT "CORRECTED",TAB(13);F7,B7,M7,M8
1390 PRINT "FOR ASYM. FLOW"\PRINT
1395 F2=(F7-F2)/X1*100\B2=(B7-B2)/X1*100
1397 M5=M5-M7\M6=M6-M8
1400 PRINT "UNCORRECTED",TAB(13);F2,B2,M5,M6
1405 PRINT "    ERROR",TAB(16);"(% OF CHAMBER WIDTH)",TAB(42);
1406 PRINT "(MICRONS/SEC/V/CM)"
1410 PRINT \PRINT TAB(22);"ASYMMETRIC INDEX = ";F6
1415 REM  STATISTICAL ROUTINE - GENERATES CONFIDENCE INTERVALS
1416 REM  FOR AVERAGE MOBILITY
1420 Q1=SQR(E2/(N-2))\Q2=S1/N
1430 R3=Q1*SQR(1+1/N+N*(F7-Q2)^2/ABS(N*S2-S1^2))
1435 R4=Q1*SQR(1+1/N+N*(B7-Q2)^2/ABS(N*S2-S1^2))
1455 FOR J=1 TO 4\R5(J)=T(J)*R3\R6(J)=T(J)*R4\NEXT J
1475 PRINT \PRINT
1476 PRINT "**********CONFIDENCE INTERVAL ESTIMATE***********"
1480 PRINT
1482 PRINT "    FSP",TAB(13);"MOB(FSP)",TAB(29);"INTERVAL  % CONFIDENCE"
1485 PRINT F7,M7,R5(1),C6(1)
1490 FOR I=2 TO 4\PRINT ,,R5(I),C6(I)
1500 NEXT I\PRINT
1510 PRINT "    BSP",TAB(13);"MOB(BSP)",TAB(29);"INTERVAL  % CONFIDENCE"
1515 PRINT B7,M8,R6(1),C6(1)
1520 FOR I=2 TO 4\PRINT ,,R6(I),C6(I)\NEXT I
1600 REM  HISTOGRAM ROUTINE
1605 REM  DETERMINE THE ACTUAL MOBILITY OF EACH CELL FROM
1606 REM  REFERENCE CURVE
1610 FOR J=1 TO N
1615 LET M(J)=M7+(M(J)-(A(1)+A(2)*X(J)+A(3)*X(J)^2))
1617 NEXT J
1620 REM  ORDER MOBILITY ARRAY WITH INCREASING NEGATIVE VALUES
1624 FOR J=1 TO N\LET L=J\LET M1=M(J)
[illegible] THEN 1650
[illegible]
[illegible] NEXT [illegible] M(J)=M1\NEXT [illegible]
[illegible] PRINT \PRINT
[illegible]
[illegible] RESOLUTIONS
[illegible] CLASS [illegible]
[illegible] PRINT "2=.03,.02 CLASS WIDTHS,3=.05,.02,.01 CLASS WIDTHS"
[illegible] PRINT "WHERE UNITS ARE MICRONS/SEC/V/CM"\INPUT [illegible]
[illegible] PRINT [illegible]
[illegible] MOBILITY [illegible] GRAM****
[illegible] PRINT \PRINT
```

```
1707 PRINT "     RANGE",TAB(16);"N    FREQUENCY"
1708 PRINT "-------------  --  ---------"
1710 REM  DETERMINE UPPER MOBILITY LIMIT WHICH IS AN EVEN
1711 REM  MULTIPLE OF HISTOGRAM CLASS WIDTH
1715 W4=INT(M(1)/H(L)+1)*H(L)\W5=W4-H(L)
1725 REM  GENERATE FREQUENCIES FOR EACH BAR OF THE HISTOGRAM
1730 J=1
1735 N1=0

1740 IF M(J)<=W5 THEN 1770 \N1=N1+1\J=J+1
1755 IF J<=N THEN 1740

1765 REM  WRITE OUT HISTOGRAM

1770 PRINT W4;TAB(7);"- ";W5;TAB(16);N1;TAB(20);
1774 IF G4=1 THEN 1780

1775 FOR K=1 TO N1\PRINT "* ";\NEXT K

1776 IF G4=0 THEN 1790

1780 FOR K=1 TO N1\PRINT "*";\NEXT K

1790 PRINT \W4=W5\W5=W5-H(L)

1805 IF J<=N THEN 1735

1810 NEXT L\PRINT \PRINT \PRINT \PRINT
1811 G5=G5+1\IF G5=2 THEN 1815
1812 PRINT "CONTRACT FREQUENCY SCALE IN HISTOGRAM (Y=1,N=0)";
1813 INPUT G4

1814 IF G4=1 THEN 1700
1815 IF G1=1 THEN 990
1820 PRINT "DO ANOTHER RUN (Y=1,N=0)";\INPUT N3
1825 IF N3=0 THEN 32767
1830 GO TO 100
8000 REM  MATRIX INVERSION BY ELIMINATION WITH PARTIAL PIVOTING
8005 E4=1.00000E-07
8010 REM  CONSTRUCT IDENTITY MATRIX D(I,J)=I
8015 FOR I=1 TO 3
8020 FOR J=1 TO 3
8025 IF I<>J THEN 8040
8030 D(I,J)=1
8035 GO TO 8045
8040 D(I,J)=0
8045 NEXT J
8050 NEXT I
```

```
8055 REM  LOCATE MAXIMUM MAGNITUDE C(I,K) ON OR BELOW MAIN DIAGONAL
8060 D4=1
8065 FOR K=1 TO 3
8070 IF K=3 THEN 8170
8075 I1=K
8080 C1=ABS(C(K,K))
8085 K1=K+1
8090 FOR I=K1 TO 3
8095 IF C1>=ABS(C(I,K)) THEN 8110
8100 I1=I
8105 C1=ABS(C(I,K))
8110 NEXT I
8115 REM  INTERCHANGE ROWS I1 AND K IF I1 NOT EQUAL TO K
8120 IF I1=K THEN 8170
8125 FOR J=1 TO 3
8130 C5=C(I1,J)
8135 C(I1,J)=C(K,J)
8140 C(K,J)=C5
8145 D5=D(I1,J)
8150 D(I1,J)=D(K,J)
8155 D(K,J)=D5
8160 NEXT J
8165 D4=-D4
8170 REM  TEST FOR SINGULAR MATRIX
8180 IF ABS(C(K,K))<=E4 THEN 8280
8185 D4=C(K,K)*D4
8190 REM  DIVIDE PIVOT ROW BY ITS MAIN DIAGONAL ELEMENT
8195 D6=C(K,K)
8200 FOR J=1 TO 3
8205 C(K,J)=C(K,J)/D6
8210 D(K,J)=D(K,J)/D6
8215 NEXT J
8220 REM  REPLACE EACH ROW BY LINEAR COMBINATION WITH PIVOT ROW
8230 FOR I=1 TO 3
8235 C6=C(I,K)
8240 IF I=K THEN 8260
8245 FOR J=1 TO 3
8250 C(I,J)=C(I,J)-C6*C(K,J)
8255 D(I,J)=D(I,J)-C6*D(K,J)
8257 NEXT J
8260 NEXT I
8270 NEXT K
8275 RETURN
8280 PRINT "SINGULAR MATRIX FOR K=";K
8285 GO TO 32767
9000 PRINT "GRAPH DEPTH-MOBILITY DATA AND REFERENCE PARABOLA (";D3;")"
9001 PRINT "(SWITCH TO TEKTRONIX (Y=1,N=0)"); :INPUT D

9010 IF D=0 THEN 1215
9015 PRINT CHR$(27)&CHR$(12)
9020 PRINT TAB(11);"DEPTH-MOBILITY DATA AND REFERENCE PARABOLA (";D3;")"
9022 REM  DETERMINE MAXIMUM ABSOLUTE MOBILITY
9025 V8=M(1)
9030 FOR I=1 TO N\IF M(I)>2 THEN 9045
9035 IF M(I)>V8 THEN 9040 \V8=M(I)
9040 NEXT I\GO TO 9050
9045 PRINT "RESCALE MOBILITY AXIS"\RETURN
```

```
9048 REM  DRAW AXES
9050 CALL "MOVE"(50,100)\CALL "DRAW"(50,700)
9060 CALL "DRAW"(1013,700)\CALL "DRAW"(1013,100)
9065 CALL "DRAW"(50,100)
9070 Y8=ABS(Y8)\Y8=INT(Y8+3)
9075 Y7=INT(600/Y8)
9080 FOR J=1 TO Y8\Y9=INT(Y7*J+100)
9082 IF J<>2 THEN 9085 \CALL "MOVE"(50,Y5)
9083 CALL "DRAW"(1013,Y9)\GO TO 9090
9085 CALL "MOVE"(50,Y9)\CALL "DRAW"(60,Y9)
9090 Y5=INT(Y9-10)\CALL "MOVE"(20,Y5)\CALL "ALFA"
9095 J1=2-J\PRINT J1\NEXT J
9100 FOR J=1 TO 9\J1=INT(J*107+50)
9105 CALL "MOVE"(J1,100)\CALL "DRAW"(J1,110)
9110 J1=INT(J1-25)\J2=.1*J
9115 CALL "MOVE"(J1,80)\CALL "ALFA"
9120 PRINT J2\NEXT J
9125 CALL "MOVE"(400,50)\CALL "ALFA"
9130 PRINT "CHAMBER DEPTH (MM)"
9135 J1=INT(1070*X1+50)
9140 FOR J=1 TO 30\LET L=2*J-1
9145 LET L1=INT(100+10*(L-1))
9150 LET L2=INT(100+10*L)
9155 CALL "MOVE"(J1,L1)\CALL "DRAW"(J1,L2)
9160 NEXT J

9200 REM  PLOT DATA POINTS
9205 FOR I=1 TO N
9210 LET Z1=INT(1070*X(I)+50)
9215 LET Z2=2-M(I)\LET Z2=INT(Y7*Z2+100)
9220 CALL "PINT"(Z1,Z2)\NEXT I
9230 REM  PLOT PARABOLA
9231 M=INT(Y7*(2-A(1))+100)

9232 CALL "MOVE"(50,M)
9235 FOR J=1 TO 200

9240 LET X=5.00000E-03*J

9245 IF X>X1 THEN 9280

9250 LET M=A(1)+A(2)*X+A(3)*X^2

9255 LET X=INT(1070*X+50)

9260 LET M=2-M\LET M=INT(Y7*M+100)

9265 CALL "DRAW"(X,M)

9270 NEXT J

9280 CALL "MOVE"(0,0)

9300 CALL "ALFA"

9305 IF G1=1 THEN 10100
9310 RETURN

9900 REM ORDER MOBILITY ARRAY WITH INCREASING NEGATIVE VALUES
9902 FOR I=1 TO N\LET M1(I)=M(I)\NEXT I
9904 FOR J=1 TO N\LET L=J\LET M1=M1(J)
```

```
9906 FOR K=J TO N\IF M1(K)<=M1 THEN 9910
9908 LET L=K\LET M1=M1(K)
9910 NEXT K\LET M1(L)=M1(J)\LET M1(J)=M1\NEXT J
9912 PRINT \PRINT
9915 REM GENERATE 1-3 HISTOGRAMS AT 1-3 RESOLUTIONS
9920 PRINT "HISTOGRAM(S) REQ'D (0=NONE,1=.05 CLASSWIDTH,"
9921 PRINT "2=.05,.02 CLASS WIDTHS,3=.05,.02,.01 CLASS WIDTHS,"
9922 PRINT "WHERE UNITS ARE MICRONS/SEC/V/CM)";\INPUT H
9930 FOR L=1 TO H\PRINT \PRINT
9932 PRINT "****MOBILITY HISTOGRAM****"
9933 PRINT "     (COATED CHAMBER)"\PRINT
9935 PRINT "    RANGE",TAB(16);"N   FREQUENCY"
9937 PRINT "-------------  --  ----------"
9938 REM DETERMINE UPPER MOBILITY LIMIT WHICH IS AN EVEN
9940 REM MULTIPLE OF HISTOGRAM CLASS WIDTH
9942 W4=INT(M1(J)/H(L)+1)*H(L)\W5=W4-H(L)
9946 REM GENERATE FREQUENCIES FOR EACH BAR OF THE HISTOGRAM
9948 J=1
9950 N1=0
9952 IF M1(J)<=W5 THEN 9956 \N1=N1+1\J=J+1
9954 IF J<=N THEN 9952
9956 REM WRITE OUT HISTOGRAM
9958 PRINT W4;TAB(7);"- ";W5;TAB(16);N1;TAB(20);
9960 FOR K=1 TO N1\PRINT "* ";\NEXT K
9962 PRINT \W4=W5\W5=W5-H(L)
9964 IF J<=N THEN 9950
9966 NEXT L\PRINT \PRINT \PRINT \PRINT
9970 GO TO 590
10020 REM COMPUTE AVERAGE MOBILITY AND ERRORS
10025 M4=0\FOR I=1 TO N\LET M4=M4+M(I)\NEXT I
10030 A(1)=M4/N\A(2)=0\A(3)=0
10035 E1=0\E2=0\E3=0
10040 FOR I=1 TO N
10045 LET V6=A(1)\LET V6=V6-M(I)
10050 LET E1=E1+V6\LET E2=E2+ABS(V6)\LET E3=E3+V6^2
10055 NEXT I\S5=SQR(E3/(N-1))
10060 PRINT "GRAPH DEPTH-MOBILITY DATA & AVERAGE MOBILITY"
10061 PRINT "(SWITCH TO TEKTRONIX)  (Y=1,N=0)";\INPUT D
10070 IF D=0 THEN 10100
10075 PRINT CHR$(27)&CHR$(12)
10080 PRINT TAB(11);"DEPTH-MOBILITY DATA & AVERAGE MOBILITY (";D$;")"
10085 GO TO 9025
10100 PRINT "OUTPUT ERROR ANALYSIS (Y=1,N=0)";\INPUT Q
10105 IF Q=0 THEN 1820
10110 PRINT \PRINT "              ERROR ANALYSIS"
10115 PRINT \PRINT "   AVERAGE MOBILITY =",A(1)
10120 PRINT
10125 PRINT "       SUM OF ERRORS              = ",E1
10130 PRINT "       SUM OF ABSOLUTE ERRORS     = ",E2
10135 PRINT "       SUM OF SQUARES OF ERRORS   = ",E3
10140 PRINT "       STANDARD DEVIATION         = ",S5
10145 REM CONFIDENCE INTERVALS FOR AVERAGE MOBILITY
10150 FOR J=1 TO 4\R5(J)=T(J)*S5\NEXT J
10165 PRINT \PRINT
10190 PRINT "**********CONFIDENCE INTERVAL ESTIMATES**********"
10195 PRINT
10200 PRINT "AVERAGE MOBILITY",TAB(22);"INTERVAL   %CONFIDENCE"
10205 PRINT A(1),TAB(25);R5(1),C6(1)
10210 FOR I=2 TO 4\PRINT TAB(25);R5(I),C6(I)
10215 NEXT I\PRINT
10220 GO TO 9900
32767 END
```

Chapter 5.

Two Electrode Systems for Use with the Zeiss Cytopherometer.

OPERATION OF THE ZEISS CYTOPHEROMETER WITH $Zn/ZnSO_4$ ELECTRODE SYSTEM OF TENFORDE ET AL.

Procedure for Microscope Electrophoresis

Cytopherometry procedure has been covered in great detail by Seaman (152), Tenforde (167), Streibel (163) and Milito (116). A general checklist description of this procedure follows:

Setup

The disassembled glassware was submerged 1 hr in a 10X dilution of chromic acid one day prior to the experiment. The electrophoresis chamber, positioned in the cytopherometer, was also given a 1 hr treatment with this chromate solution using a 2 ml pipette and a rubber connecting tube for filling. Both the chamber and glassware were rinsed and then soaked in 2 x H_2O overnight to remove chromate ions from the glass surfaces. The following day, the glassware was drained and air dried while the appropriate water thermostat was connected to the cytopherometer, filled with 2 x H_2O, adjusted to the proper temperature, and turned on to equilibrate. (In lieu of refilling the reservoir with fresh water for each experiment to prevent the growth of mold on

the surfaces of the chamber and its water jacket, 0.5 mg/ml Na Azide was added to the bath water.) The addition of ice to the reservoir sped equilibration to lower temperatures. Each zinc electrode was carefully filed to remove surface oxide and then fitted tightly to its proper electrode chamber (larger stopper to larger diameter chamber). Four teflon stopcocks were assembled to the glassware (without grease), two one-inch pieces of connecting rubber tubing (0.4 cm i.d.) were fitted to the sidearms, and a six-inch piece of tubing was joined to the outlet pipe on the left-hand assembly. Each half of the glassware, in turn, was held upright over a sink for the following procedure.

A 25 ml pipette was filled with electrophoresis buffer and connected to the rubber hose at the side arm. (Buffer from one 500 ml bottle was used throughout a given experiment for consistency; this volume was adequate for setup, cell suspensions, and flushing.) Buffer was then introduced into the glassware slowly to avoid bubble formation until its level entered the flush tube. Both stopcocks were then closed with 1/8 turn and the pipette removed to fill the flush tube completely. Replacing the pipette at the sidearm, opening both stopcocks and applying suction removed all trapped bubbles from the system. The stopcocks were then closed, the glassware held horizontally, and the electrode chamber filled with a saturated solution of $ZnSO_4$ to its brim through its vent using a Pasteur pipette. All bubbles were removed and the vent was corked.

Both halves of the glassware, filled with buffer and electrode solution, were then bolted to their plexiglass backing, and the plexiglass, in turn, was bolted to the cytopherometer stage while guiding

the rubber tubing at each sidearm onto the chamber ends. The left end of the assembly was then lowered by rotating the stage counterclockwise and a 25 ml pipette, filled with electrophoresis buffer and attached to the drain tube, was used to prime the sidearms, chamber, and sample inlet tube. All bubbles were removed by simultaneous pressure from the pipette and from squeezing the connecting tubes. The chamber was leveled and then flushed by filling the sample inlet tube with buffer, controlling its level with the stopcock at the left-hand sidearm, and collecting buffer from the drain tube in a 500 ml beaker. To prevent the reintroduction of bubbles and the time-consuming procedure for their removal, the sample inlet tube was never entirely drained.

In preparation for physical chemical measurements on the cell suspension (or suspending buffer), the 50 ml centrifuge tube was filled with 30 ml of sample and placed in the jacketed water bath along with the empty pycnometer and the clean barrel of the conductivity probe to temperature equilibrate. The conductivity bridge was then turned on to the "line" position to warm up.

The fine focus micrometer was set at zero and its locking screw loosened. With its illuminator on, the microscope was focused on the vertical lines scored equidistantly on the inside front surface of the Zeiss chamber, first using the coarse focus, then the fine focus. The micrometer locking screw was then tightened at the zero position and the coarse focus was not touched for the remainder of the experiment. This micrometer calibration depends on eye refraction and must be repeated for each individual. The number of squares of the eyepiece reticule, to the nearest tenth, observed between neighboring vertical

lines was noted on a cytopherometer data sheet, designed and mimeographed to provide a form which organized all recorded data. By advancing the fine focus micrometer, the microscope was then focused on the horizontal scratches scored equidistantly on the inside back surface of the chamber. The number of reticule squares observed between these lines, to the nearest tenth, was recorded. The four digit micrometer reading at this position was recorded as the chamber width (depth). See Figure 10. The electrical leads were clipped to the electrodes, the stopcocks positioned for electrical continuity, and the current turned up to the desired amperage (usually 1 mA). Resulting voltages in excess of 600 V usually indicated the presence of bubbles trapped in a stopcock; they were removed by disconnecting the power and repeating the final priming procedure with buffer. Amperage was more accurately measured and adjusted using a volt ohm meter (Simpson) temporarily connected in series between the right electrode and its power clip. Amperage and voltage were then recorded and both stopwatches wound fully.

Cell Preparation for Microscope Electrophoresis

A cell suspension containing >90% single cells was obtained by using a 5 ml pipette to disperse fixed erythrocytes. An EDTA treatment developed by Thompson (172) was used for tissue-cultured cells. (See Cell Preparation for Electrophoresis.) Cells were washed and resuspended in electrophoresis buffer at 2-5 x 10^6 cells/ml. A 6 ml suspension proved to be a minimum working volume for each experiment; 40 ml was optimal, allowing viscosity and conductivity measurements on

the cell suspension rather than on the suspending buffer. If the cells were unfixed, the cell stock remained on ice during the experiment.

Data Taking

In a typical experiment one hour was required to time 50-70 cells, using the following procedure.

The cytopherometer inlet tube was carefully drained of buffer to a level just above its stopcock, and 6 ml of cell suspension from the cell stock was introduced by Pasteur pipette. About 3 ml of this sample was admitted to the chamber followed by a 2 min pause for temperature equilibration and dissipation of the cells' momentum. If a substantial drift remained, it was minimized by adjusting the corks at each electrode vent to equalize the fluid pressure at both ends of the chamber. Cells near the front and back chamber walls were timed first because their numbers decreased during typical experiments. A well-defined cell was focused on, and the field switch rolled to the left, marked "L". The time required for the geometrical center of the cell to cross a convenient integral number of reticule squares as it moved left was recorded. The field was then reversed and the cell timed for the same distance in the opposite direction. This distance was normally one reticule square for slowly moving cells, and two or more squares for fast cells, such that their migration time always exceeded two seconds and was typically seven seconds. Cells moved toward the anode (at the left end for "L", the right end for "R") unless they were close to the chamber walls where direction reversals were sometimes noted. Reversals are caused by the increasing electro-osmotic buffer flow near the walls which forces cells having a low

enough mobility to move against the electric field force. Four data were recorded on the work sheet for each cell measured: the four digit micrometer reading ("X"), the number of reticule squares traversed ("RET"; equal for the left and right measurement, negative to indicate a reversal), and migration time, to the nearest tenth of a second, to the left ("SECL") and to the right ("SECR"). The velocities to the left and right for each cell were calculated and averaged by computer to correct for possible net fluid drift through the chamber at the time of measurement. About 50 cells were usually timed at positions throughout the chamber depth. The work sheet suggests four measurements every 0.1 mm (1/2 turn) on the micrometer. A micrometer reading of zero at the front wall, the chamber thickness, the amperage and voltage, and the chamber level were all rechecked, and adjusted if necessary, at least once during each experiment. If the majority of cells had sedimented from view, the chamber and sidearm glassware were first flushed with buffer from the left and right flush tubes and the chamber was replenished with 3 ml fresh cell suspension. Very infrequently poor focus definition required a realignment of the microscope phase contrast optics.

Trouble Shooting

Three recurring problems for the cytopherometer, their probable causes and the corrective measures are covered below.

If the cells do not move after pressing the field switch, the cause is probably one of the following: the stopcocks are not positioned for electrical continuity; a leak at one electrode cork has created an airgap below the sintered glass; a stopcock bore contains

air and requires flushing to remove it; one of the power clips is not connected to its electrode; or the power supply has blown a fuse.

If the cells move in only one direction independently of the field direction, the problem is excessive drift. This can be caused by a leak occurring at an inadequately sealed joint in the glassware, by unbalanced fluid pressure at the electrode vents or from unleveled glassware, or by temperature instabilities. If the glassware is leveled and sealed, and temperature equilibrium has been reached, drift can usually be minimized by adjusting the fluid pressure exerted by the corks at the electrode vents.

If reversals (cell moves toward cathode) are observed throughout the chamber depth, a net electroosmotic flow is occurring because the system is not completely sealed. The usual remedy in this case is to top up each electrode at its vent and firmly seal it with a cork. Beyond this, the glassware can be disassembled, cleaned with chromic acid, and reassembled using new rubber joints while checking for cracks. Some of these corrective procedures warrant rescue of the cell sample from the inlet tube using a Pasteur pipette.

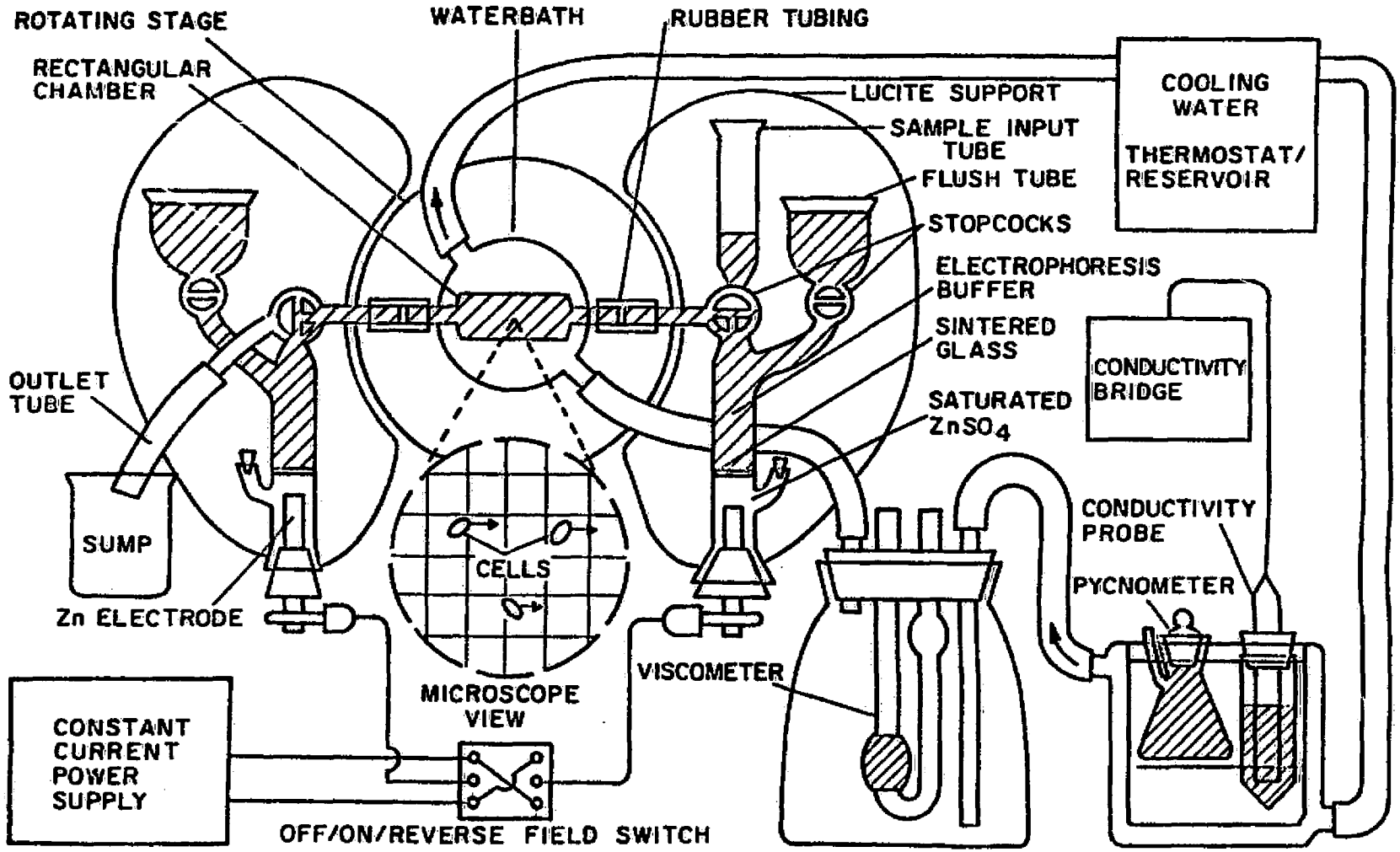
ROTATING STAGE
RECTANGULAR CHAMBER
WATERBATH
RUBBER TUBING
COOLING WATER
THERMOSTAT/ RESERVOIR
LUCITE SUPPORT
SAMPLE INPUT TUBE
FLUSH TUBE
STOPCOCKS
ELECTROPHORESIS BUFFER
SINTERED GLASS
SATURATED $ZnSO_4$
CONDUCTIVITY BRIDGE
OUTLET TUBE
SUMP
CELLS
CONDUCTIVITY PROBE
PYCNOMETER
Zn ELECTRODE
VISCOMETER
MICROSCOPE VIEW
CONSTANT CURRENT POWER SUPPLY
OFF/ON/REVERSE FIELD SWITCH

Use of the
ZEISS - CAM-APPARATUS MICROELECTROPHORESIS SYSTEM
with Ag/AgCl/KCl Electrodes

I. PREPARATION OF ELECTRODES

1) The solid silver electrodes must be scrupulously clean and dry prior to coating with AgCl. Clean as follows:
   (a) Immerse in conc. ammonia solution to remove old coating (use hood).
   (b) Polish with fine emery paper.
   (c) Rinse in 95% ethanol (handle with forceps and 'Kimwipes').
   (d) Rinse in ether.
   (e) Allow to dry.

2) Assemble an electrochemical cell using a spare silver electrode and a constant current power supply. Immerse both electrodes in 0.1M HCl so that they are parallel to each other (for optimum coating uniformity).
   (a) With the spare electrode as anode, apply ca. 50mA for some 10-15 s. Vigorous gassing will occur from the electrode to be chlorided. Remove this electrode from the electrolyte and re-immerse to remove gas bubbles.
   (b) Reverse the polarity and apply 2-3 mA or less. Coating uniformity will be improved by using lower currents and longer times.

II. ASSEMBLY OF MICROELECTROPHORESIS APPARATUS

Refer to fig.1 for an exploded view of the CAM-APPARATUS electrode housings.

1) Ensure that all O-rings and the sintered glass discs are seated firmly.
2) The glass two-way stopcocks should fit snugly into the plexiglass ports and must be held tightly by the knurled screws.

3) Fill the electrode chambers with 0.15 M KCl ensuring that no air bubbles are trapped anywhere within the chambers. Insert the electrodes allowing the glass-impregnated teflon tapers to form an efficient seal.

N.B. If buffers of lower than physiological ionic strength are to be used it is desirable to use a KCl solution of comparable molarity in the electrode chambers.

4) Attach the plexiglass blocks to the matching metal plates. These can then be mounted directly on the Zeiss Cytopherometer stage. Using silicone rubber, or similar, tubing, join the rectangular electrophoresis chamber to the short lengths of glass tubing inserted into the plexiglass housings.

5) Attach syringe housings to the filling ports to serve as funnels. Flush the system with distilled water, removing KCl solution which has leaked through the sintered glass discs. Load the system with buffer being careful to remove all air bubbles between the two stopcocks.

6) Attach the constant-current power supply leads to the electrodes and switch on.

N.B. Typical operating voltages are in the range 150-200 volts. Refer to Table I for typical operating currents for standard buffers.

III. EXPERIMENTAL PROCEDURE

1) Check that the water-bath is adequately filled with clean water. (Use of double-distilled water will help to minimise microbial growth.) Regular draining of the complete system is necessary.

N.B. The pump and thermostat unit contain mercury switches and, therefore, must be disconnected from electrical power whenever they are placed in an horizontal position.

2) Adjust the temperature to 25±0.2 °C by balancing thermostat control of the heating coils against the flow of cold tap-water through the pump cooling coil.

3) Check electrical continuity of the electrophoresis system --voltage and current readings should fall near the values shown in Table I.

4) After equilibration of the electrophoresis chamber to 25 °C, and with the phase optics correctly aligned (see Zeiss Manual for alignment procedure), the chamber depth and magnification readings may be carried out as follows:

   (a) Using the coarse and fine adjustments on the micrometer, focus on the vertical lines etched onto the inside of the front wall of the chamber. Ensure that the chamber flat is vertical. Do not touch the coarse focus again.

   (b) Set the micrometer fine adjustment to zero.

   (c) Measure the line spacing in units of eyepiece reticule divisions.

   (d) Now focus on the horizontal lines etched onto the back wall of the chamber and note the micrometer reading.

   (e) Measure the line spacing on the back wall in units of eyepiece reticule divisions.

   N.B. The front and back wall focus and corresponding micrometer readings should be repeatable. On account of wear of the micrometer movement it is desirable to check periodically for uniformity of response of this adjustment by measuring the depth of the chamber starting from different initial positions of the fine adjustment. In use, the calibrated fine adjustment must be used only over the range of uniform response.

5) Load the chamber with cell suspension--a suitable concentration being ca. 10^6 /ml. If the concentration is too high interaction between individual particles will occur and focussing at the deeper levels of the chamber will be difficult. Close both stopcocks and adjust the rotating stage so that the chamber is horizontal as indicated by the bubble level.

6) Check that, in the absence of an applied electric field, cells do not drift in one direction or another. Cells should merely fall under gravity in this situation. Drifts may arise through improper sealing, presence of bubbles, or to the non-establishment of temperature equilibrium.

7) Mobility data is collected throughout the chamber depth. For each cell in focus record the micrometer depth reading and the times for left and right traversal of a fixed number of reticule divisions. The latter is also recorded and will vary depending on the depth of the measurement.

N.B. (i) Transit times should be in the region of 5-10 seconds. Shorter times may lead to Brownian motion errors and operator timing errors. Inaccuracies due to particles falling out of focus, etc., may have a pronounced effect if much longer times are used.

(ii) Velocity reversals may occur near the front and back walls. These are recorded by assigning a negative sign to the number of reticule spacings traversed.

8) Periodic checks should be made of temperature, current, voltage, levelling, and drift.

9) The <u>viscosity</u> and <u>electrical conductivity</u> of the buffer solution at 25°C must be determined.

(a) Electrical Conductivity Measurement:

A #3403 conductivity cell in conjunction with a Model 31 conductivity bridge (Yellow Springs Instrument Company, Inc.) is used to determine buffer electrical conductivity, ensuring that the buffer temperature is 25 °C.

(b) Viscosity Measurement:

An Ostwald viscometer and a 25 ml Kimax pycnometer are used to measure buffer viscosity.

(i) Rinse viscometer with double-distilled water.
(ii) Load with 4 ml 2xdH_2O and measure flow times until two consecutive readings are comparable. (Ensure that water-bath is at 25 °C, at which temperature the flow time is 76-80 seconds.)
(iii) Load with buffer and repeat (ii).
(iv) Rinse viscometer with distilled water and acetone and store dry.
(v) Weigh clean and dry pycnometer.
(vi) Fill with double-distilled water and weigh.
(vii) Fill with buffer solution and weigh.
(viii) Rinse with distilled water and acetone and store dry.
(ix) Calculate viscosity of buffer at 25 °C using

$$\eta^{25}_{buff} = 0.8904 \times \frac{\text{weight(buffer)}}{\text{weight (water)}} \times \frac{\text{time(buffer)}}{\text{time (water)}}$$

where $\eta^{25}_{H2O} = 0.8904$.

IV. DISASSEMBLY AND CLEANING

1) Remove electrodes and store in KCl solution.

2) Remove plexiglass housings and rinse thoroughly with distilled water. Leave to dry. Complete disassembly is not normally required unless the sintered glass discs need replacing.

3) Cleaning of the electrophoresis chamber may be performed in situ:

   (a) Rinse with distilled water.

   (b) Fill with formaldehyde solution and leave for 15-20 minutes.

   (c) Rinse with 95% ethanol.

   (d) Rinse with ether.

   (e) Leave to dry.

   N.B. (i) Cleaning should be accomplished by the least drastic method possible to avoid destruction of the glass surfaces or the adsorption of extraneous materials, either of which can produce changes in the electro-osmotic flow of liquid across the surfaces.

   (ii) If the above cleaning procedure is not sufficient try 30% formic acid and/or 6% NaCl solution.

   (iii) If a detergent is used, the chamber must be thoroughly washed, first with a dilute solution of hydrochloric acid and then with large volumes of water to ensure complete removal of the detergent.

   (iv) Cleaning agents containing chromate ions are not recommended, since these ions, which are polyvalent and highly toxic, are very strongly adsorbed to glass and can only be removed by washing in flowing water for 24 hours.

   (f) The outer surfaces of the chamber will occasionally become dirty necessitating removal of the chamber and cleaning with tissue.

V. DATA ANALYSIS

Data are processed by a computer program originally written in FORTRAN by R.A. Gaines and converted to BASIC for use on the Departmental PDP 11/10 computer by L.D. Plank.

Use of the BASIC program CYTOLP:

1) Use disk labelled TODD.
2) The raw data are loaded into virtual file storage using the program CYTSTR. This will accommodate up to 250 sets of readings of depth, reticules traversed, and left and right traversal times.
3) Call up CYTOLP and run.

N.B. Additional features:

(i) Two histograms may be superimposed on the graphics terminal by using the program HISTOP.

(ii) A chi-squared analysis of the difference between two histograms may be accomplished using CHISQ. This program also has provision for performing a Student's t-test for the difference between two population means assuming the population variances are unknown and unequal.

(iii) To combine two virtual files and analyse as one file call up CYTOCOM.

TABLE I Typical Buffer Conductivities and Cytopherometer Operating Conditions at 25 °C.

BUFFER	IONIC STRENGTH	CONDUTIVITY mmho/cm	TYPICAL CURRENT mA	TYPICAL VOLTAGE V
D-1	0.015	0.8	0.85*	300
PBG-Sucrose	0.030	1.6	0.9	160
Saline -Bicarb.	0.145	13	8.0	180

*This is the lowest current achievable with the Zeiss power supply unless a bypass resistor is incorporated.

A small investment could save your valuable machine, time and MATERIAL

CAM-APPARATUS

13 MACFARLANE CLOSE, IMPINGTON, CAMBRIDGE. ENGLAND
TELEPHONE: HISTON (CODE: 022023) 2176
(REGD. ENGLAND 1691068)

MEHRISHI MK3 ELECTRODE CHAMBERS and Ag/AgCl/KCl ELECTRODES ASSEMBLIES SUITABLE FOR MOUNTING IMMEDIATELY, WITHOUT ANY MODIFICATIONS OR ANY ENGINEERING, ON AN EXISTING MACHINE - CELL ELECTROPHORESIS APPARATUS / CYTOPHEROMETER, EQUIPPED WITH AN ELECTROPHORESIS CHAMBER OF A CIRCULAR OR RECTANGULAR CROSS SECTION. [Prog.Biophys.Mol.Biol.,1972, 25:1-70,Pergamon].

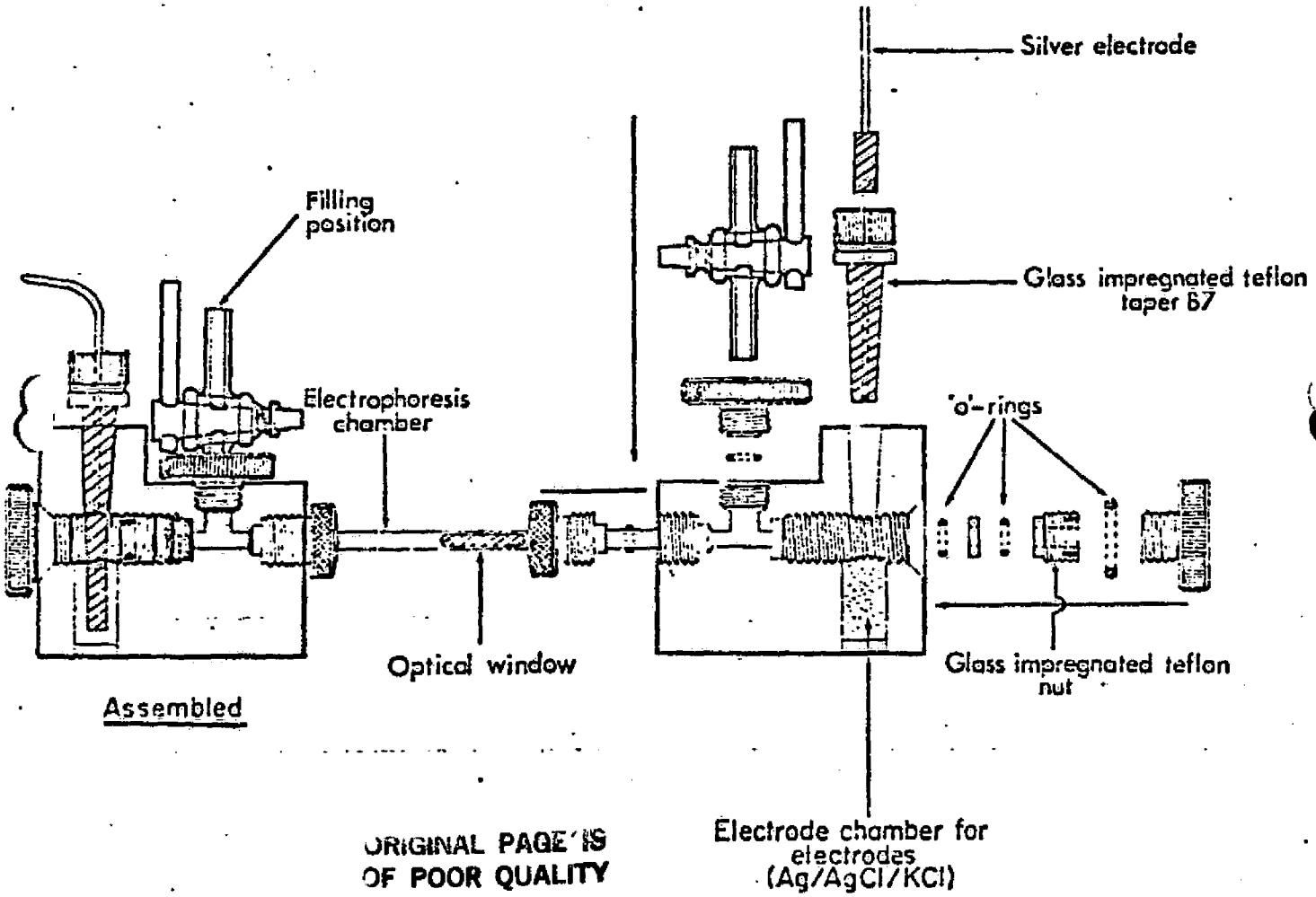

FIGURE 1

'Exploded' View for ease of ASSEMBLY

Banks: 1. Lloyds Bank Ltd., 36 Trinity Street, Cambridge, England. Account No. 00841977
2. Deutsche Bank AG, Schwanthalerstrasse 32, Munchen, Germany Kontonummer: 51161435
3. Barclays Bank S.A., 6 Rond-Point des Champs Elysées, Paris, 75008. Compte No.050775d67.
PARTNERS: DR. J. MEHRISHI, PhD (CANTAB), MRCPATH, FIBIOL., CCHEM., FRIC. MRS. M.A MEHRISHI.

CAM-APPARATUS

13 MACFARLANE CLOSE, IMPINGTON, CAMBRIDGE, ENGLAND

TELEPHONE: HISTON (CODE: 022023) 2176

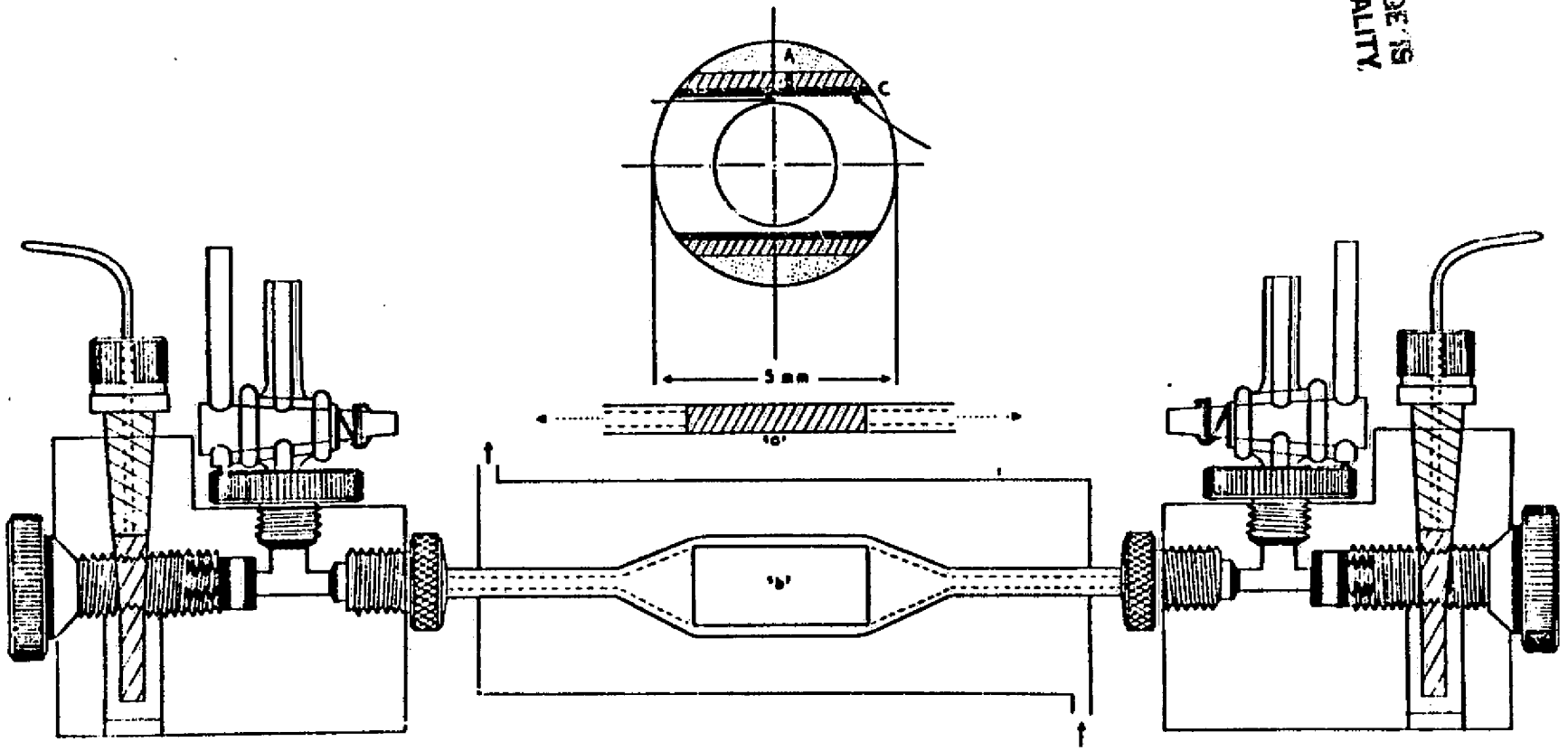

Microelectrophoresis Cell

(a) circular cross-section (vol: 0·8 ml)
(b) rectangular cross-section (vol: 1·5 ml)

Chapter 6.

Electrophoretic Mobility of Cells in a Vertical Ficoll Gradient.

ELECTROPHORETIC MOBILITY OF CELLS IN A VERTICAL FICOLL GRADIENT

Lindsay D. Plank, Paul Todd, M. Elaine Kunze, and Richard A. Gaines

It was found experimentally in early work that the upward migration of living cells and test particles under the influence of a constant electric field in a low-conductivity Ficoll gradient occurs at nearly constant velocity. In the course of migrating for 2 - 3 hr over a distance of 2 - 4 cm upward moving particles encounter changing density, viscosity, conductivity, and neutral-polymer concentration. All of these factors affect migration rate, but the most important are viscosity and neutral polymer concentration. Decreasing viscosity as the particles migrate upward has the effect of speeding them up; decreasing neutral-polymer (Ficoll) concentration, on the other hand, slows particle migration, since electrophoretic mobility increases approximately linearly with neutral-polymer concentration. Neutral polymers interact with the cell surface to effectively raise its zeta potential. An analytic function was developed from the known dependence of these physical variables on migration distance; it expresses migration velocity as an explicit function of position in the density gradient. It predicts an almost linear increase in velocity of about 12 - 16% (depending on cell type) over the working region of the gradient. It has been numerically integrated by computer and found to correctly predict cell migration distance-vs.-time curves without the use of any fitted parameters. These resulting migration curves follow the expected slowly-varying exponential form that closely resembles a straight line. The ability to determine standard electrophoretic mobilities from such curves depends on knowledge of the effect of Ficoll on the zeta potential of the cell type being separated.

Supported by National Cancer Institute Grant ROl-CA-24090.

RESULTS

The effect of varying Ficoll concentration on cell electrophoretic mobility (EPM) was determined by microelectrophoresis of glutaraldehyde-fixed rat and rabbit erythrocytes (RBC) in various concentration of Ficoll in "ceiling" buffer (for buffer compositions, see Chapter 12) at low ionic strength, $\Gamma/2 = 0.030$ M Figure 1 shows that anodic mobility increases linearly with Ficoll concentration, as predicted from the work of Brooks et. al. Thus the effective zeta potential of cells will decrease as cells migrate upward through a gradient of upward-decreasing Ficoll concentration.

This variable is included in the migration equation, in which migration velocity V (x) is implicityly dependent upon migration distance x:

$$V(X) = \frac{\mu(x)\,\eta(H_2O)\,I}{\eta(x)\,A\,K(x)} - \frac{2a^2 g\,[Po - \rho(x)]}{9\,\eta(x)} \qquad (1)$$

and the variables that depend on migration distance are:

$$\eta(x) = be^{ax} \qquad \text{viscosity} \qquad (2)$$

$$K(x) = K_1 + K_2x + K_3x^2 \qquad \text{conductivity} \qquad (3)$$

$$\rho(x) = r_1 + r_2x \qquad \text{density} \qquad (4)$$

$$\mu(x) = m_1 + m_2x \qquad \text{mobility (from Fig. 1).} \qquad (5)$$

By using these explicit functions and equation (1) it is possible to derive the time T required to migrate distance x:

$$T = \int_0^x \frac{dx}{v(x)} = \frac{Q(x)\,e^{ax}dx}{C(x)} \qquad (6)$$

in which Q(x) is a quadratic function of x, and C(x) is a cubic function of x, derived by combining coefficients from equations (3), (4), and (5). Equation (6) was integrated numerically by computer for various cases, and Figure 2 shows an example in which the upward migration of fixed rat RBC's was predicted using the data of Figure 1 and a 2-8% Ficoll gradient under the conditions specified in the diagram.

Below the break in the graph, migration is almost linear with time; actually, it is a slowly-rising exponential function (equation 6). Above the break the inverse dependence, Q(x)/C(x), becomes mildly apparent.

Figure 3 indicates that, in the real experimental situation, equation (6), the dashed lines, very closely predicts the upward electrophoretic migration of fixed rat and rabbit erythrocytes.

Once it was established that a single value of EPM could be used to successfully predict migration distance, equation (6) was applied to the prediction of the distribution on the density-gradient column of cells subjected to a specific electrophoresis procedure. The EPM distribution was determined for fixed rat RBC's by microelectrophoresis; this is presented in Figure 4, which predicts a mean EPM of 1.22 ± 0.06 μm-cm/V-sec at 4°C, the operating temperature of the density gradient. Each histogram subclass in Figure 4 was subjected to the calculation of migration distance using equation (6), and the resulting distributions of cells on the density gradient column were determined at various times. These are shown in Figure 5, which includes an experimental profile for comparison. The experimental data indicate that the cells did not migrate as far as predicted, and the coefficient of variation was greater, probably owing to cell band distortion that results from the cell collection procedure.

CONCLUSION

From simple physics and the known dependence of EPM on neutral polymer (Ficoll) concentration it is possible to predict the upward anodic electrophoretic migration of cells in a Ficoll density-gradient column. Predictions are consistent with experimental data, and both theoretical and experimental plots of migration distance vs. time are approximately linear. From these facts it is possible to characterize a cell population by its EPM found by density-gradient electrophoresis, and at 4°C with no viscosity correction, one can define Ficoll-column mobility as

$$\mu_F = \frac{x K A}{tI} \qquad (7)$$

where I=current, A=column cross-sectional area, K=conductivity, and x/t is a good approximation of v(x). The predicted distribution of cells on the column is narrower than that observed; this is probably due to the increase in apparent bandwidth that occurs during the collection of cells in fractions from the column.

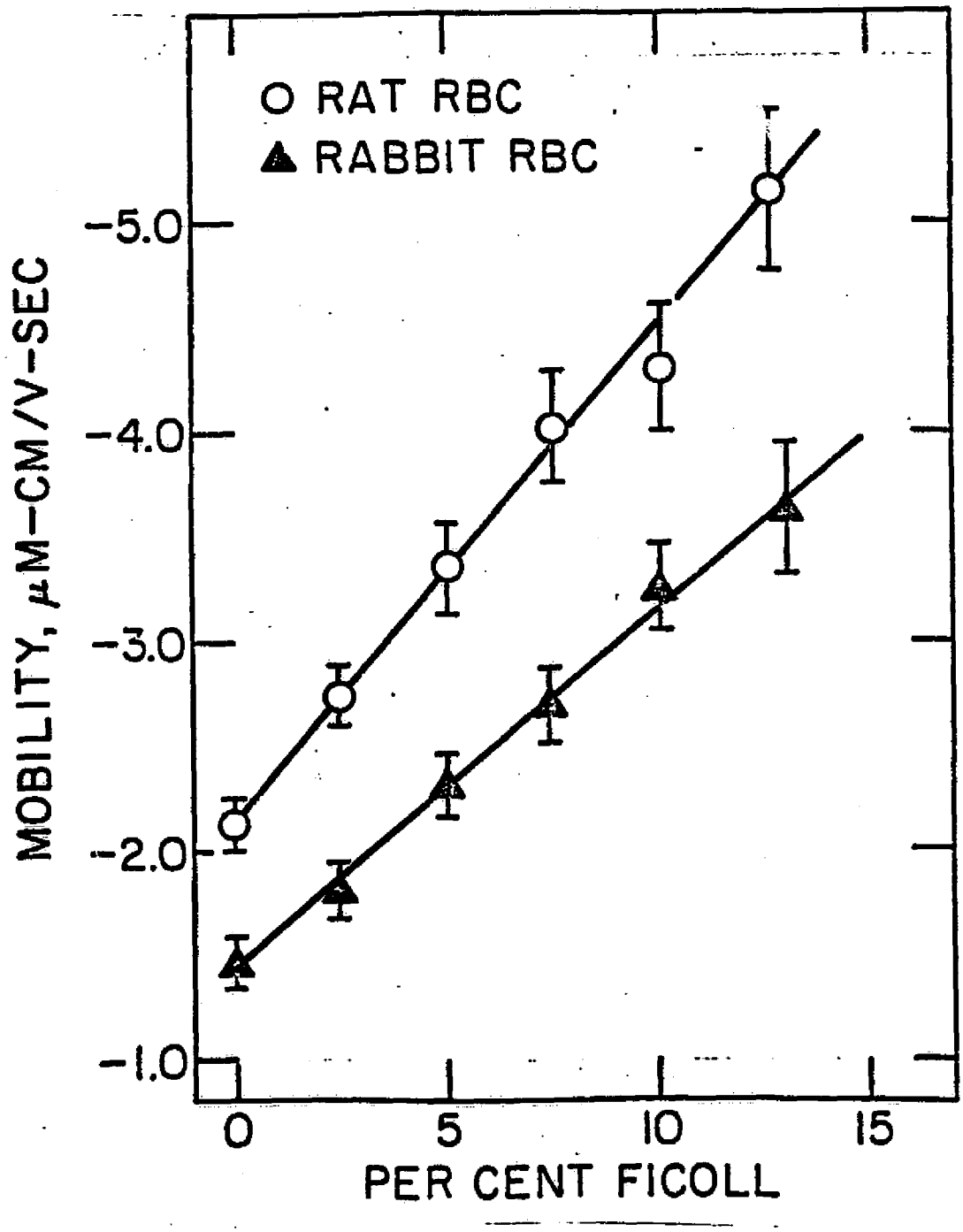

Figure 1. Dependence upon Ficoll concentration of the electrophoretic mobilities of fixed rat and rabbit erythrocytes.

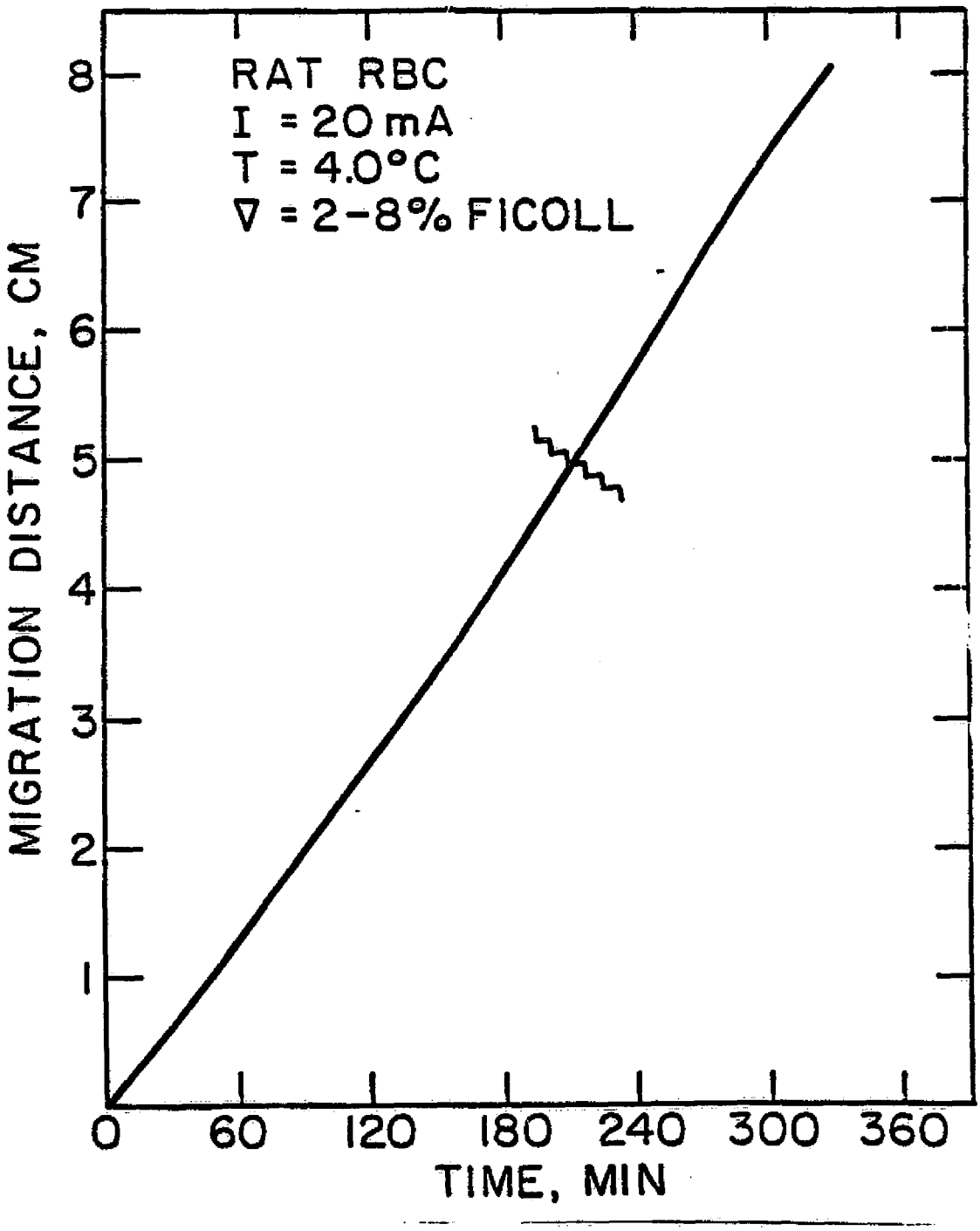

Figure 2. Predicted electrophoretic upward migration of fixed rat erythrocytes in a Ficoll gradient under the conditions indicated on the graph.

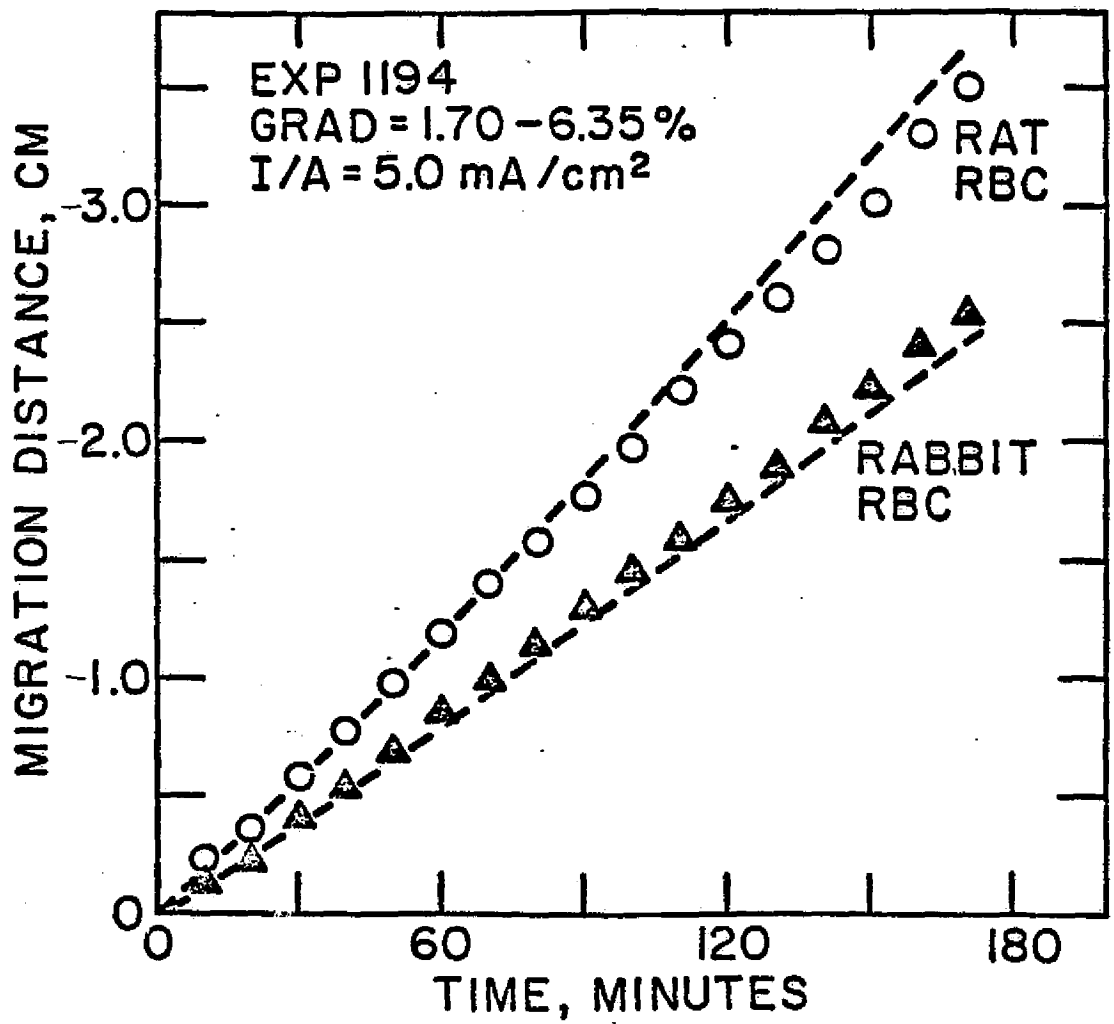

Figure 3. Comparison of predicted and experimental migration plots of fixed rat and rabbit erythrocytes subjected to upward electrophoresis in a Ficoll gradient under conditions indicated on the graph.

Figure 4. Electrophoretic mobility distribution of fixed rat erythrocytes in density-gradient electrophoresis buffer at 4°C and at 25°C. This distribution was used to produce the profile in Figure 5.

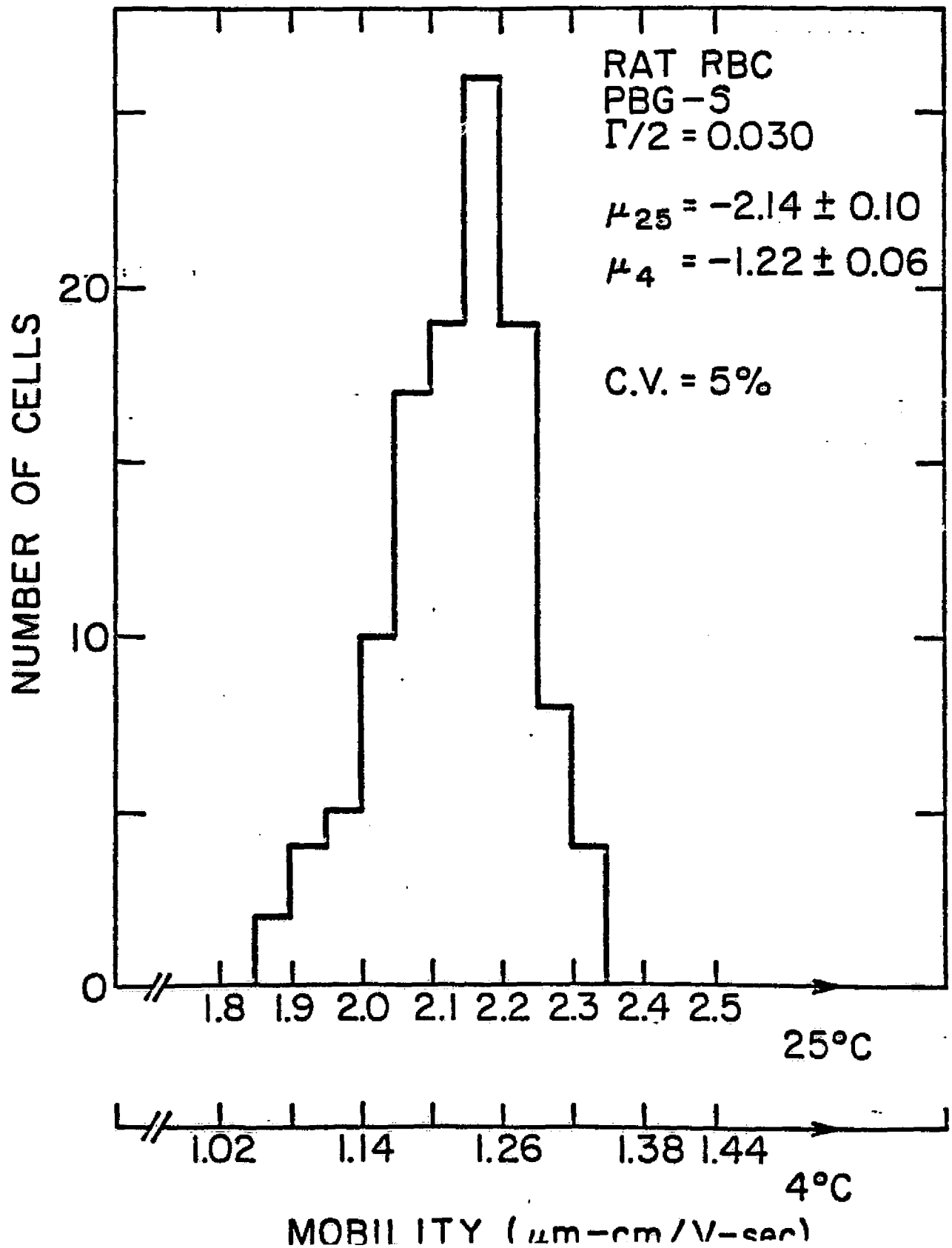

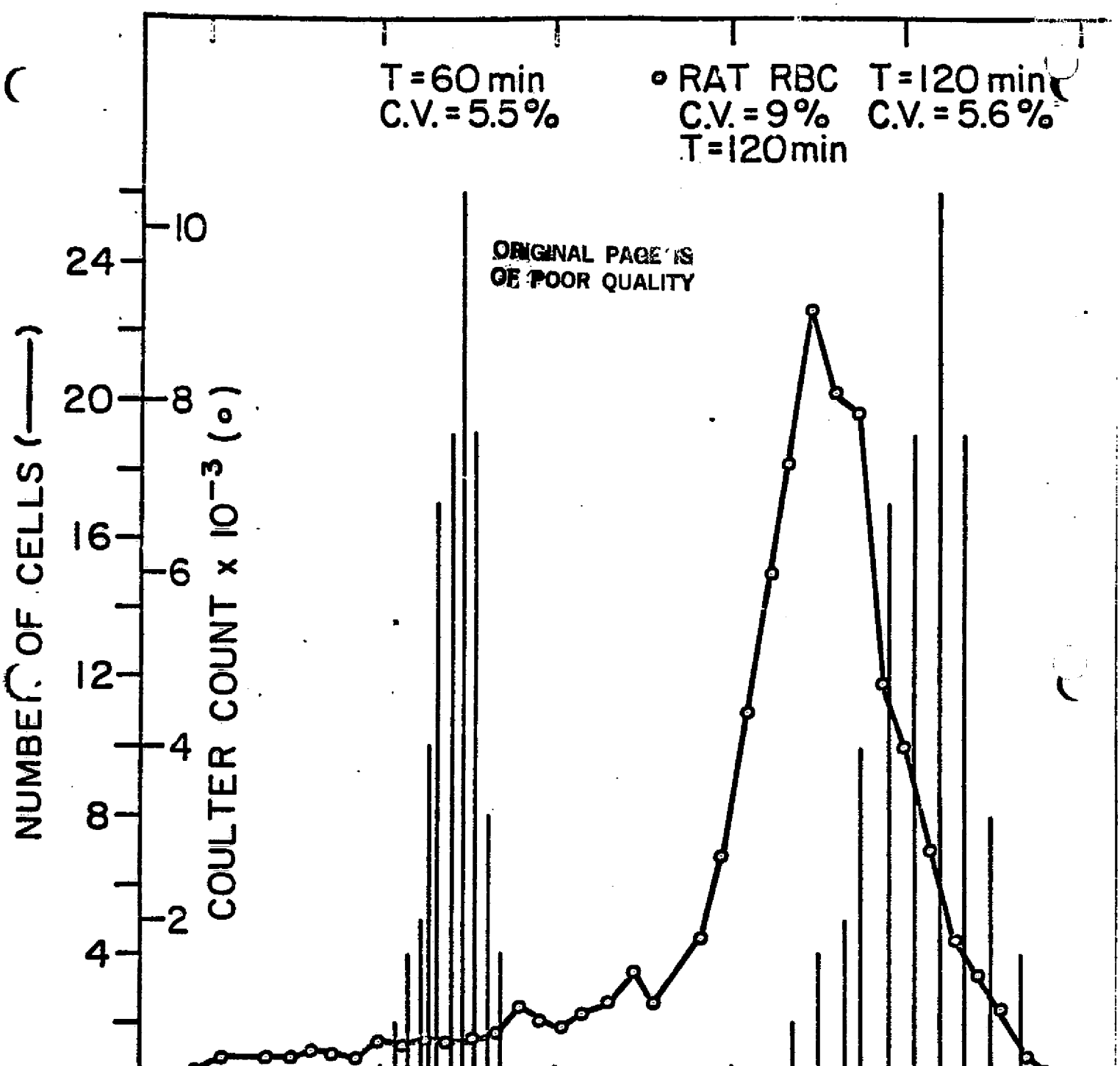

Figure 5. Predicted and observed distributions of fixed rat erythrocytes subjected to upward density gradient electrophoresis and collected in fractions by pumping the gradient out the top of the column. Vertical bars represent predictions on the basis of the distribution of Figure 4 and equation (6).

Chapter 7.

Preliminary Studies on Density Gradient Electrophoresis of Cells in a Reversible Gel.

Presented at American Electrophoresis Society Meeting 1984

DENSITY GRADIENT ELECTROPHORESIS OF CELLS IN A REVERSIBLE GEL

Lindsay D. Plank, M. Elaine Kunze, Richard A. Gaines, and Paul Todd

Althouse Laboratory, The Pennsylvania State University, University Park, Pennsylvania 16802

Density gradient electrophoresis permits the separation of cell types according to surface charge density with very high resolution. Any source of flow compromises the resolving power of density gradient electrophoresis. Although procedures have been devised to successfully counteract electroosmotic and convective flows, the final collection of separands requires that they be pumped out of the electrophoresis column. Experiments were therefore designed to test the hypothesis that this flow could also be eliminated by trapping the separated bands in a gel, from which they could subsequently be collected with high resolution by slicing thin bands from the cylindrical gel. Glutaraldehyde-fixed rat and rabbit erythrocytes were used as test particles in a phosphate-buffered isotonic Ficoll-sucrose density gradient in a 2.2 cm diameter, thermostated vertical glass column (Prep. Biochem. 3, 383, 1973). A special column design permitted passage of a plunger in at one end and the formed gel out at the other. Two types of agarose were used as gel polymers: Electrophoresis grade agarose (J. T. Baker Chemical Co.) at final concentrations of 0.1 to 0.25% and SeaPrep(TM) ultralow gelling agarose (Marine Colloids Div. FMC Corp.) at a final concentration of 1.5%. Electrophoretic saparability of the test particles and fluid stability were tested independently in the range of temperatures (32 - 55 C) at which the agaroses were liquid and found to be relatively unaffected. The experiments demonstrated that the higher temperature required and the presence of agarose compromised neither the stability of the density gradient nor the migration properties of the cells.

This research was supported by National Aeronautics and Space Administration Contract NAS9-15584.

DENSITY GRADIENT ELECTROPHORESIS OF CELLS IN REVERSIBLE AGAROSE GELS

M. E. Kunze, L. D. Plank, R. A. Gaines, and P. Todd

403 Althouse Laboratory
The Pennsylvania State University
University Park, Pennsylvania 16902

INTRODUCTION

Two of the factors that affect achievable resolution in the separation of cells by density-gradient electrophoresis are related to the procedure of obtaining cells after they have been separated. Disturbance of cell-containing zones as they are removed from the column and sedimentation of cells from one zone to another compromise the purity of fractions harvested by drop collection. The elimination of the time and motion involved in pumping or draining liquid from the column after cell separation should therefore improve electrophoretic resolution. Disturbing fractionation procedures could be avoided if the cells could be trapped in a gel matrix after separation and the gel sliced into bands for the collection of fractions without perturbing the cell-containing zones. Trapping separated cells in a gel would also have applications in remote operations such as column electrophoresis aboard the space shuttle and in semi-automatic devices that might be used in the future.

Experiments were therefore undertaken to assess the feasibility of using reversible gels in density-gradient electrophoresis in a vertical column. Fixed erythrocytes were used as test particles and, after considering several gel-forming polymers, agarose was chosen for testing as gel matrix material. The migration of test particles in the reversible gel and their ability to be trapped in position were tested. Fractionation procedures were not tested in this study.

MATERIALS AND METHODS

Cells. Rat and rabbit erythrocytes were diluted from fresh, unheparinized blood into 0.067 M Sorensen's buffer and washed and fixed in the same buffer in 2.5% glutaraldehyde for 10 min. After two more centrifugations in the same buffer the cells were stored in 0.145 M NaCl, 0.1 mM Na bicarbonate (1,2).

Gels. Two types of agarose were used.

The other, SeaPrep(TM) is an ultralow gelling temperature agarose (Marine Colloids Div., FMC Corp., Rockland, ME). Because this agarose remains fluid at room temperature, it is especially useful with live cells.

Electrophoresis. The column electrophoresis method of Boltz et al. was used (3,4,5) with some modifications. An all-glass column was constructed so that both ends could be opened completely for gel extrusion. This arrangement required additional adaptations as described in Figure 1. Polyacrylamide gel plugs formed in the side-arms and ends isolated the electrophoresis column from the electrodes. Two-hole rubber stoppers formed the ends of the columns. The gel plugs were formed with the column oriented so that gravity established the plug shapes and, when necessary, balloons were inflated in the electrode vessels to provide a surface against which gels could form. Buffer solutions and

electrode solutions were as previously described (4,5).

Procedure. In the case of regular agarose, it was dissolved in "C-1" buffer (5) normally used to for the density gradient, but Ficoll was omitted while sucrose was at isotonic concentration. The final agarose concentration was 0.2%, which is liquid above 50 C and solid below 30 C. Thus, the column temperature was held at 37 C with thermostat water at that temperature while the agarose solution was admitted at the bottom of the column, followed by the cell suspension (fixed rat and rabbit erythrocytes, 20 million/ml each). The temperature remained at 37 C until the end of cell separation, and the column was cooled with thermostat water at 4 C until the gel solidified for extrusion. In the case of Sea Prep agarose it was possible to use a procedure more compatible with cell viability. A normal Ficoll density gradient was used (3,5), and agarose was dissolved at 1.5% in all solutions at 37 C. The column was loaded from the bottom, first with "C-1" buffer, then with gradient, cells, and "floor"(5) all containing agarose at 37 C. The column temperature was then brought to 32 C where Sea Prep remains liquid, and upward cell electrophoresis was performed. The column temperature was slowly reduced to below 15 C, and the gel was extruded through the top of the column after removal of overlying materials.

RESULTS

The results of a cell separation with ordinary agarose at 37 C are illustrated in Figure 2, which consists of photographs taken every 30 min as upward cell migration proceded. Although a clear separation of the two types of erythrocytes (rat and rabbit) occurred, the temperature required was incompatible with cell viability. No density gradient was used, yet the fluid column remained stable at the operating temperature.

Before SeaPrep agarose was used in conjuntion with a Ficoll gradient preliminary evaluations of electrophoresis at the elevated temperature were made, as it is normal to operate the column at 4 C with this density gradient. The shallow density gradient remained stable through a three-hour test at 32 C, as indicated by Figure 3. Over a similar period of time the electrophoretic migration of a zone of fixed rat erythrocytes was normal, as indicated in Figure 4. It was found possible to shift, during a successful separation of rat and rabbit erythrocytes, from 10 C to 32 C without compromising the migration pattern of the cells (Figure 5). Thus the density gradient and electrophoretic pattern in the column were found to be stable through a wide temperature range.

The migration of rat erythrocytes was examined in the 1.5% SeaPrep Ficoll gradient column and found to be normal, as can be seen ifn Figure 6. The migration was linear, as predicted (7), but the band was broadened, possibly due to the time allowed for temperature equilibration before applying current. The column was cooled slowly to 10 C and extruded in a 4 C coldroom. It was found that cooling too rapidly after the completion of electrophoresis can lead to convection that compromises band sharpness.

DISCUSSION

The reversible gel procedure is, in principal, usable for density-gradient cell separation. To this point it has not been proven to improve resolution of separation, but it has the potential of providing a harvesting mechanism where

drop collection is not feasible, such as in zero-g column electrophoresis or in the separation of cells containing a very dense subpopulation that sediments during harvesting. A reversible gel density gradient could also be used for the preparation of gradients for transportation or sale where gradient forming equipment is unavailable or undesirable. The use of this technique, if suitable temperature control had been available, aboard Shuttle flight STS-3 could have averted the loss of ~~recovered~~ cells through loss of freezing capacity after recovery of the frozen, separated cell samples (8).

REFERENCES

1. T. S. Tenforde. Microelectrophoretic Studies on the surface chemistry of the red blood cell. Adv. Biol. Med. Phys. 13, 43 (1972).

2. R. C. Boltz, Jr., P. Todd, R. A. Gaines, R. P. Milito, J. J. Docherty, C. J. Thompson, M. F. D. Notter, L. S. Richardson, and R. Mortel. Cell electrophoresis directed toward clinical cytodiagnosis. J. Histochem. Cytochem. 24,16-23 (1976).

3. R. C. Boltz, Jr., P Todd, M. J. Streibel, and M. K. Louie. Preparative electrophoresis of living mammalian cells in a stationary Ficoll gradient. Prep. Biochem. 3, 383 (1973).

4. P. Todd, W. C. Hymer, L. D. Plank, G. M. Marks, M. E. Kunze, V. Giranda, and J. N. Mehrishi. Separation of functioning mammalian cells by density-gradient electrophoresis. In Electrophoresis '81, Ed. R. C. Allen and P. Arnaud, W. DeGruyter Co., Berlin (1981) pp. 371-382.

5. R. C. Boltz, Jr. and P. Todd. Density gradient electrophoresis of cells in a vertical column. In Electrokinetic Separation Methods. Ed. P. G. Righetti, C. J. van Oss, and J. W. Vanderhoff. Elsevier/North-Holland, Amsterdam (1979), pp. 229-250.

6. R. A. Gaines. Physical evaluation of density gradient electrophoresis of cells. Thesis, The Pennsylvania State University (1981)

7. L. D. Plank, M. E. Kunze, and P. Todd. Electrophoretic mobility of cells in a vertical Ficoll gradient. Electrophoresis (to be submitted).

8. D. R. Morrison and M. L. Lewis. Electrophoresis tests on STS-3 and ground control experiments: A basis for future biological sample selections. In Proc. 33rd Intern. Astronautical Fed. Congress, IAF Paper No. 82-152, ~~in press~~ (1983)

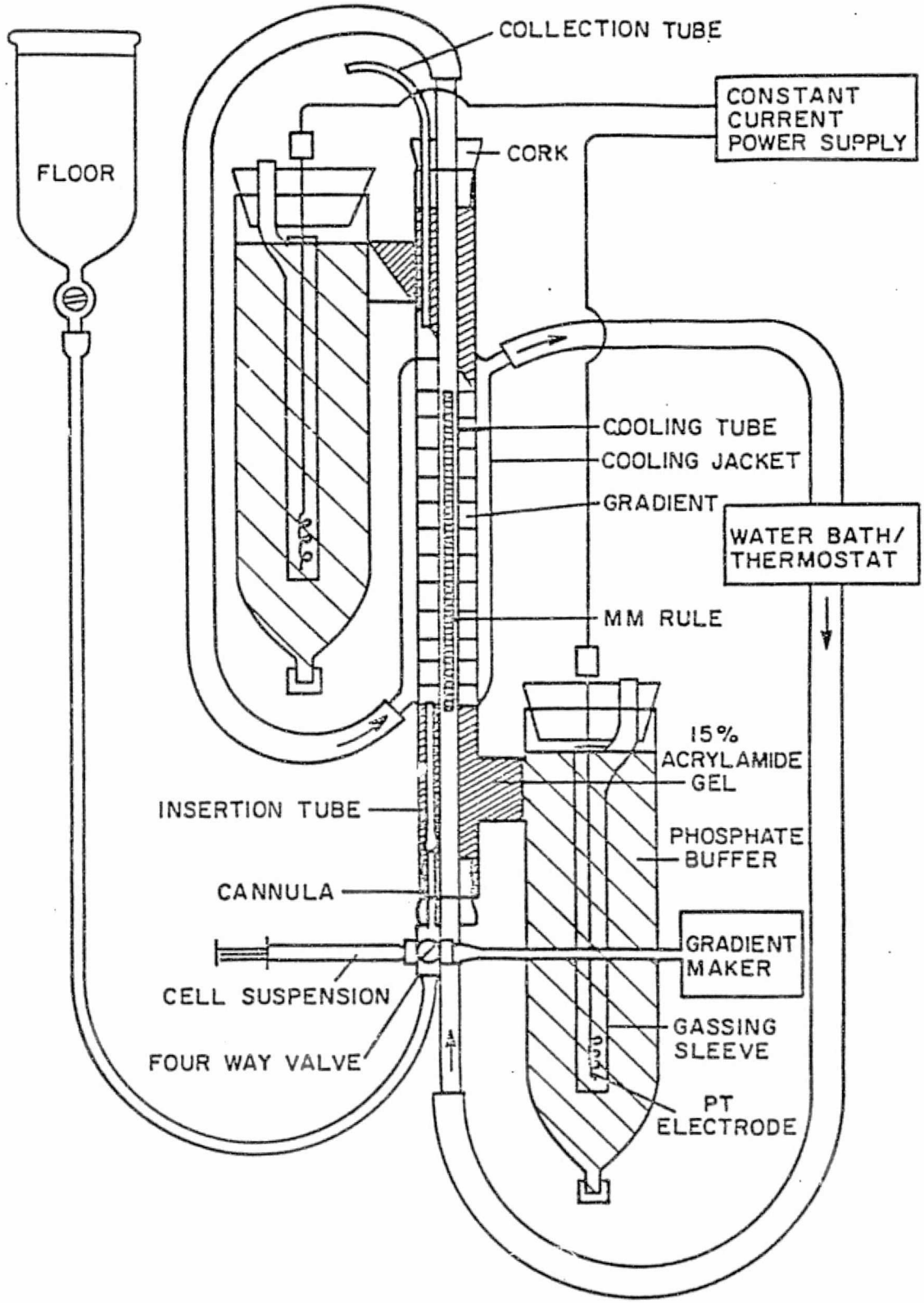

Figure 1. All-glass electrophoresis column for the separation of cells in reversible gels.

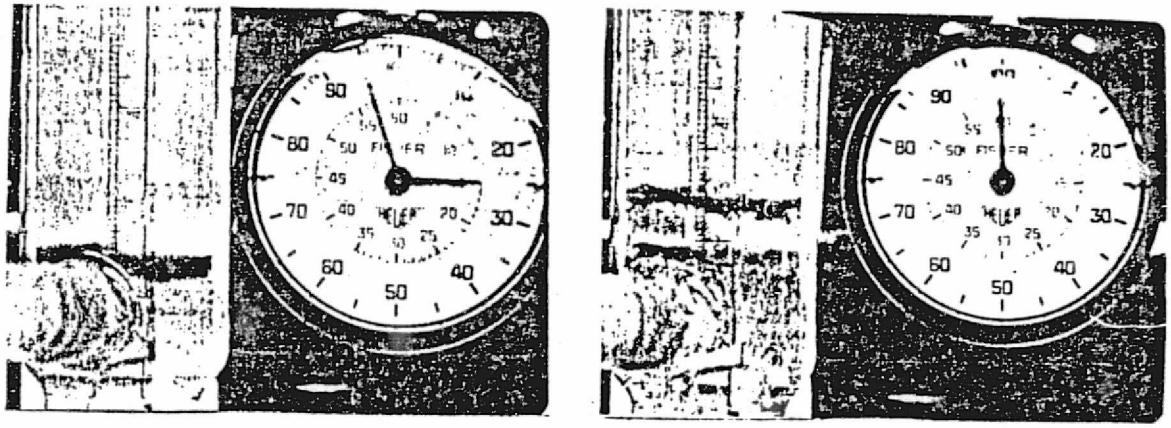

Figure 2. Photographs of the progression of separation of fixed rat and rabbit erythrocytes during upward electrophoresis in 0.2% agarose.

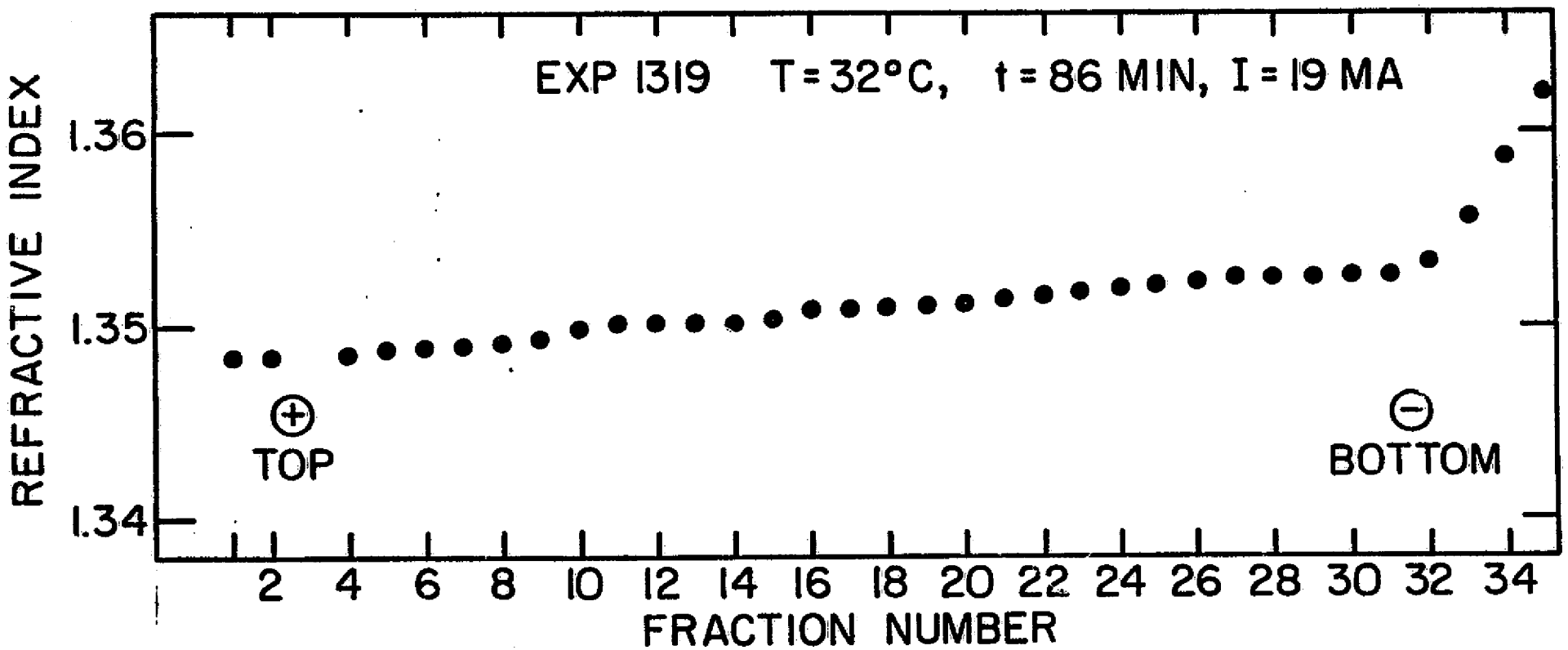

Figure 3. Refractive index profile of a Ficoll density gradient after 86 min of operation of the column at full current at 32 C, indicating that gradient was stable throughout this operating regimen.

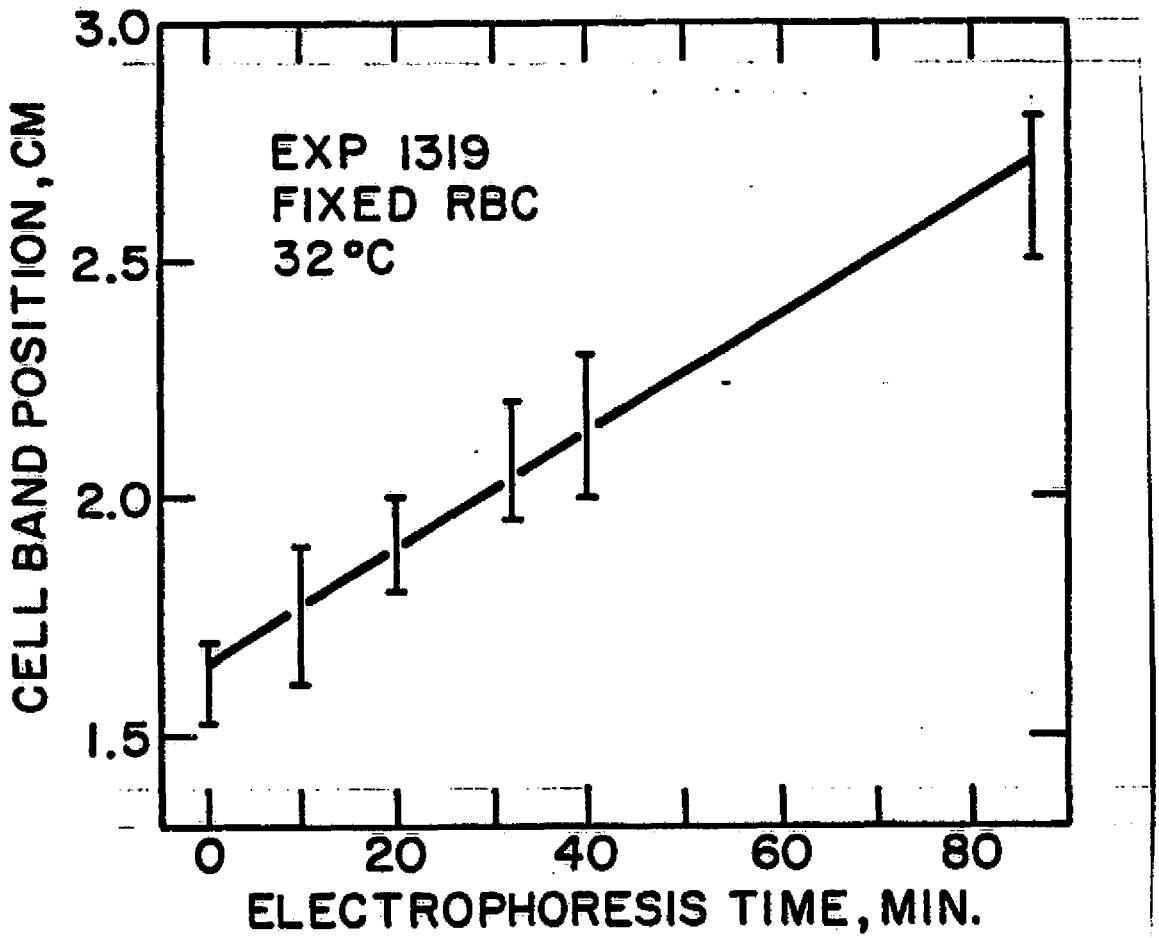

Figure 4. Linear migration of fixed rat erythrocytes in a Ficoll gradient at 32 C, indicating normal migration behavior of cells on the column operated at full current at the higher temperature.

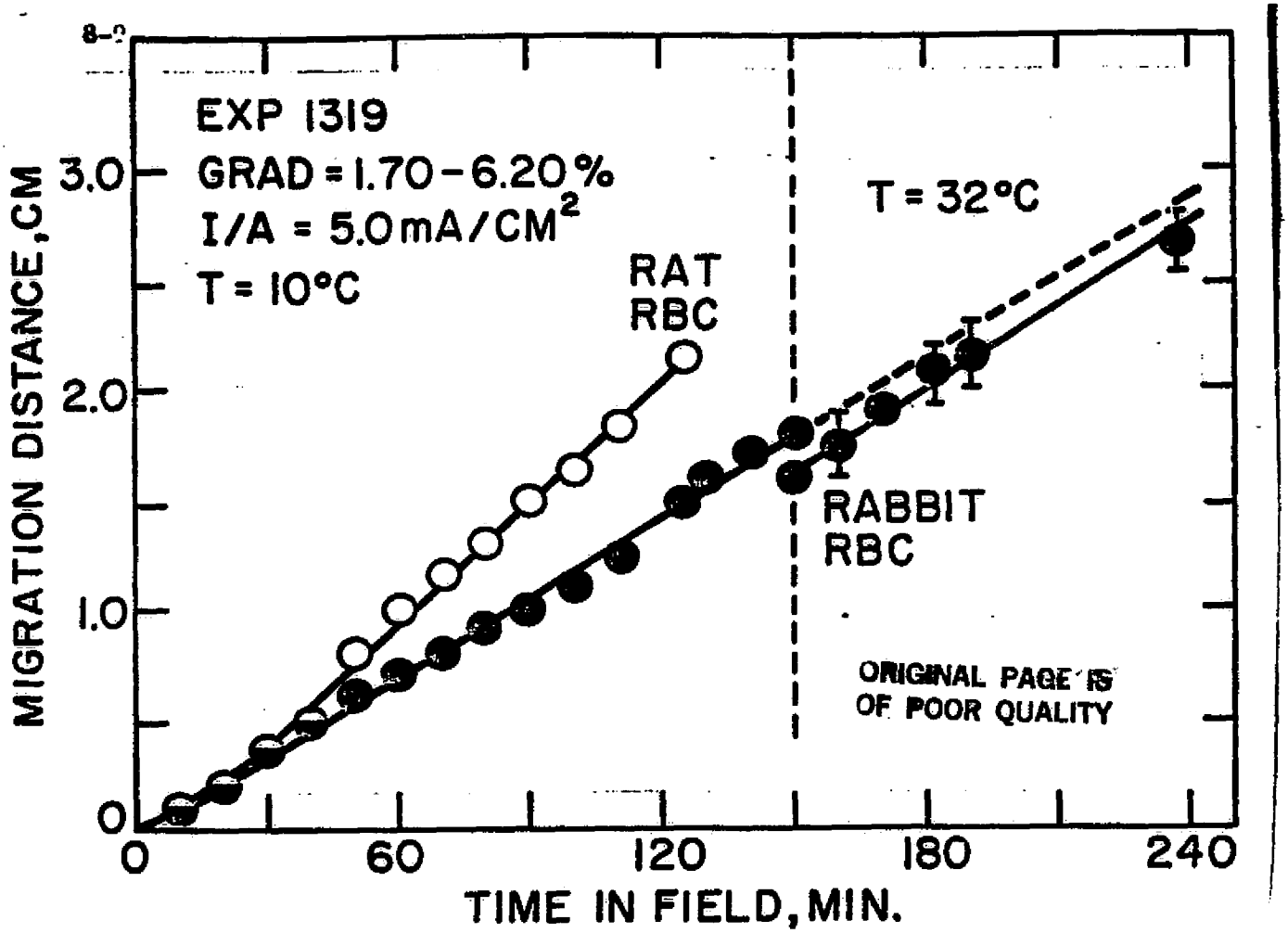

Figure 5. Linear migration of rat and rabbit erythrocytes through a Ficoll gradient at 10 C and continued linear migration of rabbit erythrocytes through an upward temperature shift to 32 C. The cell band position moved downward due to sedimentation while the current was off during effecting of the temperature shift.

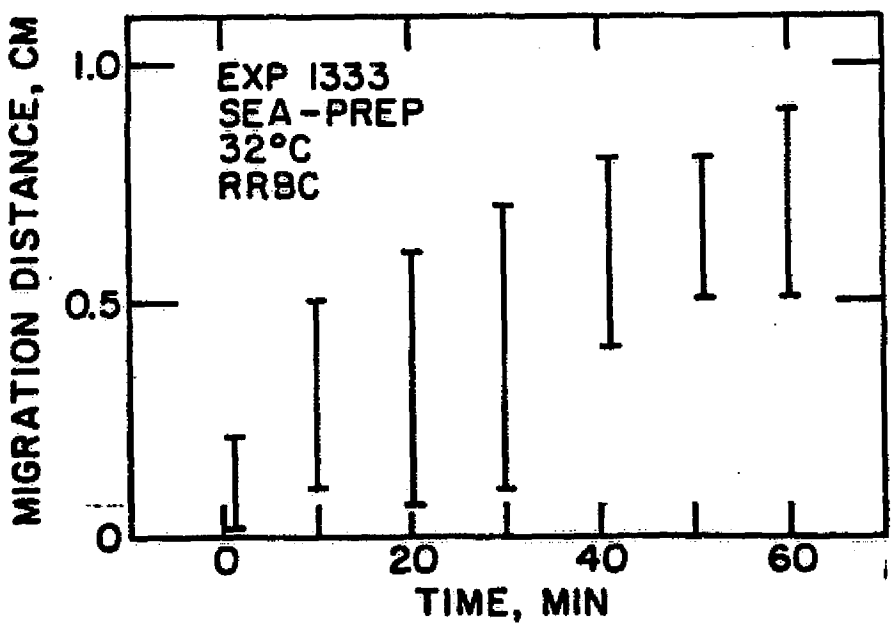

Figure 6 Linear migration of fixed rat erythrocytes through a Ficoll gradient at 32 C with 1.5% SeaPrep(TM) agarose dissolved in the buffers. The column was solidified after migration had finished..

Chapter 8.

Free Zone Electrophoresis: Study of Erythrocyte and Cultured-Cell Interactions.

FREE-ZONE ELECTROPHORESIS OF ANIMAL CELLS I. EXPERIMENTS ON CELL-CELL INTERACTIONS

Paul Todd and Stellan Hjertén
Institute of Biochemistry, Biomedical Center, University of Uppsala, Box 576, S-751 23 Uppsala, Sweden

Summary

Free-zone electrophoresis is the horizontal electrophoresis of materials introduced into a rotating quartz tube as dense zones. The progress of electrophoretically migrating zones is monitored by scanning the tube with an ultraviolet photometer. The absence of fluid flows in the direction of migration permits direct measurement of electrophoretic velocities of any material (small molecules, macromolecules, particles, cells). As sedimentation is also orthogonal to electrokinetic motion, effects of particle-particle interaction on electrophoretic mobility can be studied by free-zone electrophoresis. Fixed erythrocytes at high concentrations, mixtures of fixed erythrocytes from different animal species, and mixtures of cultured human cells were studied in low ionic strength buffers. The electrophoretic velocity of fixed erythrocytes was not altered by increasing cell concentration or by the mixing of erythrocytes from different species. Concentrations up to 2 x 10^9 cells/ml were used. When zones containing cultured human glial cells and neuroblastoma cells were permitted to interact during electrophoresis, altered migration patterns occurred. As in the case of molecule-molecule interactions previously studied by free-zone electrophoresis, cell-cell interactions appear to depend upon cell type.

Introduction

Free-zone electrophoresis (FZE) in a rotating tube (1) has been applied to the study of proteins (2) and cells (3) in buffers of widely varying composition. The method has been applied also to the study of the interaction of samples in two zones when the zones electrophoretically collide with one another (1-4). Any subsequent mobility changes are attributable to the occurrence of a chemical reaction during collision.

The interaction of animal cells during electrophoresis in free fluid is difficult to evaluate due to droplet, or zone, sedimentation at high cell concentrations (5). But Omenyi and Snyder (6) have presented data that erythrocytes might interact at high concentration, and evidence concerning cell-cell interaction was sought in experiments with human and rabbit erythrocyte mixtures in the microgravity environment, where zone sedimentation does not occur (7). The results of microgravity experiments, although consistent with a lack of cell-cell interaction, were not firm and unambiguous; the optical images available for analysis did not show two clearly separated peaks (7-9). Previous studies using FZE (3) indicated a lack of aggregation of fresh erythrocytes under all conditions of ionic strength and buffer composition tested; however, microorganisms aggregated under a wide variety of buffer conditions at high concentration and high field strength. This aggregation occurred abruptly after prolonged exposure (ca. 30 min.) to high fields.

Because zone sedimentation does not affect electrophoretic migration in FZE, and because this method also reveals interactions that affect electrophoretic migration, FZE was chosen as a means of exploring possible effects of animal cell interactions on electrophoretic mobility.

Materials and Methods

Cells. Human erythrocytes were obtained from a 47-year-old healthy male donor by venipuncture and immediately diluted into isotonic phosphate buffer containing 0.01% EDTA as anticoagulant. After three rinses in this buffer the cells were suspended in 2.5% paraformaldehyde in isotonic phosphate buffer at ambient temperature (19-24 °C) for 2 weeks. Rabbit erythrocytes were obtained from a 6-month-old healthy New Zealand white rabbit by ear venipuncture and treated subsequently in the same manner as the human RBC's (7). The cells were washed 3 times in electrophoresis buffer "D-1" prior to experiments. Two strains of cultured human cells were used: Normal human cells of glial origin, "787CG" and neuroblastoma cells "SKNSH-5YSY", kindly supplied by Dr. S. Pahlmann of the Wallenberg Laboratory, Uppsala. They were suspended from monolayer culture by rinsing 5 min in 0.02% EDTA in phos-phate-buffered isotonic saline (PBS) and incubating 5 min at 37°C in 0.25% trypsin (1-300) in PBS. The action of trypsin was stopped by the addition of complete culture medium (Eagle's Minimum Essential Medium) containing 10% fetal bovine serum. Cells were removed from medium by centrifugation and suspended in buffer C-1 with 3.4% Ficoll (6.2% sucrose) to discourage sedimentation and aggregation.

Buffers. The blood-collection buffer and the cell-fixation buffer are described in Table 1, which lists the concentrations of the ingredients. The electrophoresis buffer used for RBC electrophoresis, designated "D-1", and the buffer "C-1" used for cultured human cell electrophoresis are also described in Table 1.

Electrophoresis. The free-zone electrophoresis apparatus (1), consists of a thermostated rotating horizontal tube coated with methylcellulose to prevent electroosmotic

backflow. The RBC experiments reported here were performed with the following parameters: temperature, 14°C; tube rotation speed, 70 rpm; tube diameter, 3.0 mm; conductivity of buffer, 0.90 mmho/cm; applied current, 0.80 mA; optical monitoring wavelength, 320 nm or 290/320 nm ratio; column scanning interval, 5 min; column scanning time, 1 min (with field turned off). Cells were introduced in two starting bands at the "origin" of the tube 2 cm apart at concentrations of 2 x 10^9 cells/ml. The cultured human cell experiments were performed under the following conditions: temperature 3°C; conductivity of buffer, 1.5 mmho/cm; applied current, 4.0 mA; potential, 1450 V. Other conditions were the same as for RBC experiments. Optical scans were recorded, usually at 5 min intervals, on paper with an analog strip-chart recorder.

Table 1. Composition of buffers used in human and rabbit erythrocyte collection and fixation and in the free-zone electrophoresis tube and electrodes (concentrations are mM or %)

COMPONENT	BLOOD COLLECTION	RBC FIX	TUBE D-1	ELECTRODE D-1	ELECTRODE C-1
Na_2HPO_4		53.7	1.76	1.76	8.10
NaH_2PO_4		13.5			
KH_2PO_4			0.367	0.367	1.47
NaCl	145.0	150.0	6.42	6.42	
KCl			0.889	0.889	2.65
$MgCl_2$					0.48
Na_2EDTA	4.0		0.336		
Glucose			222.0		55.5
Sucrose					199.0
Dimethylso			5%		
Paraformaldehyde		1.5%			
Conductivity (mmho/cm)			0.9		1.5
Ionic Strength (g-ions/litre)			0.015		0.030

Fractions of electrophoretically-separated human cells were collected from the tube with the long, thin needle normally used for inserting samples zones. Each fraction corresponded to a 2 cm interval along the tube. Each collected fraction was added directly to 5 ml of complete culture medium in a 60 mm plastic culture dish. The number of each cell type per microscope field was counted in ten fields by phase contrast microscopy 28 hours later. The two cell types were distinguishable in phase contrast at 160x total magnification. Figure 1 indicates the principle of multiple sample zone insertion, and figure 2 is a photograph of two erythrocyte zones inserted at different locations in the tube.

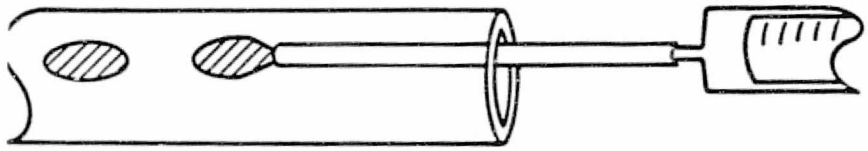

Figure 1. The insertion of multiple zones into the rotating free-zone electrophoresis tube.

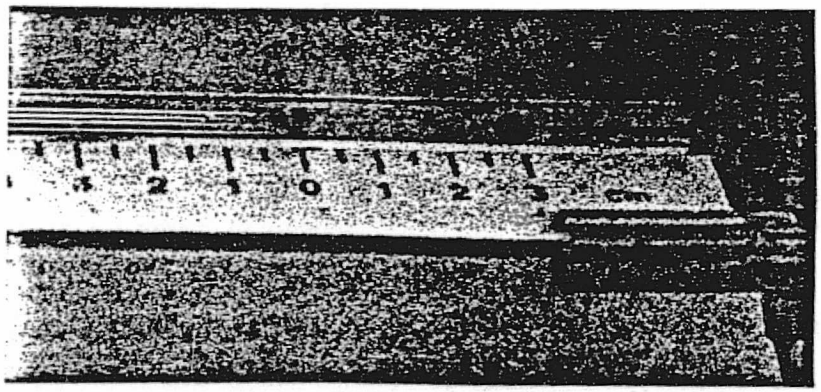

Figure 2. Photograph of 2 zones of erythrocytes inserted into the rotating free-zone electrophoresis tube.

Results

Cell-cell interaction was not found to be a significant factor in the electrophoresis of fixed erythrocytes. Figure 3 is a series of optical scans of the free-zone electrophoresis tube at various intervals after the initiation of electrophoretic migration of two cell zones initially 2 cm apart. The human cell zone ("H") migrated through the rabbit cell zone ("R") without any modification of its velocity or zone shape.

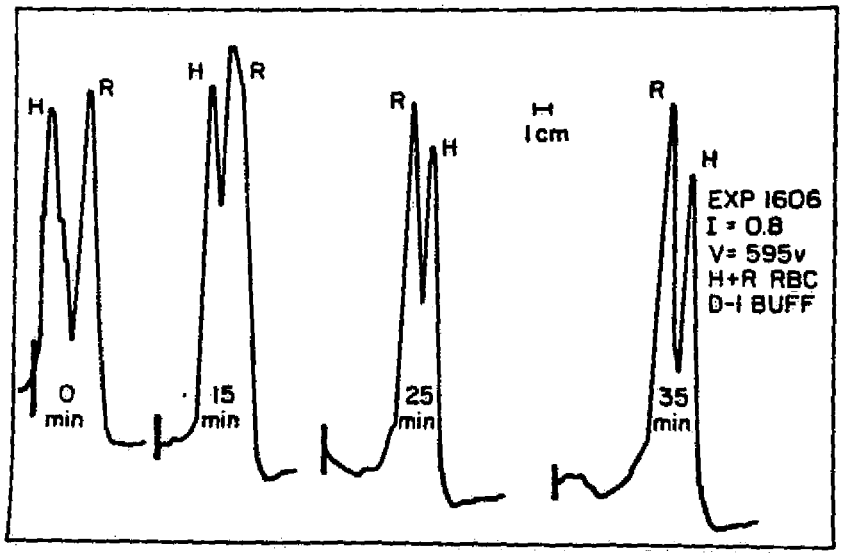

Figure 3. Optical scans of migrating zones of fixed human ("H") erythrocytes and fixed rabbit ("R") erythrocytes. Each zone contained 2 x 10^9 cells.

Cell-cell interaction was found to occur in living, non-erythroid cells. Figure 4, lower panel, is a graph of the migration of a rapidly moving zone of cultured glial cells through a lower-mobility zone of cultured neuroblastoma cells. These cells interacted when the zones collided, and the aggregates that formed were visible so their motion in

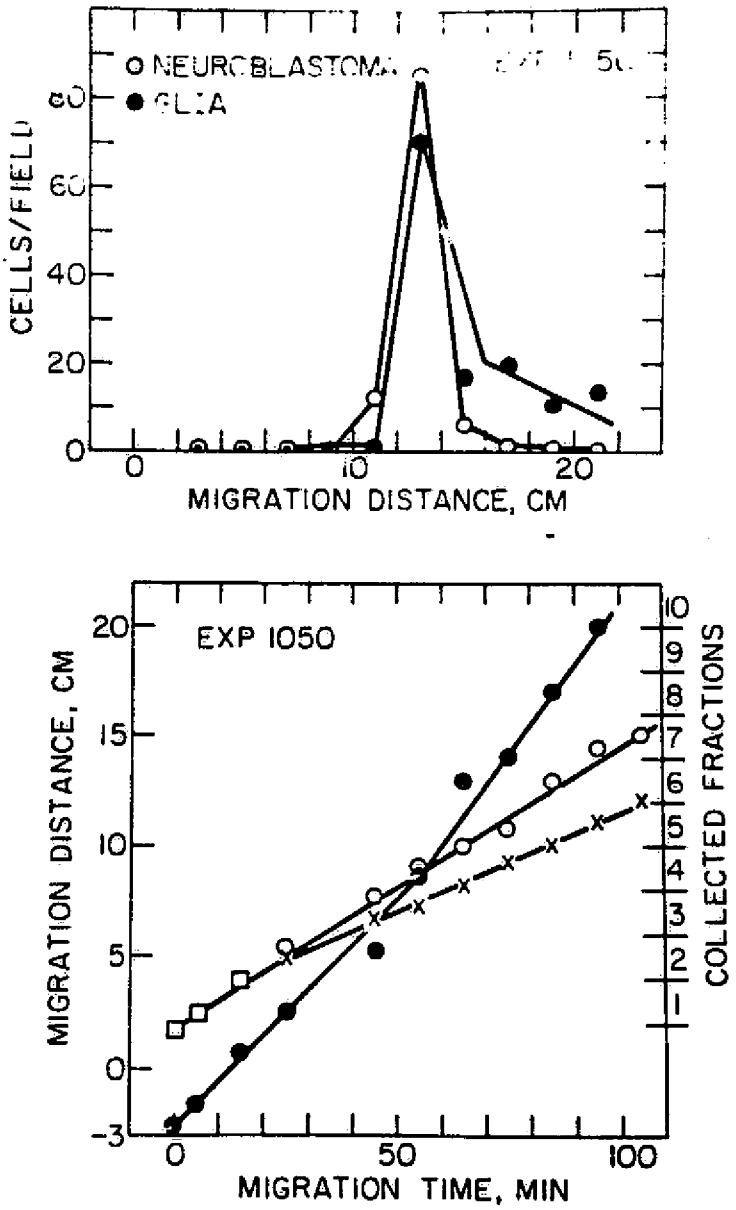

Figure 4. Electrophoretic migration profile (top) and distance migrated vs time (bottom) of human neuroblastoma (circles) and glial (dots) cells inserted as zones initially separated by 4 cm. The glial cell zone (1.4×10^3 cells) with a higher mobility, collided with the neuroblastoma cell zone (1.3×10^4 cells) after 30-50 min of migration, during which aggregates formed and migrated more slowly (indicated by x's). The two individual cell types continued to migrate with their original mobilities. The aggregates that formed during collision contained both cell types as indicated by their simultaneous presence in fraction 6 in the top figure, where the glial cell count has been multiplied by 5.

the field could be followed. Their mobility was lower than that of the individual cell types. After the field was switched off, and the cells were collected from the tube in 2 cm increments, most of the cells of both types appeared in the fraction that contained the aggregates.

Discussion

This study has confirmed previous findins (3) that erythrocytes do not interact with one another in a way that affects electrophoretic mobility and has extended these findings to very high cell concentrations, mixtures of cells from different species, and conditions encountered in preparative cell electrophoresis. On the other hand, living animal cells do interact, consistent with earlier observations involving microbial cells and leukocytes (3,4).

Acknowledgements

We thank Irja Johansson and Karin Elenbring for superb technical assistance. This research was supported by the International Union Against Cancer (UICC) through a Yamagiwa-Yoshida Visiting Cancer Research Fellowship and by the Universities Space Research Association (USRA) through a Visiting Scientist Grant.

References

1. Hjerten, S.: Free Zone Electrophoresis. Almqvist and Wiksells Bktr., Uppsala, 1967.

2. Karlsson, E., Eaker, D. L., and Porath, J.: Biochim. Biophys. Acta 127, 505 (1966).

3. Hjerten, S.: In Cell Separation Methods (Ed. H. Bloemendal) Elsevier/North-Holland Biomedical Press, Amsterdam, 1977, pp. 119-128.

4. Agarwal, K. N. and Hjerten, S.: Acta Endocrinol., Suppl. 93, 53 (1964).

5. Boltz, R. C., Jr., and Todd, P.: Electrokinetic Separation Methods (Eds. P. G. Righetti, C. J. van Oss, and . Vanderhoff) Elsevier/North-Holland Biomedical Press, Amsterdam, 1978, pp. 229-250.

6. Omenyi, S. N., Snyder, R. S., Absolom, D. T., Neumann, A. W., and van Oss, C. J.: J. Colloid Interface Sci. 81, 420-409 (1981).

7. Snyder, R. S., Rhodes, P. H., Herren, B. J., Miller, T. Y., Seaman, G. V. F., Todd, P., Kunze, M. E., and Sarnoff, B. E.: Electrophoresis (submitted 1984).

8. Sarnoff, B. E., Kunze, M. E., and Todd, P.: Adv. Astronaut. Sci. 53, 139-148 (1983).

9. Todd, P.: In Cell Electrophoresis '84 (Eds. W. Schutt, V. Thomanek, E. Knippel, and J. Richly), W. deGruyter, Berlin, 1985.

REPRINTED FROM
FEDERATION PROCEEDINGS
VOL. 39, NO. 6, MAY 1980
PRINTED IN THE U.S.A.

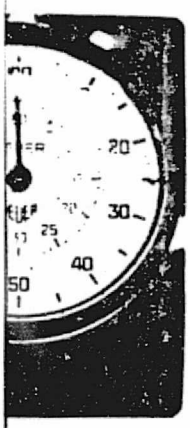

Figure 2. ...ed rat and rabbit erythrocytes

FREE-ZONE ELECTROPHOESIS OF ANIMAL CELLS. Paul Todd and Stellan Hjertén*. Institute of Biochemistry, The Biomedical Centre, University of Uppsala, S75 123 Uppsala, Sweden.

Free-zone electrophoresis consists of horizontal electrophoresis of samples applied in a small liquid zone in a horizontal capillary tube rotating at 60 rpm. The rotation and narrowness of the tube prevent purterbations due to sedimentation and convection from affecting motion in the direction of the applied electric field. Ultraviolet absorption scanning is used to determine the location of sample materials in the tube. This method has been used to determine mobilities of macromolecules and bacterial cells; experiments were therefore undertaken to test it in analytical and preparative animal cell electrophoresis. Fixed erythrocytes from rat, rabbit, and chicken and cultured living human cells were used as test particles. Cells were electrophoresed in a Ficoll-containing medium having conductivity of 0.5 mmhos/cm; field strengths used were around 100 V/cm. Migration rates were around 20 cm/h, and cells differing in mobility by 20% were separated by 4 cm. True mobility distributions of fixed test cells were determined, and coefficients of variation were around 4%. Separated cells were removed by syringe, and fractions 86-99% pure were obtained. The maximum separated sample size was 3×10^7 cells, and viable cell fractions were obtained when living cultured cells were used. Free-zone electrophoresis is a very effective analytical method for animal cells and is a useful preparative tool in certain applications. (Supported in part by a Yamagiwa-Yoshida Memorial International Cancer Study Grant).

PART III.

CELL CULTURE TECHNOLOGY

Chapter 9.

The Use of Econazole for the Prevention of Fungal Contamination.

9-1

IN VITRO Vol. 19, No. 3 (Part I), March 1983

AN EVALUATION OF ECONAZOLE, AN ANTIFUNGAL AGENT, FOR USE IN QUANTITATIVE CELL CULTURE EXPERIMENTS

M. ELAINE KUNZE[1] AND PAUL TODD

Molecular and Cell Biology Program, The Pennsylvania State University, 403 Althouse Laboratory, University Park, Pennsylvania 16802

(Received November 4, 1982; accepted December 15, 1982)

SUMMARY

Econazole, an imidazole derivative with high antifungal activity, was tested for cytotoxicity using five sensitive tests of human cell function in vitro: colony forming efficiency, growth rate, cell cycle distribution of a permanent epithelioid cell line (T-1E), and attachment efficiency and urokinase production by early passage human embryonic kidney cells. None of these endpoints was detectably affected by 1 μg/ml Econazole in serum containing medium. At 3 μg/ml, Econazole reduced slightly the growth rate of T-1E cells but did not detectably affect the other end points.

Key words: Econazole; antifungal agents; human kidney cells; antimycotics; toxicity of antimycotic.

INTRODUCTION

Wyler et al. (1) announced that Econazole (1-[2, 4-dichloro-β- (*p*-chlorobenzyloxy)-phenetyl]-imidazole) is an efficient antifungal agent that is not toxic to mammalian cells in culture. The quantitative toxicological tests used were the ability of cells to replicate virus, rate of DNA synthesis, and rates of RNA and protein synthesis. It was concluded that 1 μg/ml could be used safely and, on the basis of these tests, would not be toxic to cells. Many applications of modern cell culture include the requirement that individual cells form colonies when plated at low density. This end point is one of the most sensitive tests of viability because it requires that several cell functions remain unaffected. Furthermore, the rate at which single cells multiply to form colonies is a yet more sensitive test of cellular metabolic and molecular integrity. We therefore performed a series of experiments in which effects of Econazole on plating efficiency, cell multiplication rate, and progression through the cell cycle were evaluated.

Certain cell purification procedures subject cells to higher than normal risk of fungal contamination. A biochemical or secretory function is frequently demanded of cells after separation. The effect of Econazole on the ability of early passage cultured human embryonic kidney cells to attach and secrete urokinase into medium was therefore also evaluated.

MATERIALS AND METHODS

Cells chosen for the study of colony formation, growth rate, and cycle progression were human T-1 epithelioid cells. These aneuploid cells proliferated in cultures of normal human kidney (2) and have been used extensively in plating efficiency experiments (3,4). It is possible that they are an early isolate of HeLa cells (5). They were propagated in Eagle's minimum essential medium supplemented with 10% newborn or fetal bovine serum, 100 U/ml streptomycin, and 100 μg/ml penicillin, at 37° C in 3% CO_2, 100% relative humidity incubator. Plating efficiency and growth rate experiments were carried out in the usual way (4).

Human embryonic kidney cells were purchased as primary monolayer cultures from M. A. Bioproducts, Inc. (Walkersville, MD) and subcultured in Medium 199 with 10% newborn and 5% fetal bovine serum, 100 U/ml streptomycin, and 100 μg/ml penicillin. These cells were tested for their ability to produce urokinase in urokinase

[1]To whom reprint requests should be addressed.

TABLE 1

COMPOSITION OF UROKINASE PRODUCTION MEDIUM

Component	Grams/Liter	Milliosmolar	Milliliters of Stock
NaCl	5.21	179	
KCl	0.56	9	
$CaCl_2 \cdot 2H_2O$	0.37	7.5	
$MgSO_4 \cdot 7H_2O$	0.57	4.6	
$NaHCO_3$	0.80	21	
$NaH_2PO_4 \cdot H_2O$	0.23	3.3	
NaOH, 1 *N*			1.56
Glycine	6.0	80	
Glutamine	0.29	2	
Glucose	1.0	5.6	
Lactalbumin hydrolysate	5.0	42	
Human serum albumin	1.0		
Phenol Red, 0.5%			0.5
Eagle's Vitamins 100X			10.0

production medium consisting of Eagle's vitamins, Hanks' salts, lactalbumin hydrolysate, 0.1% human serum albumin, and 80 m*M* glycine (Table 1).

Econazole (Cilag-Chemie Ltd., Schaffhausen, Switzerland) was a gift from Dr. Heinz Möhl of Cilag-Chemie Ltd. It was dissolved at 1 or 3 μg/ml in complete medium from a 100x stock solution in distilled H_2O which was routinely stored at 4° C.

Urokinase activity was assayed either by the amidolytic effect on the substrate S-2444, pyroglutamylglycylarginyl-*p*-nitroanilide, manufactured by AB Kabi Diagnostica, Stockholm, Sweden (6), or by the fibrin plate method, using the following procedure.

Ten milliliters of bovine fibrinogen (75% clottable) (Miles Laboratories, Elkhart, IN) at 5 mg/ml was placed in a petri dish and clotted with 0.2 ml of thrombin (bovine, Miles Laboratories) at 15 U/ml. Both reagents were dissolved in 0.1 *M* Tris pH 8.0. The clotted plate was allowed to stand for up to 1 h. Twenty microliters of sample were added to the surface of the clot which was incubated at room temperature for 15 to 24 h, and the major and minor diameters of the elliptical lysis zones were measured. Solutions of the International Reference Preparation of urokinase were used to obtain standard curves of lysis area vs. CTA (Committee on Thrombolytic Agents) units.

Cellular DNA content was measured by fluorescent flow cytometry using a modified Bio/Physics Systems, Inc. (now Ortho Instruments, Bedford, MA) Cytofluorograf 4800 A (7) after staining the cells by the acriflavine-Feulgen procedure (8). The resulting cellular DNA distributions were analyzed by computer programs written by Wood (9,10) for simplified analysis and comparison of the distributions.

TABLE 2

PLATING EFFICIENCIES OF HUMAN T-1E CELLS IN ECONAZOLE

Econazole (μg/ml)	Plating Efficiencies (%)
0	61.3 ± 1.7
1	55.3 ± 2.4
3	62.0 ± 1.0

RESULTS

Plating efficiency. The plating efficiency of cultured human T-1E cells was not affected by a range of concentrations of Econazole considered effective in fungus control, as indicated in Table 2.

Attachment efficiency. The percent of early passage cultured human kidney cells able to attach and spread within 18 h was not affected by Econazole present at recommended useful concentrations, as indicated in Table 3.

Growth rate. Econazole at 1 μg/ml did not introduce growth or division delay, nor did it modify the colony doubling time of human T-1E cells, as the growth curves of Fig. 1 indicate. At 3 μg/ml there seemed to be a 10% increase in doubling time, but no indication of division delay.

Cycle phase distribution. Consistent with the lack of growth curve modification was the finding

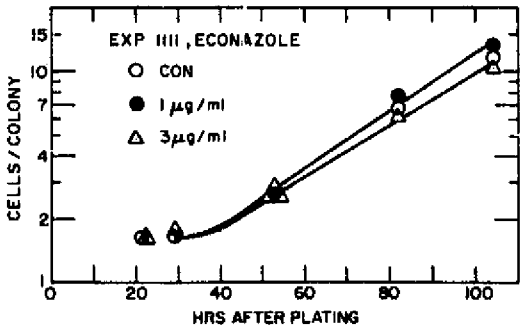

FIG. 1. Growth curves of colonies of human epithelioid T-1E cells in 0 (*circles*), 1 (*dots*), and 3 (*triangles*) μg/ml Econazole as assayed by phase microscopic examination of 50 to 100 colonies in growing cultures.

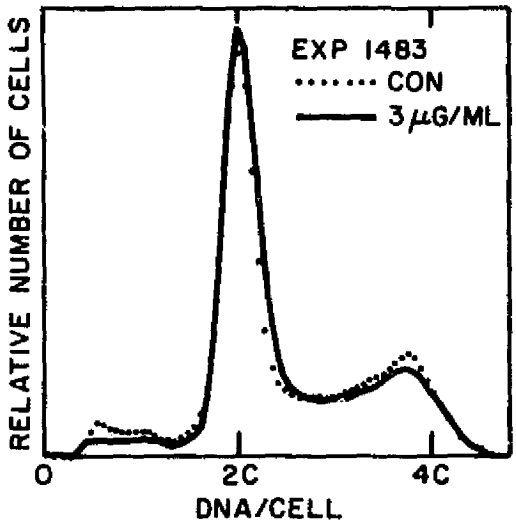

FIG. 2. DNA distributions of cell populations exposed to 0 (*dotted curve*) and 3 (*solid curve*) μg/ml Econazole. The difference between the two distributions is the same as the difference between pairs of identically treated populations.

that 1 μg/ml Econazole produced no noticeable modification in cellular DNA distributions when applied to human T-1E cells for 48 h, as comparison of the DNA distributions in Fig. 2 shows. Also, 3 μg/ml had no noticeable effect. The integrated differences between the DNA distributions of control cells and cells treated with 1 and 3 μg/ml were, respectively, 3.94 ± 0.87% and 4.36 ± 4.25%. These differences are too small to be significant, inasmuch as identically treated cultures, including controls, when pairs were compared differed by 5.01 ± 3.50% in the same experiments. Apparently Econazole does not perturb progression through the human cell cycle by the introduction of delays in specific phases.

Specific enzyme production. The production of urokinase by cultured human embryonic kidney cells in high glycine, serumless production medium is not altered by 1, 3, and 5 μg/ml of Econazole, as indicated by the results of fibrin plate tests and colorimetric assays shown in Table 4. After 4 d in Econazole, standard cultures produced 55 CTA U/ml of urokinase, and cultures treated with 3 μg/ml Econazole produced 60 CTA U/ml. The similar size of the thrombolytic zones also implied that no change occurred in the type of urokinase produced; that is, the treated and control cultures produced plasminogen activators with the same molecular weights.

TABLE 3

EFFECT OF ECONAZOLE ON 24 H ATTACHMENT EFFICIENCY OF HUMAN EMBRYONIC KIDNEY CELLS – PASSAGE 3

Econazole μg/ml	% Cells Attached
0	77 ± 6
1	83 ± 5
3	82 ± 5

TABLE 4

UROKINASE PRODUCTION OF HUMAN EMBRYONIC KIDNEY CELLS IN ECONAZOLE

Econazole (μg/ml)	Fibrin Plate (CTA U/ml)	S-2444 (CTA U/ml)
0	55	52.5
1	50	40.8
3	60	56.4
5	45	48.5

DISCUSSION

On the basis of five additional sensitive tests of cell function in vitro, it seems that Econazole at 1 μg/ml has a negligible effect, and its cytotoxicity at this concentration is sufficiently low to indicate that it is a safe antifungal agent for quantitative cell culture research. At 3 μg/ml, Wyler et al. (1) observed detectable inhibition of macromolecular synthesis; this is consistent with the observation (Fig. 1) that this concentration slightly slowed the growth rate of a permanent cell line. Nevertheless, it was reported that 3 μg/ml can counteract heavy fungal contamination, and it seems that very minute cell damage accompanies treatment with this concentration. In substantial agreement with Wyler et al., we recommend use of Econazole at 1 μg/ml as antifungal agent in quantitative cell culture experiments.

REFERENCES

1. Wyler, R.; Murbach, A.; Möhl, H. An imidazole derivative (Econazole) as an antifungal agent in cell culture systems. In Vitro 15: 745–750; 1979.
2. van der Veen, J.; Bots, L.; Mes, A. Establishment of two human cell strains from kidney and reticule sarcoma of lung. Arch. Ges. Virusforsch. 8: 230–245; 1958.
3. Barendsen, G. W.; Beusker, T. L. J.; Vergroesen, A. J.; Budke, L. Effects of different ionizing radiations on human cells in tissue culture. II. Biological experiments. Radiat. Res. 13: 841–849; 1960.

4. Todd, P. Heavy-ion irradiation of cultured human cells. Radiat. Res. Suppl. 7: 196-207; 1967.
5. Nelson-Rees, W.A.; Daniels, D.W.; Flandermeyer, R. R. Cross-contamination of cells in culture. Science 212: 446-452; 1981.
6. Gallimore, M.; Fareid, E. Studies on human plasma inhibitors of plasmin, plasma kallikrein, trypsin, thrombin and urokinase using chromogenic substrate assays. Kakkar, V. V. ed. Chromogenic substrates. New York: Academic Press; 1978.
7. Leary, J. F.; Todd, P.; Wood, J. C. S.; Jett, J. H. Laser flow cytometric light scatter and fluorescence pulse width and pulse rise-time sizing of mammalian cells. J. Histochem. Cytochem. 27: 315-320; 1979.
8. Trujillo, T. T.; Van Dilla, M. A. Adaptation of the fluorescent-Feulgen reaction to cells in suspension for flow microfluorometry. Acta Cytol. 16: 26-30; 1972.
9. Deford, L. S.; Buss, E. G.; Todd, P.; Wood, J. C. S. Estimation of haploid cell content of parthenogenetic turkey embryos: a cytofluorometric study. J. Exp. Zool. 210: 301-306; 1979.
10. Wood, J. C. S. Flow cytometric life cycle analysis in cellular radiation biology. University Park, PA: The Pennsylvania State Univ.; 1982. Thesis.

We thank Vincent Giranda for technical assistance. The International Reference Preparation of urokinase was supplied by WHO International Laboratory for Biological Standards, Holly Hill, Hampstead, London.

This research was supported by U.S. Public Health Service Grant R01-CA-24090 from the National Cancer Institute, National Institutes of Health, and National Aeronautics and Space Administration Contract NAS-9-15584.

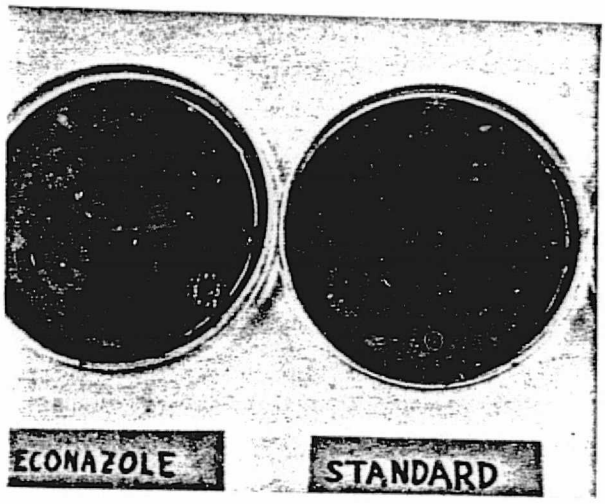

Figure 4. Lysis zones formed in the fibrin plate assay of human kidney cell urokinase. The 100-mm plate on the right contains zones formed by aliquots of WHO urokinase standard. These are used to develop a standard curve in every experiment. The plate on the left contains two lysis zones (left side) produced by urokinase activity of 0.2 ml of production medium from control human kidney cell cultures and two lysis zones (right) produced by identically-treated cultures that contained econazole.

Chapter 10.

Evaluation of Low-Ionic-Strength Buffers for Freezing and Electrophoresis of Cultured Human Cells.

TASK I. Development and testing of electrophoresis solutions.

I.1. Development of optimal buffer system.

Of the four types of buffers proposed for testing, two have been explored: low ionic strength electrophoresis buffer with and without density-gradient material. When the ability of cells to attach and spread was used as viability criterion it was found that the electrophoresis routine was better tolerated when Ficoll was present. Table 1 shows the results of a viability study that began with a poor-viability population of primary human fetal kidney (HFK-1) cells at the first passage.

Three cell lines have been utilized so far in various aspects of the project, including the other tasks (below). Human T-1 cells originated from a biopsy of a kidney of an adolescent male in 1957 (1) and have been in continuous use in the project laboratory. Cell strain "HFK" (our designation) was obtained at first passage from Grand Island Biological Co. Aliquots were frozen at second passage, and it was propagated to the 13th passage. Cell strain "HFK-1" has been used in several experiments at the first and second passage. HFK consisted mainly of fibroblasts, and HFK-1 has a high epithelioid cell content. The chromosomes of HFK were examined, and the cells were found to be euploid.

The stock medium for cell electrophoresis is described in Table 2. In this solution are dissolved density-gradient solutes such as sucrose and Ficoll to bring the osmolarity to 0.30. Its ionic strength is less than 0.01M, and its conductivity is usually 0.0011 mho/cm. (2).

Methods for viability determination have included direct microscopic counting of the percent cells attached and spread within 24 hr of plating test cultures or electrophoretically separated fractions. In terms of the project objectives, this seems to be the most relevant test. The Cytograf viability assay concept has been tested, and Figure 1 shows, as expected that blue-stained cells scatter less light into the 0.8 - 3.3° angular interval than do unstained cells. Experiments are continuing using a HeNe laser with the Los Alamos flow cytophotometry system "FMF II" currently on loan from the Environmental Protection Agency. This apparatus permits optimization of the light-scatter detection angle so that stained cells will be maximally discriminated (3).

I.2. Ionic strength tolerances.

All cultured cells tested so far appear to be highly tolerant of the low (less than 0.01 M) ionic strength of electrophoresis buffers (see also Table 1). This finding is consistent with the experience of the ASTP MA-011 experimenters, who used "A-1" buffer with 0.0097 M ionic strength. It is presumed, therefore, that the full range of ionic strength between 0.14 M (physiological) and 0.01 M is acceptable.

I.3. Testing of viability at non-standard pH's.

Studies have not yet been initiated on this aspect of the project, which will be important only if isoelectric focusing studies are contemplated.

I.4. Optimum inorganic salt concentrations.

Low (Na^+) seems to be acceptable as long as the osmolarity is maintained with neutral solutes (glucose, sucrose, Ficoll). The standard buffer is 1.6 mM Na^+ (Table 2) compared to 8.1 mM used in the MA-011 buffer. However, our buffer contains 4.1 mM K^+ and 0.5 mM Mg^{+++} while the A-1 buffer contains only 0.37 mM K^+ and no Mg^{+++}. Preliminary experiments indicate that EDTA is very toxic.

TASK II. Optimization of freezing and thawing.

II.1. Determination of optimum additive concentrations

The use of 10% DMSO had always been satisfactory in our customary procedure (5). Strain HFK did not survive after thawing, and the cells' morphology was clearly indicative of severe membrane damage. The method of trypsinizing is currently under investigation as an etiologic factor in low post-freezing viability. The optimization of trypsinization will be entered into the project before DMSO and glycerol concentration studies continue.

II.2. Determination of optimum freezing rate.

Due to conditions just described, studies have not yet been initiated on this aspect of the project.

TASK III. Procedure for evaluation of separated cells.

III.1. Standard culture conditions.

A 1-to-6 dilution of cells suspended in electrophoresis medium directly into growth medium (Eagle's BME + 10% fetal calf serum) in a 60 mm culture dish for each fraction has worked extremely well. Cells of the strain HFK-1 do very well in "maintenance medium" consisting of Medium 199 plus 5% fetal calf serum. There is very little cell multiplication, and cells are not lost from the vessel surface. They attach readily in both media. Passing cultures of this strain at high density has resulted in a lack of fibroblast overgrowth and maintenance of epithelioid, granular morphology.

Electrophoretic fractions of HFK and HFK-1 attach and spread within 1 hr after plating 1 ml of cells suspended in low-ionic strength electrophoresis buffer into 4 ml of Eagle's BME + 10% fetal calf serum. The use of 15% serum was not found to improve the viability of cells plated from frozen stocks.

TASK I. Development and testing of electrophoresis solutions.

The testing of buffers and media continued, using additional new human kidney cell explants obtained from Microbiological Associates, Inc. These were designated HFK-6 through HFK-9. The earlier source, Grand Island Biological Company, is no longer supplying human kidney cells. During this 6-month reporting period a problem requiring additional research arose. Fetal calf serum became scarce then essentially unavailable. Alternatives tested for the growth of HFK-7 and HFK-8 cells included Calf serum, newborn calf serum, donor calf serum, "bobby" calf serum, and bovine (adult) serum. No qualitative differences were observed between cultures of these cells grown in fetal and newborn calf sera at 10% concentration in Eagle's BME. If anything, newborn serum was better (EXP 1064). A more quantitative evaluation was made using our colony-forming human cell line T-1E, which shares phenotypic properties with HeLa cells. It was found (EXP 1069) that plating efficiencies were not significantly different whether fetal, newborn, calf, or bovine sera were used at 10% concentration and that growth curves in fetal and newborn sera were indistinguishable. Experimentation therefore continued using newborn calf serum on a routine basis.

Comparisons between PBG and A-1 buffers continued at various stages of cell preparation and electrophoresis. The formulae for these solutions were given in the previous progress report. Emphasis was placed on the effect of spending 4 hr at 4°C in the two buffers containing DMSO or glycerol on the cells' ability to attach and spread in culture and to form confluent monolayers. The regular culture medium "BME-10" was used as control standard. The effects of 5% DMSO or glycerol were compared in complete medium, and it was found (EXP 1036) that without freezing DMSO produced denser cultures than glycerol in 72 hr, and the cultures in the two solutions were comparable after 96 hr. Supernatants contained cells that later attached in both cases, and cells from both treatments ultimately produced confluent sheets. When 5% glycerol was used in A-1 or PBG buffers (EXP 1037) for storage at 4°C for 4 hr it was found that A-1 plus glycerol led to slightly higher viability than PBG plus glycerol, as shown in Table 1. It is concluded that, if cells are not to be frozen, A-1 buffer is slightly better. However, see below under "freezing" task.

Another step in the procedure was examined, namely the use of EDTA or scraping in place of trypsinizing to prepare cells for electrophoresis. Although neither procedure was as gentle as our usual trypsinization it was clear that incubation of monolayers in 0.37% EDTA in Puck's Saline A (PSA), which produced 48% attached and flat cells in 24 hr was superior to scraping cells in PSA and no EDTA, which produced less than 20% cells attached and spread in 24 hr (EXP 1062). Due to an earlier decision to try to avoid trypsinization in future electrophoresis runs, cell dispersal for electrophoresis is now being done with 0.37% EDTA in PSA. Monolayers are incubated 10 min in this solution, and suspending fluid is added to dilute the EDTA.

TASK II. Optimization of freezing and thawing.

It was previously reported that freezing and thawing of HFK cell suspensions resulted in large numbers of non-adherent but apparently viable cells. These cells were subjected to further study, and no evidence could be found that they are capable of proliferation (EXP 1024). Attempts to evaluate their DNA content by laser flow cytofluorometry failed when it was found that the 4N HCl used in Feulgen hydrolysis destroyed these cells (EXP 1027, 1039). It is tentatively concluded that these are dead cells whose unattached carcasses do not readily lyse or otherwise disappear from cultures. Cells with this peculiar behavior have not been found in large numbers in recent explants.

Glycerol and DMSO (5%) were compared as freezing agents in complete medium (EXP 1036). Cells frozen 18 days in liquid nitrogen attached more quickly after thawing in glycerol than in DMSO. On the second and third days, however, the cultures were indistinguishable. When 5% glycerol was used in A-1 or PSB and cells were frozen 2 days, the results shown in Table 2 (EXP 1037) were obtained, and it was concluded that PSB is superior to A-1 when cells are frozen in glycerol, despite the above finding that cells in A-1 buffer survive better when freezing is not part of the procedure.

The effect of incubation time after thawing and before adding medium was investigated. By allowing cells to attach 1 hr and removing medium and replating the supernatant while changing medium on the attached cells, it was possible to conclude that 75% of the cells (HFK-6) attach in the first 2 hr after thawing and that they tolerate the residual DMSO (diluted to about 0.8%) for this 2-hr period (EXP 1083).

In a combined 3-day freezing test of glycerol vs. DMSO and A-1 vs. PBG it was found, as indicated in Table 3 (EXP 1060) that combining glycerol and DMSO was very bad for the cells, otherwise glycerol and DMSO were about the same in A-1 buffer, but in this particular test glycerol appeared to be better than DMSO in PBG; however, the fraction of cells that also spread in 24 hr was actually greater in DMSO--28% vs. 13%. Cells spread more slowly yet (10-12% in 24 hr) in the A-1 buffer solutions.

The results of freezing and thawing experiments to date slightly favor the use of 5% DMSO in PBG, but it is also evident that 5% glycerol in A-1 is really not very different. It seems that 50-60% viability (in terms of cell attachment in culture) is to be expected under several of the conditions tested. The present data do not give very strong reasons for making recommendations of any particular combination of buffer and freezing agent.

Table 1. Effect of medium composition on the viability of cells stored at 4°C for 4 hr.

MEDIUM	PER CENT CELLS ATTACHED AFTER 24 HR	48 HR	72 HR	96 HR
"BME-10"	95	100	Confluent	Confluent
A-1 + 5% glycerol	76	77	77	Confluent
PBG + 5% glycerol	68	63	70	81

Table 2. Effect of medium composition on the viability of cells frozen in liquid nitrogen for 2 days.

MEDIUM	PER CENT CELLS ATTACHED AFTER 24 HR	48 HR	72 HR	96 HR
A-1 + 5% glycerol	29	19	20	23
PBG + 5% glycerol	39	45	33	53

Table 3. Effect of medium composition on the attachment of cells frozen in liquid nitrogen for 3 days and examined 24 hr after thawing.

BUFFER	% GLYCEROL	% DMSO	% CELLS ATTACHED
A-1	5	0	57
"	5	5	0
"	0	5	57
"	0	10	0
PBG	5	0	72
"	5	5	0
"	0	5	49
"	0	10	48

Table 1. Viability of HFK-1 cells at first passage under various simulations of electrophoresis treatment. The ability to attach and spread in culture was used as viability criterion.

MEDIUM	TREATMENT	VIABILITY
PBG + 6.8% sucrose	30 min. 25°C	42%
PBG + 6.8% sucrose	4 hr. 4°C	44%
PBG + 5.9% sucrose + 5.0% Ficoll	4 hr. 4°C	66%

Table 2. Composition of phosphate-buffered glucose medium (PBG).

COMPONENT	MW	g/l	M
KCl	74.56	0.20	0.00268
$MgCl_2 \cdot 6H_2O$	203.33	0.10	0.00049
$Na_2 HPO_4$	141.96	1.15	0.00810
$KH_2 PO_4$	139.09	0.20	0.00144
Glucose	180.16	10.00	0.05551

Table 3. Composition of zero-g electrophoresis buffer used in viability tests (A-1).

COMPONENT	MW	g/ℓ	M
NaCℓ	58.45	0.380	0.00642
Na_2HPO_4	94.98	0.167	0.00176
KH_2PO_4	136.09	0.050	0.000367
Na_2EDTA	372.24	0.125	0.000336
Glucose	180.16	40.0	0.222
Glycerol	92.10	47.34	0.514

Chapter II.

Separation of Functioning Mammalian Cells by Density Gradient Electrophoresis.

Reprint from:
Electrophoresis '81 · Editors: Allen, Arnaud

SEPARATION OF FUNCTIONING MAMMALIAN CELLS BY DENSITY-GRADIENT ELECTROPHORESIS

Paul Todd, W.C. Hymer, Lindsay D. Plank, Gary M. Marks, M. Elaine Kunze, Vincent Giranda

Althouse Laboratory, The Pennsylvania State University, University Park, Pennsylvania 16802

J.N. Mehrishi

Department of Medicine, Addenbrookes Hospital, University of Cambridge, Cambridge, England CB2 2QQ

Introduction

One of the promises of preparative cell electrophoresis is its ability to purify functioning, living animal cells in useful quantities. One of several such methods is density-gradient electrophoresis. When a low-ionic-strength, isotonic gradient of Ficoll and sucrose is used in a glass column at 4°C, the physical factors that determine the upward velocity of cells combine to produce a nearly-constant migration rate. Density-gradient electrophoresis has been applied to suspended cells prepared from freshly dispersed tissues, cultured-cell monolayers, and naturally suspended cells from body fluids (1, 2, 3, 4). It is the purpose of this report to briefly describe recent work performed at the Pennsylvania State University consisting of further physical characterization of density-gradient electrophoresis and the results of a small number of recent applications to living cells. The most popular uses of preparative cell electrophoresis have been in the field of immunology, and this is true of density-gradient electrophoresis (4, 5). Some rather more unusual applications will be discussed here. All of the research reported here used the

apparatus and methods described by Boltz et al. (6). Columns without a central cooling finger were used.

Electrophoretic Cell Migration in a Ficoll Gradient

As cells migrate upward through a decreasing Ficoll concentration in the electrophoresis column they encounter changes in viscosity, density, and conductivity. In addition, Ficoll itself affects electrophoretic mobility (1, 6, 7). The effect of Ficoll was determined quantitatively by the microscopic method of cell electrophoresis using the Zeiss cytopherometer and determination of mobilities from complete velocity parabolas corrected for asymmetric electroosmotic backflow (2, 8). A linear increase of the mobilities of various erythrocytes with increasing Ficoll concentration was found. From the remaining known and measured properties of the cells and solutions (9) it is possible to predict the upward migration velocity of cells under the influence of the combined forces of gravity and the applied electric field. The resulting mathematical relationship, when integrated numerically, produces a migration plot (distances vs. time) such as that shown in Figure 1. Because migration velocity depends slightly, but roughly linearly, upon migration distance, an exponential function is expected, but, as Figure 1 indicates, this is a slowly rising exponential function which is indistinguishable from a straight line within the accuracy of most distance measurements. The electrophoretic mobility, μ, normally defined as migration velocity per unit field strength in μm-cm/V-sec, was therefore determined in these studies by dividing the distance migrated by the electrophoresis time and dividing this ratio by the constant field strength.

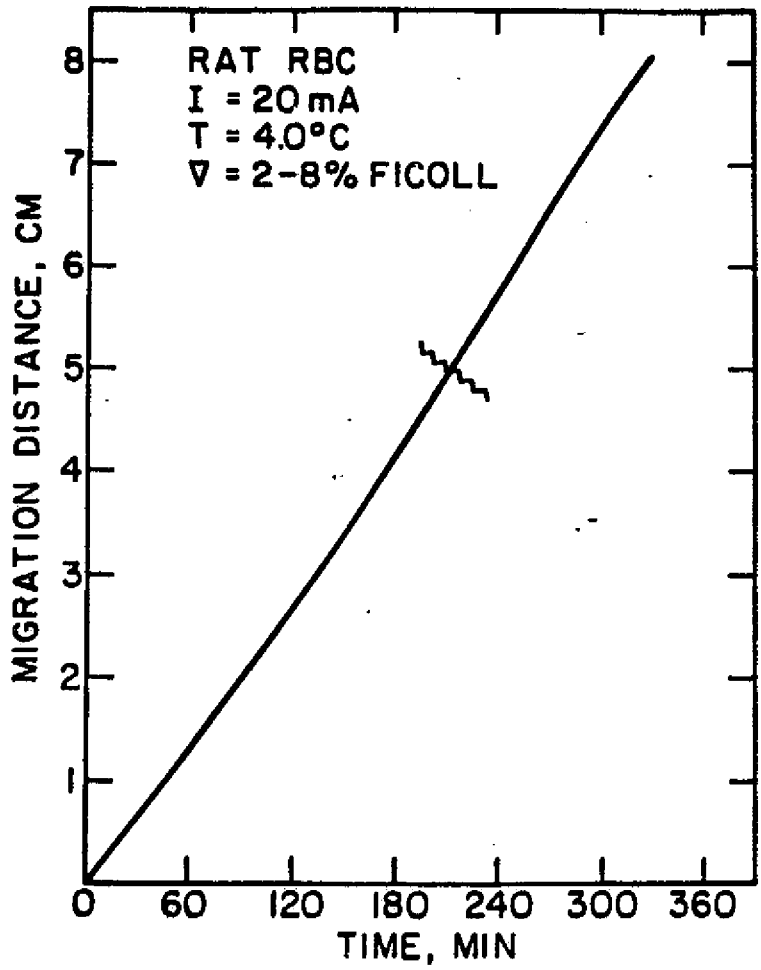

Figure 1. Plot of migration distance vs. time for upward migration of erythrocytes in a Ficoll gradient. The graph was determined by numerical integration of the relationship between cell velocity and the varying properties of the gradient: viscosity, density, conductivity, and Ficoll concentration. Below the break shown near the middle of the curve the numerical integration is approximated satisfactorily by an exponential function resulting from the assumption that cell velocity depends linearly on migration distance.

Effect of Cell Cycle Phase on Electrophoretic Mobility

Cells from a long-term cultured epithelial line designated "T-1" (10, 11) were cultured in monolayers in plastic flasks and suspended in electrophoresis buffer by detachment with

EDTA. After subjecting the suspended cells to density-gradient electrophoresis, fractions were collected, and the DNA content of individual cells was measured by flow cytometry using the staining method of Trujillo et al. (12) and flow cytometry with a Bio/Physics Systems, Inc. Cytofluorograf (13). The cellular DNA distribution of individual fractions revealed that low-mobility fractions were enriched in cells in the G2 phase of the cell cycle (Figure 2). However, the mobility distributions of cells in different phases of the cycle are broad (14), and the data of Figure 2 reveal only, as found by Forrester (14), that there is a general trend toward lower mobilities as cells progress through the cycle.

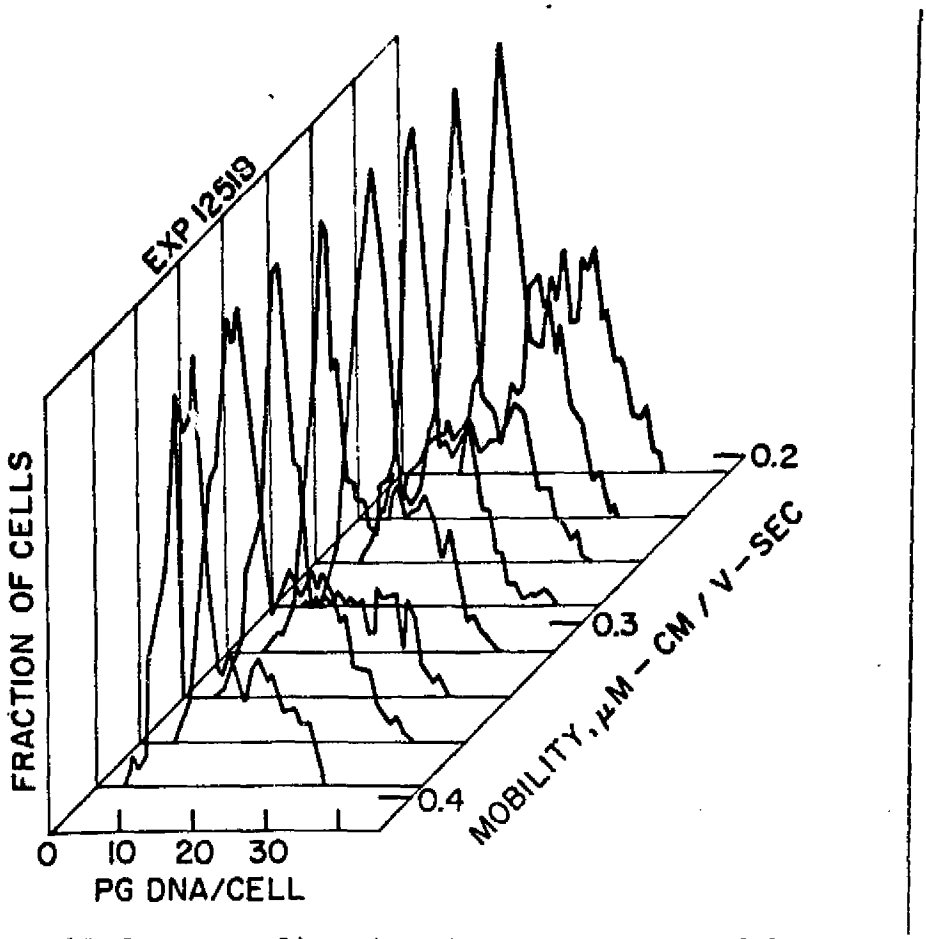

Figure 2. Cellular DNA distributions of cultured human T-1 cells in fractions collected after density-gradient electrophoresis. DNA content per cell was calibrated biochemically (15). Higher mobility fractions were depleted, while lower mobility fractions were enriched, with respect to cells in the G2 phase of the cell cycle.

Urokinase-producing Cells in Human Embryonic Kidney Cell Cultures

Human urokinase, a plasminogen activator produced in the kidney, is being considered as a therapeutic agent for thrombosis (16). Electrophoretically purified cultured human embryonic kidney cells are considered a potentially efficient source of this material (17), and electrophoretic purification attempts have been reported (18). Cells from early-passage culture, designated "HFK-18", were propagated in monolayers in plastic flasks and suspended in electrophoresis buffer by detachment with EDTA. After subjecting the suspended cells to density-gradient electrophoresis, fractions were collected and cultured in complete medium. Just before these cultures became confluent the complete medium was replaced by a high-glycine, incomplete medium into which urokinase-producing cells secreted their product. Urokinase activity was measured in CTA units by a calibrated fibrin-plate method (19) every 3-4 days after this medium change. Figure 3 indicates that most electrophoretic fractions contain cells that produce urokinase and, in this particular culture, the highest mobility fractions produced the highest levels of urokinase activity per cell.

Freshly Dispersed Lymphocytes from the Irradiated Mouse Spleen

Radiation therapy often leads to lymphopenia in treated cancer patients (20). It had previously been found that lymphocyte population changes in thymus lymphocytes of irradiated mice could be followed by analytical electrophoresis as a function of time after irradiation and that a clear rise and fall of the proportion of high-mobility (presumably cortical) cells occurs (21). Similarly, spleens of control and irradiated mice were excised 9 hr after exposure to 5.5 Gy of ^{60}Co gamma radiation; lymphocytes were teased away from stromal tissue and purified by the magnetic removal of macrophages and the removal by

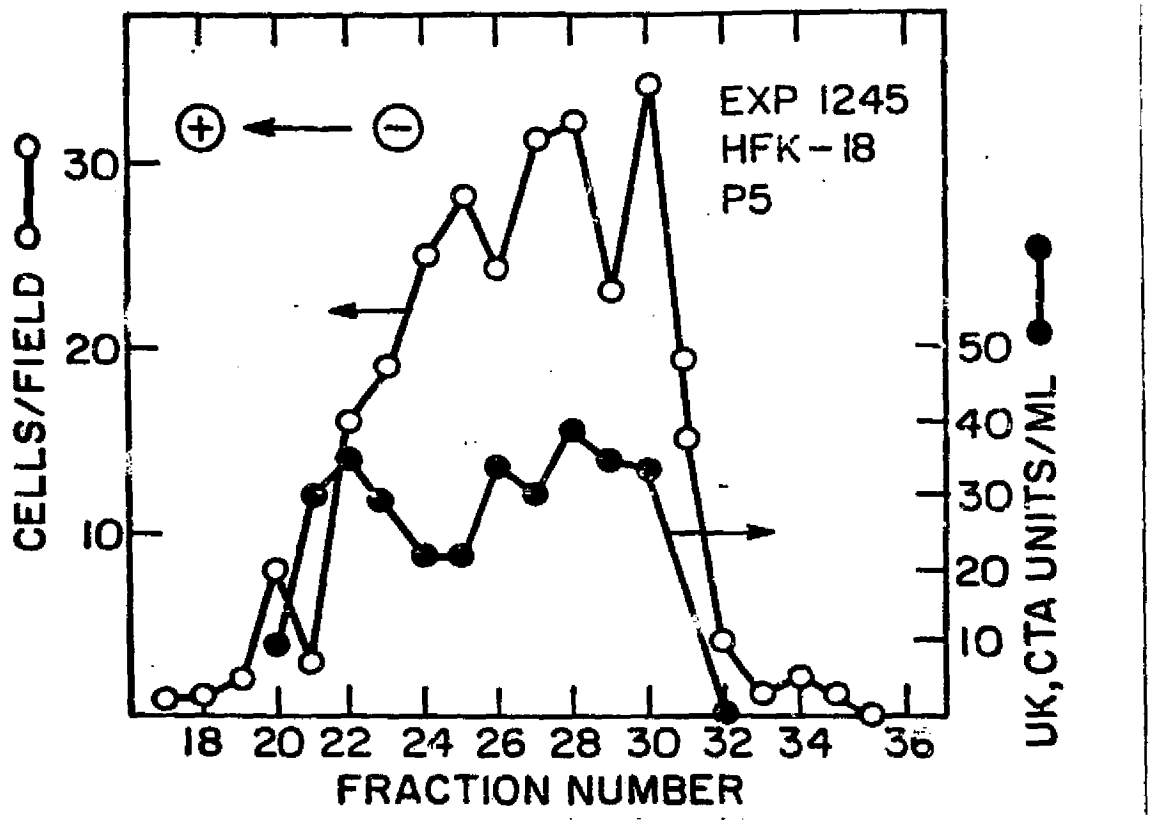

Figure 3. Density-gradient electrophoretic profile of cultured human embryonic kidney cells "HFK-18" at the fifth passage in vitro. Cells per field (O) in each fraction was determined by phase-contrast microscopy of cultures in dishes; urokinase activity (●) was determined by a fibrin-plate method (19). High mobility cells showed a high specific activity.

centrifugation of erythrocytes (22). The resulting lymphocyte suspensions were subjected to density-gradient electrophoresis, fractions were collected, and the number of cells per fraction in the 5.0-6.3 μm diameter range was determined by Coulter counter. The results shown in Figure 4, which is a distribution of cell number vs. electrophoretic fraction, indicates that there was a preferential loss of cells from the low-mobility cell population after irradiation. The high-mobility fraction has been reported to consist mainly of T-lymphocytes in adult mice (23). From this result we conclude that non-T-lymphocytes are preferentially reduced in number in the spleens of irradiated mice.

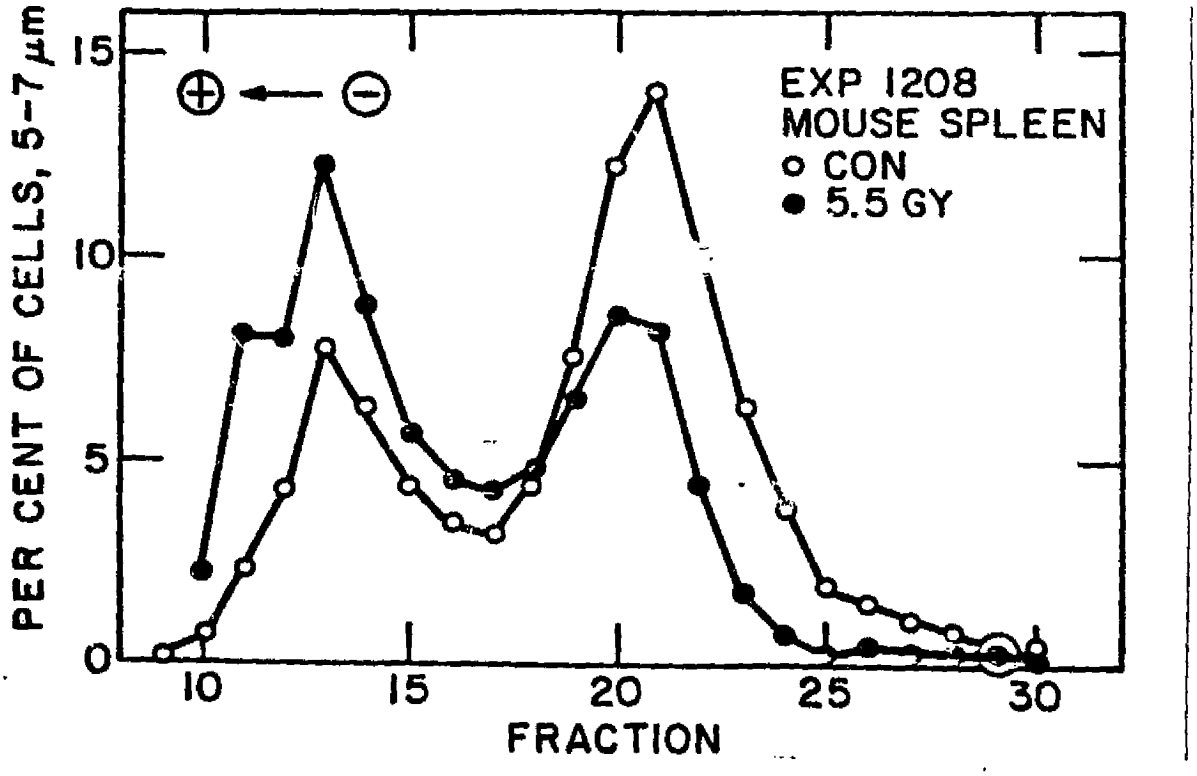

Figure 4. Density-gradient electrophoretic profile of 5.0-6.3 μm cells in fractions collected from columns to which were applied splenic lymphocytes from control (O) and irradiated (●) mice. The percent cells in the low-mobility (presumably non-T) population was preferentially reduced 9 hr after exposure to 5.5 Gy.

Suspended Somatotrophin-producing Cells from the Rat Anterior Pituitary

Purified populations of live somatotrcphin-producing cells have numerous potential applications, including implantation for growth enhancement (24), production of mRNAs for gene cloning, investigation of single-cell responses to releasing agents (25), the study of other functions of somatotrophs (26), and hormone production in vitro (27). Preparative cell electrophoresis is one of the methods that is potentially applicable to this particular cell purification problem. Somatotrophin-secreting cells constitute about 30 percent of the cells in the mammalian adenohypophysis so their electrophoretic mobility

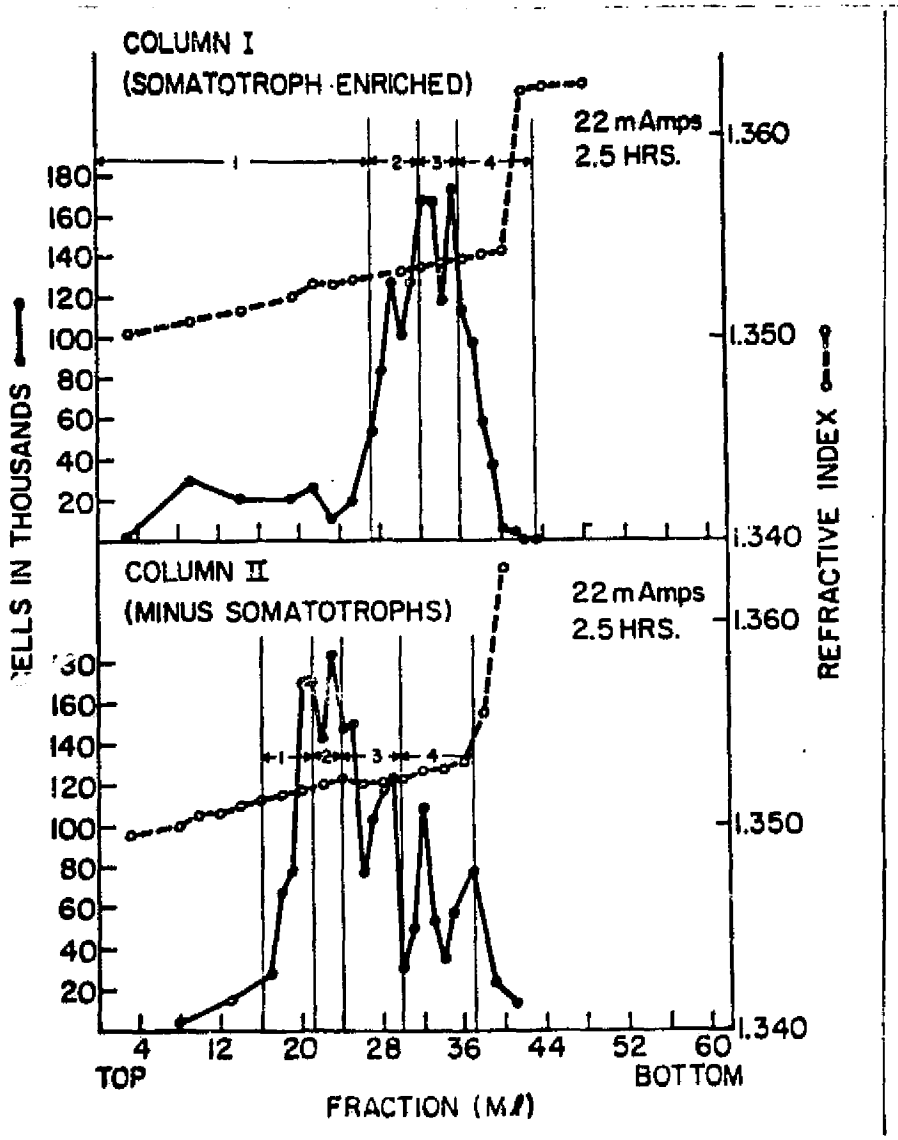

Figure 5. Electrophoretic profiles of suspended rat anterior pituitary cells after enrichment (upper panel) or depletion (lower panel) of somatotrophs by centrifugation. Bands 1, 2, 3, and 4 define fractions that were pooled for radioimmunoassay of hormone per 1000 cells. Band 4 in the upper panel was richest in somatotrophs, and their specific activity was nearly twice that of centrifugally purified somatotrophs.

cannot be determined by analytical cell electrophoresis methods. Heavily granulated rat somatotrophs were separated to ca. 80% purity by a single centrifugation procedure (28) consisting of layering freshly dispersed cells over 28% bovine serum albumin (BSA) (density 1.069 g/cm^3) which in turn was layered over a

dense, 34% BSA, layer. Centrifugation produced two rat pituitary cell bands, band I at the top interface and band II at the intermediate interface. Cells in band II were enriched somatotrophs. The electrophoretic mobility distribution of these partially purified cells was determined by density-gradient electrophoresis. At the same time electrophoretic fractions were collected and assayed for growth hormone content so that specific mobilities could be associated with specific levels of hormone production per cell. Two electrophoresis columns were used to simultaneously separate cells in centrifugal bands I and II. The separation profiles (Figure 5) reveal obvious differences in the mobility distributions between bands I and II. Radioimmunoassay of pooled fractions of cells from this separation experiment showed that the specific activity of cells from band 4 (lowest mobility group) in the upper panel of Figure 5 was 872 ng of growth hormone per 1000 cells, whereas pooled fractions represented by bands 1, 2, and 3 had 300 $\pm$ 50 ng/1000 cells. Cells from all fractions from column II (lower panel of Figure 5) had only 30 ng/1000 cells. These data suggest that a small pool of somatotrophs that contain relatively large quantities of hormone can be separated from other cell types on the basis of their low electrophoretic mobility.

Discussion and Summary

The fact that cell migration in Ficoll density-gradient electrophesis is nearly linear allows meaningful separations and analyses to be performed by density-gradient electrophoresis. In specific research projects it was found that the electrophoretic mobility of logarithmically growing cells from a long-term cultured human cell line depends on cell cycle phase. Preparative electrophoresis makes this experiment possible in the absence of artificial synchronization of the cells. Electrophoretic subpopulations of cells from human embryonic kidney

are enriched in cells that produce urokinase, a plasminogen activator used in thrombolytic therapy. Preparative electrophoresis concentrates larger numbers of these senescing cells than could be done by the selection of single clones. Electrophoretic separation of freshly dispersed lymphocytes from the irradiated mouse spleen indicates a preferential loss of low-mobility ("non-T") cells. Freshly dispersed cells from the rat anterior pituitary have a low-mobility subpopulation that is rich in somatotrophs that contain growth hormone after electrophoretic purification. Preparative electrophoresis permits the post-separation use of functional assays to unequivocally identify classes of cells having known electrophoretic mobilities. These research examples also indicate the utility of preparative electrophoresis, especially including density-gradient electrophoresis, in producing populations of functioning cells for further study or use in the production of cell products.

Acknowledgments

We thank Mrs. Gertrud Barsch, Mrs. Mary Hershey, | Mr. Michael Hatfield, and Mr. Charles Goolsby for excellent technical assistance. This work was supported by National Aeronautics and Space Administration Contracts NAS 9-15583, NAS 9-15566, and NAS 9-15584, and by Public Health Service Grant R01-CA-24090 from the National Cancer Institute.

References

1. Boltz, R. C., Jr., Todd, P., Gaines, R. A., Milito, R. P., Docherty, J. J., Thompson, C. J., Notter, M. F. D., Richardson, L. S., Mortel, R.: J. Histochem. Cytochem. 24, 16-23 (1976).
2. Thompson, C. J., Docherty, J. J., Boltz, R. C., Jr., Gaines, R. A., Todd, P.: J. gen. Virol. 39, 449-461 (1978).

3. Hammerstedt, R. H., Keith, A. D., Boltz, R. C., Jr., Todd, P.: Arch. Biochem. Biophys. 194, 565-580 (1979).

4. Platsoucas, C. D., Griffith, A. L., Catsimpoolas, N.: J. immunol. Meth. 13, 145-152 (1976).

5. Platsoucas, C. D., Good, R. A., Gupta, S.: Proc. natl. Acad. Sci. U.S. 76, 1972-1976 (1979).

6. Boltz, R. C., Jr., Todd, P.: In Electrokinetic Separation Methods (Righetti, P. G., van Oss, C. J., Vanderhoff, J. W., eds.) Elsevier/North-Holland, Amsterdam (1979) pp. 229-250.

7. Brooks, D. E.: J. colloid interface Sci. 43, 714-726 (1973).

8. Gaines, R. A.: Thesis, The Pennsylvania State University, (1981).

9. Boltz, R. C., Jr., Todd, P., Streibel, M. J., Louie, M. K.: Prep. Biochem. 3, 383-401 (1973).

10. Barendsen, G. W., Beusker, T. L. J., Vergroesen, A. J., Budke, L.: Radiat. Res. 13, 841-849 (1960).

11. Nelson-Rees, W. A., Flandermeyer, R. R., Daniels, D. W.: Science 209, 720-722 (1980).

12. Trujillo, T. T., Van Dilla, M. A.: Acta Cytologica 16, 26-30 (1972).

13. Leary, J. F., Todd, P., Wood, J. C. S., Jett, J. H.: J. Histochem. Cytochem. 27, 315-320 (1979).

14. Brent, T., Forrester, J. A.: Nature 215, 92-93 (1967).

15. Todd, P.: Radiat. Res. 61, 288-297 (1975).

16. Urokinase Pulmonary Embolism Trial: J. Amer. Med. Assoc. 214, 2163-2172 (1970).

17. Barlow, G. H., Rueter, A., Tribby, I.: In Proteases and Biological Control (Reich, E., Rifkin, D. B., Shaw, E., eds.) Cold Spring Harbor Press, Cold Spring Harbor, NY (1975) pp. 325-331.

18. Allen, R. E., Rhodes, P. H., Snyder, R. S., Barlow, G. H., Bier, M., Biguzzi, P. E., Van Oss, C. J., Knox, R. J., Seaman, G. V. F., Micale, F. J., Vanderhoff, J. W.: Sep. Purif. Meth. 6, 1-28 (1977).

19. Astrup, T., Müllertz, A.: Arch. Biochem. Biophys. 40, 346-351 (1952).

20. Sternswärd, J., Jondal, M., Vanky, F., Wigzell, H., Sealy, R.: Lancet 1, 1352-1356 (1972).

21. Mehrishi, J. N., Hiesche, K. D., Révész, L.: Studia Biophysica 73, 63-69 (1978).

22. Bøyum, A.: Scand. J. clin. lab. Invest. 21, suppl. 97, 77 (1968).

23. Catsimpoolas, N., Griffith, A. L., Gupta, S., Good, R. A., Platsoucas, C. D.: In Electrophoresis '79 (Radola, B. J., ed.) W. de Gruyter, Berlin/New York (1980) pp. 607-622.

24. Weiss, S. J., Berglund, R., Turpen, C., Hymer, W. C.: Fed. Proc. 36, 363 (1977).

25. Hymer, W. C., Page, R., Kelsey, R. C., Augustine, E. C., Wilfinger, W., Ciolkosz, M.: In Synthesis and Release of Adenohypophyseal Hormones (McKerns, K. W., Jutis'z, M., eds.) Plenum, NY (1979) pp. 126-168.

26. Wallis, M.: Nature 284, 512 (1980).

27. Tashjian, A. H.: Biotechnol. Bioeng. 11, 109 (1969).

28. Hymer, W. C., McShan, W. H.: Cell Biol. 17, 67-86 (1963).

Key Words and Index Terms

density-gradient electrophoresis
cell electrophoresis
kidney cells, human, cultured
lymphocytes, mouse spleen, irradiated
spleen lymphocytes, mouse, irradiated
cell cycle, electrophoresis and
anterior pituitary, electrophoresis of cells from
growth hormone, production of by separated cells
somatotrophin, separation of cells that produce
Ficoll, in cell electrophoresis

Chapter 12.

Electrophoretic Mobilities of Erythrocytes in Various Buffers.

ELECTROPHORETIC MOBILITIES OF ERYTHROCYTES IN VARIOUS BUFFERS

L. D. Plank, M. E. Kunze, and P. Todd

INTRODUCTION

The calibration of space flight equipment has grown to depend upon a source of standard test particles, and the test particle of choice has become the fixed erythrocyte. Erythrocytes from different species have different electrophoretic mobilities. Most buffers used in space electrophoresis applicatons have low conductivity and hence low ionic strength. Electrophoretic mobility depends upon zeta potential, which, in turn depends upon ionic strenth. Zeta potential decreases with increasing ionic strength, so cells have high electrophoretic mobility in space electrophoresis buffers than in typical "physiological" buffers, which have ionic strength = 0.145 g-ions/l. Therefore, a series of experiments was conducted to characterize the electrophoretic mobilities of fixed human, rat, and rabbit erythrocytes in 0.145 M salt, the standard experimental condition, and buffers of varying ionic strength, temperature, and composition, in order to assess the effects of some of the unique combinations used in space buffers.

Several effects had to be assessed: glycerol or DMSO (dimethylsulfoxide) were under consideration for use as cryoprotectants. The effect of these substances, if any, on erythrocyte electrophoretic mobility was therefore important to know. The choice of buffer partly depended upon cell mobility (owing to operating constraints of the EEVT apparatus). Primary experiments with kidney cells established the choice of buffer and cryoprotectant. A non-standtard temperature was anticipated in the EEVT experiment, so the temparture dependence of EPM in the suitable buffer had to be determined. Since there was a loss of ionic strength control in the course of preparing columns for flight, the efffects of small increases in ionic strength over the expected low values were also in need of evaluation.

MATERIALS AND METHODS

Approximately 10 different buffers were used in EPM measurements that were performed over the 6-year project period. Most of these are described, with respect to composition, ionic strength, conductivity, and osmolarity, in Table 1. In addition, the buffer designated "C-2", one of the glucose-sucrose Boltz buffers originally developed for density gradient electrophoresis, is described in Table 2.

Rat erythrocytes were collected by cardiac puncture or exsanguination after cervical dislocation. For fixation they were collected into 0.067 M Ssorensen's buffer and fixed in formaldehyde by Seaman's method or in glutaraldehyde by Tenforde and Glaeser's method. Human and rabbit blood were collected by venipuncture and fixed in the same way.

Measurements of EPM were performed using the Zeiss "Cytopherometer" with a rectangular chamber and Cam-Apparatus electrodes or with the "Pen Kem 3000" automated electrokinetic analyser. In the former case, cells at all depths through the chamber were clocked (by hand), and the resulting data were recorded on a DEC PDP-11 or Zenith Z100 miocrocumpter for fitting of assymetric parabolas and analysing them into histograms of cell count vs. mobility, using the BASIC RT-11 programs developed by L. D. Plank on the basis of the work of R A. Gaines (Chapter 4).

RESULTS

During the 1980-1982 calendar years numerous EPM measurements were mmade on fixed human erythrocytes; the raw list of resulting mobilities is given in table 3. The other standard particle chosen of use on EEVT was fixed rabbit erythrocytes, which have about 0.55 the mobility of human erythrocytes, although the literature values tend to vary by about 15% around this ratio. Table 4 is as raw list of rabbit erythrocyte mobilities. From these two tables it was possible to derive the final mobility values most relevant to the EEVT experiment; these are the human and rabbit erythrocyte mobilities in buffer D-1, finally chosen for the flight experiment, and 0.145 M NaCl in bicarbonate buffer, the standard buffer for erythrocyte electrokinetic mauseruemts. These measurements are summarized in Tables 5 and 6. All values are corrected ot the viscosity of water at 25 degrees C.

During the final months before flight an invonsistency arose concerning the EPM of the cells fixed by G. V. F. Seaman to be used as the flight standards. Measurements at McDonnel-Douglas Astronaoutics Corp. (MDAC) yielded unexpectedly high mobilities, and measurements at Marshall Space Flight Center (MSFC) yielded unexpectdely low mobilities. These discrepancies were resolved when it was found that the MDAC samples had become contaminated, and they also had high mobilities when measured at the Pennsylvania State Universtiy (PSU) (Table 3, lines 1 and 2), and when the same viscosity corrections were applied to data obtained at MSFC (Figure 1) and PSU (Tables 3 and 4) the mobiliteis and standard deviations were essentially the same. Thus, the ACTUAL mobilities agreed upon, that would apply in D-1 buffer at 25 degress, are those seen in Figure 1, prepared by Dr. R. S. Snyder of MSFC, using Rank Bros. electrophoresis microscope with circular chamber.

The several questions that arose in the ccurse of this study were answered as follows:

1. Cells that were studied at MDAC had higher mobility, especially those that had been stored in D-1 buffer at MSFC.
2. Mobility in D-1 is consistently higher than in A-1, but only bo 0.1 - 0.2 unit.
3. Mobililties measured in saline in all laboratories are correct.
4. The lowest mobilities meeasured were 2.31 and 2.35; these were made in D-1 without DMSO, in the Cytopherometer and Pen Kem, respectively.
5. Using higher current did not increase mobility.
6. The range of reliable mobilities (3/82) of formalin-fixed human erythrocytes is 2.54 - 2.79.
7. Deriving mobililties from whole velocity parabolas does not increase measured mobility. If anything, parabola mobilities are about 0.1 - 0.2 unit less that mobilities derived from stationary-plan-only measurements.
8. Glutaraldehyde-fixed cells do not have higher mobility than formalin-fixed cells.

Another method used in the course of the research was density gradient electrophoresis, using the same fixed cells as standards. So that this work could be related to the microgravity studies, absolute mobility measurements were also made in C-1 buffer (Table 3 and 4) and verified using the Pen Kem 3000 Automated Electrokinetic analyser, using glutaraldehyde fixed rat erythrocytes rather than human (Figure 2).

Conductivity and temperature of the column buffers in the EEVT were not exactly as planned, so post-flight analysis depended upon understanding the

effects of changing the concentration (and hence ionic strength, conductivity, viscosity, etc.) of D-1 buffer. The dependence of mobility on ionic strength is well known (Heard and Seaman, 1960). The buffers used in evaluating the ionic strength dependence of RBC mobility using the Cytopherometer are listed in table 7, and a graph of EPM vs. ionic strength is given as Figure 4. An example of the study of the effect of temperature using the Cytopherometer is given in Figure 5, in which complete velocity parabolas are presented at two temperatures in D-1 buffer. A series of such experiments was conducted and the final results are presented in Table 8, where EPM as a function of both temperature and buffer concentration is given.

Table 2. Composition of buffer C-2 used in density gradient electrophoresis systems.

COMPONENT	GRAMS/LITER	MOLEC. WT.	MILLIMOLARITY
KCl	0.2	74.55	2.68
$MgCl_2 \cdot 6H_2O$	0.1	203.23	0.49
Na_2HPO_4	0.48	141.98	3.38
KH_2PO_4	0.84	136.09	6.17
Glucose	10	180.16	5.55
Sucrose	68	342.3	198.7

Conductivity (mmho/cm)	0.87
Viscosity (cP)	1.10

Table 1. Compositions of Buffers Used in Microscopic Electrophoresis of Cells Prepared From Monolayer Cultures.

	CONCENTRATIONS, MILLIMOLES/LITER									
Buffer Name	$MgCl_2$	NaCl	KCl	KH_2PO_4	Na_2HPO_4	Glucose	Sucrose	$NaHCO_3$	$\Gamma/2$	mmho* K cm
Standard Saline	0	145.0	0	0	0	0	0	0.30	0.145	12.5
.12	0.48	89.7	2.65	1.47	8.10	55.5	19.9	0	0.120	9.2
.09	0.48	59.8	2.65	1.47	8.10	55.5	80.1	0	0.090	6.8
.06	0.48	29.9	2.65	1.47	8.10	55.5	14.0	0	0.060	4.2
.03	0.48	0	2.65	1.47	8.10	55.5	199	0	0.030	1.5
1 mM Phosphate	0.48	0	2.65	0.15	0.81	55.5	199	0	0.015	0.5
Josefowicz		13.0		[10 mM Tris]		290 (sorbitol)			0.015	~1.5
1/30 Seligmans + 0.61 mM NaAc	0	4.36	.089	.0245	.0175	0.185	280	0.28	0.005	
D-1	0	6.42	0	0.367	1.76	222	0	0	0.015	0.9
A-1 + .336 mM EDTA + 5% glycerol (A-1) + 5% DMSO (D-1)	0	6.42	0	0.367	1.76	222	0	0		

Table 3
List of fixed human RBC mobilities from individual experiments, corrected to viscosity of water at 25°C.

MOBILITY	BUFFER	DATE	SPECIAL CONDITIONS
2.74 ± 0.12	D-1 from MDAC	3/4/82	Sent in formalin-saline
2.83 ± 0.13	D-1 made at PSU	3/4/82	Sent in formalin-saline
2.31 ± 0.18	D-1 without DMSO	10/7/81	
1.99 ± 0.11	C-1 ($\Gamma/2$ = 0.030)	7/28/81	
2.76 ± 0.18	D-1	7/15/81	
3.02 ± 0.20	D-1	6/30/81	
1.76 ± 0.13	C-1 ($\Gamma/2$ = 0.030)	5/20/81	
1.69 ± 0.11	C-1 ($\Gamma/2$ = 0.030)	4/14/81	
1.47 ± 0.12	C-1 ($\Gamma/2$ = 0.030)	3/20/81	
3.05 ± 0.09	D-1	11/12/80	
2.05 ± 0.11	D-1 made at MSFC	10/23/81	Meas. at MSFC
2.40 ± 0.30	D-1	8/21/81	Pen-Kem, 0059
2.35 ± 0.15	D-1 without DMSO	8/21/81	Pen-Kem 0057
1.76 ± 0.12	C-2 ($\Gamma/2$ = 0.015)	8/21/81	Pen-Kem 0063
2.76 ± 0.16	D-1 without DMSO	3/10/82	Seaman-MSFC cells (7/20/81)
2.67 ± 0.11	D-1	3/10/82	
2.54 ± 0.15	A-1	3/10/82	
2.70 ± 0.14	D-1	3/12/82	I = 0.5 mA
2.64 ± 0.17	D-1	3/12/82	I = 0.9 mA
2.78 ± 0.13	D-1	3/12/82	I = 0.5 mA, Front S. P.
1.35 ± 0.06	0.145 M NaCl, 10^{-4} M $NaHCO_3$	3/12/82	Front S. P. meas. only
1.24 ± 0.06	0.145 M NaCl, 10^{-4} M $NaHCO_3$	3/12/82	Parabola
2.79 ± 0.13	D-1	3/12/82	F.S.P. only, after saline
2.59 ± 0.15	D-1	3/12/82	Parabola
1.10 ± 0.08	0.145 MNaCl, 10^{-4} M $NaHCO_3$	3/14/82	Seaman-formald 7/20/81
1.02 ± 0.08	0.145 MNaCl, 10^{-4} M $NaHCO_3$	3/14/82	PSU Glut. 10/23/80 cells
1.13 ± 0.07	0.145 MNaCl, 10^{-4} M $NaHCO_3$	3/14/82	pH 6.9
1.28 ± 0.07	0.145 MNaCl, 10^{-4} M $NaHCO_3$	3/14/82	pH 9.1
1.10 ± 0.08	0.145 MNaCl, 10^{-4} M $NaHCO_3$	8/21/81	Pen-Kem 0055 Rat RBC
1.10 ± 0.08	0.145 MNaCl, 10^{-4} M $NaHCO_3$	8/21/81	Pen-Kem 0053 Rat (repeat)
2.65 ± 0.15	D-1	3/15/82	Pool of 274 cells, 4 runs

Table 4
List of fixed rabbit erythrocyte mobilities from individual experiments, corrected to viscosity of water at 25°C

MOBILITY	BUFFER	DATE	CONDITIONS
0.93 ± 0.28	C-1	4/11/78	
1.08 ± 0.07	($\Gamma/2$ = 0.0299)	6/30/80	
1.47 ± 0.14	C-1	7/3/80	
0.51 ± 0.07	0.145	7/8/80	
0.79 ± 0.08	PBG-sucrose-NaCl (0.090)	7/9/80	
2.11 ± 0.09	B-3 ($\Gamma/2$-0.007)	7/14/80	
2.50 ± 0.18	B-2/5% Ficoll (0.0299)	7/16/80	
3.35 ± 0.34	B-2/10% Ficoll (0.0299)	7/16/80	
2.83 ± 0.27	B-2/7.5% Ficoll (0.0299)	7/23/80	
1.91 ± 0.15	B-2/2.5% Ficoll (0.0299)	7/25/80	
3.51 ± 0.28	PBG-Sucr./12.5% Ficoll (0.0299)	7/28/80	
0.82 ± 0.06	PBG-Sucr. NaCl ($\Gamma/2$ = 0.060)	7/29/80	
0.63 ± 0.09	PBG-Sucr. NaCl ($\Gamma/2$ = 0.120)	8/30/80	
0.98 ± 0.07	PBG-Sucr. NaCl ($\Gamma/2$ = 0.060)	8/25/80	
1.29 ± 0.09	C-1	10/15/80	
1.47 ± 0.11	C-1	12/9/80	
1.82 ± 0.11	PBG Sucr. Ficoll 2.5% (0.030)	12/9/80	
2.30 ± 0.15	5.0%		
2.70 ± 0.17	7.5%		
3.25 ± 0.20	10%		
3.63 ± 0.31	12.5%		
2.18 ± 0.11	D-1 ($\Gamma/2$ = 0.015)	2/20/81	
0.96 ± 0.09	C-1 (0.030)	5/20/81	
1.62 ± 0.12	D-1	6/19/81	
1.89 ± 0.13	D-1	6/30/81	
1.22 ± 0.11	C-1 (0.030)	9/21/81	
1.41 ± 0.12	C-1 Ficoll 2.5%	9/21/81	
1.53 ± 0.13	5.0%		
1.70 ± 0.18	C-1 Ficoll 7.5%		
1.80 ± 0.20	C-1 Ficoll 10.0%		
0.30 ± 0.05	0.145		Pen Kem 0055
0.35 ± 0.10	0.145		Pen Kem 0053 (repea

Table 5 Human RBC mobilities

corrected to the viscosity of water at 25°C

BUFFER	MOBILITY	DATE	CONDITIONS
D-1, no DMSO	2.31 ± 0.18	10/7/81	
D-1, no DMSO	2.35 ± 0.15	8/1/81	Pen-Kem 3000
D-1, no DMSO	2.76 ± 0.16	3/10/82	Seaman cells from MSFC
D-1	2.67 ± 0.11	3/10/82	Seaman cells from MSFC
A-1	2.54 ± 0.15	3/10/82	Seaman cells from MSFC
D-1	2.59 ± 0.15	3/12/82	Complete parabola (usual)
0.145 NaCl, 10^{-4} $NaHCO_3$	1.10 ± 0.08	3/14/82	Seaman formald. 7/20/81
0.145 NaCl, 10^{-4} $NaHCO_3$	1.02 ± 0.08	3/14/82	PSU glut. 10/23/80
0.145 NaCl, 10^{-4} $NaHCO_3$	1.13 ± 0.07	3/14/82	pH 6.9
0.145 NaCl, 10^{-4} $NaHCO_3$	1.28 ± 0.07	3/14/82	pH 9.1
D-1	2.65 ± 0.15	3/15/82	Pool of 274 cells, 4 runs

Table 6 Rabbit RBC mobilities

corrected to the viscosity of water at 25°C

BUFFER	MOBILITIES	DATE	CONDITIONS
D-1	1.62 ± 0.12	6/19/81	
D-1	1.89 ± 0.13	6/30/81	
0.145 NaCl, 10^{-4} $NaHCO_3$	0.51 ± 0.07	7/8/80	

Table 7

Conductivity, K (mmho/cm), and ionic strength, $\Gamma/2$ (M), for buffers used to determine cell mobilities, concentrated D-1 buffer, and flight column buffers.

MEDIUM	$\Gamma/2$	K(25°C)
D-1	0.015	0.95
C-1	0.030	1.5
C-2	0.015	0.5
0.145	0.145	12.5
B-3	0.007	
B-3'	0.060	4.2
B-3"	0.120	9.2
2XD-1	0.030	1.52
1.5XD-1	0.0225	1.29
1.25XD-1	0.0165	1.03
1.0XD-1	0.015	0.97
019	0.0237	1.306
049	0.0190	1.142

Table 8. Temperature dependence of the electrophoretic mobility of glutaraldehyde-fixed human erythrocytes as a function of temperature in D-1 and 1.25 concentrated D-1 buffer, corrected for H_2O at 25°C.

TEMPERATURE	ELECTROPHORETIC MOBILITY μm-cm/V-sec	
°C	IN D-1	IN 1.25 x D-1
12.0	2.41 ± 0.31	2.41 ± 0.18
14.0	2.76 ± 0.21	2.52 ± 0.30
20.0	2.59 ± 0.26	2.45 ± 0.26
25.0	2.70 ± 0.27	2.62 ± 0.36

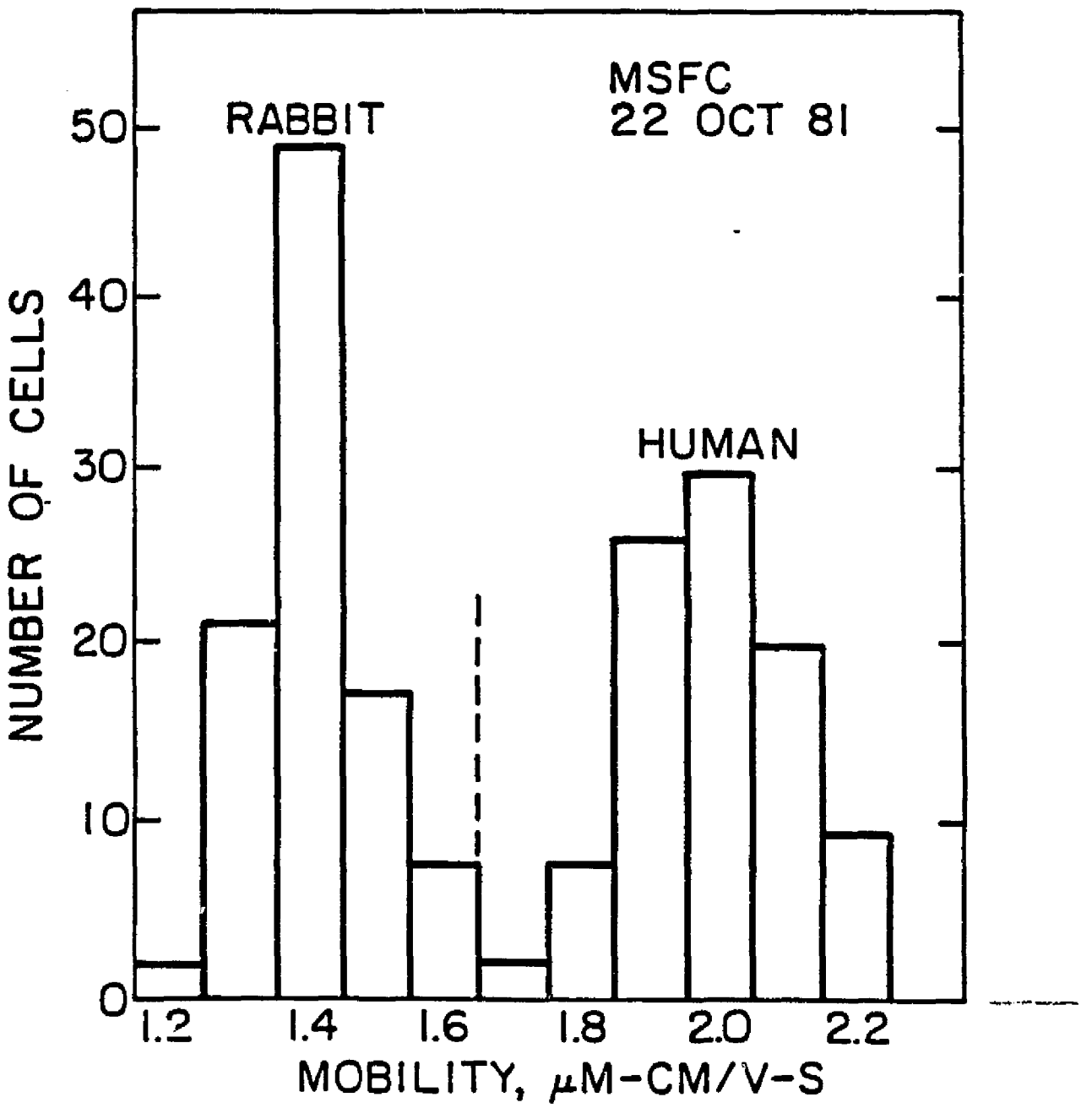

Figure 1. Electrophoretic mobility distributions of formaldehyde-fixed rabbit and human erythrocytes in D-1 buffer as determined using Marshall Space Flight Center's Rank microscopic electrophoresis apparatus by measuring velocities at the stationary position in a cylindrical chamber at 25 C.

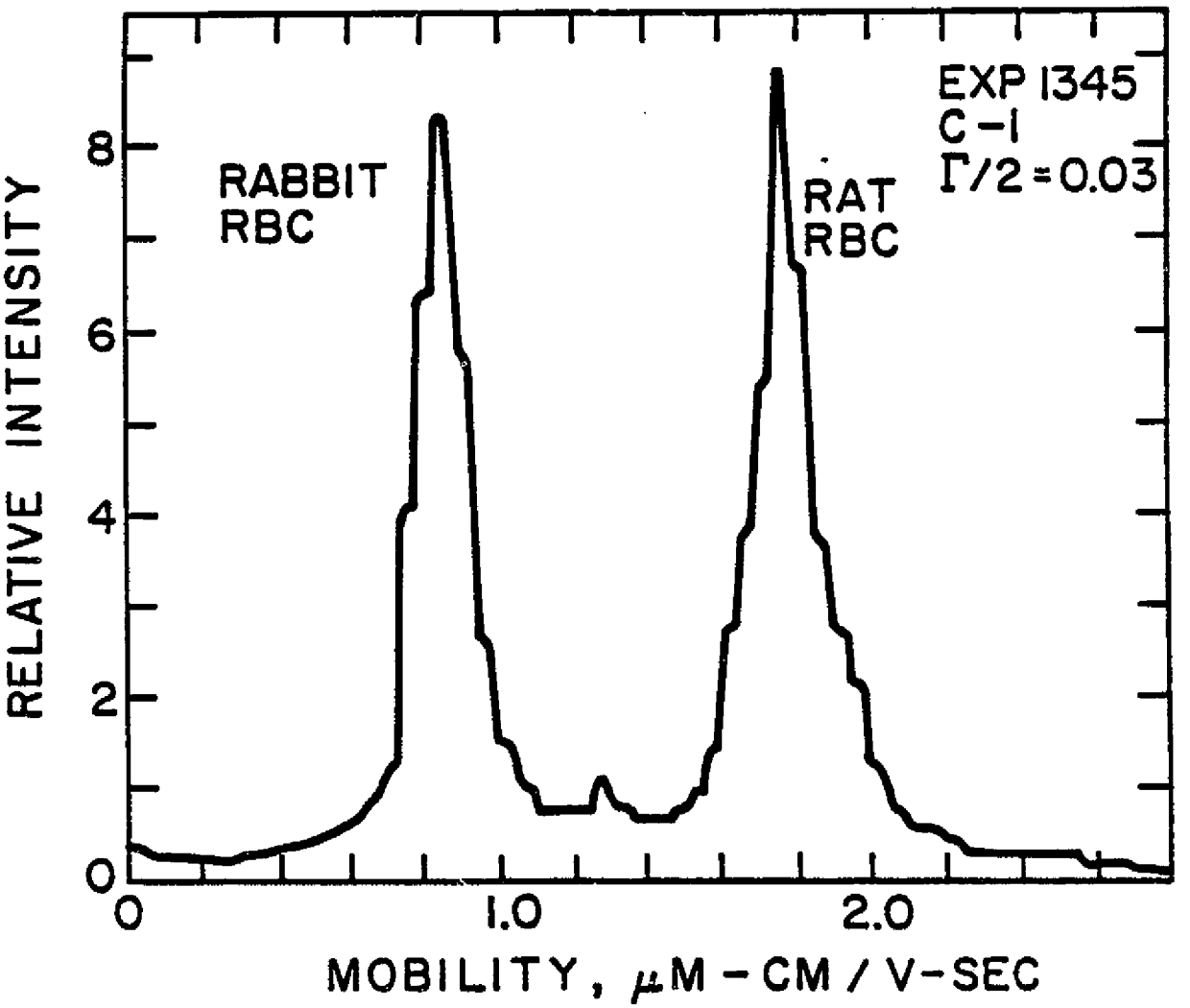

Figure 2. Electrophoretic mobility distribution of glutaraldehyde-fixed rat and rabbil erythrocytes mixed together in equal concentrations in C-1 buffer, measured using the Pen Kem "3000" automated laser light-scattering electrokinetic analyzer.

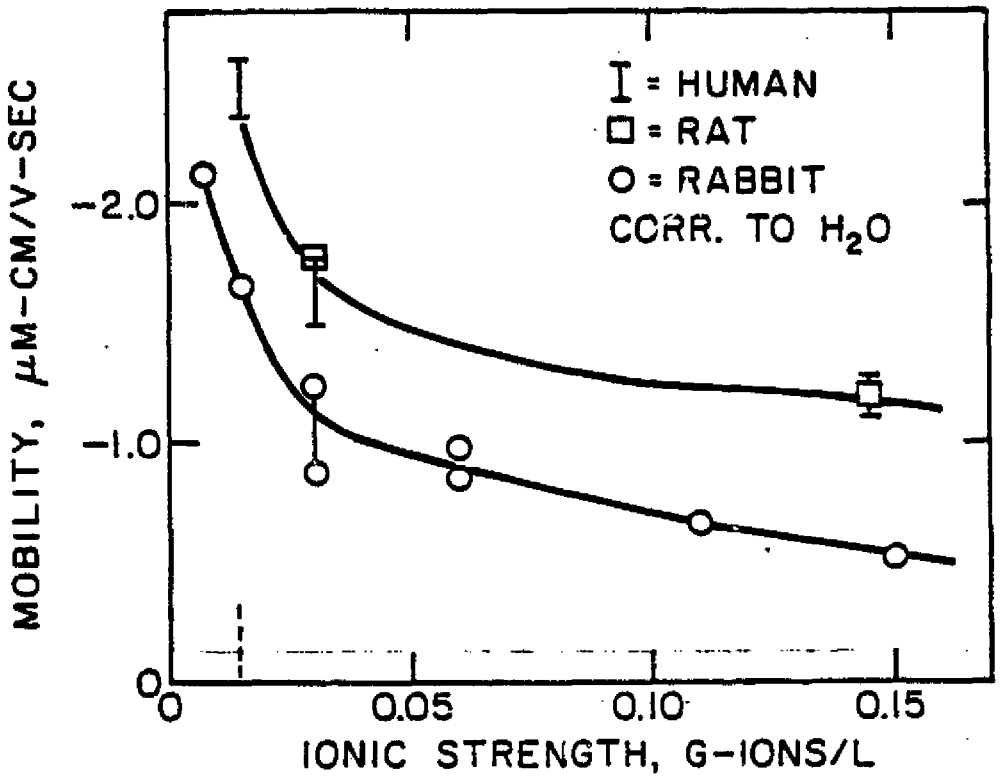

Figure 4. Electrophoretic mobility of fixed human, rat, and rabbit erythrocytes as a function of ionic strength in various buffers (Table 11) using pre-existing laboratory data.

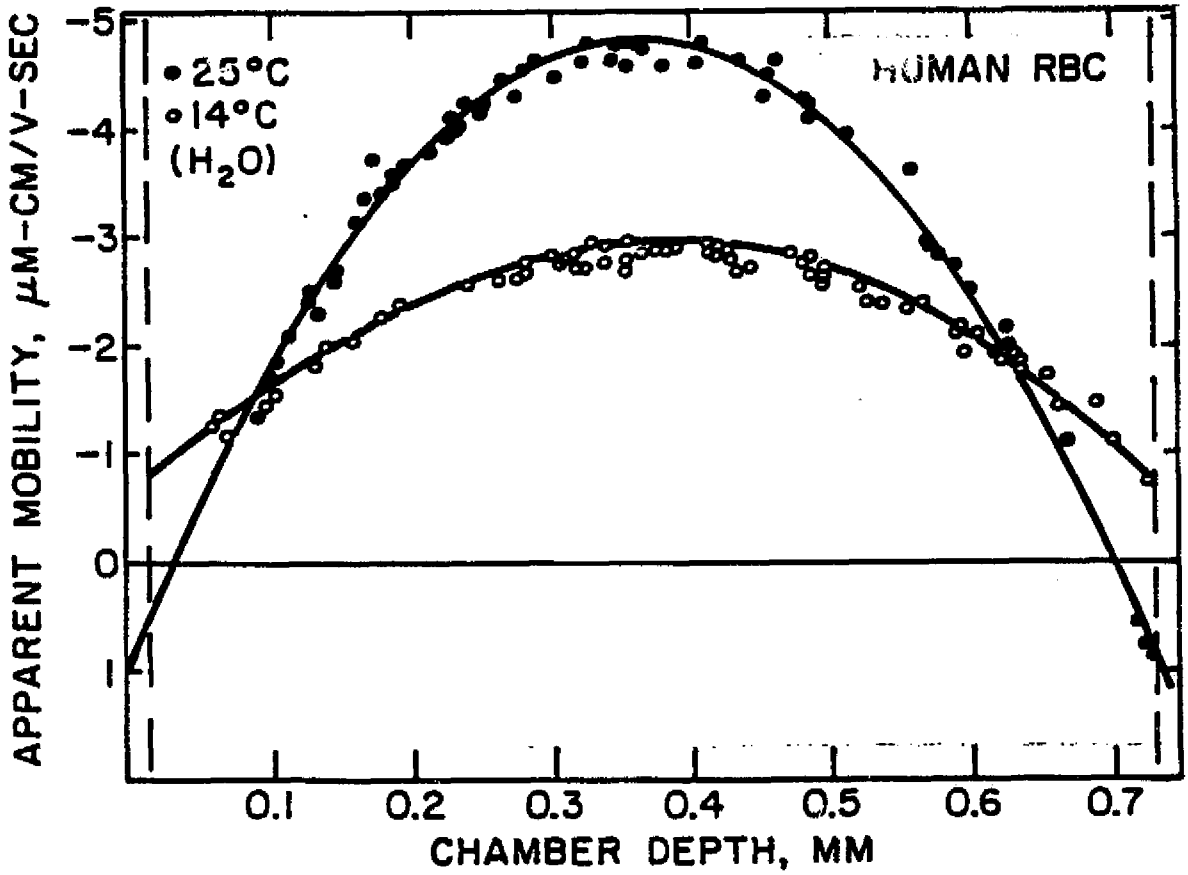

Figure 5. Mobility parabolas for glutaraldehyde-fixed human erythrocytes in D-1 buffer (1.0X) at two temperatures.

Chapter 13.

Effects of Method of Detachment on Electrophoretic Mobility of Mammalian Cells Grown in Monolayer Culture.

Effects of Method of Detachment on Electrophoretic Mobility of Mammalian Cells Grown in Monolayer Culture

L. D. Plank, M. E. Kunze and P. Todd

INTRODUCTION

A variety of proteolytic and mucolytic enzymes, mechanical procedures, and changes in the ionic environment, especially Ca^{++} chelation, have been routinely used for dispersal of monolayer-grown cells. If either chelating agens or mechanical dispersion are used alone, the cell yield is often low and suspensions of single cells are difficult to obtain. Confluent monolayers treated with EDTA tend to be released from their surfaces in sheets, and clumpts of cells remain even after further incubation in EDTA (Snow and Allen, 1967). Crude trypsin is the most popular dispersal agent and is known to contain a variety of contaminating enzymes (Rinaldini, 1958; Waymouth, 1974; Pine et al., 1969) which may contribute in many cases to the dispersal of cells (Pine et al., 1969). Reports of a variety of cell injuries resulting from the activity of proteolytic enzymes have appeared. These include adverse effects on cellular metabolism and viability (Berry et al., Gunther et al., Hebb and Chu, Weiss, 1958; Malucci, Konigsberg, Edwards, et al., Kellner et al.) as well as specific injury to the cell surface (Seaifecta, Lehmkuhlod, Haltzer et al.) Snow and Allen ( ) have reported the release of macromolecules containing bound amino sugars from cells in tissue culture after harvesting with crude trypsin, Crystalline trypsin, and EDTA. Further, crystalline trypsin was shown to be least harmful to cell integrity as judged by trypan blue uptake.

There is considerable evidence that both crude trypsin and crystalline trypsin treatment removes surface sialoglycopeptides from monolayer grown celsl (Snow and Allen, 1967; Shen and Ginsburg, 1969; Vogel, 1978) ascites tumor cells (Langley and Ambrose, 1964, 1967; Gasic and Gasic, 1962 a and b, Codington, 1970) and human (Cook et al., 1960) and beef erythrocytes (Walter et al., 1972). It is noteworthy that Cook et al., 1962) found no release of

sialic acids from Ehrlich ascites tumor cells after treatment with crude trypsin. EDTA treatment, however, does not release surface sialic acids from cells in tissue culture (Snow and Allen, 1970; Vogel, 1978) but is expected to remove calcium from the cell periphery (Weiss, 1967) (Borle, 1966).

Crude trypsin preparations from different sources are know to vary markedly in their compsoition with regard to contaminating enzyme activities (Speicher, 1977). A number of studies have investigated the effects of proteolytic enzymes and chelating agents on the e.p.m. of mammalian cells (Seaman and Ulntlerbreck, 1963; Tenforde, 1979; Hayry et al., 1965; Fike and van Oss, 1976; Brent and Forrester, 1967; Ponder, 1951; Seaman and Heard, 1960; Thompson et al., 1978; Thompson 1977; Molito 1977; Weiss 1966; Woo and Cater, 1972).

Crystalline trypsin has been shown to reduce the e.p.m. of human red blood cells by approximately 30% when measured in physiological saline (Seaman and Uhlenbruck, 1962, 1963; Ponder, 1951). Appreciable reduction in e.p.m. has also been observed in chimpanzee and dog erythrocytes whereas those of hose, ox, pig and sheep exhibited small decrements or no change (Seaman and Uhlenbruch, 1962, 1963).

In the case of monolayer cultures, adequate controls are difficult to achieve. Adherent cell types which also grow in suspension have been investigated by Brent and Forrester (1967) and by Fike and van Oss (1976). The former group concluded that EDTA dispersal of Hela cells probably does not affect the e.p.m. when measured at physiological ionic strength. Likewise, no significant change in the e.p.m. of RPMI 1846 cells after EDTA treatment was observed by Fike and van Oss (1976). These authors reported that crude trypsin, however, caused a significant increase in zeta potential and identical mobilities were reported for the treated suspension cells and for the trypsin

dispersed monolayer cells. A low ionic strength buffer (0.015 g.ions/l) was used in this work.

The effects of trypsin and EDTA dispersal on the e.p.m. of anchorage-dependent cells have generally been considered in comparison with a mechanical dispersal technique. Hayry et al. (1965) reported that the e.p.m. of Hela cells in physiological saline was reduced significantly after disaggregation with trypsin when compared with the mobility of mechanically dispersed cells which was similar to that obtained by EDTA dispersal. Simon-Reuss (1964) also compared the effects of scraping and crude trypsin dispersal on a variety of primary and continuous cell types. Mobility measurements in standard saline could not detect any significant differences between the two treatments. A novel approach was adopted by Fike and Van Oss (1976) who determined the zeta-potential of intact cell monlayers by measuring the electro-osmotic flow velocity in their capillary chamber on the inner surface of which a confluent layer of cells was present. Their results indicated that both EDTA and mechanical scraping caused no significant change in zeta potential but that trypsin dispersal resulted in an aprpeciable decrease in the two cell types examined.

In the present work, the effects on zeta potential of EDTA dissociation of monolayer cultures was compared with the effects of detachment by exposure to hypotonic medium followed by mechanical agitation. Gaffney and McElwain (19) had used briefe expsoure to hypotonic salt solution to selectively detach mitotic cells from monolayers. In our lab, all cultures were routinely subcultivated approximately 24 hours prior to harvesting so that subconfluent monolayers only were dispersed. This protocol enabled single cell suspensions to be obtained by EDTA treatment. In all the adherent cell cyptes examined crude trypsin dispersal resulted in signficantly decreased zeta potentials when

compared with dispersal by EDTA. This was true for low and intermediate values of buffer ionic strength as well as for physiological saline. Identical values of e.p.m. were invariably obtained after harvesting by trypsin compared with trypsin-EDTA. Two lines of evidence thus show that trypsin, not EDTA, modifies the charge composition of the cell periphery. In chinese hamster cell lines, the hyptonic medium removal method resulted in lower e.p.m. than that obtained for EDTA dispersal. Trypsan blue viability measurements indicated that the former method was more damaging to cellular integrity. EDTA and hypotonic medium dissociation of T-1E cells, however, resulted in similar mobility readings. After maintenance in spinner culture, following trypsin dispersal the e.p.m. was significantly higher than that of the EDTA dispersed cells. The effect of EDTA treatment on the spinner-maintained cells has not been investigated.

Measurements of e.p.m. provide an indixe of net surface charge density at the hydrodynamic slip plane of a cell (Briton and Lauffer, 1958). All studies ot date have shown that the vertebrate cell surface exhibits a neagative seta potential. Sialic acid groups have been implicated as an important determinant of this negative charge in many cell types (Seaman and Heard, 1960; Cook, Heard and Seaman, 1961; Wallach and Eyler, 1961; Forrester, Ambrose and MacPherson, 1962). The contribution from other anionic groups in the cell periphery will vary according to cell type and conditions of measurement. "The further away from the electrokinetic surface of a cell an ionized group is, the less will be its projected contribution at the plane of the zeta potential." Lowering the ionic strength of the buffer in which electrophoretic mobility determinations are made results in extension of the Debyi shielding distance which means that the net surface charge density measured is averged over a greater depth of the cell periphery (Seaman and Heart, 1960).

After incubation with trypsin-EDTA, the e.p.m. of the mouse lymphoma cells at intermediate ionic strength (0.03) was significantly higher than that of untreated cells. EDTA treatment had no appreciable effect on the e.p.m. of control cells. Weiss (1967) has remarked that this latter result could indicate that either the majority of the chelated calcium is bound to anionic groups in the glycocalyz whicha re appreciably deeper than 20A from the hydrodynamic shear plane, or univalent cations readily mask any superficial anionic sites revealed by calcium removal. Woo and Cater (1972) demonstrated that incubation of hepatoma ascites cells with trypsin resulted in a 22% reduction of mobility. Weiss 91966) found, however, no significant change in the mobility of murine sacroma 37 ascites cells after incubation with crystalline trypsin. Both these studies used physiological ionic strength buffers. Weiss (1967) has also observed the effect of EDTA incubation on the mobility of murine sarcoma cells and found no detectable change.

This study was undertaken to assess the effects of trypsin and EDTA dissociation on cellular electrophoretic mobility and viability in view of the importance of maintaining cell integrity and electrophoretic heterogeneity for preparative electrophoresis experiments. Primary human embryonic kidney cultures used in this work possess morphologically distinguishable subpopulations which may well be separable electrohoretically, as has been achieved for rabbit kidney cortex cells by Heidrich and Dew (1977) and Vandewalle et al. (1982). Although no consistent reduction in electrophoretic heterogeneity following trypsin treatment as compared with other treatments was observed in the present work, the greater surface charge alterations seen following trypsin dispersal could yet be detrimental to separation. The variability of different trypsin batches in enzyme composition and activity (Speicher) also may affect reproducibility of a separation protocol based on

surface charge differences. The apparently less severe effect of EDTA dispersal on the electrokinetic surface needs to be considered along with the reduced viability sometimes seen following this treatment.

MATERIALS AND METHODS

The electrophoresis buffer composition is given in Table 1. Cells were removed from subconfluent cultures by incubation in 0.37% EDTA in Puck's saline A (composition given in Table 2) or the same solution with 0.03% crude trypsin added. Cells were centrifuged out of these solutions and washed and resuspended in D-1 buffer for electroporesis. The Zeiss Cytopherometer with Cam-Apparatus electrodes was used to obtain mobility hisotgrams from the analysis of the complete cell flow parabola.

RESULTS

A parabola giving cell velocity vs. chamber depth is shown in Fig. 1., and the mobility histograms are shown in Fig. 2. Due to the small number of cells available for measurement in the chamber there is no statistically significant difference between the histogram obtained with cells dispersed with trypsin and EDTA and that for cells dispersed with EDTA only. In any case, trypsin treatment did not reduce the electrophoretic mobilities.

The combination of cell dispersal with EDTA and suspensions in D-1 buffer still does not lead to fully satisfactory viability. Table 4 summarizes the results of a preliminary experiment designed to test the ability of D-1 buffer on its own to disperse cells. This experiments was based on a recently announced finding that DMSO at 10% concentration disaggregates actin-containing microfilaments in epithelioid cells in culture. The results indicate that D-1 buffer does disperse cells, but that it might selectively suspend cells with

low viability, since the traditional method employing EDTA in Puck's saline A led to much higher viability, as measured by percent attachment in 24 hours. Variant of this experiment are to be performed in the near future.

Table 1. Composition of D-1 Buffer, Low Ionic Strength Medium for Cell Freezing and Electrophoresis.

COMPONENT	GRAMS/LITRE	MOLARITY
NaCl	0.380	0.00642
Na_2HPO_4	0.167	0.00176
KH_2PO_4	0.050	0.000367
Na_2EDTA	0.125	0.000336
Glucose	40.0	0.222
DMSO	50.0	0.64

Table 2. Composition of Puck's Saline A, Used as the Medium for Cell Dispersing AGents Trypsin and EDTA

COMPONENT	g/ℓ
NaCℓ	8.00
KCℓ	0.40
$NaHCO_3$	0.35
$Na_2HPO_4 \cdot 7H_2O$	0.09
KH_2PO_4	0.06
Na_2EDTA	0.20
Glucose	1.00
Phenol red	0.01

Table 4. Effect of Method of Cell Removal on Viability (attachment in 24 hr) of Strain HFK-15 (Passage 5) Cells Plated in BME + 10% Newborn Calf Serum (Experiment 1212)

DISPERSING SOLUTION	INCUBATION TIME, 37°C	% ATTACHED IN 24 HR	DENSITY IN 24 HR
D-1 buffer	10 min	46	Sparse
0.37% EDTA in Puck's Saline A	20 min	85	Confluent

Figure 1. Cell velocity vs. distance from the front wall of the Zeiss cytopherometer electrophoresis chamber. Cells are HFK-15, passage 5, resuspended with 0.03% trypsin and 0.37% EDTA in Puck's saline A.

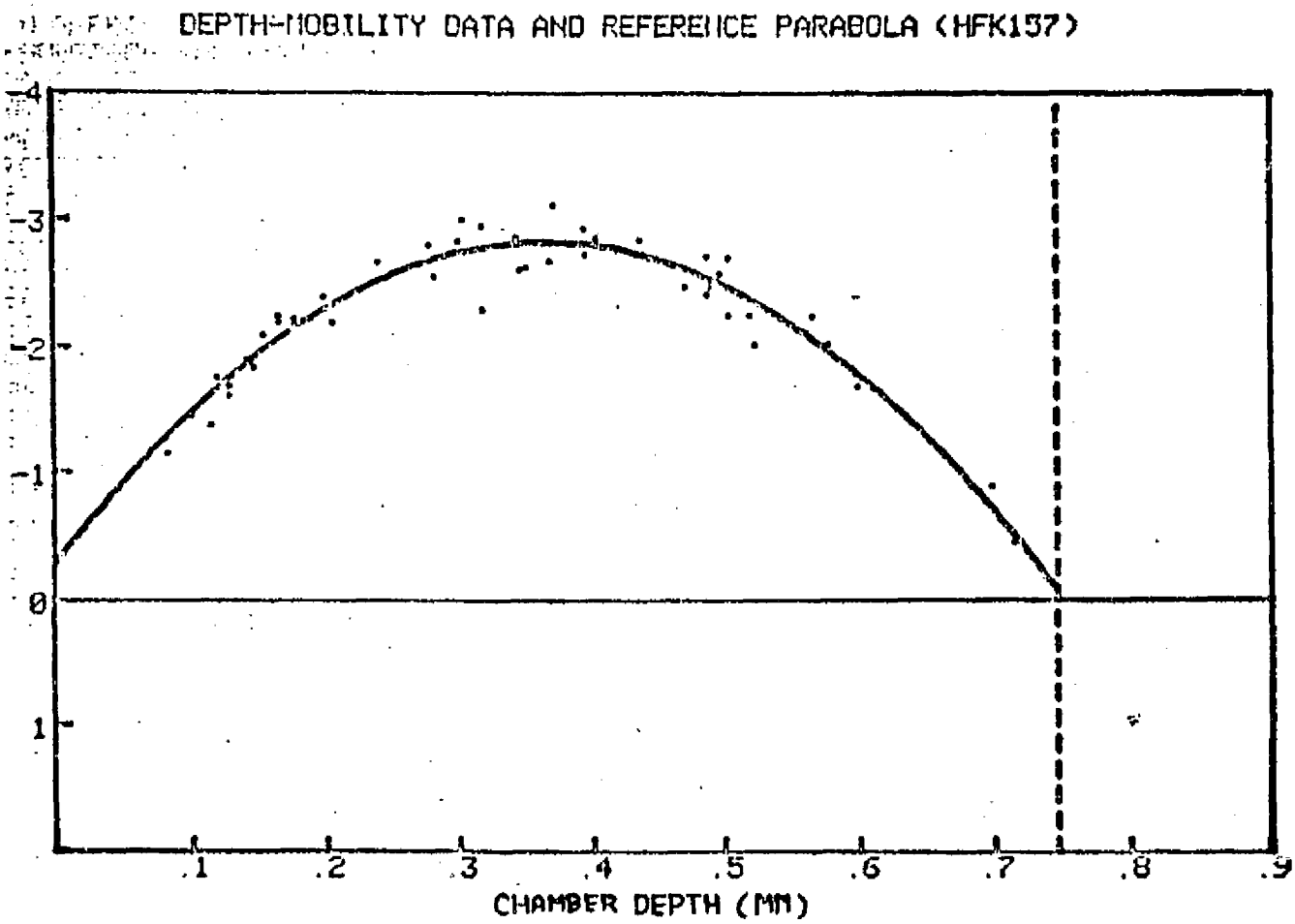

Figure 2. Electrophoretic mobility histograms of HFK15 cells, passage 5, in D-1 buffer after suspension in EDTA or EDTA plus trypsin.

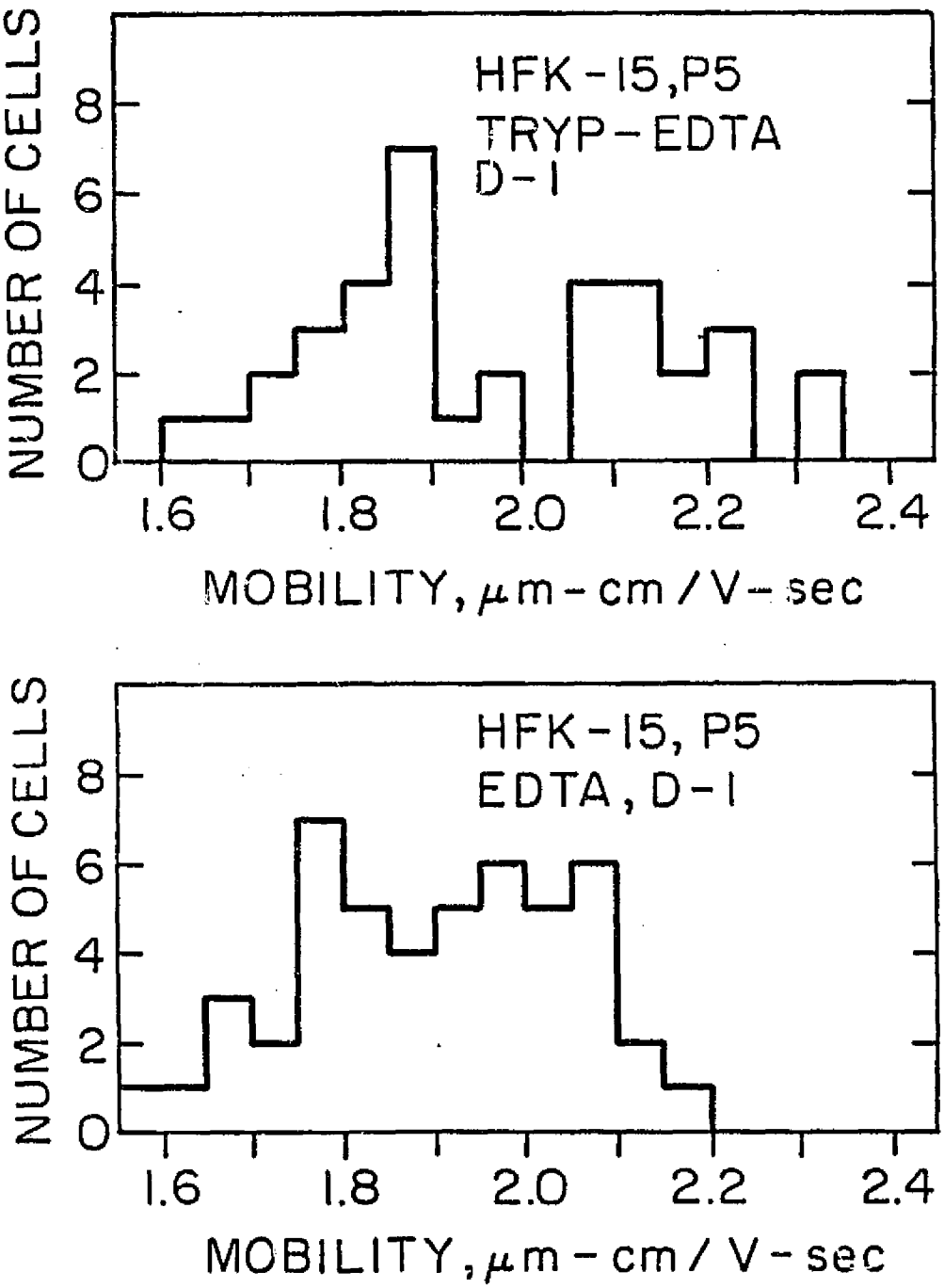

Chapter 14.

Density Gradient Electrophoretic Separation of Living Mammalian Cells: Effect of Position in the Cell Cycle.

PREPARATIVE ELECTROPHORESIS OF CULTURED HUMAN CELLS: EFFECT OF CELL CYCLE PHASE

M. E. Kunze, P. Todd, C. Goolsby, and J. T. Walker

ABSTRACT

Human epithelioid T-1E cells were cultured in suspension and subjected to density gradient electrophoresis upward in a vertical column. Three lines of evidence indicated that the most rapidly migrating cells were at the beginning of the cell cycle and the most slowly migrating cells were at the end of the cell cycle. The most rapidly migrating cells divided 24 hr later than the most slowly migrating cells. Colonies developing from slowly migrating cells had twice as many cells during exponential growth as did the most rapidly migrating cells, and the numbers of cells per colony at any time was inversely related to the electrophoretic migration rate. DNA measurements by fluorescence flow cytometry indicated that the most slowly migrating cell populations were enriched in cells that had twice as much DNA as the most rapidly migrating cells. It is concluded that electrophoretic mobility of these cultured human cells declines steadily through the cell cycle and that the mobility is lowest at the end of G_2 phase and highest at the beginning of G_1 phase.

INTRODUCTION

Changes in cell shape (1), surface interactions (2), and surface composition (3) through the cell cycle imply that significant cell surface modifications occur. Presumably some aspects of these surface modifications are manifested in the form of surface charge density changes that are detectable by cell electrophoresis. The electrophoresis of synchronized cells requires large numbers of narrowly-synchronous cells in suspension with undamaged surfaces. Such cell populations are extremely difficult

to obtain. An early attempt at synchronous cell electrophoresis was made by Brent and Forrester (4) who collected mitotically detached HeLa cells from mitotically-enriched (5) populations in monolayer culture. The mitotically-collected cells had a much higher electrophoretic mobility (EPM) than did asynchronous cells growing in suspension (see Table 1). Subsequent cultivation of asynchronous cells in suspension led to a decrease in EPM, which rose again at the time of the next synchronous mitosis. These experiments were performed by microscopic electrophoresis at ionic strength approximately 0.16 M.

Nearly all other experiments on the EPM of synchronous cells have been performed using suspension-grown cells. Mayhew and O'Grady partially synchronized RPMI 41 sarcoma cells by double thymidine block and measured EPM as a function of time. A mitotic peak occurred 14-17 hr (15% mitotic cells) after thymidine release, and at this time EPM was highest, about -1.3 μm-cm/V-sec (see Table 1). During DNA synthesis cells had mobilities similar to or lower than asynchronous cells. After cell division the mobility fell sharply (6,7) and appeared to rise again around G_2 or the next mitosis. Neuraminidase-treatment of double-thymidine and cold-shock synchronized cells eliminated the cyclic variation of EPM (7). Shank and Burki (8) reported that the EPM of L5178Y mouse lymphoma cells synchronized in suspension by sequential thymidine and colcemic blockades did not change through the cell cycle (see Table 1). They suggested that cells that are normally non-adherent have no need to change surface features through the cell cycle, so EPM may also be expected to remain constant. However, Gersten and Bosmann (9) studied the same cells with the same synchronizing procedure but measured EPM at much lower ionic strength and found that EPM fell from a maximum of -2.0 during G_1 phase to a constant value of about -1.7 during S phase and rose again at the next cell division.

Despite rather substantial differences in the cell systems studied to date, it is possible to discern a mild concensus in the findings. EPM is highest at one or both ends of the cell cycle. By examining the published data it can be seen that EPM is definitely high at the very beginning of the cell cycle (early G_1), but it is less certain that EPM is high at the end of the cycle, sinceall experiments reported to date report measurements made after considerable desynchronization and hence in the presence of early G_1 cells. All cell synchronizations were also accomplished by the use of abnormal metabolic conditions, such as excess thymidine S-phase blockade, colcemid M-phase blockade, and cold shock.

In view of the above state of affairs and our own research objectives, the study of radiation effects on EPM, a series of experiments was undertaken to determine whether human T-1E cells experienced modulation of EPM throgh the cell cycle, whether cyclic changes in EPM occur in the absence of metabolic synchronization, and, if so, whether EPM is high at both or only one end of the cell cycle. To achieve these objectives, asynchronous T-1E cells were grown in suspension without metabolic synchronization and subjected to preparative density gradient electrophoresis, subsequent to which individual electrophoretic subpopulations of cells were subjected to DNA distribution analysis by fluorescence flow cytometry.or growth analysis to determine position in the cycle following electrophoresis.

MATERIALS AND METHODS

Human T-1E cells were maintained as monolayer cultures in Eagle's Minimum Essential Medium according to routines previously described (10). In preparation for experiments, suspensions were prepared using 0.03% crude trypsin in Puck's Saline A, and cells were diluted to 3×10^5/ml in complete medium and transferred to spinner flasks for cultivation in

24 hr. These asynchronous cells were centrifuged out of the complete medium and resuspended in electrophoresis buffer (11) for electrophoretic separation at low (0.030 M) ionic strength in a Ficoll gradient (11). After electrophoresis for approximately 2.5 hr at 19 mA, cells were collected, usually under sterile conditions, in fractions pumped out the top of the column. In some instances cells were then cultured in monolayers for growth or colony formation measurements, and in some instances cells were fixed and stained for flow cytometry (12). Growth curves were determined by periodic counting of the number of cells in each of about 100 colonies by phase contrast microscopy as a function of time after plating cells in 60 mm culture dishes, as previously described (13).

RESULTS

When human T-1E cells were subjected to density gradient electrophoresis and collected in 3-drop fractions (high resolution) the electrophoretic profile given in Figure 1 was found. The circles indicate the number of visible colonies formed in each culture prepared from the individual fractions by collecting three drops of column effluent directly in 60 mm culture dishes with 5.0 ml of complete medium. The plotted dots represent the ratio of colonies formed to cells per unit area in the starting culture prepared from each fraction. The electrophoretic profile is a broad double- or triple-peaked distribution, but there is not clear trend in plating efficiency vs. fraction number. When selected fractions were examined microscopically for the determination of average number of cells per colony it was found that the rapidly migrating fractions (40-50) had fewer cells per colony than did slowly migrating fractions (60-68) during logarithmic phase growth (65.5 hr after plating). Furthermore, the number of cells per colony at this stage increased with fraction number in a regular

fashion between fractions 50 and 60. In other words, more slowly migrating cells gave rise to larger colonies. These results are seen in Figure 2. The slowly-migrating cells could give rise to more rapidly growing colonies or colonies that enter logarithmic growth sooner. The complete growth curves of selected fractions, given in Figure 3, indicate that the growth rates do not differ significantly, but the growth curve of the most slowly migrating fraction (dots) leads the growth curve of the most rapidly migrating fraction (circles) by as much as 18 hr. The more accurate growth curves from a lower-resolution electrophoresis experiment, given in Figure 4, confirm this finding. Cells from slowly-migrating fractions multiply sooner, but not faster, than cells from rapidly-migrating electrophoretic fractions.

Growth curves of asynchronous T-1E cells determined by counting cells per colony can be analysed to show that large colonies correspond to cells plated in the later part of the cycle (G_2 phase, for example), and small colonies correspond to cells plated in the G_1 phase. Thus Figure 5 shows that the growth curve for the 20% largest colonies in a population starts with a delay of 0-2 hr, and the growth curve for the 20% smallest colonies in a population starts with a delay of 19-23 hr (about one cycle time). The smallest colonies started growth with a division delay of about 1 cycle, implying that they had to pass through nearly a full cycle before dividing. It is deduced from this type of analysis that, in normal cultures, large colonies correspond to single cells plated in G_2 phase, and small colonies correspond to cells plated in early G_1 phase. This principle was applied to growth curves of cells from specific fractions distributed throughout the high-resolution electrophoretic profile shown in Figure 6, and it can be seen in Figure 7 that the most

rapidly migrating cells were the last to divide (fraction 15), while the most slowly migrating cells divided first (fraction 33).

In a similar series of experiments growth curves were determined with greater time resolution during the first two cell cycles after electrophoresis, and Figure 8 shows that evidence for synchronous waves of division exist and that they occur at different times in cells from different electrophoretic fractions; in slowly migrating fractions they occur before they do in rapidly migrating fractions.

When collected fractions were subjected to DNA analysis by flow cytometry it was found that rapidly migrating fractions (high apparent mobility fractions in Figure 9) were nearly devoid of G_2 cells and very low in S cells, but slowly-migrating fractions (0.5 - 0.6 apparent mobility units in Figure 9) were enriched in G_2 cells. These differences are seen more clearly in Figure 10, in which fractions 16 (high mobility) and 22 (low mobility) are compared on the same scale.

To determine whether or not this finding of electrophoretic enrichment of cells in specific phases of the cell cycle applies to other cell types, experiments were also performed in which mouse lymphoma L5178Y cells were grown in logarithmic phase in Fischer's medium (14) with 10% newborn calf serum, subjected to density gradient electrophoresis, and analysed for DNA content by flow cytometry. In complete analogy with Figure 10 for T-1E cells, these cells also shown electrophoretic enhancement of G_1 cells in rapidly migrating fractions and of G_2 cells in slowly migrating fractions.

DISCUSSION

The migration rate of cells in density gradient electrophoresis depends upon their position in the cell cycle, and rapidly migrating fractions are clearly enriched in early G_1 cells, while slowly migrating fractions are enriched in G_2 cells. Preliminary evidence indicates that this principle applies to more than one cell type. The results of the density-gradient electrophoretic studies are consistent with the hypothesis that EPM is highest at the beginning of the cell cycle, as shown in several previous reports (4,6,7,9). Published results, strictly interpreted, do not indicate a rise in EPM during G_2 phase, and the present results are consistent with lowest EPM occurring at G_2 phase.

Density-gradient electrophoresis differs from microscopic analytical electrophoresis in many ways, including the necessity to use low ionic strength buffers and the presence of the sedimentation component in the cell migration velocity. Although provisions are made for the gradient to be very close to neutral buoancy throughout the separation process, it is possible that sedimentation plays a significant role cell separation by this method, and this possibility is under continuing investigation.

Table 1. Summary of published experiments in which EPM was measured on synchronized cultured mammalian cells.

Cell Type	Conditions	Buffer	Mobility	Ref.
HeLa	Asynchronous, suspension	0.146 M NaCl 0.01 M PO_4	-0.98±0.06	(4)
	Asynchronous, EDTA from monolayer	0.01 M PO_4	-1.06±0.10	(4)
	Synchronous, mitotic	0.01 M PO_4	-1.41±0.11	(4)
	Synchronous, mitotic, EDTA-treated	0.01 M PO_4	-1.36±0.10	(4)
RPMI 41	Asynchronous	50% HBSS + 5% sucrose	-1.05±0.02	(6)
	Mitotic (15% in M)	50% HBSS + 5% sucrose	-1.29±0.03	(6)
L5178Y	Synchronized or asynchronous, throughout cycle	M/15 PO_4	-1.12	(8)
L5178Y	Mitosis and early G_1 phase	.0145 M NaCl 0.6 mM $NaHCO_3$ 4.5% sorbitol	-2.0	(9)
	S-phase	4.5% sorbitol	-1.7	(9)

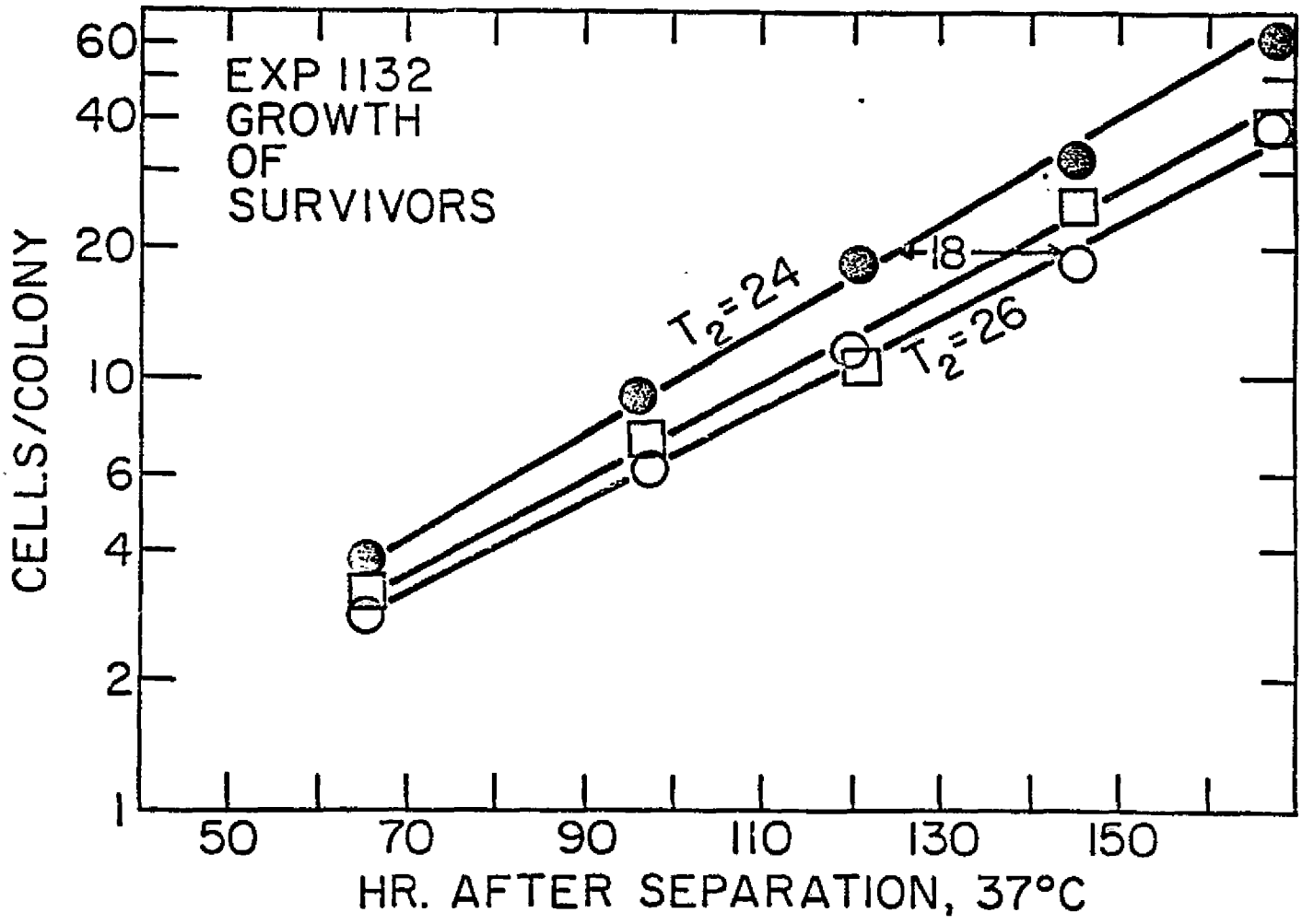

Figure 3. Growth curves determined in cultures obtained from selected fractions from the electrophoretic separation experiment described in Figure 1. Dots correspond to slowly migrating cells, and circles correspond to rapidly migrating cells. T_2 = doubling time in hr.

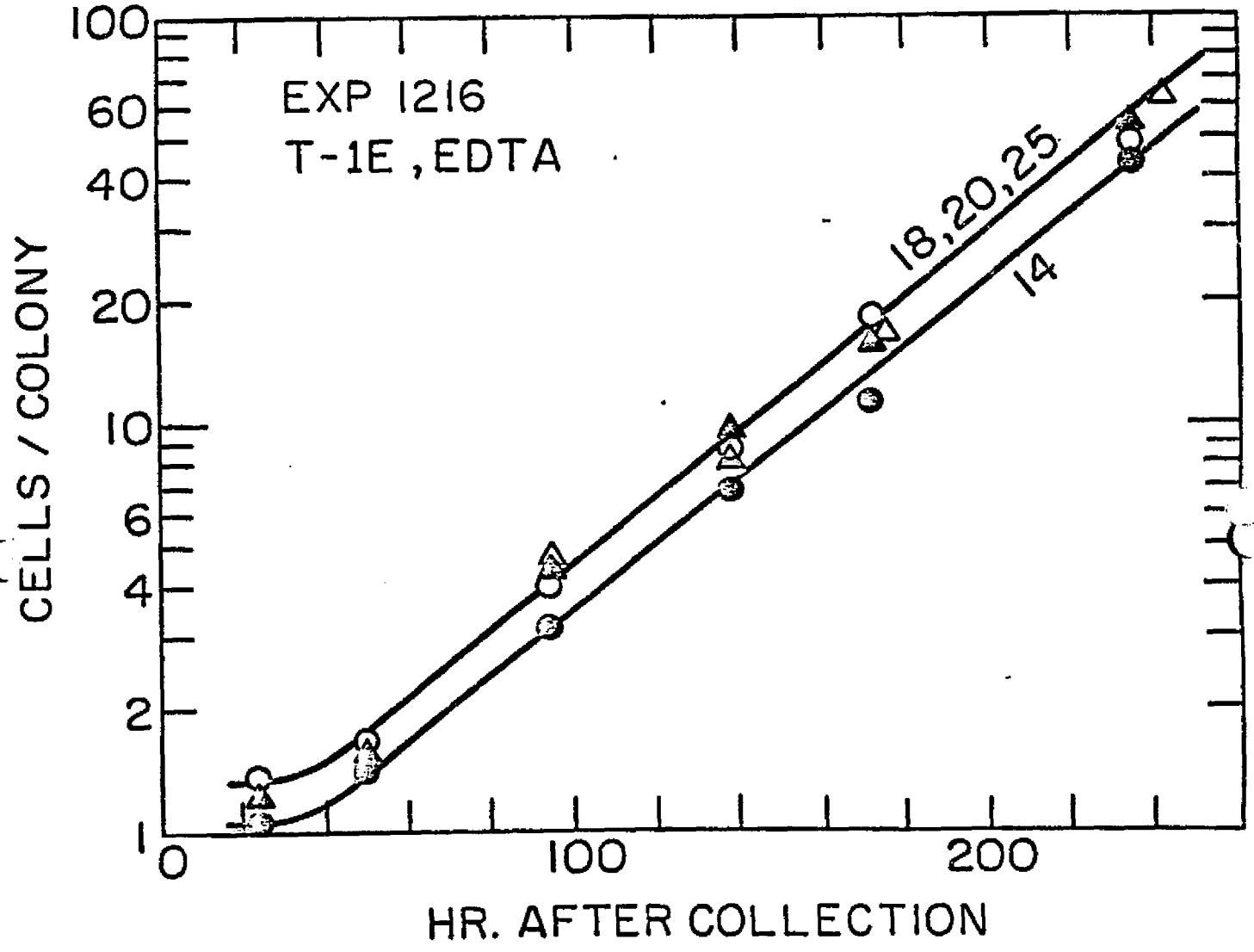

Figure 4. Complete growth curves of cells obtained from four electrophoretic T-1E cell fractions. The most rapidly migrating fraction (14) grew at the same rate as cell from other fractions, but with a delay.

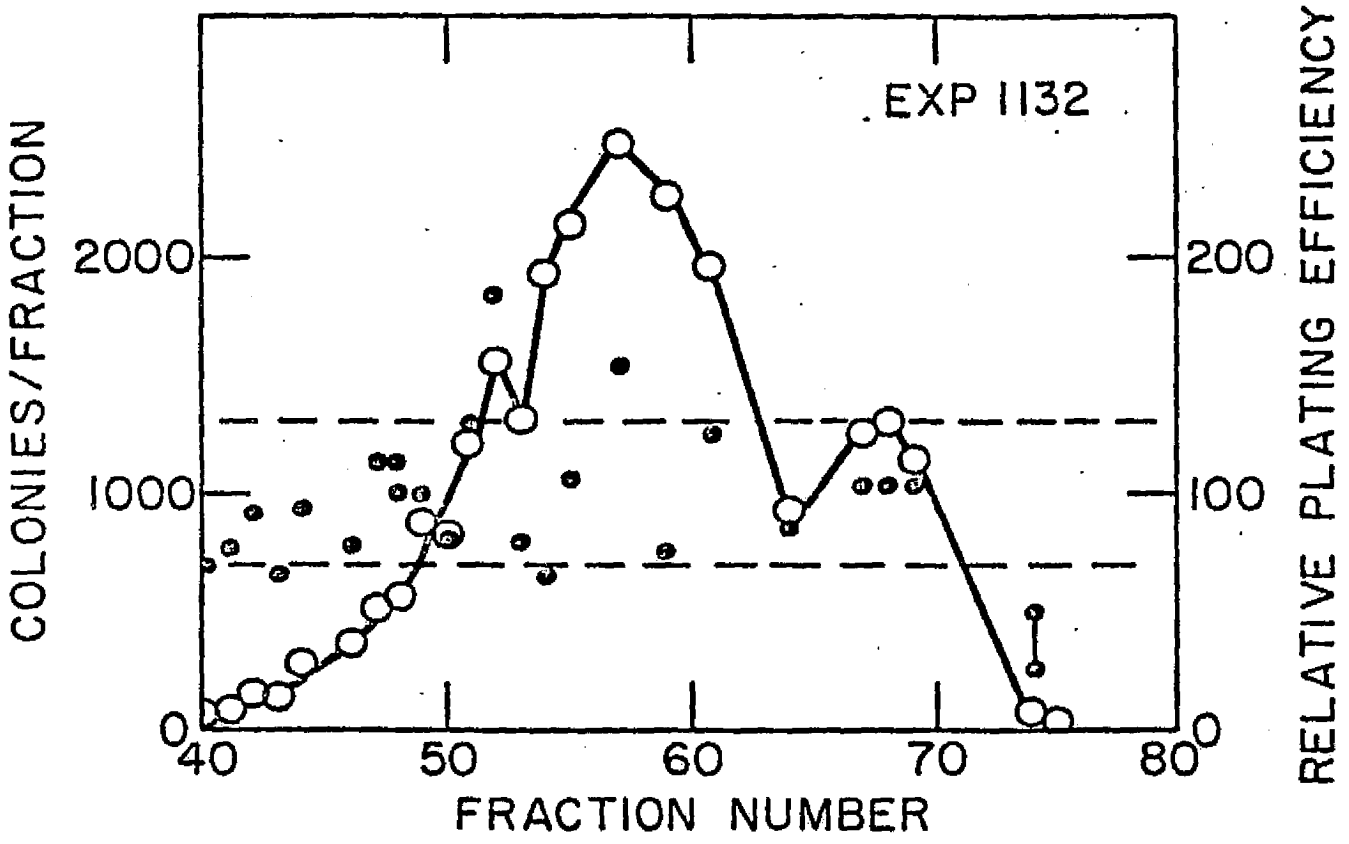

Figure 1. Electrophoretic profile of colony-forming T-1E cells (circles) collected from the density gradient electrophoresis column. Dots show relative values of colonies formed per cell per unit area in initial cultures, and dashed lines mark the standard deviations of this relative ratio. Electrophoresis was from right to left, so low fraction numbers correspond to rapidly migrating cells, and this condition applies to all subsequent figures.

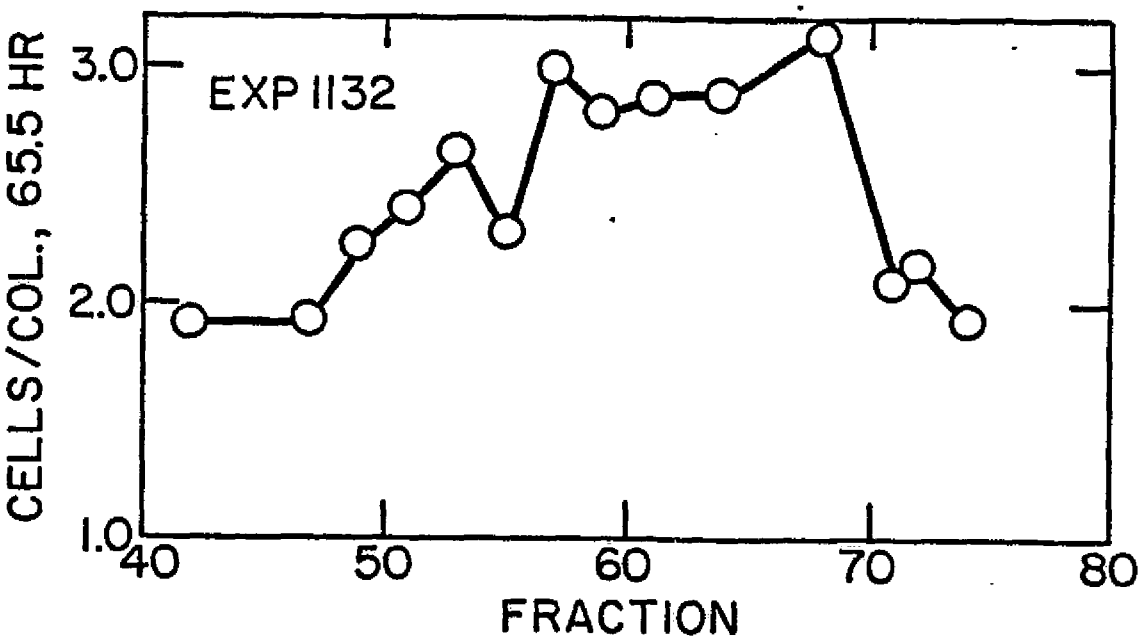

Figure 2. Cells per colony 65.5 hr after collection of cells from the electrophoretic separation described in Figure 1. With the exception of the extremely slow cells, rapidly migrating cells had fewer cells per colony that slowly migrating cells.

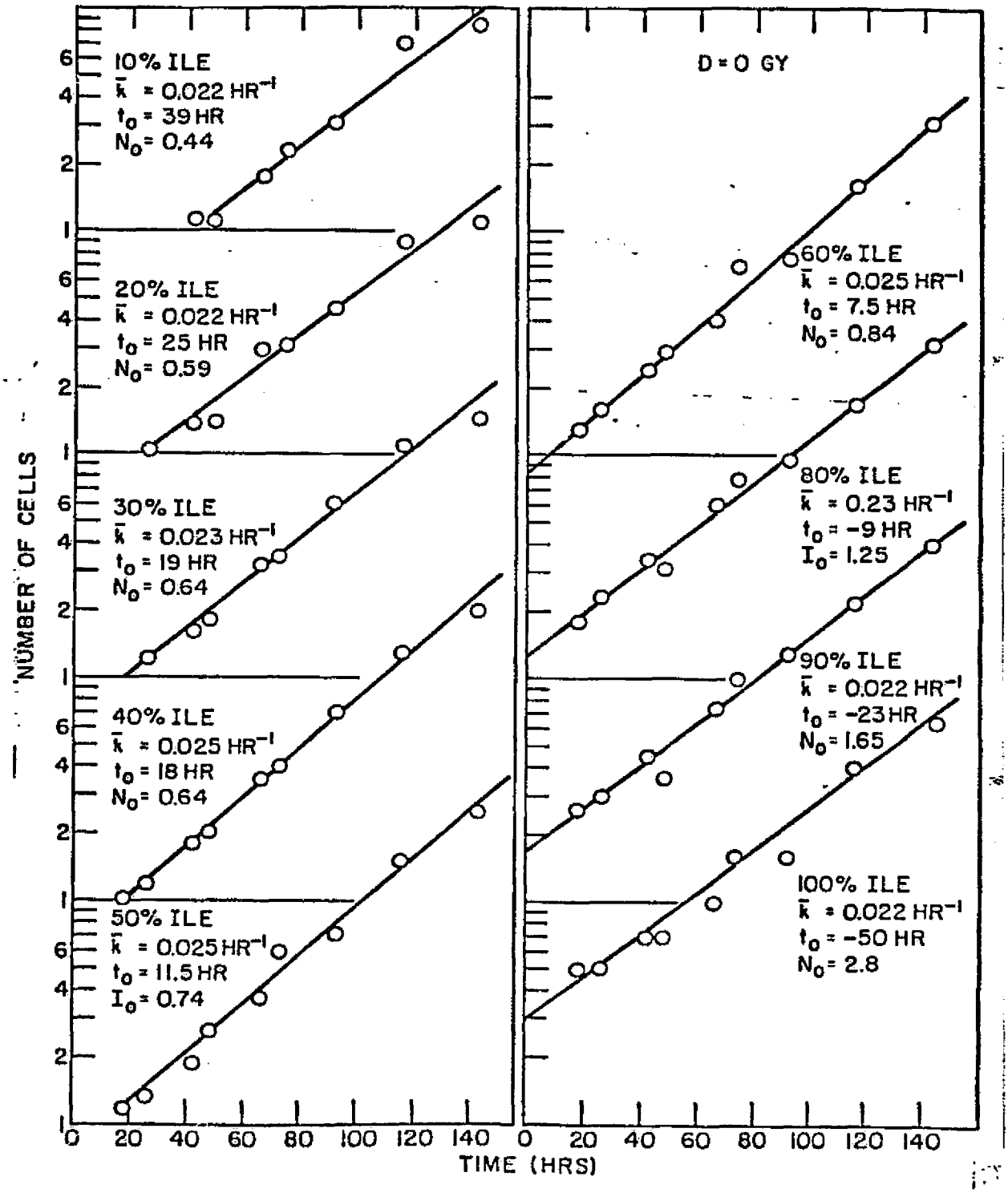

Figure 5. Growth curves of colonies of T-1E cells according to percentile colony size. Smaller colonies grow at the same rate but begin growth at different times.

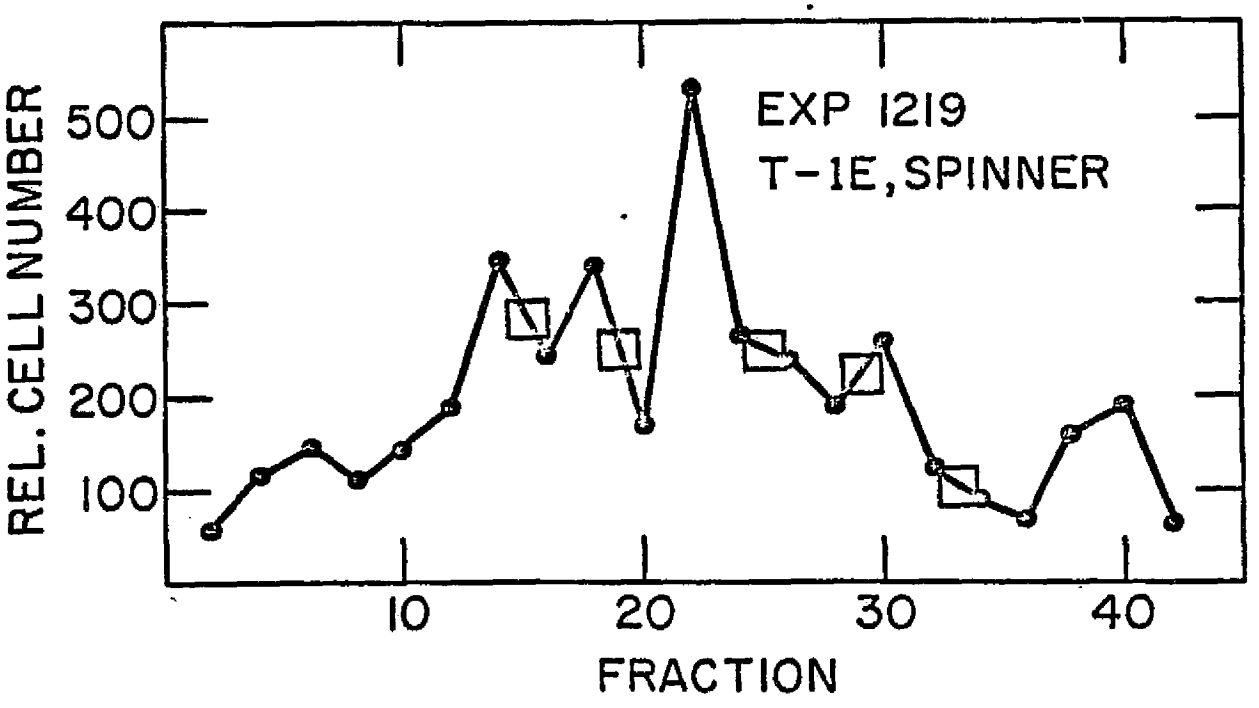

Figure 6. Density gradient electrophoretic separation of human T-1E cells at high resolution. Cell numbers were determined by Coulter counting, and squares represent the positions of the 5 fractions used in the determination of the 5 growth curves of Figure 7.

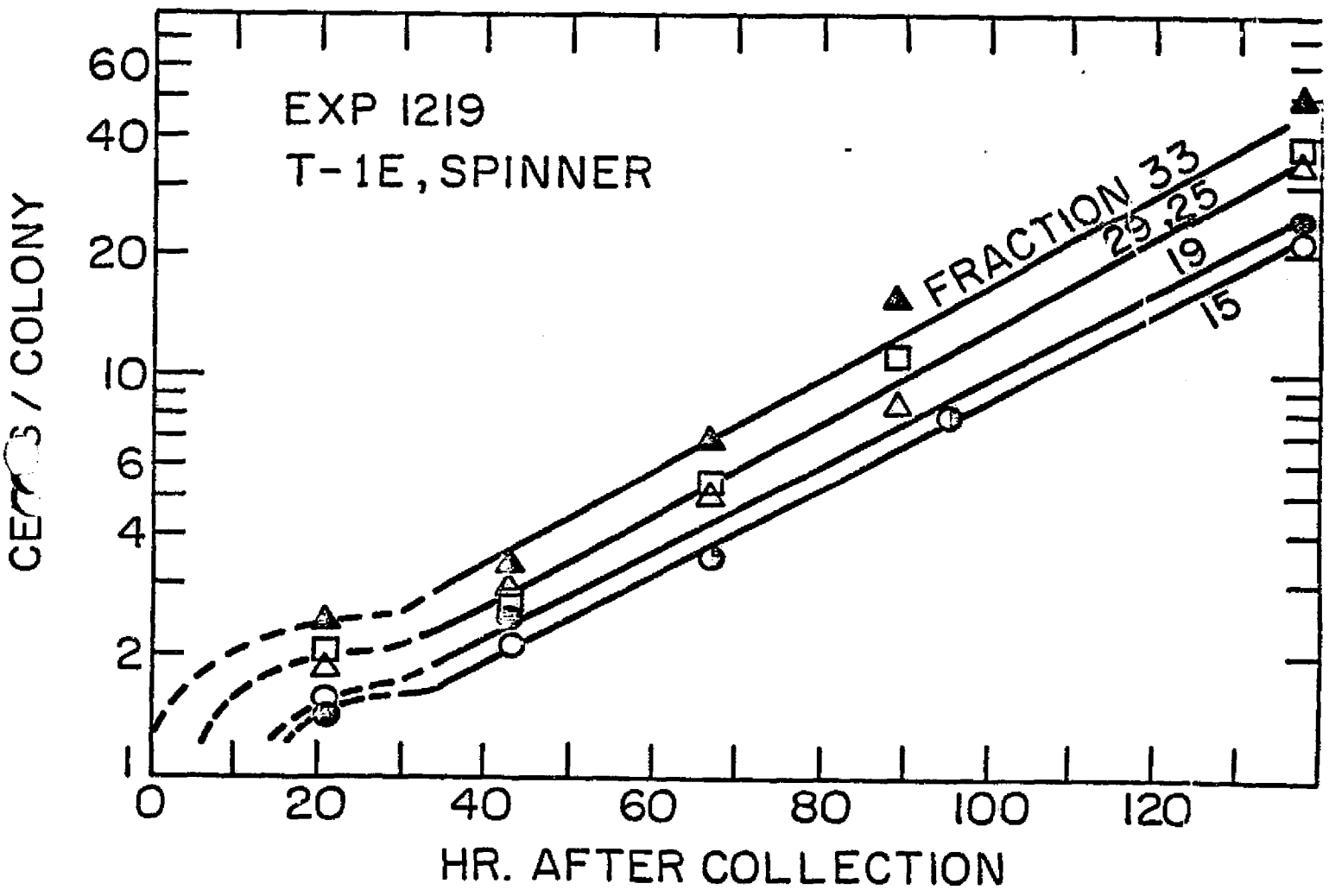

Figure 7. Growth curves of 5 electrophoretically separated fractions of T-1E cells (see Figure 6). Cells from all fractions grew at the same rate but began growth at different times.

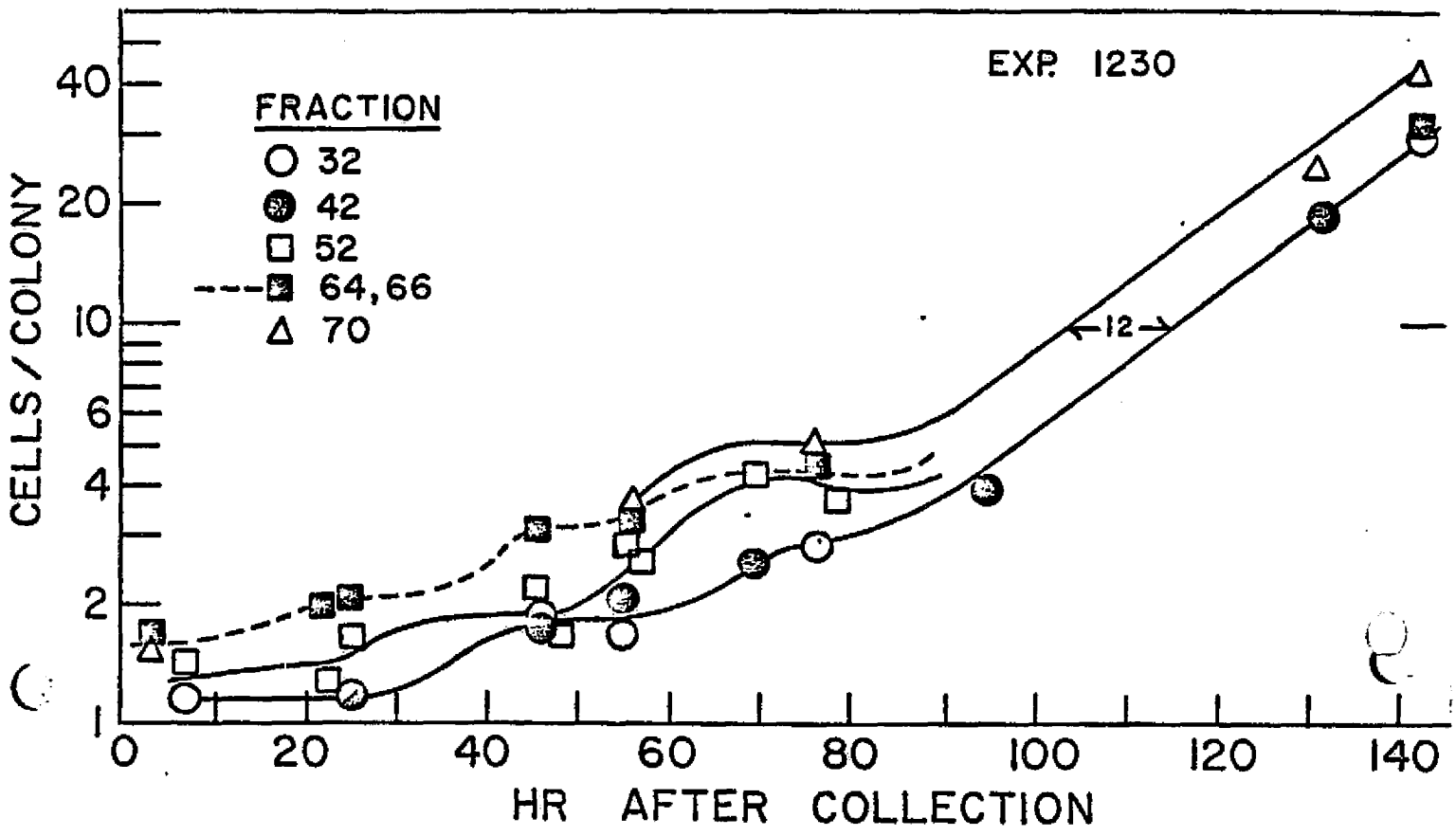

Figure 8. Early growth of cells from 5 fractions of electrophoretically separated human T-1E cells. Evidence for the first doubling in cell number occurs earliest in slowly-migrating fractions and latest in rapidly migrating fractions. Evidence for the second doubling in cell number follows the same pattern, and final extent of growth is correspondingly related to fraction number.

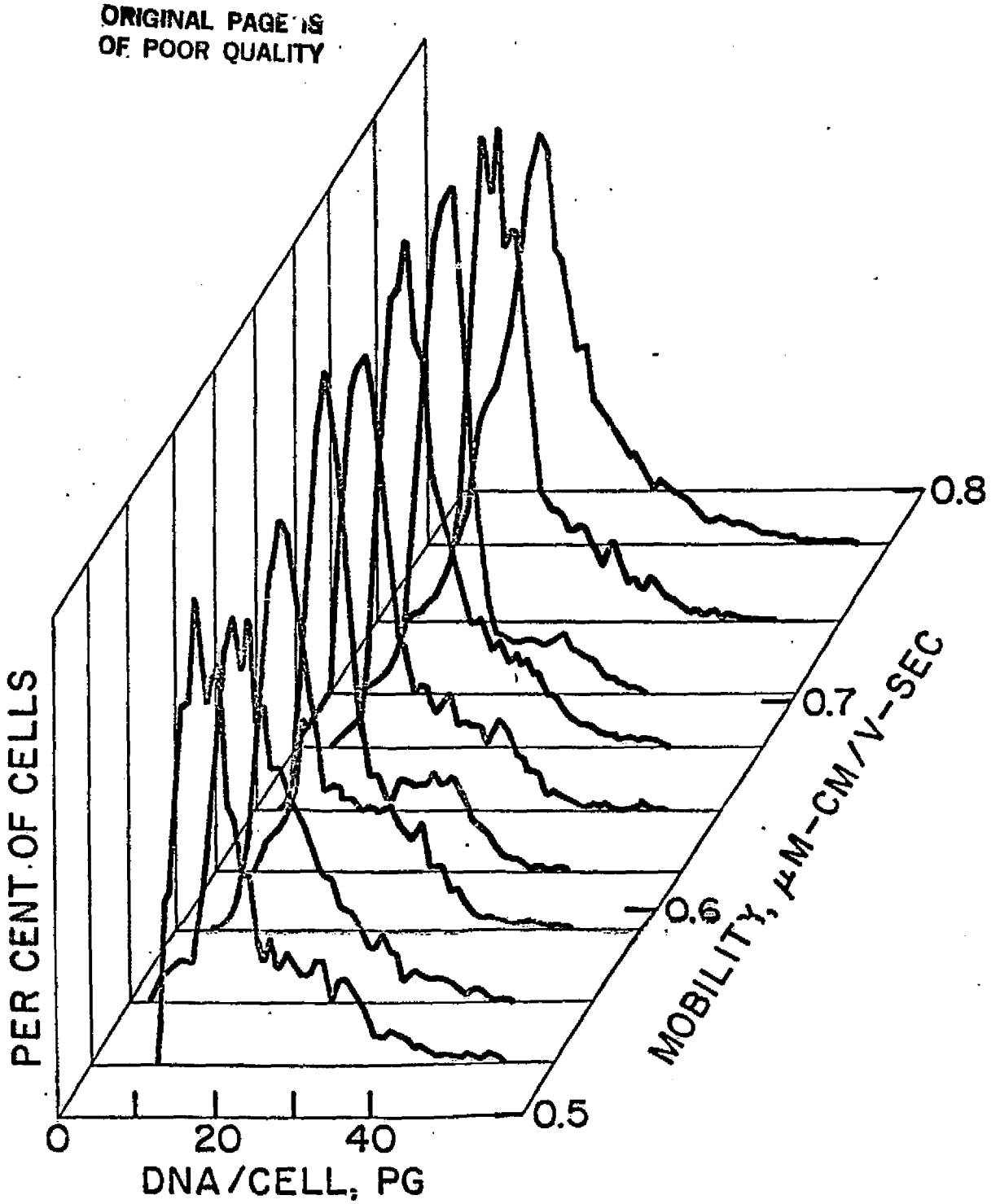

Figure 9. Cellular DNA distributions of 9 electrophoretic fractions of T-1E cells separated at low resolution. The mobility parameter is the uncorrected apparent value and not absolute mobility.

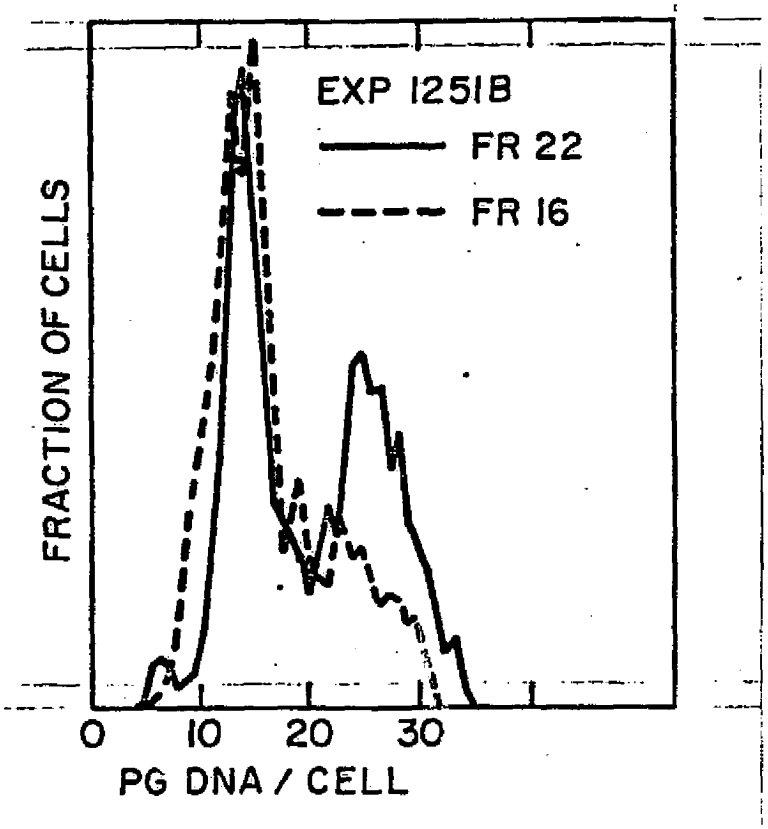

Figure 10. Direct comparison of cellular DNA distributions of fractions 16 and 22 (fast and slow, respectively) from the experiment of Figure 9. The slowly migrating fraction is enriched in, and the rapidly migrating fraction is depeleted of, G_2 cells.

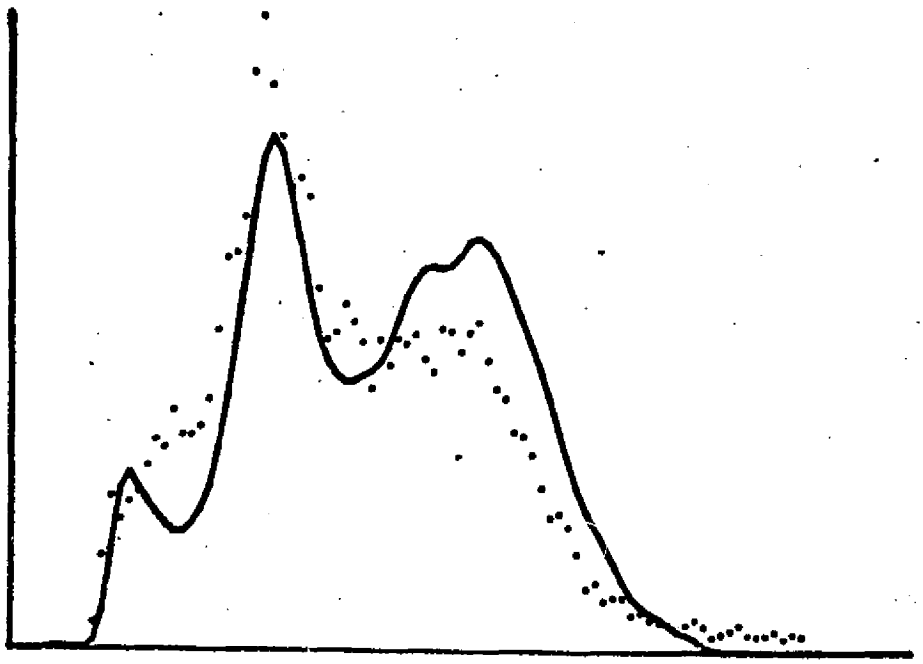

Figure 11. Comparison of cellular DNA distributions of rapidly and slowly migrating fractions of mouse lymphoma L5178Y cells after density-gradient electrophoresis. The slowly migrating fraction is enriched in G_2 cells (solid curve).

N85-31759

SIZE AND DNA DISTRIBUTIONS OF ELECTROPHORETICALLY SEPARATED CULTURED HUMAN KIDNEY CELLS

M. E. Kunze, L. D. Plank, and P. Todd

SUMMARY

The application of electrophoretic purification to the problem of purifying cultured cells according to function presumes that the size of cycle-phase of a cell will not be an overriding determinant of its electrophoretic velocity in an electrophoretic separator. Experiments were therefore performed in which the size distributrions and DNA distributions of fractions of cells purified by density gradient electrophroesis were determined. No systematic dependence of electrophoretic migraction upward in a density gradietn column upon either size or DNA content were found. In contrast, human leukemia cell populations, which are more uniform with respect to function and found in all phases of the cell cycle during exponential growth, separated on a vertical censity gradient electrophroesis column according to their size, which is easily shown to be strictly cell-cycle dependent.

RESULTS

In third-passage cultures of heterogeneous populations of human embryonic kidney cells (HFK-9) the size distributions of various electrophoretic fractions suggest that cell size and electrophoretic migration are not related in a systematic and significant way. See Figure 1.

In third-passage cultures of heterogeneous populations of human embryonic kidney cells (HFK-) the DNA distributions of various electrophoretic fractions suggest that cell cycle phase and electrophoretic migration are not related in a systematic and significant way. See Figure 2.

In third-passage cultures of homogeneous populations of human B lymphoma cells (line "RAJ") the DNA distributions of various electrophoretic fractions suggest that cell cycle phase and electrophoretic migration are related in a systematic and significant way. In other experiments it was determined that the effect of cell size on sedimentation velocity during upward migration is responsible for the slower migration of the larger, G2, cells. See Figure 3.

14-21 Figure 1. Coulter volume distributions indicate that there is no systematic variation in cell size with electrophoretic fraction number. Apparently sedimentation is not an important factor in the vertical separation of HFK cells.

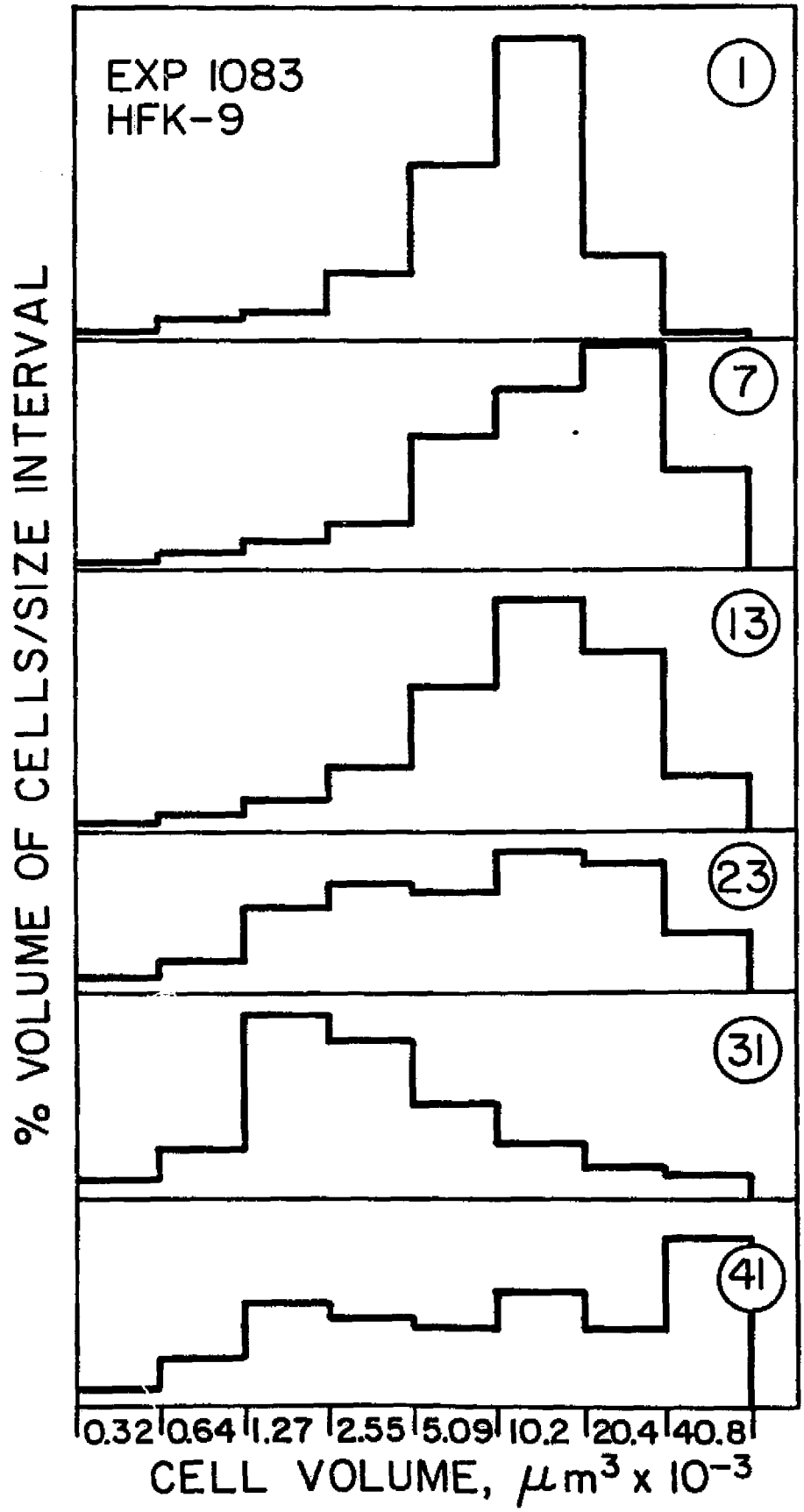

FIGURE @

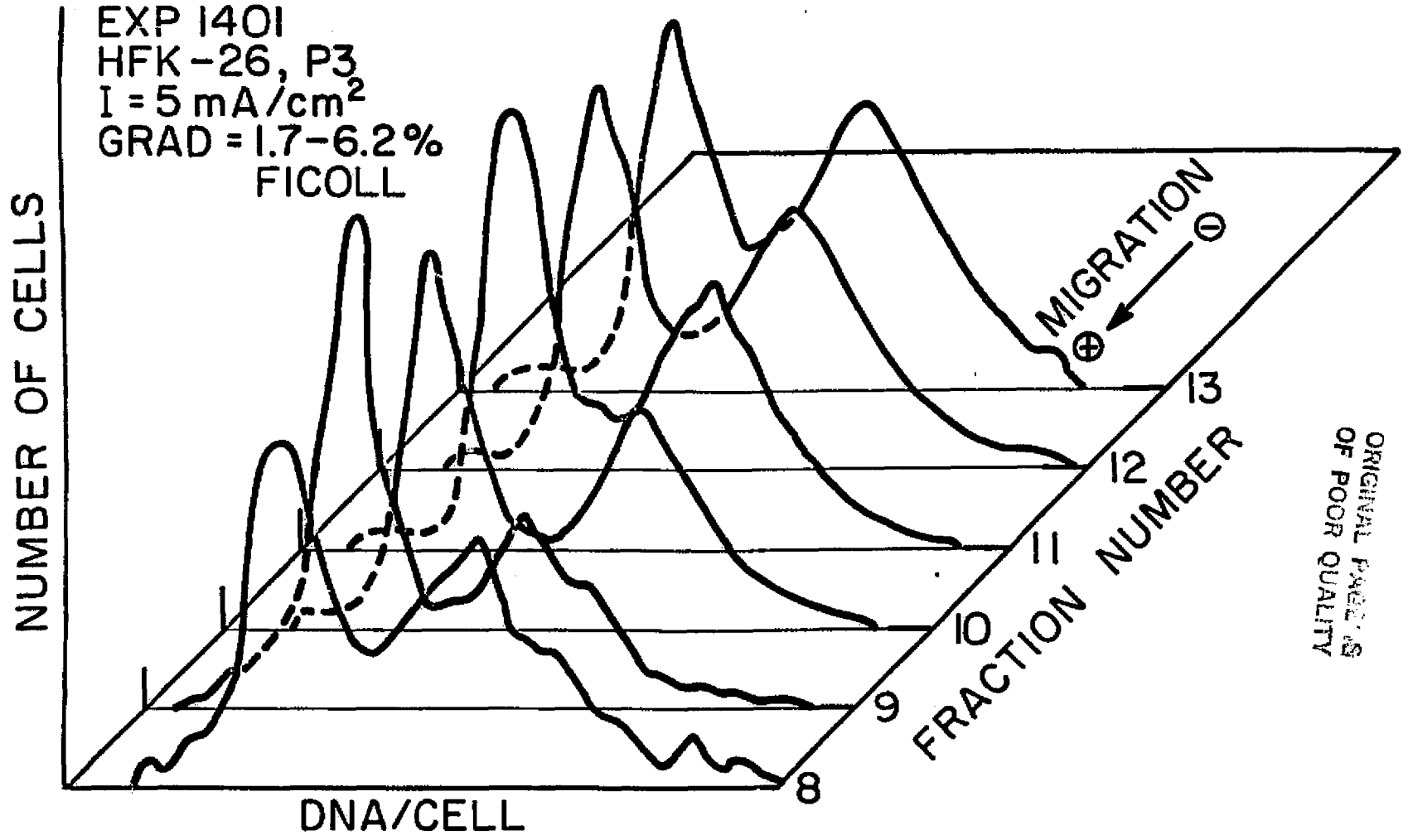

FIGURE 3

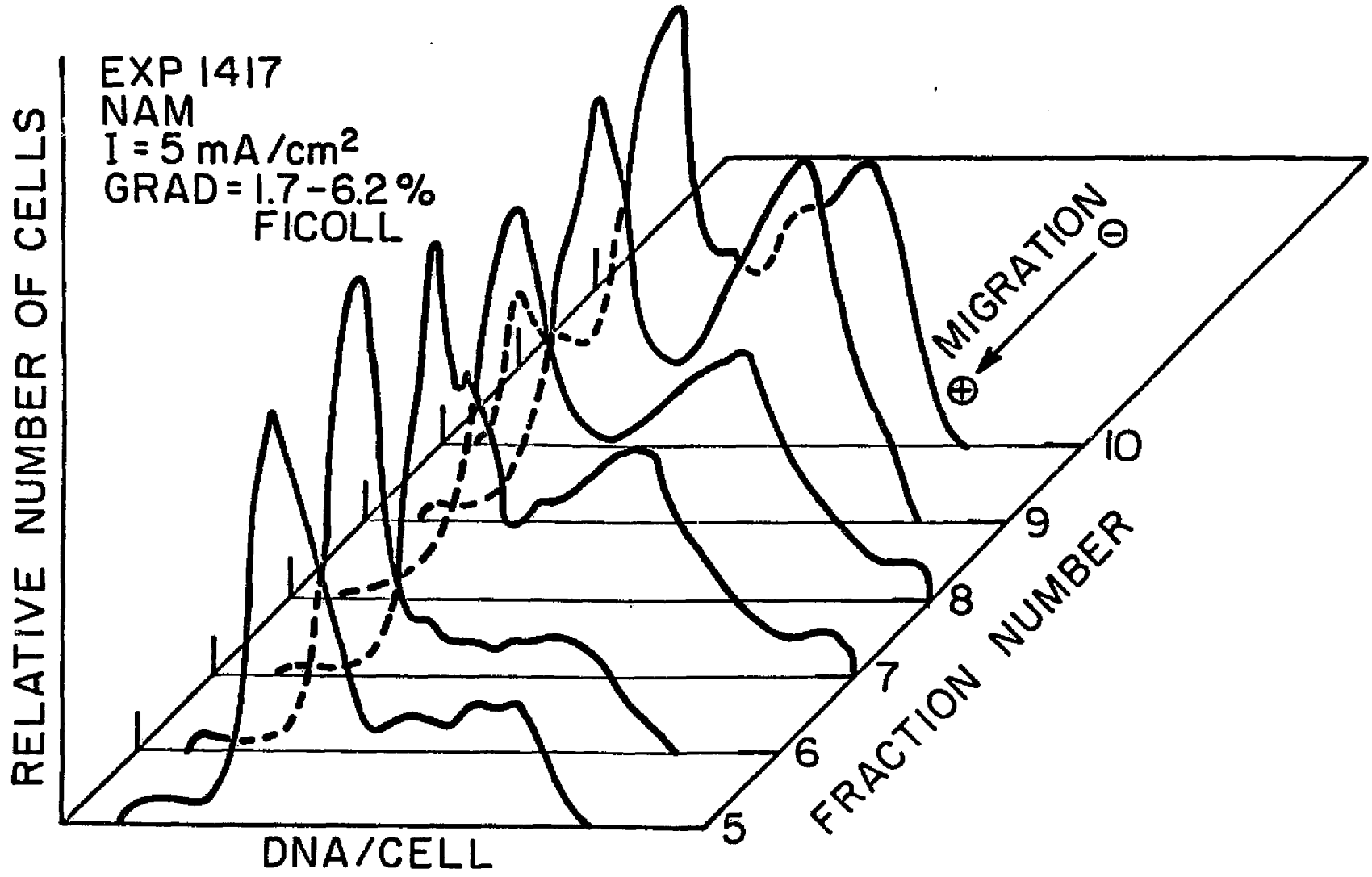
EXP 1417
NAM
I = 5 mA/cm²
GRAD = 1.7-6.2%
FICOLL
RELATIVE NUMBER OF CELLS
DNA/CELL
MIGRATION
⊕
⊖
5
6
7
8
9
10
FRACTION NUMBER

N85-31760 14-24

THE ROLE OF CELL SIZE IN DENSITY GRADIENT ELECTROPHORETIC SEPARATION OF MOUSE LEUKEMIA CELLS ACCORDING TO POSITION IN THE CELL CYCLE

Lindsay D. Plank, M. Elaine Kunze, and Paul Todd

When cultured mouse leukemia cells, line L5178Y, are subjected to upward electrophoresis in a density gradient, the more slowly migrating cell populations are drastically enriched in G2 cells. Figure 1. As published data indicate that this cell line does not change electrophoretic mobility through the cell cycle the possibility that increased sedimentation downward on the part of the larger G2 cells caused this separation was explored.

When two different cell populations were investigated, one of them deliberately enriched with G2 cells by exposure to ionizing radiation 24 hr previously, the log phase population was found to migrate upward faster than the G2 population, and a similar difference between their velocities could be calculated on the basis of a 1 um diameter difference between the two cell populations. The solid lines in Figure 2 are calculated on this basis.

To furher explore this question, G2 and G1 enriched populations were isolated by Ficoll density gradient sedimentation. Figure 3.

The bottom fraction was enriched in G2 cells Figure 4), and the top fraction was enriched with G1 cells (Figure 5), especially when compared with starting material (Figure 6).

The electrophoretic mobilities of these two cell populations did not differ significantly from one another. Figure 7.

Cell diameter dependent migration curves were calculated on the basis of the theory mentioned previously, and they were found to differ. Figure 8. This exercise predicts families of migration curves that differ when cell size is considered as a parameter.

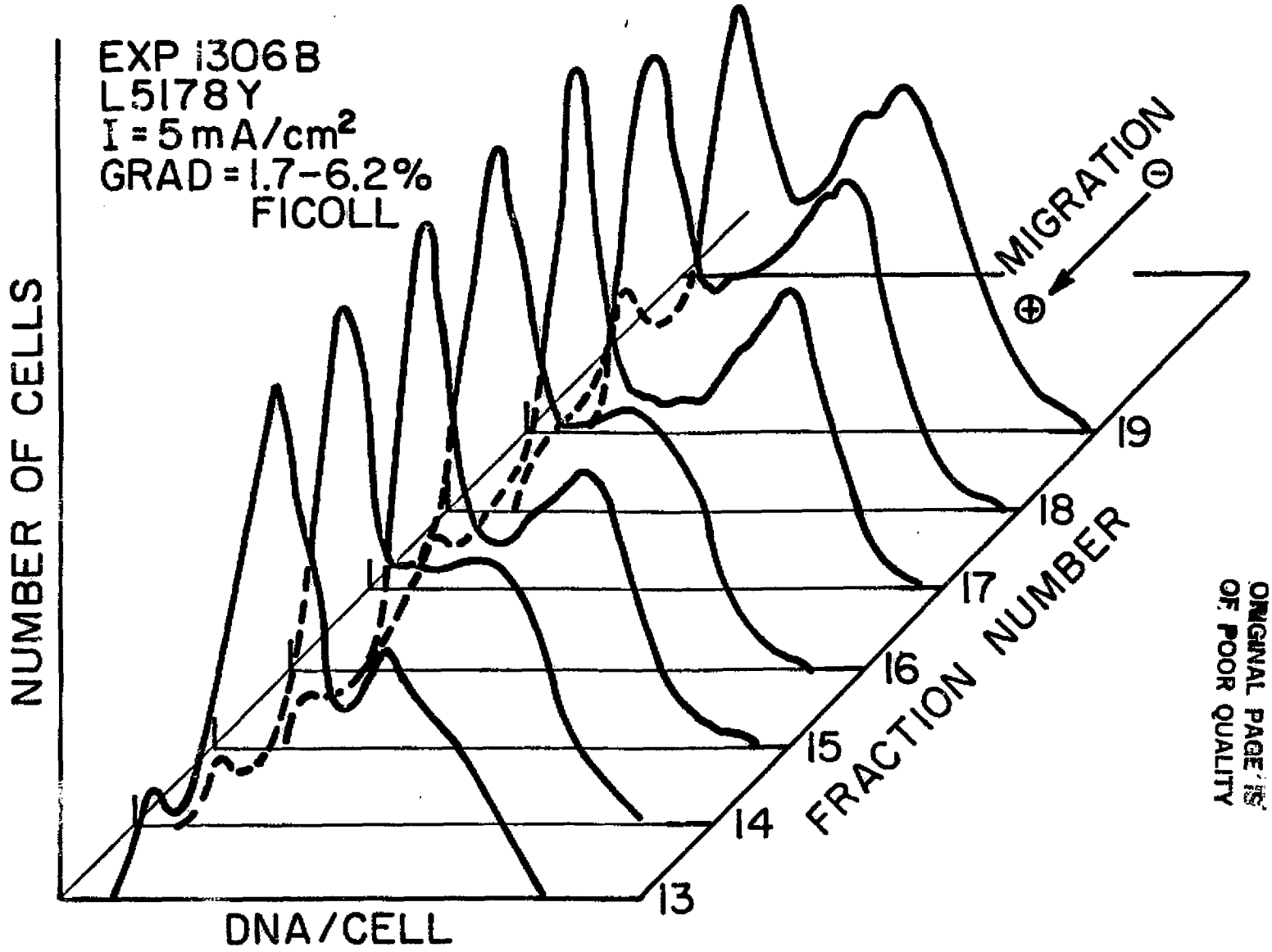

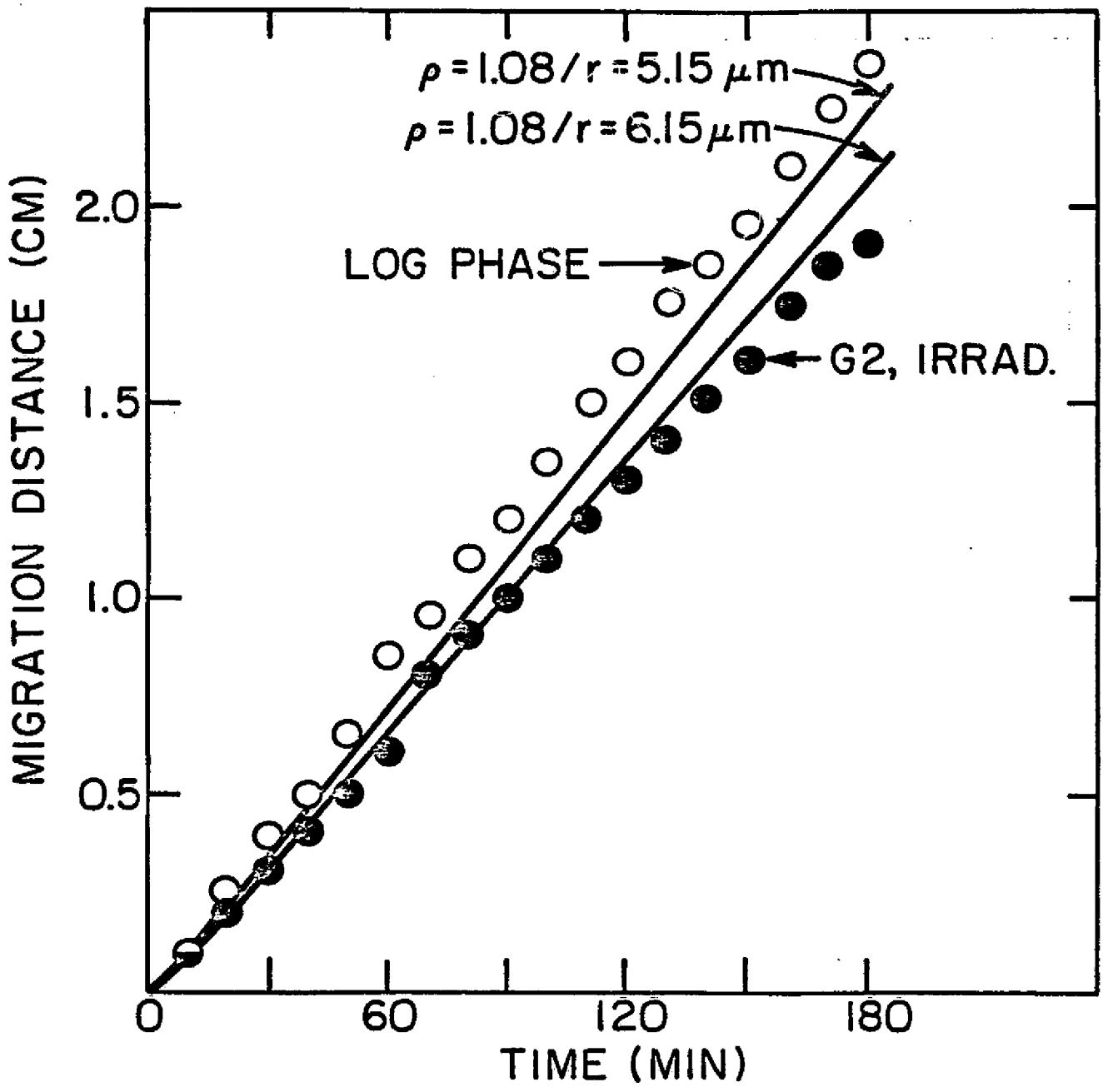
ρ = 1.08/r = 5.15 μm
ρ = 1.08/r = 6.15 μm
LOG PHASE
G2, IRRAD.
MIGRATION DISTANCE (CM)
2.0
1.5
1.0
0.5
0
60
120
180
TIME (MIN)

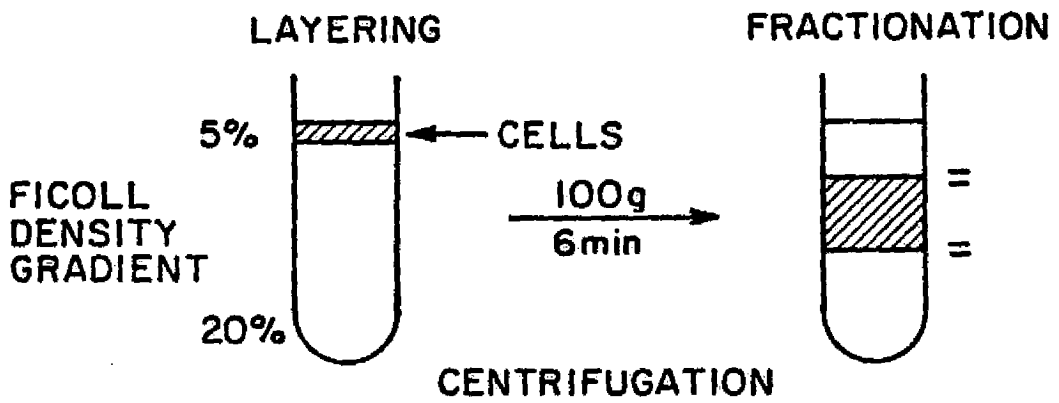
LAYERING
FRACTIONATION
5%
CELLS
FICOLL
DENSITY
GRADIENT
100g
6min
20%
CENTRIFUGATION

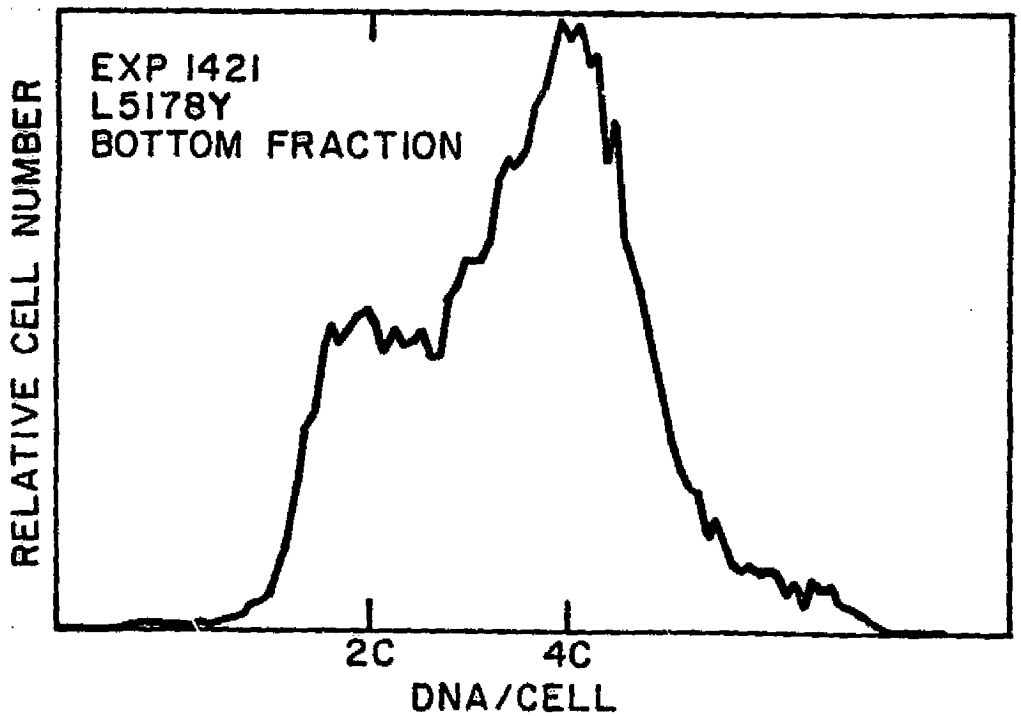
EXP 1421
L5178Y
BOTTOM FRACTION
RELATIVE CELL NUMBER
2C
4C
DNA/CELL

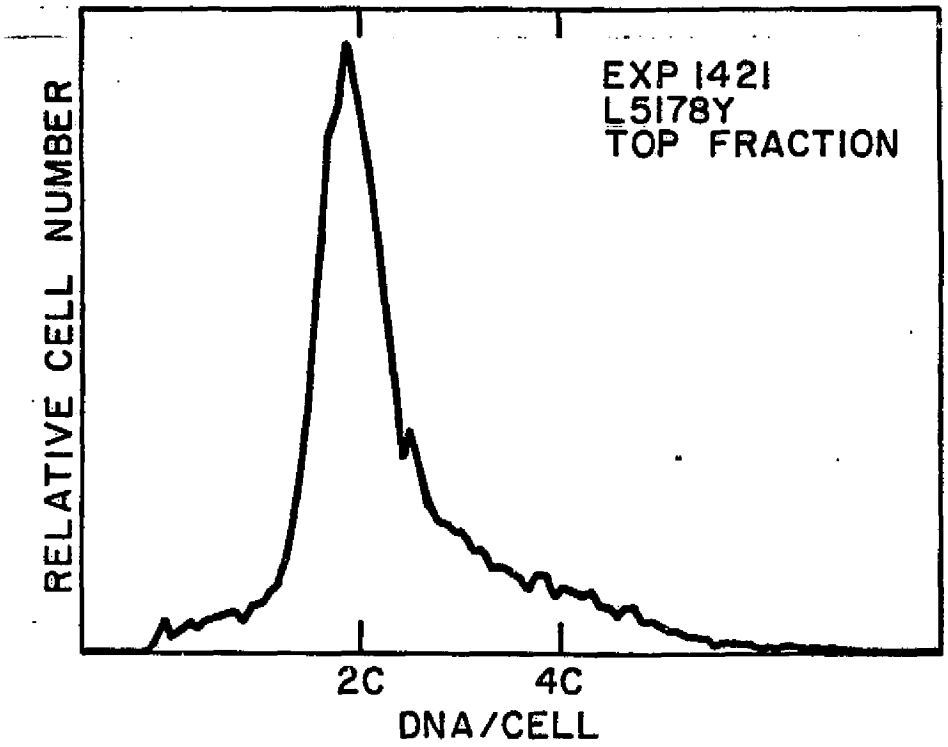

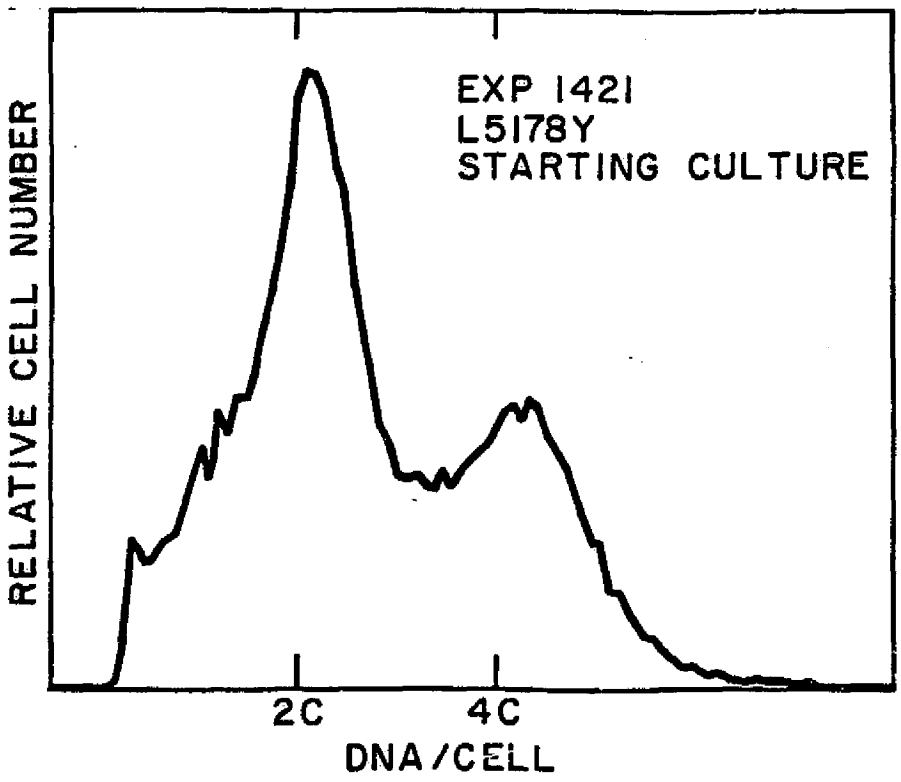

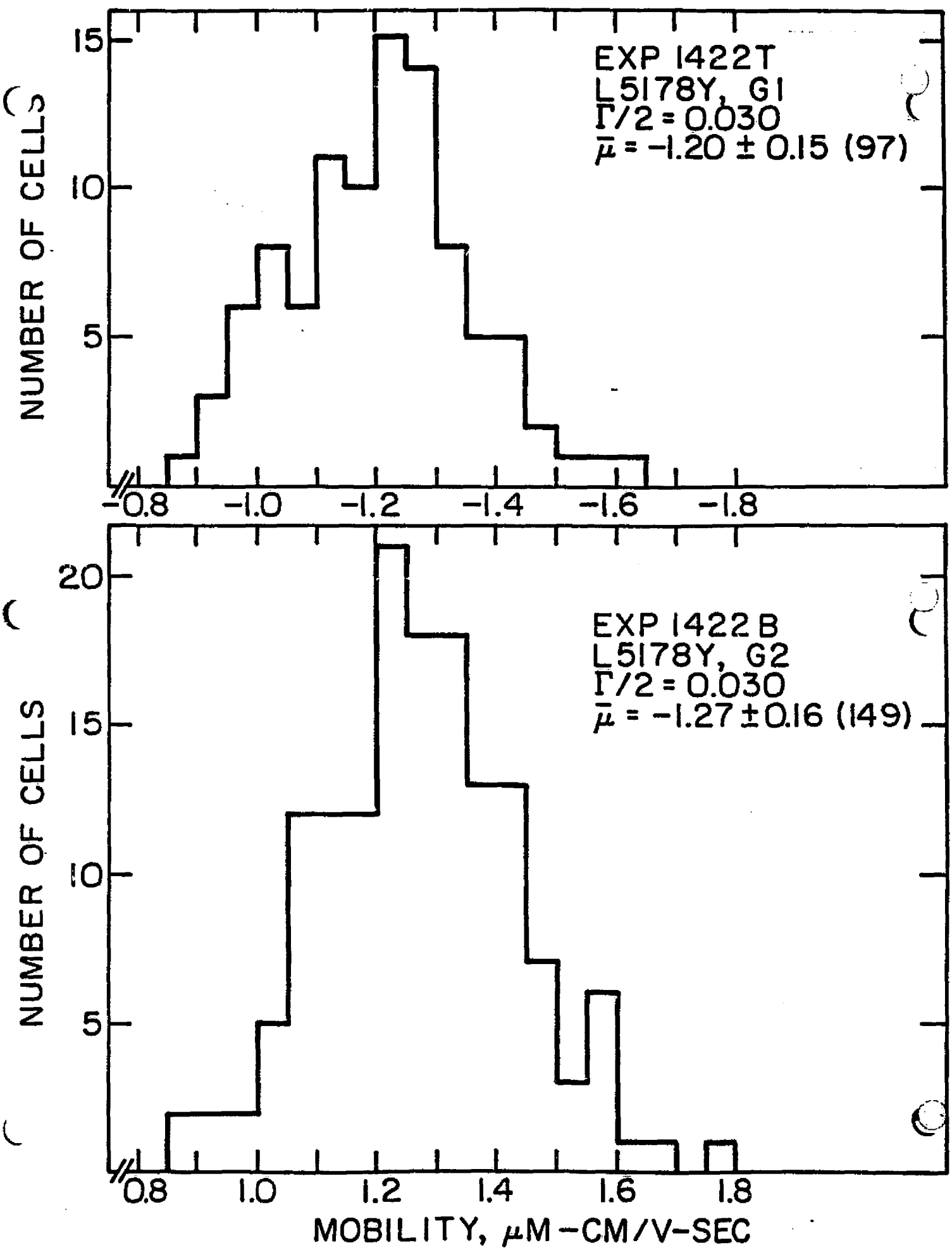
EXP 1422T
L5178Y, G1
Γ/2 = 0.030
$\bar{\mu}$ = −1.20 ± 0.15 (97)
NUMBER OF CELLS
15
10
5
−0.8
−1.0
−1.2
−1.4
−1.6
−1.8
EXP 1422B
L5178Y, G2
Γ/2 = 0.030
$\bar{\mu}$ = −1.27 ± 0.16 (149)
NUMBER OF CELLS
20
15
10
5
0.8
1.0
1.2
1.4
1.6
1.8
MOBILITY, μM−CM/V−SEC

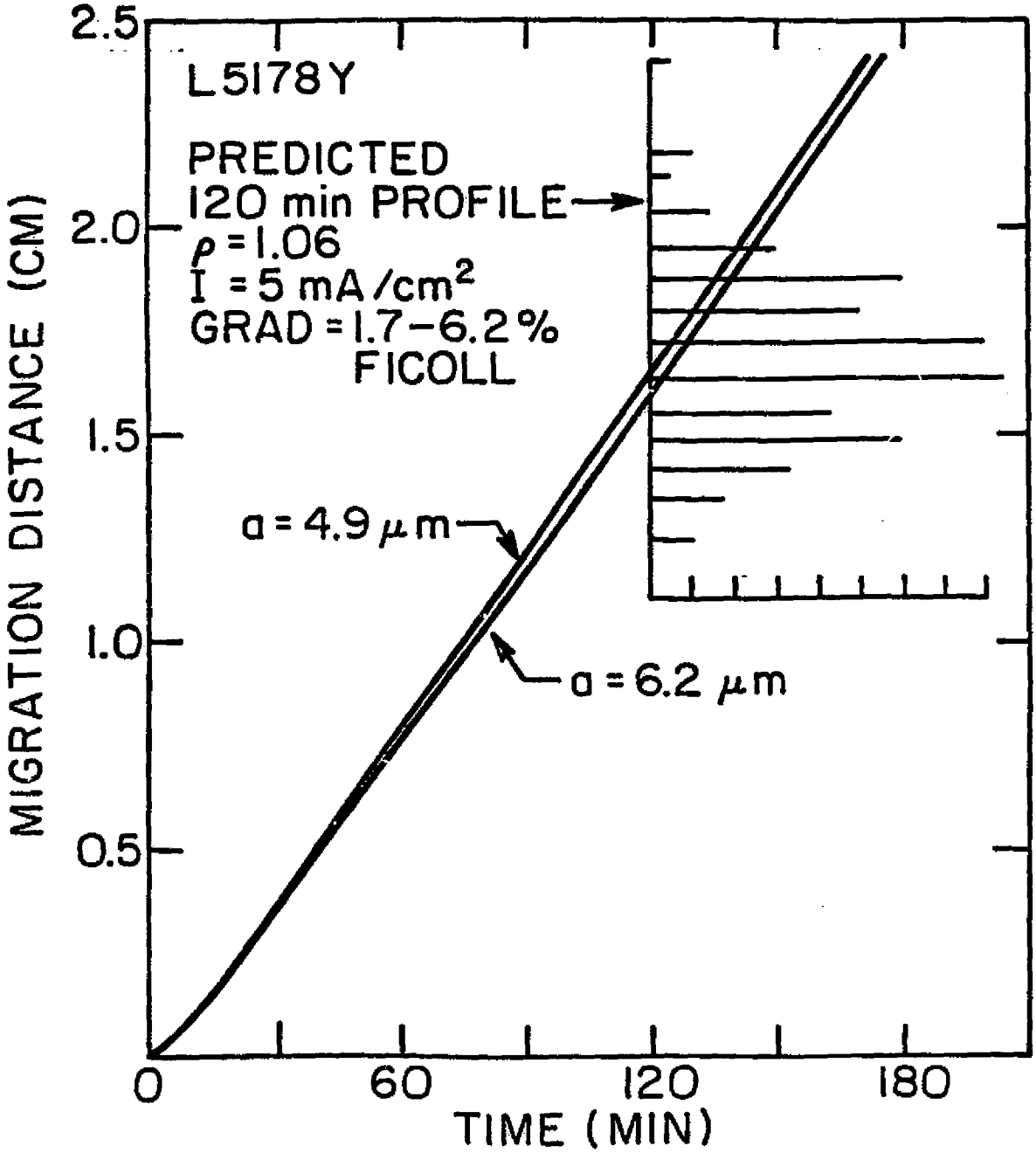
L5178Y
PREDICTED
120 min PROFILE
ρ = 1.06
I = 5 mA/cm²
GRAD = 1.7–6.2 %
FICOLL
a = 4.9 μm
a = 6.2 μm
MIGRATION DISTANCE (CM)
TIME (MIN)
2.5
2.0
1.5
1.0
0.5
0
60
120
180

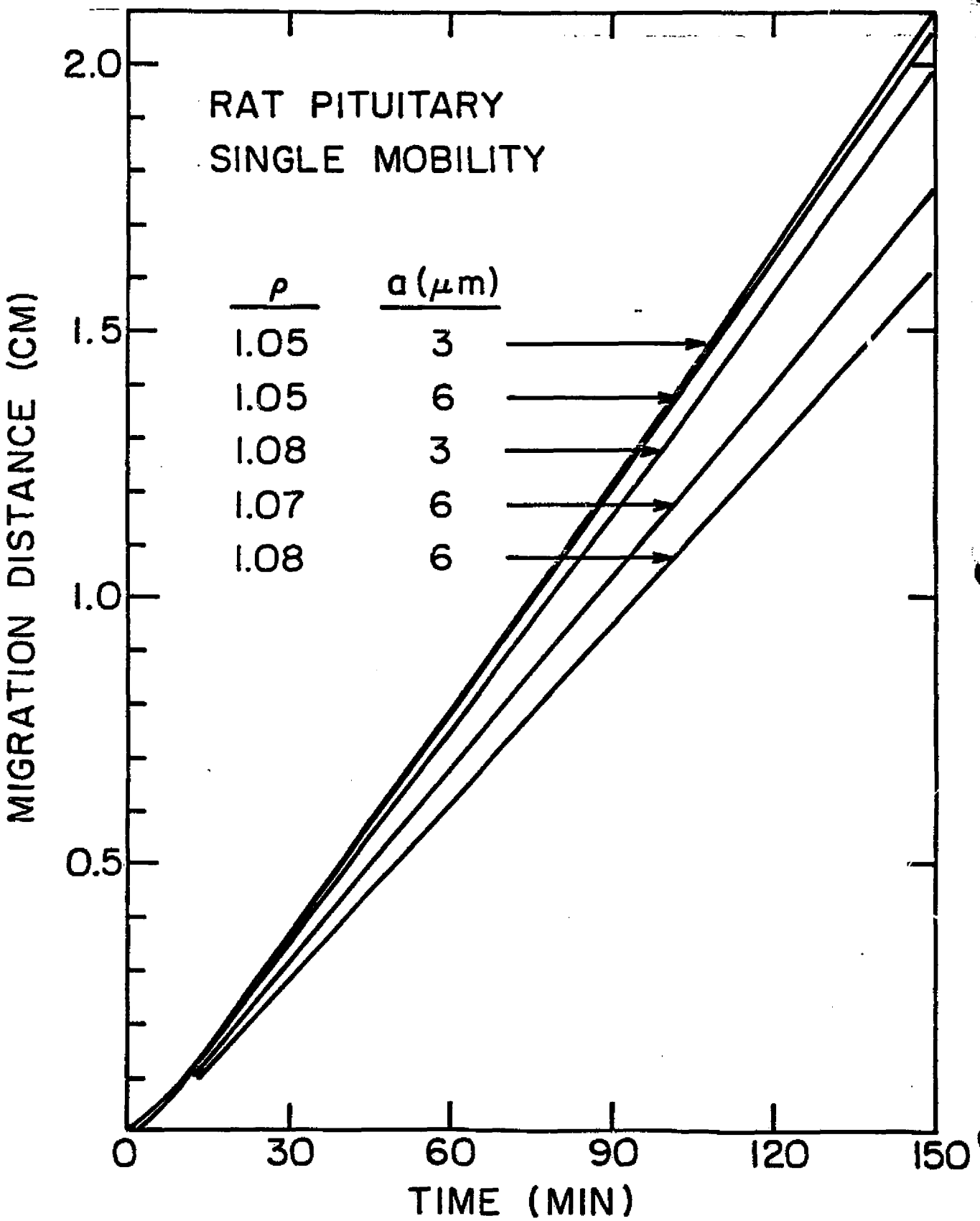
RAT PITUITARY
SINGLE MOBILITY
ρ
a (μm)
1.05
3
1.05
6
1.08
3
1.07
6
1.08
6
MIGRATION DISTANCE (CM)
2.0
1.5
1.0
0.5
0
30
60
90
120
150
TIME (MIN)

Chapter 15.

Electrophoretic Mobilities of Cultured Human Embryonic Kidney Cells in Various Buffers.

INTRODUCTION

This interim report was prepared in response to an immediate need for data on the electrophoretic mobility distributions of cells in the new D-1 buffer and the interlaboratory standardization of urokinase assay methods. In addition, a table of cell strains and recent data on cell dispersal methods are included.

1. ELECTROPHORETIC MOBILITIES OF KIDNEY CELLS IN D-1 BUFFER

It was decided among laboratories that glycerol in A-1 buffer should be replaced by dimethylsulfoxide (DMSO); therefore, a need developed for electrophoretic mobility data on cultured human embryonic kidney cells subjected to electrophoresis in this buffer. The buffer composition is given in Table 1.

Cells were removed from subconfluent cultures by incubation in 0.37% EDTA in Puck's saline A (composition given in Table 2) or the same solution with 0.03% crude trypsin added. Cells were centrifuged out of these solutions and washed and resuspended in D-1 buffer for electrophoresis. The Zeiss Cytopherometer with Cam-Apparatus electrodes was used to obtain mobility histograms from the analysis of the complete cell flow parabola. A parabola giving cell velocity vs. chamber depth is shown in Fig. 1., and the mobility histograms are shown in Fig. 2. Due to the small number of cells available for measurement in the chamber there is no statistically significant difference between the histogram obtained with cells dispersed with trypsin and EDTA and that for cells dispersed with EDTA only. In any case, trypsin treatment did not reduce the electrophoretic mobilities.

4. TESTING OF DISPERSAL PROCEDURES

The combination of cell dispersal with EDTA and suspensions in D-1 buffer still does not lead to fully satisfactory viability. Table 4 summarizes the results of a preliminary experiment designed to test the ability of D-1 buffer on its own to disperse cells. This experiment was based on a recently announced finding that DMSO at 10% concentration disaggregates actin-containing microfilaments in epithelioid cells in culture. The results indicate that D-1 buffer does disperse cells, but that it might selectively suspend cells with low viability, since the traditional method employing EDTA in Puck's saline A led to much higher viability, as measured by percent attachment in 24 hours. Variants of this experiment are to be performed in the near future.

Table 1. Composition of D-1 Buffer, Low Ionic Strength Medium for Cell Freezing and Electrophoresis

COMPONENT	GRAMS/LITRE	MOLARITY
NaCl	0.380	0.00642
Na_2HPO_4	0.167	0.00176
KH_2PO_4	0.050	0.000367
Na_2EDTA	0.125	0.000336
Glucose	40.0	0.222
DMSO	50.0	0.64

Table 2. Composition of Puck's Saline A, Used as the Medium for Cell Dispersing Agents Trypsin and EDTA

COMPONENT	g/ℓ
NaCℓ	8.00
KCℓ	0.40
$NaHCO_3$	0.35
$Na_2HPO_4 \cdot 7H_2O$	0.09
KH_2PO_4	0.06
Na_2EDTA	0.20
Glucose	1.00
Phenol red	0.01

Table 3. Short Table of Human Kidney Cell Lot Data and Experimentation

CELL LINE	START DATE	CO.	LOT #	FREEZE	MAX PSG	UK TEST	MEDIUM	STOP DATE	ELECTRO PHORESIS	REMARKS
HFK	8/21/78	GIB	D-110	YES	14		BME	11/12/78	YES	
HFK-1	10/25/78	GIB	83010TE	YES	13		BME	2/14/79	YES	
HFK-2	12/13/78	GIB	81812TE	YES	9		BME	2/18/79	YES	
HFK-3	3/7/79	GIB	70503TE	NO-	4	YES	BME	4/3/79	YES	Used Up Cells
HFK-4	3/30/79	GIB	90204TE	YES	4		BME	4/30/79	YES	Last To Mold
HFK-5	4/28/79	GIB	93004TE	NO-	3		BME	5/16/79	YES	Last To Mold
HFK-6	7/24/79	MAB	HEK7923	YES	4		BME	8/10/79	YES	Contamination
HFK-6S	7/24/79	MAB	HEK7923	NO-	5		BME	10/12/79	YES	Non-attaching
HFK-7	9/6/79	MAB	HEK8251		6		BME	11/26/79	YES	Senescence
HFK-7S	9/6/79	MAB	HEK8251		6		BME	10/30/79	YES	Non-attaching
HFK-8	11/27/79	MAB	HEK8988	YES	6		BME	12/17/79	YES	
HFK-9	1/22/80	MAB	HEK9470		5		BME	4/13/80	YES	
HFK-10	3/18/80	MAB	HEK9933		8		BME	5/8/80	YES	
HFK-11	5/14/80			YES	5		BME	6/11/80	YES	
HFK-12	7/2/80	MAB	HEK0711	YES	1	YES	BME	7/11/80	NO	
HFK-13	7/8/80	MAB	HEK0804	YES	7	YES	BME	8/7/80		
HFK-14	9/15/80	MAB	HEK20.1246	YES	4	YES	BME	10/8/80		
HFK-15	10/21/80	MAB	HEK1466	YES	4	YES	BME		YES	Still Going

Table 4. Effect of Method of Cell Removal on Viability (attachment in 24 hr) of Strain HFK-15 (Passage 5) Cells Plated in BME + 10% Newborn Calf Serum (Experiment 1212)

DISPERSING SOLUTION	INCUBATION TIME, 37°C	% ATTACHED IN 24 HR	DENSITY IN 24 HR
D-1 buffer	10 min	46	Sparse
0.37% EDTA in Puck's Saline A	20 min	85	Confluent

Figure 1. Cell velocity vs. distance from the front wall of the Zeiss cytopherometer electrophoresis chamber. Cells are HFK-15, passage 5, suspended with 0.03% trypsin and 0.37% EDTA in Puck's saline A.

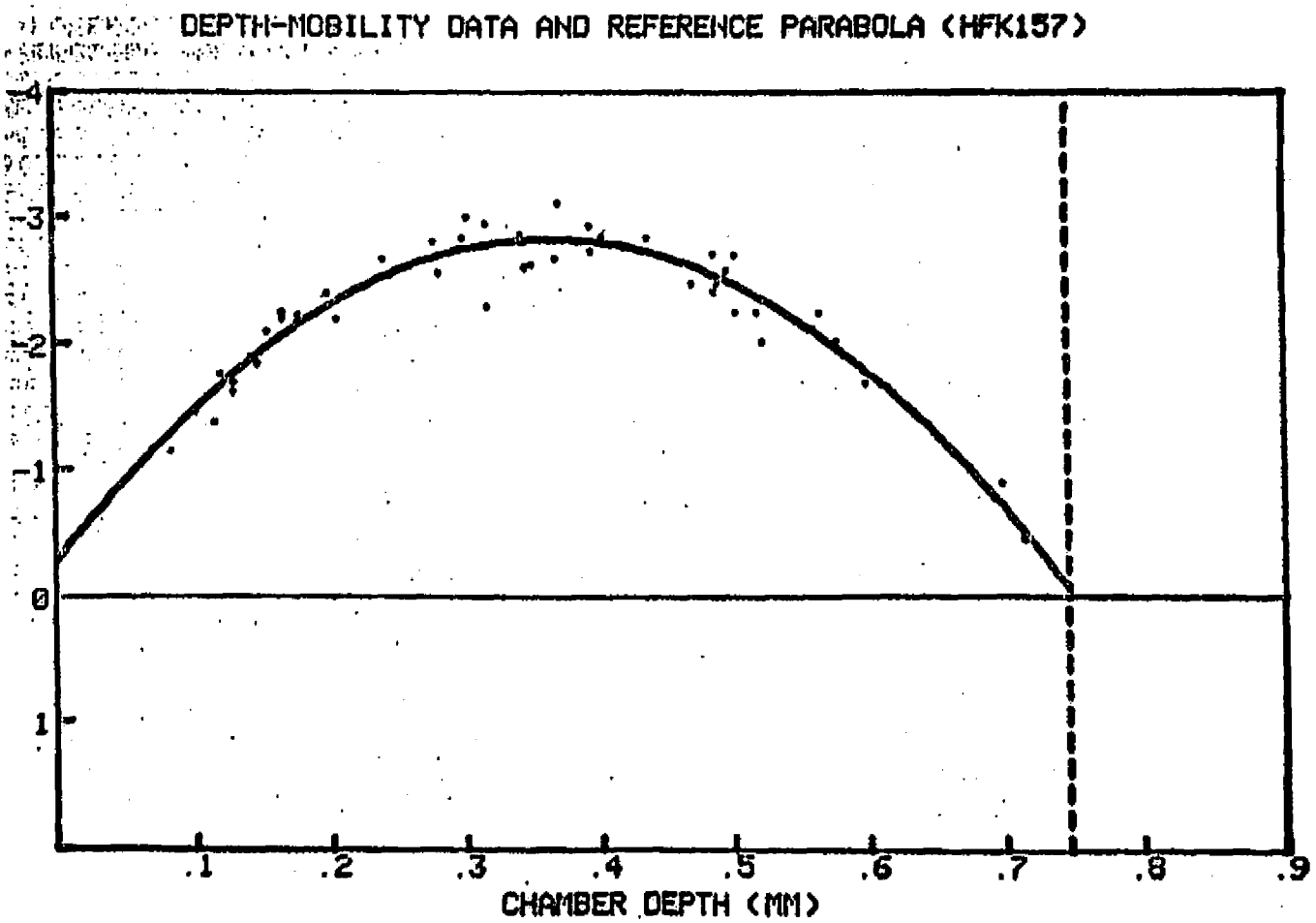

Figure 2. Electrophoretic mobility histograms of HFK-15 cells, passage 5, in D-1 buffer after suspension in EDTA or EDTA plus trypsin.

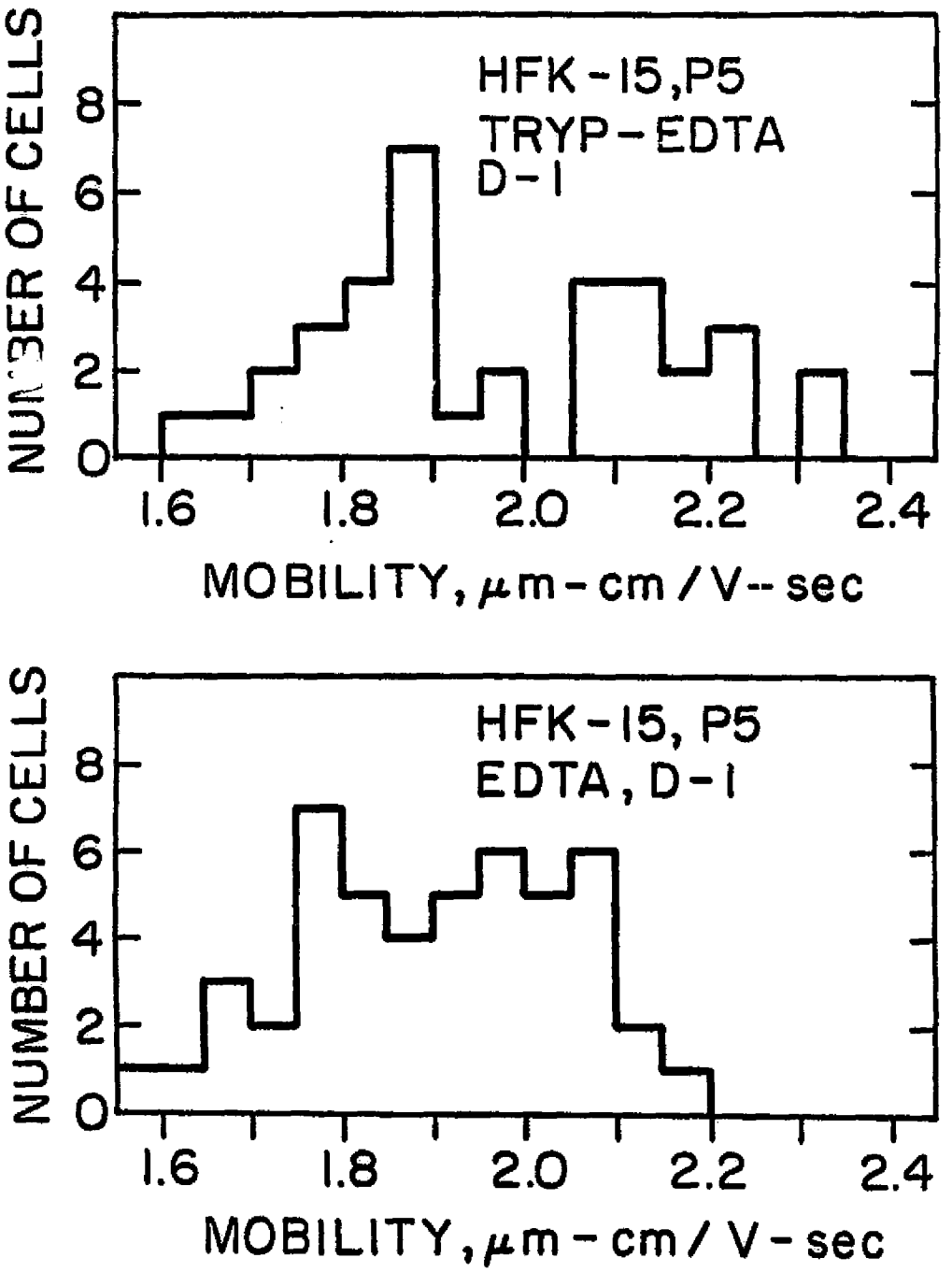

Mobilities of two cell lots determined using the Pen Kem 3000 Automated electrophoretic analyser. Early passage cells are clearly more heterogeneous in D-1 buffer than late passage cells.

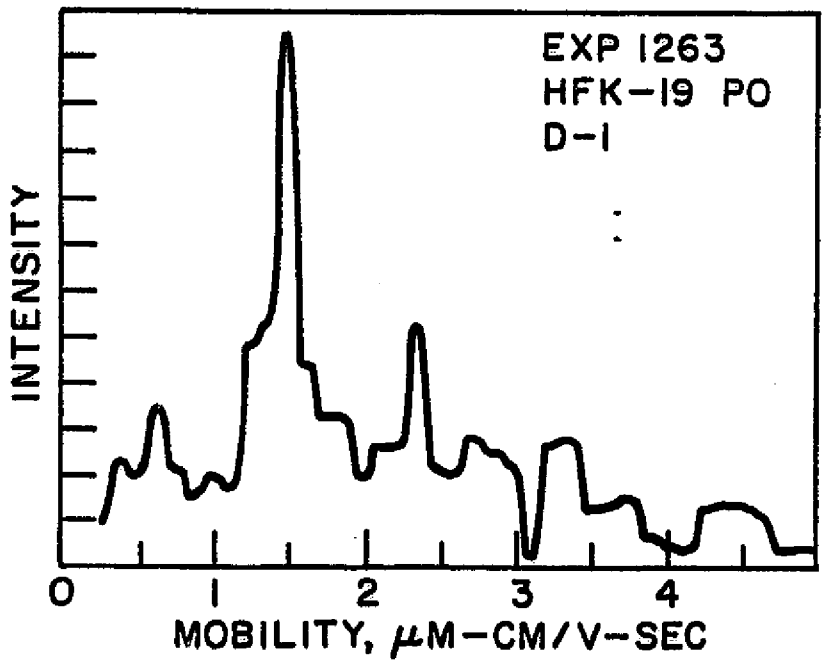

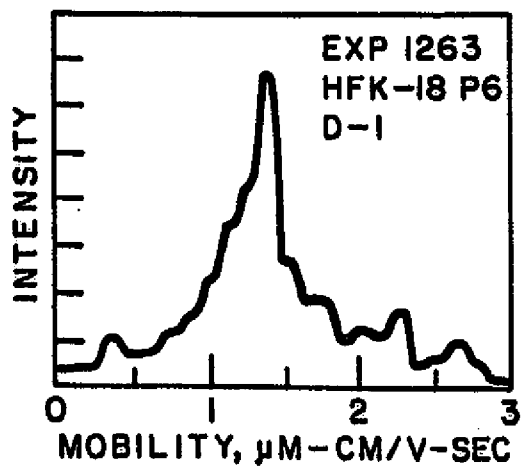

KIDNEY CELL ELECTROPHORESIS III. EFFECT OF PASSAGE NUMBER ON ELECTROPHORETIC MOBILITY DISTRIBUTIONS OF CULTURED HUMAN EMBRYONIC KIDNEY CELLS

M. Elaine Kunze

N85-31762

A systematic investigation was undertaken to characterize population shifts that occur in cultured human embryonic kidney cells as a function of passage number in vitro after original explantation. This approach to cell population shift analysis follows the suggestion of Mehreshi, Klein and Revesz that purturbed cell populations can be characterized by electrophoretic mobility distributions if they contain subpopulations with different electrophoretic mobilities. It has been shown that this is the case with early-passage cultured human embryo cells.

The figure below shows that, in the case of strain "HFK-40" a downward trend in mean mobility was found during the first three passages in vitro, and this shift is mainly due to the reduction in the fraction of cells with high mobility (-1.6 to -1.8).

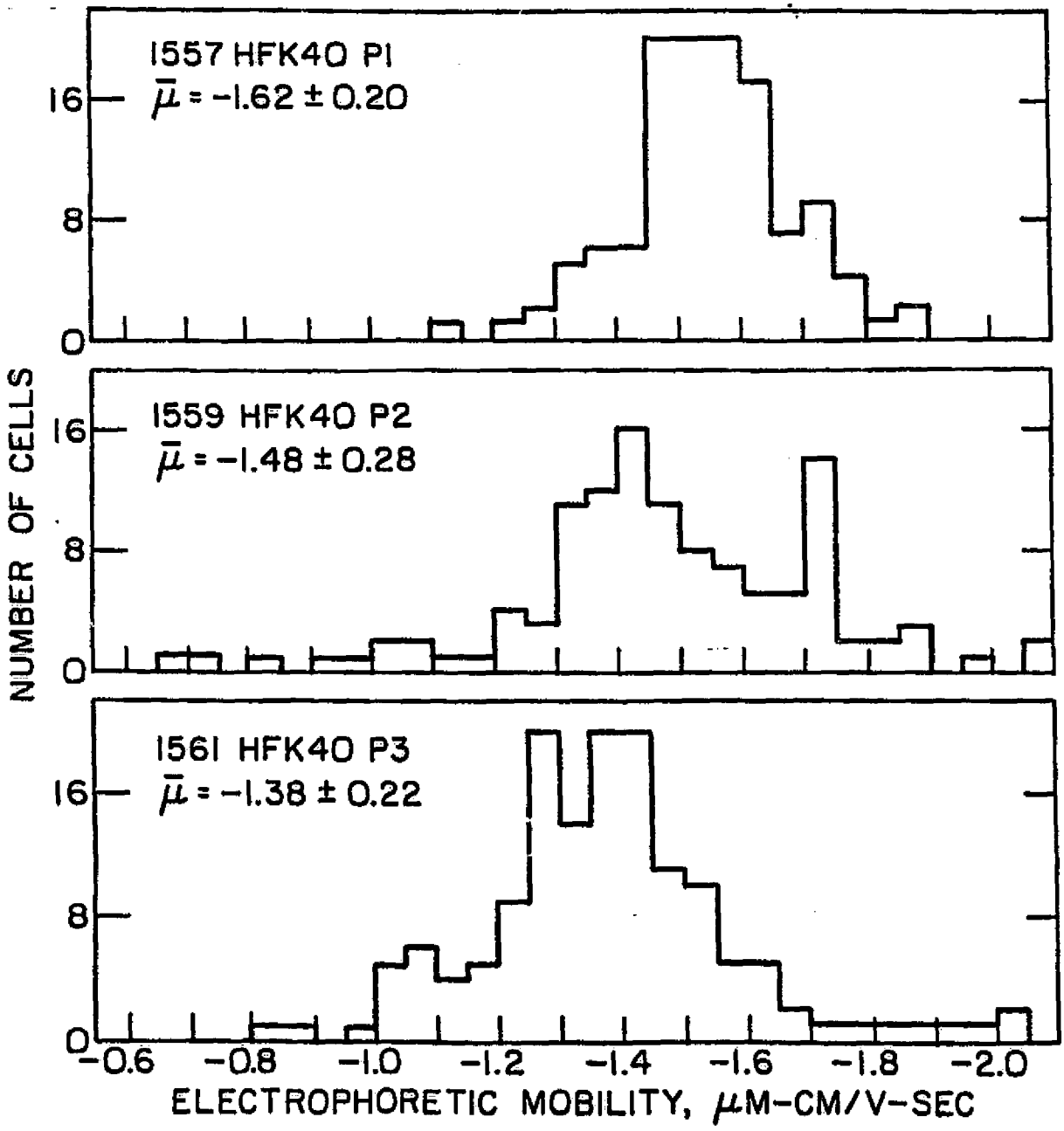

Chapter 16.

Density Gradient Electrophoresis of Cultured Human Embryonic Kidney Cells.

DENSITY GRADIENT ELECTROPHORESIS OF CULTURED HUMAN EMBRYONIC KIDNEY CELLS

L. D. Plank, M. E. Kunze, V. Giranda, and P. Todd

INTRODUCTION

Ground-based confirmation of the electrophoretic heterogeneity of human embryonic kidney cell cultures, the general characterization of their electrophoretic migration, and observations on the general properties of cultures derived from electrophhoretic subpopulations were the objectives of this research. To accomplish these objectives, the following sub-projects were undertaker:

1. The relationship between cell migration in a density gradient electrohoresis column and cell electrophoretic mobility.

2. Comparison of the mobility and heterogeneity of cultured human embryonic kidney cells with those of fixed rat erythrocytes as model test particle.

3. Examination of electrohoretically separated cell subpopulations with respect to size, viability, and culture characteristics.

RESULTS

1. The relationship between cell migration in a density gradient electrophoresis column and cell electrophoretic mobility.

The composition of the buffer used for making the density gradient (Boltz et al., 1973) is given in Table 1. The mixing of Ficoll and sucrose in this buffer in the gradient maker gives an upward gradient of sucrose and a downward gradient of Ficoll, which has changing conductivity, viscosity, and effect on cell zeta potentials as a function position in the column. The dependence of conductivity on Ficoll concentration is given in Figure 1.

It was pointed out in an earlier report that standard test particles (fixed rat, chick, and rabbit erythrocytes (RBC)) were being used to calibrate the migration of cells in the density gradient column against the traditional analytical electrophoresis method using the Zeiss Cytopherometer. Careful measurements of conductivity, viscosity, temperature, osmolarity, and density have now been made throughout the gradient. In addition, it was necessary to measure the effect of Ficoll on the mobility of test particles in the column electrophoresis buffer, owing to the well-known effect of neutral polymers on effective zeta potential. Figure 2 clearly indicates that Ficoll increases zeta potential, and the results predict that cellular zeta potential will decrease as cells migrate up the column toward lower Ficoll concentrations. By using this complete

information set it is possible to predict the velocity a charged particle will have at any position in the column. The mathematical function corresponding to these dependencies can be integrated to produce a migration function (Fig. 3) that is approximately quadratic near the bottom of the column and inverse exponential near the top. This function correctly predicts the shapes of RBC migration plots (Fig. 4) and comes within 15% of predicting the absolute value of the distance migrated by rat RBC's under the conditions described in Fig. 3.

Continuing data analysis and experimentation indicate that the agreement between theory and experiment is actually much better, and algorithms are being developed to convert density-gradient fraction numbers into mobility units.

2. Comparison of the mobility and heterogeneity of cultured human embryonic kidney cells with those of fixed rat erythrocytes as model test particle.

During an attempt to prepare a temporary spinner culture for electrophoresis of HFK cells at the 10th passage it was found that most of the cells died in suspension within 6-10 hr. and were not suitable for electrophoretic separation. The culture was re-plated and saved until the surviving cells re-grew to confluence over a 75 cm^2 area. The resulting separated bands of RBC's and HFK cells were clearly visible (Figure5) in scattered light, so the migration of the bands could be monitored by eye for determination of migration rates, as shown in Fig. 6. The average HFK cell migration rate is about 0.67 - 0.72 as great as that for fixed rat RBC's. Although the profile at the end of the separation was dominated by RBC's it could be shown by using Coulter volume analysis that the added RBC's separated cleanly from the HFK cells. This separation is easier to visualize when the data are plotted on relative scales as in Figure 7. The HFK cells seem to occupy a single peak, so there is very little evidence for heterogeneity. This is not surprising, considering the selected nature of the cells. Each fraction was examined by phase microscopy after it had been plated in a 60 mm Falcon tissue culture dish, and additional heterogeneity was found. Fraction 8, the most populous fraction in culture (see Figure 8) contained viable cells which multiplied in suspension without attaching to anything. Fraction 6 contained fibroblasts that attached and spread and formed monolayers. Fractions 12-15 consisted mainly of dead cells. Direct observations of fractions in cultures yielded information about purity, as shown in Figure 9. The purest fractions contained 97.8% HFK cells and 99.8% fixed RBC's; these were 3 fractions apart (about 1.5 cm in this case). Coulter volume analysis also facilitates the determination of peak compositions. Figure 10, which presents three volume histograms, shows that the starting mixture was mostly RBC's (channels 6 & 7) and that channels 5 & 6 include debris and some RBC's while channels 11 & 12 account for most of the HFK cells. Fraction 5 is mainly RBC's, while fraction 10 is mostly HFK cells and debris. Cultures of fractions 6 & 8 have been maintained for further characterization.

Early passage cells of strain HFK-1 were subjected to density gradient electrophoresis after mixing with fixed rat erythrocytes (RBC). The resulting electrophoretic profile indicated that the electrophoretic mobility of the modal HFK-1 cells is about 70% that of the fixed RBC's in the Ficoll gradient and the non-adherent cells had about 60% the mobility of RBC's. Non-adherent ("round") cells were fewer in number than attaching cells, and their average mobility was lower. This particular population was not studied for its urokinase activity. See Figure 11.

Most experiments to date have involved the collection of large-volume (0.5 - 1.0 ml) fractions, and in these early experiments high resolution separations were not the goal. Experiments in which 0.25 ml fractions are collected have begun with cell strain HFK-1. Fractions of 1.0 ml volume have given a resolution of $\Delta\mu$(min) 0.054 μm-cm/V-sec per fraction after 4 hr of separation, and the harvesting of 0.25 ml (5 drop) fractions provides resolution of $\Delta\mu$(min) 0.01 μm-cm/V-sec. Fractions of HFK-1 cells have been collected at this latter resolution for fibrin slide analysis. The data of Figure 4 form the basis of these calculations. Figure 7 provides additional insight into resolution. The RBC and HFK cell peaks are separated by 4 fractions and are 1.5 and 2.0 fractions wide, respectively. These numbers give

$$\frac{\Delta x}{\tau_x} = \frac{4}{3.5} = 1.14$$

as the classical separability resolution.

3. Examination of electrohoretically separated cell subpopulations with respect to size, viability, and culture characteristics.

By combining the results of this work period with those presented in previous progress reports it becomes clear that different primary cultures produce different electrophoretic mobility profiles. Some additional examples are presented here. Cell strain HFK-7 produced copious quantities of non-adherent cells, and the electrophoretic migration plot of Fig. 12 indicates quite clearly that the non-adherent cells belonged to a completely different mobility class from the fibroblasts, which dominated this cell strain at the 6th passage, when this separation was performed. The morphology of the cells in the fractions was determined by phase-contrast microscopy of the plated cultures. As was found to be the case with other HFK strains, this cell strain was much more heterogeneous at earlier passages. Fig. 13 shows the migration plot (EXP 1028) of a separation experiment with strain HFK-7 at passage #2, which is the earliest possible culture passage available to us for study. In this experiment alternating fractions were plated and counted so that quantitative counts (including volume distributions) and evaluations in culture could be obtained on adjacent fractions. This is the procedure followed in about 75% of the HFK separation experiments. The density gradient electrophoretic distribution profile, Fig. 14, confirms that these cells are very broadly distributed with respect to electophoretic mobility. Although 60 pairs of fractions were collected over a 12-cm migration distance in this experiment, electrophoretic heterogeneity was not manifested as a number of sharp peaks but as a broad distribution. Both cases have been seen in past experiments, but sharp peaks are more likely to appear when smaller fraction are collected.

A very homogeneous population of (epithelioid) kidney cells designated HFK-10 was found to have a narrow electrophoretic profile after density gradient electrophoresis. In Figure 15 it is seen that nearly all of the viable cells were found in only in the narrow band between fractions 49-58, and that fractions above and below this band contained mainly unattaching, non-viable cells. The Coulter counts of these fractions (dta not shown) matched this profile. Further evidence of the homogeneity of this population is found in the Coulter volume distributions of three widely-separated fractions in Figure 16.

Different starting materials have produced different results. Figure 17 presents a density-gradient electrophoretic profile of cells trypsinized from passage 10 of strain HFK. The starting population consisted only of about 10^5 cells, and Coulter volume analysis was the only procedure applied to each fraction. Although most of the cells in the starting culture were fibroblastic, there is evidence for considerable electrophoretic heterogeneity. Fractions numbered 35 or higher consisted of clumped cells which sedimented farther during upward electrophoretic migration. When only large clumps were counted (Channel 13 on Coulter Counter TA II) they were found principally near the bottom of the gradient; Their distribution is indicated by the empty circles. None of the fractions from this experiment were saved for further culturing.

Over the entire period of the project all kidney cell cultures of reasonable quality have been subjected to density gradient electrophoresis, so that several dozen experiments have been performed using this technique. The solutions used in the columns have in all cases been those described in Table 1.

Figures 19 through 33 constitute a catalog of electrophoretic profiles of a variety of kidney cell cultures. Many of these have been presented in earlier reports, but some trends are now beginning to emerge. Early results, Figure 19, confirmed that human kidney cell cultures are electrophoretically heterogeneous and therefore present the possibility of separating cells according to function. Figures 20 and 21 illustrate that it is possible to determine electrophoretic mobility profiles of different classes of cells identified by size in the Coulter volume analyser. At least one size class, Channel 12, had a bimodal mobility distribution.

In highly heterogeneous populations, such as described in Figs. 22, 24, and 25, there is a high-mobility population of cells that are non-

viable by microscopic in vitro criteria. This appears to be a very consistent observation. As indicated previously, as well as in Fig. 25, strain HFK-10 had a very large population of very-low-mobility viable cells. There is no evidence that these are UK producers. Figures 26 through 29 portray a computerized version of the analysis described in Fig. 21, namely the determination of the electrophoretic profiles of cells in specific volume classes as determined by Coulter volume spectrometry. Again, multimodal electrophoretic distributions are found within size classes.

Figures 30 through 33 describe electrophoretic profiles of recently-acquired cell strains, and it can be seen that microscopic evaluation continues to reveal a high-mobility fraction of cells with low viability. Cultures from these fractions are to be analysed for UK production also.

Table 1. Composition of phosphate-buffered glucose (PBG) and PBG-sucrose, which is PBG with 6.8% sucrose to give isosmolarity.

COMPONENT	MW	g/l	M
KCL	74.56	0.20	0.00268
$MgCl_2 \cdot 6H_2O$	203.33	0.10	0.00049
Na_2HPO_4	141.96	1.15	0.00810
KH_2PO_4	139.09	0.20	0.00144
Glucose	180.16	10.00	0.05551

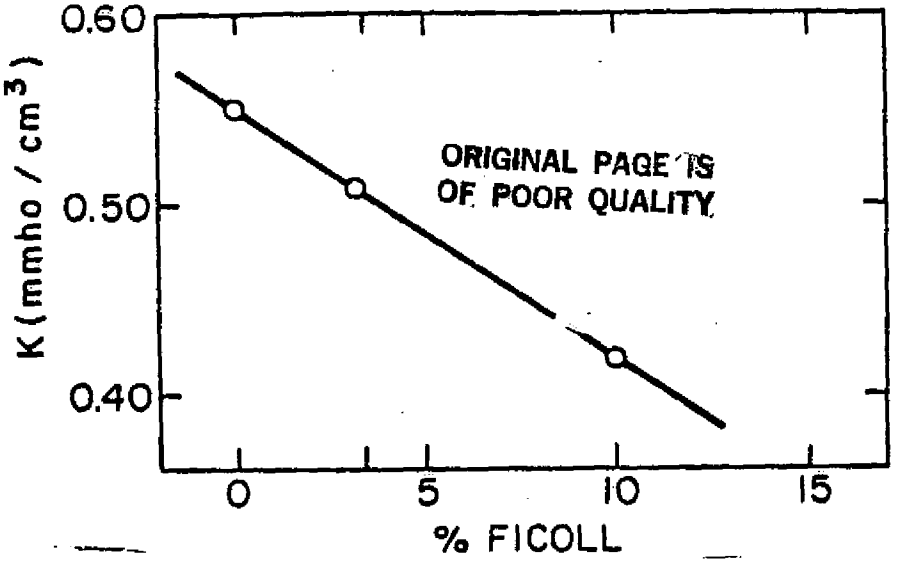

Figure 1. Conductivity of Ficoll-sucrose solution mixtures used in density gradient column electrophoresis. The apparent conductivity falls with increasing Ficoll concentration.

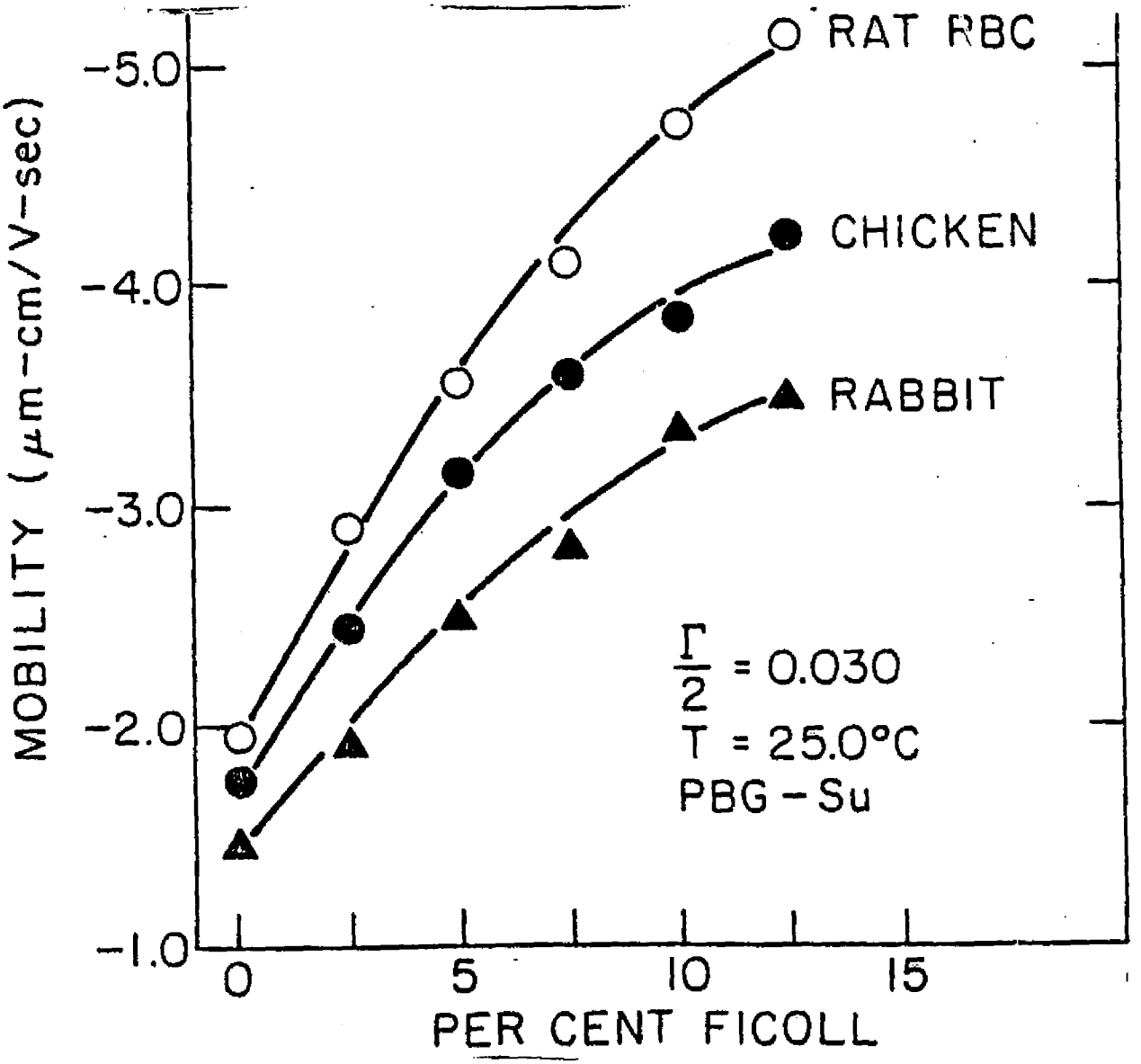

Figure 2. Fixed erythrocyte mobilities as a function of Ficoll concentration in phosphate-buffered glucose medium used for density gradient electrophoresis. Measurements were made using the Zeiss Cyto-

Figure 3. Predicted migration curve for fixed RBC's subjected to electrophoresis upward through a Ficoll gradient under typical experimental conditions.

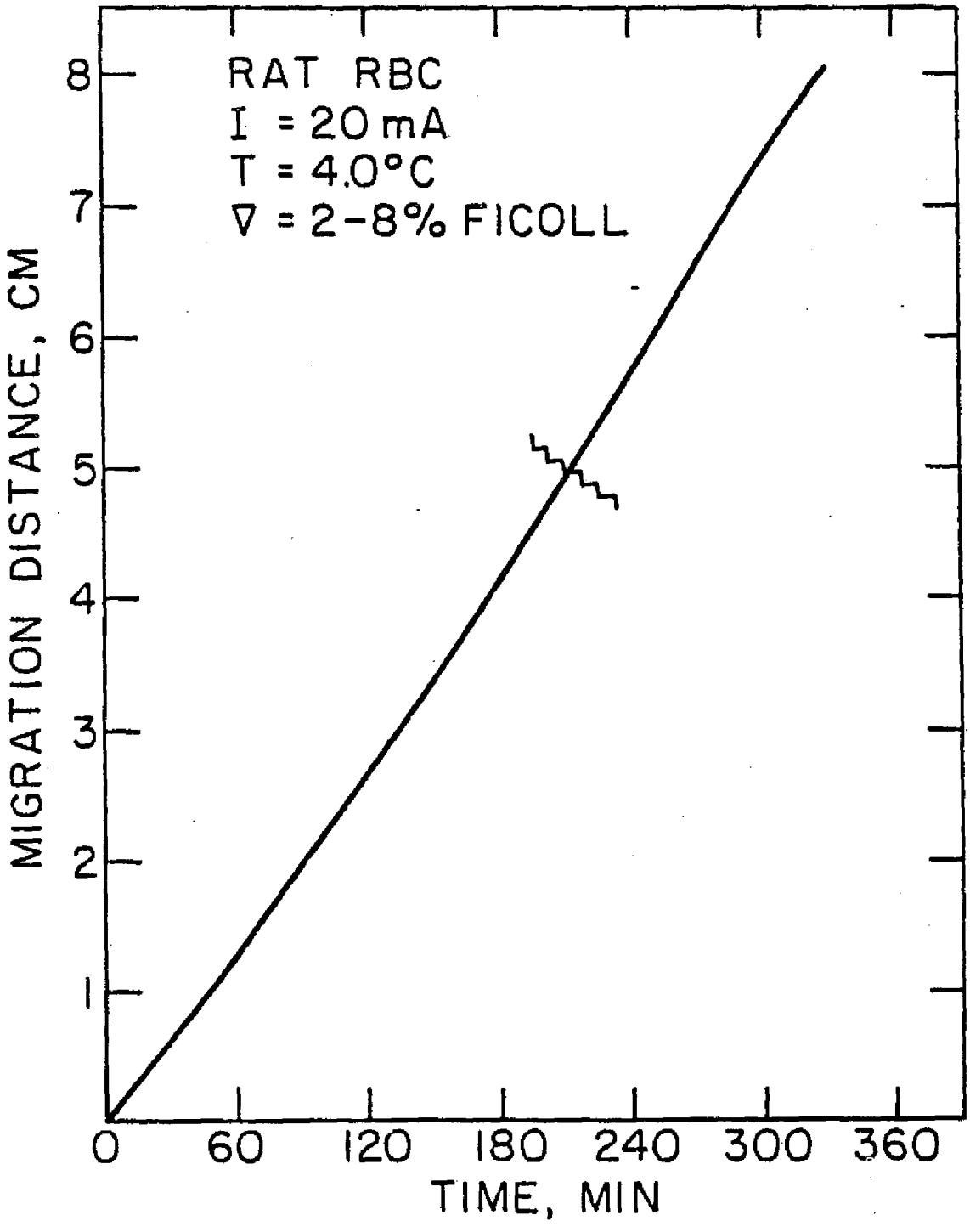

Figure 4. Comparison of migration plots for fixed rat and rabbit RBC's with the predicted function calculated for rat RBC's (solid line). Same physical conditions as in Fig. 14.

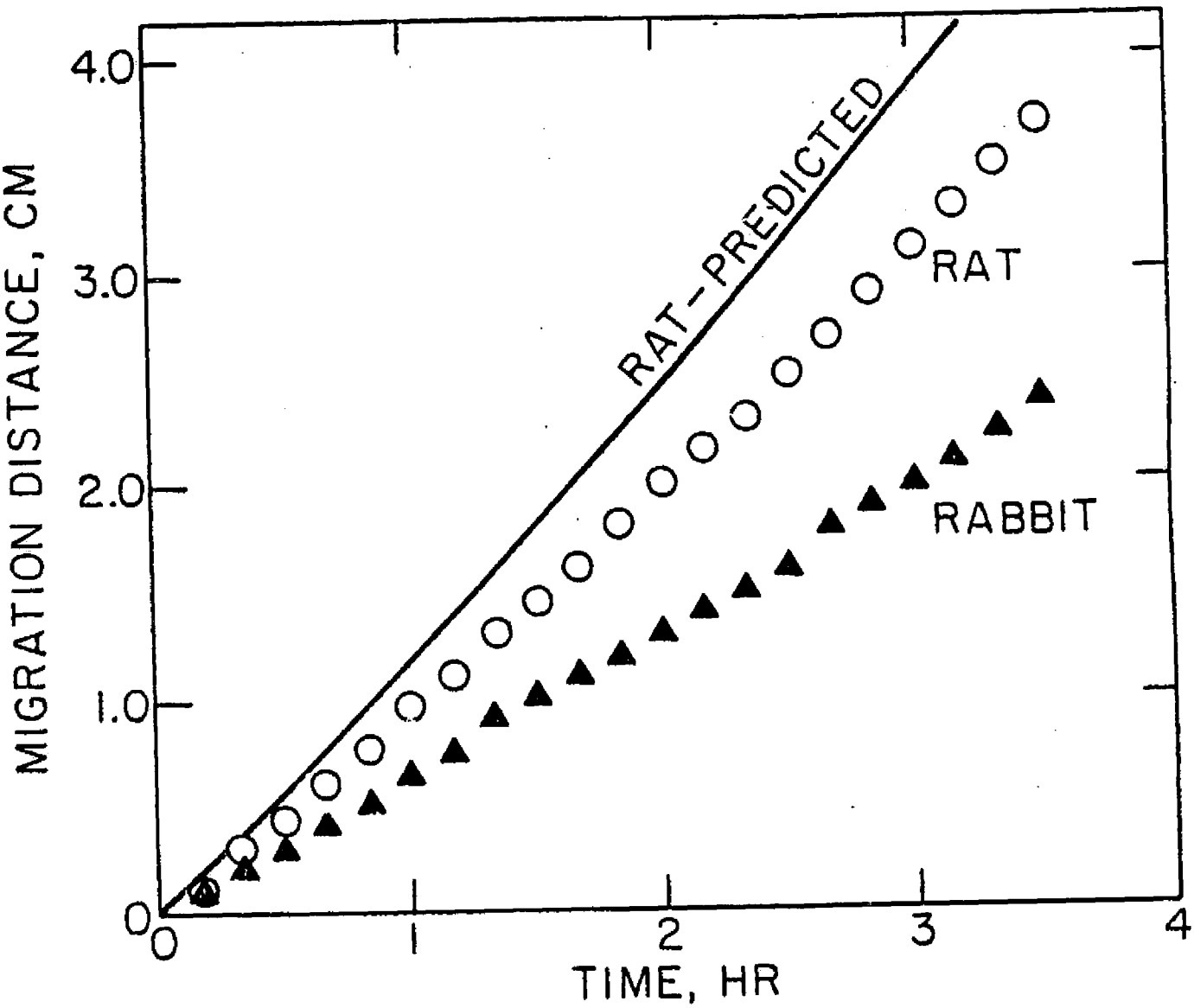

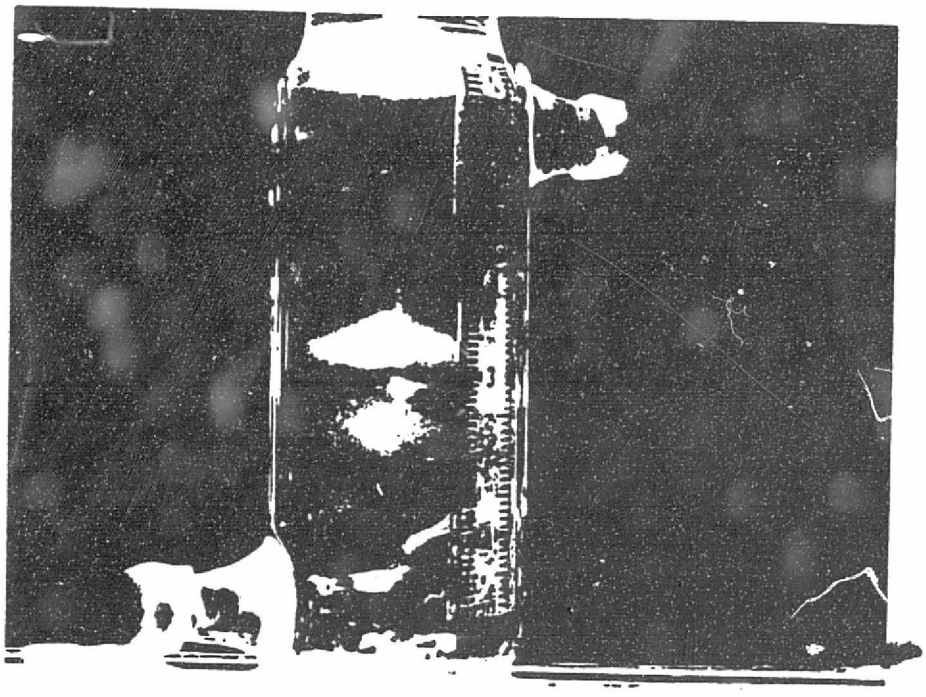

Figure 5. Photograph of red blood cell marker band (upper band) and broader band of HFK cells (lower band) after 3.0 hr of electrophoresis in the Ficoll gradient. The numbers on the scale give migration distance in cm.

Figure 6. Plot of the migration distance vs. time of electrophoresis of fixed rat red blood cells (circles) and HFK cells that had been selected by suspension culture (dots).

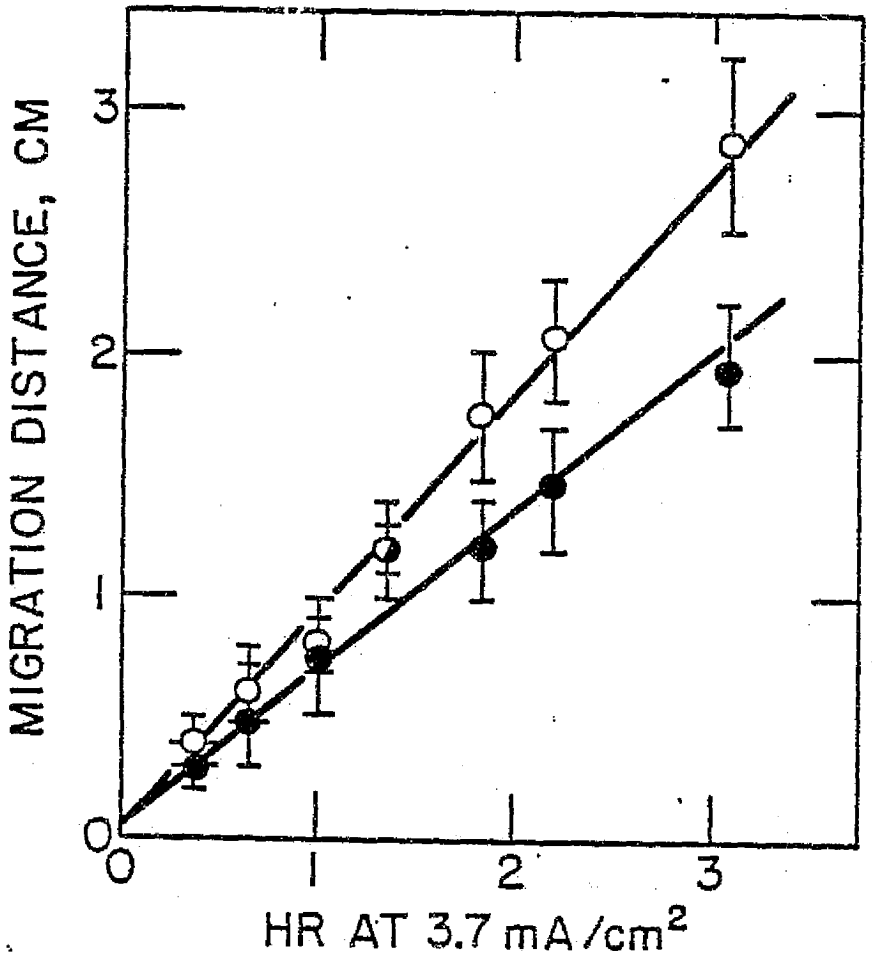

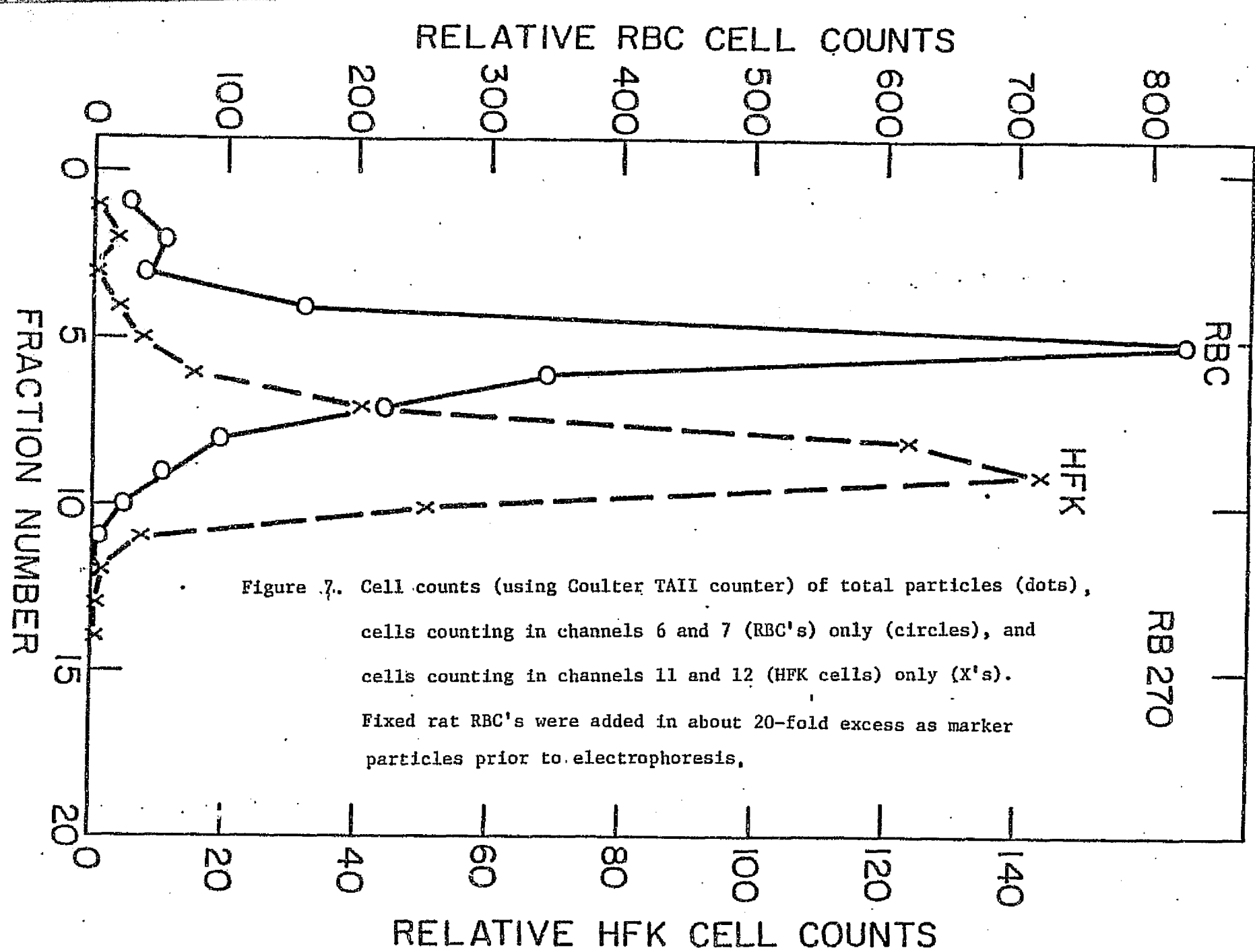

Figure 7. Cell counts (using Coulter TAII counter) of total particles (dots), cells counting in channels 6 and 7 (RBC's) only (circles), and cells counting in channels 11 and 12 (HFK cells) only (X's). Fixed rat RBC's were added in about 20-fold excess as marker particles prior to electrophoresis.

FIGURE 7.

Figure 8. Microscopic counts of fixed red blood cells (RBC) and HFK cells from the experiment described in figure 5. Fractions were collected directly into culture dishes and counted in the inverted phase contrast microscope 24 hr after harvesting. The large peak at fraction #8 consisted of multiplying, non-attaching cells.

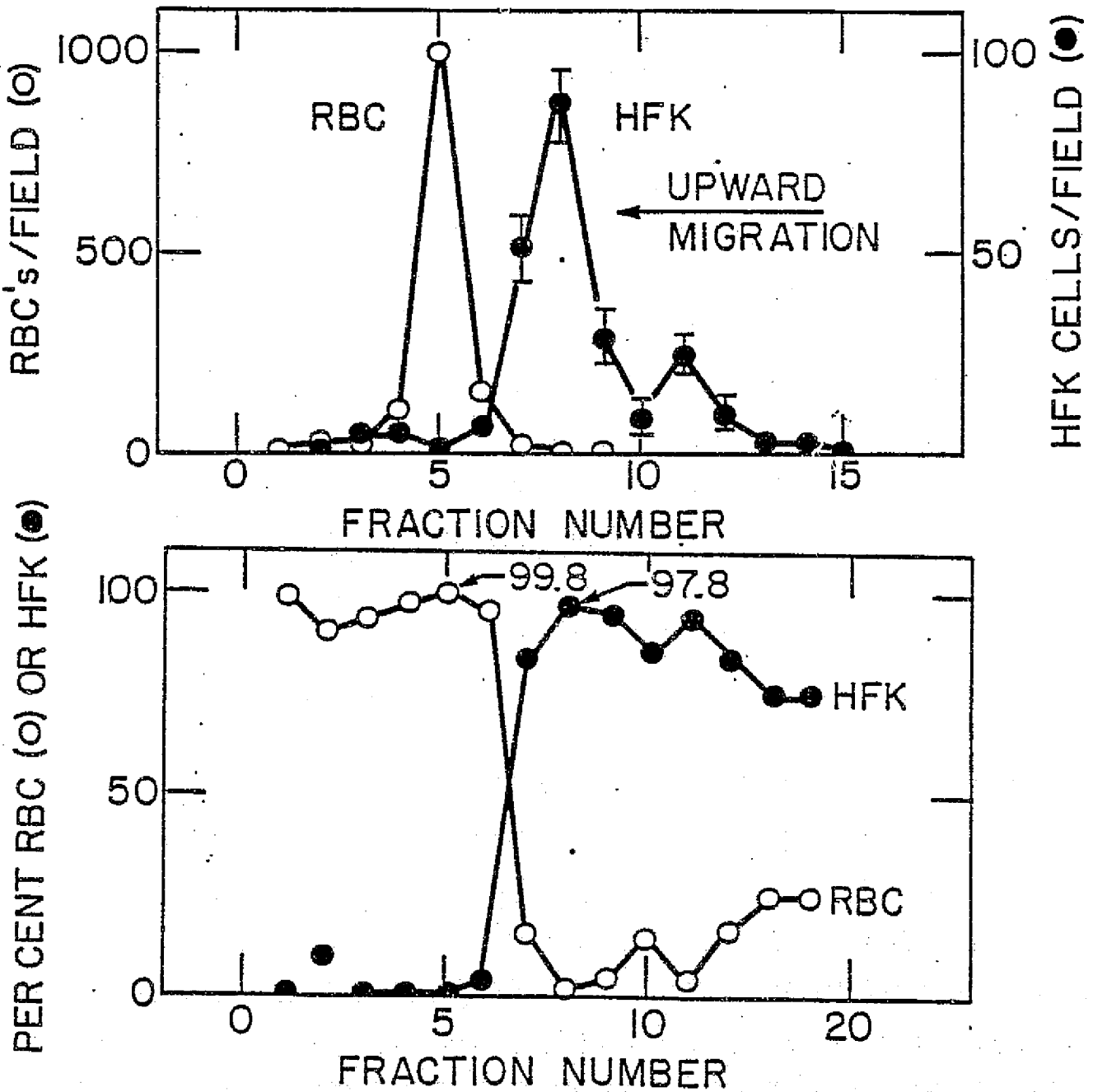

Figure 9. Evaluations of purity of fractions harvested from the experiment of figure 5. Microscopic counts were made of percent RBC's (circles) and percent HFK cells (dots) in each fraction. The maximum purity of each is indicated in percent at the top of the graph.

FIG. 10
CAPTION NEXT PAGE

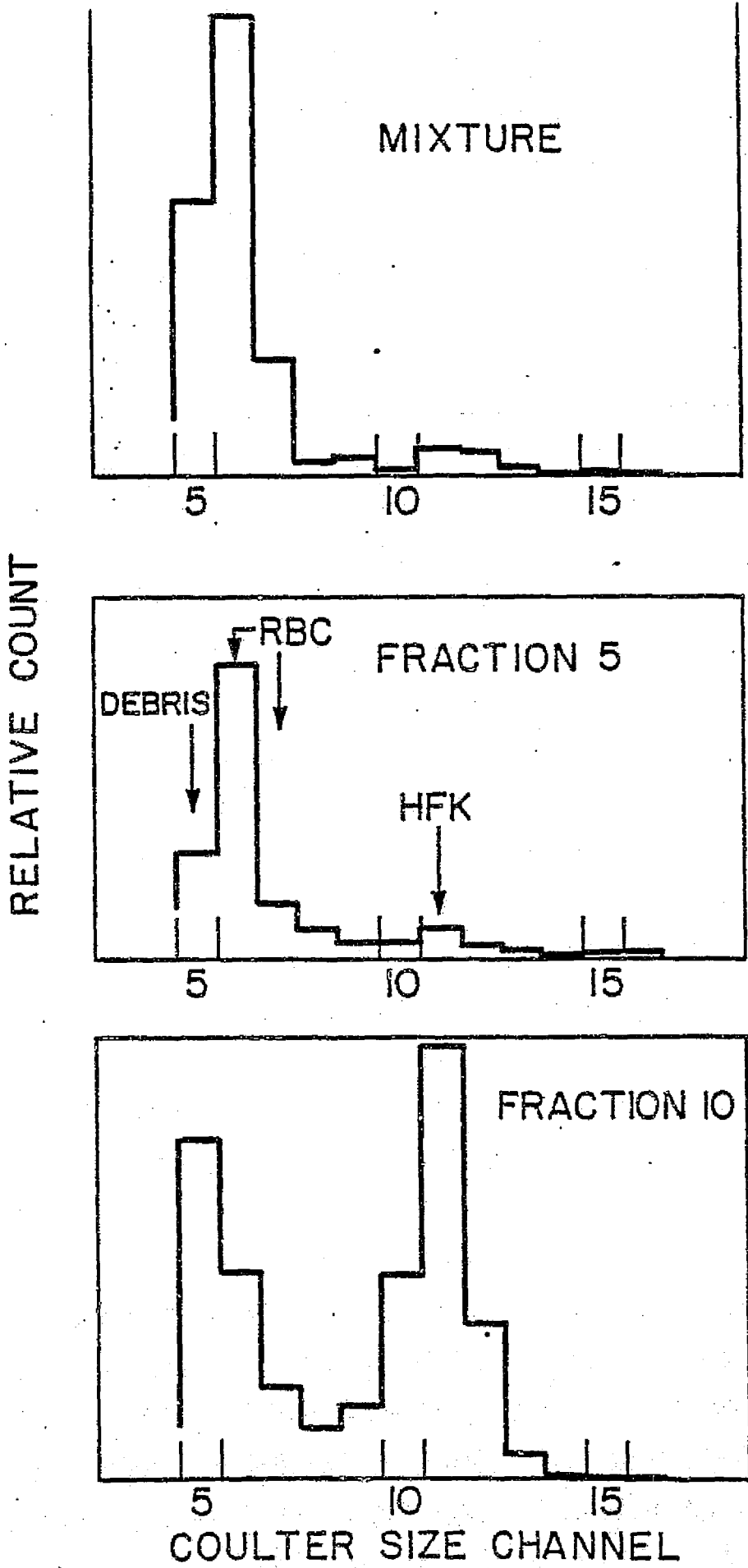

Figure 10. Coulter volume distributions of a starting mixture of marker fixed rat RBC's and HFK cells (top panel). Channel 10 corresponds to 10 μm diameter spheres, and each channel corresponds to a factor of 2 in volume. There are 16 channels, but particle counts in channels 1-4 are discriminated against, because they account mainly for debris and particles in counting solution. RBC's are counted in channels 6 and 7, and cultured cells are counted in channels 11 and 12. The volume distribution of fraction 5 (Figure 5) shows that most of the particles are RBC's (middle panel). The volume distribution of fraction 10 (Figure 5) shows that most of the particles are cultured cells (bottom panel). SEE PREVIOUS PAGE.

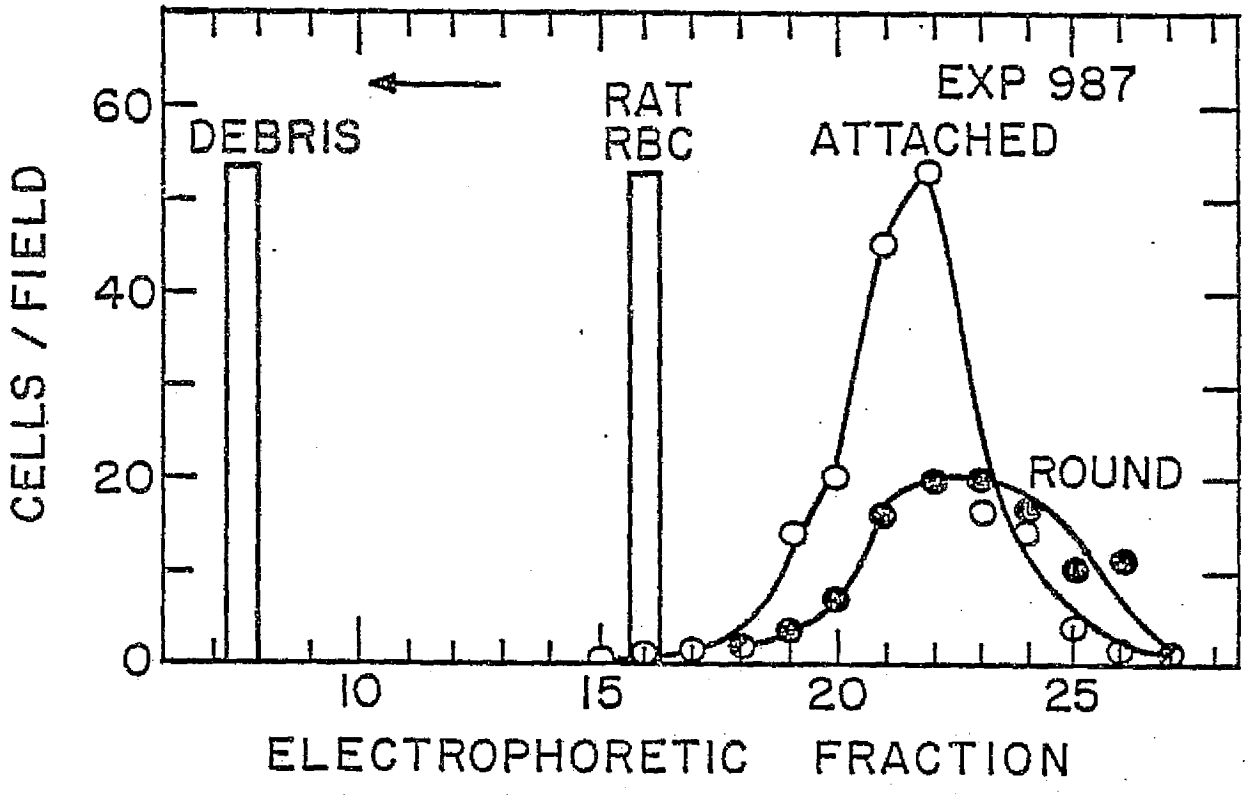

Figure 11. Density gradient electrophoretic profile of early-passage HFK-1 cells co-electrophoresed with fixed rat red blood cells as markers. The mobility of the kidney cells in the peak fraction is estimated to be 70% of that of the RBC's. Fractions were collected directly into culture vessels, and the number of cells per 16X field was counted 24 hr later.

Figure 12. Distance migrated in the density gradient column as a function of time of electrophoresis of human kidney HFK-7 cells. The lower envelope describes the migration of a narrow band consisting of round, non-adherent cells, and the upper envelope describes the migration of a broadly distributed band of cells consisting mainly of fibroblasts. The culture was in its 6th passage.

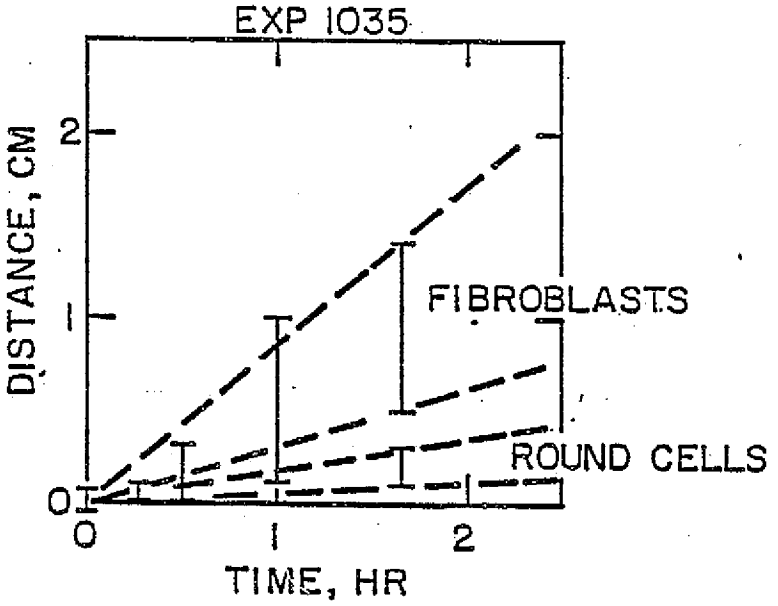

Figure 13. Electrophoretic migration of HFK-7 cells at the 2nd passage, as in Fig. 1. The uppermost envelope describes the migration of an extremely diffuse band of cells having a mixture of morphologies. The electrophoretic heterogeneity of this early-passage culture is reflected in the distribution shown in Fig. 3, in which the fraction numbers correspond to the numbers on the right axis of this migration plot.

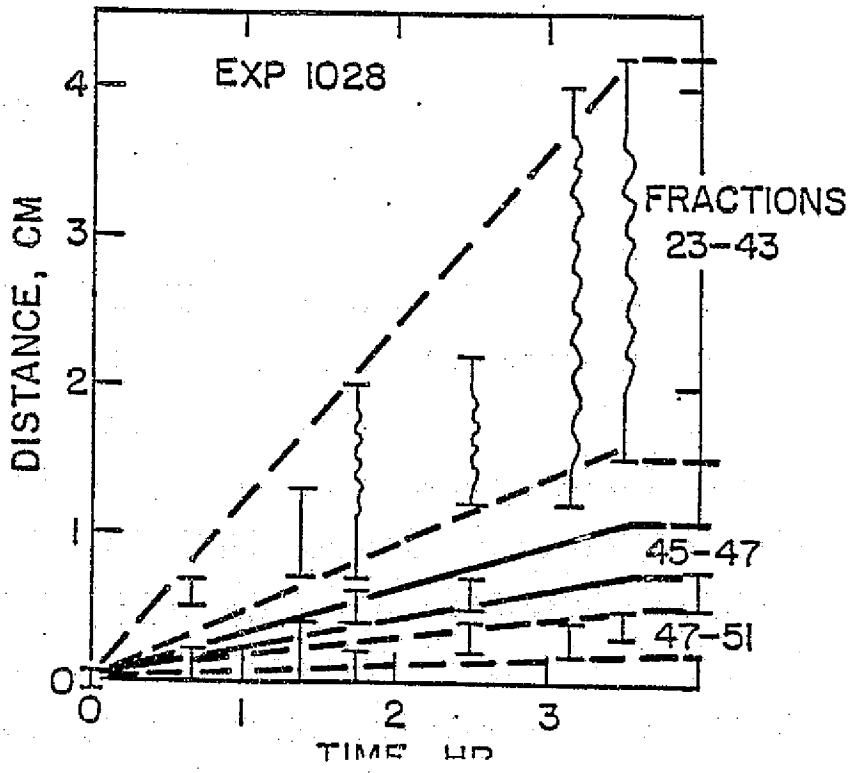

Figure 14. Electrophoretic profile of HFK-7, 2nd passage, cells subjected to density gradient electrophoresis for 3.75 hr and harvested in 1 ml fractions. Fraction numbers correspond to numbers in Fig. 2. Electrophoresis was upward, from right to left on the plot.

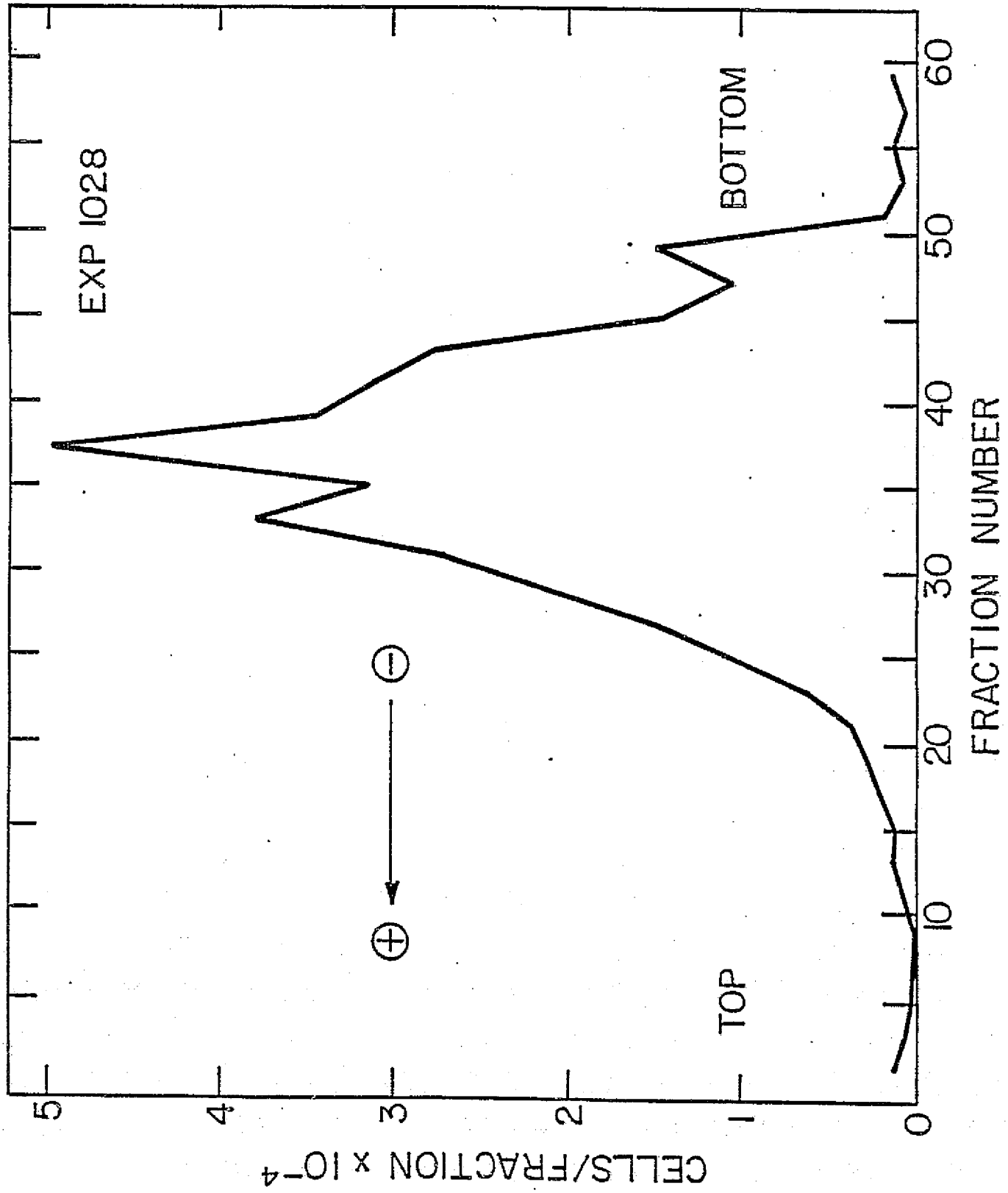

Figure 15. Electrophoretic profile of HFK-10 cells that attached and did not attach in culture. The profile corresponds to that determined by Coulter counting. The starting population was morphologically homogeneous (epithelioid).

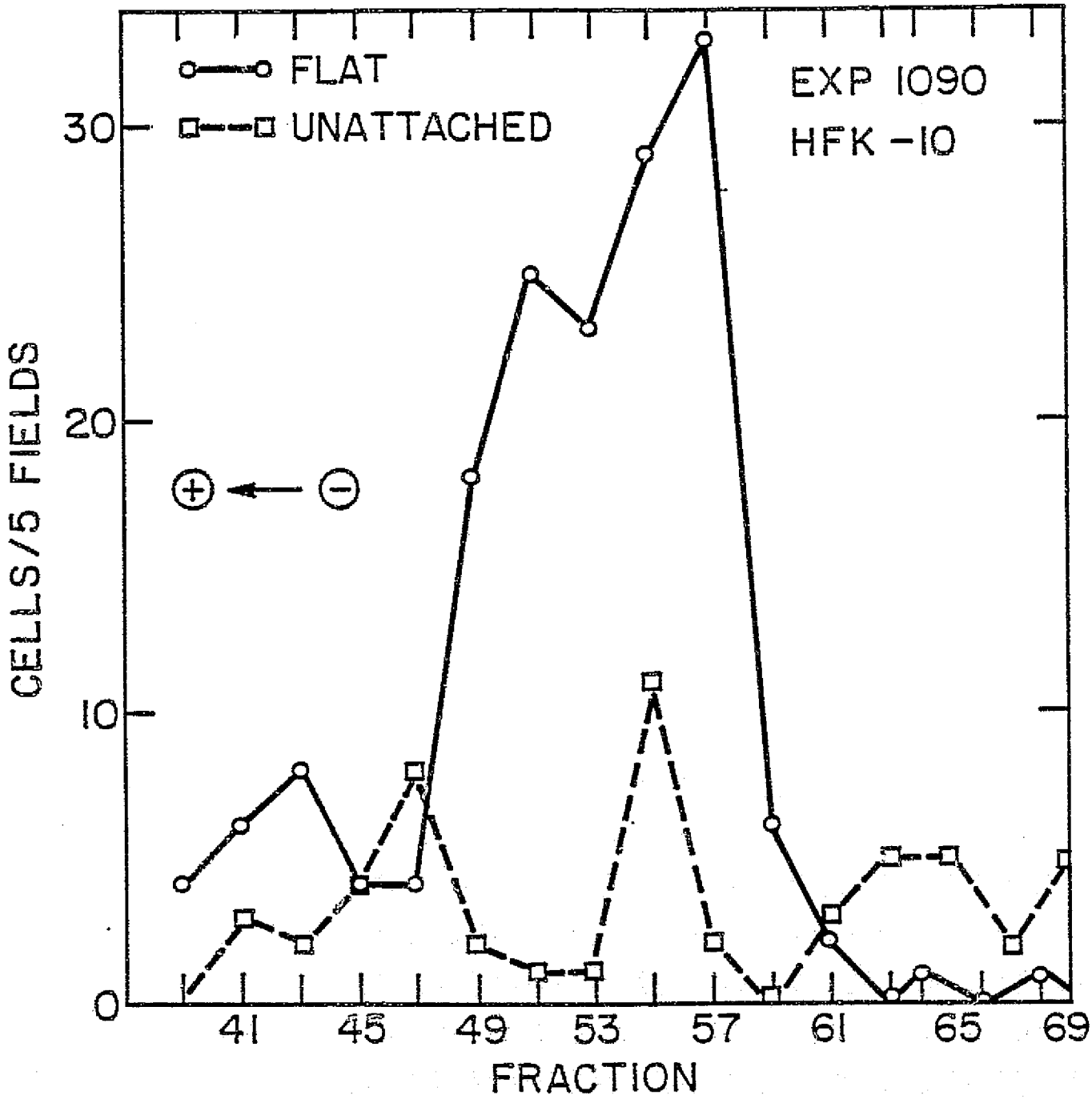

Figure 16. Coulter volume distributions indicate that different fractions of electrophoretically separated HFK-10 cells were similar in size. This observation is consistent with the observation that the starting population was morphologically homogeneous, and electrophoretically separated fractions did not differ morphologically.

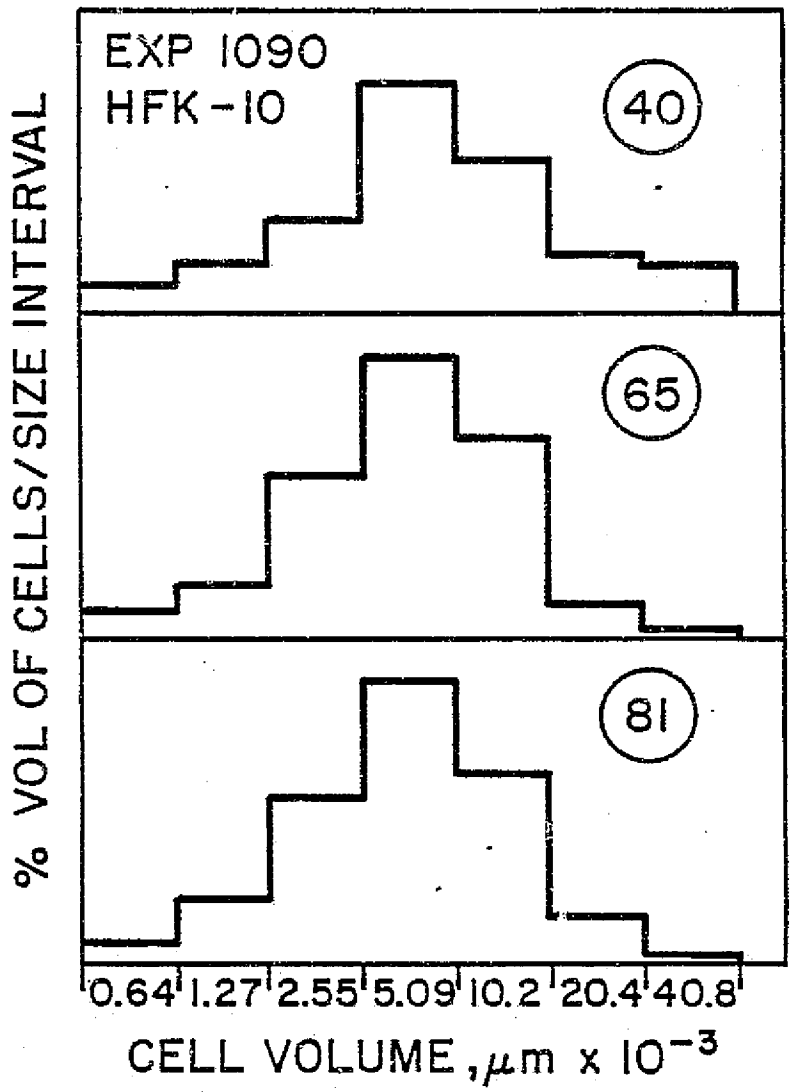

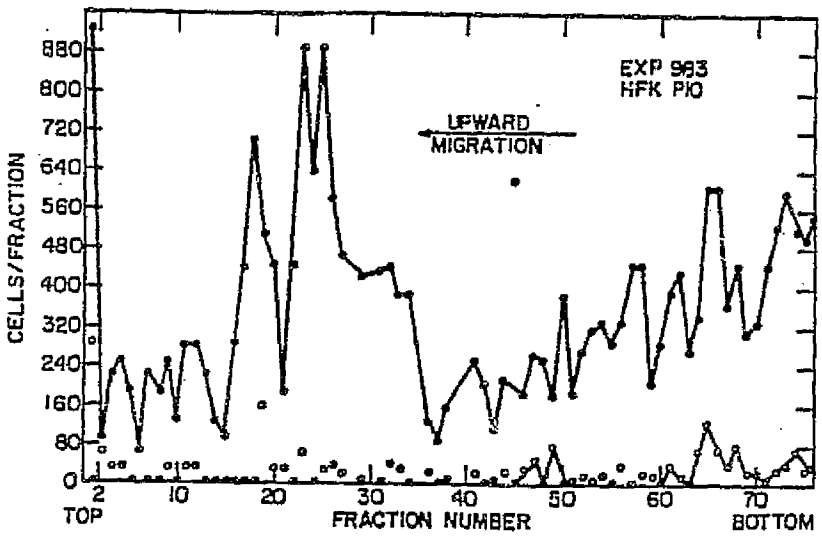

Figure 17. Electrophoretic profile of HFK cells at the 10th passage after explanting. Approximately 1.5 x 10^5 cells were suspended from a flask culture using 0.25% "trypsin" and 0.01 M EDTA. They were applied to the bottom of the density gradient and electrophoresed upward for 5.0 hr, and 10-drop fractions were collected from the top of the column. Fractions were Coulter counted for single cells (dots) and clumps of cells (circles). Counts in fractions greater than #40 are indicative of clumped cells that sedimented during electrophoresis.

Figure 19. Cell counts in cultures two weeks after collection of density-gradient electrophoretic fractions of HFK-3 cells. Suspended cells were non-adherent and were determined by Coulter counting of the supernatant medium in each culture. Attached cells were determined by trypsinizing each monolayer and Coulter counting. Volume distributions were obtained for both components of each cultured fraction. Electrophoretic migration was toward the left.

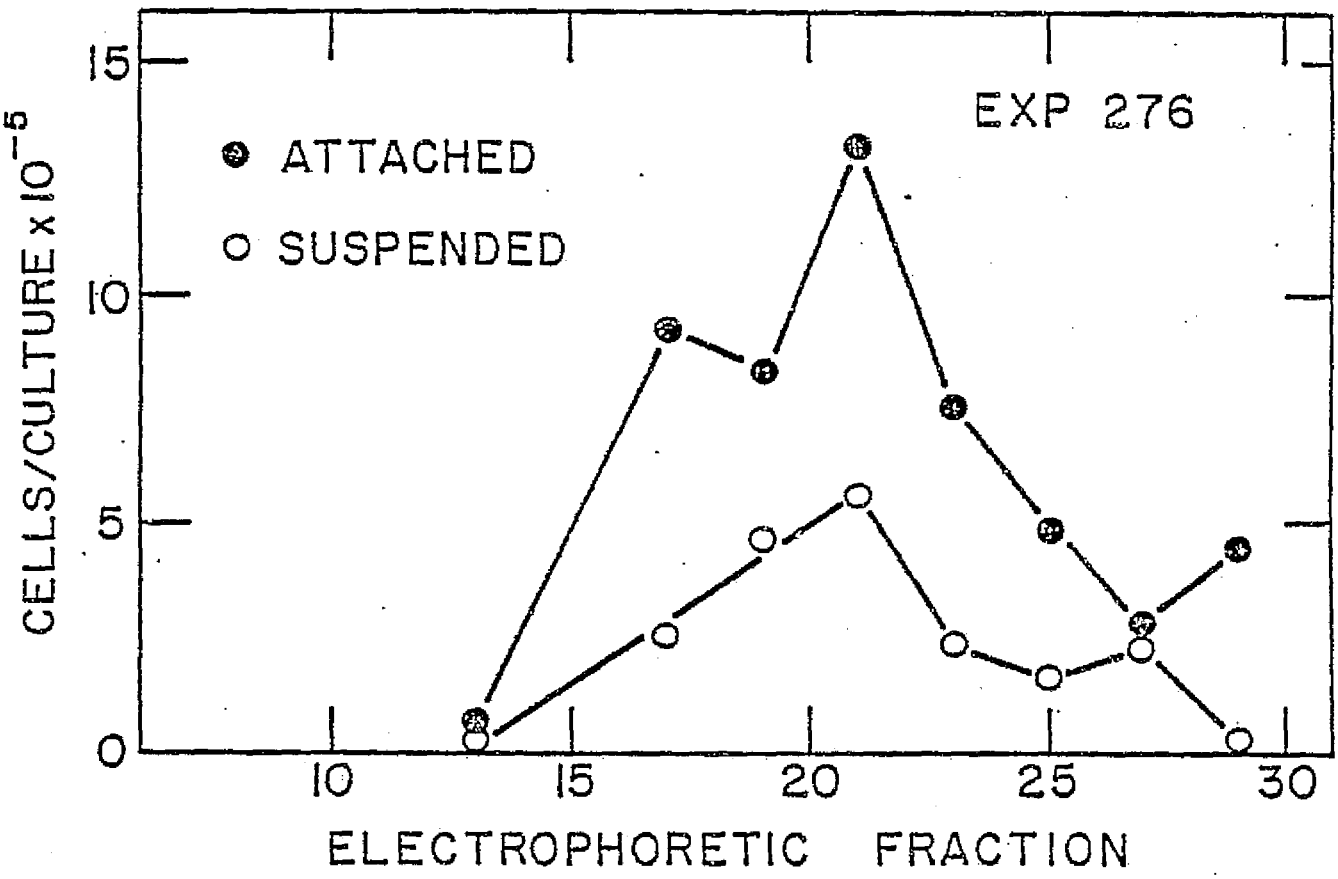

Figure 20. Electrophoretic profile of HFK-9 cells, passage 4, as determined by Coulter counts of harvested fractions after density gradient electrophoresis. The size classes (large) corresponding to Coulter volume channels 9 through 14 are included in the cell count. Electrophoretic heterogeneity is evident, with at least a trimodal distribution. Page 16-23

Figure 21. Electrophoretic profiles from the same experiment as in Fig. 20. In this case the distributions of cells having specific sizes were determined by plotting only the cell counts in individual Coulter channels. Channel 12 cells, for example, consist of at least two electrophoretic subpopulations. Page 16-24.

Figure 22. Electrophoretic profile of HFK-10 cells as determined by phase contrast microscopy of cultures from each fraction made by plating 10-drop fractions in 5 ml of complete medium (BME + 10% fetal bovine serum). Attached cells are distinguished from dead cells. This page.

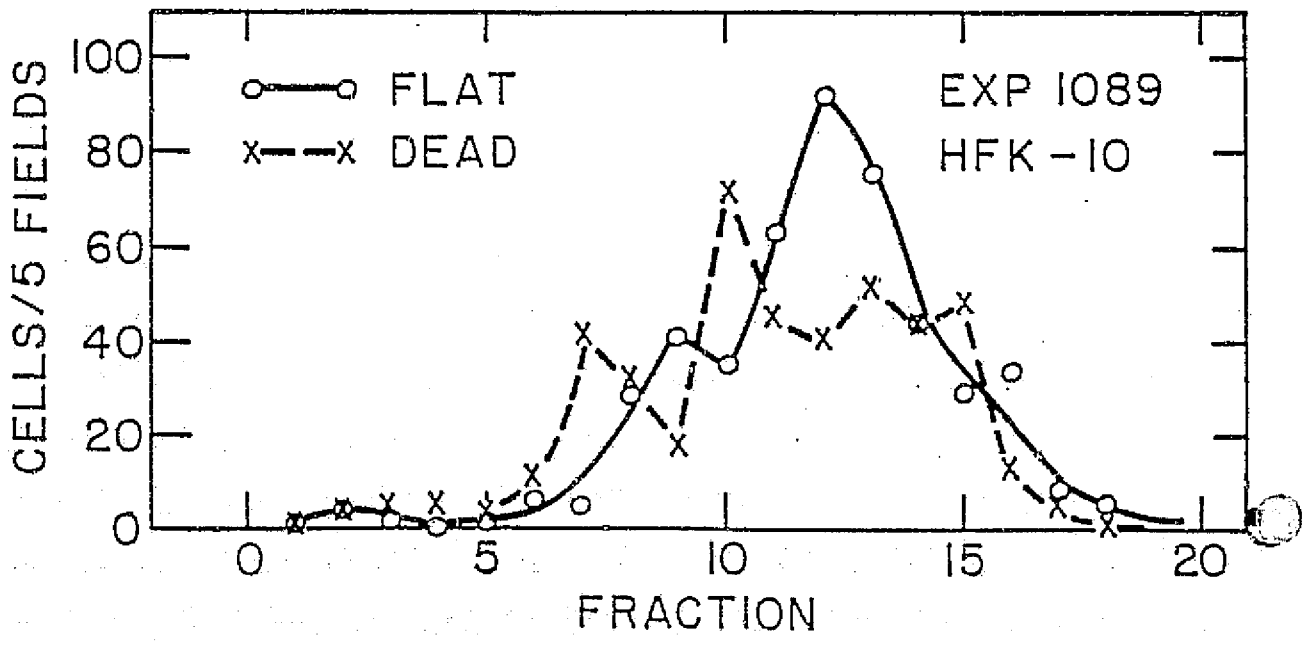

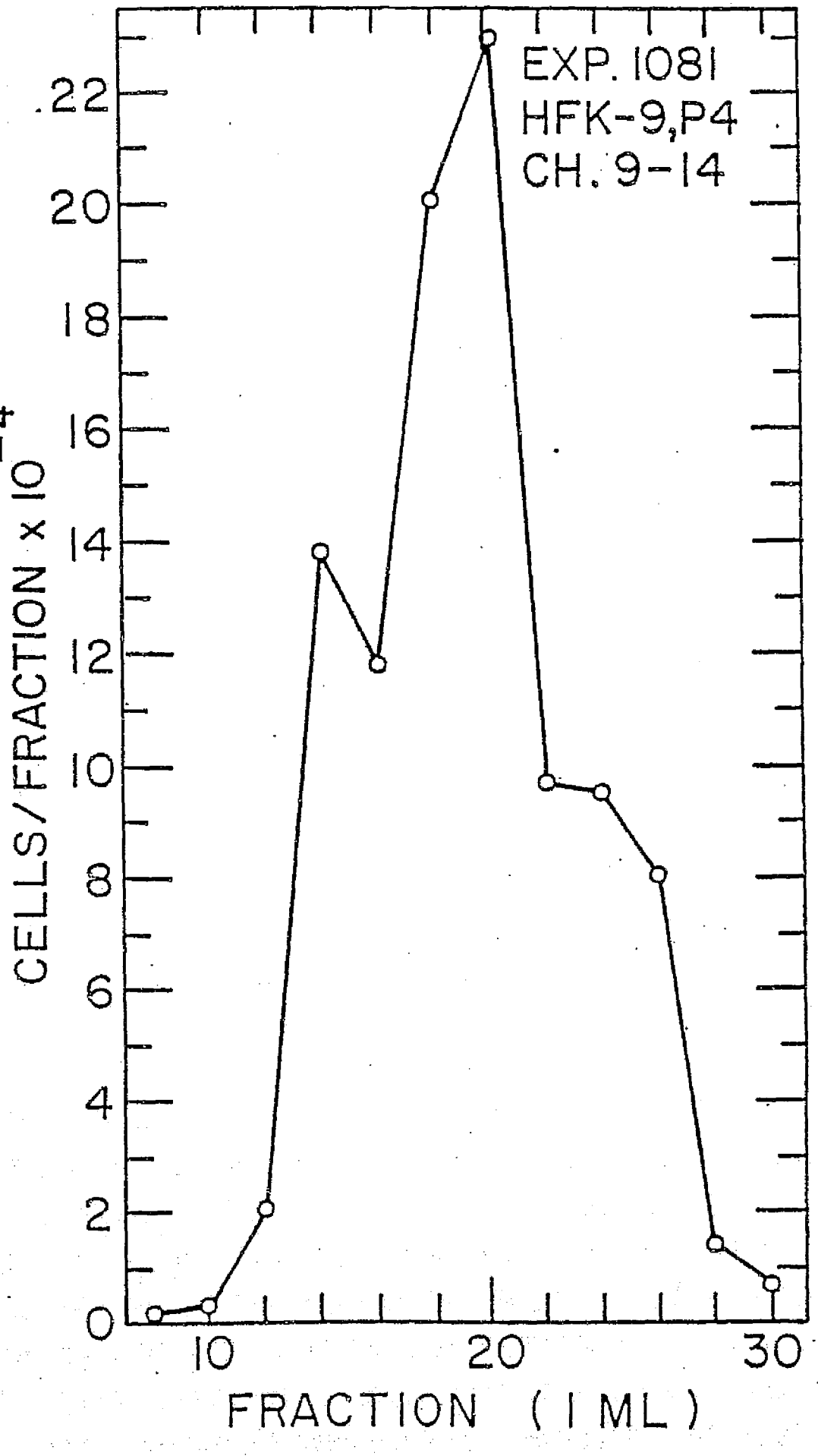
EXP. 1081
HFK-9,P4
CH. 9-14
CELLS/FRACTION x 10^{-4}
0
2
4
6
8
10
12
14
16
18
20
.22
10
20
30
FRACTION (1 ML)

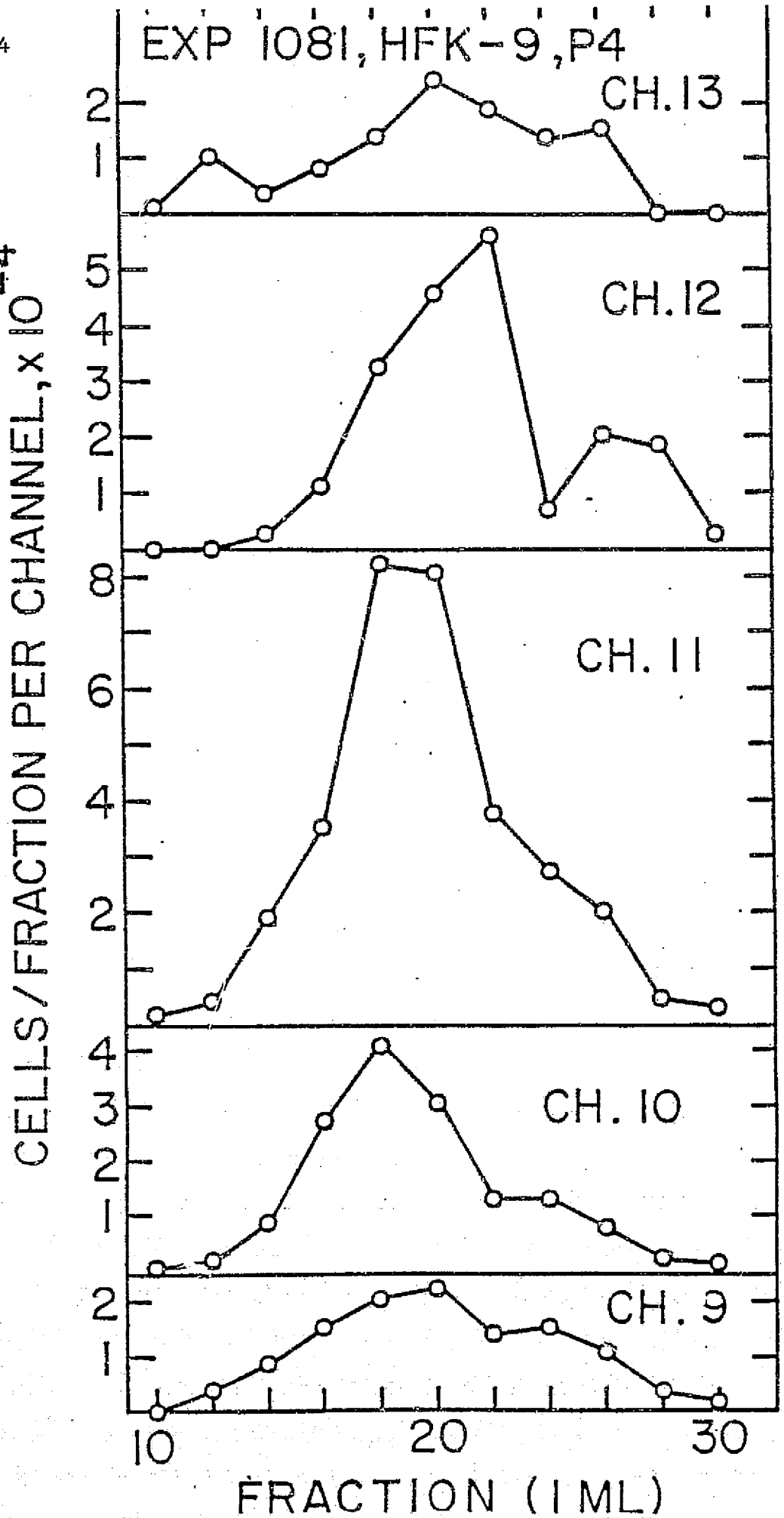
EXP 1081, HFK-9, P4
CH. 13
CH. 12
CH. 11
CH. 10
CH. 9
CELLS/FRACTION PER CHANNEL, x 10⁻⁴
FRACTION (1 ML)
10
20
30

Figure 21

Figure 23. Electrophoretic profile of all cells after density gradient electrophoresis of HFK-10 cells.

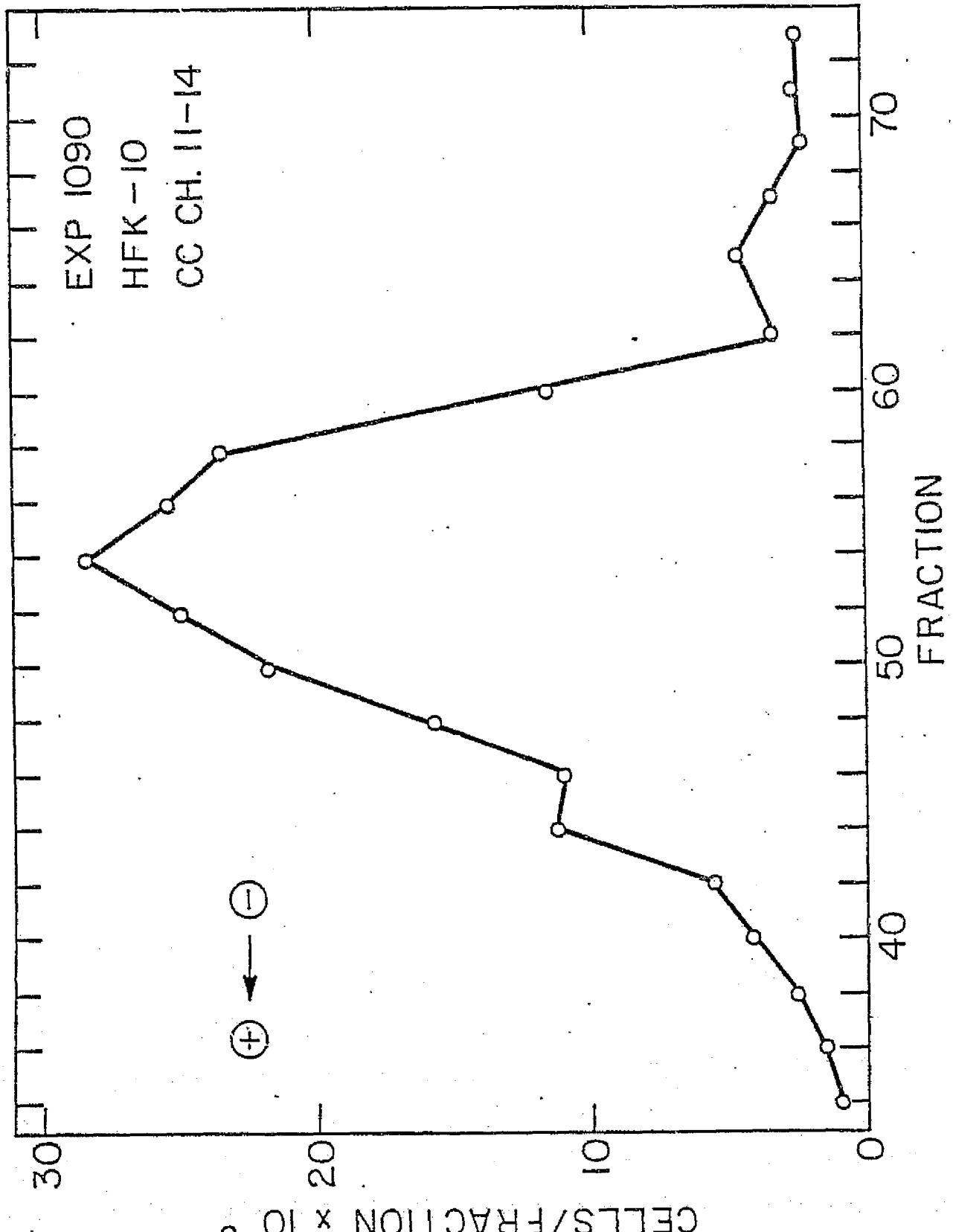

Figure 24. Microscopic counts of cultures in same experiment as shown in Fig. 23. Dead cells predominate at very high and very low mobilities.

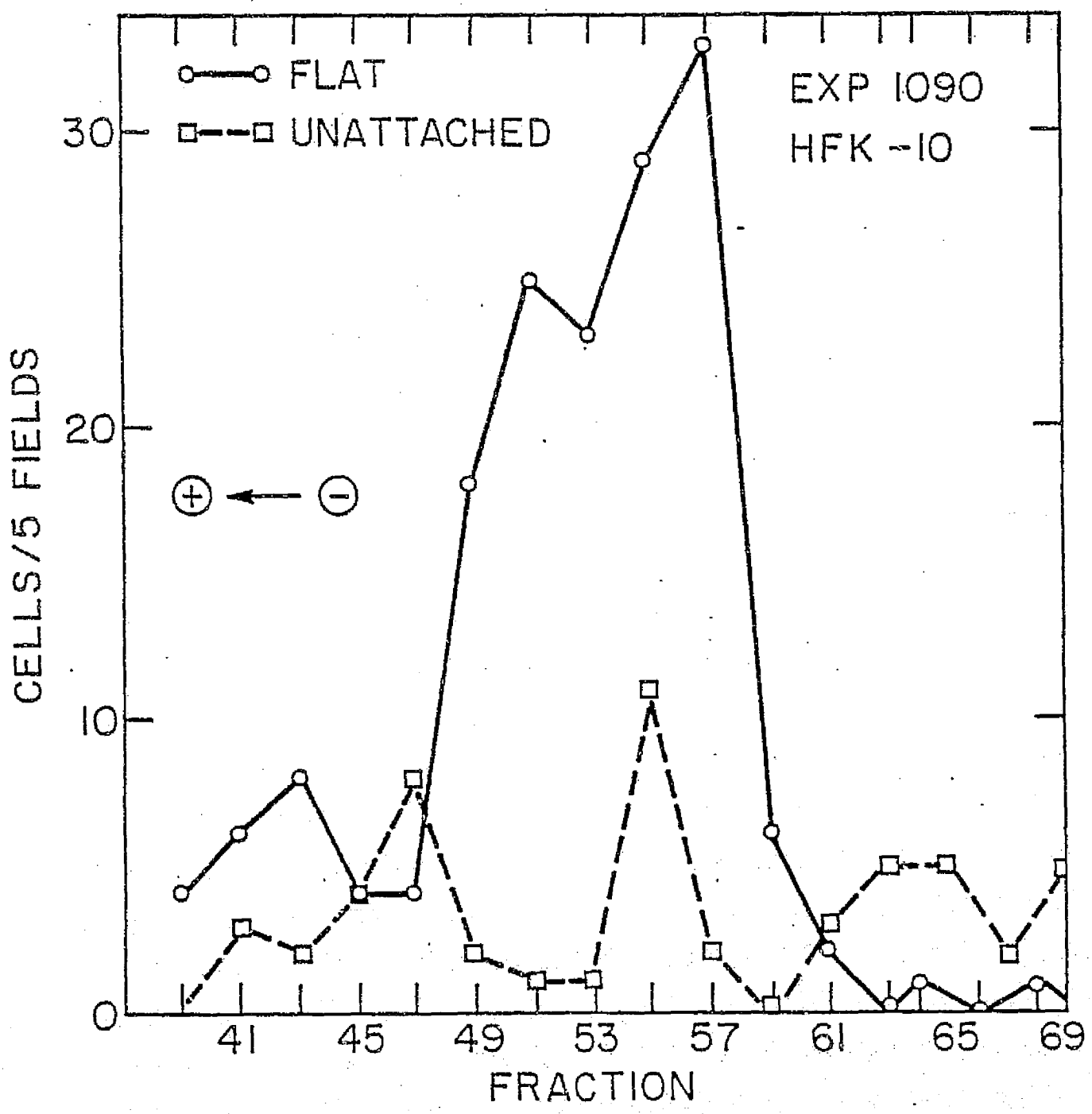

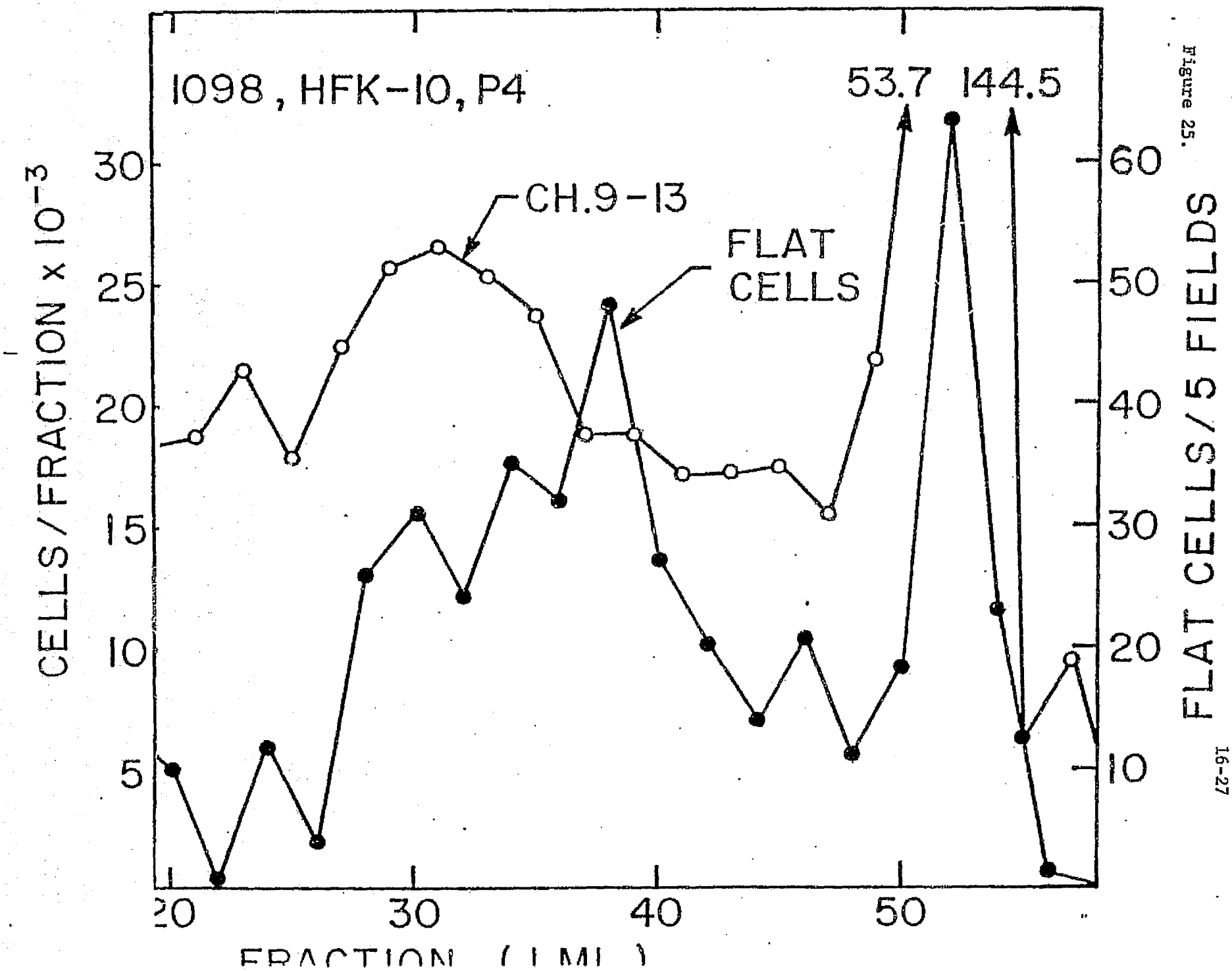
1098, HFK-10, P4
53.7
144.5
CH.9-13
FLAT CELLS
CELLS/FRACTION x 10^{-3}
FLAT CELLS/5 FIELDS
30
25
20
15
10
5
60
50
40
30
20
10
20
30
40
50
FRACTION (1 ML)

Figure 25.

Figure 25. Combined electrophoretic profiles of HFK-10 cells, passage 4, as determined by phase contrast microscopy of cultured fractions (dots) and by Coulter counting of all cells (circles). A highly viable, very-low-mobility subpopulation of cells existed in HFK-10 cultures. The high mobility cells (fractions 15-25) showed very low viability in culture. Page 38.

Figure 26. Electrophoretic profile of HFK-13 cells, passage 5, as determined by Coulter counting of all cells and storing counts in individual Coulter volume channels on computer disk. This page.

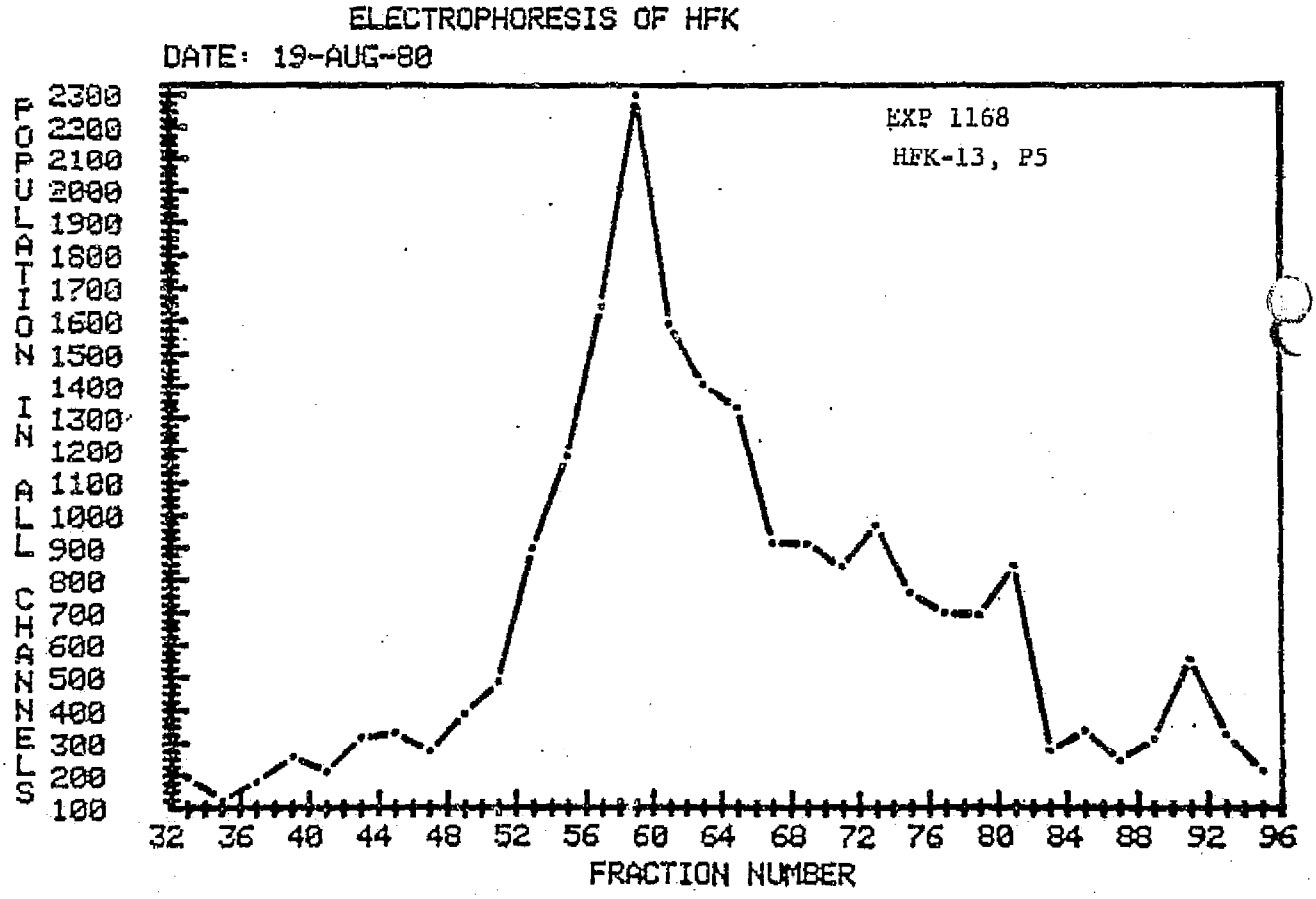

Figures 27-28-29. Electrophoretic profiles of specific size classes of HFK-13, Passage 5, cells: Coulter channels 5 and 6 (small), 9 (medium), and 13 plus 14 (large) respectively. Data from the experiment of Fig. 26. Plots were developed from stored files of the complete data set (all individual Coulter volume channels) for the experiment. Exp 1168.

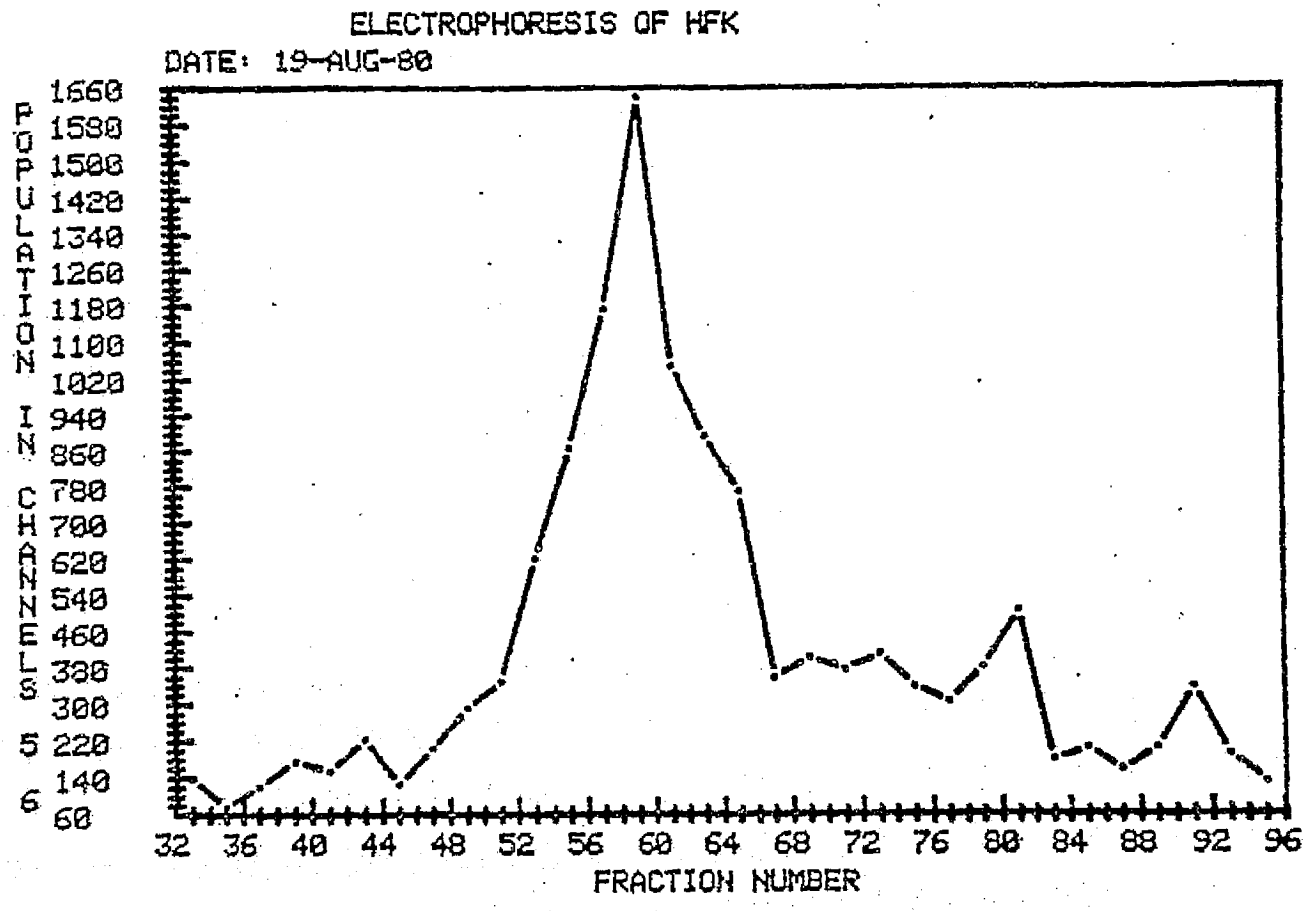

Figure 28.

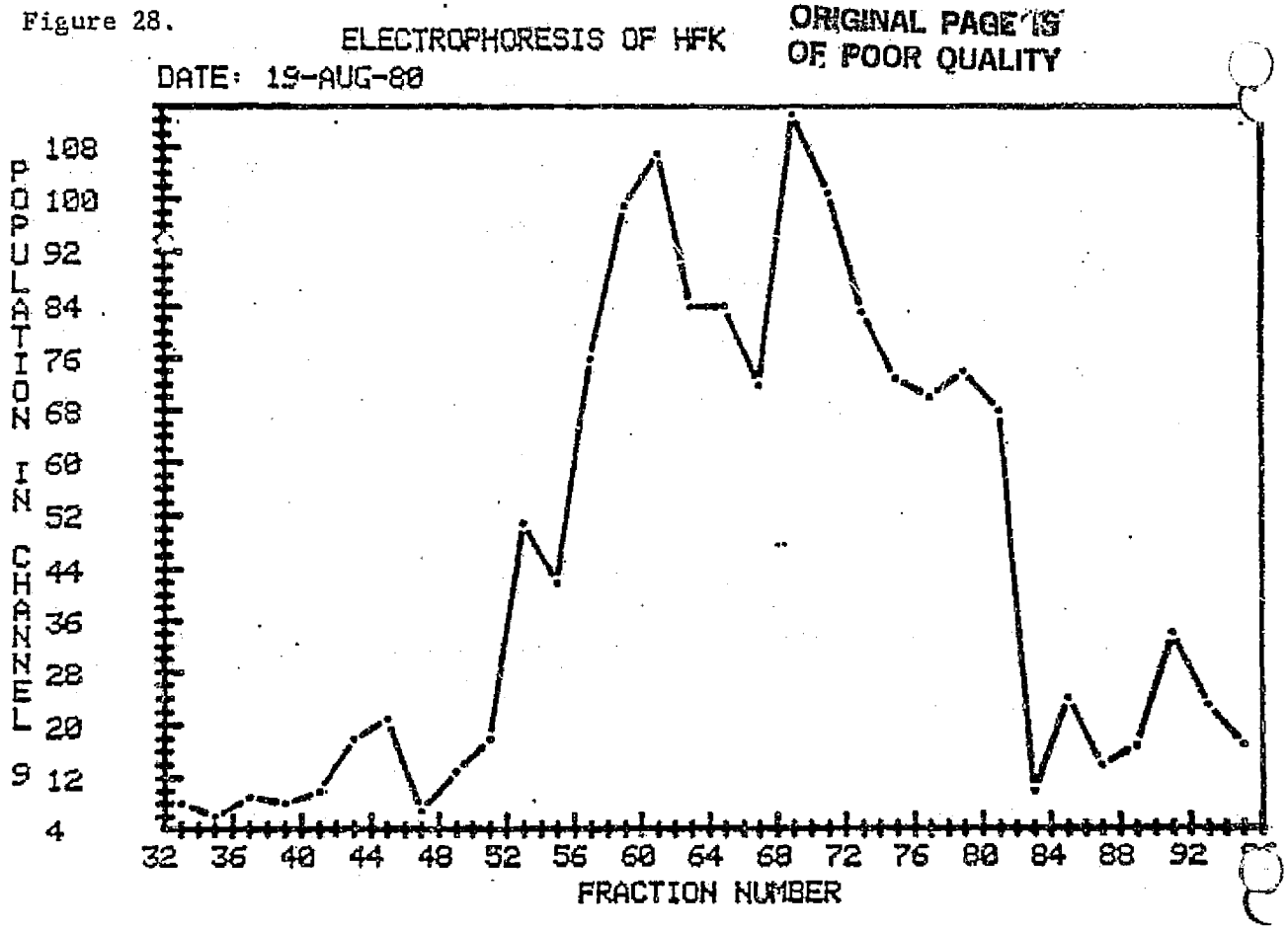

Figure 29.

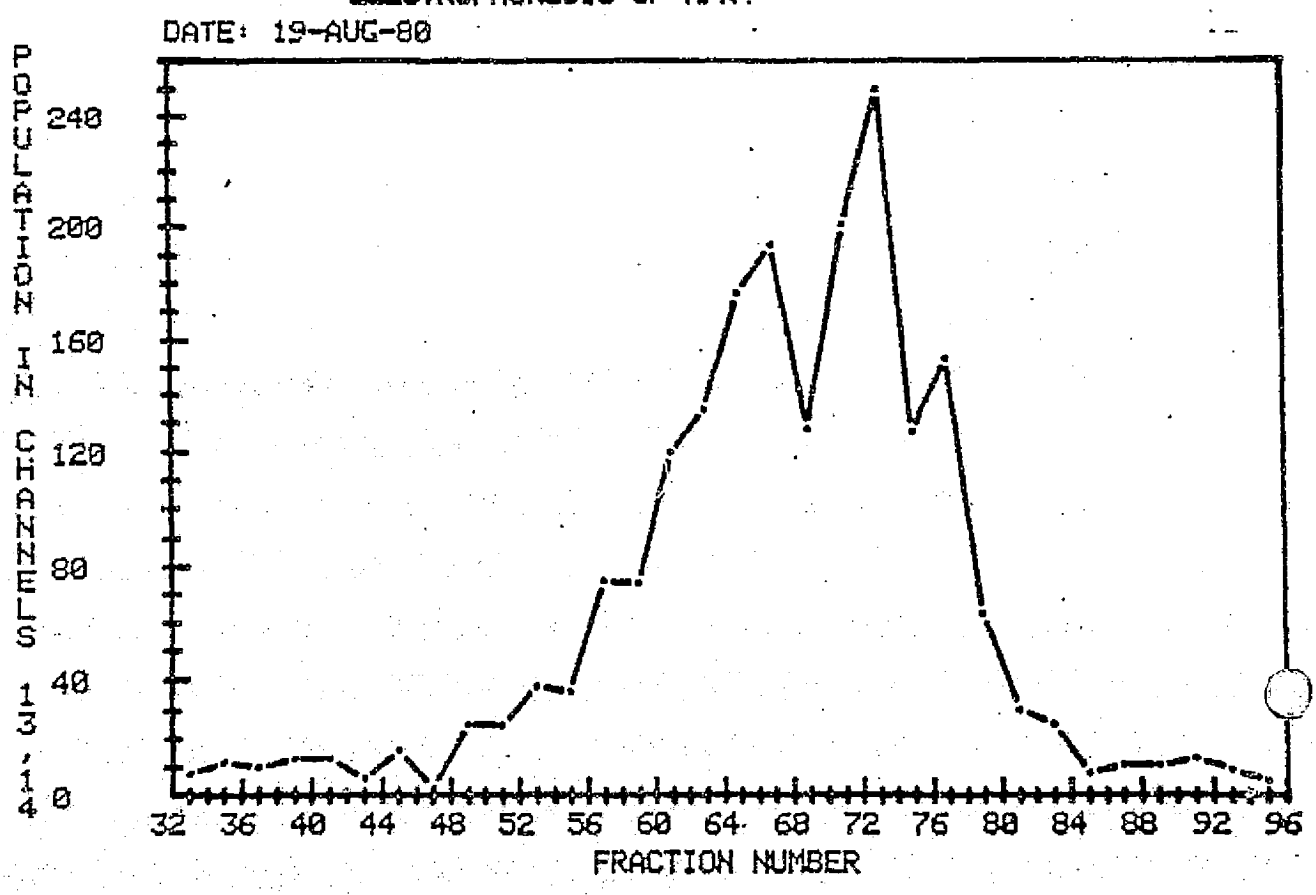

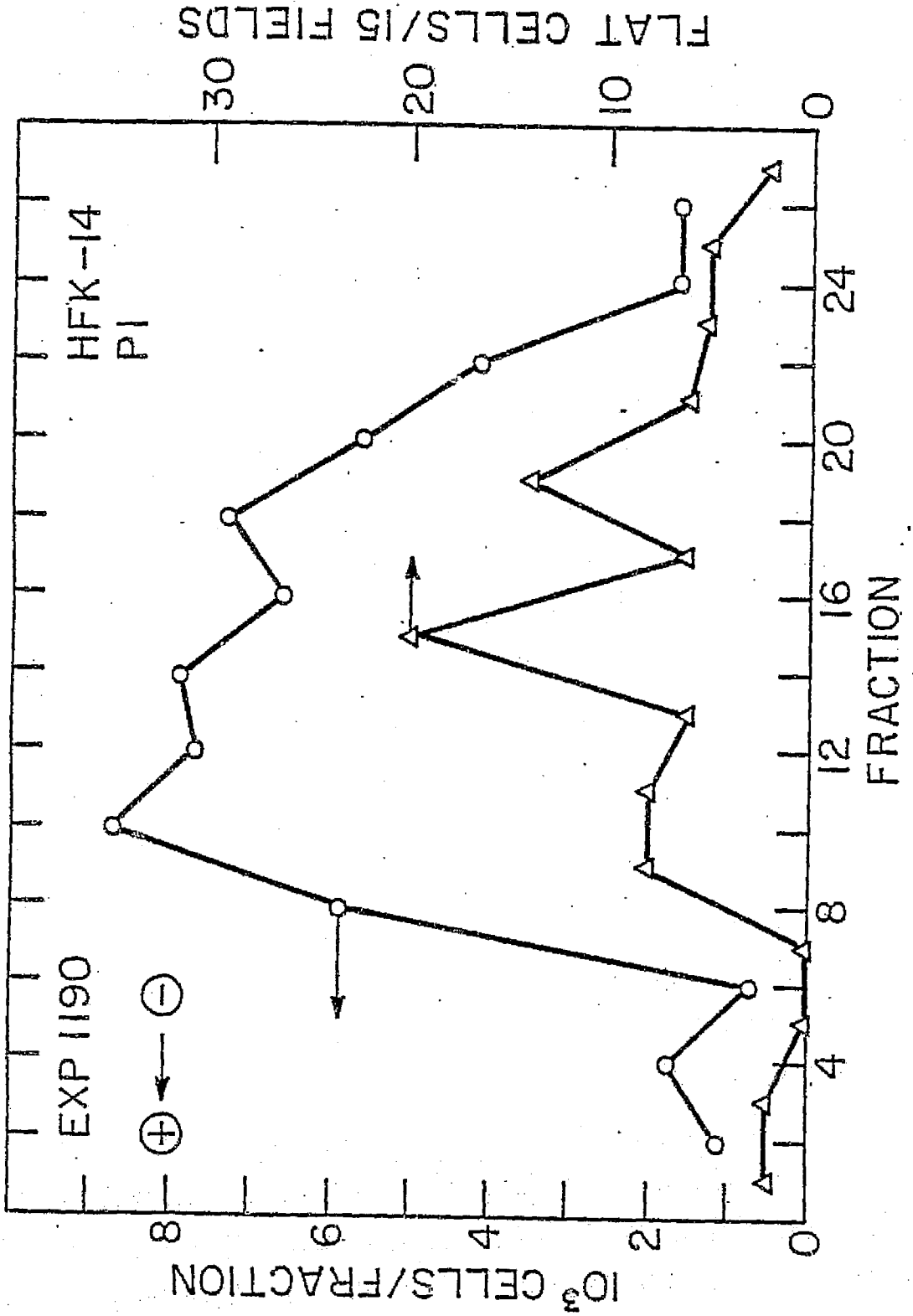

Figure 30. Electrophoretic profile of HFK-14 cells, passage 1, as determined by Coulter count with volume selection and by microscopy of cultures of collected fractions. This profile also shows that higher mobility cells had lower viability.

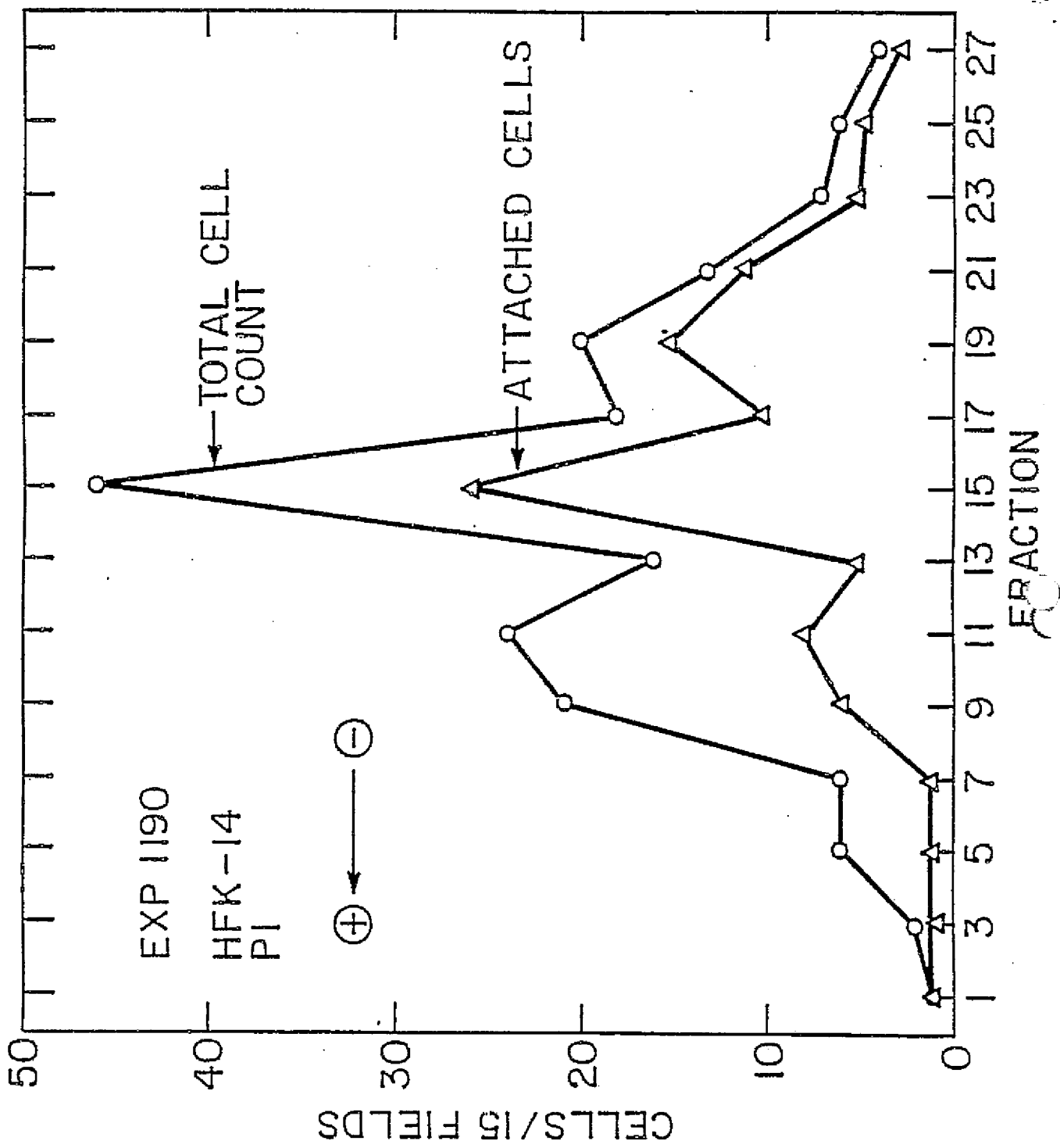

Figure 31. Electrophoretic profile of HFK-14 cells, passage 1, as determined by counting cells per microscopic field in cultures of collected fractions. In this culture, higher mobility cells had lower viability.

C-4

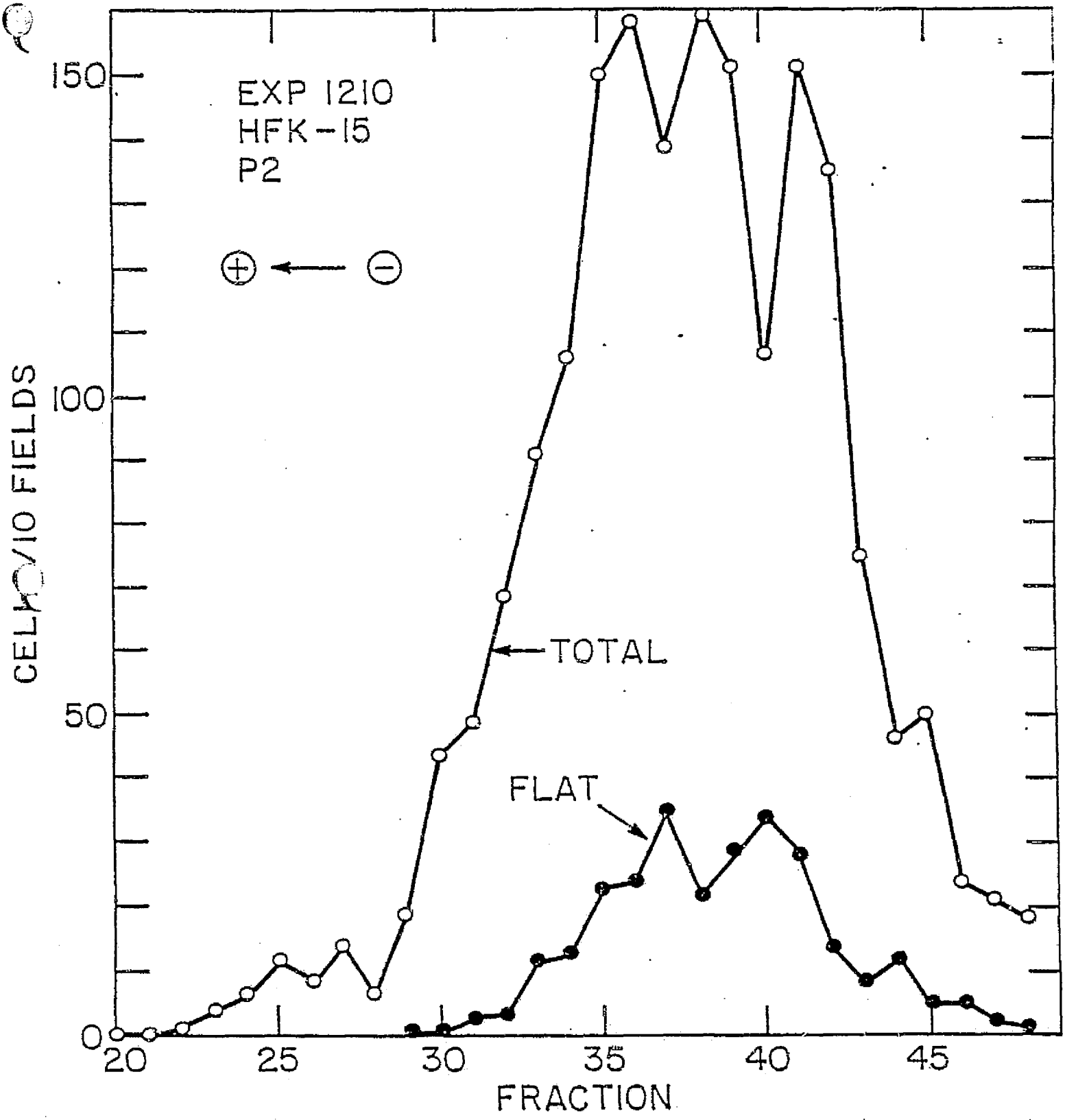

Figure 32. Electrophoretic profile of HFK-15 cells, passage 2, as determined by counting cells per microscopic field in cultures of collected fractions. Post-separation viability was low in

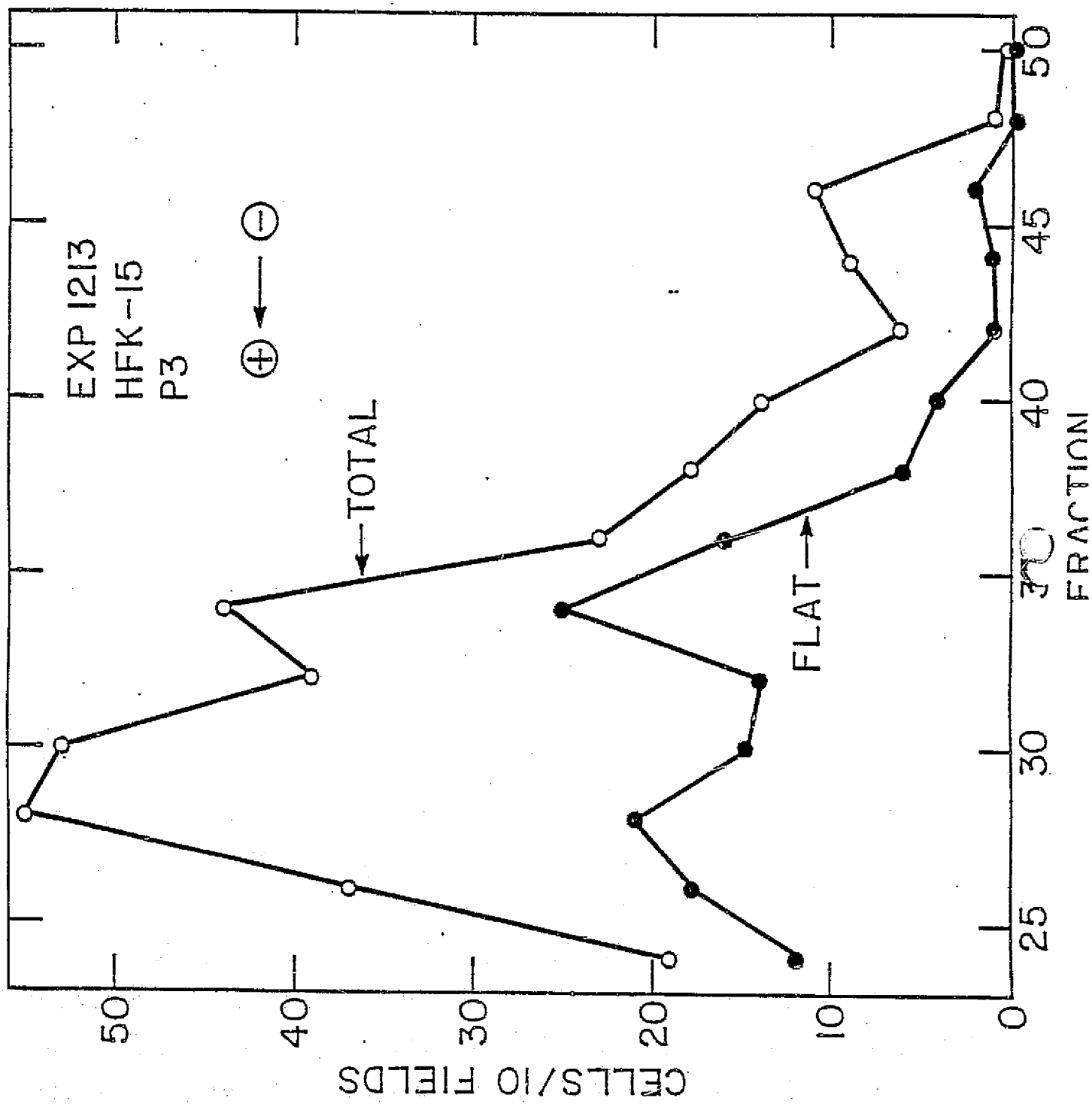

Figure 33. Electrophoretic profile of HFK-15 cells, passage 3, as determined by counting cells per microscopic field in cultures of collected fractions. In this culture higher mobility cells had lower viability. Exp 1213.

Chapter 17.

Identification and Quantitation of Morphological Cell Types in Electrophoretically Separated Human Embryonic Kidney Cell Cultures.

Kimberly B. Williams, M. Elaine Kunze, and Paul Todd

IDENTIFICATION AND QUANTITATION OF MORPHOLOGICAL CELL TYPES IN ELECTROPHORETICALLY SEPARATED HUMAN EMBRYONIC KIDNEY CELL CULTURES

Kimberly B. Williams, M. Elaine Kunze, and Paul Todd

ABSTRACT

Four major cell types have been identified by phase microscopy in early-passage human embryonic kidney cell cultures: small and large epithelioid, domed, and fenestrated cells. Fibroblasts are also present in some explants. The per cent of each cell type changes with passage number as any given culture grows; as a general rule, the fraction of small epithelioid cells increases, while the fraciton of fenestrated cells, always small, decreases further. When fibroblasts are present, they alway increase in percentage of the total cell population. Electrophoretic separation of early-passage cells showed that the domed cells have the highest electrophoretic mobility, fibroblasts have an intermediate high mobility, small epithelioid cells have a low mobility, broadly distributed, and fenestrated cells have the lowest mobility. All cell types were broadly distributed among electrophoretic subfractions, which were never pure but only enriched with respect to a given cell type.

INTRODUCTION

Primary human embryonic kidney cells, when placed in culture, maintain several differentiated functions (Leighton et al., Bernik and Kwaan, Taub et al., Sato), and these are reflected biochemically as well as morphologically. Commercializable biochemical products are produced by some of these subpopulations, so their purification and characterization has both scientific and practical value. The correlation of a morphological property with a biochemical function, as has been done in the case of the pancreas, liver, and anterior pituitary, for example, would greatly facilitate the purification of biochemically specific kidney cells for study and applications.

MATERIALS AND METHODS

Human embryonic kidney cells were purchased from MA Bioproducts, Inc., Rockville, Maryland, as fresh sheets of cells prepared from human embryonic kidneys. Some of these were subcultured for experiments through passage 1 2, 3, etc. using a 1:2 or 1:4 split ratio, some were frozen at these passages for subsequent study, and some were used immediately for experiments. They were propagated in Medium 199 with 10% fetal bovine serum. Electrophoretic separations were accomplished using the density gradient procedures and equipment described by Boltz et al. (1973, 1977). Morphological types were scored on the basis of appearance of cells, as shown in the photographs of Figure 1 and the sketches of Figure 2, under phase contrast at a total magnification of 200X. The two sizes of epithelioid cells were sometimes lumped into a single class. Approximately 1,000 cells wer counted per datum.

RESULTS

Epithelioid cells were found to be the dominating cell type in early-passage cultures. Fenestrated cells, although very conspicuous by their bizarre appearance, were always very few in number, almost never constituting more than 10% of any culture. Table 1 is a sketch of the growth patterns found in early-passage cultures derived from three different explants. Although gross differences are seen with respect to the per cent of each cell type in

each culture strain, their growth trends are very consistent. As days pass in culture and the number of monolayer cells increases, the fraction of fenestrated cells always decreases, the fraction of fibroblasts always increases (when they are present), and domed cells appear to increase at about the same rate as the overall culture growth. This finding is also expressed in Figure 3, which is a plot of percentage of each cell type vs. days in 2nd passage culture.

Electrophoretic separation of early-passage cells into subfractions by density gradient electrophoresis never yielded pure populations of any of the 5 cell types, but nearly all fractions were enriched with respect to one or more of the cell types. Figure 4 is a plot of the per cent of each cell type in each electrophoretic subfraction. Electrophoresis was upward, and the column was harvested from the top, so low fraction numbers correspond to high electrophoretic mobility and vice versa. Domed cells were nearly 3 times as frequent in high-mobility fractions as in low-mobility fractions, while exactly the reverse was true of epithelioid cells. These two cell types constituted more than 95% of the initial starting population, so their distributions should be reflexive of one another. The maximum number of fibroblasts appeared at the center of the electrophoretic distribution, while fenestrated cells were found only in the lowest mobility fractions.

REFERENCES

R. E. Allen, P. H. Rhodes, R. S. Snyder, G. H. Barlow, M. Bier, P. E. Bigazzi, C. J. van Oss, R. J. Knox, G. V. F. Seaman, F. J. Micale, and J. W. Vanderhoff. Column electrophoresis on the Apollo-Soyuz Test Project. Sep. Purif. Meth. _6_, 1-59 (1977).

G. H. Barlow, S. L. Lazer, A. Rueter, and R. Allen. Electrophoretic separation of human kidney cells at zero gravity. In D. R. Morrison, Ed. _Bioprocessing in Space_, NASA TM X-58191, Lyndon B. Johnson Space Center, January 1977, pp. 125-142.

M. B. Bernick and H. C. Kwaan. Plasminogen activator activity in cultures from human tissues; an immunological and histochemical study. J. Clin. Invest. _48_, 1740-1753 (1969).

Boltz, R. C.,Jr., Todd, P., Streibel M. J., and Louie, M. K.: Preparative Biochem. _3_, 383-401 (1973).
Biomedical Press, Amsterdam, 1978, pp. 345-355.

Boltz, R. C., Jr., and Todd, P.: In Electrokinetic Separation Methods (Eds. P. G. Righetti, C. J. van Oss, and J. Vanderhoff) Elsevier/North-Holland Biomedical Press, Amsterdam, 1978, pp. 229-250.

R. A. Gaines. _A Physical Evaluation of Density Gradient Cell Electrophoresis_. Thesis. The Pennsylvania State University, University Park, Pennsylvania, 1981.

G.-G. Heidrich and M. E. Dew. Homogeneous cell populations from rabbit kidney cortex. J. Cell Biol. _74_, 780-788 (1983).

W. C. Hymer. Separation of Cells from the Rat Anterior Pituitary Gland. In _Cell Separation: Methods and Selected Applications_, Vol.3, pp. 163-194. Edited by T. G. Pretlow and T. Pretlow. Academic Press, NY (1983).

J. Leighton, L. W. Estes, S. Mansukhani, and Z. Brada. A cell line derived from normal dog kidney (MDCK) exhibiting qualities of papillary adenocarcinoma and of renal tubular epithelium. Cancer _26_, 1022-1028 (1970).

J. Leighton, Z. Brada, L. W. Estes, and G. Justh. Secretory actrivity and oncogenicity of a cell line (MDCK) derived from canine kidney. Science _163_, 472-473 (1969).

J. A. Lever. Inducers of mammalian cell differentiation stimulate dome formation in a differentiated kidney epitheoial cell line (MDCK). Proc. Natl. Acad. Sci. U. S. A. _76_, 1323-1327 (1979).

D. Livingston and M. Taub. Growth of functional proximal tubule cells from rabbit kidney in defined medium. Fed. Proc. _40_, 1710 (1981).

E. O. Major, S. Ehlke, and M. Lampert. Selection of somatic cell hybrids between BK virus transformed BHK-21 and human embryonic kidney cells to study viral gene expression. J. Virol Methods _1_, 139-147 (1980).

D. R. Morrison and M. L. Lewis. Electrophoresis tests on STS-3 and ground control experiments: a basis for future biological sample selections. In _33rd International Astronautical Federation Congress_, Paper No. 82-152 (1983).

D. R. Morrison, G. H. Barlow, C. Cleveland, R. Grindeland, W. C, Hymer, M. E. Kunze, J. W. Lanham, M. L. Lewis, B. E. Sarnoff, P. Todd, and W. Wilfinger. Electrophoretic separation of kidney and pituitary cells on STS-8. Adv. Space Res. (in press, 1984).

D. R. Morrison, M. L. Lewis, C. Cleveland, M. E. Kunze, J. W. Lanham, B. E. Sarnoff, and P. Todd. Properties of electrophoretic fractions of human embryonic kidney cells separated on Space Shuttle flight STS-8. Adv. Space Res. (in press, 1984).

C. A. Rabito and D. A. Ausiello. Effect of cell-substratum interaction on hemicyst formation by MDCK cells. In Vitro _16_, 461-468 (1980).

M. Taub, L. Chuman, M. H., Saier, and G. H. Sato. The growth of a kidney epithelial cell line (MDCK) in hormone-supplemented serum-free media. Proc. Natl. Acad. Sci. U.S.A. _76_, 3338-3342 (1979).

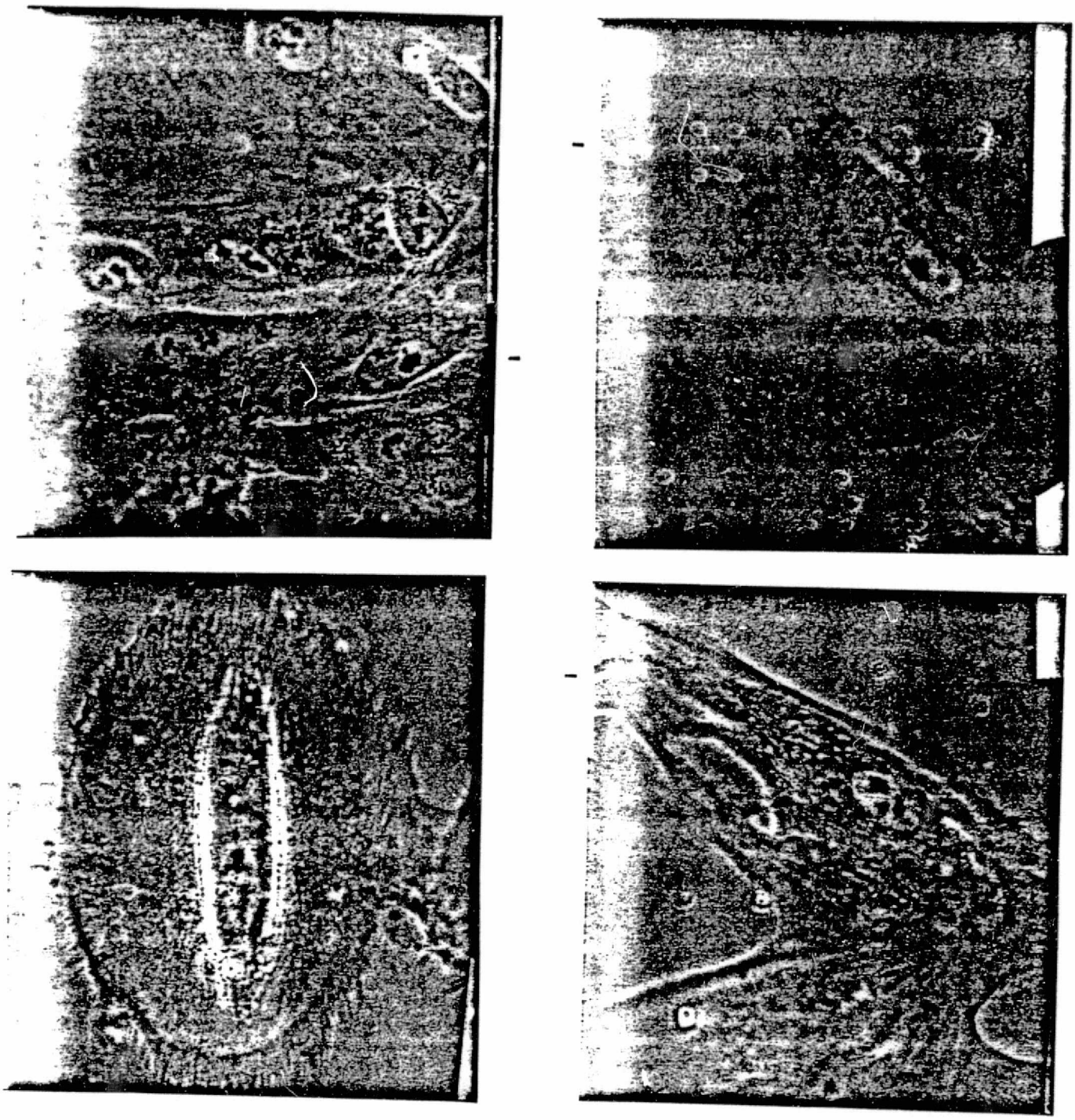

Figure 1. Phase-contrast micrographs of the 4 major cell types (other than fibroblasts) found in early-passage human embryonic kidney cell cultures. Upper left: small epithelioid, upper right large epithelioid, lower left: domed, lower right: fenestrated.

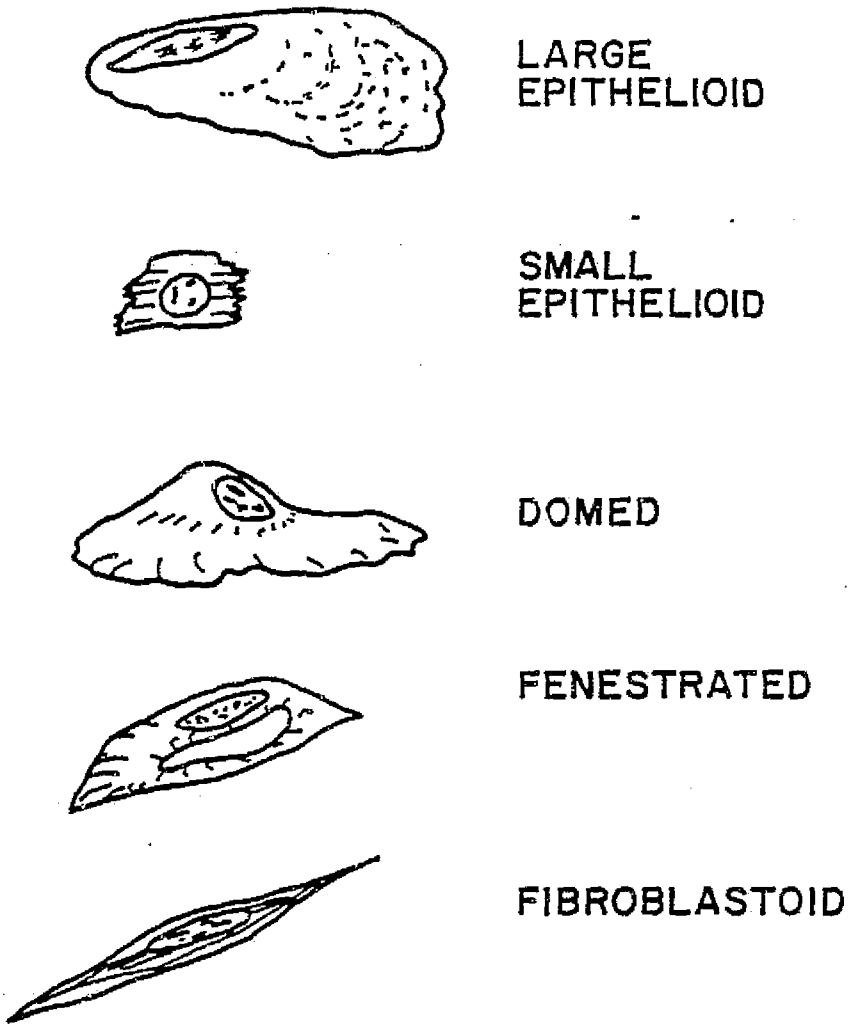

Figure 2. Sketches of the 5 major identifiable cell types found in early-passage human embryonic kidney cell cultures.

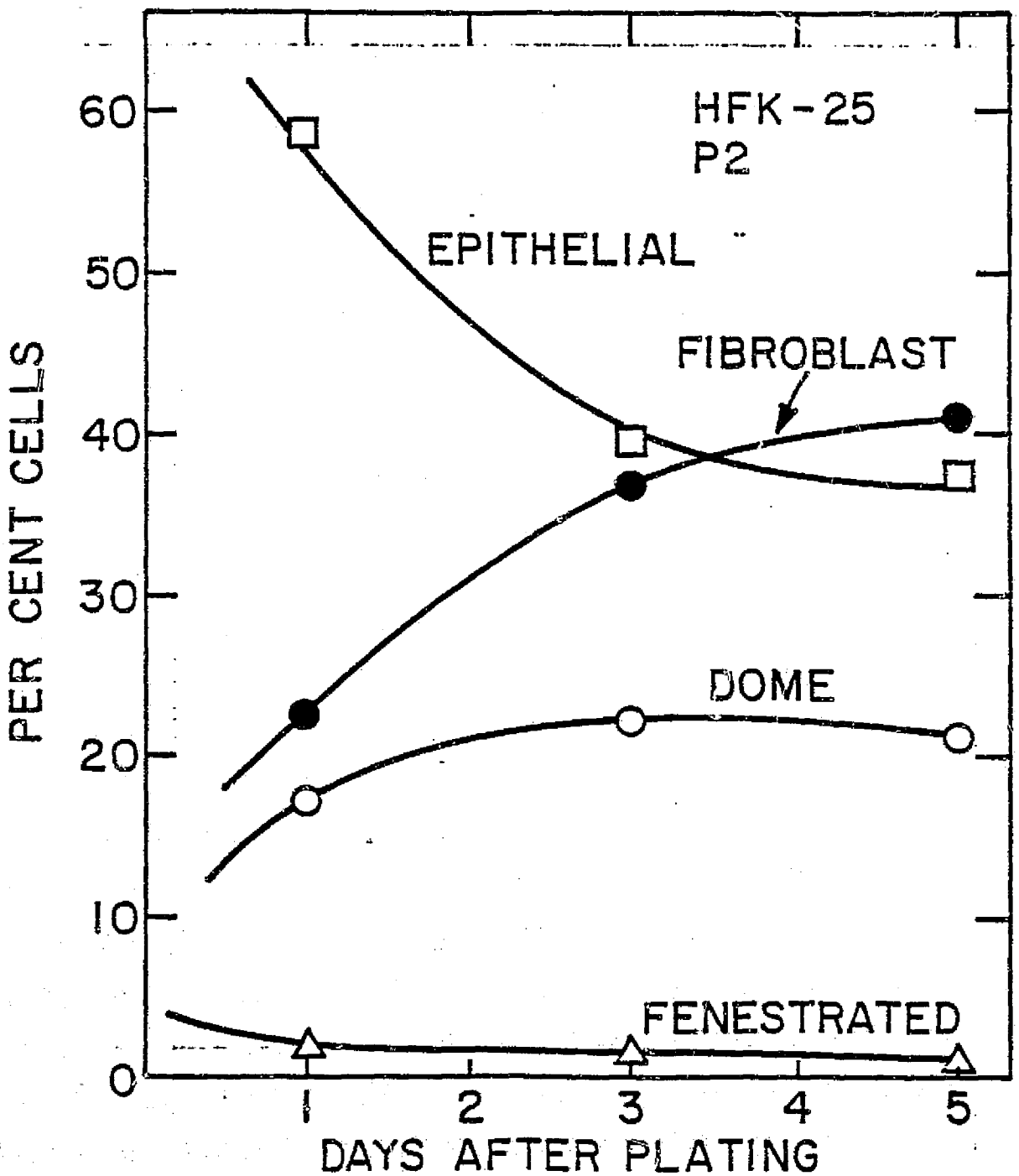

Figure 3. Per cent of each cell type as a function of time after plating a 2nd passage culture of human embryonic kidney cell strain HFK-25.

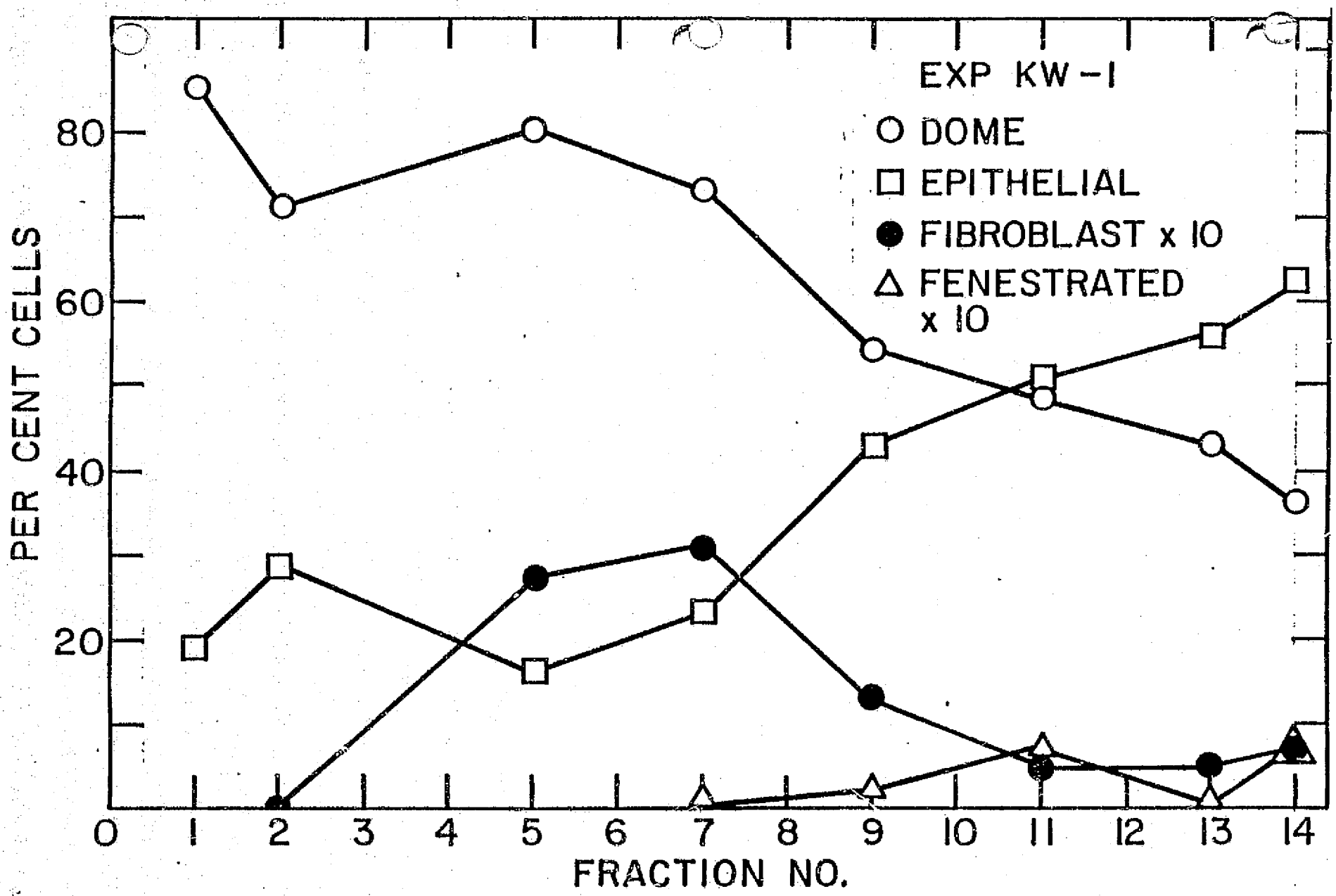

Figure 4. Density gradient column electrophoretic profile of human embryonic kidney cell culture strain HFK at the 2nd passage in culture. A trypsinized cell suspension was subjected to 2 hr of upward electrophoresis in a Ficoll gradient (Boltz et al., 1973, 1977), and 0.5-ml fractions were collected from the top of the column. Electrophoretic migration was thus from right to left on the graph. The per cent domed and fibroblastoid cells has abeen multiplied by 10 to make their distributions clearer.

Chapter 18

Urokinase Production by Electrophoretically Separated Human Embryonic Kidney Cells.

KIDNEY CELL ELECTROPHORESIS V. UROKINASE PRODUCTION BY ELECTROPHORETICALLY SEPARATED CULTURED HUMAN EMBRYONIC KIDNEY CELLS

M. E. Kunze, L. D. Plank, V. Giranda, K. Sedor, and P. Todd

INTRODUCTION AND RATIONALE

Urokinase is a plasminogen activator found in urine (Celander and Guest, 1960). Relatively pur preparations have been tested in Europe, Japan and the United States for the treatment of deep vein thrombosis and other dangerous blood clots. This treatment method appears to have great potential, but a single dose requires material prepared from nearly 100 man-days of urine. Human embryonic kidney cell cultures have been found to produce urokinase at much higher concentrations, but less than 5% of the cells in typical cultures are producers (White and Barlow, 1970; Huseby et al., 1977). Since humman diploid cells become senescent in culture the selection of clones derived from single cells will not provide enough material to be useful, so a bulk purification method is needed for the isolation of urokinase producing cell populations. Preparative cell electrophoresis was chosen as the method, since evidence exists (Knox, 1978) that human embryonic cell cultures are richly heterogeneous with respect to electrophoretic mobility, and preliminary electrophoretic separations on the Apollo-Soyuz space flight produced cell populations that were rich in urokinase production (Allen et al., 1977). Similarly, erythropoietin is useful in the treatment of certain anemias and is a kidney cell product, and electrophoretically enriched cell populations producing this product have been reported (Allen et al., 1977). Thus, there is a clear need for diploid human cells that produce these products, and there is evidence that such cells should be separable by free-flow cell electrophoresis.

Progress made in the Project Laboratory

Human embryonic kidney cells have been acquired from commercial producers and given serial names: HFK-1, HFK-2, etcs. The cell strains have been subcultured and/or frozen in liquid nitrogen. Microscopic and density gradient electrophoresis have been applied to these populations, and evidence has been found favoring the notion that urokinase producing cells should be separable by preparative electrophoresis, such as free-flow electrophoresis.

Human kidney HFK-3 cells at the first passage were separated by density gradient electrophoresis, and fractions were grown in culture in 5 ml complete medium in 60 mm tissue culture dishes for two weeks. After the supernatant was sampled for urokinase activity it was sampled for non-adherent cells. The monolayers were trypsinized and also counted. It appeared from the cell-count profile that fractions containing the high numbers of attached cells also contained high numbers of unattached cells. Coulter volume spectrometry revealed that non-adherent cells were smaller than attached cells by as much as a factor of 4 in volume. The fractions highest in cells did not coincide with maximum urokinase production. It, therefore, appears that urokinase producing cells were a rather small proportion of this particular explant and that UK activity was high, on a per cell basis, in the lower-mobility fractions.

Similar separation experiments were performed at passage 1 and passage 2 of strain HFK-3, and specific cell fractions were found to produce UK in both cases. Unfortunately, the applied electric fields were not the same in the two experiments, so the fractions could not be directly related. In both cases, UK producing cells appeared to be at least biomodically distributed among the collected fractions. It is possible that there will be more than one electrophoretic population of cells producing UK in cultures in general. The cell population described by the data of Figure 8 behaved similarly. There were two electrophoretic peaks of urokinase producing cells, and there was evidence for two populations whose UK production increased between day 12 and day 13 in culture after electrophoretic separation. In these experiments UK activity was assayed on aliquots of supernatant culture medium using the colorimetric 4-methoxy-2-naphthylamide method. Activity units per viable cell in separated fractions have not yet been determined.

Figures 9 through 12 show UK production in cultures of cells grown from collected fractions in density-gradient electrophoresis experiments. The distribution of UK production relative to total cells varies among cell strains and passage numbers. For example, in Fig. 9 UK production occurred in cells with higher mobility than the majority; whereas, in Fig. 11 UK production followed total cells/fraction rather closely. Strain HFK-10 persistently had a large population of very low mobility cells (Fig. 12), and UK production occurred in cells with higher mobility. Figures 9 and 10 illustrate computerization of UK activity calculations which will finally make possible the expression of UK production in electrophoretic fractions in CTA units/million cells/day.

The profile of UK production closely parallels the number of cells PLATED per vessel in Figure 13, but when the actual number of cells per vessel is counted at the time of the UK assay, it is found that there is a distinct peak of high-UK producing cells in cultures derived from near the front of the band of migrating cells (Figure 14). This finding will be found consistent with many other experiments, including those conducted in microgravity. This finding was repeated in the case of cell strain HFK-18 (Figure 15) and subsequently with cell strain 8514 using continuous flow electrophoresis. This result also reveals that high UK producers multiplied much less than their lower-mobility counterparts.

In summary, electrophoretic separations have produced populations of viable adherent and non-adherent cells and cell fractions capable of producing differing amounts of UK upon subsequent cultivation. There may be more than one electrophoretic cell subpopulation capable of UK production.

Table 1. COLUMN ELECTROPHORESIS BUFFERS
(300 mOsm approx.)

Ionic strength = 0.030 g ions/l

	Composition in g/l				
	PBG	CEILING (LIGHT)	HEAVY	FLOOR (15%)	FLOOR (20%)
KCl	0.2	0.2	0.2	0.2	0.2
$MgCl_2.6H_2O$	0.1	0.1	0.1	0.1	0.1
KH_2PO_4 anhyd.	0.2	0.2	0.2	0.2	0.2
Na_2HPO_4 anhyd.	1.15	1.15	1.15	1.15	1.15
Glucose	10.0	10.0	10.0	10.0	10.0
Sucrose	-	68.0	51.0	42.5	34.0
Ficoll 400	-	-	100.0	150.0	200.0

Table 2.
Preparation of Gradient Electrophoresis Buffers:

1. Prepare DOUBLE-STRENGTH PBG according to the following recipe:

	g/l	ml. from 100g/l stock solns.
KCl	0.4	4.0
$MgCl_2.6H_2O$	0.2	2.0
KH_2PO_4	0.4	4.0
Na_2HPO_4	2.30	23.0
Glucose	20.0	-

2. To prepare 1 litre of, for example, heavy solution, dissolve 100.0g Ficoll and 51.0g sucrose in 500 ml double-strength PBG plus approximately 300 ml twice-distilled H_2O; then make up to 1 litre with 2xdH_2O.

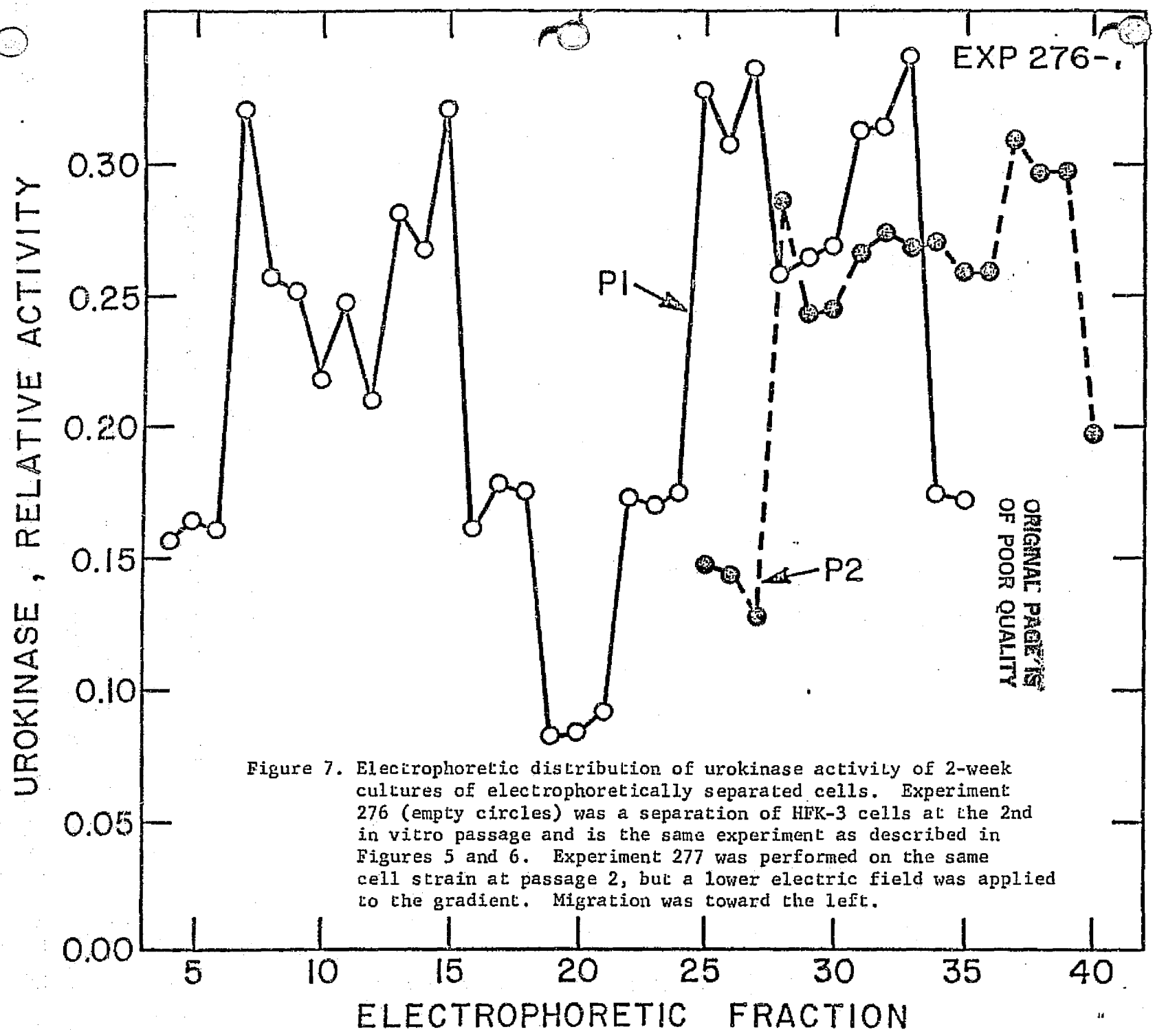

Figure 7. Electrophoretic distribution of urokinase activity of 2-week cultures of electrophoretically separated cells. Experiment 276 (empty circles) was a separation of HFK-3 cells at the 2nd in vitro passage and is the same experiment as described in Figures 5 and 6. Experiment 277 was performed on the same cell strain at passage 2, but a lower electric field was applied to the gradient. Migration was toward the left.

Figure 8. Urokinase activity of supernatants of cultures of cells separated by density gradient electrophoresis. The same cultures were sampled on successive days, and increased production was found in high and low, but not intermediate, mobility cells.

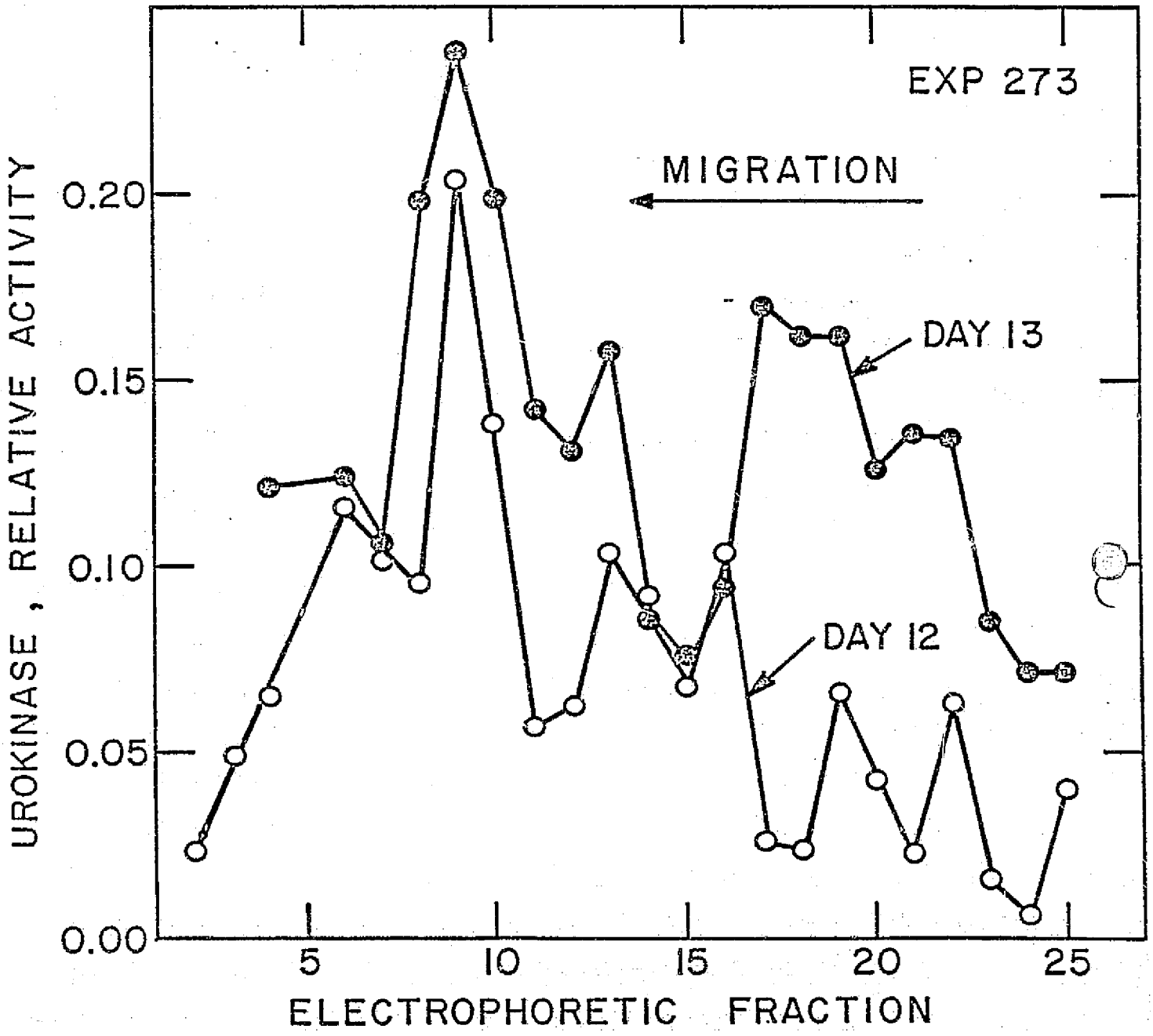

Figure 9. Electrophoretic profile of HFK cells, passage 11, and urokinase activity of selected fractions 2 days after electrophoretic separation.. Exp 985.

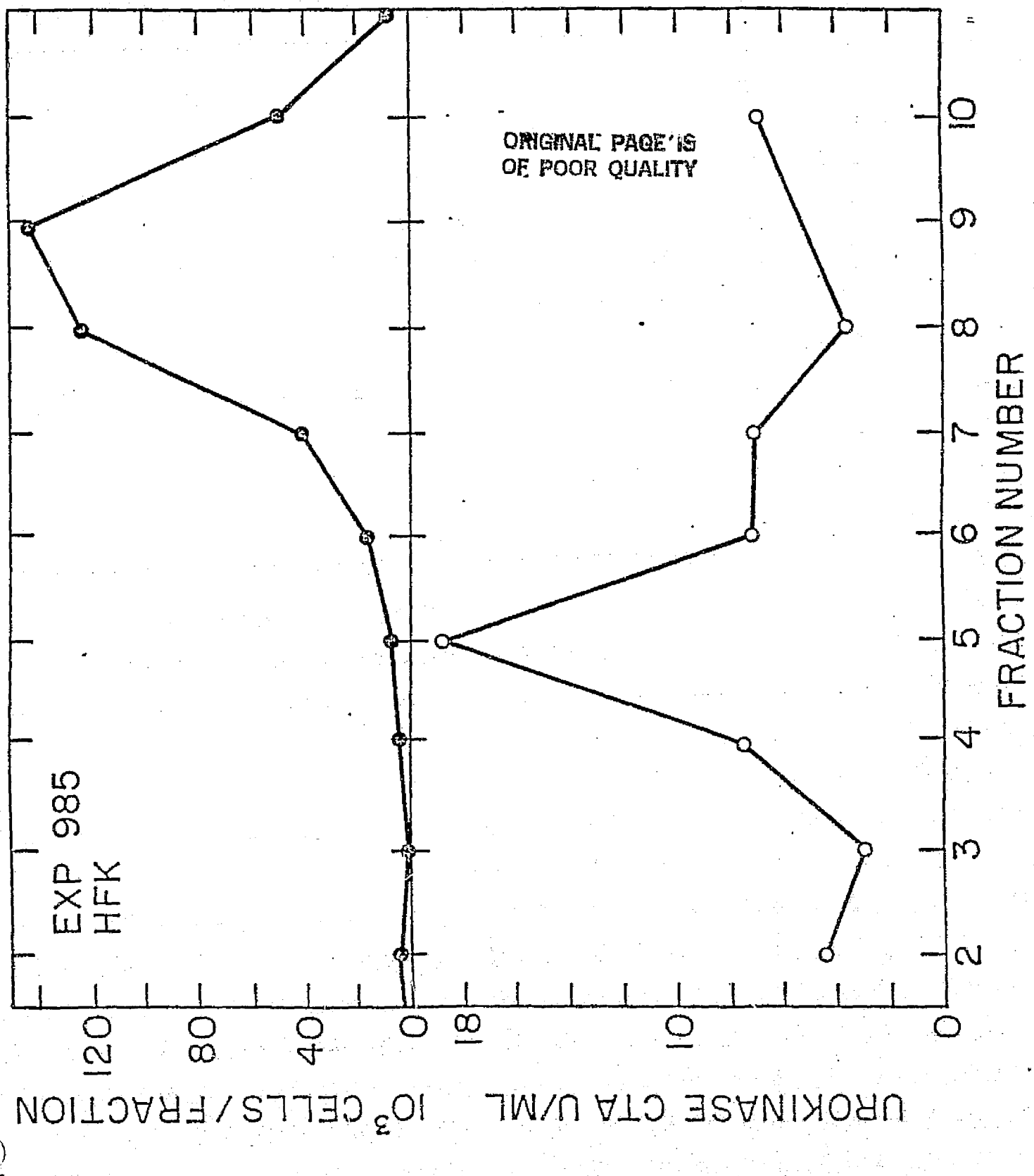

Figure 10. Urokinase activities in cultured electrophoretically separated cell fractions. Matching cell counts not given. Upper plot: optical density units. Lower plot: CTA units. Exp RB270.

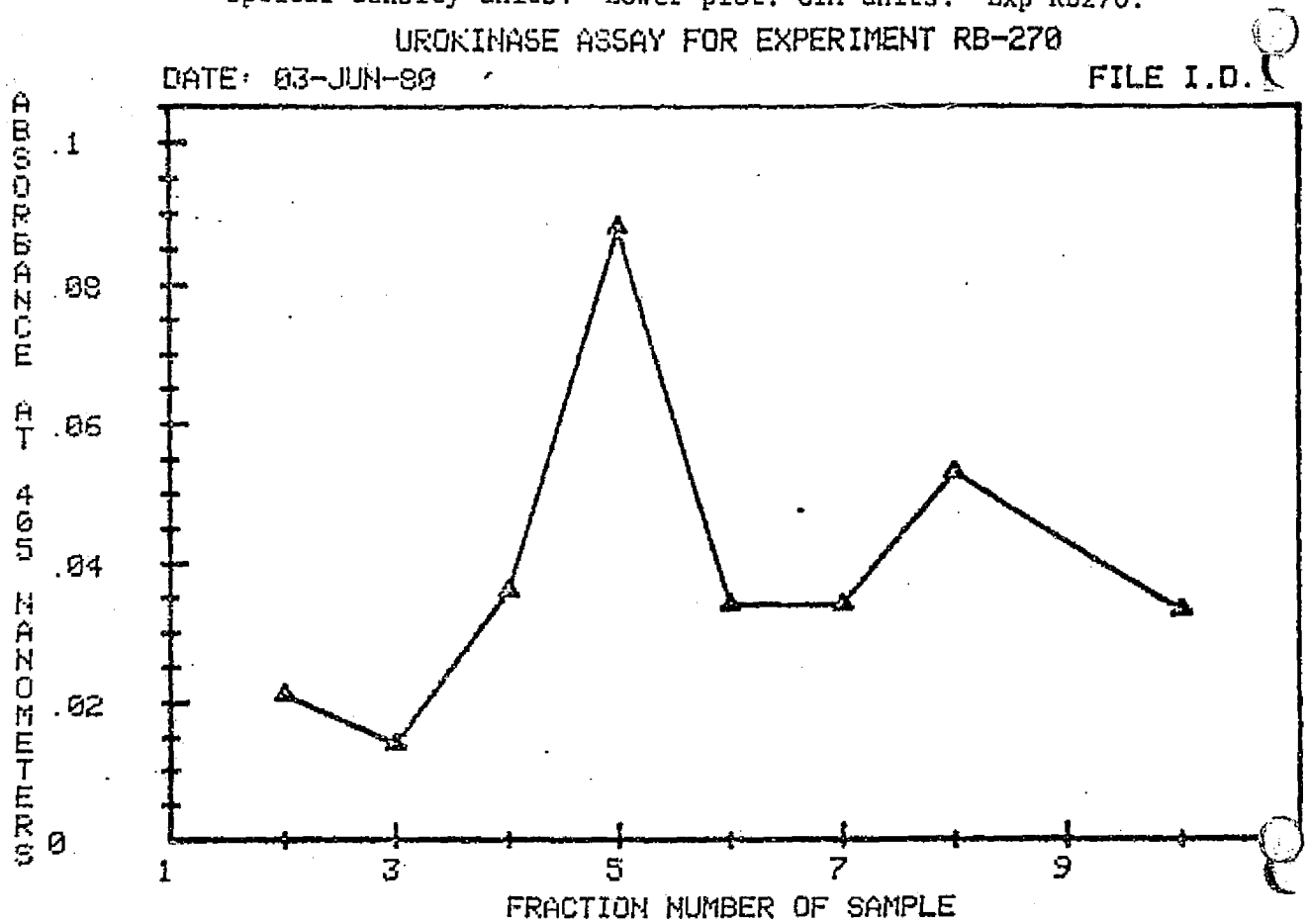

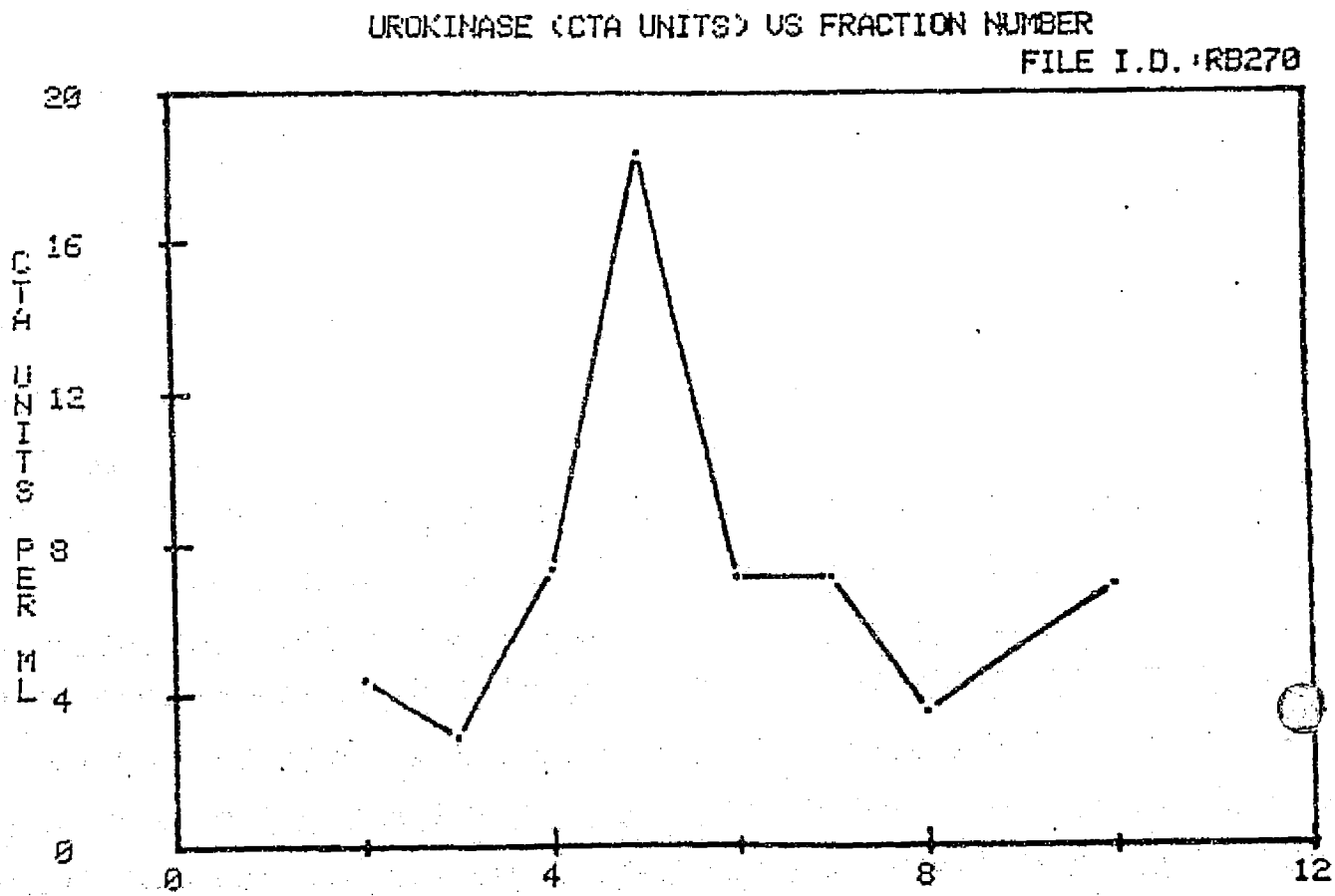

Figure 11. Electrophoretic profile of HFK-9 cells, passage 4, and urokinase activity of selected cultured fractions 1 and 6 days after electrophoretic separation. Exp 1077.

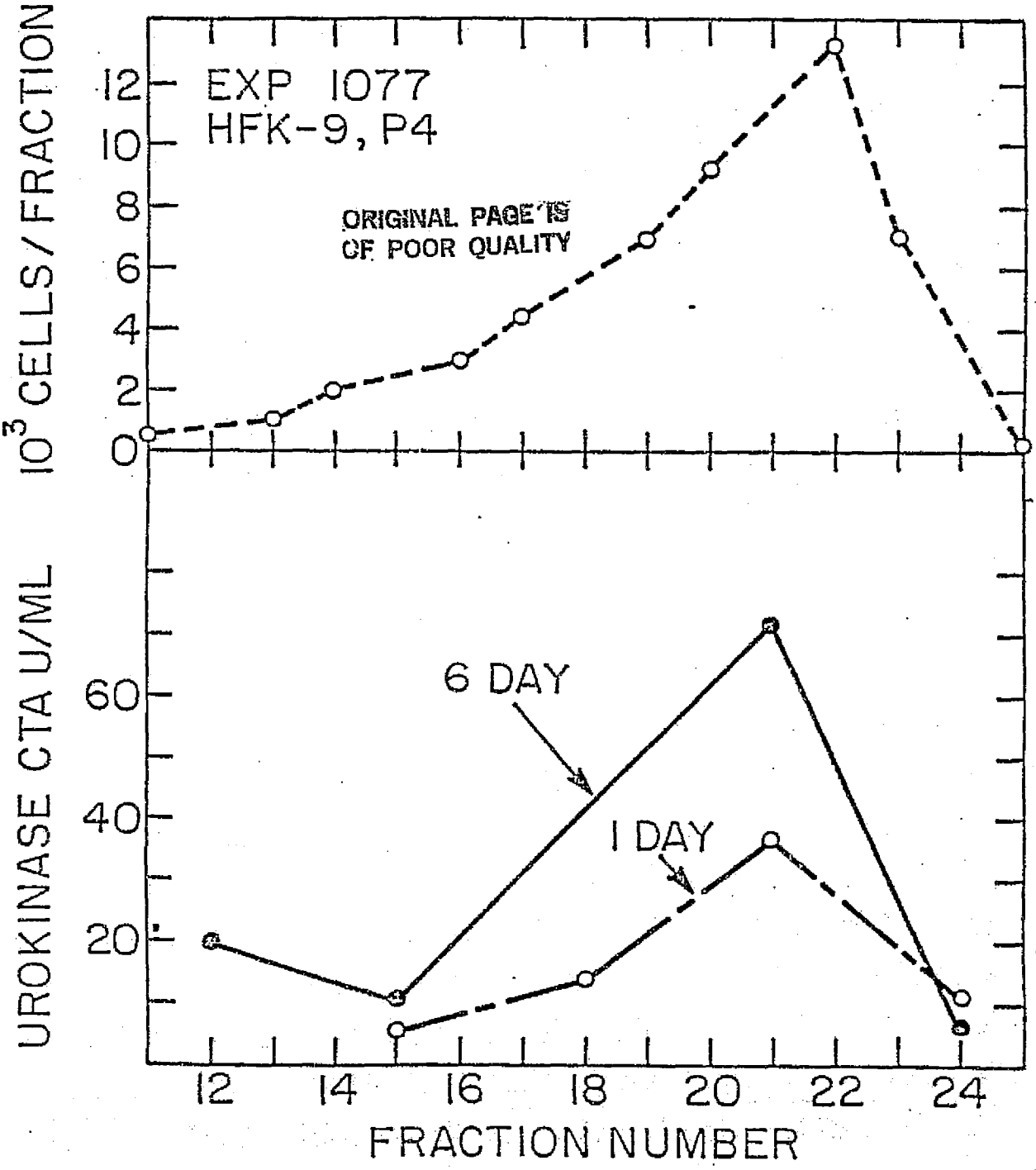

Figure 12. Electrophoretic profile of HFK-10 cells, passage 4, and urokinase activity of selected cultured fractions 11 days after electrophoretic separation. Exp 1098.

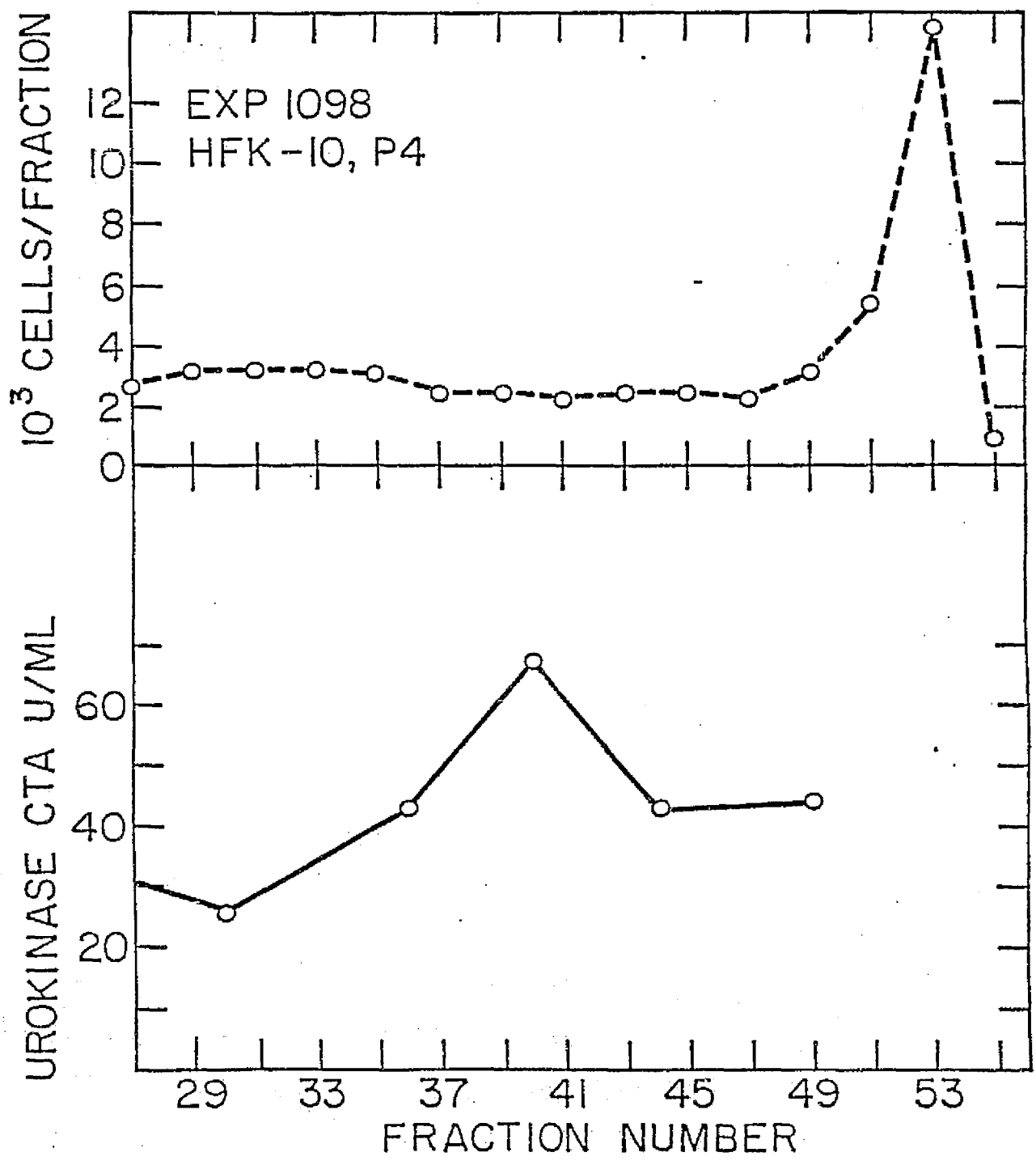

Figure 13. Electrophoretic profile of cell strain HFK-17 at passage 3 and UK production measured 16 days after culturing the electrophoretic fractions. The number of "cells per well" corresponds to the number of cells plated in each fraction.

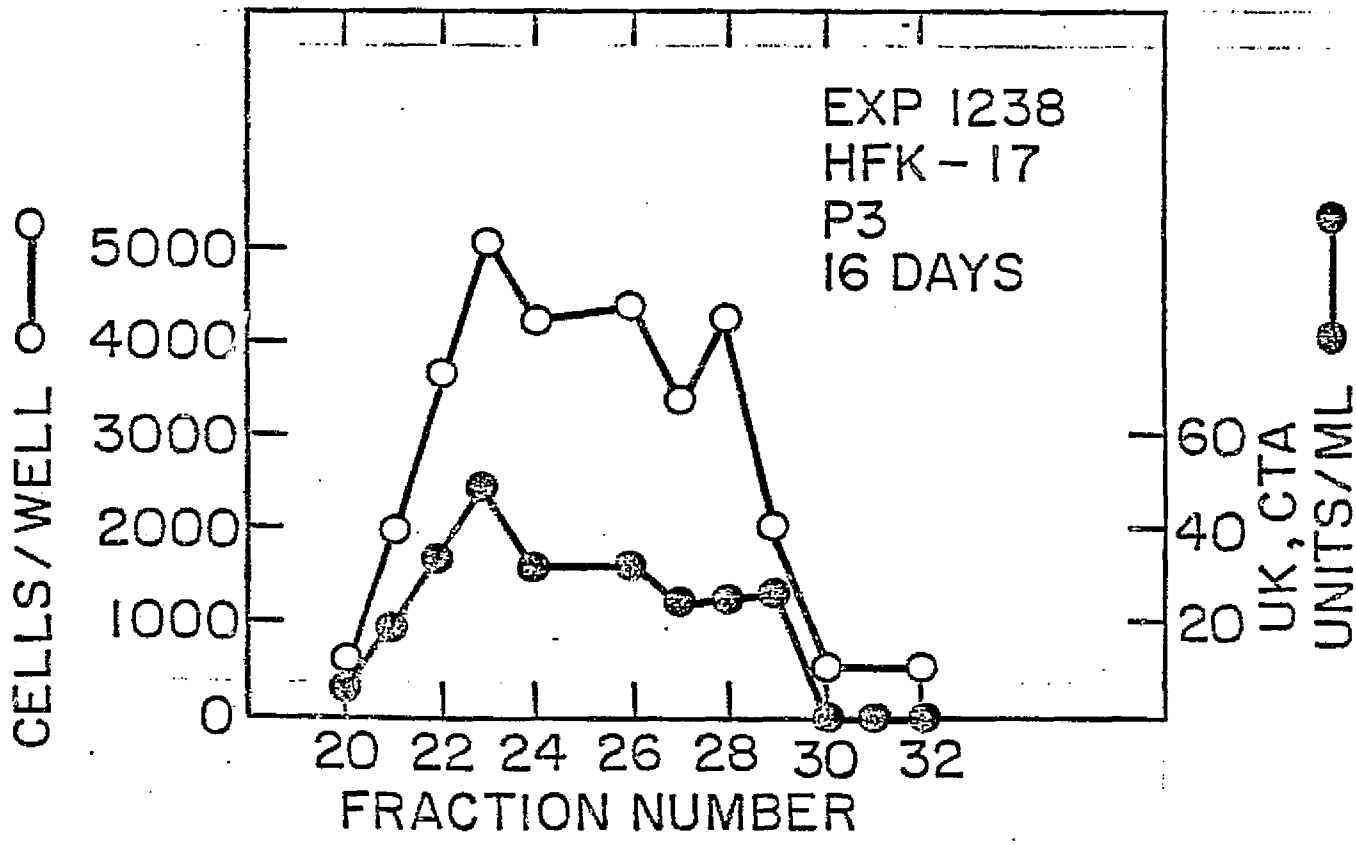

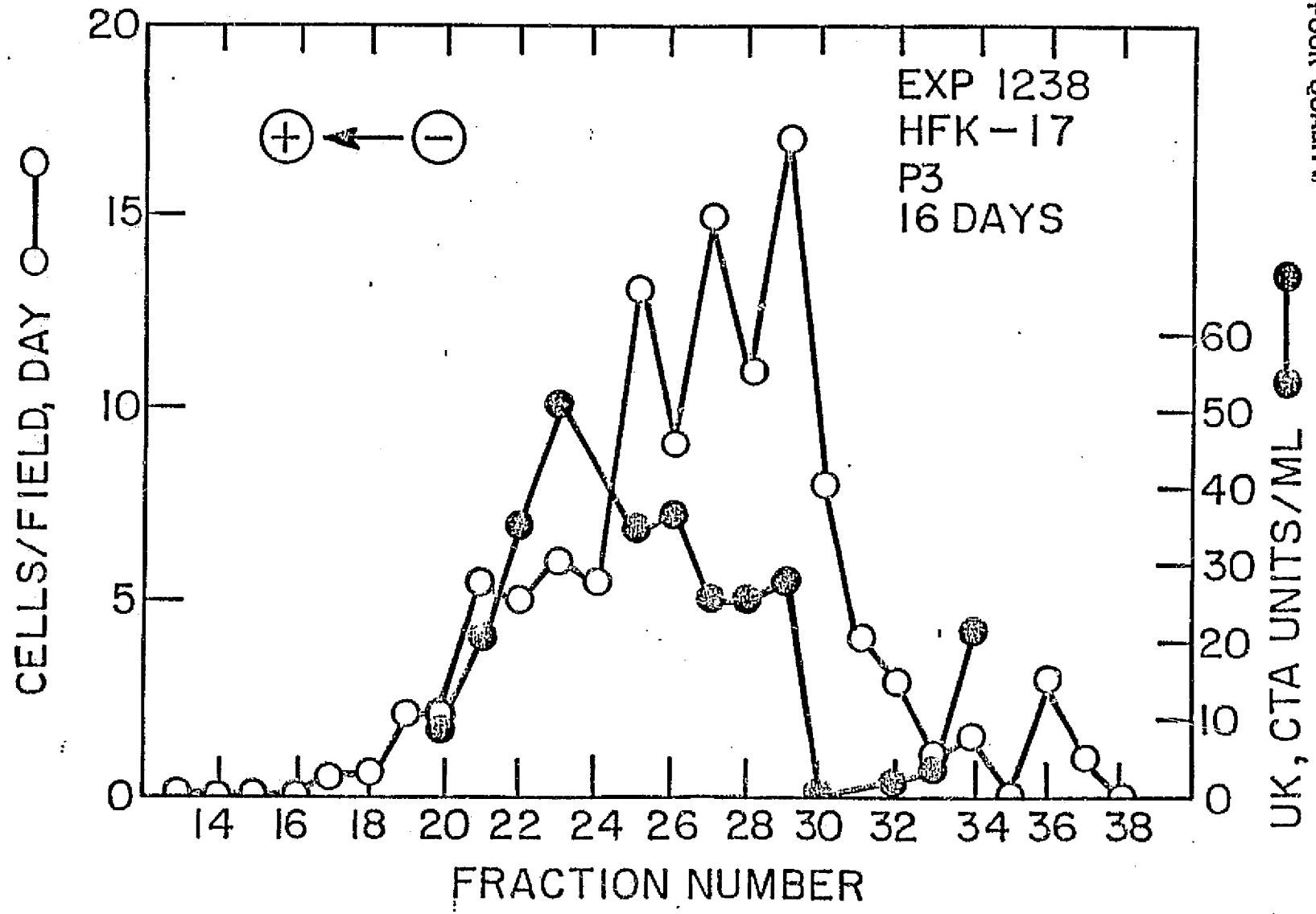

Figure 14. Same as Figure 13, but the number of cells per fraction was determined on the basis of microscopic counts of cell density, thereby representing the number of cells pr[illegible]t at the time of the UK assay.

Figure 15. Confirmation of the result of Figure 14; an identical electrophoretic profile of both cell number and UK production in the case of a different cell strain at a later passage. In strain HFK-18, high mobility cells are also very efficient UK producers and apparently the least prolific with respect to multiplication.

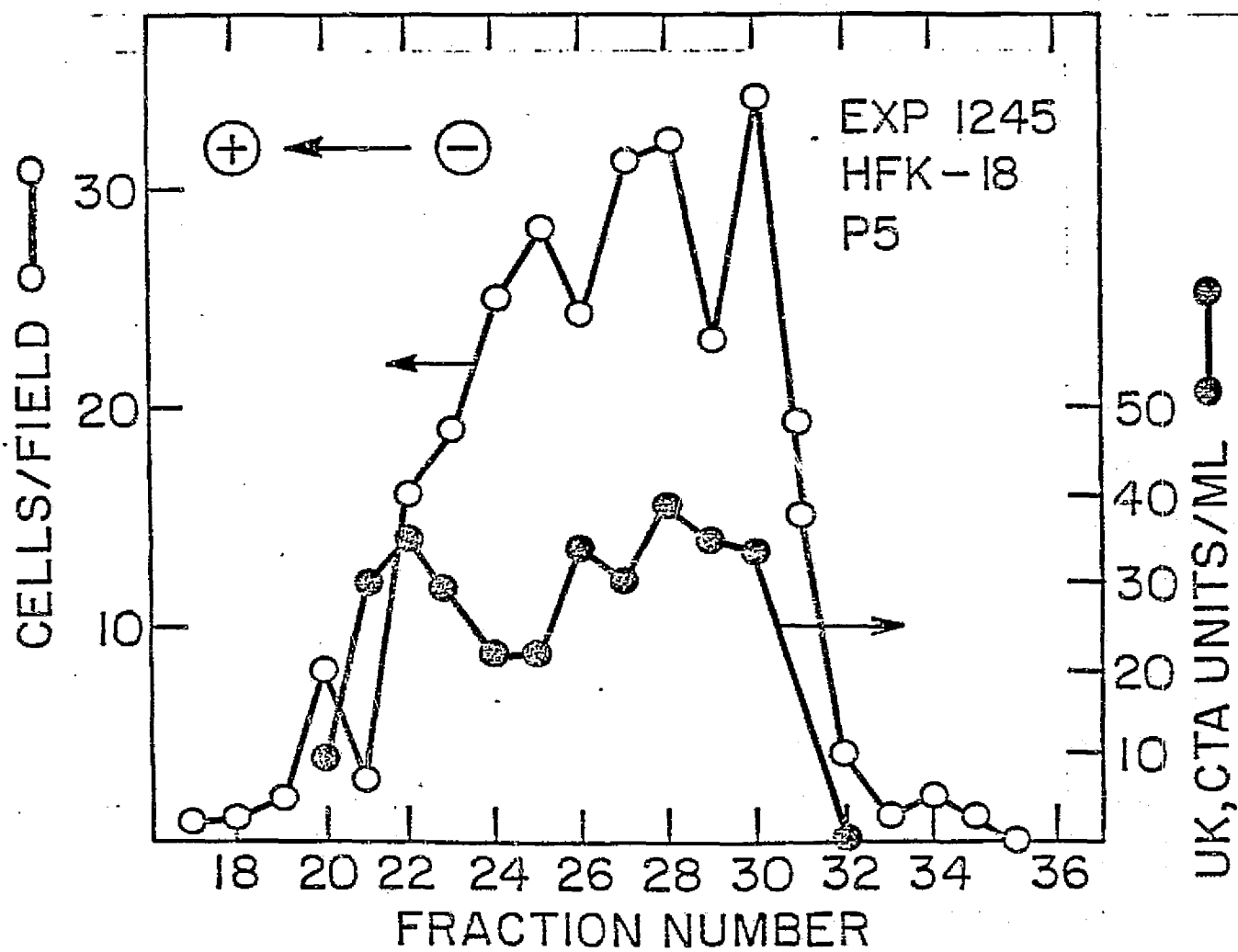

Chapter 19

Electrophoretic Studies on Human Embryonic Kidney Cell Strain 8514.

SUMMARY ELECTROPHORETIC DATA BASE ON HUMAN EMBRYONIC KIDNEY CELL STRAIN 8514

L. D. Plank, M. E. Kunze, M. V. Arquiza, D. R. Morrison, and P. Todd

To properly plan the EEVT and CFES experiments with human embryonic kidney cells, first a candidate cell lot had to bechosen on the basis of electrophoretic heterogeneity, growth potential, cytogenetics, and urokinase production. Cell lot 8514 from MA Bioproducts, Inc. was chosen for this purpose, and several essential analytical electrophoresis experiments were performed to test its final suitability for these experiments.

In order of appearance, the experimental results are:

1. A test of the reproducibility of EPM distributions, using third-passage cells as a model (experiments 1492 and 1430).

2. Comparison with rat erythrocytes evaluated during the same test interval.

3. Effect of trypsin and EDTA or EDTA alone on EPM distribution.

4. Subdivision of EPM distribution into 3 arbitrary mobility subgruops, fast, intermediate, and slow.

5. Simulation of the subgroup structure for computer projections.

6. Simulation of cell migration under the conditions of the EEVT experiment.

7. Simulation of cell migration under the conditions of the EEVT experiment, but with increased electroosmotic tube wall mobility.

8. Effect of storage conditions in a simulated space-flight CFES experiment on the EPM distributios.

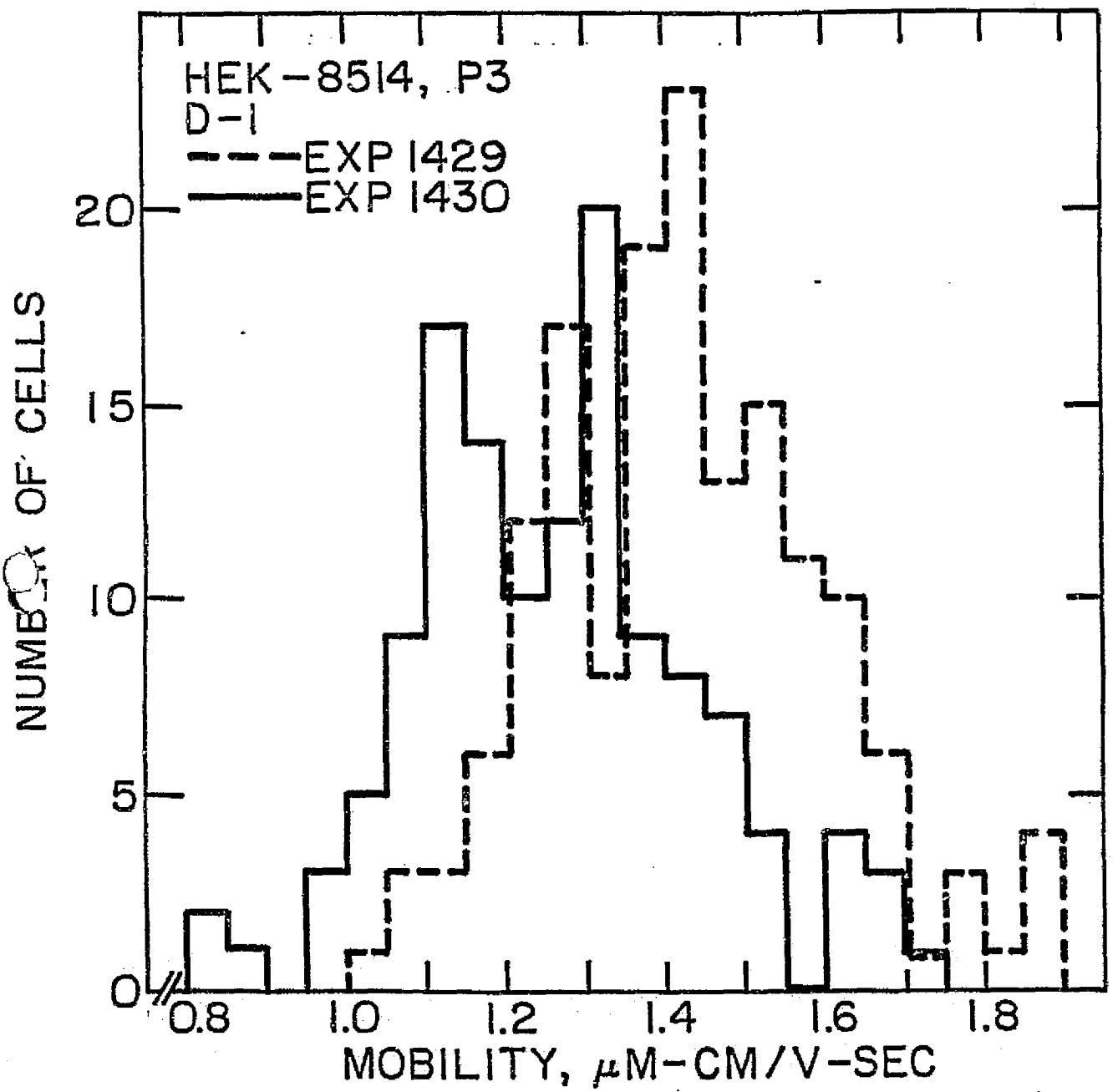
HEK-8514, P3
D-1
EXP 1429
EXP 1430
NUMBER OF CELLS
0
5
10
15
20
0.8
1.0
1.2
1.4
1.6
1.8
MOBILITY, μM-CM/V-SEC

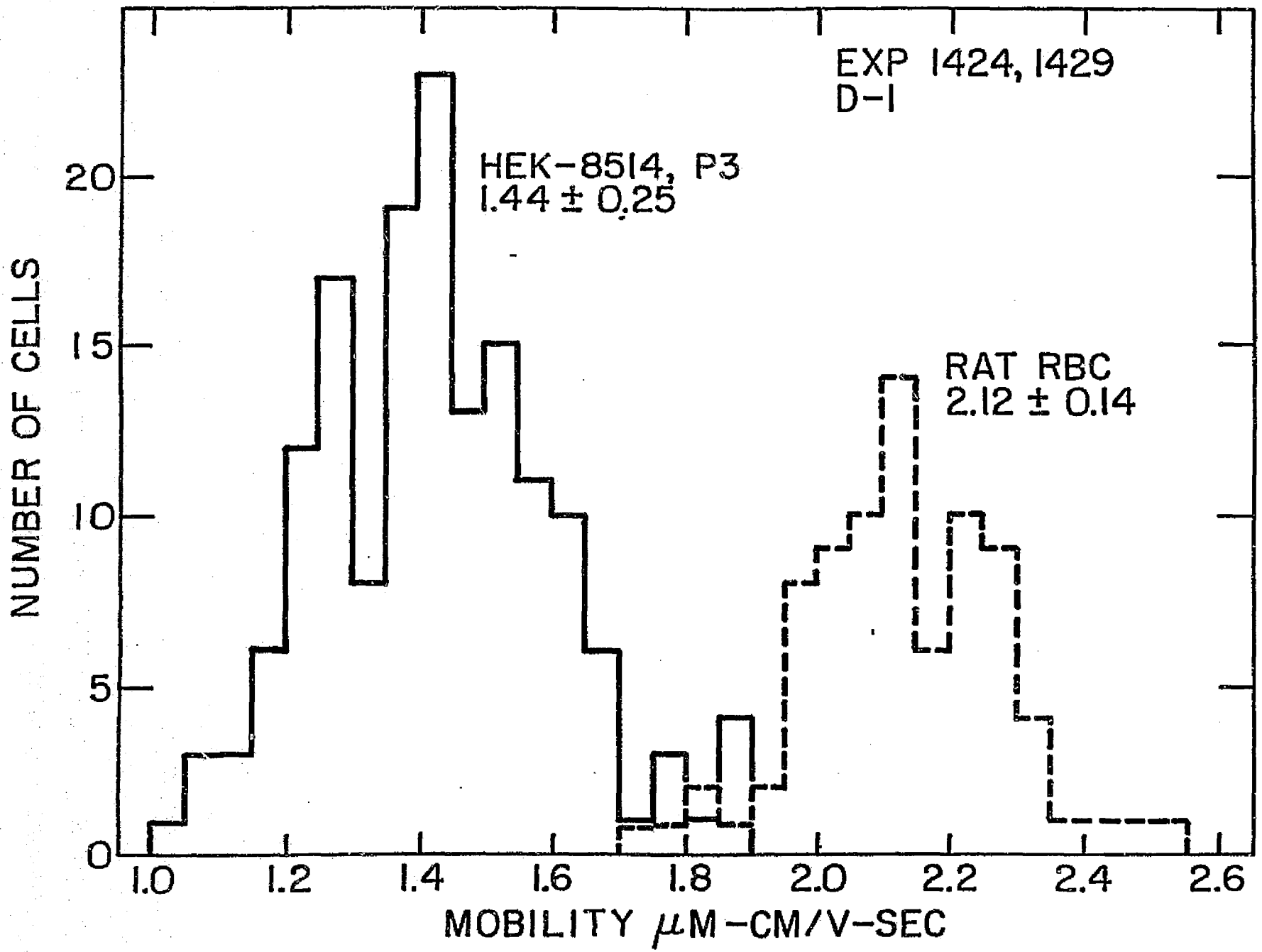
EXP 1424, 1429
D-1
HEK-8514, P3
1.44 ± 0.25
RAT RBC
2.12 ± 0.14
NUMBER OF CELLS
0
5
10
15
20
1.0
1.2
1.4
1.6
1.8
2.0
2.2
2.4
2.6
MOBILITY μM-CM/V-SEC

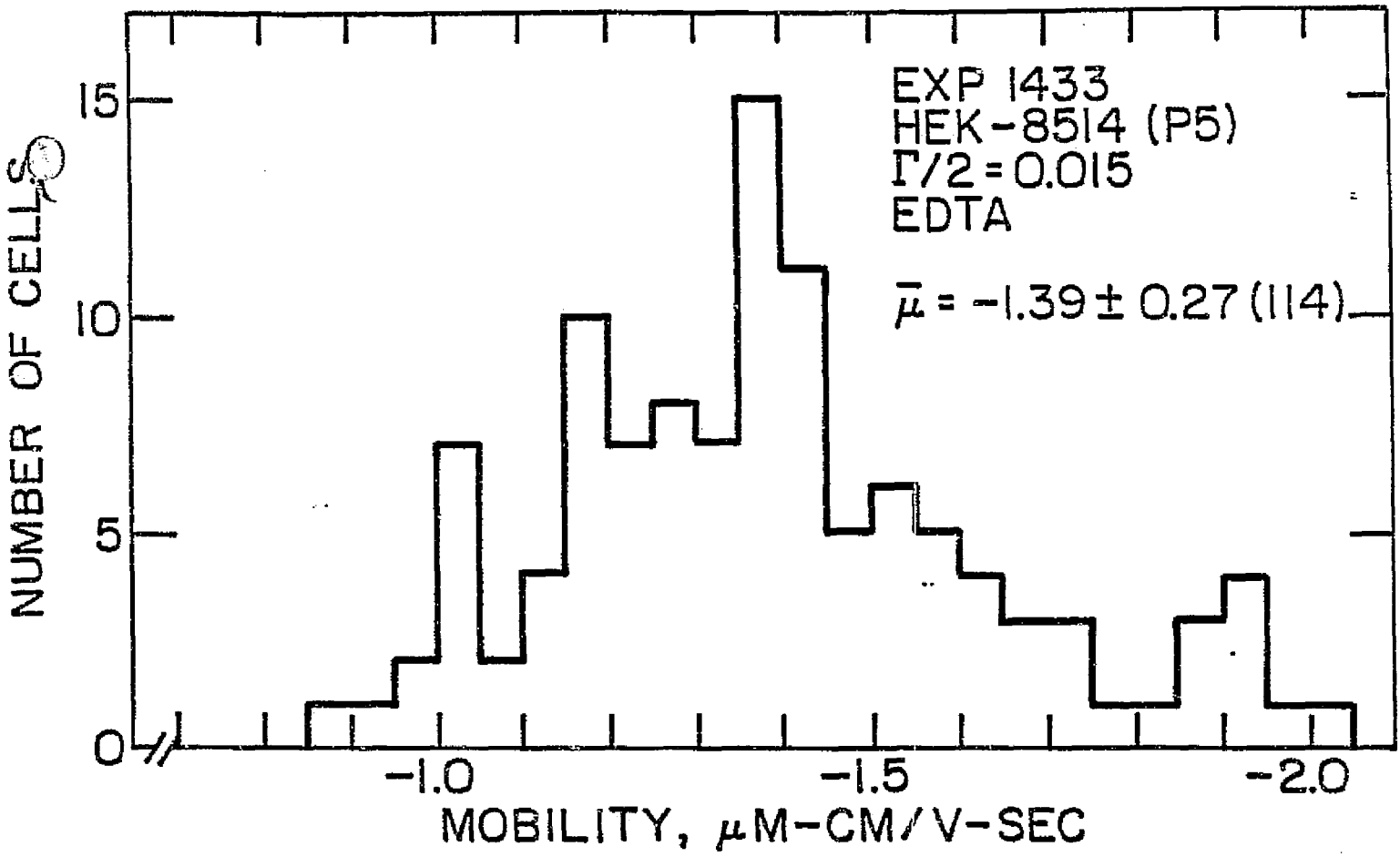
EXP 1433
HEK-8514 (P5)
Γ/2 = 0.015
EDTA
$\bar{\mu}$ = −1.39 ± 0.27 (114)
NUMBER OF CELLS
15
10
5
0
−1.0
−1.5
−2.0
MOBILITY, μM-CM/V-SEC

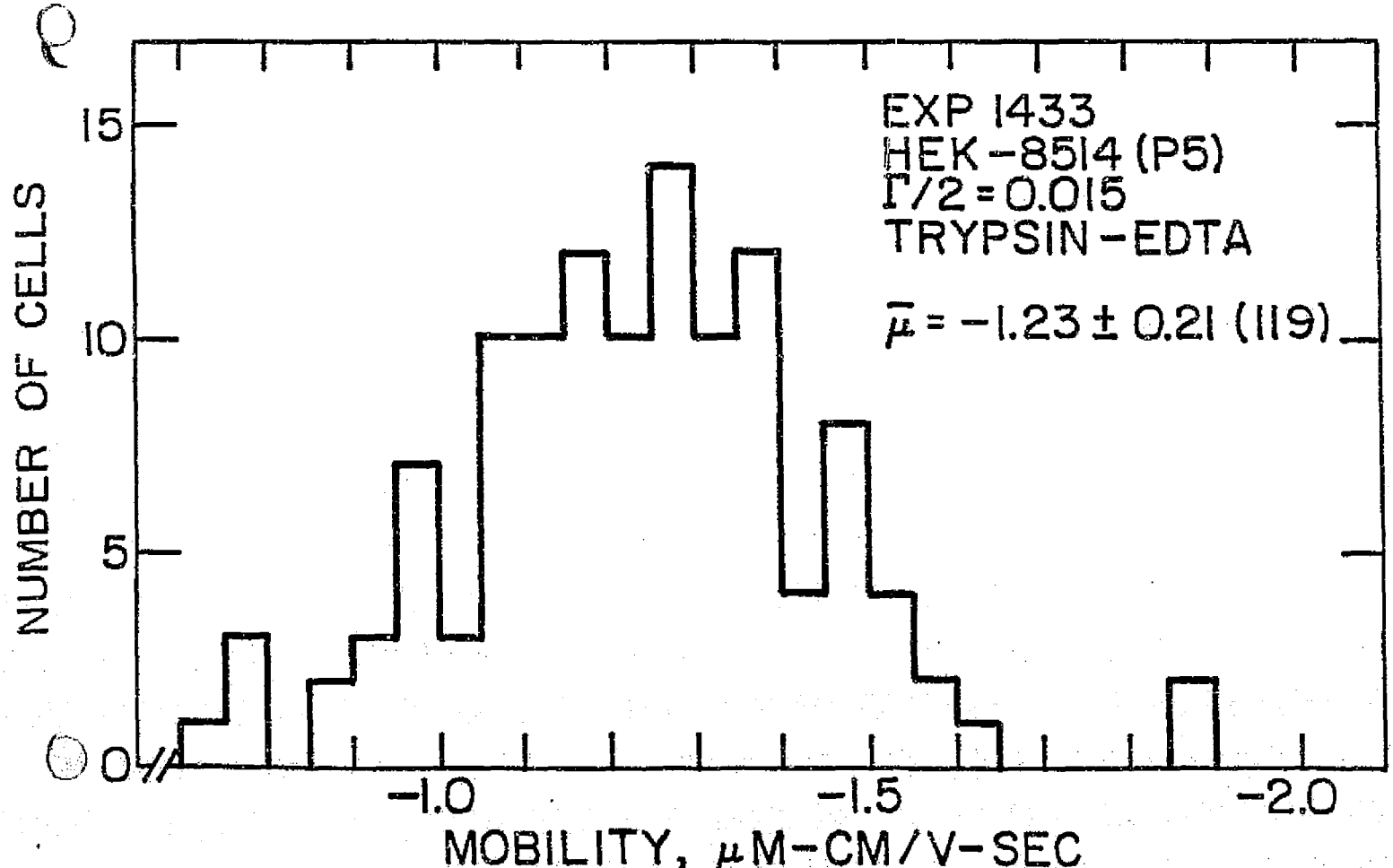
EXP 1433
HEK-8514 (P5)
Γ/2 = 0.015
TRYPSIN-EDTA
$\bar{\mu}$ = −1.23 ± 0.21 (119)
NUMBER OF CELLS
15
10
5
0
−1.0
−1.5
−2.0
MOBILITY, μM-CM/V-SEC

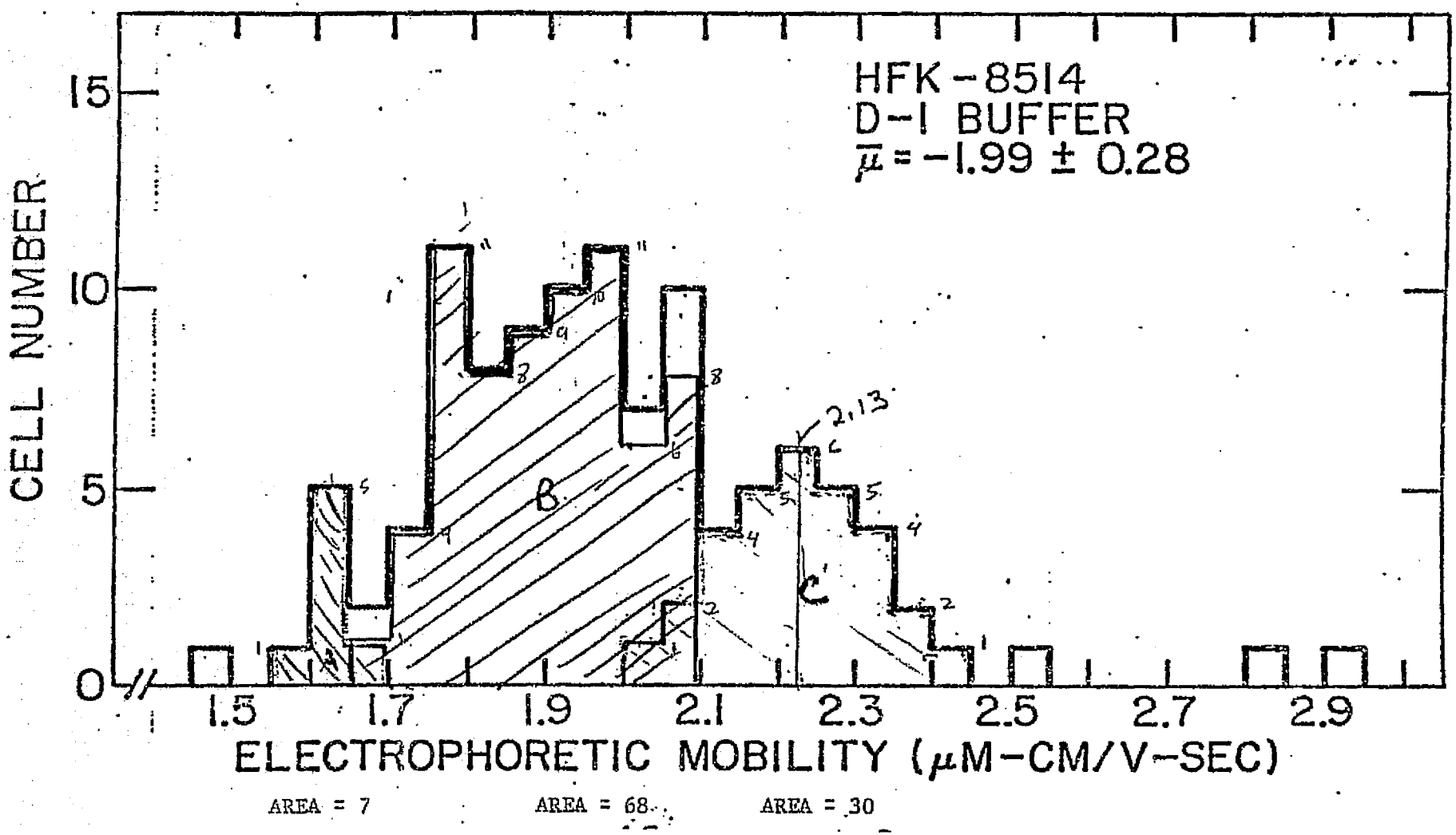
HFK-8514
D-1 BUFFER
$\bar{\mu}$ = -1.99 ± 0.28
CELL NUMBER
0
5
10
15
1.5
1.7
1.9
2.1
2.3
2.5
2.7
2.9
ELECTROPHORETIC MOBILITY (μM-CM/V-SEC)
B
C'
2,13
AREA = 7
AREA = 68
AREA = 30

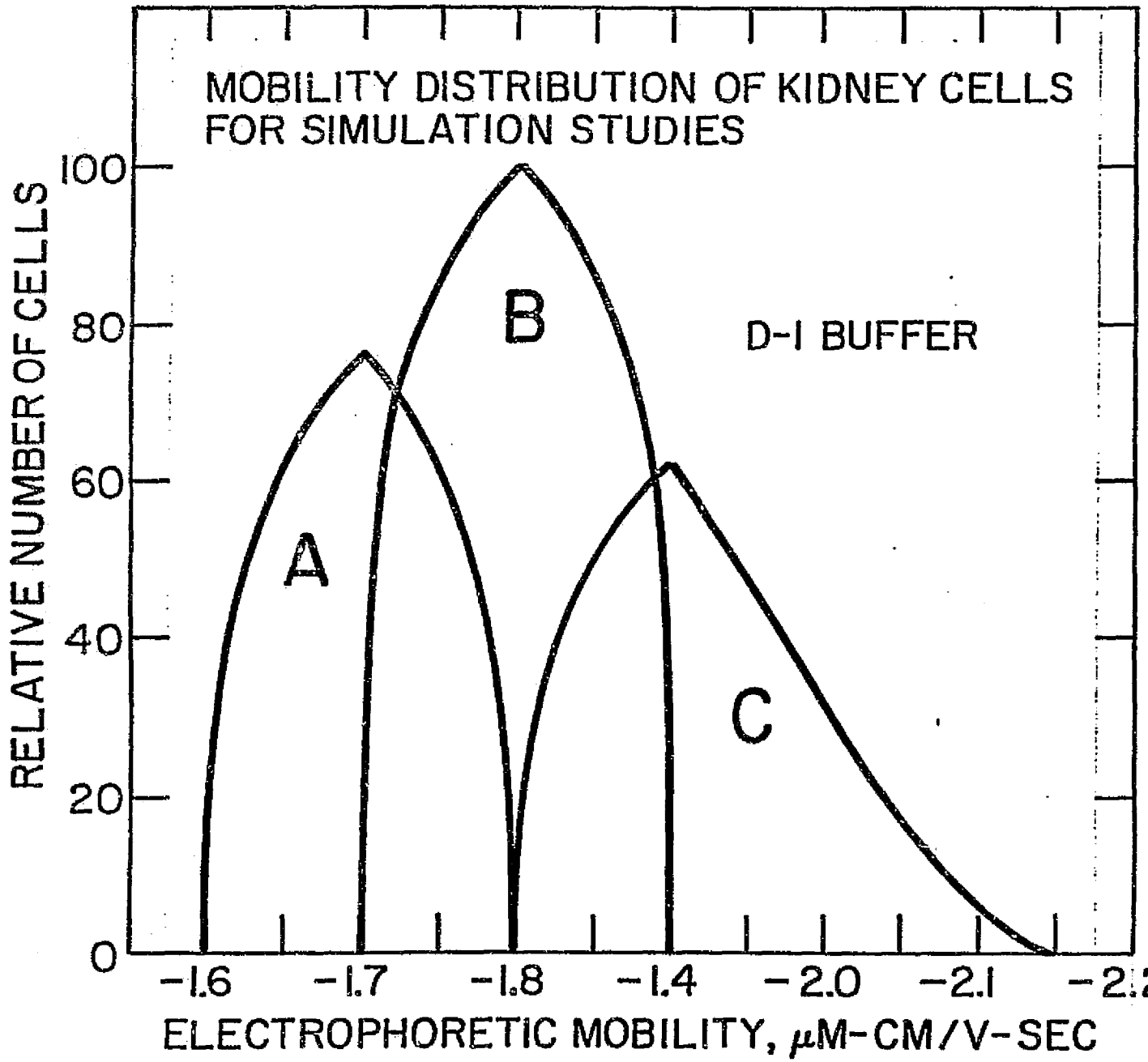
MOBILITY DISTRIBUTION OF KIDNEY CELLS
FOR SIMULATION STUDIES
D-I BUFFER
A
B
C
RELATIVE NUMBER OF CELLS
100
80
60
40
20
0
-1.6
-1.7
-1.8
-1.4
-2.0
-2.1
-2.2
ELECTROPHORETIC MOBILITY, μM-CM/V-SEC

New mobility data

H2K 8514

CTUAL PARTICLE PROFILE AT THIS POINT IN TIME FOR THE GIVEN SET OF CONDITIONS

TIME TO THIS STAGE = 2705.63 SECONDS OR = 45.09 MINUTES

(SCALE IN CENTIMETERS)

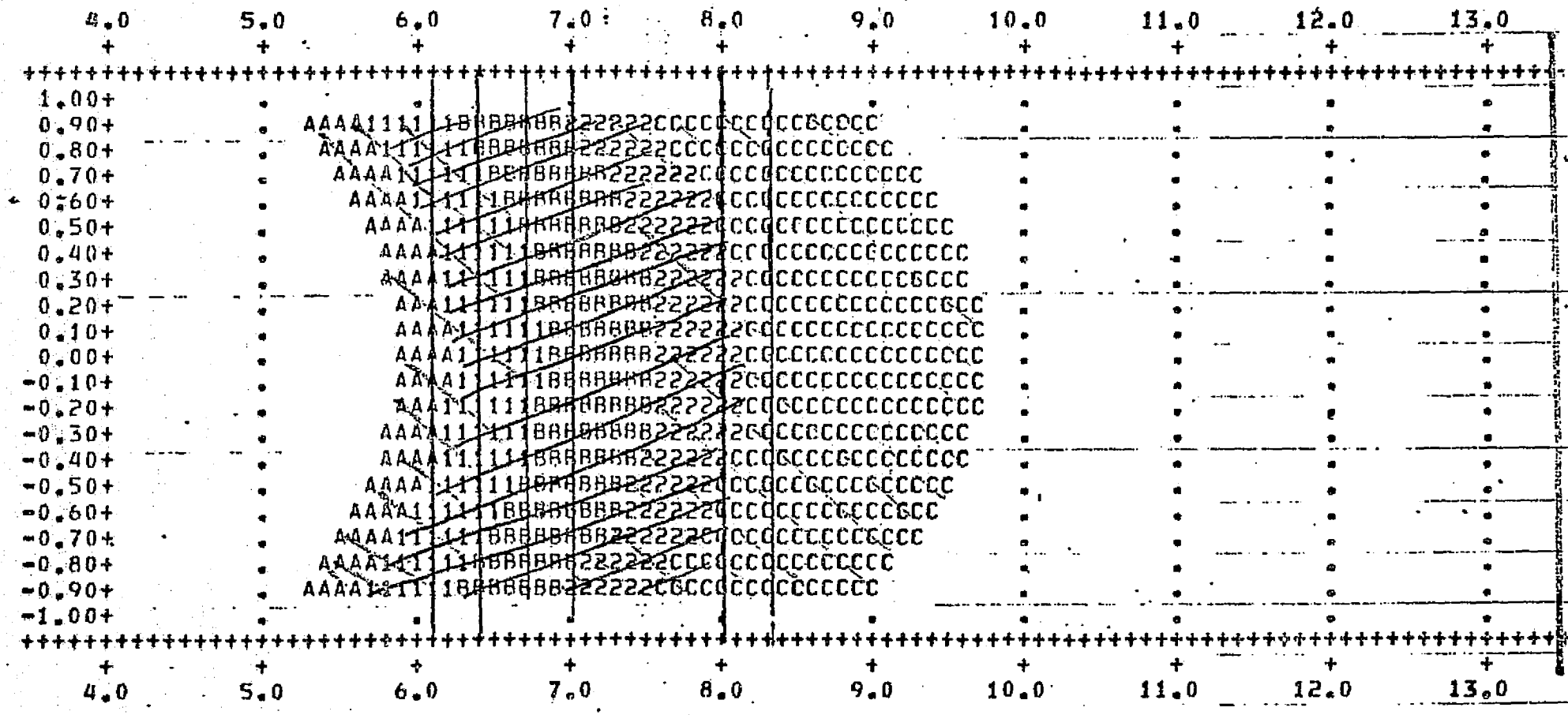

A = PARTICLE NO. 1 B = PARTICLE NO. 2 C = PARTICLE NO. 3

R	LEAD	TRAIL	LEAD	TRAIL	LEAD	TRAIL
0.9000	6.2424					

New mobility data HEK LOT 6514

ACTUAL PARTICLE PROFILE AT THIS POINT IN TIME FOR THE GIVEN SET OF CONDITIONS

U_{hc} = 0.0(

F_f = 18.6V

TIME TO THIS STAGE = 3607.51 SECONDS OR = 60.13 MINUTES

ORIGINAL PAGE IS OF POOR QUALITY

(SCALE IN CENTIMETERS)

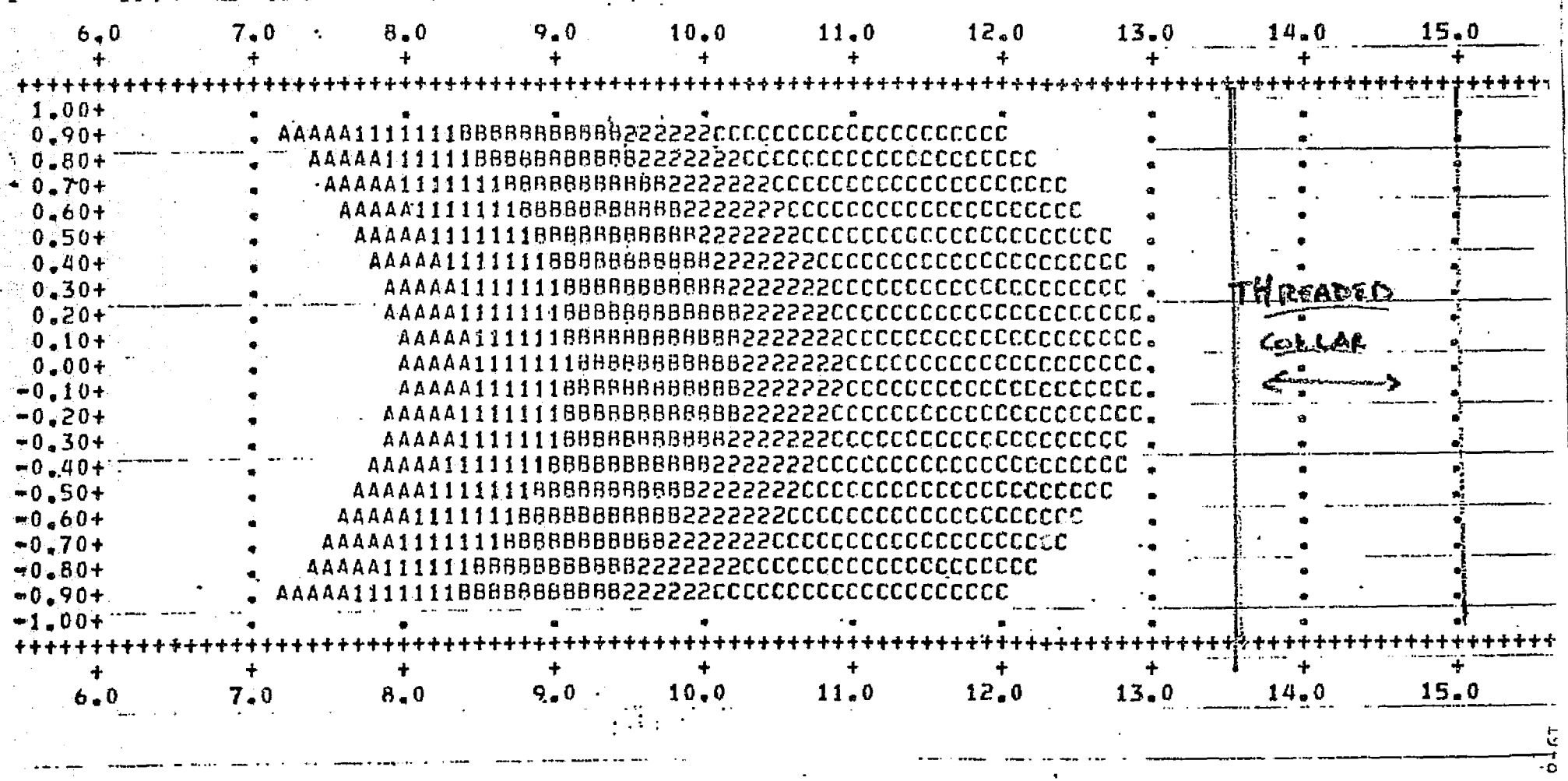

PARTICLE NO. 1 | PARTICLE NO. 2 | PARTICLE NO. 3

R | LEAD | TRAIL | LEAD | TRAIL | LEAD | TRAIL

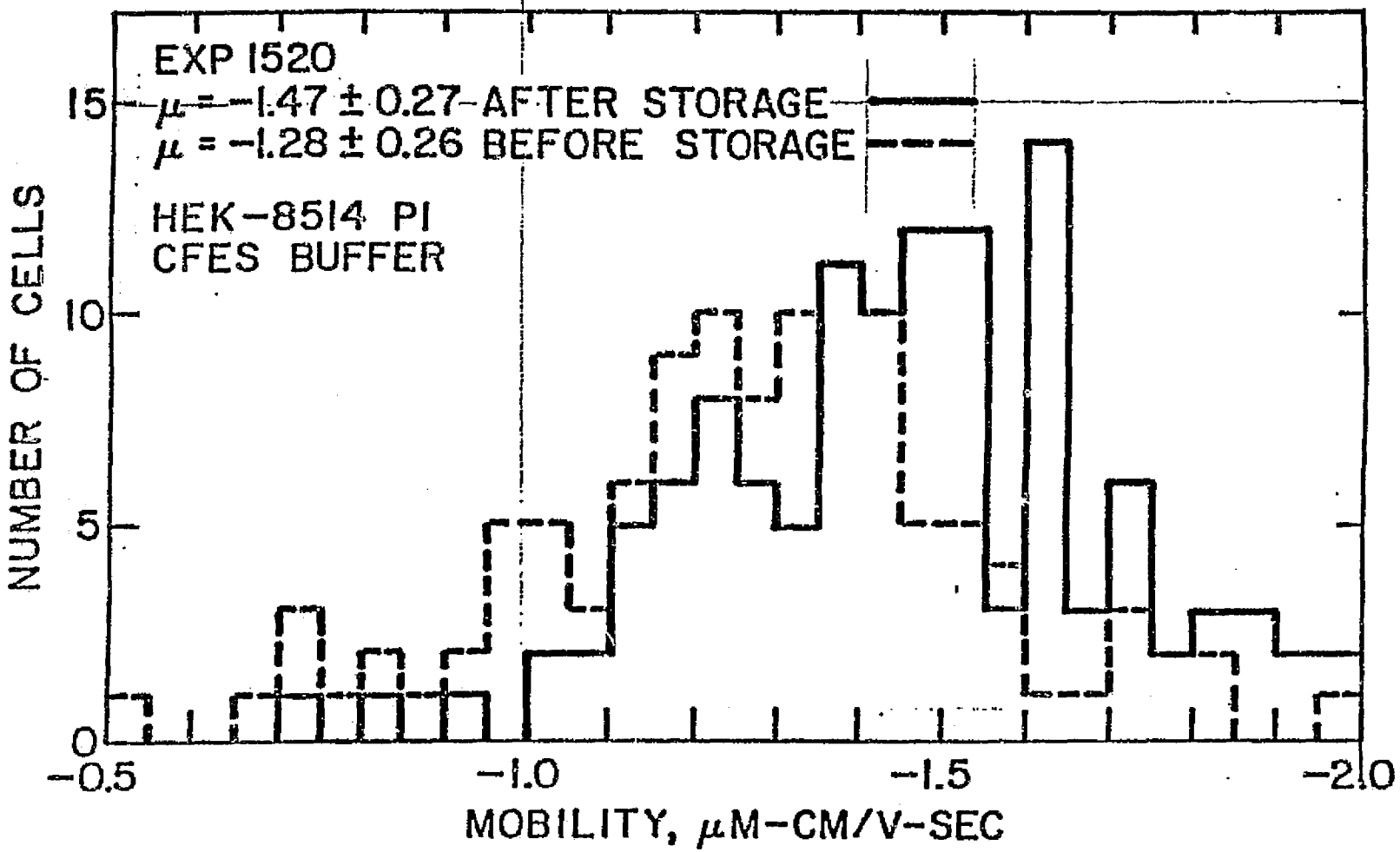
EXP 1520
μ = −1.47 ± 0.27 AFTER STORAGE
μ = −1.28 ± 0.26 BEFORE STORAGE
HEK−8514 PI
CFES BUFFER
NUMBER OF CELLS
0
5
10
15
−0.5
−1.0
−1.5
−2.0
MOBILITY, μM−CM/V−SEC

Chapter 20

A Review of Kidney Cell Growth in Serum-Free Medium.

A Critical Synopsis: Continuous Growth of Proximal Tubular Kidney Epithelial Cells in Hormone-supplemented Serum-free Medium. (Chuman, Fine, Cohen, and Saier. J. Cell Biol. 94, 506-510. 1982)

SUMMARY:

The kidney forms urine and reabsorbs electrolytes and water. This study used kidney cell lines and hormone-supplemented serum-free medium; the hormones were insulin, transferrin, vasopressin, cholesterol, prostaglandins, hydrocortisone, and triidothyronine. In general, epithelial cell lines are polar and form hemisycsts. The Madin-Darby canine kidney(MDCK) cell line used is distal tubule-like. LLC-PK_1 cells are derived from pig kidneys and have the properties of different kidney segments.

The LLC-PK_1 cells with proximal tubule properties were maintained in hormone-supplemented serum-free medium. Seven factors(the aforememtioned hormones and selenium) were needed for growth. Hormone-defined medium supported LLC-PK_1 cell growth, allowed transport(as seen by hemicyst formation), and influenced cell morphology. Vasopressin(used for growth and morphology) could be partially replaced by isobutylmethylxanthine or dibutyryl cAMP. The defined medium was used to isolate rabbit proximal tubule kidney epithelial cells free of fibroblasts.

The paper, Continuous growth of proximal tubular kidney epithelial cells in homone-supplemented serum-free medium, makes a few misguided assumptions about proximal vs distal tubules and properties of LLC-PK_1 cells, but basically provides a good model for defined media studies.

I. Background

A. Kidneys (see figure 1 and 2[24])

The functional structure of the kidney is the nephron. It is here that urine forms, beginning in the glomerulus capillary system. From the glomerulus the fluid that will become urine enters the proximal tubule (P.T.) where solutes and water are reabsorbed in equal amounts. Active sodium reabsorption drives all other transports in the P.T., e.g., passive movement of water out of the tubule and coupled reabsorption of glucose. Entering the Loop of Henle, the fluid loses water and solutes, forming a gradient that concentrates the urine so that the only reabsorption needed in the distal (D.T.) and collecting tubules (C.D.) is fine tuning.[24]

B. Hormones

The hormones examined in the paper were insulin, transferrin, cholesterol prostaglandins, hydrocortisone, and triidothyronine. In vivo, the hormones act and interact onspecific tissues. Insulin causes glucose release, but has little effect on glucose transport in the kidney. Transferrin is a β-globulin that combines with iron to transport it in the plasma. Vasopressin(antidiuretic hormone--ADH) controls reabsorption of water in the kidney's late distal tubule and collecting duct. Cholesterol forms cholic acid in the liver, leading to bile formation. Prostaglandins cause vasoconstriction or vasodilation. Prostaglandin E_2 is produced in the kidney and causes vasodilation. Hydrocortisone(cortisol) stimulates gluconeogenesis in the liver by mobilization of amino acids from extra-cellular fluid. Triidothyronine is present in small amounts, but is very potent at increasing metabolic rate.

C. Epithelial Cells in Culture

Studies of epithelial cells in culture have many advantages: (1) minimum variability among samples. Genetic differences are reduced by developing samples from the same precursors, and differences in nutrition, endocrinology, and age can be eliminated. (2) large amounts of homogeneous material can be grown. (3) samples can be stored frozen and examined later. (4) cultures of a single cell type can be developed and genetically dissected to discover cell function mechanisms.

Cereijido and associates(1979) found epithelial cell lines in culture to be polar and form hemicysts(fluid filled spaces.) The reason for polarity is unclear, but polarity is attachment dependent with the basolateral plasma membrane facing the supporting surface and the apical membrane facing the medium(see figure 3).[2] The direction of transport can be determined by watching fluid movements and specific polar budding of enveloped viruses.[1] Hemicyst(dome) formation is unique to confluent epithelia and is seen in kidney,[8,10] mammary gland, liver,[15] and urinary bladder[6] cells. Rabito, et al (1980) found hemicyst formation dependent on transepithelial transport and cell substratum adhesion strength which is modified by, for example, dibutyryl cyclic AMP. When adhesion strength increased, hemicyst formation decreased.[16]

Hemicyst formation is stimulated by cAMP, theophylline, or papaverine.[23] Hemicyst formation can not be used to quantify transport since formation depends on epithelial ability to seal in transported fluid, amount of adhesion of basal membrane to the surface, and rate of transport; however, it can be used as an indicator of transport in new cell lines.[18]

Kidney cell function can be determined in culture by such things as transepithelial transport, hormone and drug control of transport, and hormone secretion. Cell culture could overcome kidney studies' problems of too much and too little--too much variety in whole kidney extracts and too little material in dissected kidney segments. A totally defined medium in which kidney epithelial cells grow and differentiate could facilitate selection of cell of interest and study of their function.[6]

D. Madin-Darby Canine Kidney Cell Line (MDCK)

Hull, et al (1976) suggested the MDCK cell line has the properties of distal tubule epithelial kidney cells. Cereijido(1978) and Hull(1976) independently found dome formation due to active fluid transport from top to bottom occured with a specific trans-epithelial electric potential and microvilli facing into the media. The electron microscope showed structural polarity, microvilli facing the medium, smooth membrane across from the solid support, and individual cells joined by tight junctions(see figure 3.)[19] Cereijido, et al (1978) saw abnormal cytological characteristics like large nuclei and abnormal mitotic figures. When these cells were injected into chick embryos, metastatic lesion developed.[2] MDCK cells lack the specific enzyme markers of proximal tubule(P.T.) kidney cells.[19] Rindler and associates(1979) stimulated adenylate cyclase(an enzyme involved in ATP to cAMP pathways) activity with vasopressin, oxytocin, prostaglandins, glucogon, cholera toxin, and isoproterenol in MDCK cell lines. Cyclic AMP[22] and cell differentiation inducers[11] stimulate hemicyst formation.

E. Pig-derived Cell Line($LLC-PK_1$)

Hull, et al(1976) examined the $LLC-PK_1$ cell line derived from

pig kidneys that have undergone mutations and property changes in culture so that it has characteristics unlike any segment of the kidney. Hemicyst formation and tight junctions lead to cell sheet epithelial transport in LLC-PK_1 cells.[8] Goldring and associates(1978) found adenylate cyclase activity sensitive to vasopressin and calcitonin.

II. Continuous Growth of Proximal Tubular Kidney Epithelial Cells in Hormone-supplemented Serum-free Medium.

A. Materials and Methods

Basic cell culturing techniques were used: LLC-PK_1 cells were grown in Dulbecco's modified Eagles medium supplemented with horse and fetal bovine serum or hormones. Rabbit proximal tubule kidney epithelial cells were microdissected and grown in the hormone defined medium.

B. Results

The hormones added to the medium were transferrin, insulin, hydrocortisone, triidothyronine, vasopressin, prostaglandin E_1, cholesterol, and selenium. Transferrin(MDCK--5 μg/ml, LLC-PK_1--μg/ml), insulin(MDCK--5 μg/ml, LLC-PK_1--10 μg/ml),or selenium(both--5 x 10^{-8}M) deleted from the hormone defined medium reduced LLC-PK_1 relative growth to about 40% of the defined medium control growth. Hydrocortisone(MDCK--2 x 10^{-7}M, LLC-PK_1--5 x 10^{-8}M) and triidothyronine (both--10^{-9}M) were used for growth stimulation, and ~~either's~~ absence reduced growth to 75% and 60%, respectively. Adenylate cyclase activity was stimulated by vasopressin(10 μU/ml) in LLC-PK_1 and prostaglandin E_1(25 ng/ml) in MDCK, either's absence reduced growth to about 30%. Cholesterol(10^{-8} M) was added only to LLC-PK_1 cells, and its absence reduced growth to 70%. With all other hormone

concentrations normal, each hormone was varied in concentration. Transferrin and insulin dose response curves rose quickly to the defined medium concentration then dropped. Triidothyronine, hydrocortisone, and cholesterol curves continued upward; vasopressin curve rose quickly then remained fairly constant.(See figure 4.) There was no growth inhibition for any of the concentrations.

LLC-PK_1 cells grew slower in the defined medium(doubling time = 26.4 h, serum = 21.6 h) with a lower efficiency(70% vs 97%.) Hemicysts formed with equal frequency in the defined and serum media. Vasopressin requirements for growth was partially replaced by isobutylmethylxanthine or dibutyryl cAMP, which caused similar morphological changes to vasopressin. Electron microsoopy showed the LLC-PK_1 cells to be similar in either medium, except the brush boarder was denser, but shorter microvilli in the hormone serum. MDCK cells grew in LLC-PK_1 defined medium, but with no hemicyst formation; however, LLC-PK_1 cells did not grow in MDCK defined medium.

LLC-PK_1 defined medium was used to isolate primary cultures of carefully microdissected P.T. of kidneys. When testing P.T. specificity, cortical collecting duct also grew in the medium; therefore, the medium was not selective for P.T. cells.

C. Discussion

LLC-PK_1 cell line of presumed P.T. origin grew in a serum-free medium similar to that needed by the MDCK line. Medium specificity was indicated by LLC-PK_1 cells rapid growth without serum, hemicyst formation similar to that in serum, and epithelial isolation from a microdissected P.T. from rabbit kidney. Some other factor for growth was not in the defined medium since cells grew faster in serum. This was also seen by primary cultures of carefully micro-

dissected P.T. from rabbit kidney. Some other factor for growth was not in the defined medium since cells grew faster in serum. Also, primary cultures of P.T. epithelial cells did not differentiate (no dense microvillous brush boarder.) The defined medium could be used to determine cell surface receptors of LLC-PK_1 cells, molecular growth requirements for the cells, hormonal dependencies for expression of biochemical traits, also for isolation of P.T. epithelial cells in other species.

III. Critique

LLC-PK_1 cells were assumed to be proximal tubular; however, these cells have properties of other kidney segments. The glucose transport is similar to proximal tubules;[21] adenylate cyclase activity is similar to that in the ascending limb of the loop of Henle;[3] and high trans-epithelial resistance like the collecting duct.[7] It would be hard to convince a renal physiologist that LLC-PK_1 cells act as anything but LLC-PK_1 cells. However, the specific action, e.g., fluid transport, may be studied in these cells as a general process.

Microdissection of proximal tubule segments has been successful,[24] but the experimenters should have double checked the P.T. segment culture by using other tests like specific enzyme markers like maltase, trehalase, sodium-dependent glucose uptake, and p-amino hippurate(PAH) uptake.[19] In the results, collecting duct segments also grew in the defined medium, yet the conclusions state the medium could be used for isolation of P.T. epithelial cells in other species.

There were other hormones that affect kidneys that may have been used to further study the P.T. vs D.T. question. Aldosterone

stimulates sodium reabsorption and potassium secretion in the D.T. Angiotensin causes water and salt retention. ADH(vasopressin) could also be used as a D.T. and P.T. parameter because ADH causes water reabsorption only in D.T. and C.D. of the kidney.

Being picky, several "data not shown" statements were included in the results. If the data is not shown, we should not be expected to believe without seeing. (This should not be a test of faith and trust.

Finally, cultured cells are not a system. Perhaps the effects of hormones on biochemical traits can be examined in culture, but it would be a pure model with difficulties in extrapolating into in vivo situations. Hormones interact with each other in the body, as do tissues and systems. Without these interactions, I wonder how practical cultured cells would seem from a physiologist's viewpoint.

Figure 1. Cross section of the kidney.

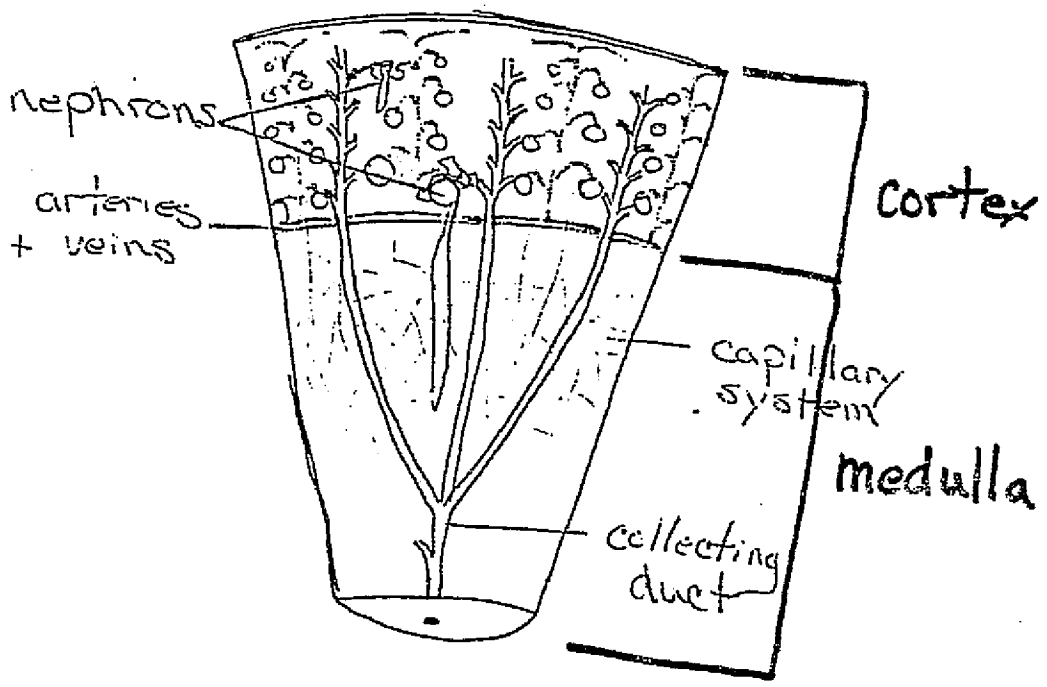

Figure 2. Kidney nephrons.

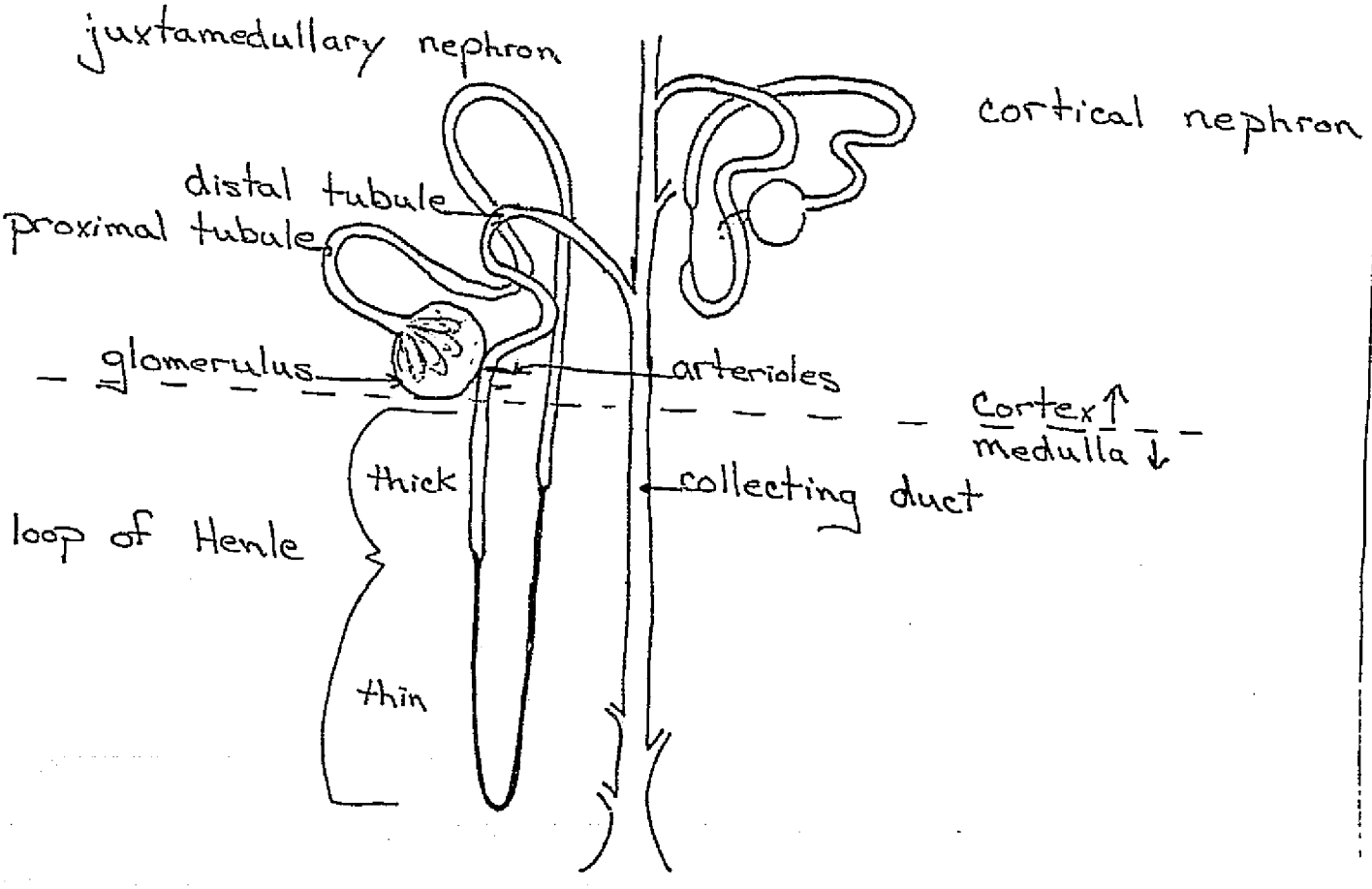

Figure 3. Schematic epithelial cell line.

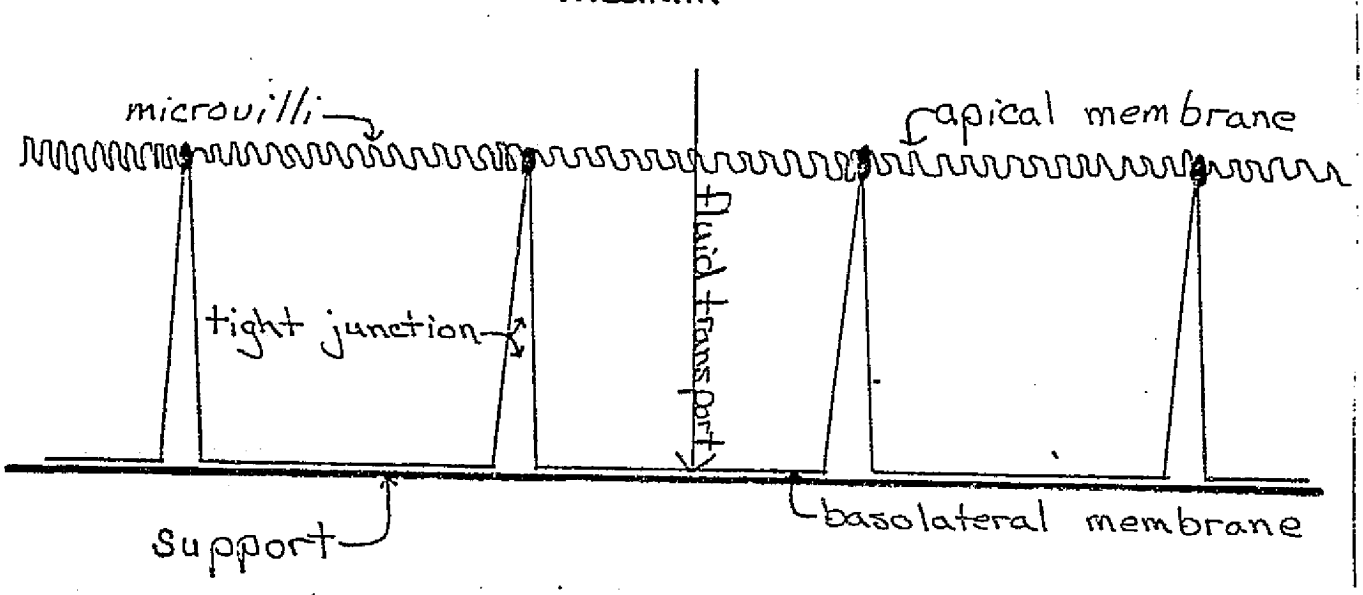

Figure 4. Dose response curves.

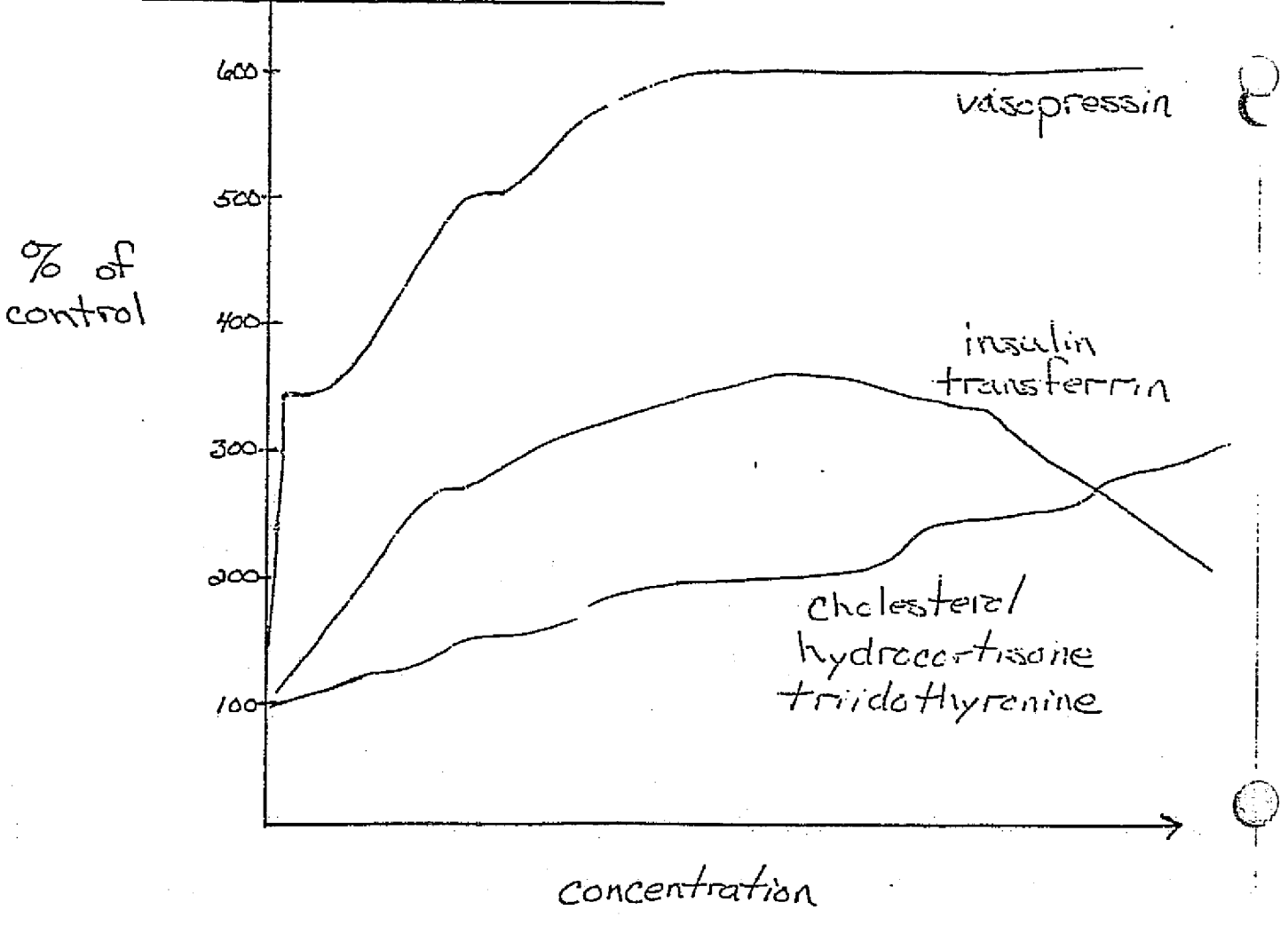

REFERENCES

1. Boulan, E.R., and Sabatini, D.D. Asymmetric budding of viruses in epithelial monolayers: a model system for study of epithelial morphology. Proc. Natl. Acad. Sci. 75: 5071-5075, 1978.

2. Cereijido, M., Robbins, E.S., Dolan, W.J., Rotunno, C.A., and Sabatini, D.D. Polarized monolayers formed by epithelial cells on a permeable and translucent support. J. Cell Biol. 77: 853-880, 1978.

3. Chabardes, D., Imbert-Teboul, M., Montegut, M., Clique, A., and Morel, F. Distribution of calcitonin-sensitive adenylate cyclase activity along the rabbit kidney tubule. Proc. Natl. Acad. Sci. 73: 3608-3612, 1976.

4. Goldring, S.R., Dayer, J.M., Ausiello, D.A., and Krane, S.M. A cell strain cultured from porcine kidney increases cyclic AMP content upon exposure to calcitonin and vasopressin. Biochem. Biophys. Res. Commun. 83: 434-440, 1978.

5. Handler, J.S., Perkins, F.M., and Johnson, J.P. Studies of renal cell function using cell culture techniques. Am. J. Physiol. 238: F1-F9, 1980.

6. Handler, J.S., Steele, R.E., Sahib, M., Wade, J.B., Preston, A.J., Lawson, N., and Johnson, J.P. Toad urinary bladder epithelial cells in culture: maintenance of epithelial structure, sodium transport and response to hormones. Proc. Natl. Acad. Sci. 76: 4151-4155, 1979.

7. Helman, E.I., Grantham, J.J., and Burg, M.B. Effect of vasopressin on electrical resistance of renal cortical collecting tubules. Am. J. Physiol. 220: 1815-1832, 1971.

8. Hull, R.N., Cherry, W.R., and Weaver, G.W. The origin and characteristics of a pig kidney cell strain LLC-PK_1. In Vitro 12: 670-677, 1976.

9. Leighton, J., Estes, L.W., Mansukhani, S., and Brada, Z. A cell line derived from normal dog kidney(MDCK) exhibiting qualities of papillary adenocarcinoma and of renal tubular epithelium. Cancer. 26: 1022-1028, 1970.

10. Leighton, J., Brada, Z., Estes, L.W., and Justh, G. Secretory activity and oncogenicity of a cell line (MDCK) derived from canine kidney. Science. 163: 472-473, 1969.

11. Lever, J.A. Inducers of mammalian cell differentiation stimulate dome formation in a differentiated kidney epithelial cell line (MDCK). Proc. Natl. Acad. Sci. 76: 1323-1327, 1979.

12. Misfeldt, D.S., Hamamoto, S.T., and Pitelka, D.R. Transepithelial transport in culture. Proc. Natl. Acad. Sci. 73: 1212-1216, 1976.

13. Livingston, D., and Taub, M. Growth of functional proximal tubule cells from rabbit kidney in defined medium. Fed. Proc. 40: 1710, 1981.

14. Mullin, J.M., Weibel, J., Diamond, L., Kleinzeller, A. Sugar transport in LLC-PK$_1$ cell line: similarity to mammalian kidney and effect of cell density. J. Cell Physiol. 104: 375-389,1980.

15. Owens, R.B., Smith, H.S., and Hacket, A.J. Epithelial cell culture from normal glandular tissue of mice. J. Natl. Cancer Inst. 53: 261-266, 1974.

16. Rabito, C.A., and Ausiello, D.A. Na^+-dependent sugar transport in a cultured epithelial cell line from pig kidney. J. Membr. Biol. 54: 31-38, 1980.

17. Rabito, C.A., and Ausiello, D.A. Effect of cell-substratum interaction on hemicyst formation by MDCK cells. In Vitro. 16: 461-468, 1980.

18. Rabito, C.A.,Tchao, R., Valentich, J., and Leighton, J. A tissue culture model to study transport functions in epithelial membranes. J. Gen. Physiol. 70: 15a, 1977.

19. Rindler, M.J., Chuman, L.M., Shaffer, L., and Saier, M.H. Retention of differentiated properties in an established dog kidney epithelial cell line (MDCK). J. Cell Biol. 81: 635-648,1979

20. Taub, M., Chuman, L., Saier, M.H., and Sato, G.H. The growth of a kidney epithelial cell line (MDCK) in hormone-supplemented serum-free media. Proc. Natl. Acad. Sci. 76: 3338-3342, 1979.

21. Ullrich, J.J. Renal tubular mechanisms of organic solute transport. Kidney Int. 9: 134-148, 1976.

22. Valentich, J.D., Tchao, R., and Leighton, J. Functional control of transporting epithelia by cAMP and divalent cation. J. Cell Biol. 70: 330A, 1976.

23. Valentich, J.D., Tchao, R., and Leighton, J. Hemicyst formation stimulated by cAMP in dog kidney cell line (MDCK). J. Cell Physiol. 100: 291-304, 1979.

24. Wideman, R.F. Personal communications. 1983.

Chapter 22

Fibrin Slide Method of Identifying Urokinase-Producing Cells in Culture

THE FIBRIN SLIDE ASSAY FOR DETECTING UROKINASE ACTIVITY IN HUMAN FETAL KIDNEY CELLS

KATHRYN SEDOR

This paper deals directly with the Fibrin Slide Technique of Hau C. Kwaan and Tage Astrup. This relatively simple assay involves two steps: the formation of an artificial clot and then the addition of an enzyme (UROKINASE) to dissolve the clot. The actual dissolving away of the clot is detected by the appearance of holes (lysis zones) in the stained clot.

In this paper, the procedure of Kwaan and Astrup will be repeated, along with modifications and suggestions for improvements based on experience with the technique.

The method of Kwaan and Astrup for a Histochemical Fibrin Slide Technique as it appeared in Laboratory Investigation, Volume 17, No. 2, was used throughout the experiment. The procedure was tried a total of five times on seperate occasions. The first two experiments involved the initial cell lot that was present in the laboratory. The second two experiments involved a more recent cell lot that was heartier than the initial line. Finally, the last experiment dealt with a particular fraction of cells that had been run through electrophresis and then cytospun onto slides. The procedure varied slightly from experiment to experiment and these differences are described below.

MATERIALS:

Solutions

BARBITAL BUFFER---0.05M barbital, 0.10M NaCl, 0.25% gelatin. pH to 7.8.

PHOSPHATE BUFFER--ionic strenght=0.15; mix 9g NaH_2PO_4 and 10.65g Na_2HPO4. add distilled water to make 1 liter. pH to 7.75.

THROMBIN----------20 NIH units/ml of 0.9% NaCl, originally 2500u/ml. add 0.1ml of 2500u/ml thrombin and 12.7ml 0.9% NaCl.

FIBRINOGEN---------0.005g plasminogen, 7.15ml phosphate buffer, 0.05ml fibrinogen.

UROKINASE----------Needed:245, 120, 60, 30, 15, and 1.5CTA units/ml. We had urokinase in dilutions of 1750, 1000, 400 and 200CTA units/ml. Dilutions were made accordingly with the barbital buffer.

HARRIS' HEMATOXY-
LIN STAIN----------Hematoxylin 0.5g, ammonium alum or aluminum ammonium sulfate 5.0g, sodium iodate 0.1g dissolve in 70.0ml in distilled water and filter.

FORMALDEHYDE, 10% solution

METHANOL, 50% solution

HANKS' BALANCED SALTS 1X solution

Sources for cells enzymes, etc.

CELLS: Human Fetal Kidney /// GIBCO
Urokinase- Crude Powder /// SIGMA
Fibrinogen-type I, Bovine Blood ///SIGMA
Thrombin, from Bovine Blood ///SIGMA
Plasminogen, Human /// Worthington Enzymes

METHODS:

ORIGINAL in brief:

1. on ordinary precleaned microscope slides, an area of 2.5 X 4.0cm was delineated with waterproof ink.
2. 10λ of thrombin solution was spread evenly over this area and allowed to dry quickly at room temperature.
3. Then, 60λ of fibrinogen solution was applied and spread quickly with a glass rod, evenly distributing the solution by gentle tilting.
4. Slides were placed on a horizontal glass plate in a moist chamber at room temperature for 1 hour to complete clot formation.

5. Cell suspensions were usually prepared as a smear on the glass slide, either by simple drying or after brief fixation in 50% methanol and then covered.
6. The slides were then incubated for appropiate lengths of time in a moist chamber at 37°C.
7. The incubated slides were fixed in 10% formaldehyde solution for 1 hour, if necessary,after pretreatment in formalin vapor.
8. After staining with Harris' Alum Hematoxylin without acetic acid, the slides were mounted in glycerine jelly.
9. For comparison, solutions of urokinase (or tissue activator) were applied with a glass capillary (diameter 1.5mm) delivering approximately 5λ by gently touching the fibrin film.

ADAPTED:

1. Steps 1--4 same.
2. Cell suspension preparation varied, see below.
3. Slides were incubated for one hour at 37°C.
4. Cells were fixed only in a 10% formaldehyde solution, with fixation time varying with each experiment, see below.
5. Steps 8-9 same.

CONDITIONS ON EACH EXPERIMENT

EXPERIMENT I

Slides U1-6, E1-4

Confluent HFK cells were trypsinized and centrifuged in a solution of equal parts of Hanks Balanced Salts and 50% methanol. After centrifugation for 10 minutes at 1400rpm, the supernatant was removed, The remaining cells were added to the slide and allowed to air dry. Cells were from the slower growing lot.

The 37°C incubation was carried out in the incubator without CO_2, however the slides were open to the air resulting in partial drying.

Slides were fixed in formaldehyde for 30-60 minutes and stained with hematoxylin twice, once for 2 minutes and then again for 20 minutes.

EXPERIMENT II

Slides $U_2$1-6, E1-4

Repeat of Experiment I, the same cell lot and procedure.

EXPERIMENT III

Slides U_c1-6, NCI,II, Ex_c1-12

Cells, from the same lot as above, were grown directly on the microscope slides until fairly confluent. Then, they were rinsed with Hanks Balanced Salts and then with distilled water. The procedure that followed was the same as above with the exceptions of a 1 hour fixation in formaldehyde and 20 minutes of staining in hematoxylin.

EXPERIMENT IV

Slides U_D1-6, θ cont, E_D1-12

Cells in this experiment were from a newer, heartier lot than before. These cells were also grown directly on the slides but only for 24 hours. The slides were then rinsed with Hanks to remove the excess media.

During the 37° incubation, a moist chamber was used to prevent the slides from drying out. This chamber was put into the moist incubator for 1 hour. Finally, the slides were fixed in formaldehyde overnight and then stained for 40 minutes in hematoxylin.

EXPERIMENT V

Slides U_E1-2, RB262 2-78

Cells were obtained from an electrophretic fraction from the newer HFK lot. These cells were cytospun onto the slides and kept cold until use. The procedure was then the same as the above.

RESULTS:

Rapid inspection of the stained slides showed that all the slides had a "Swiss cheese" appearance; it looked as though holes had been poked in the light stained clot.

These characteristic holes were seen on all the slides: the urokinase controls, the negative controls and the experimental slides.

Staining with the hematoxylin would yield color in the following degrees: Complete areas of no color (lysis zones?), light staining (fibrin clot?), and dark staining (cells and other debris).

DISCUSSION:

In veiwing the slides, I had thought that the first few experiments had worked as expected because the urokinase control slides seemed to decrease in the number of 'holes' that it contained depending on the urokinase concentration that was added. Then, I happened upon the negative controls which showed the same 'holes' but not to the same degree.

None of the slides with cells showed any good zones of lysis within the area of the premarked square. One interesting thing that was observed was that the cells had the ability to 'eat' away at the black marker that was being used. This would cause problems in containing the forming clot in the necessary boundaries on the slide.

Another problem dealt with the staining time. Initially a 2 minute stain was tried with little success. Next a 20 minute time was employed. Finally, a 40 minute staining period was tried with the best results. Even with the 40 minute staining period, the fibrin clot stained very lightly in comparison with the cells, which took the stain extremely well.

Incubation time in the 37^{o}C chamber was a problem with this experiment. According to Kwaan and Astrup, when the clot is made over the smear of cells, the

time required for formation and stabilization of the clot makes the proper incubation period less well defined. Also, the incubation time is dependent on the particular cell type that is being tested as well as the different manufactures for the standard urokinase. According to the original paper, with longer incubation times, even a weakly active site will be detected.

According to Kwaan and Astrup, "to achieve a detailed and discrete localization of active sites, the fibrinogen must be rich in plasminogen, low in inhibitor content with clottability above 85-90%, containing no spontaneous fibrinolytic activity (including such caused by bacterial contamination), be free of citrate and be soluble at high concentration (about 1%) without sedimentation. We have found no commercial preparations which fulfill all of these criteria, in particular, they arelow in plasminogen and therefore low in sensitivity to activators." (1)

Perhaps this would be a good place to start to work on the assay-determine exactly what combination of ingredients yield the best clot. By keeping all solutions filtered and cold, this cuts down on the bacterial contamination so that should not be a problem. It could be possible to change the incubation time for the clot formation to give a better result.

To determine the best incubation time in the 37^{o}C chamber, a quick test will have to be run with each new batch of urokinase standards, if there is any intention of correlating the different experiments. This is easily done by placing samples of each dilution on the same slide and then incubating for various periods of time and then comparing the results. Once this is done, it will be possible to scan an experimental slide and determine the actual concentrations of activator present based on the degree of lysis.

In summation, I think that after the best clot mixture is determined the assay will yield good results. Staining and reading the slides at this time may be no problem if the right mixture is discovered.

REFERENCES:

1. Kwaan, Hau C. and Astrup, Tage, 17, Demonstration of Cellular Fibrinolytic Activity by the Histochemical Fibrin Slide Technique." Laboratory Investigation. No. 2, pages 140-5, 1967.

Chapter 23

Calculations and Recommendations Concerning Physical Characteristics of the EEVT Apparatus.

RECOMMENDATIONS AND CALCULATIONS CONCERNING PHYSICAL CHARACTERISTICS OF THE EEVT APPARATUS

Several issues arose during the course of preparing for the flight of EEVT on STS-3, and these involved several institutions. Although this is not a formal report, it envelopes some of the correspondence and documents that highlight the discussions that occurred during the establishemnet of certain policies pertinent to the execution of the EEVT experiment.

Documents concerning the issues are presented in the following order:

1. The possibility of mixing latex spheres with kidney cells as standard electrokinetic markers.

2. Tube breakage and the potential fo the development of leaks and bubbles.

3. Effects of the shape of the sample gate on the electric field and the outward migration of cells -- M. Reynolds.

4. Suggestions for reducing electroosmosis by decreasing the diameter of the sample -- J. O. N. Hinckley.

5. Predictions of the effects of modified sample dimensions on electroosmotic band spreading -- F. J. Micale.

1. THE POSSIBILITY OF MIXING LATES SPHERES WITH KIDNEY CELLS

Spheres mixed with monolayers of kidney cells were found to be unrecoverable from the cultures. This finding was consistent with published observations that cultured cells grown in the rpesence of 1 million latex particles/ml medium incorporate the spheres into the cytoplasm by phagocytosis.

Parks, et al.: Proc. Natl. Acad. Sci. _76_, 1962 (1979).
Veomett et al.: Proc. Natl. Acad. Sci. _71_, 1999 (1974).

2. TUBE BREAKAGE AND LEAKAGE

Two additional possible sources of on-board difficulties were discussed. Electrophoresis tube breakage has bo be taken somewhat more seriously than in the past. One tube has already broken in the laboratory in the absence of unusual stresses while it was empty. Judging from the natur3 of the fracture (it showed concoidal fracture surfaces) there must have been a flaw in the tube created during fabrication. It is recommended that after fabrication, tubes be subjected to optical ;analysis, such as UV schlieren testing or whatever quality control testing is traditionally done by glassblowers when glass parts are fabricated for critical or high-stress applications. Several tubes that were processed on Apollo 14, Appollo 16, and ASTP developed bubbles. It is suggested that the formation of bubbles might be due to the evapoartion of water following its diffusion through the plastic containers, especially those with thin walls (bags) used for electrode buffer recycling. Water diffusing out and air diffusing in while liquids are held in plastic is a relatively common problem. Perhaps measures that retard this process would help prevent bubble formation in electrode buffer in future experiments. This notion should be tested in the laboratory very soon, bu simply letting water (or buffer) stand in the system for a few days and turning it on as if in a run. The bubbles which may have formed, however, might not have the same effect on the earth's surface as in microgravity, for the simple reason that the principal force on bubbles at 1 g is buoyancy, whereas the principal force in orbit is electrophoresis, which would sweep bubbles to one end of the electrophoresis tube from the electrode buffer compartment.

Reply to Attn of. SD5-81-MR-02

JAN 29 1981

Dr. F. J. Micale
Center for Surface & Coating Research
Sinclair Laboratory, Bld. 7
Lehigh University
Bethlehem, PA 18015

Dear Dr. Micale:

This is to confirm our conversation yesterday on Dr. Paul Todd's visit with you at Lehigh University on Feb. 5, 1981.

We would like to have the following areas discussed:

1. Sample Slide Size

Enclosed is a cross section sketch of the current sample slide in relation to the delrin sleeve and glass electrophoresis column. The current sample size is 0.188 inches, the sketch reflects a possible larger opening of 0.240 inches. Our experiments have demonstrated that we can get 3 to 3.5 times more cells in this larger diameter. We would appreciate your views on the feasibility of increasing this opening, and the problems related to such an increase in size.

2. Coating Procedure

We would like you to go over in detail the coating procedure for the glass tubes. In particular how you determine the electroosmotic values for the tubes.

3. Mobility Data

We hope that you've had time to run our mobility data that we sent. Between your results and Dr. Todd's we should be able to determine the length of time we need to run the kidney cells on EEVT.

4. Latex Bead-Red Blood Cells

There have been some discussions on the feasibility of running some of your latex beads along with red blood cells as markers in EEVT. What do you think of this idea?

We hope that you and Dr. Todd will have enough time to discuss all these areas. We really appreciate you taking the time to help us make EEVT a success. Thank you again for your help.

Sincerely,

Mike,

Michael A. Reynolds, Ph. D.
Biomedical Applications Branch

cc:
Dr. P. Todd, Penn State

ORIGINAL PAGE IS
OF POOR QUALITY

Calculation of effect of cells in the sample gate on electric field through sample gate.

The electrophoresis unit may be considered as an electrical circuit:

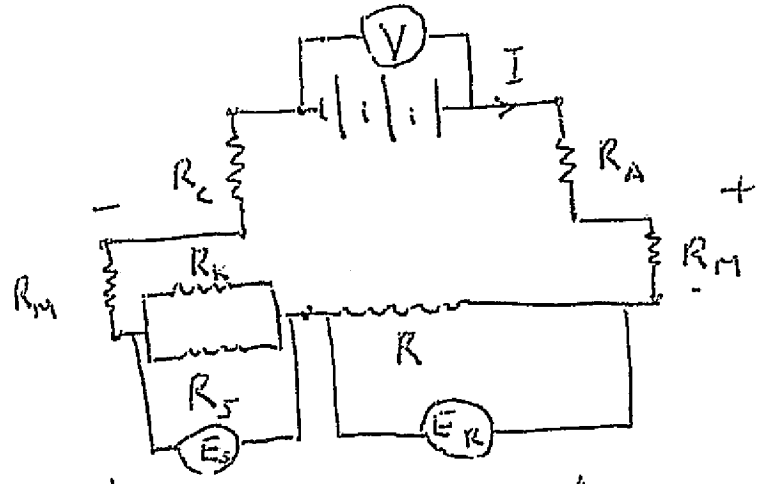

V = voltage at power supply

R_K = resistance in the sample slide due to kidney cells

R_S = resistance in the sample slide due to buffer

R = resistance of column

E_R = field strength across electrophoresis column

E_S = field strength across sample slide opening

I = applied current, held constant at power supply

l = length of hole; thickness of slide

$$E_s = \frac{I}{k_o A} = \frac{I l}{k_o A l} = \frac{I l}{k_o (V - V') + k_o' (V')}$$

$$\frac{E_{s,\text{with}}}{E_{s,\text{without}}} = \frac{\frac{I l}{k_o (V - V') + k_o' V'}}{\frac{I l}{k_o V}} = \left[\frac{k_o (V - V')}{k_o V}\right]^{-1}$$

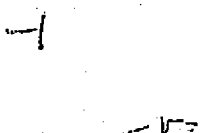

$$\therefore \quad \frac{E_{\text{with cells}}}{E_{\text{without}}} = \left(\frac{V - V'}{V}\right)^{-1}$$

$V = \pi r^2 l = \pi (0.305)^2 0.15 = 0.044 \text{ cm}^3$

$\pi (0.305)^2 0.3 = 0.088$

$r = \frac{.24''}{2} = \frac{0.61}{2} = 0.305 \text{ cm}$

$l = 0.15 \text{ cm} \quad 0.3 \text{ cm.}$

$k_o = 0.9 \text{ mmho/cm} = 0.9 \times 10^{-3} \text{ mho/cm}$

$V' = 6 \times 10^6 \text{ cells} \times 5000 \mu m^3/\text{cell} = 3 \times 10^{10} \mu m^3 \times 10^{-12} \frac{\text{cm}^3}{\mu m^3}$

$1 \mu m = 10^{-4} \text{ cm}$

$1 \mu m^3 = 10^{-12} \text{ cm}^3$

$V' = 0.03 \text{ cm}^3$

$$\frac{E_{\text{with}}}{E_{\text{without}}} = \left[\frac{0.088 - 0.030}{0.088}\right]^{-1} = \frac{88}{88 - 30} = 1.52$$

34% of vol = cells

APPENDIX B

A Gel-Halo Sample Pellet: the best of both worlds? Stubby Zones without a Constricted Sample Gate. by J. O. N. Hinckley

This reduces cell quantity, in the same way as does a narrower bore sample gate. The cells are confined to the center of the gate, inside a halo of electrolyte (D-1 buffer, here) immobilized by gel, which halo mechanically retains the ice pellet in position prior to thaw. The gel halo can be retained by the same gentle ridge as is contemplated for the ice pellet, and the ice pellet can be likewise retained within the gel halo.

The gel should be a very low EEO agarose, made up in D-1 buffer to have identical conductivity. It should be cast in the gate. The hole in the gel for the ice pellet could be made by a cast preform, removable on insertion of the ice. Further, the rear of the gate could be a continuous agarose film, further retaining the cells from contact with the rear of the gate and the Spectrapore/agarose/fit assembly, if desired. The pellet is inserted or frozen in situ (nb gel behavior on freezing etc - but bearable, or use a glycol-loaded gel).

The current lines now go straight through the gel, and there are no corner backwaters or field problems. However (see under field-bending below), there may be merit in ensuring that the thawed pellet has a conductivity similar to the halo, event if this differs from the bulk D-1 conductivity in the column.

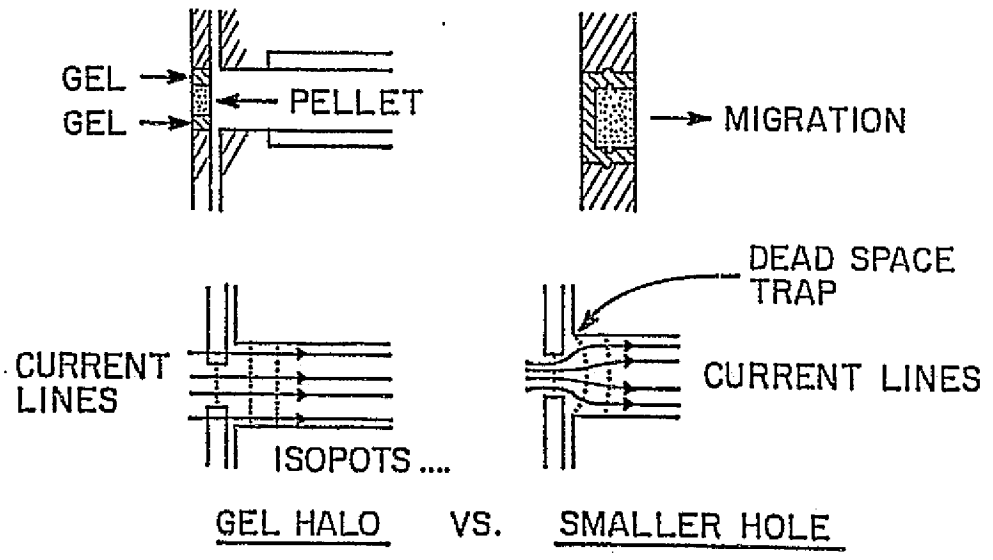

Electroconvection

This occurs in free solution electrophoresis, in the experience of Philpot (1971 personal communication, 1973 in print briefly), and follows from field theory: according to Gauss-Coulomb's Law a variation in space of field strength must give rise to a local non-neutrality. The effect is observable in non-uniform electric field, where it is a source of leakage current in liquid transformer and high voltage insulating oils, and can even be used as an adjunct cooling circulation. (One would therefore expect it as a disturbance in dielectrophoresis, Pohl's method).

Wherever there is a non-uniform field, we should be alert for electroconvention and dielectrophoretic effects (negligible compared with electrophoresis in DC and uniform fields). Electroconvection is related to EEO - just that in EEO the non-neutraility is due to adsorption equilibria between wall and bulk solution, rather than due to field non-uniformity.

The rule is avoid non-uniformities of bore e.g. sample gate, if narrow. Why look for trouble?

Entrainment and stubby zones.

This spectre I conjured up in 73/74 alo, and suggested its relation to the waisting and bullet heads of Apollo 16 runs, which did not seem all so parabolic, but rather like gobs of chewing gum slowly detaching----------.

----- in that any charge difference (cf. EEO) between clear buffer and a zone of cells would give rise to an electrconvective situation, where it is less energetic for a zone to travel through clear buffer as a single quasi-macro-particle than for each cell to swim through its own fluid medium surrounding it. Thus liquid would be entrained by the zone, if there was buffer in hydraulic parallel. That is, a stubby zone could perhaps entrain buffer, and as it moves forward, the counterflow would be peripheral to the zone rather than intrazonal and equally

integrated across the tube section. Or, regard suspension as cosity, cohesion, a hecting slip-pla-----

I do not know what the figures would be when plugged in, or if this is real. But it might be nice to know, before we get too deep into stubby zones. Conventional zones across the whole lumen section might be a safer conservation choice.

Field- bending, and stubby zones, and the gel-halo

Another effect of both stubby zones and the gel-halo idea is this. Cells tend to be electrically insulating, so replacement of some of a volume of buffer by a similar volume of suspended cells would reduce the conductivity of the buffer, in some proporation to the concentration of the suspension. Therefore, a stubby zone distorts its local electrical field (leading to electroconvention, etc?), which in turn affects the migration speed and pattern. I'll be that one didn't get into the computer programs. It applies to the gel-halo concept - which is why I think the halo should be made to have the same conductivity as the thawed pellet.

Such field-bending may also be involved in the Apollo 16 anomalies. The effects of field-bending on a stubby zone are anticipated in the picture:

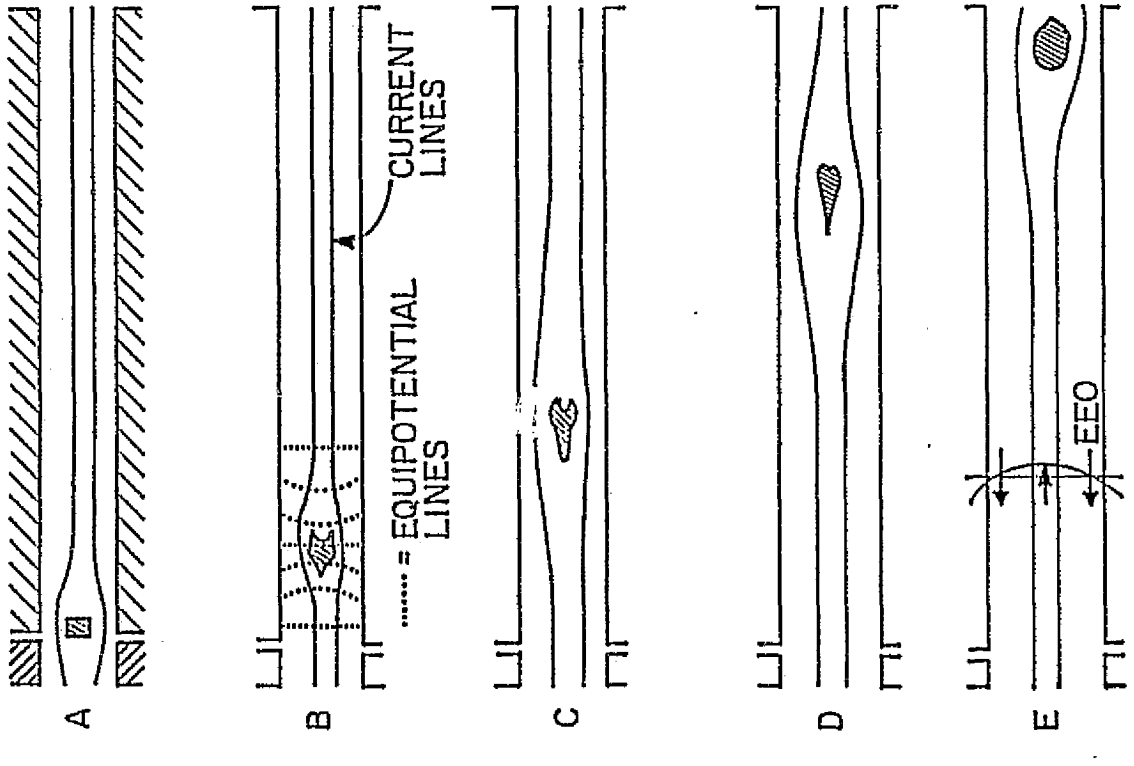

Lehigh University

F.J. Micale
Associate Professor of Chemistry

Center for Surface and Coatings Research
Francis MacDonald Sinclair Memorial Laboratory 7
Bethlehem, Pennsylvania 18015
telephone (215) 861-3596

March 27, 1981

Dr. Mike Reynolds
SD5-80-MR012
Johnson Space Flight Center
NASA RD #1
Houston, Texas 77058

Dear Mike:

Enclosed are the results of the computer calculations for a simulated distribution of kidney cells (enclosed). The calculations were made for different values of electro-osmotic flow, U_{os}, and ratio of sample diameter to channel diameter, R. Results are also available (not enclosed) as a function of time. A copy of these results are being sent to Paul Todd.

Call if there are any questions.

Best regards.

Sincerely,

Nato Micale

F. J. Micale

FJM/kd
enclosure

T = 1 HR, R = 0.96, U_{OS} = −0.06, E = 18.6 V/CM, U(HUM) = −2.05 ± 0.11, U(RAB) = −1.05 ± 0.09

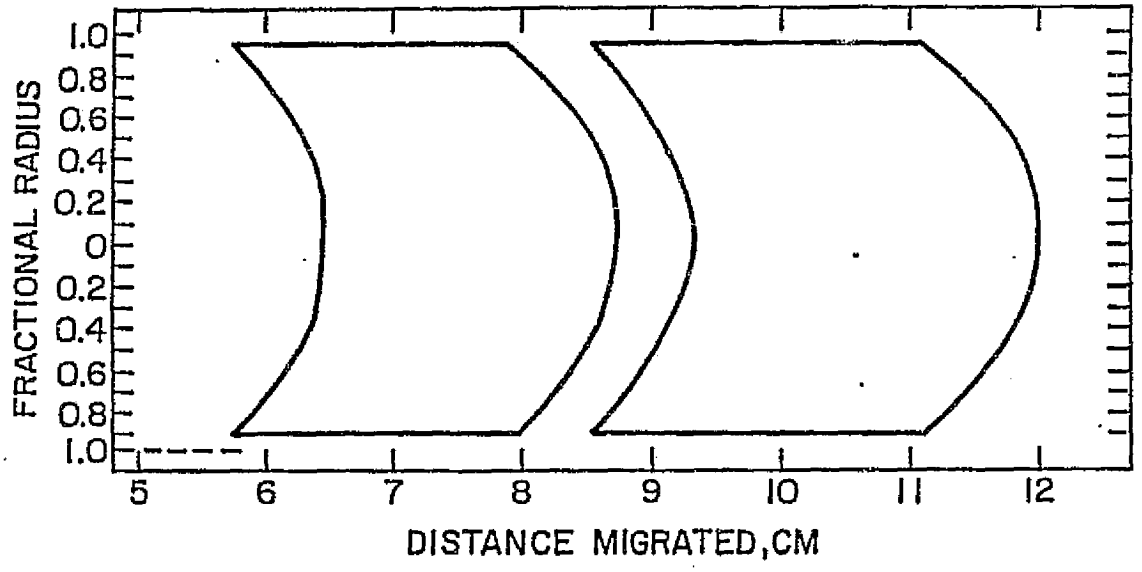

T = 1.0 HR, R = 0.75, U_{OS} = −0.06, E = 18.6 V/CM, U(HUM) = −2.05 ± 0.11, U(RAB) = −1.05 ± 0.09

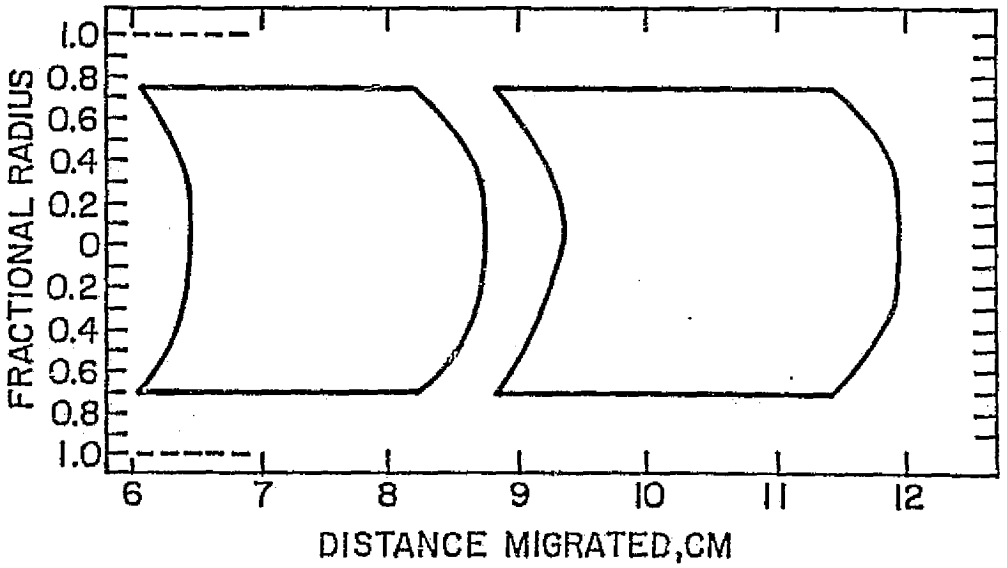

Chapter 24

Final Report on Detailed Performance of the EEVT Experiment on Shuttle Flight STS-3.

Evaluation of Results of Cell Electrophoresis Experiments on Space Shuttle STS-3 including Pre-Flight and Post-Flight Laboratory Experiments

Semi Annual Progress Report

Contract NAS 9-15584

Paul Todd
403 Althouse Laboratory
The Pennsylvania State University
University Park, Pennsylvania 16802

This special report emphasizes Shuttle experiment results, including relevant pre flight and post flight laboratory experiments and calculations. It therefore includes work of Marshall and Johnson Space Centers integrated into the data and narrative. Introductory sections for example, were written in part by R. S. Snyder

INTRODUCTION

In free fluid zone electrophoresis experiments in the microgravity environment of space, sample and equipment complexity has increased from electrophoresis of soluble dyes on Apollo 14,[1] polystyrene latex on Apollo 16[2] and viable cells on the Apollo-Soyuz Test Project (ASTP)[3,4]. Zone electrophoresis in cylindrical columns has been the method of choice because basic phenomena of electrophoresis, electroosmosis and any second-order fluid disturbances could be evaluated by photography and post-flight fraction analysis.

The ASTP experiments which fractionated viable cells, introduced considerable experimental and equipment difficulties. The biological samples were taken into space as frozen disks to assure both biological viability during pre-flight storage and sample conformation at the beginning of electrophoresis. The columns were frozen after electrophoresis to preserve the positions of separated biological cells and to preserve the cells for subsequent post-flight analysis and culturing. The use of multiple columns required a separable connector between the electrode buffer circulation system and the electrodes of the individual columns, as shown in Fig. 1. Electrode buffer circulation was required to carry electrode gases to the phase separators. All operations on the ground and in space were done without introducing microbial contamination as proven by the sterile culture of kidney cells sustained after the flight. All systems, however, did not work in flight for all experiments, and the Electrophoresis Equipment Verification Test (EEVT) was designed to repeat the most promising parts of the ASTP experiment with equipment that had been more thoroughly operated and tested in the laboratory before flight. The equipment worked as planned in space during the third Space Shuttle mission (STS-3), and photographs of the two columns with red blood cells were obtained. Information on the final distribution of the human and rabbit cells was lost when the frozen columns melted before sections could be cut and analyzed. This report analyzes the photographs and describes the pre-flight and post-flight experiments that were done to understand the resulting data.

BACKGROUND

Review of Relevant ASTP Observations.

The column electrophoresis experiment conducted on the Apollo-Soyuz Test Project (ASTP) was intended to separate model particles and biological cells by zone electrophoresis in the microgravity environment of orbital flight. The model particles, aldehyde-treated red blood cells from rabbit, human and horse, were used to test the column coating procedures developed to eliminate electroosmotic fluid flow and to emulate the inter-particle aspects of an electrophoretic separation without the added technical problems of sterility, cell viability, and particle heterogeneity. Additional columns contained human peripheral blood lymphocytes, cultured human embryonic kidney cells, and native red blood cells. Each experiment was performed in duplicate to determine reproducibility of cell fractionation.

Only two columns from the four space experiments (eight columns) yielded results that encouraged further investigation: an enhanced urokinase production was measured from specific fractions of separated kidney cells, and good photographs of the fixed red blood cell separation showed the absence of electroosmotic fluid flow. Nevertheless, neither of these experiments were without deficiencies. The two freeze-thaw cycles of the kidney cells substantially reduced cell viability, and the urokinase analyses were made with very few cells. Kidney cells were also found, unexpectedly near the point of sample insertion. This was not expected on the basis of ground-based mobility measurements, thus the cells may have been retarded while leaving the insertion slide. The frozen column of red blood cells, whose separation was photographed in space, fractured while in the slicing apparatus. Frozen disks containing the blood cell fractions which could then be reconstructed to give a profile of the red cell populations were therefore not obtained. A knowledge of the precise to explain photographs which showed a distinct leading band of cells (presumably horse) followed by a broader band of mixed cells (human and rabbit).

Objectives of RBC Experiments on STS-3

The objectives of the red blood cell experiments on ASTP were to provide a visual check on the electrophoretic process and especially electroosmotic flow in space as well as to provide test separations of non-degradable standard particles for comparison with the separations of the three viable cell types studied on ASTP. Since electroosmosis was minimized in the ASTP columns and was not considered a problem for the Shuttle experiment, the objective of the reflight EEVT was less technical and more scientific in its scope. Determination of the maximum concentrations of cells that can be separated in column electrophoresis was a significant goal. Two of the eight columns were available for red cell experiments, so two concentrations of human and rabbit RBC mixtures were used.

During ASTP, dimensions of the column and sample insertion slide were chosen on the basis of compromise. The column internal diameter of 0.625 cm could not be increased without increasing the radial gradient of temperature and temperature dependent parameters such as viscosity and conductivity. The column length was suitable for the range of cell mobilities, the moderate applied electric field (~15 V/cm) and the available electrophoresis time interval (one hour). The cylindrical sample insertion disk was 0.476 cm diameter and 0.318 cm thick. The diameter was made less than the internal diameter of the column to minimize the influence of any residual electroosmotic fluid flow at the column wall. The thickness was chosen on the basis of compromise that provided enough cells to be fractionated and collected and grown in culture, and adequate resolution of separation.

The number of fixed red blood cells loaded into each 0.06 ml sample slide on ASTP was 5.2×10^6 rabbit, 3.4×10^6 human and 7.3×10^6 horse cells for an overall concentration of 2.6×10^8 cells/ml. The EEVT experiment compared the electrophoretic behavior of this concentration of cells with that of cells 10 times as concentrated.

Human and rabbit cells were selected because they are of similar size not different mobility, and the concentration effect could be established with two species. Although horse cells as used on ASTP or cat cells which were available for STS-3 have substantially higher mobilities than human cells, they have substantially higher mobilities than human cells they have a significantly smaller size, and adding them would add another factor to the analysis, so a third cell type was not used. The human and rabbit cells are easily separated by continuous flow electrophoresis at concentrations of 2×10^8 cells/ml as Fig. 2 shows. Continuous flow electrophoresis has also separated fixed red blood cell populations (cow and turkey) at 10^9 cells/ml, although the separated bands are broad due to effects such as droplet sedimentation[5]. Density gradient gradient electrophoresis is also limited by droplet sedimentation at RBC concentrations around 5×10^8 cells/ml[6]. Thus, one EEVT sample slide had a total of 2×10^8 cells/ml and the other slide had 1×10^9 cells/ml with equal numbers of fixed human and rabbit cells in each slide. Each erythrocyte has a biconcave discoid shape with a volume of about 90 cubic microns. The volume concentration of 1×10^9 cells/ml is thus approximately 10%, and 2×10^8 cells/ml occupies 2% of the starting buffer volume. Thus cell migration and separation were studied at two starting concentrations.

Objectives of Kidney Cell Experiments on STS-3

Only one column on ASTP yielded separated, live human embryonic kidney (HEK) cells. The fractions each contained very few cells, and cell viability was extremely low. Nevertheless, post-flight evidence was found for the existence of electrophoretic fractions enriched in cells that produce urokinase (UK), erythropoietin (ESF) or granulocyte conditioning factor (HGCF)[3,4]. The objectives of the EEVT experiment were to evaluate the reproducibility of of microgravity electrophoretic separation of living cells, to separate cells with highly viability despite two freeze-thaw cycles, and to optimize the physical

conditions of cell separation. Owing to the uncertain heterogeneity of the starting material the experimental design does not assess resolution in microgravi but improved separability was sought in comparison to density-gradient electrophoresis[7] or continuous-flow electrophoresis, as in Fig. 3, which shows distributions of cells and UK activity after separation of HEK cells in McDonnell-Douglas Continuous Flow Electrophoretic Separator.

Effort were made to increase cell yield and cell viability in the EEVT experiment and to assess reproducibility directly. An increase in cell yield was achieved by increasing the sample volume by ~30%-compared to ASTP apparatus by increasing the sample-holder diameter to 0.584 cm. Viability was increased by the use of "D-1" buffer, in which the cryprotectant was DMSO rather than glycerol as was used in "A-1" buffer on ASTP. Reproducibility was to be achieved by using 6 identical columns.

ANALYSIS OF ELECTROPHORESIS EXPERIMENTS ON SHUTTLE FLIGHT STS-3

1. Pre-flight characterization of fixed human erythrocytes

Table 1 lists some pertinent measurements of the electrophoretic mobility of glutaraldehyde or formaldehyde fixed human RBC's in D-1 buffer and saline. A general value of 2.60 $\pm$ 0.15 ($\pm$ S.D.) seems to apply. This is higher than that determined at MSFC, as indicated in Figure 4. The expected values in saline and the expected dependence of mobility on pH do not reveal unique features of the method of measurement that would explain the discrepancy readily.

2. Pre-flight characterization of fixed rabbit erythrocytes

Table 2 lists some measurements of fixed rabbit RBC electrophoretic mobility in D-1 buffer. In all cases the fixation utilized glutaraldehyde, and a reasonable value was found in saline. Generally, the mobility in D-1 was 1.70 $\pm$ 0.22 μm-cm/V-sec. Figure 4, however, favors mobility of formaldehyde-fixed rabbit RBC's in D-1 of about 1.45 μm-cm/V-sec.

3. Pre-flight characterization of human embryonic kidney cells

Numerous experiments were performed in which early-passage human embryonic kidney cell strain HEK-8514, passage 5, were subjected to density gradient electrophoresis and/or microscopic electrophoresis. Figure 5 shows that the distribution is very broad, has a mode around 1.3, and is slightly narrowed and shifted downward by trypsinization.

4. Conclusions concerning RBC mobility measurements

Mobility in D-1 is consistently higher than in A-1, but only by 0.1 - 0.2 unit. Mobilities measured in saline are in agreement with published values. The lowest human RBC mobilities in D-1 were 2.31 and 2.35; these were made in D-1 without DMSO, in Cytopherometer and Pen-Kem, respectively. The range of reliable mobilities of formalin-fixed human RBC's is 2.54 - 2.79. Deriving mobilities from whole velocity parabolas does not increase the measured mobility. If anything, mobilities determined

from parabolas are 0.1 - 0.2 unit less. Glutaraldehyde-fixed cells do not have higher mobility than formalin-fixed cells.

5. Pre-flight determination of electrophoresis column resistances

Figure 6 is a sketch of the measurements used in determining resistances of the various column components. Using these dimensions and K = 1.05 mmho/cm and 0.762 mmho/cm at 23°C at 10°C, respectively, the component resistances are,

for the glass column at 23°C:

$$R = \frac{15.0 \text{ cm}}{1.05 \times 10^{-3} \text{ mho/cm} \times \frac{1}{4}\pi (0.635)^2} = 45.11 \text{ k}\Omega \quad (1)$$

for the dummy slide at 23¼C:

$$R = \frac{0.3226 \text{ cm}}{1.05 \times 10^{-3} \text{ mho/cm} \times \frac{1}{4}\pi (0.208)^2} = 9.04 \text{ k}\Omega \quad (2)$$

for the sample slide at 10°C:

$$R = \frac{0.3226 \text{ cm}}{0.762 \times 10^{-3} \text{ mho/cm} \times \frac{1}{4}\pi (0.610)^2} = 1.45 \text{ k}\Omega \quad (3)$$

for the electrode chamber at 23°C:

$$R = \frac{0.75 \text{ cm}}{1.05 \times 10^{-3} \text{ mho/cm} \times \frac{1}{4}\pi (0.650)^2} = 2.15 \text{ k}\Omega \quad (4)$$

and, by difference, for the membranes between both electrodes and the column:

$$R \text{ (2 mem)} = \frac{V \text{ meas}}{I} - 45.11 - 9.04 - 2.15 = 13.7 \text{ k}\Omega \quad (5)$$

From these calculations and the conductivity of the flight buffer at any temperature, general formulae were developed for the column resistances. With a dummy slide in place: $R_{TOT} = \frac{61.37}{K} + 13.74$ (6)

With a sample slide in place: $R_{TOT} = \frac{52.98}{K} + 13.74$ (7)

for conductivity, K, in mmho/cm.

The electric field strength in the column must always be calculated from the relationship

$$E = I/KA$$

using the conductivity K rather than the voltage across the column. If there is a bubble in the column, for example, or any other discontinuities in conductance, the total column resistance does not reflect the conductivity at the position of the cells, where the field must be known. Considering the assembly as resistors in series,

$R_T = 2R_E + R_S + R_C$ where R_E = electrode compartment resistance

R_C = column resistance

$R_C = 1/KA$

R_S = sample slide resistance

Under ideal conditions

$$R_C = R_T - 2R_E - R_S = (1 - 2R_E/R_S - R_T/R)R_T = CR_T$$

where C = constant, so a measurement of the total column resistance R_T and the length of the column l will give the average field strength throughout the column

$$\bar{E} = V_C/l = IR_C/l = ICR_T/l,$$

which is the same as E = I/KA.

But if a buble is introduced a new resistance is added to the circuit, and

$R_T = 2R_E + R_S + R_C + R_B$ where R_B = bubble resistance

then $R_C = CR_T - R_B$

and $V_C = ICR_T - IR_B$

where the value <u>measured in flight</u> is $V_T = IR_T$, which will be high, and not

proportional to V_C. The true field strength will be

$$E = ICR_T/l - IR_B/l_B$$

where l_B = length of the bubble. This is not the same as $\bar{E}$ given above. If a bubble is present, the measured voltage on the EEVT apparatus cannot be used to estimate field strength. Unless it can be ascertained with certainty that a particular column did not contain a bubble, its field must be calculated from $E = I/KA$ using the best value of K for that column, determined before flight and corrected for inflight temperature using the empirical formula, equation (7), and the conductivity-temperature curve of Fig. 7.

6. Pre-flight determinations of electrophoresis column conductivities

Individual measurements on the columns loaded for flight indicated that the conductivity of the buffer in each column was different. This was explained by differential degassing of the solutions in each column and differential water loss, resulting in different electrolyte concentrations in the different columns. The conductivities were measured at various temperatures, and the resistance of column #067 was measured at two temperatures to obtain D-1 conductivity-temperature curves. These curves were scaled, as shown in Fig. 7, for purposes of predicting column voltages in each case under the conditions of flight, when T = 12-14°C. The conductivities were calculated using Equation (6), and they are shown in Table 3 at the temperatures at which they were measured.

7. Pre-flight predictions of column voltages during flight

From the conductivity measurements and the temperature curve of Fig. 7, applied to equation (7), the expected column voltages at 12°C and 14°C during flight were calculated. These are summarized in Table 4, along with the electroosmotic mobilities of the corresponding columns for later use in predicting band migration.

8. Pre-flight predictions of cell migration profiles

The electrophoretic mobility distributions of Figs. 4 and 5 were used, along with the electroosmotic mobility values in Table 4 to estimate the distances specific parts of the cell bands in each column would migrate. The expected positions of the foward and rearward boundaries of the cell bands are included in Table 5, and diagrams of the band profiles expected at the end of 60 min are in Figure 8.

9. In-flight observations of column voltages

Figure 9 summarizes column voltages at every minutes during the operation of the 6 columns that contained HEK-8514 cells. The legend at the right end of the figure shows the plotting symbols and the predicted voltages for each of the numbered columns.

A steady voltage rise was seen in three of the columns, implying that heating by the current may have been expanding a bubble of significant diameter compared to the column. With two exceptions the voltages ended higher than predicted. Tables 6 and 7 summarize the in-flight voltages of columns 019 and 049, respectively. These columns contained fixed red cells and were photographed with thermal cover off every 10-12 min. These times are denoted by asterisks (*), and small voltage and temperature excursions can be seen, especially as plotted in Figures 10 and 11. Under these conditions one would expect variable cell migration rates.

10. In-flight observation of cell migration

When astronaut voice-downs of the cell migration distances were heard, it was determined that the fixed RBC's did not migrate as far as expected, they did not separate into two distinct bands, and the migration rate may not have been constant. The data are shown in Fig. 12, and drawings of the cell bands from the photographs that were taken during flight are shown in Fig. 13 and 14. These, too, reveal that the cells did not migrate as far as expected and that they did not form two distinct bands.

11. Analysis of column photographs

Negative photographs of the columns were scanned along a position just off the center of the projection of the long axis of the column using a film densitometer (Fig. 1. which produced a strip-chart record of uncalibrated light transmission vs. uncalibrated position. Densitometer readings were listed numerically, and absolute distances were established using Risso marks on the camera and the positions of landmarks such as column thermistors. These numerical readings are listed in Tables 8 and 9, as a function of time, for the two columns.

Pairs of these optical scans were analyzed using a program in BASIC/RT-11 which matched the scans along the axis of migration, normalized them, and subtracted one from the other. Usually, as in Figure 16, a scan of the baseline is determined

at 11 min, before cells appear, and displayed as a solid curve. The scan containing a cell band is displayed as a dotted curve. The baseline has considerable structure, owing to the reflectance of the column and the method of illumination. The difference appears as a broad peak of relative light absorption vs. column position.

Figures 17 and 18 show optical absorption profiles as a function of time for colums 019 and 049, respectively. As previously noted, migration was not as rapid as expected, the cell bands were not sharp, and there is a lack of clear structure in the absorption profiles that is evidence of human and rabbit cell separation.

12. Comparison of results and redictions

In Table 10 the predicted 52-minute migration distances of human (μ = 2.05 μm - cm/V-sec) and rabbit (μ = 1.45 μm - cm/V-sec) cells (Figures 1 and 2 in columns 019 and 049 are compared with the positions of the leading and trailing edges of the observed, optically-scanned cell bands (Fig. 17 and 18). The cells did not migrate as far as predicted.

13. Post-flight analysis of buffer effects

The conductivities of the columns were variable because the electrolyte concentrations were variable owing to the buffer degassing procedure during pre-flight loading of the columns. The ionic strength was therefore different in each column. The cell mobilities measured in D-1 buffer would therefore not apply under the conditions of the flight experiments. Laboratory values of human and rabbit (and rat, which is similar to human) fixed erythrocytes' mobilities are plotted against ionic strength in Fig. 19, using pre-existing laboratory data. The ionic strengths and conductivities of the media used are shown in Table 11. To enter Fig. 16 to obtain mobilities it was necessary to determine the ionic strengths of the buffers in columns 019 and 049. From their conductivities at 25°C, namely 1.306 and 1.142 mmho/cm, respectively, determined from Fig. 5, and the plot of $\Gamma/2$ vs. K for D-1 in Fig. 17, the ionic strengths of the two columns were estimated to be 0.0237 and 0.0190, respectively. From Fig. 16 corrected mobilities are found as given in Table 12. The validity of these mobilities in the orbital experiments is based on the relative insensitivity of mobility to temperature changes.

Table 1. Human RBC mobilities

corrected to the viscosity of water at 25°C

BUFFER	MOBILITY	DATE	CONDITIONS
D-1, no DMSO	2.31 ± 0.18	10/7/81	
D-1, no DMSO	2.35 ± 0.15	8/1/81	Pen-Kem 3000
D-1, no DMSO	2.76 ± 0.16	3/10/82	Seaman cells from MSFC
D-1	2.67 ± 0.11	3/10/82	Seaman cells from MSFC
A-1	2.54 ± 0.15	3/10/82	Seaman cells from MSFC
D-1	2.59 ± 0.15	3/12/82	Complete parabola (usual)
0.145 NaCl, 10^{-4} $NaHCO_3$	1.10 ± 0.08	3/14/82	Seaman formald. 7/20/81
0.145 NaCl, 10^{-4} $NaHCO_3$	1.02 ± 0.08	3/14/82	PSU glut. 10/23/80
0.145 NaCl, 10^{-4} $NaHCO_3$	1.13 ± 0.07	3/14/82	pH 6.9
0.145 NaCl, 10^{-4} $NaHCO_3$	1.28 ± 0.07	3/14/82	pH 9.1
D-1	2.65 ± 0.15	3/15/82	Pool of 274 cells, 4 runs

Table 2. Rabbit RBC mobilities

corrected to the viscosity of water at 25°C

BUFFER	MOBILITIES	DATE	CONDITIONS
D-1	1.62 ± 0.12	6/19/81	
D-1	1.89 ± 0.13	6/30/81	
0.145 NaCl, 10^{-4} $NaHCO_3$	0.51 ± 0.07	7/8/80	

Table 3

Conductivities of buffer in each column, based on column resistance measurement at 23°C (3/18/82) and assuming membrane resistance = 13.7 kΩ.

COL	R_{TOT}	$K = \frac{61.37}{R_{TOT}-13.7}$	T°C K
017	76.05	0.984	22
019	64.02	1.22	22
026	66.23	1.168	23
032	62.89	1.248	23
037	76.63	0.975	23
046	72.62	1.041	23
048	75.93	0.986	23
049	73.37	1.028	23
067	78.86	0.941	22
068	71.79	1.056	23
073	71.48	1.062	22
080	75.53	0.992	23
081	71.53	1.061	23
082	78.13	8.952	23

Table 4

Summary of predicted column voltages and electrosmotic mobilities (μm-cm/V-sec).

SERIAL	COLUMN	V (12°C)	V (14°C)	EEO
1	019	236.8*	.229.7*	0.023
2	081	280.6	270.3	0.020
3	048	302.4	288.1	0.030
4	080	304.4	291.9	0.023
5	068	293.4	280.9	0.059
6	026	254.9*	245.9*	0.064
7	046	302.4	288.1	0.075
8	049	280.1	268.6	0.087

Table 5. SUMMARY OF EXPECTED COLUMN VOLTAGES

RUN	COLUMN	V (12°C)	V (14°C)	MIGRATION DISTANCES FRONT	TAIL	(cm)
1	019	236.8*	229.7*	8.7	6.8	
2	081	280.6	270.3	11.6	6.7	
3	048	302.4	288.1	12.5	7.3	
4	080	304.4	291.9	12.7	7.4	
5	068	293.4	280.9	12.1	7.0	
6	026	254.9*	245.9*	10.3	6.0	
7	046	302.4	288.1	12.9	6.9	
8	049	280.1	268.6	10.7	6.6	

* Lower than specified range

Table 6. Column temperatures and voltages at one-minute intervals for column 019 and sample slide 03, 10^9 human and rabbit fixed erythrocytes/ml. *Indicates column uncovered for photography.

TIME (MIN)	TEMP. (°C)	VOLTAGE (V)	TIME (MIN)	TEMP. (°C)	VOLTAGE (V)
0	11	003	41	20	264
1	12	273	42	16	269
2	13	264	43	15	273
3	13	267	44	14	277
4	13	264	45	14	274
5	14	267	46	14	278
6	14	263	47	14	278
7	14	262	48	14	277
8	14	262	49	14	277
9	14	265	50	14	281
10	14	263	51	16	274*
11	16	260*	52	19	264*
12	18	257*	53	16	273
13	15	256	54	15	272
14	14	262	55	14	277
15	14	265	56	14	278
16	14	265	57	14	278
17	14	265	58	14	280
18	14	269	59	13	005
19	14	267	60	12	005
20	14	265	61	15	005*
21	17	262*	62	12	003
22	19	256*	63	8	005
23	16	258	64	5	005
24	15	265	65	1	005
25	14	264	66	-2	005
26	14	267	67	-6	005
27	14	269	68	-8	005
28	14	266	69	-11	005
29	14	269	70	-13	005
30	14	266	71	-06	003
31	14	273	72	-7	003
32	14	269	73	-8	002
33	18	266*	74	-9	005
34	19	265*	75	-11	002
35	18	263	76	-13	005
36	17	265	77	-16	005
37	17	263	78	-18	005
38	17	273	79	-20	005
39	17	273	80	-22	005
40	17	271			

Table 7. Column temperatures and voltages at one-minute intervals for column 049 and sample slide 04, 2 x 10^8 human and rabbit fixed erythrocytes/ml. *Indicates column uncovered for photography.

TIME (MIN)	TEMP. (C°)	VOLTAGE (V)	TIME (MIN)	TEMP. (C°)	VOLTAGE (V)
1	11	297	32	12	282
2	12	290	33	14	280*
3	12	288	34	18	274*
4	12	286	35	12	277
5	12	286	36	12	276
6	12	285	37	12	278
7	12	283	38	12	278
8	12	283	39	12	282
9	12	283	40	12	280
10	12	285	41	12	283
11	17	279*	42	12	281*
12	19	276*	43	19	272*
13	13	277	44	13	274
14	13	278	45	12	278
15	12	283	46	12	278
16	12	285	47	12	280
17	12	282	48	12	285
18	12	278	49	12	278
19	12	280	50	12	285
20	12	278	51	11	282
21	12	283	52	17	278*
22	18	277	53	19	277*
23	20	273	54	12	275
24	12	273	55	12	280
25	12	277	56	12	283
26	11	277	57	12	280
27	12	280	58	28	283
28	12	280	59	16	284
29	12	280	60	42	005
30	11	280	61	34	007
31	12	280	62	29	007
			63	35	004

Table 8. Arbitrary numerical light transmission vs. position on Column 019.

DISTANCE (mm)	TRANSMISSION AT 11 MIN	22 MIN	41 MIN	51 MIN
20	195	75	75	180
21	200	75	152	109
22	295	78	191	290
23	370	80	243	321
24	400	78	191	290
25	380	135	263	353
26	372	135	268	353
27	355	352	268	345
28	365	390	245	345
29	370	388	210	345
30	378	400	160	314
31	360	381	128	290
32	390	400	104	272
33	400	397	89	257
34	410	402	81	250
35	383	385	80	242
36	410	400	80	236
37	125	170	78	78
38	410	419	80	190
39	417	420	80	178
40	432	440	79	172
41	460	450	78	170
42	460	453	80	170
43	460	461	78	159
44	490	490	85	130
45	555	550	100	120
46	560	570	145	95
47	620	600	175	85
48	610	600	260	81
49	610	610	374	80
50	630	623	352	79
51	630	630	520	78
52	645	650	642	76
53	671	670	648	76
54	670	670	662	76
55	625	627	680	80
56	645	660	637	91
57	720	742	688	99
58	730	740	750	99
59	735	755	730	100
60	762	761	758	100
61	735	661	760	95
62	750	750	750	89
63	750	771	760	88
64	727	740	760	9[illegible]
65	758	760	742	118
66	750	767	767	92
67	745	760	758	165
68	740		770	310
69	740		780	550
70				615
71				550

C-5

Table 9. Arbitrary numerical light transmission vs. position on Column 049.

DISTANCE (mm)	TRANSMISSION AT	11 MIN	22 MIN	33 MIN	42 MIN	52 MIN
20		95	82	215	135	160
21		95	82	163	132	162
22		105	95	170	132	165
23		272	188	192	286	320
24		338	232	347	350	391
25		325	222	350	367	412
26		325	145	347	373	88
27		330	166	350	365	400
28		335	192	350	364	401
29		340	244	335	372	415
30		382	339	350	377	430
31		390	409	350	365	435
32		350	355	360	389	436
33		370	364	375	370	442
34		353	352	367	360	432
35		371	372	365	360	441
36		372	381	360	345	435
37		370	368	344	351	420
38		110	110	200	140	180
39		390	387	228	370	415
40		392	387	260	371	400
41		410	403	330	380	410
42		410	411	412	377	405
43		418	422	490	392	402
44		429	430	495	390	430
45		450	443	495	391	463
46		492	486	560	422	500
47		509	512	552	368	505
48		540	525	590	273	520
49		542	548	592	230	537
50		551	535	605	300	540
51		560	550	605	400	528
52		585	560	636	505	528
53		609	570	646	590	545
54		617	580	646	611	540
55		635	611	660	660	550
56		645	619	686	690	540
57		650	625	687	690	505
58		680	625	708	690	430
59		655	625	690	685	330
60		685	672	713	714	295
61		699	686	760	745	365
62		686	670	745	720	474
63		682	670	751	726	564
64		682	670	767	726	638
65		693	670	760	718	640
66		682	678	742	721	696
67		674	660	749	678	715
68		680	668	764	715	750
69		700	690	788	740	760

Table 10

Comparison of predicted 52-minute linear cell migration distances with positions of leading and trailing edges of bands:

COLUMN	FIELD (14°C)	CELL μ	X (obs)	X (calc)
019	10.95	2.05	65	70.0
019	10.95	1.45	35	49.5
049	13.28	2.05	59	85.0
049	13.28	1.45	43	60.1

Table 11

Conductivity, K (mmho/cm), and ionic strength, Γ/2 (M), for buffers used to determine cell mobilities, concentrated D-1 buffer, and flight column buffers.

MEDIUM	Γ/2	K(25°C)
D-1	0.015	0.95
C-1	0.030	1.5
C-2	0.015	0.5
0.145	0.145	12.5
B-3	0.007	
B-3'	0.060	4.2
B-3"	0.120	9.2
2XD-1	0.030	1.52
1.5XD-1	0.0225	1.29
1.25XD-1	0.0165	1.03
1.0XD-1	0.015	0.97
019	0.0237	1.306
049	0.0190	1.142

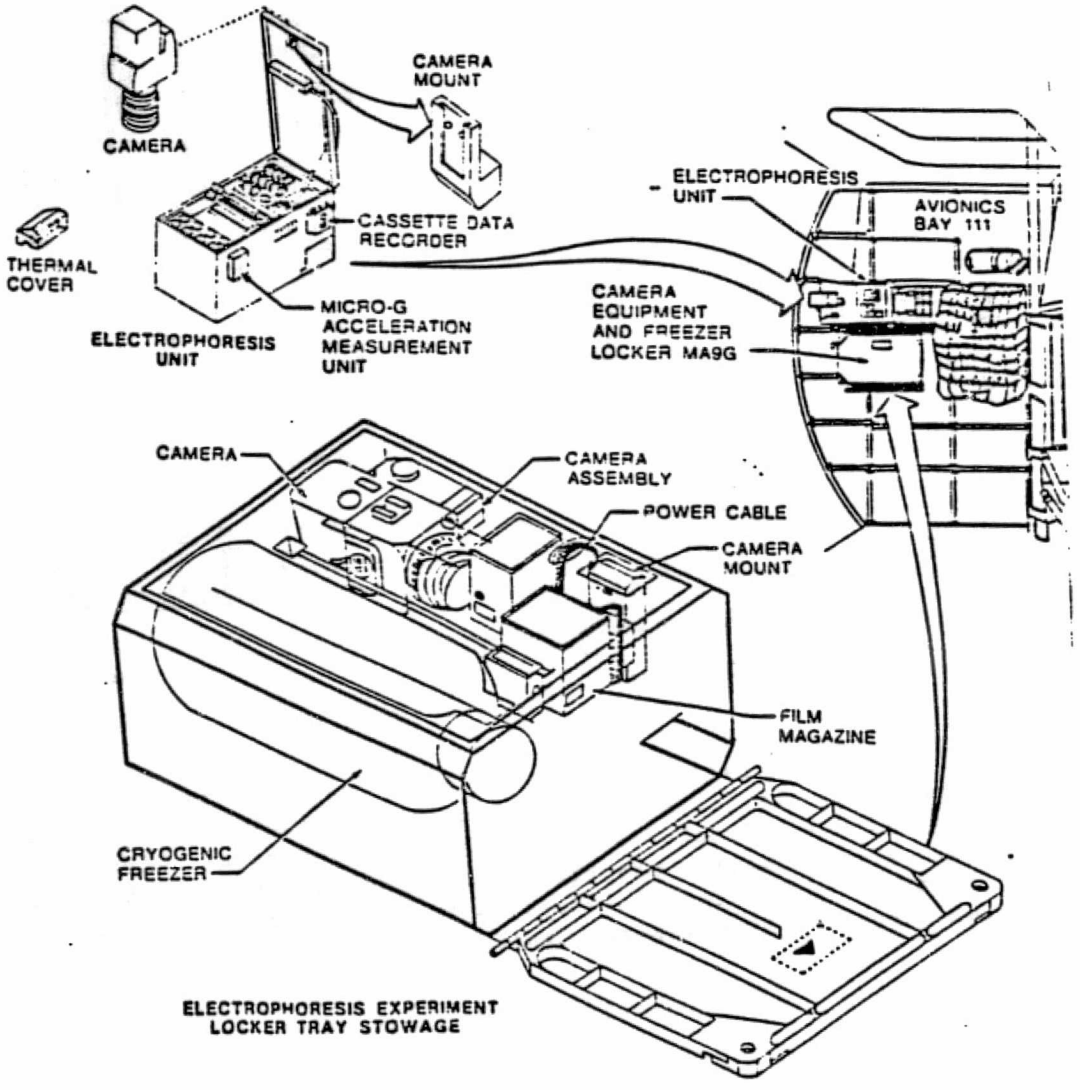

Fig. 1. Electrophoresis equipment used on STS-3. Reprinted by permission of Dr. D. Morrison.

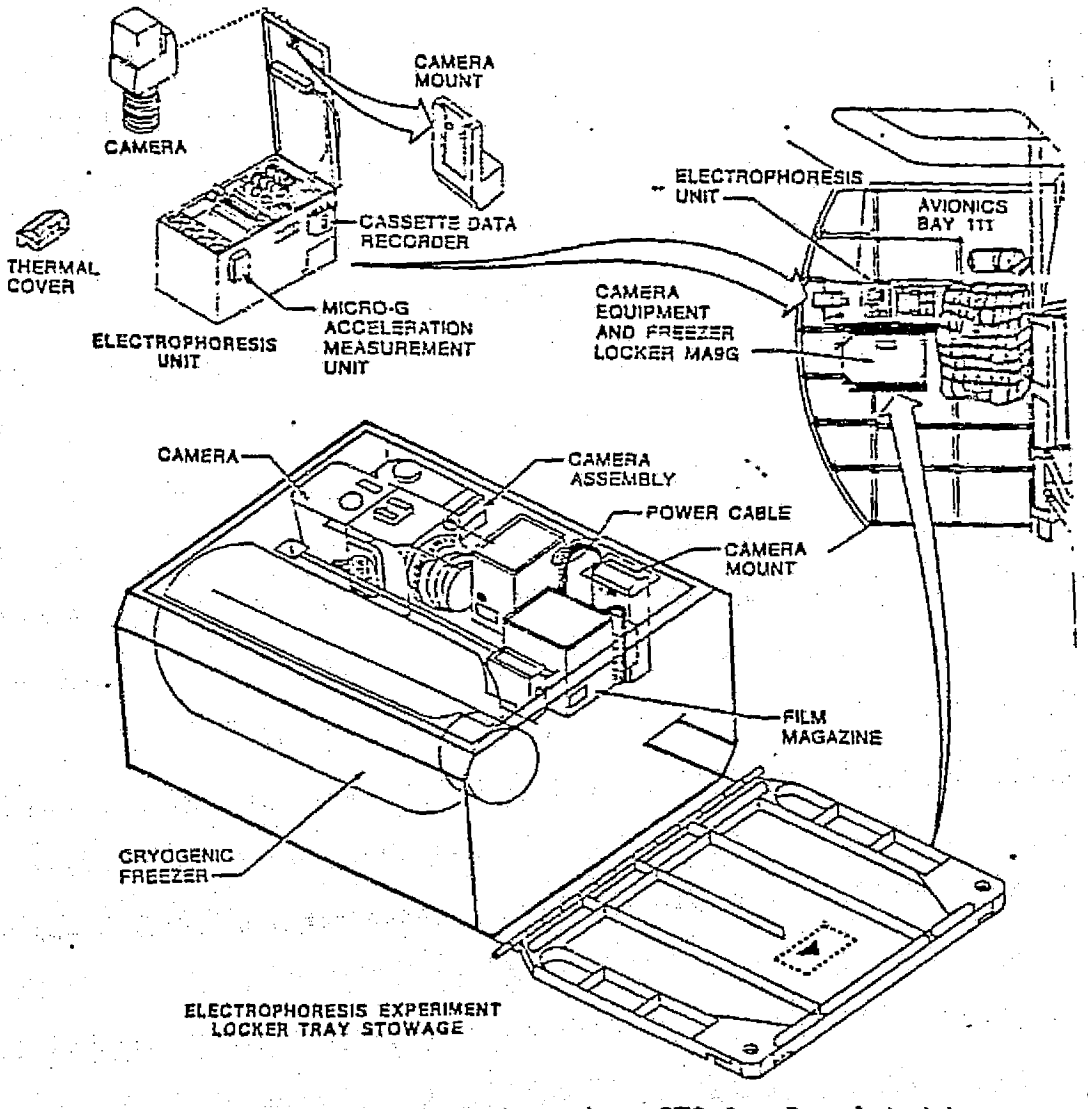

Fig. 1. Electrophoresis equipment used on STS-3. Reprinted by permission of Dr. D. Morrison.

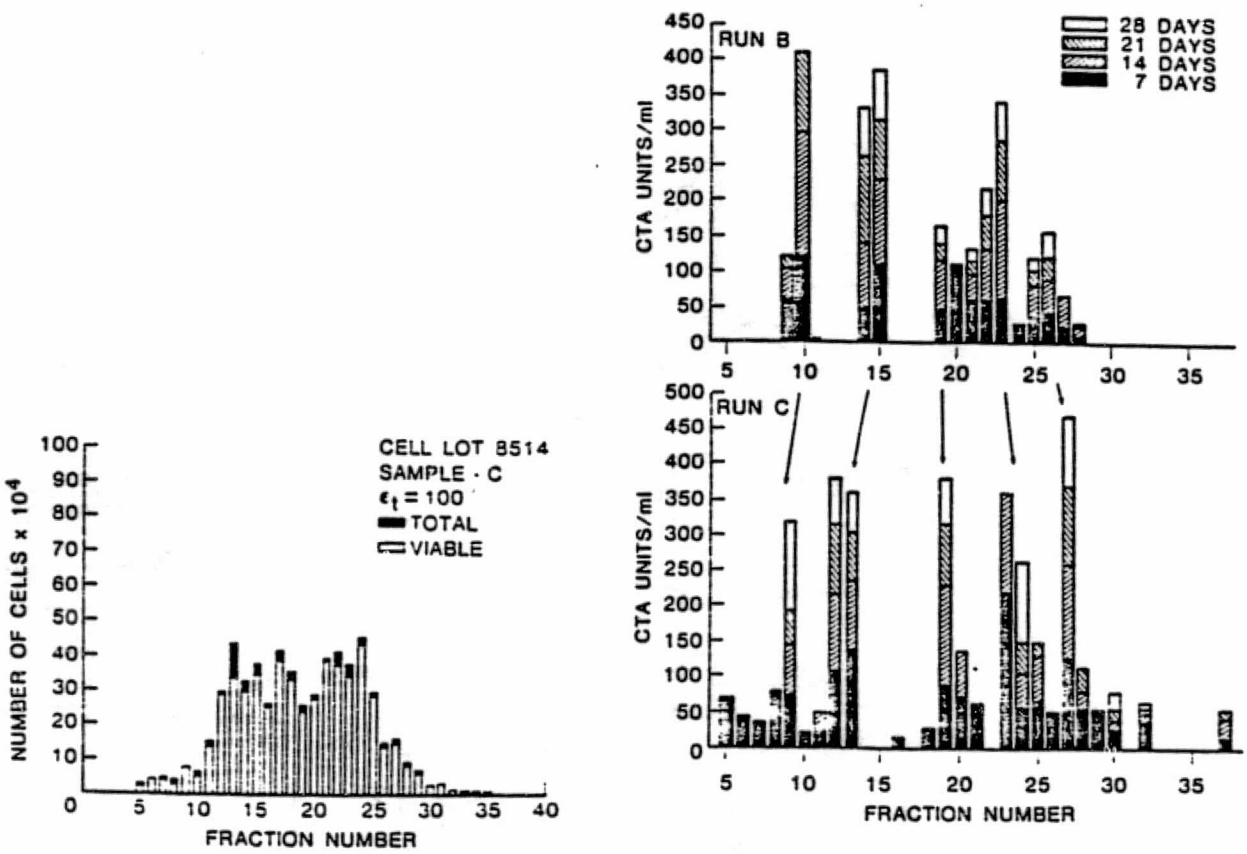

Figure 3 Electrophoretic profile of living cultured human embryonic kidney cells, HEK-8514, and of urokinase-producing fractions separated by continuous-flow electrophoresis. The McDonnell Douglas "CFES" continuous-flow electrophoretic separator was used. Left: Number of cells per fraction. Right: Cumulative urokinase production by separated cells as a function of fraction number. (Morrison and Lewis, 1983)

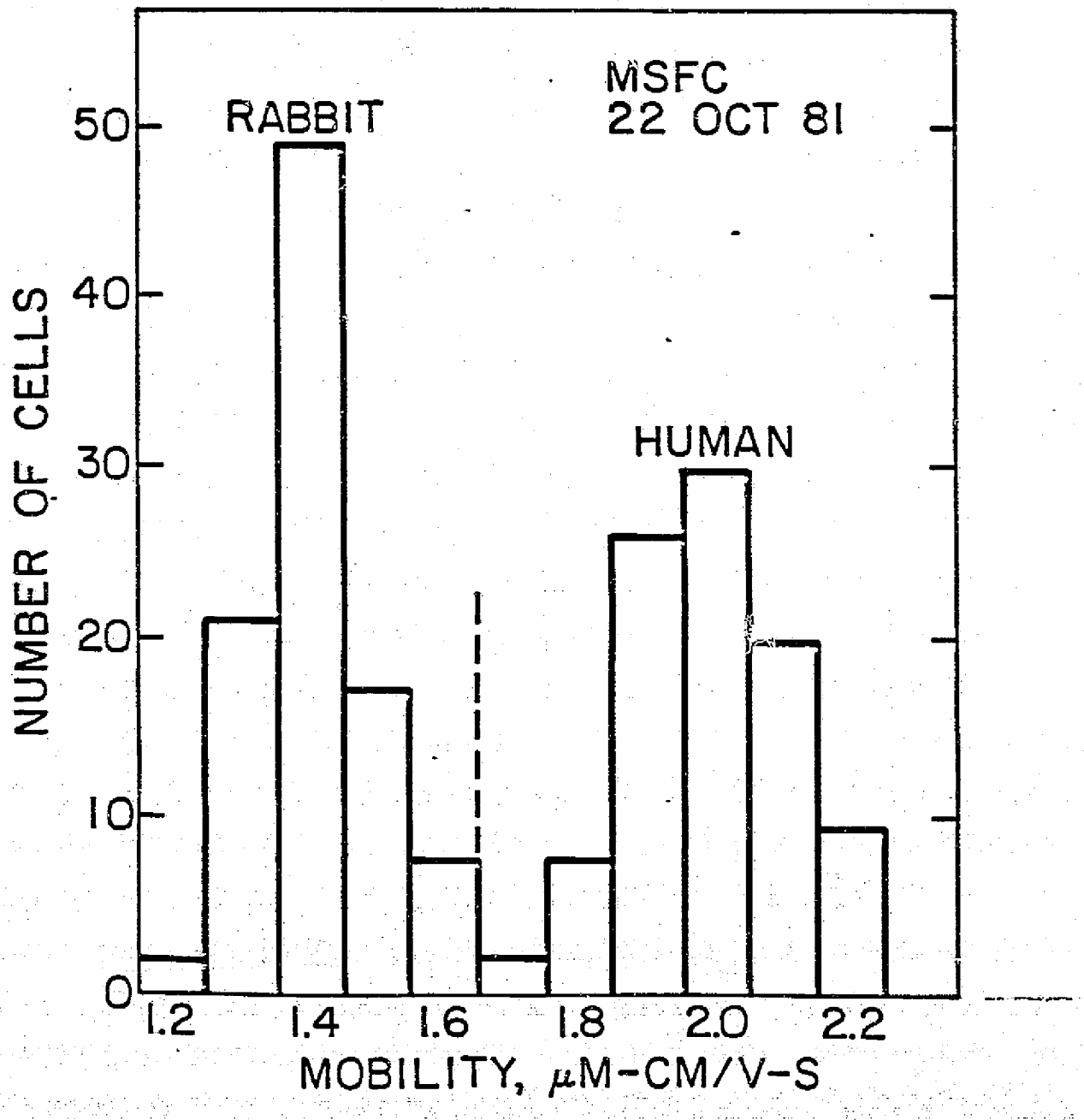

Figure 4. Electrophoretic mobility distributions of formaldehyde-fixed rabbit and human erythrocytes in D-1 buffer as determined using Marshall Space Flight Center's Rank microscopic electrophoresis apparatus by measuring velocities at the stationary position in a cylindrical chamber at 25 C.

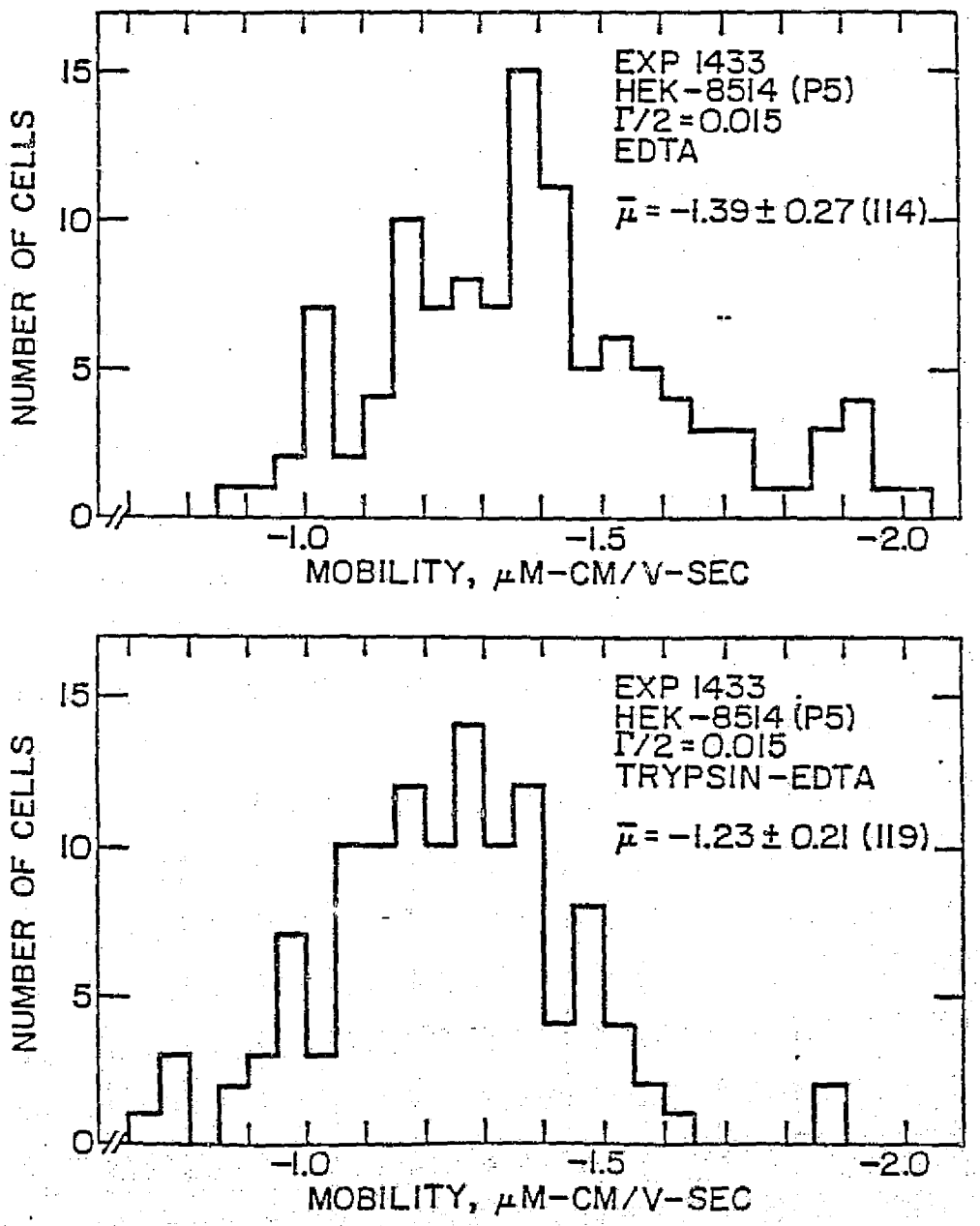

Figure 5. Electrophoretic mobility distributions of living human embryonic kidney cells, HEK-8514 at passage 5, in D-1 buffer after preparation of suspensions with EDTA (top) or with EDTA plus trypsin (bottom). Distributions were determined from mobility parabolas in the rectangular chamber of a Zeiss "Cytopherometer".

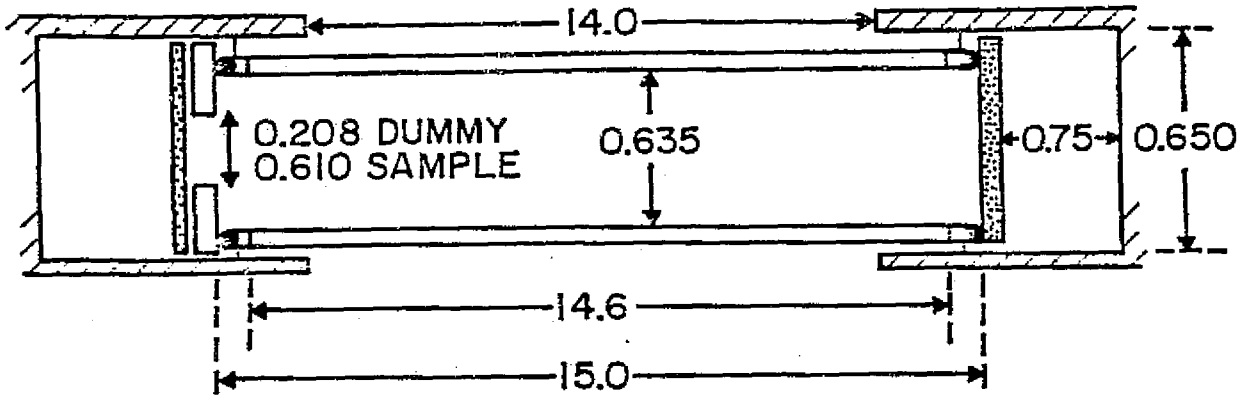

Figure 6. Sketch (not to scale) indicating dimensions of electrophoresis columns and their parts as used in calculating resistances.

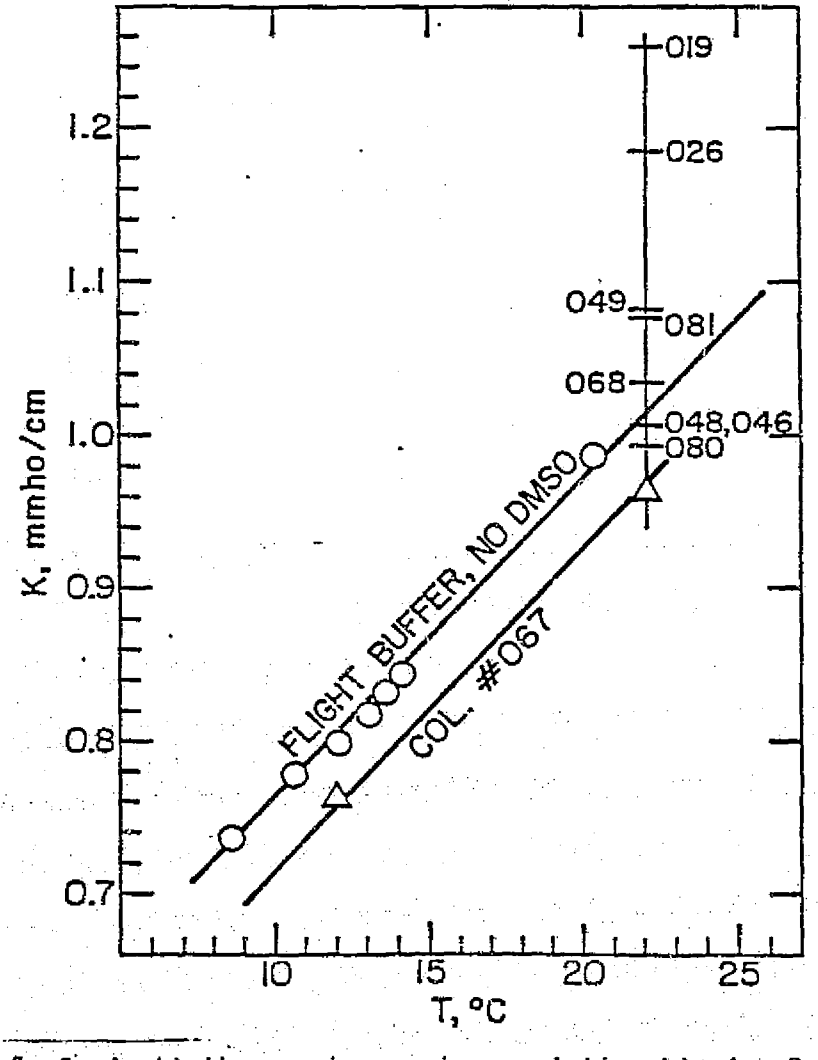

Figure 7. Conductivity vs. temperature relationship for D-1 buffer without DMSO but as prepared for flight (circles), conductivity as measured in a back-up column just prior to flight (triangles), and conductivities at 22 C of buffers in the 8 columns used for flight.

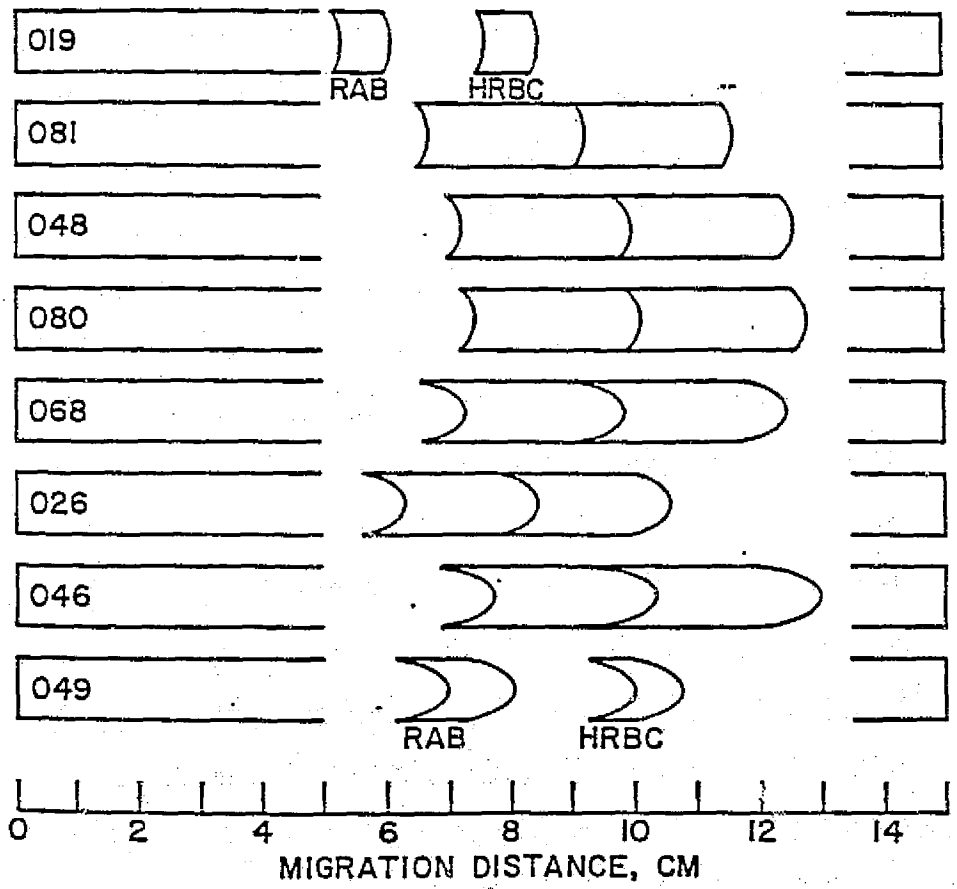

Figure 8. Predicted cell distributions at the end of EEVT experiments in the planned order of column runs aboard STS-3. HRBC = fixed human red blood cells; RAB = fixed rabbit red blood cells. Columns 2-7 contained human embryonic kidney cells.

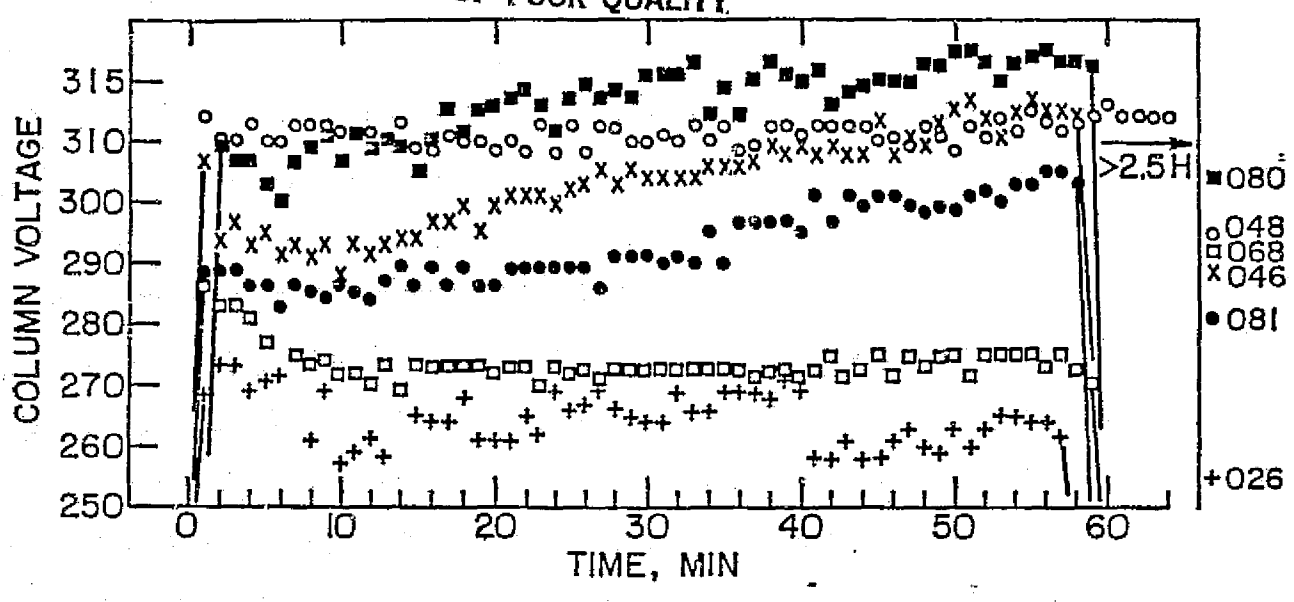

Figure 9. Voltage readings at each minute during the operation of the six kidney-cell electrophoresis columns aboard STS-3. Predicted values (from Table 4) are shown with the corresponding plotting symbol for each column at the right end of the graph. Column 048 continued to operate for over 2.5 hr.

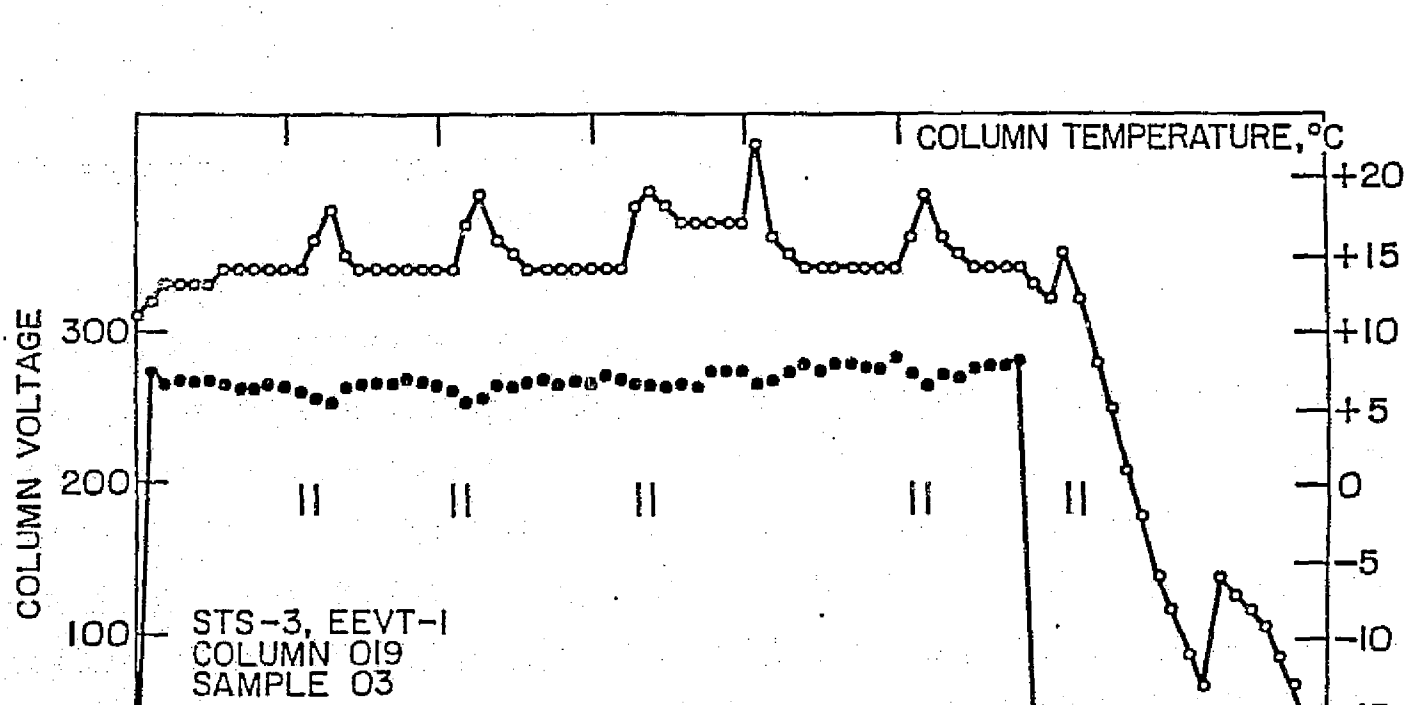

Figure 10. Voltage and temperature readings at each minute during operation of NBC electrophoresis column 019 (1.0E09 cells/ml) aboard STS-3. The right end of the temperature curve shows cooling and freezing profile that was characteristic of all of the columns. Intervals of reduced cooling capacity during photography are indicated by paired vertical bars.

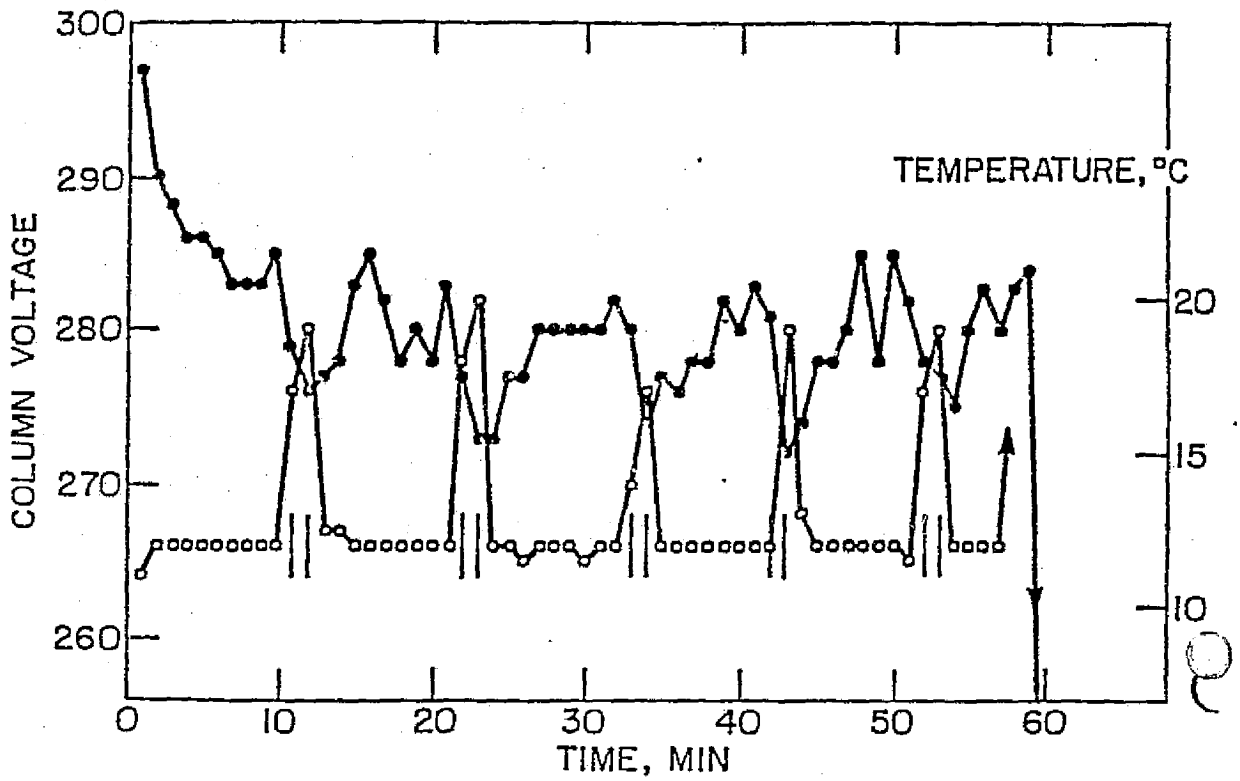

Figure 11. Voltage and temperature readings at each minute during operation of REC electrophoresis column 049 (2.0E08 cells/ml) aboard STS-3. Expanded scales emphasize voltage and temperature excursions during photography, indicated by paired vertical bars.

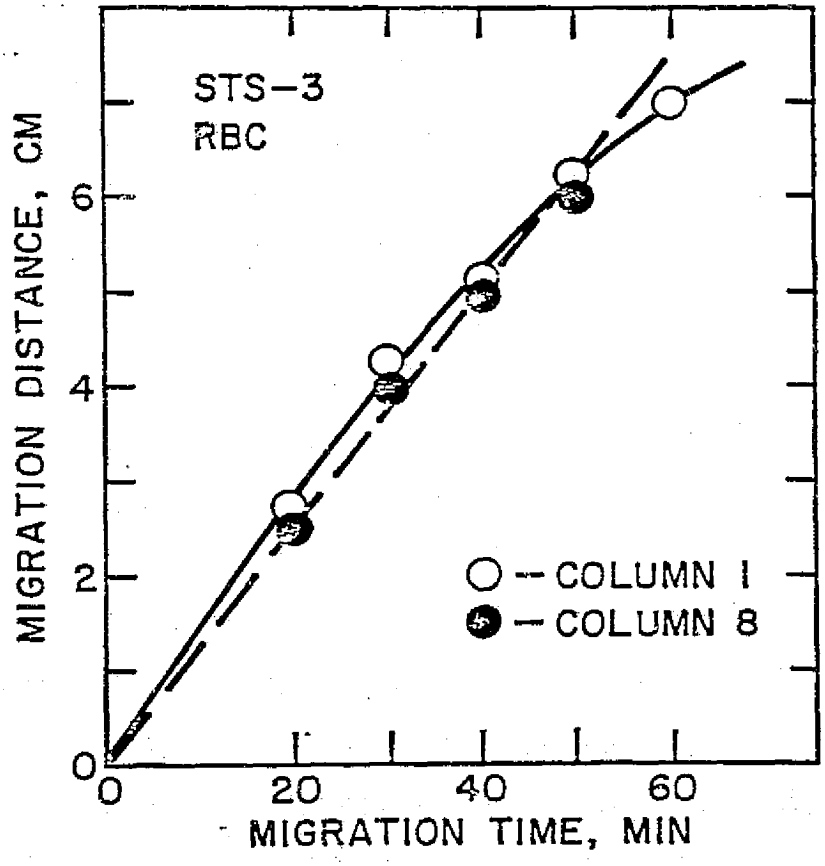

Figure 12. Migration distances of cells in columns 019 (1.0E09 cells/ml, circles) and 049 (2.0E08 cells/ml, dots) as stated by astronauts during STS-3 flight. The distances correspond to positions of the leading edge of the fastest cell population.

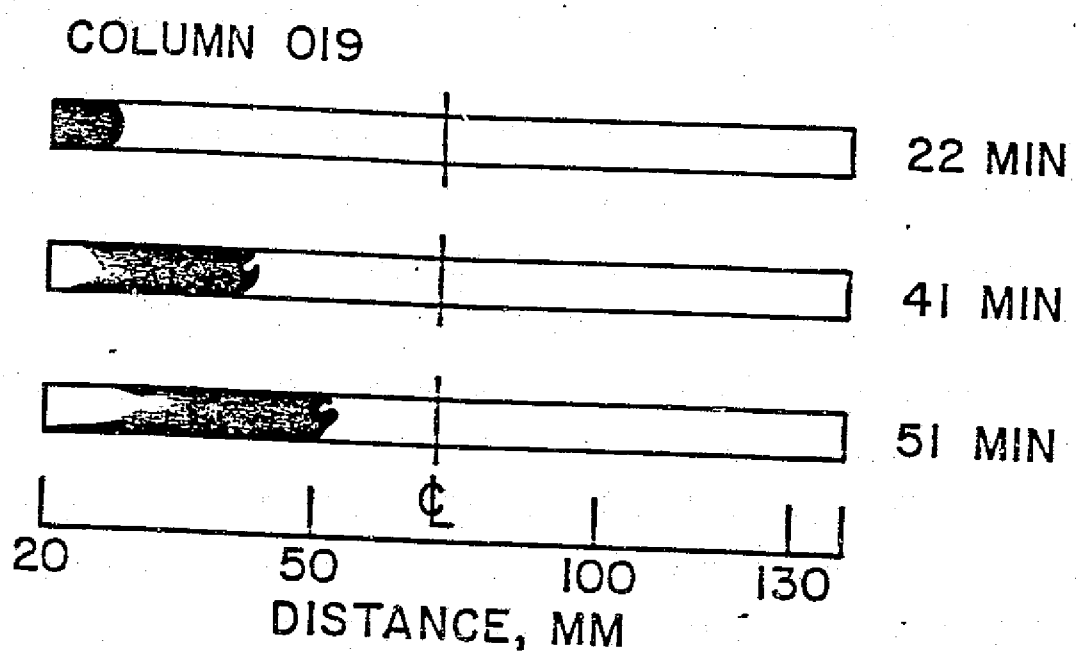

Figure 13. Tracings of photographs of column 019 taken during operation on STS-3 (1.0E09 cells/ml).

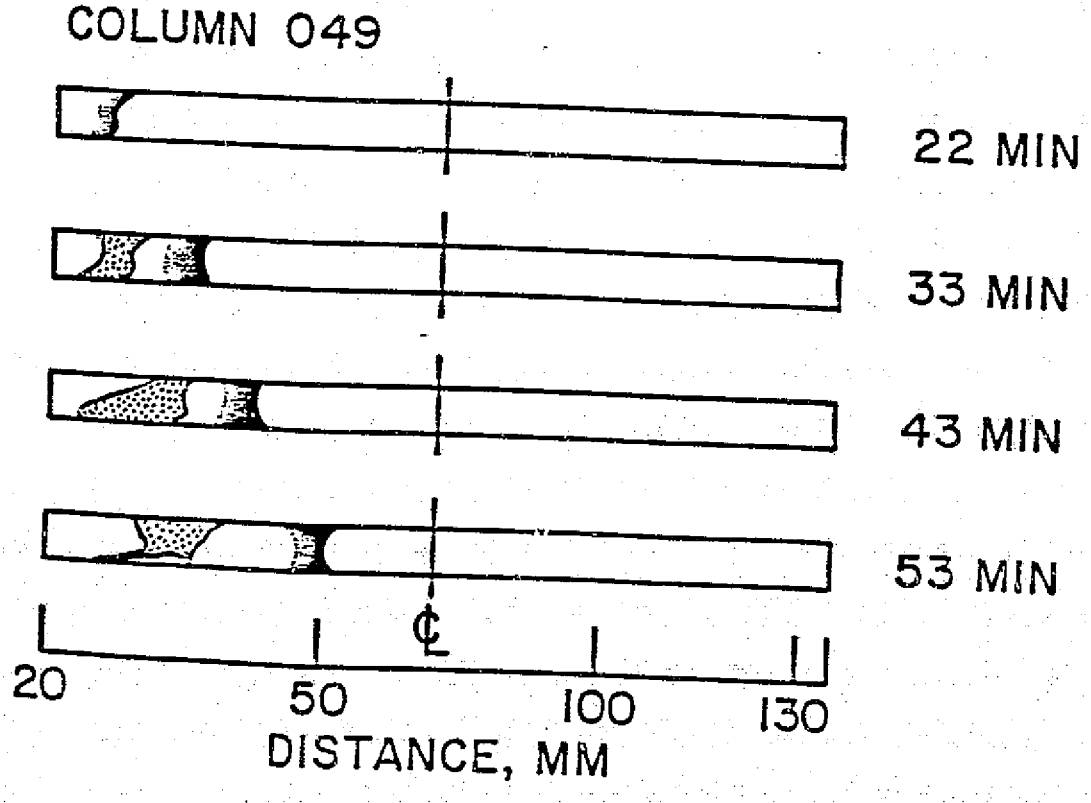

Figure 14. Tracings of photographs of column 049 taken during operation on STS-3 (2.0E-08 cells/ml).

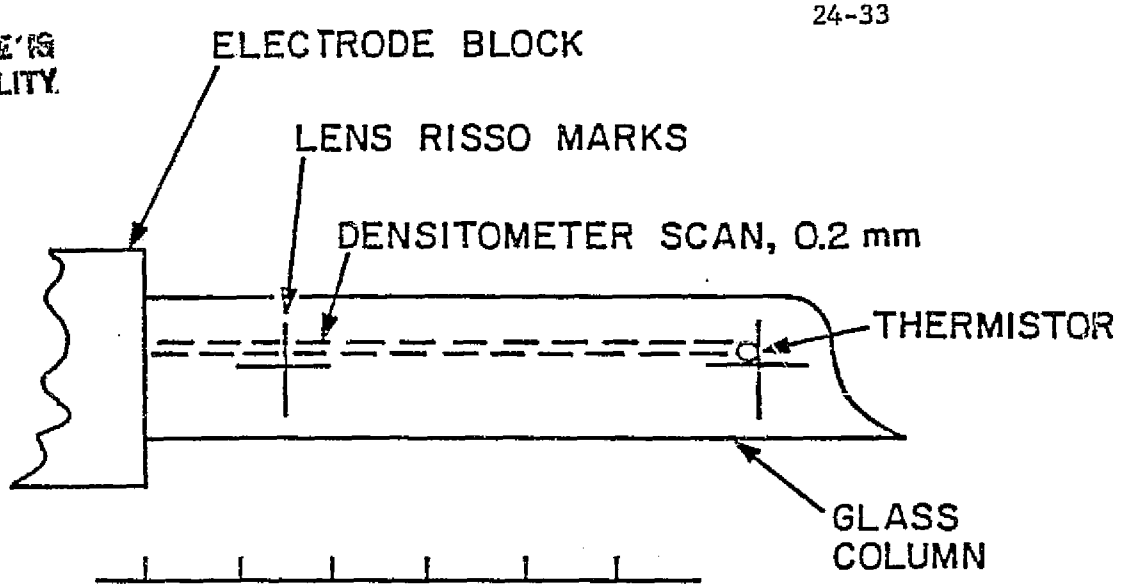

Figure 15. Sketch, not to scale, indicating procedure for densitometer scanning and determining positions of scan on photographic negatives of electrophoresis columns. Scans were off center to avoid Risso marks of camera lens. Electrode blocks and Risso mark (at 38.0 mm) were used as landmarks.

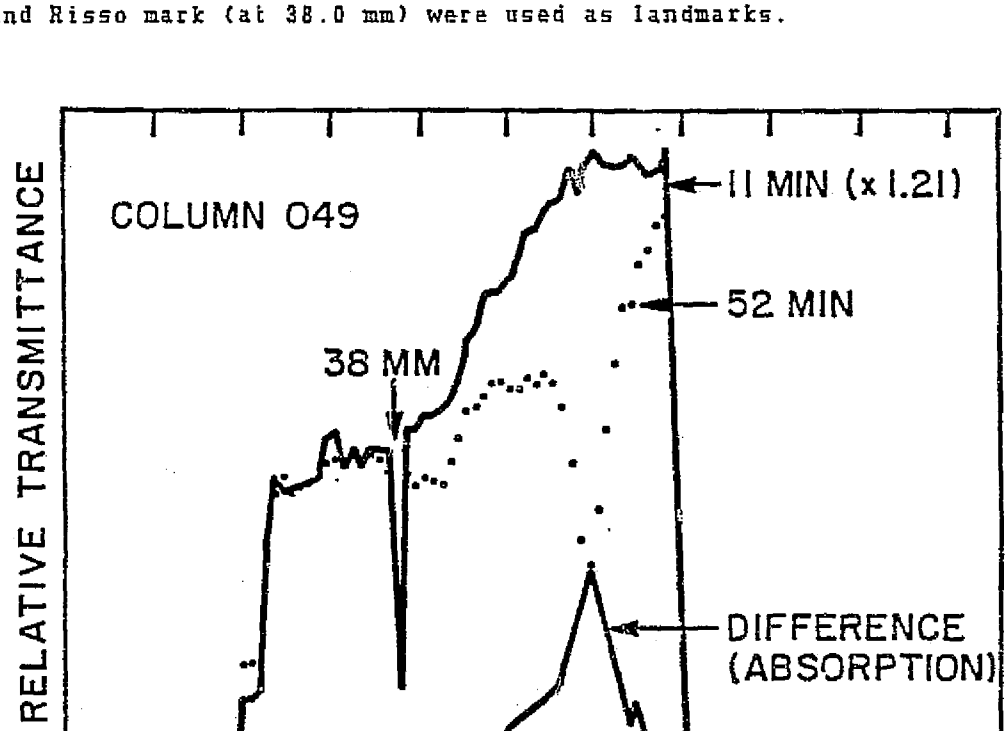

Figure 16. Relative transmittance as a function of column position on densitometer scans of inflight photographic negatives. The procedure for extracting relative absorption data is illustrated. In this case, a scan at 11 min (no cells present) is used as baseline and normalized by computer to equal the relative transmittance of the 52 min scan at both ends, where cells are also absent. The two distributions are shifted horizontally, if necessary, so that the discontinuities due to Risso marks coincide. The two scans are subtracted to give relative absorption as a function of distance.

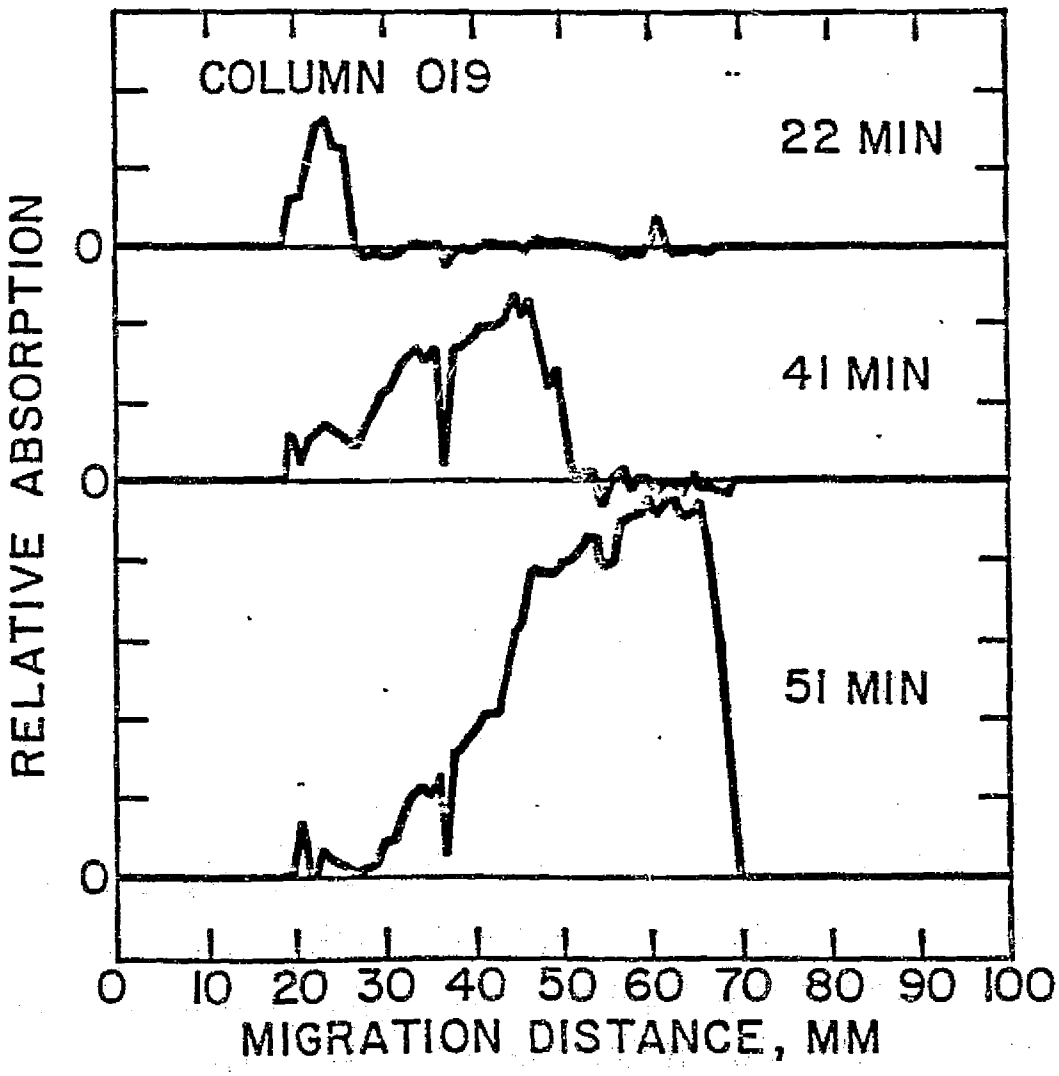

Figure 17. Relative absorption as a function of column position as determined from densitometer scans of negatives of photographs of column 019 (1.0E09 cells per ml) after 22, 41, and 51 min of operation during STS-3 flight.

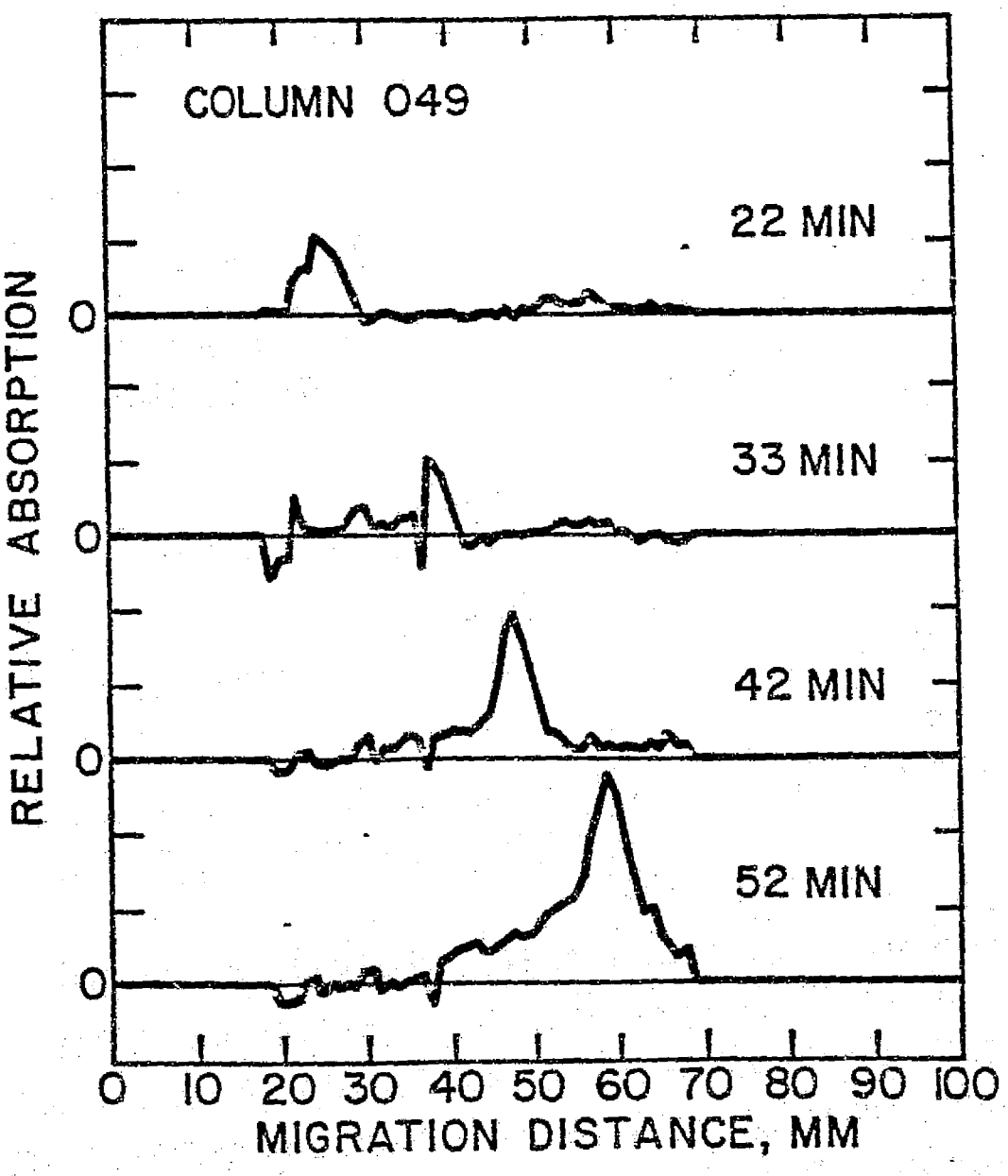

Figure 18. Relative absorption as a function of column position as determined from densitometer scans of negatives of photographs of column 049 (2.0E08 cells per ml) after 22,33,42,and 52 min of operation during STS-3 flight.

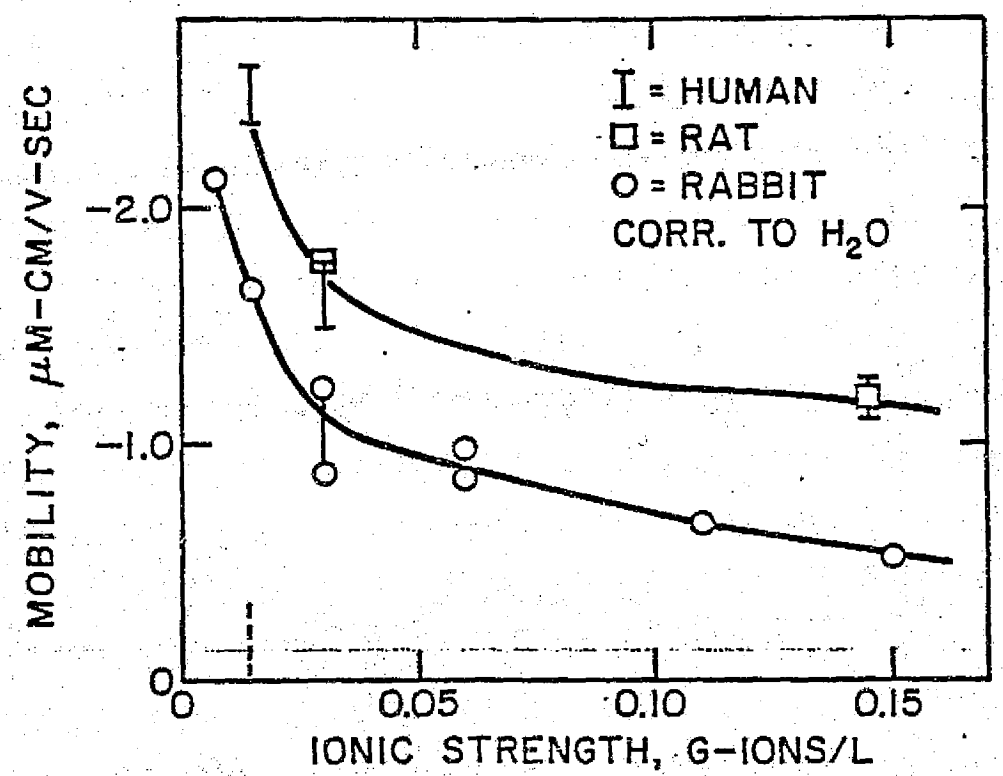

Figure 19. Electrophoretic mobility of fixed human, rat, and rabbit erythrocytes as a function of ionic strength in various buffers (Table 11) using pre-existing laboratory data.

Chapter 25

Analysis of results of STS-3 experiments: comparison with laboratory measurements of electrophoretic mobility.

AMERICAN ASTRONAUTICAL SOCIETY

Reprinted from *Space Manufacturing 1983, Volume 53, Advances in the Astronautical Sciences*, edited by James D. Burke and April S. Whitt, 1983. Published for the American Astronautical Society by Univelt, Inc., P.O. Box 28130, San Diego, California 92128.

AAS 83-212

ELECTROPHORETIC PURIFICATION OF CELLS IN SPACE: EVALUATION OF RESULTS FROM STS-3

Burton E. Sarnoff, M. Elaine Kunze, and Paul Todd*

Processes under consideration for zero-g manufacturing in space include electrophoretic purification of cells and molecules for pharmaceutical application. The absence of convection and sedimentation at zero-g permits up to 400-fold improvements in purification efficiency, because higher field strength and particle concentrations are possible. An electrophoresis experiments ("EEVT") performed on Space Shuttle Flight STS-3 had as its goal the investigation of the electrophoretic behavior of animal cells in suspension more concentrated than possible on earth. The results of this collaborative experiment with Marshall Space Flight Center and Johnson Space Center investigators were evaluated by simulating the conditions of temperature, ionic strength, and buffer composition (but not cell concentration) in laboratory electrophoresis experiments. The resulting laboratory values of electrophoretic mobilities were compared with those determined by computerized analysis of in-flight photographs taken during two separate experiments at 11-minute intervals by the STS-3 astronauts. The comparison of laboratory results with STS-3 results indicates that zero-g electrophoresis of very high cell concentration (1×10^9 cells/cm^3) is possible and not unexpectedly different from the electrophoresis of normal cell concentrations at unit gravity.

INTRODUCTION

When placed in an electric field, particles with a net electrical surface charge experience a force proportional to their surface charge density. If biological samples are placed in a liquid conducting medium, they migrate under the influence of this force. Since different types of biological cells may have different surface charge densities a mixture of such cells can be separated by observing their migration distance in a timed experiment. This principle, cell electrophoresis, is under consideration for commercial applications.

* *403 Althouse Laboratory, The Pennsylvania State University, University Park, Pennsylvania 16802*

An electric field in a conducting medium gives rise to an electric current which in turn produces Joule heating. On Earth such heating gives rise to convective mixing which limits the resolution of cell type separation. Droplet sedimentation, another problem encountered in earth-bound experiments, occurs when solute molecule diffusion causes localized density instability of cell-containing fluid zones (higher density fluid above lower density fluid which leads to the rapid settling of cell-containing droplets). This limits the cell concentration that can be used. In a microgravity environment, these two problems are avoided.

Electrophoretic mobility, μ, is defined as the velocity of cells in medium per unit electric field; the units are customarily μm/sec per volt/cm. Mobilities in different media and temperatures can be compared by making appropriate viscosity corrections.

Earlier space experiments, such as those on Apollo 14, Apollo 16, Skylab 4, and the Apollo-Soyuz Test Project [1-4], indicated that separation by electrophoresis was possible in the microgravity environment. Various equipment problems resulted in the design of another detailed experiment to establish future space bio-processing procedure. The Electrophoresis Equipment Verification Test (EEVT) was flown on Shuttle flight STS-3 in March, 1982.

PROCEDURES

The Electrophoresis Experiments aboard STS-3

Eight cell samples were aboard STS-3 for the EEVT. Six were Human Embryonic Kidney (HEK) cell cultures. Two were mixtures of human and rabbit aldehyde-fixed red blood cells (RBC). The medium was D-1 buffer, a solution of water, salts and glucose with five percent DMSO added as a cryopreservative.[5]

Figure 1 shows the Electrophoresis Unit and its stowage on the Shuttle. Fifteen cm glass tubes with inside diameter of 0.635 cm were filled with D-1 at Kennedy Space Center. The cells were frozen in 0.318 cm thick sample slides and stowed in the cryogenic freezer before launch. Astronauts placed each glass electrophoresis column with its associated electrode chambers in the electrophoresis unit. The frozen sample slide was inserted at the cathode (left) end. Figure 2 shows the arrangement with the slide thumb grip just below the leftmost Rizzo mark. During operation, a thermoelectric cooling cover was placed over the column to compensate for the Joule heating and therefore to maintain constant temperature. The cover was removed at ten minute intervals, and the progress of cells was photographed. Figure 2 shows a series of such photographs for the column labeled 049, which contained 2×10^8 erythrocytes/ml in its sample slide. The other RBC column, 019, contained 1×10^9 erythrocytes/ml. The RBC columns provided a control from which to assess the migration of the kidney cells. Kidney cell migration could not be observed directly because they are transparent. The applied electric field was 13-17 V/cm during each 60 min experiment. After electrophoresis, all columns were frozen to maintain position and structure of the cell bands. The frozen

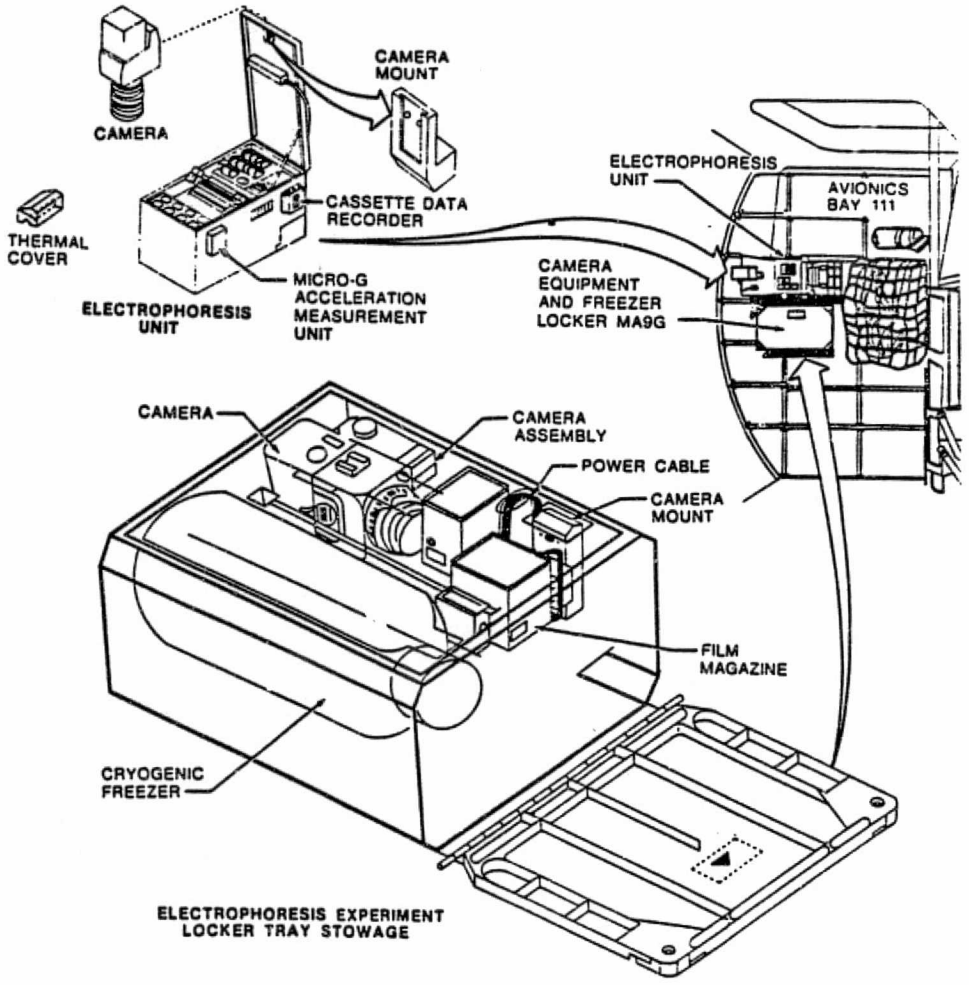

Fig. 1. Electrophoresis equipment used on STS-3. Reprinted by permission of Dr. D. Morrison.

columns were to be sliced, and cultures were to be grown from separate bands of HEK cells, as purification of the cell type that produce high levels of the kidney enzyme urokinase, which activates the dissolution of blood clots,[6] was the goal. The freezer that was used to transport the columns to Houston lost its liquid nitrogen coolant charge. The columns thawed and materials for post-flight processing were lost.[5] Thus photographic, voice-down, temperature, voltage, and preflight observations were the only data that remained for analysis.

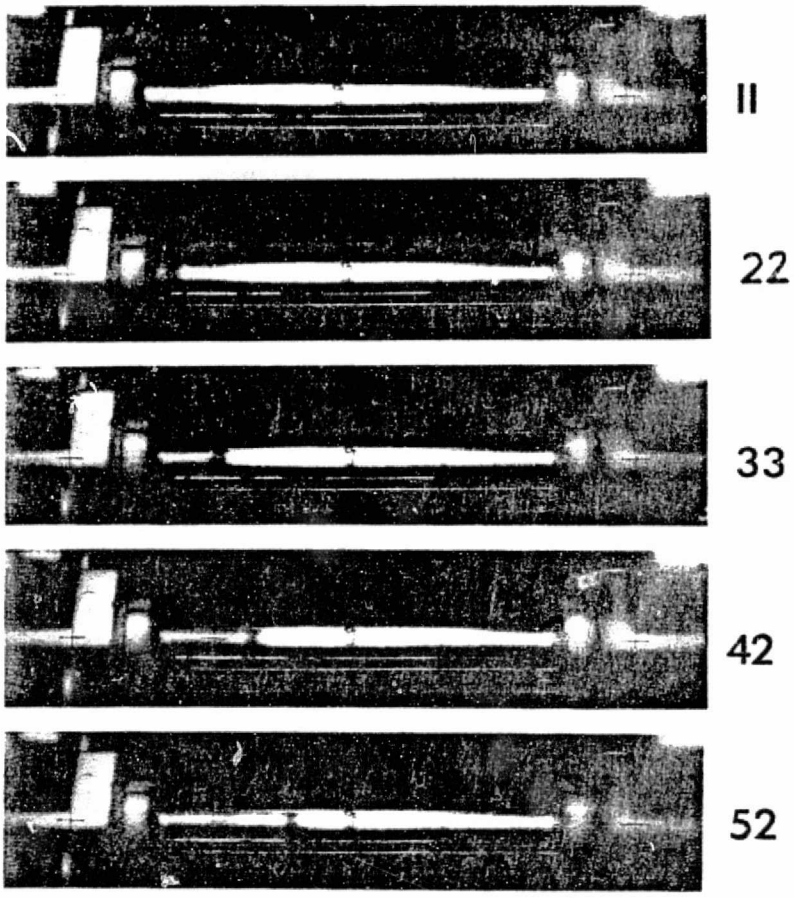

Fig. 2 Series of Column 049 photographs. Elapsed time from beginning of run in minutes is on right side. A thermistor is located in the column glass at 7.5 cm.

Microdensitometer scans of the column photographic negatives were taken 0.2 mm wide just beside the centerline of the columns. The density profile of the first photograph of each series (in which cell bands were absent), provided the baseline for computerized analysis of cell band densities in the column. Figure 3 shows the optical absorption analysis for Column 049 at different times. The light-absorption peak rises as it progresses because of the nonlinearity of the film and the presence of glare on the column surface. Given a column current of 3.84 mA and voltage about 290 V, the cell bands were expected to migrate about 30 mm farther than observed. Voltage readings were lower than the specified range, indicating column conductance higher than predicted.

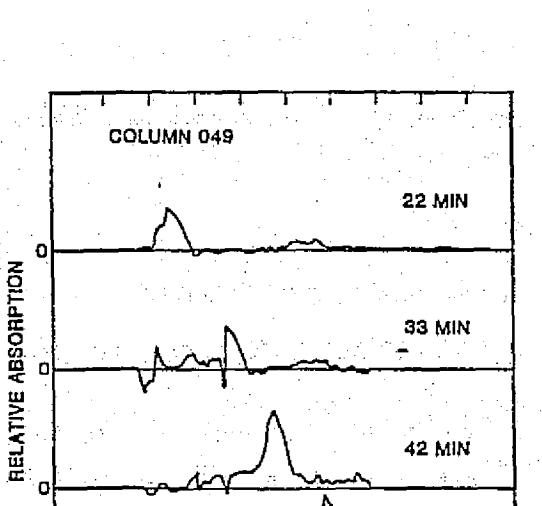

Fig. 3. Computer analysis of microdensitometry data from photographic negatives of Column 049, showing cell band positions. The small spike at 37 mm corresponds to the Rizzo mark at 37 mm in Figure 2.

Retrospective determination of the applied electric field

Prior to filling the columns the D-1 buffer was degassed in a vacuum. Unfortunately, this procedure also removed water, and concentrated the salts, thereby raising the conductivity of the buffer. Each column was under vacuum for a different length of time, so each had a unique conductance. The concentration of solutes in Columns 019 and 049 is estimated to have been between 1.0 and 1.25 times the standard D-1 concentration of all solutes.

Analysis of in-orbit voltage and temperature data provided values of the originally unknown conductivities of the buffer in Columns 019 and 049. Voltage drops across various circuit elements give, by subtraction, the actual voltage across the columns. Knowing the current through the column yields the resistance by Ohm's law and hence the conductance and conductivity. Resistance values were determined for the following circuit elements: the column, two electrode chambers, two membranes that interface the columns and electrodes, and the sample slide.

Resistance of 2 membranes was determined by preflight observations. A column with buffer of known conductivity has resistance at 23°C:

R_c = 15.0 cm/(1.05 mmho/cm)(π/4)(0.635 cm)^2 = 45.11 Kohm

At 23°C the substitute sample slide (with small diameter, for ground operations) has resistance:

R_d = 0.318 cm/(1.05 mmho/cm)(π/4)(0.206 cm)^2 = 9.073 Kohm

The total electrode to column path length has resistance at 23°C:

R_e = 0.75 cm/(1.05 mmho/cm)(π/4)(0.635 cm)^2 = 2.26 Kohm

By difference, the membranes have resistance:

R_{2m} = (Vmeas/I) - R_c - R_d - R_e = 13.56 Kohm

From these calculations and the conductivity K of flight buffer at any temperature, general formulae were developed for the column resistance.

R_{TOT} = C/K + B/K_o + 13.56 · Kohm

where: C = 49.06 cm^{-1} from geometries of columns and sample slide
K = unknown conductivity of column buffer
B = 2.368 cm^{-1} from geometry of electrode chamber
K_o = 1.03 mmhos/cm. conductivity of electrode buffer

K is determined by setting R_{TOT} = V/I and solving:

K = 49.06/(V/I - 15.86)

For column 019, at T = 14°C, V was determined by least squares analysis of V vs. T (for the early part of run 019, before the effects of a bubble become apparent) and was 265.6 V, so K = 0.9203 mmho/cm.
For Column 049, at 12° (V also determined by least squares analysis of V vs T), K = 0.855 mmho/cm. From these values for K, the electric field was determined from the column cross-sectional area A:. E = I/KA. For Column 019, E = 3.84 mA/(0.920 mmho/cm)$\frac{\pi}{4}$ (0.635 cm)^2 = 13.2 V/cm. In Column 049, E = 14.5 V/cm.

Laboratory Measurement of Electrophoretic Mobilities

The electrophoretic mobility of cells in suspension was determined using the Zeiss cytopherometer fitted with a rectangular chamber[7] and equipped with reversible Ag/AgCl/KCl electrodes (Cam-Apparatus, Impington, Cambridge, U.K.) as described by Mehrishi.[8] The velocities of 70 cells were measured in both directions as a function of depth in the chamber. The expected electroosmotic flow parabola was fitted to the velocity data by a computer program that incorporated corrections for magnification and asymmetric flow prior to defining the stationary levels in the chamber.[9] This program computed the average mobility and its standard deviation.

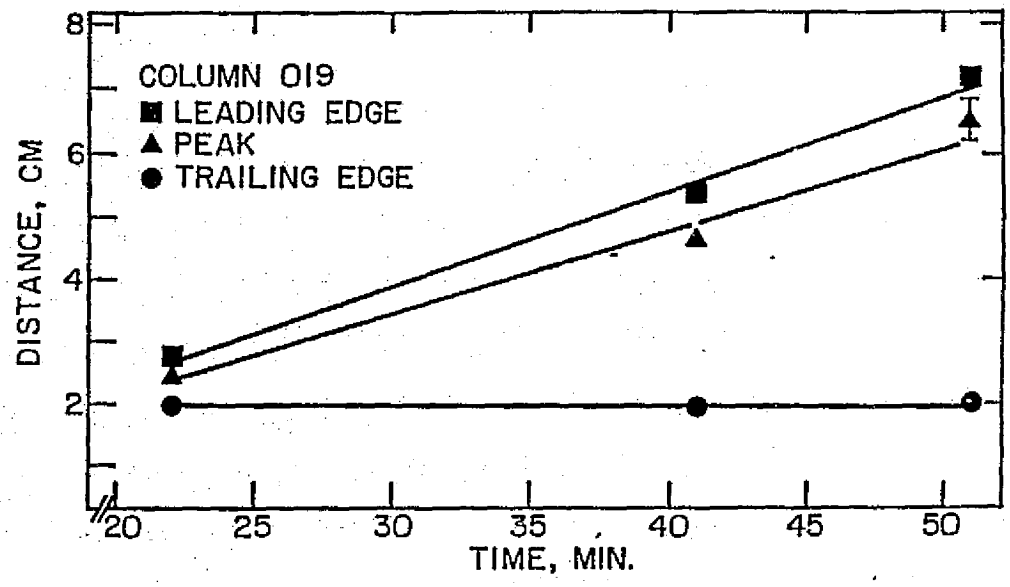

Fig. 4. Cell migration distance versus time for Column 019. The photograph at 31 min was underexposed and not usable for analysis. The absorption peak had spread considerably by 51 minutes.

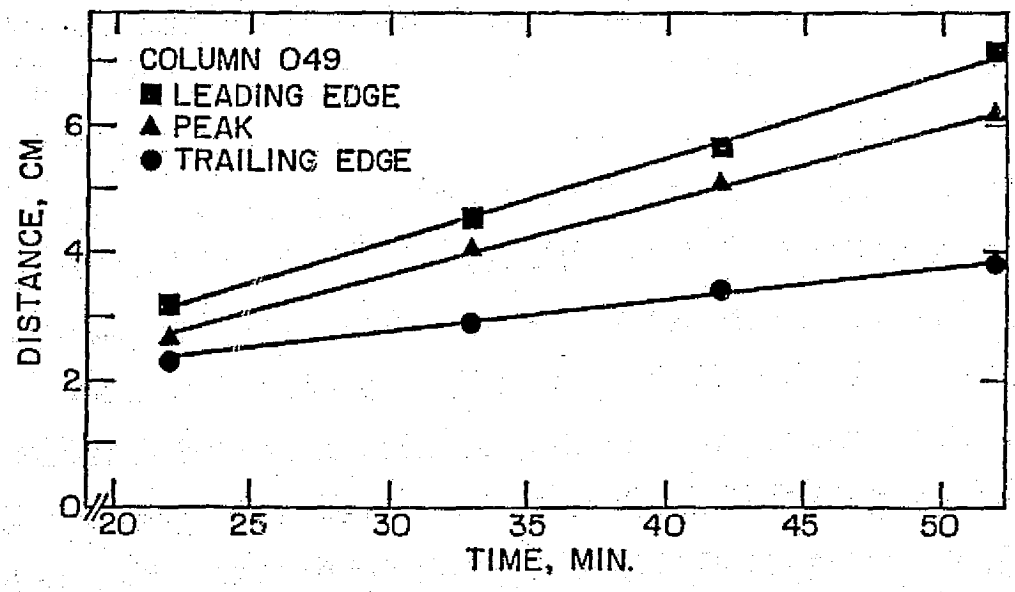

Fig. 5. Cell migration distance versus time for Column 049.

RESULTS

Electrophoretic Mobilities of Cells in the Flight Experiments

Figures 4 and 5 show the distance migrated vs time for the two RBC experiments. The slope of each line gives the slowest, most frequent and fastest cells in each band. Although only three points are available in Figure 4, it appears that the particle velocity was not quite constant in Column 019, apparently due to the formation of a bubble in the column. From these slopes and the electric field calculations, electrophoretic mobilities were calculated. The distribution of velocities represents a mixture of human and rabbit RBC mobilities. Table 1 shows these results.

Electrophoretic Mobilities of Cells in Simulation Experiments

Electrophoretic mobilities of fixed human RBC's were measured at 12, 14, 20, and 25°C in D-1 buffer and in D-1 buffer deliberately made at 1.25 times its normal concentration. Thus the laboratory simulation experiments covered the ranges of temperature, viscosity, conductivity, and ionic strength that occurred in the flight experiments. The relevant measurements of electrophoretic mobility are included in Table 1 for comparison with the mobilities measured in space.

Table 1

ELECTROPHORETIC MOBILITIES OF FIXED HUMAN AND RABBIT RED BLOOD CELLS IN SPACE AND OF FIXED HUMAN RED BLOOD CELLS IN D-1 BUFFERS IN SIMULATION EXPERIMENTS.

COLUMN	TEMPERATURE °C	POSITION	ELECTROPHORETIC MOBILITIES μm/sec per V/cm IN SPACE	IN D-1	IN 1.25xD-1
019	14	FAST	-1.59	-1.66± 0.13	-1.41±0.17
		PEAK	-1.42		
		SLOW	----		
049	12	FAST	-1.52	-1.42±0.18	-1.28±0.10
		PEAK	-1.32		
		SLOW	-0.83	0.94±0.12*	

*Rabbit RBC mobility measured in D-1 buffer at 25°C and corrected to 12°C using the ratio of mobilities of human RBC at 12°C and 25°C.

CONCLUSION

Although red blood cell migration and separation as observed through photographic records of the EEVT experiments aboard Shuttle STS-3 were not as expected, the cell mobilities and migrating band profiles are consistent with the results of laboratory simulation experiments. It thus appears that zero-g electrophoresis of very high cell concentrations (1×10^9 red blood cells/ml) is possible and not unexpectedly different from the electrophoresis of normal cell concentrations at unit gravity in the ground-based laboratory.

ACKNOWLEDGMENT

We acknowledge the enthusiastic particpation of all who made the flight of EEVT possible, especially astronauts Gordon Fullerton and Jack Lousma. The flight package was prepared for launch by Dr. Dennis Morrison, group leader, and P. Rhodes, Dr. M. Lewis, Dr. G. H. Barlow, and Mr. A. K. Love. We thank Dr. L. D. Plank and Mr. C. Goolsby for laboratory electrophoresis and computer assistance and Drs. R. S. Snyder and G. V. F. Seaman for technical guidance and leadership. This work was supported by National Aeronautics and Space Administration Contract NAS 9-15584.

REFERENCES

1. E. C. McFannan, A. C. Krupnick, R. N. Griffin and L. R. McCreight. "Electrophoresis separation in space-Apollo 14." National Aeronautics and Space Administration Report NASA TMX-64611 (1971).

2. R. S. Snyder. "Electrophoresis demonstration on Apollo 16." National Aeronautics and Space Administration Report NASA TMX-64724 (1972).

3. M. Bier, J. O. N. Hinckely and A. J. K. Smolka. "Potential use of isotachophoresis in space." Protides of the Biol. Fluids Vol. 22, H. Peeters, Ed., Pergamon Press Ltd., Oxford, 1975, pp. 673-678.

4. R. E. Allen, G. H. Barlow, M. Bier, P. E. Bigazzi, R. J. Knox, F. J. M. Micale, G. V. F. Seaman, J. W. Vanderhoff, C. J. Van Oss, W. J. Patterson, F. E. Scott, P. M. Rhodes, B. H. Nerren and R. J. Harwell. "Electrophoresis technology." In Apollo-Soyuz Test Project Summary Progress Report vol. 1, National Aeronautics and Space Administration Report NASA SP-412 (1977), pp. 307-334.

5. D. R. Morrison and M. L. Lewis. "Electrophoresis test on STS-3 and ground control experiments: a basis for future biological sample selections." In Proc. 33rd International Astronautical Federation Congress, in press, 1983.

6. M. B. Bernick and H. C. Kwaan. "Plasminogen activator activity in cultures from human tissues; an immunological and histochemical study." J. Clin. Invest. vol. 48, No. 7, 1969, pp. 1740-1753.

7. M. Kunitz. "A cell for the measurement of cataphoresis of ultramicroscopic particles." J. Gen. Physiol. vol. 4, 1923, pp. 413-418.

8. J. N. Mehrishi. "Molecular aspects of the mammalian cell surface." Progr. Biophys. Molec. Biol. vol. 25, 1972, pp. 1-20.

9. A. Gaines. A Physical Evaluation of Density Gradient Cell Electrophoresis: Thesis. The Pennsylvania State University, University Park, Pennsylvania, 1981.

Chapter 26

Simulation of Zero-G Blood Cell Electrophoresis using Free Zone Electrophoresis

N85-31773

FREE ZONE ELECTROPHORESIS SIMULATION OF STATIC COLUMN ELECTROPHORESIS IN MICROGRAVITY ON SHUTTLE FLIGHT STS-3

Paul Todd and Stellan Hjertén

Institute of Biochemistry, Biomedical Research Centre, University of Uppsala, Box 576, S-751 23 Uppsala, Sweden

Two experiments had been performed on U. S. Space Shuttle flight STS-3 to test the hypothesis that in microgravity cell-cell interactions do not compromise the separability or modify the electrophoretic mobility of animal cells at very high concentrations. Fixed human and rabbit erythrocytes were observed to migrate at constant velocity for 1 hr, but densitometer scans of photographs of columns in which cells were migrating did not demonstrate a distinct separation of the two cell types, although the leading edge of the cell band, presumably human erythrocytes, migrated at the predicted velocity (Snyder et al., Electrophoresis, submitted 1984; Sarnoff et al., Adv. Astronaout Sci. 53, 139, 1983). Free zone electrophoresis, in which the rotation of a 3 mm i.d. tube counteracts convective flow and sedimentation orthogonal to a horizontal electric field, was used as a method to simulate static column electrophoresis on Shuttle flight STS-3. The electrophoretic conditions were simulated as closely as possible: current density, buffer composition and conductivity, temperature, and cell concentrations. The positions of cell zones were determined every 5 min by scanning spectrophotometry, and, as in the microgravity experiments, migration rates were found to be constant and independent of cell concentration up to 2 billion cells/ml. Zone broadening due to increased cell concentration was found to be negligible relative to that due to electrophoretic heterogeneity. An unequal concentration of the two cell types and the introduction of a small amount of electroosmosis at the chamber wall resulted, after 1 hr of electrophoresis, in a band of mixed cells identical to that found in a microgravity experiment on STS-3.

This research was supported by a visiting investigator grant from Universities Space Research Association and by National Aeronautics and Space Administration Contract NAS9-15584.

REPORT ON RESEARCH PROJECT: SIMULATION OF ZERO-G RED BLOOD CELL ELECTROPHORESIS USING FREE-ZONE CELL ELECTROPHORESIS IN THE INSTITUTE OF BIOCHEMISTRY, BIOMEDICAL CENTER, UNIVERSITY OF UPPSALA

Paul Todd, 403 Althouse Labortory, University Park, Pennsylvania 16802
Host: Stellan Hjerten, University of Uppsala

INTRODUCTION

This project was designed to test principles that were also under test in the Shuttle flight STS-3 zero-G electrophoresis experiment ("EEVT") and to provide an explanation for some of the observations that were made. Specifically, two of the eight electrophoresis columns processed during the STS-3 mission contained mixtures of human and rabbit erythrocytes fixed with formaldehyde and suspended at different cell concentrations in order to determine whether or not cell concentration affects cell migration, especially when cell concentration higher than those that can be stably maintained in 1-G are used. Zero G was thus used as a test environment for determining cell concentration effects, and the experiments also probed the limits of usable cell concentrations for future zero-G cell separations, such as those using McDonnell-Douglas' continuous-flow zero-G electrophoretic separator (CFES). Only photographic results were available from the red blood cell (RBC) experiments about STS-3, and these showed a single visible band migrating at the predicted velocity of human cells in the low-concentration sample, and a very broad, tapering band the front of which migrated at the predicted velocity of human cells and the tail of which migrated near the predicted velocity of rabbit cells. It was expected that two clear bands of cells would be seen migrating independently at the velocities of the two cell types. The inability to retrieve the separated cells after the STS-3 flight made it impossible to analyse fractions of the column for the types of cells they contained. Thus is was not known whether rapidly migrating cells in the high-concentration (2 x 10'9 cells/ml) column were exclusively human cells or whether all positions in the column contained both cell types at the end of the run.

Experiments were therefore designed to replicate, as closely as possible in 1-G, the conditions of the STS-3 RBC experiments. Free zone electrophoresis was the method of choice, since it minimizes the role of gravity in cell migration. The physical conditions of the STS-3 experiments were used, and human and rabbit RBC's fixed by the same method were the test particles. The effects of cell concentration, electroosmotic mobility, and sample composition were tested in order to seek explanations for the STS-3 results and to provide data on cell concentration effects for future zero-G separations on the CFES.

MATERIALS AND METHODS

CELLS. Human erythrocytes were obtained from a 47-year-old healthy male donor by venipuncture and immediately diluted into isotonic phosphate buffer containing 0.01% EDTA as anticoagulant. After three rinses in this buffer the cells were suspended in 2.5% paraformaldehyde in isotonic phosphate buffer at ambient temperature (19-24 deg C) for 2 weeks. Rabbit erythrocytes were obtained from a 6-month-old healthy New Zealand white rabbit by ear venipuncture and treated subsequently in the same manner as the human RBC's.
These were the conditions specified for the fixed RBC's that were used on the STS-3 mission (Snyder et al.,1983). The cells were washed 3 times in

electrophoresis buffer "D-1" prior to experiments using the same buffer in the continuous flow electrophroesis apparatus.

BUFFERS. The blood-collection buffer and the cell-fixation buffer are described in Table 1, which lists the concentrations of the ingredients. The electrophoresis buffer, designated "D-1" is similarly described in Table 2.

ELECTROPHORESIS. The free-zone electrophoresis apparatus was invented an constructed by S. Hjerten, in whose thesis it is described in complete detail (Hjerten, 1964). It consists of a thermostated rotating horizontal tube coated with methylcellulose to prevent electroosmotic backflow. The experiments reported here were performed with the following parameters: temperature, 14 deg C; tube rotation speed, 70 rpm; tube diameter, 3.0 mm; conductivity of buffer, 0.90 mmho/cm; applied current, 0.80 mA; optical monitoring wavelength, 320 nm or 290/320 nm ratio; column scanning interval, 5 min; column scanning time, 1 min (with field turned off). Cells were introduced in one or two starting bands at the "origin" of the tube at concentrations of cells/cm^2 similar to those used on the STS-3 mission and corresponding to 1 x 10^8 to 4 x 10^9 cells/ml. Cells were either mixed or single type, depending on the experimental objective. Cells were exposed to the electric field for approximately two hours, after which, in most cases, the field was reversed for cell migration back to the origin. Optical scans were recorded, usually at 5 min intervals, on paper with an analog strip-chart recorder.

DATA ANALYSIS. Strip-chart records were analysed on the basis of optical scanning peaks, whose positions and widths were measured manually. Peak positions were corrected for scale factors and apparatus error, and peak widths were converted to standard deviations and coefficients of variation. These geometric data were, in turn, converted to electrophoretic mobilities (EPM's) and EPM standard deviations by using the geometrical and electrical constants of the experiments and fitting a straight line (method of least squares) through the corrected peak position points plotted against time. A computer program was written in BASIC to accomplish this task, and it is outlined in Table 3.

RESULTS

UNMIXED CELLS. The first experiments were designed to determine the effect of cell concentration on EPM, if any. Migration velocities of human RBC's introduced at 2 x 10^8 and at 4 x 10^9 cells/ml migrated with the same velocity. The same result was found when rabbit RBC's were used at these concentrations. Thus no intrinic effect of cell concentrtation on EPM in D-1 buffer at 14 deg C seems to exist. The area density range that was tested was approximately 4 x 10^6 to 8 x 10^7 cells/cm^2, based on sample input volume of 6 microliters. This is similar to the cell densities encountered on the STS-3 mission experiments.

MIXED CELLS. Cells of the two types were mixed in equal concentrations (2 x 10^8 each/ml), and each cell type was found to migrate exactly as in unmixed suspensions. However, when cells were mixed at 2 x 10^9/ml each, heavy band overlap was observed, and no true "gap" existed between the bands, even at maximum separation after nearly two hours. The peaks of the distributions of both cell types migrated with the predicted velocity, nevertheless. Continued

experimentation led to the conclusion that the quality of separation in free-zone electrophoresis of high cell concentrations depended upon the quality

of the input band (how narrow it could be made) and the quality of the tube coating (how low the electroosmotic mobility could be maintained). Figure 1 indicates that input bands at high cell concentrations are rather broad (copy of a photo). Figure 2 indicates the quality of separation that can nevertheless be achieved by free-zone electrophoresis at this cell concentration when sample band width and electroosmosis are minimized.

SIMULATION. An attempt was made to produce a distribution that resembled the optical scans obtained during the electrophoresis of high mixed cell density on STS-3 at the end of the run ("Column 019"). By having half as many rabbit cells as human cells and a considerable electroosmotic mobility, such a distribution was reproduced in the laboratory (Figure 3). Increased electroosmotic mobility of the electrophroesis tube was confirmed in this case by observing the rapid formation of a parabolic pattern (5-10 min) by crystal violet in the presence of the electric field.

Table 1. Composition of buffers used in human and rabbit erythrocyte collection and fixation. Cells were stored for two weeks in fixation buffer at ambient (19-23 deg C) temperature.

COMPONENT	CONCENTRATION (M) IN BUFFERS FOR COLLECTION	FIXATION
Na_2HPO_4		0.0537
NaH_2PO_4		0.0135
NaCl	0.145	0.150
Na_2EDTA	0.004	
Paraformaldehyde	0.0	1.5%

Table 2. Composition of D-1 buffer used in free-zone electrophoresis tube and in free-zone electrohoresis electrodes.

COMPONENT	CONCENTRATION (mM) IN TUBE D-1	ELECTRODE D-1
Na_2HPO_4	1.76	1.76
KH_2PO_4	0.367	0.367
NaCl	6.42	6.42
KCl	0.889	0.889
Na_2EDTA	0.336	0.0
Glucose	222	0.0
Dimethylsulfoxide	5%	0.0

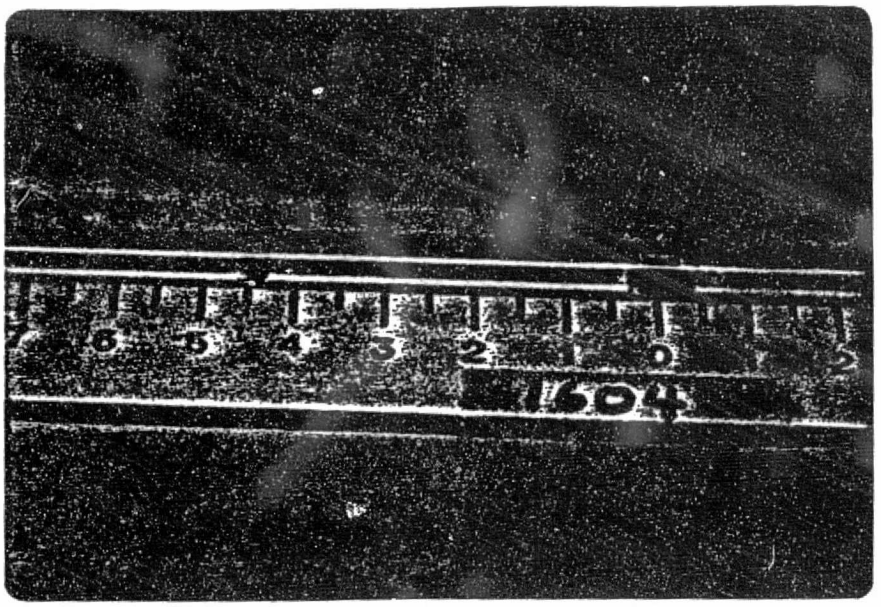

Figure 1. Photograph of rabbit and human RBC mixtures immediately after insertion into the free-zone electrophoresis tube. The left band contains 2 x 10^8 cells/ml each, and the right band contains 2 x 10^9 cells/ml each. approximately 4 microliters of sample were admitted in each case.

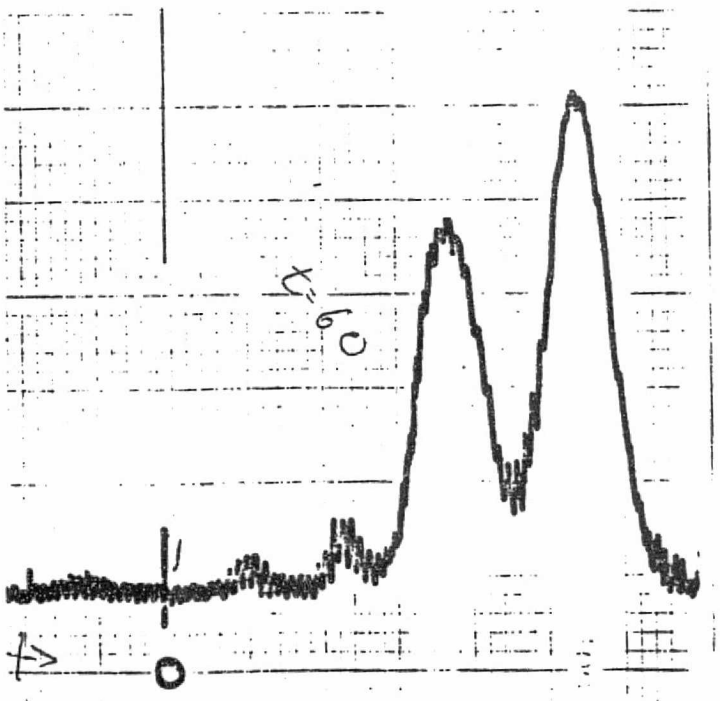

Figure 2. Strip-chart record of the separation of 2 x 10^9/ml each human (right, leading band) and rabbit (left, trailing band) RBC's under optimized free-zone electrophoresis. "O" marks the origin, and the leading band migrated 11 cm in 60 min.

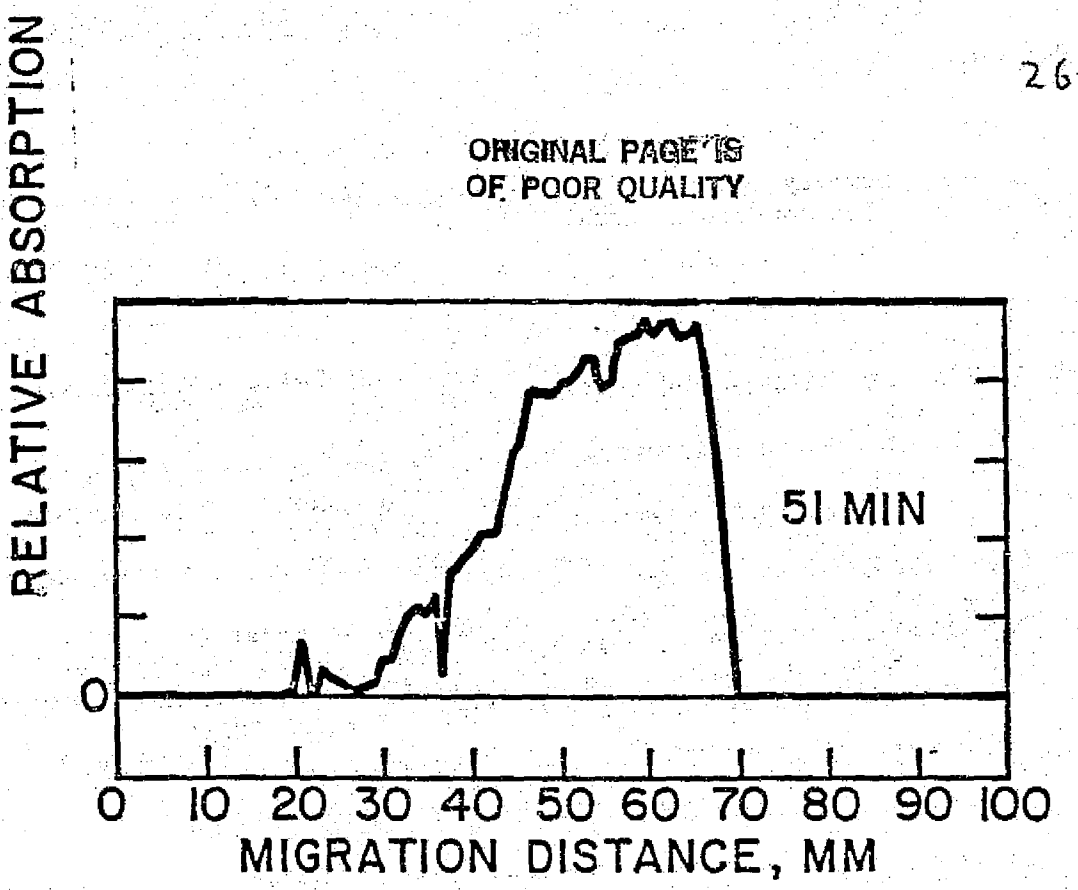

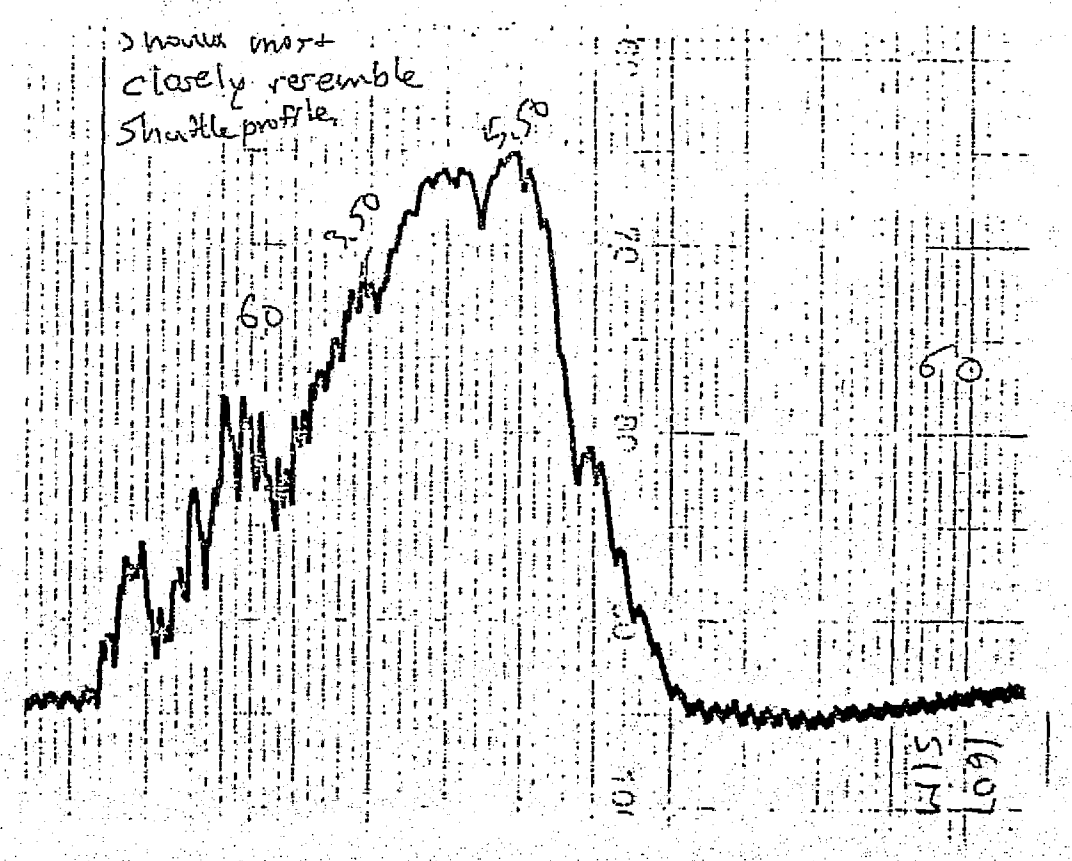

Figure 3. Top: Optical scan of negative of photo taken 51 min after the initiation of electrophoresis of "Column 019" on STS-3 mission (Sarnoff et al., 1983; Morrison and Lewis, 1983). Bottom: Strip-chart record of electrophoretic separation of 1 x 10^9/ml rabbit and 2 x 10^9/ml human RBC's in free-zone electrophoresis tube with some electroosmosis, 60 min after the beginning of electrophoresis.

Table 3. Summary outline of BASIC program "FZEANAL" for processing of free-zone electrophoresis data.

```
10 PRINT "FZEANAL.BAS PROGRAM FOR FREE ZONE ELECTROPHORESIS DATA ANALYSIS"
12 PRINT "WANT TO SEE DESCRIPTION OF PROGRAM (Y=1,N=0)";:INPUT QZ
13 IF QZ=0 GOTO 110
22 PRINT  "LINES 10-100=REM STATEMENTS,DIMENSIONS,OPTIONS,ORGANIZATION"
24 PRINT "100-1000=INPUT ROUTINES + DATA CORRECTION ALGORITHMS FOR CURRENT"
25 PRINT "            MIGRATION DISTANCE, TIME, AND PEAK WIDTH"
26 PRINT "1000-2000=CALCULATION OF CUMULATIVE MOBILITIES AND DATA PRINT-OUT"
28 PRINT "2000-3000=CREATION OF DATA FILES"
29 PRINT "3000-4000=ACCESS AND CONVERSION OF DATA FILES ON DISK"
30 PRINT "4000-5000=CALCULATION OF MEAN MOBILITIES BY LEAST SQUARES FIT"
33 PRINT "5000-6000=SCREEN GRAPHICS FOR PLOTTING MIGRATION DISTANCE VS. TIME"
40 PRINT "8000-9000=SUMMARY OF VARIABLES IN ORDER OF APPEARANCE"
```

Chapter 27

Factors that affect free fluid electrophoresis: A summary of Microgravity studies on STS-3, STS-4, and STS-6.

N85-31774

Microgravity Electrophoresis: A Study of the Factors that Affect Free-Fluid Separations

ABSTRACT: Electrophoresis experiments have been performed in the microgravity environment of the Space Shuttle. Test particles (fixed human and rabbit erythrocytes) migrated as expected in a static column and test macromolecules (human serum albumin, ovalbumin, hemoglobin A, and Pneumococcus polysaccharide 6B) migrated as expected in a continuous flow apparatus. The concentrations studied exceeded those that can be used in free-fluid separation and purification processes at unit gravity.

Free-fluid preparative electrophoresis, which is capable of processing higher concentrations of separands than gel electrophoresis, can be performed in a static vertical column with or without a density gradient, a vertically-flowing chamber, a horizontally-flowing chamber with a density gradient, an annular cylindrial chamber in a magnetic field, or a horizontal rotating tube (1). Considerable effort has gone into designing these devices to function at maximum sample capacity within the limits imposed by zone sedimentation and convection, two gravity-dependent processes. Protein solutions of about 0.5% and cell suspensions of about 10^7 cells/ml appear to be the maximum usable concentrations. Preparative electrophoresis experiments using test mixtures were therefore performed in the absence of gravity using a static column for cell electrophoresis (2) (Fig. 1a) and a continuous flow electrophoretic separator for electrophoretic studies on biological macromolecule mixtures (Fig. 1b).

A test particle mixture consisting of formaldehyde-fixed (3) human and rabbit erythrocytes, 0.5×10^9 each/ml was used to simulate the electrophoresis of biological cell suspensions at high concentrations. This concentration had

been demonstrated to exceed the zone sedimentation limit at unit gravity (4), and the mobilities of the cells had been determined in the buffer D-1 used in the apparatus depicted in Figure 1a. Table 1 compares the electrophoretic mobilities of the two test particles measured in the laboratory by microscopic analytical electrophoresis (5) with the mobilities of the leading and trailing edges of migrating cells determined by dividing their velocities, measured from photographs taken every 11 minutes by the STS-3 astronauts (6), by the monitored field strength, also in the photographs, of 13.5 v/cm. The mobilities are the same in microgravity at a concentration of 10^9 cells/ml as unit gravity at a concentration of 10^6 cells/ml.

A test mixture of ovalbumin and rat serum albumin at a total protein concentration of 16% was used to simulate the electrophoretic purification of a biological protein mixture. This concentration is more than 40 times the zone sedimentation limit in the apparatus of Figure 1b when operated at unit gravity and in more conventional downward-flowing continuous electrophoretic separators. Figure 2a contains the electrophoretic profiles of fractions collected at 1-g and a concentration of o.2% and the profile of fractions collected at 0-g and a concentration of 25% total protein plotted on the same scale. The two profiles are approximately the same despite an 80-fold concentration difference. The field strength in the 0-g experiment was twice as great, and the chamber thickness was twice that on the ground. The effectiveness of the separation is illustrated in Figure 2b.

A test mixture of human hemoglobin A (7) and Pneumocuccus polysaccharide 6B, a potential vaccine material (8) at concentrations of 2% and 4%, respectively, were used to simulate the electrophoresis of a crude biological supernatent. These concentrations could not be used stably in a commercial continuous-flow electrophoretic separator (9). Figure 3 is the electrophoretic profile of the separation in the apparatus of Figure 1b at 0-g.

These three earth-space comparisons were designed to test the hypothesis that, if free-fluid electrophoresis in space is to be considered as a source of biomedical research, diagnostic, or therapeutic materials (10) the necessary higher concentrations of materials can be processed without unexpected effects due to the higher concentrations per se. The results obtained indicate that such high concentrations of cells, protein mixtures, and protein-polysaccharide mixtures can be handled in a microgravity separator.

Robert S. Snyder, Percival P. Rhodes, Blair Herren
Marshall Space Flight Center
Huntsville, AL

J. Wayne Lanham
McDonnell-Douglas Astronautics Corp.
P.O. Box 516
St. Louis, MO 63166

Geoffrey V. F. Seaman
Oregon Health Sciences University
Portland, OR 97201

Paul Todd, Burton E. Sarnoff, M. Elaine Kunze
The Pennsylvania State University
University Park, PA 16802

John L. Sloyer NASA Separation Processes Br. ES73 ~~ES7~~ George C. Marshall Space Flight Ctr. Huntsville, AL 35812

Dennis R. Morrison, Marian Lewis
SD5 Bioprocessing Laboratory
L. B. Johnson Space Center
Houston, TX 77058

Table 1. Electrophoretic mobilities of fixed human and rabbit erythrocytes in "D-1" buffer in the laboratory and in space, measured at 12°C, in units of μm/sec per V/cm.

CONDITION	METHOD	CONCENTRATION (cells/ml)	RBC ~~RBS~~ MOBILITIES HUMAN	RABBIT
Space	Static column	10^9	−1.32	−0.83
Laboratory	Microscopic	10^6	−1.42 ± 0.18	−0.94 ± 0.12 *

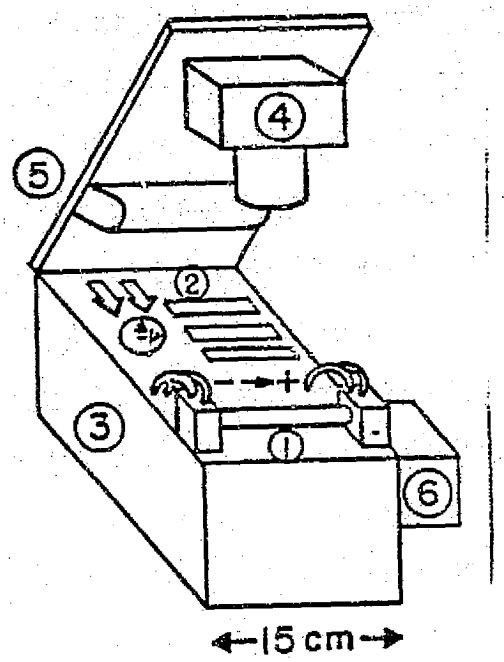

Figure 1a. Schematic diagram of static column zero-g electrophoresis device. (1) Electrophoresis column in which cells move left to right in buffer "D-1" (6.42 mM NaCl, 0.367 mM KH_2PO_4, 1.76 mM Na_2HPO_4, 222 mM glucose, 0.336 mM Na_2EDTA, 5% dimethylsulfoxide, pH 7.2, 0.015 g-ions/l ionic strength, conductivity=0.9 mmho/cm) under an applied field of 13.6 v/cm at 14°C. (2) Meters for monitoring column voltage and temperature, toggle switches, and clock in the viewing field of the camera (4), which took photographs of the meters every minute and of the columns, when there thermal cover was removed briefly, every 10 min. (3) Power supply and electrode buffer circulating system. (5) Illuminator. (6) Accelerometer for detecting small non-zero-g accelerations during cell electrophoresis.

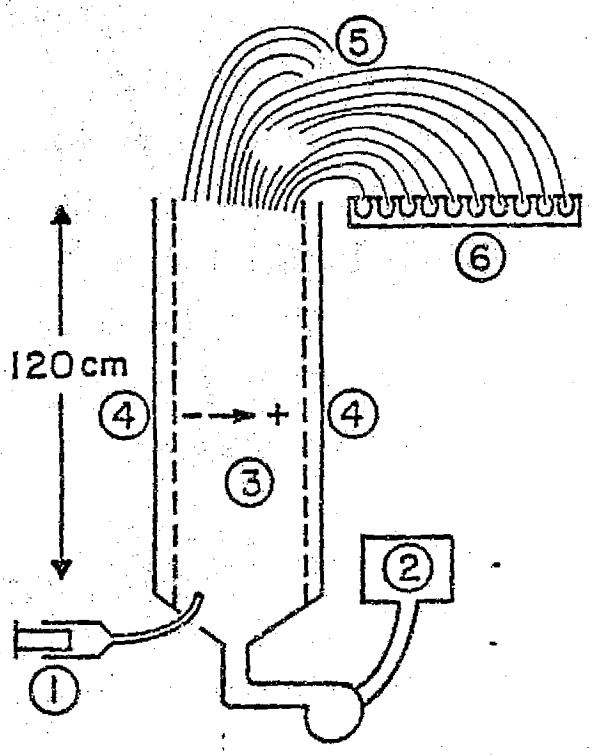

Figure 1b. Schematic diagram of continuous flow zero-g electrophoresis device. (1) Continuous sample input at 0.05 ml/min. (2) Computer-controlled pumping system for continuous buffer input at 40 ml/min into the separation chamber (3) where cells migrate from left to right in a 40 V/cm field while flowing upward. The system pumps separate buffer into the electrode compartments (4). (5) Sample collection system which divides the end of the column into 198 outlets and delivers electrophoretic subfractions to 198 receptacles (6). A modification of triethanolamine-acetate buffer of Hannig et al. was used in the chamber.

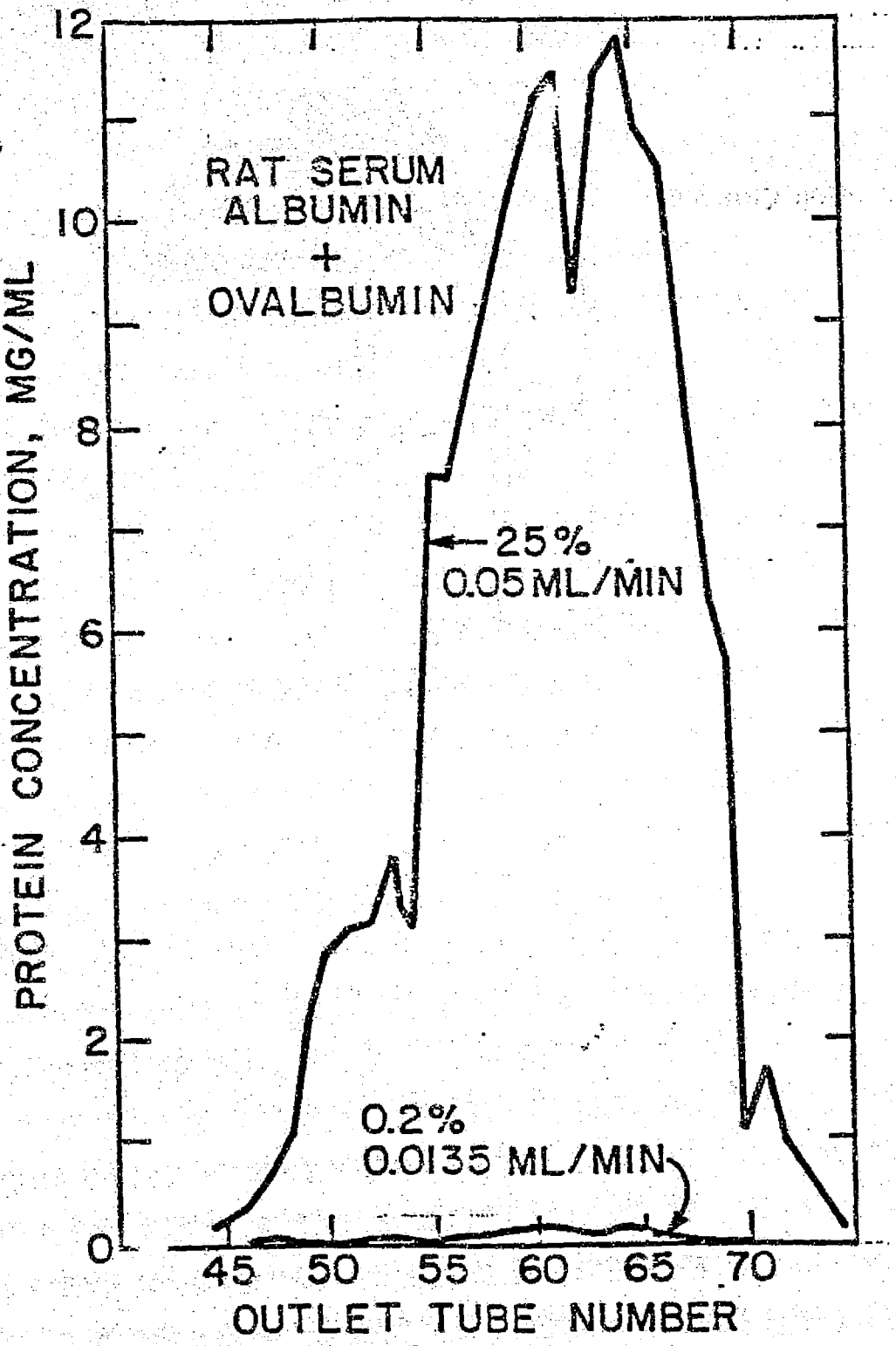

Figure 2a. Electrophoretic profile of a test mixture of rat serum albumin (low mobility component) and ovalbumin at 25% total protein concentration in zero-g in the continuous flow electrophoresis device described in figure 1b. The lower curve is the profile of the same separation under optimal laboratory conditions in the same device on the ground, plotted on the same scale. This zero-g separation resulted in a 463-fold increase in processing capacity with equivalent purity.

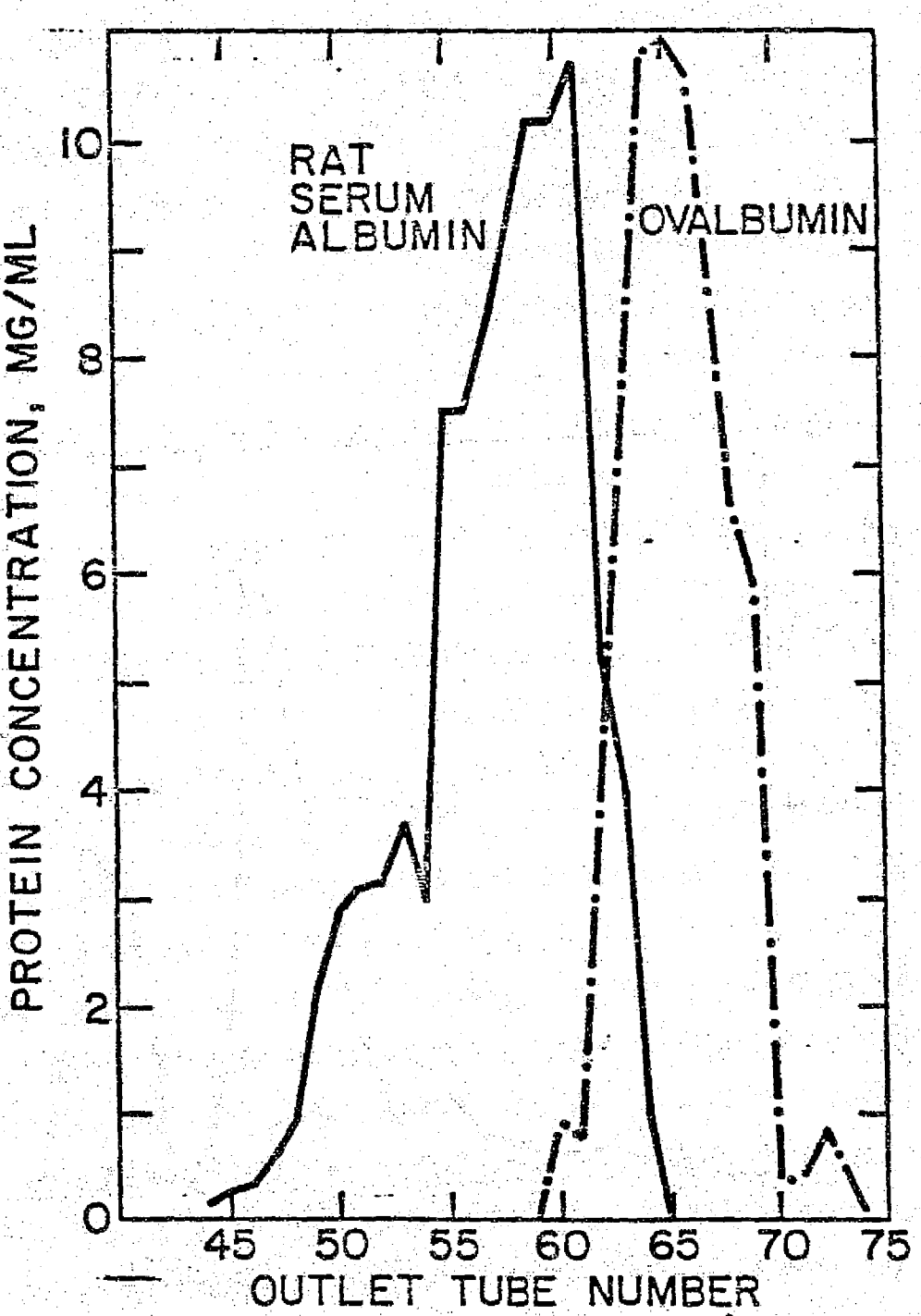

Figure 2b. The same separation as in figure 1b, with the products analysed separately. Fractions 45-57 were 100% serum albumin; fractions 65-75 were 100% ovalbumin. These products differ approximately 25% in electrophoretic mobility.

Fig. 3.

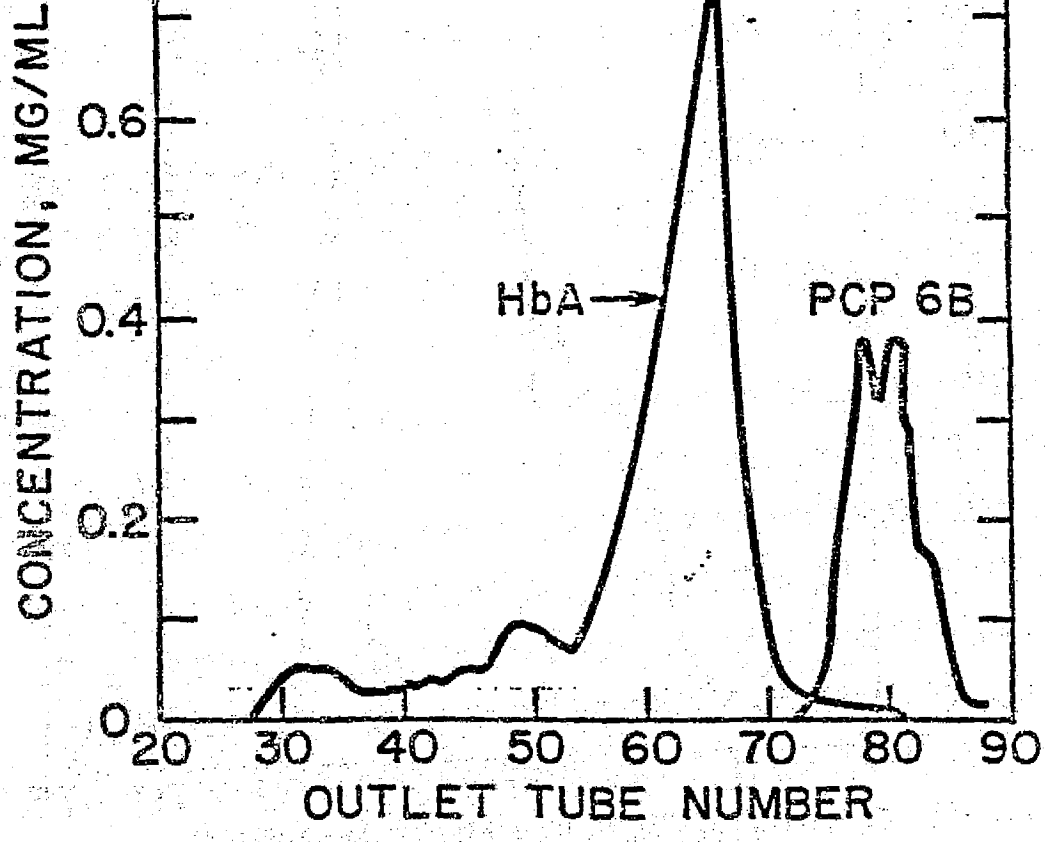

Figure 3. Electrophoretic profiles of human hemoglobin A (cyanmethemoglobin) and Pneumococcal capsular polysaccharide fraction 6B. Input sample on the continuous-flow electrophoresis device (Fig. 1b) was electrophoresis buffer containing 2% (w/v) HbA and 4% (w/v) PCP-6B. Cyanmethemoglobin A was obtained as a solution from centers for disease control (7), and PCP-6B was prepared from Pneumococcus sp. using previously-described methods (8).

REFERENCES AND NOTES

1. P. G. Righetti, C. J. vanOss, and J. Vanderhoff, Eds. Electrokinetic Separation Methods, Elsevier Amsterdam, 1979. H. Bloemendal, Ed. Cell Separation Methods, Elsevier, Amsterdam, 1977.

2. R. E. Allen, P. H. Rhodes, R. S. Snyder, G. H. Barlow, M. Bier, P. E. Bigazzi, C. J. vanOss, R. K. Knox, G. V. F. Seaman, F. J. Micale, J. W. Vanderhoff. Sep. Purif. Meth. 6, 1-60 (1977).

3. G. V. F. Seaman. In The Red Blood Cell. D. M. Surgeoner, Ed. Academic Press, NY, 1975. pp. 1135-1229.

4. R. C. Boltz, Jr., P. Todd. In Electrokinetic Separation Methods, P. G. Righetti, C. J. vanOss, and J. Vanderhoff, Eds. Elsevier, Amsterdam, 1979. pp. 229-250.

5. G. V. F. Seaman. Blood
(The erythrocyte and thrombocyte surface chemistry.)

6. D. R. Morrison and M. Lewis. International Astronautics Federation, Annual Meeting Proceedings, 1983 (in press).

7. We thank of the Centers for Disease Control, Birmingham, Ala., for kindly providing cyanmethemoglobin A in generous quantities.

8. J. L. Sloyer. Ann. Otol. Rhinol. 89, 133 (1980).

9. Desaga "FF48" (Desaga AB, Munich, GDR), beckman "CPE" (Beckman Instruments, Los Angeles, Calif.) and McDonnell-Douglas continuous-flow electrophoretic separators were used in experiments that affirm this finding. However, see J. A. L. I. Walters and W. S. Bont. Anal. Biochem. 93, 41-45 (1970).

10. J. H. Bredt, B. O. Montgomery, Astronaut. Aeronaut. , 22-41 (1975).

11. K. Hannig, H. G. Heidrich. methods Enzymol. 21, 746-761 (1974).

12. This research was sponsored by National Aeronautics and Space Administration, Office of Space Science Applications, including contracts and NAS-9-55318 to The Pennsylvania State University.

13. We gratefully acknowledge the skilled and helpful collaborations of the Shuttle astronauts of flights STS-3, 4, and 6, the technical staff of the Electrophoresis Operations in Space group of McDonnell-Douglas Astronautics Corp.

Chapter 28

Pre-flight report on cultured human embryonic kidney cell handling and cell electrophoresis.

PRE-FLIGHT REPORT ON CULTURED HUMAN EMBRYONIC KIDNEY CELL HANDLING AND CELL ELECTROPHORESIS

Prepared prior to continuous-flow electrophoretic separation experiments aboard Space Shuttle flight STS-8

by

Paul Todd
Burton E. Sarnoff
Zhan Kui Li

403 Althouse Laboratory
The Pennsylvania State University
University Park, Pennsylvania 16802

20 August 1983

PRE-FLIGHT STUDIES ON McDONNELL-DOUGLAS ASTRONAUTICS CORP. VERSION OF TRIETHANOLAMINE-ACETATE CONTINUOUS FLOW ELECTROPHROESIS BUFFER AND FLIGHT HANDLING PROCEDURES FOR CULTURED HUMAN EMBRYONIC KIDNEY CELLS

This report summarizes studies of

1. Physical properties of MDAC CFES buffer

2. Electrokinetic properties of human erythrocytes in MDAC CFES buffer

3. Electrokinetic properties of human embryonic kidney cells in MDAC CFES buffer

4. Vizbility and yield of human embryonic kidney cells subjected to flight handling procedures

and presents summary comments and recommendations.

1. Physical properties of MDAC CFES buffer

Measurements of viscosity and conductivity were made using an Ostwald viscometer for viscosity measurements with water as standard in each experiment and a YSI conductivity bridge with a cell with 0.1 cell constant. The resulgs of viscosity measurements are given in Table 1. At low temparature the solutions were found to be very viscous. The accuracy of the meaurement is about _+_ 1.5%. The results of conductivity measurements are given in Table 2. At such low conductivity it was found very easy to accidentally increase the conductivity of the buffer by pouring from one vessel to another, using certain types of labware, and aging the solutions, for example. This situation is reflected in the data; different batches can differ in conductivity, and conductivity rises slowly with storage of 500 ml in glass bottles (last 2 lines of table) or small volumes in plastic centrifuge tubes (data not shown).

Experiments were also performed in which 10^6 - 10^9 cells/ml were added to buffer during conductivity measurements. The latter concentration increased buffer conductivity by up to 20%. After removal of cells the buffer conductivity was also increased by a considerably greater amount than expected on the basis of dilution of the cell-storage solution alone after several washes. This low-ionic strength solution appears to acquire ions from glass, plastic, and fixed cells. At very high concentrations cells themselves will also be carriers of ions. Although a definitive study may still be needed, it seems that sample zones in the CFES may constitute conductance gaps during operation. However, conductivity increases of less than 20% are not serious conductance gaps.

2. Electrokinetic properties of human erythrocytes in MDAC CFES buffer

Under stable conditions the mobility of human erythrocytes in MDAC CFES buffer is 1.58 _+_ 0.08 (n=5) at 6.0 degrees C. The correction factor to the viscosity of water at 25 deg is almost exactly 2.00, so the corrected normal mobility of fresh erythrocytes 3.16 _+_ 0.16 mobility units. This value is consistent with the known ionic-strength dependence of erythrocyte mobility. From Table 3 it can be seen that sometimes the mobility of fresh cells was low (1.12-1.13). The ionic strength of the buffer is low and in the range of "membrane metastability" at pH 7.2-7.4 as described by Seaman et al. in electrophoretic studies of human erythrocytes. Raising the temperature may

destabilize the erythrocyte membrane further, as indicated in the last 3 lines of Table 3, in which the standardized EPM dropped when fresh cells were subjected to electrophoresis but not when fixed cells were used. The erythrocyte mobilities overlap heavily with those found for human embryonic kidney (HEK) cells, fixed human erythrocytes would not be suitable as a reference marker mixed with HEK cells during CFES operation.

A raw mobility histogram of fresh human erythrocytes under stable conditions in CFES buffer at 6.0 degrees C is shown in Figure 1.

3. Electrokinetic properties of human embryonic kidney cells in MDAC CFES buffer

Similar experiments were performed using human embryonic kidney cells HFK-34, passage 4 (P4), HEK-8514 (P2), and HEK-8514 (P1). The final two experiments (experiments 1520 and 1521) were studies on cells incubated 1 or 2 days after arrival from Houston without subcultivation and subjected to electrophoresis immediately after trypsinization (standard trypsin-EDTA procedure) or stored at 1.6 million cells/ml for 3 days in CFES buffer with 10% dialysed horse serum to simulate pre-run holding time on CFES operation on STS-8. The volume of the suspension was about 1.0 ml, and it was rotated at about 70 rpm at 5 degrees C in a tuberculin syringe to prevent sedimentation and attachment. See report on viability studies below.

Table 4 indicates that a wide variety of mobilities was found. This variability was acribable to variable origin of cells, passage number, and stability. In at least two important experiments it was found that freshly trypsinized cells behaved normally for the first half of an EPM measurement procedure with the Cytopherometer then an abrupt increase in buffer conductivity would occur with a corresponding modification of the mobility distribution. An example is shown in Table 4, where population 1521S1 was measured durint the first half of a run, and population 1521S2 was measured during the second half of the same run, during which the buffer conductivity doubled and so did the mean EPM. Cells that had been exposed to the STS-8 pre-run storage conditions were more stable that the freshly trypsinized cells as indicated by the absence of such mid-run changes in conductivty and mobility and by the appearance of the cells in phase contrast. There was also a substantial increase in EPM observed after storage, and Table 4 indicates increased mean EPM from about 0.8 before to about 1.4 after storage. Compare, for example 1516S to its post-storage counterpart 1516F--similarly 1521S1 with 1521F.

The EPM distributions remain broad after storage in CFES buffer and horse serum, as indicated by the histograms in Figure 2, where pre- and post-storage data are compared using mobilities corrected to water at 6 degrees, the temperature of the CFES buffer in the electrophoresis chamber in this experiment. The typical 3-subpopulation type of histogram seen in all other buffers appears to be preserved in CFES buffer at this temperature after, as well as before, storage in buffer and serum.

Figure 3 is a raw mobility histogram produced under conditions that simulate CFES operation at closely as possible. Cells (HEK 8514,P1) were stored 3 days in CFES buffer and 10% dialysed horse serum, rinsed in CFES buffer at 6 degrees and analysed electrohoretically at 6 degrees. The mean raw mobility was 1.11 $\pm$ 0.21 with a range of 0.5 to 1.76. This histogram is displayed at slighily higher resolutio than the CFES to indicate the type of

spread among fractions that might be expected. The corresponding migration distances using ET=150 would span the range cm to cm. A similar distribution is shown in Figure 4 for passage-2 cells. A large population grown up for the CFES operation on STS-8 might consist of a mixture of the cells whose mobility histograms appear in Figures 3 and 4.

Table 1. Viscosity of CFES buffer.

TEMPERATURE DEGREES C	VISCOSITY CENTIPOISE
4.0	1.764
6.0	1.792
25.0	1.077
25.0	1.084

Table 2. Conductivities of CFES buffer.

DATE PREPARED	DATE MEASURED	TEMPERATURE DEGREES C	CONDUCTIVITY mMHO/CM
4/30/83	5/2/83	4.0	0.062
4/30/83	5/2/83	5.0	0.064
7/27/83	7/28/83	5.5	0.048
7/27/83	7/28/83	5.5	0.048(after run)
7/27/83	8/04/83	5.5	0.048
7/27/83	8/08/83	5.5	0.052

TABLE 3. Electrophoretic mobilities of human erythrocytes in MDAC CFES buffer

EXPERIMENT POPULATION	FRESH CELLS	TEMPERATURE DEGREES C	ELECTROPHORETIC MOBILITIES H2O 25 DEG	CFES, T
1515H1	+	6.0	3.27±0.50	1.64±0.25
1515H2	+	6.0	3.10±0.42	1.55±0.21
1516H2	+	6.0	3.42±0.36	1.71±0.18
CFES6	+	6.0	3.04±0.26	1.52±0.13
HS002A	+	4.0	2.23±0.19	1.12±0.10
HS002B	+	5.0	2.24±0.25	1.13±0.13
CFES2	+	25.0	1.82±0.23	1.50±0.19
CFES4	-	25.0	3.00±0.22	2.48±0.18
CFES5	+	25.0	3.42±0.36	1.71±0.18

4. Viability and yield of human embryonic kidney cells subjected to flight handling procedures

A preliminary test (Experiment 1505) of the holding procedure was made using HFK-34(P2) cells. After trypsinization they were held at 4 degrees C and rotated in plastic centrifuge tubes at 15 rpm. Samples were evaluated at 24, 48, and 72 hours. The suspending medium was CFES buffer with 5% dialysed horse serum. The results were as follows:

HOURS AT 4 DEG	PER CENT YIELD	PER CENT VIABILITY
24	72.2	100
48	65.0	100
72	62.0	74

Continued research with this cell strain showed that 10% serum was slightly better than 5%, that passage through CFES buffer without serum, as in electrophoresis experiments, reduced viability to 86% immediately and to 66% after the cells spent an additional 2 days in suspension in receiving medium.

The results of the combined viability-mobility experiment 1520 are given in Table 5, in which the mobility is given in water at 6 degrees. See 1520F for values in CFES buffer.

CONCLUSIONS AND RECOMMENDATIONS

In general, the procedure for cell handling and electrophoresis of HEK-8514 cells in 1st or 2nd passage on STS-8 is acceptable if executed properly. The CFES buffer has ionic strength that is barely compatible with cell viability and membrane stability, as seen in experiments with human erythrocytes and trypan-blue staining of human kidney cells. Cells suspended in 10% dialysed horse serum for 3 days in the cold appear to be more stable than freshly trypsinized cells. 10% horse serum appears to be superior to 5% horse serum for this purpose. The mean absolute raw mobility of HEK-8514 cells in CFES buffer at 6 degrees, conductivity 0.055 mmho/cm, is 1.1 - 1.4 um-cm/V-sec, with a range of nearly a whole mobility unit. The above-described pretreatment has the effect of raising the EPM of these cells, but electrophoretic heterogeneity does not seem to be affected. Receiving medium consisting of 4X-5X F-12/DMEM (ingredients but not salts) and 20-40% serum initial concentration appears suitable; it yields about 80% viability in 2 days post treatment relative to initial post-treatment viability. It would seem reasonable to proceed with the following plan"

1. Trypsinize cells in the ground, suspend in 10% dialysed horse (or calf) serum in CFES buffer, as close to 4 deg C is possible, from just prior to launch to just prior to electrophoresis.

2. Inject sample, which will have a slight conductance gap due to the serum, into the chamber with ET consistent with mobility range 1.0 - 1.4.

3. Collect samples into isotonic medium concentrate with 20-40% serum (horse or calf) for storage until retrieval. Plate as soon as possible in F-12/DMEM based medium.

TABLE 4. Electrophoretic mobilities of HEK-8514 human embryonic kidney cells in CFES buffer

EXPERIMENT POPULATION	CONDUCTIVITY MMHO/CM	TEMPERATURE DEGREES C	ELECTROPHORETIC MOBILITIES H2O 25 DEG	CFES, T
1515S2(P2)PRETEST	0.055	6.0		0.81±.21
BS002C(P2)PRETEST	0.055	6.0	1.63±0.27	0.81±0.15
1516S(P2)PRETEST	0.13	6.0	1.55±0.30	0.78±0.15
1516F(P2)POSTTEST	0.055	6.0	2.80±0.30	1.40±0.15
1520S(P1)PRETEST	0.055	6.0		0.97±0.20
1520F(P1)POSTTEST	0.055	6.0		1.11±0.21
1521S1(P1)PRETEST	0.055	6.0	1.82±0.42	0.91±0.21
1521S2(P1)PRETEST	0.113	6.0	3.44±0.84	1.72±0.42
1521F(P1)POSTTEST	0.055	6.0	2.83±0.66	1.41±0.33

Pretest mean = 0.86±0.08 (N=5); posttest mean = 1.20±0.17 (N=3) in CFES buffer at 6.0 degrees C.

TABLE 5. RESULTS OF EXPERIMENT 1520

Suspension: Trypsin-EDTA

Cells: 1.4×10^6

Volume: 0.15 ml

Treatment: 3 days in CFES at 6°C

Measurement	Before	After
Number of cells, 10^6	1.4	1.6
Viability, %	100	81.5
Applied Current, μA	25	25
EPM, μm-cm/V-sec	1.28 ± 0.26	1.47 ± 0.27

Figure 1. Electrophoretic mobility histogram of fresh human erythrocytes in MDAC CFES buffer, 6 degrees, uncorrected.

RANGE	N	FREQUENCY
-1.2 - -1.25	1	*
-1.25 - -1.3	2	* *
-1.3 - -1.35	2	* *
-1.35 - -1.4	5	* * * * *
-1.4 - -1.45	13	* * * * * * * * * * * * *
-1.45 - -1.5	9	* * * * * * * * *
-1.5 - -1.55	9	* * * * * * * * *
-1.55 - -1.6	10	* * * * * * * * * *
-1.6 - -1.65	8	* * * * * * * *
-1.65 - -1.7	3	* * *
-1.7 - -1.75	4	* * * *
-1.75 - -1.8	3	* * *
-1.8 - -1.85	1	*

Figure 2. Comparison of two mobility histograms of first-passage HEK-8514 cells before and after spending 3 days in CFES buffer plus 10% dialysed horse serum. Mobility values shown are corrected to water at 6 degrees. The mean mobility after storage, in this experiment, was 1.11±0.21 in CFES buffer.

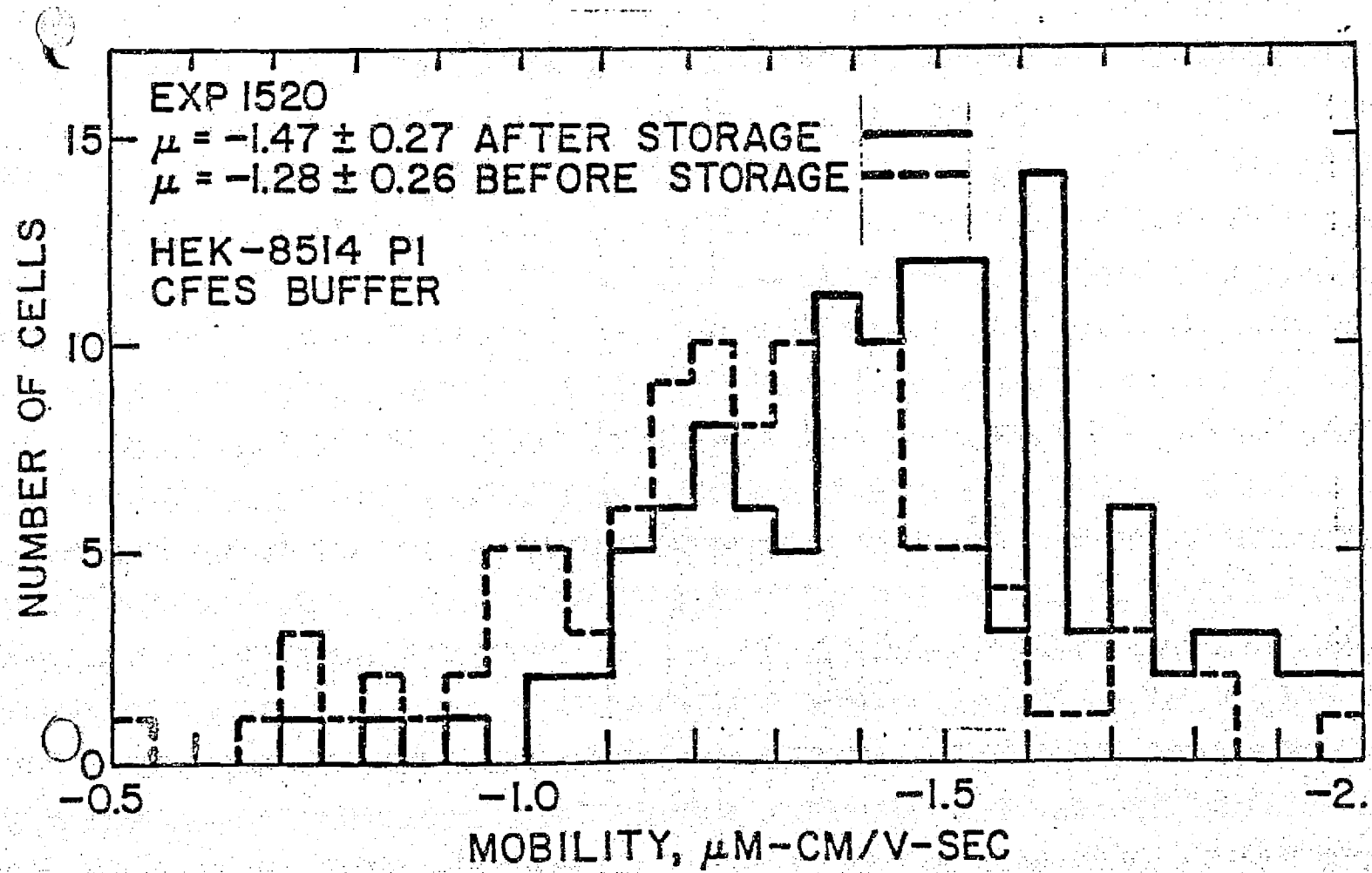

Figure 3. Raw mobility histogram of HEK-8514(P1) cells in CFES buffer at 6 degrees after 3 days of storage in CFES buffer plus 10% dialysed horse serum at 8 degrees.

RANGE			N	FREQUENCY
-1.13	-	-1.14	1	*
-1.14	-	-1.15	0	
-1.15	-	-1.16	0	
-1.16	-	-1.17	1	*
-1.17	-	-1.18	0	
-1.18	-	-1.19	1	*
-1.19	-	-1.2	1	*
-1.2	-	-1.21	0	
-1.21	-	-1.22	1	*
-1.22	-	-1.23	2	* *
-1.23	-	-1.24	0	
-1.24	-	-1.25	2	* *
-1.25	-	-1.26	5	* * * * *
-1.26	-	-1.27	6	* * * * * *
-1.27	-	-1.28	5	* * * * *
-1.28	-	-1.29	4	* * * *
-1.29	-	-1.3	3	* * *
-1.3	-	-1.31	5	* * * * *
-1.31	-	-1.32	3	* * *
-1.32	-	-1.33	6	* * * * * *
-1.33	-	-1.34	3	* * *
-1.34	-	-1.35	4	* * * *
-1.35	-	-1.36	2	* *
-1.36	-	-1.37	3	* * *
-1.37	-	-1.38	5	* * * * *
-1.38	-	-1.39	4	* * * *
-1.39	-	-1.4	4	* * * *
-1.4	-	-1.41	8	* * * * * * * *
-1.41	-	-1.42	1	*
-1.42	-	-1.43	3	* * *
-1.43	-	-1.44	0	
-1.44	-	-1.45	4	* * * *
-1.45	-	-1.46	2	* *
-1.46	-	-1.47	2	* *
-1.47	-	-1.48	3	* * *
-1.48	-	-1.49	2	* *
-1.49	-	-1.5	2	* *
-1.5	-	-1.51	2	* *
-1.51	-	-1.52	2	* *
-1.52	-	-1.53	0	
-1.53	-	-1.54	1	*
-1.54	-	-1.55	1	*
-1.55	-	-1.56	2	* *
-1.56	-	-1.57	0	
-1.57	-	-1.58	1	*
-1.58	-	-1.59	1	*
-1.59	-	-1.6	2	* *
-1.6	-	-1.61	2	* *
-1.61	-	-1.62	2	* *
-1.62	-	-1.63	0	
-1.63	-	-1.64	0	
-1.64	-	-1.65	0	
-1.65	-	-1.66	0	
-1.66	-	-1.67	0	
-1.67	-	-1.68	0	
-1.68	-	-1.69	0	
-1.69	-	-1.7	0	
-1.7	-	-1.71	1	*
-1.71	-	-1.72	0	
-1.72	-	-1.73	0	
-1.73	-	-1.74	0	
-1.74	-	-1.75	0	
-1.75	-	-1.76	0	
-1.76	-	-1.77	0	
-1.77	-	-1.78	0	
-1.78	-	-1.79	0	
-1.79	-	-1.8	1	*
-1.8	-	-1.81	1	*
-1.81	-	-1.82	0	
-1.82	-	-1.83	1	* EXP 1516F
-1.83	-	-1.84	0	

Figure 4. Same is Figure 3, but cells are in second passage.

Chapter 29

Properties of electrophoretic fractions of human embryonic kidney cells separated on shuttle flight STS-8.

Session: G.1.5.3

PROPERTIES OF ELECTROPHORETIC FRACTIONS OF HUMAN EMBRYONIC KIDNEY CELLS SEPARATED ON SPACE SHUTTLE FLIGHT STS-8

Dennis R. Morrison*, Marian L. Lewis**, Grant H. Barlow***, Paul Todd+, M. Elaine Kunze+, Burton E. Sarnoff+, and Zhankui Li+

*Johnson Space Center, Houston TX 77058, U.S.A., **Technology Inc., Houston TX 77058, U.S.A., ***Michael Reese Research Foundation, Chicago, IL U.S.A., +403 Althouse Laboratory, The Pennsylvania State Universtiy, University Park, PA 16802.

ABSTRACT

Suspensions of cultured primary human embryonic kidney cells were subjected to continuous flow electrophoresis on Space Shuttle flight STS-8. The objectives of the experiments were to obtain electrophoretically separated fractions of the original cell populations and to test these fractions for the amount and kind of urokinase (a kidney plasminogen activator that is used medically for digesting blood clots), the morphologies of cells in the individual fractions, and their cellular electrophoretic mobilities after separation and subsequent proliferation. Individual fractions were successfully cultured after return from orbit, and they were found to differ substantially from one another and from the starting sample with respect to all of these properties.

INTRODUCTION

The previous paper /1/ described the functional differences among electrophoretic subfractions of kidney and pituitary cells separated on Space Shuttle floght STS-8. This paper describes electrophoretic and morphological

differences among the progeny of cells propagated from kidney cell subfractions.

METHODOLOGY

Human embryonic kidney cells were prepared in suspension prior to flight in electrophoresis buffer containing 10% calf serum. Electrophoretic separation proceded on Space Shuttle flight STS-8 in electrophoresis buffer without serum in the McDonnell-Douglas Astronautics Corp (MDAC) continuous flow electrophoretic separator (CFES), and fractions were collected into sample bags containing culture medium and concentrated serum. Two separations were performed, designated #3 and #4, and subsequent culturing and biochemical measurements were conducted at Johnson Space Center. Fractions that yielded enough progeny cells were analysed at The Pennsylvania State University for morphology by phase-contrast microscopy and flow cytometry, and electrophoretic mobility distributions were determined with a Zeiss "Cytopherometer" /2,3/. Not all fractions were available for these analyses. Additional experimental details are given in the preceding paper /1/.

RESULTS

The electrophoretic mobility (EPM) of the starting cell population was found to be -1.47 +or- 0.27 um-cm/V-s by analytical microscopic electrophoresis using the space electrophoresis buffer. The CFES operated at E x t = 300 V-min/s (field times residence time for cells in the chamber). Fractions were collected 0.8 mm apart, and the cell stream was directed at fraction 59 in the absence of the electric field; therefore about 95% of the cells should have been distributed between fractions 80-102. In Figure 1 it is seen that 95% of the cells were distributed between fractions 93-115. The spread was as predicted, but cells migrated about 12 fractions farther than predicted on the basis of electrokinetic movement alone. The two experiments (#3 with a low cell input, and #4 with a high cell input) were in excellent agreement with with each other with respect to the distribution of cells among fractions.

The EPM distributions of progeny cells cultured from the three electrophoretic fractions that yielded adequate cells are shown in Figure 2, where it can be seen that the lowest mobility fraction studied (fraction 96) produced higher-mobility progeny, while the other two fractions produced progeny cells with mobilities relted to the farctions from which they were collected, namely -0.82 +or- 0.18 and -1.13 +or- 0.18 for fractions 103 and 113, respectively.

Four cell types were identified by phase microscopy: small epithelioid, large epithelioid, domed (phase-bright, refractile bulges in single cells) and fenestrated (1 or 2 large holes through the cytoplasm, including upper and lower plasma membrane). After subcultivation, progeny of cells from available fractions had the per cent of each cell type shown in Table 1. Fraction 110, which had the highest urokinase production /1/ was highest in per cent large epithelioid cells; low-mobility fractions were highest in domed cells.

DISCUSSION

Subsequent to electrophoretic purification in microgravity, kidney cell fractions were successfully cultured and analysed, and progeny cells grown from different subfractions were shown to be different with respect to EPM and morphology as well as with respect to products they produce.

ACKNOWLEDGMENTS

We thank the staff of Electrophoresis Operatons in Space, McDonnell-Douglas, Inc., and the STS-8 asstronauts for the excellent technical execution of the electrophoresis experiment in microgravity. This research was supported by the U. S. National Aeronautics and Space Administration.

REFERENCES

1. D. R. Morrison et al. Electrophoretic separation of kidney an dpituitary cells on STS-8. Adv. Space Res. This issue.

2. D. R. Morrison and M. L. Lewis. Electrophoresis tests on STS-3 and ground

control experiments: as basis for future biological sample elections. In _33rd Inaternation Astronautical Federation Congress_ Paper No. 82-1562, 1983.

3. L. D. Plank, W. C. Hymer, M. E. Kunze, G. M. Marks, J. W. Lanham, and P. Todd. A study of cell electrophoresis as a means of purifying growth hormone secreting cells. J. Biochem. Biophys. Meth. _8_, 275-289 (1983).

Table 1. Morphological distributions of cells in electrophoretic fractions in second passage on 10/19/83. Numbers used per cent of each cell type.

FRACTION	SMALL	LARGE	DOME	FEN	TOTAL	% GRANULAR
91	63	20	12	4	320	33
96	59	13	22	6	411	37
101	79	12	6	3	326	37
103	65	11	2	7	373	44
110	40	47	7	7	255	53
112	80	9	6	5	400	20
113	82	8	7	4	43	12
113W	75	11	7	6	33	19
116	80	8	6	6	366	19

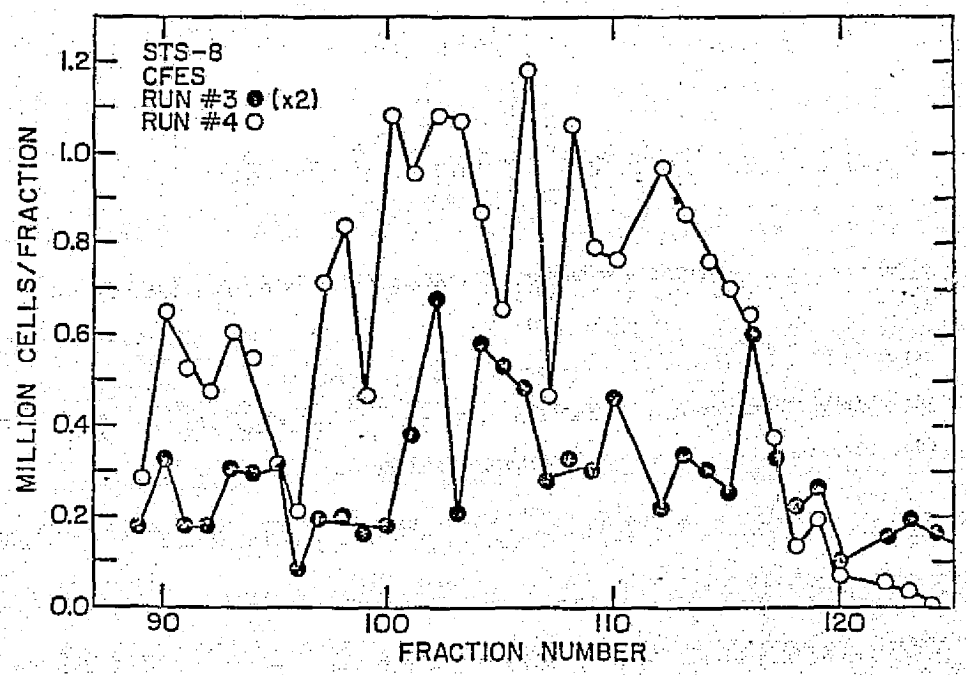

Figure 1. Number of cells collected in each electrophoretic fraction in experiments #3 and #4 on Space Shuttle flight STS-8. The cell counts in #3 have been multiplied by 2 to make the scales comparable.

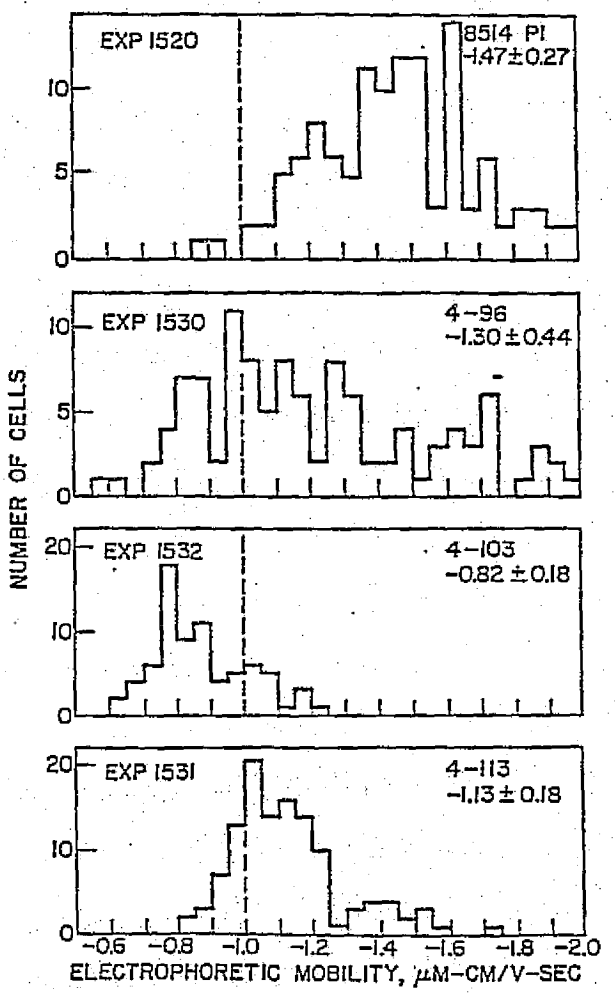

FIGURE 2. Electrophoretic mobility (EPM) distributions of starting mixture (top) and 3 fractions of human embryonic kidney cells (strain HEK-8514) separated by Continuous Flow Electophoresis in microgravi and subsequently grown in cell culture. Original EPM is linearly related to fraction number (96, 103, and 113 in this case). The low EPM fraction (number 96) differentiated into higher-EPM progeny cells.

Chapter 30

Application of light scatter theory to flow cytometry and sorting of human embryonic kidney cells.

DETECTION OF INTERNAL STRUCTURE BY SCATTERED LIGHT INTENSITY: APPLICATION TO KIDNEY CELL SORTING

N85-31777

by Charles L. Goolsby and M. Elaine Kunze

Introduction.

Scattered light measurements in flow cytometry have been successfully used to distinguish cells on the basis of differing morphology and internal structure (6,9,36,37,52,62,64,65,71-73,75,84). Differences in scattered light patterns due to changes in internal stucture would be expected to occur at large scattering angles. At these angles refraction and reflection from internal cellular structures would be expected to be larger, compared to overall cellular scattered intensity, than at low scattering angles (33). One of the most widely used methods based on internal structural differences is the discrimination of different cell types from human peripheral blood. Based on narrow forward angle and 90° scattered light measurements human leukocytes are seperated into lymphocytes, monocytes, and granulocytes (6,73) with the 90° scattered light signal increasing in that order corresponding to increasing internal structure. Visser et al (84) seperated mouse bone marrow cells into 4 groups based on a 1° versus 90° scattered light measurement and found that the cells with the most complex of internal structure had the highest 90 scattered intensity. Loken et al (52) by measuring scattered light in the 2 -8 interval were able to sort cells into red blood cells, small lymphocytes, large lymphocytes and polymorphnuclear leukocytes. By measuring the scattered light intensity in 32 angular regions between 0° and 30° Salzman et al (71,72) were able to distinquish invasive carcinoma cells from normal cells of the human uterine cervix. Jensen (37) used 90° scattered light to differentiate between leukocytes and squamous cells in gynecologic samples. Measurements of scattered intensity in 32 angular intervals between 0°and 21° by Price et al (64) demonstrated that two cell types whose intensity patterns were indistinguishable over certain angular intervals were easily separable at others. Jamieson et al (36) and Schafer et al (75) found that fibroblasts from a patient with Snadhoff's disease had a higher scattered light intensity in the 4° to 14° region than did normal human skin fibroblast lines. This increased intensity was believed to arise from increased cytoplasmic inclusions. Benson et al (9) investigated tumor cell heterogenity and developed an index of tumor aggressiveness based on 70°- 110° and 2°-25° scattered light measurements. They found that increases in the 70°-110° measurement correlated with the degree of roundness of the nucleus. Theoretical treatments of morphology and internal structure have been limited (3,42,43). In the present study we propose to investigate the effects of internal structure on light scattering in a more simplistic manner than used in previous treatments. By comparing the angular distribution of the scattered light intensity from spheres that are small compared with the size of a cell ("granules") with the scattered light intensity from a whole cell, we have attempted to predict the optimum angular regions in which to detect granulation and other internal structures.

Kidney cells

Cultured cells of embryonic human kidney origin are not as well characterized in terms of their internal structure. There exist five major cell types with differing morphologies. Photomicrographs of these different cell types are shown in Figure 1. The small and large epithelial cells are between 8 and 12 μm and 14 and 20 μm, respectively, when in suspension. The domed cells are similar in size to the large epithelial cells and form hemispherical domes above the substratum when in culture. The fenestrated cells are also of similar size to the large epithelial cells and in culture develop with "holes" which

penetrate through the cytoplasm (cytoplasm intact). The fibroblastic cells are in the 8 μm to 12 μm size range. In addition, when the cells are viewed in suspension by phase contrast microscopy there are large refractile cytoplasmic inclusions although they do not appear to be associated with any particular cell type. Even though no details of internal structural differences are known, the expression of different morphologies in culture should be indicative of differing internal structure. In addition different cultures are known to produce differing amounts of the proteolytic enzyme, urokinase, a plasminogen activator. This differential production of urokinase is an indication of different degrees of differentiation in the different cultures and might be reflected in differing morphologies or internal structure (10). Even in those cases, such as the kidney, where the morphological and structural differences are less distinct than in the pituitary scattered light measurements should still be able to distinquish different cell types.

Materials and Methods.

Numerical Procedures.

Intracellular granules were modeled as homogeneous spheres and cells were modeled as coated spheres. All scattered light distributions were calculated using Mie theory (15,55). The homogeneous and coated sphere calculations were carried out using the routines, "BHMIE" and "COAT" (15), respectively. Additional routines for calculating and plotting the results were written in Fortran IV as needed and utilizied the above programs as callable subroutines. The integrations contained in Tables 2-5 were performed by Simpson's rule. All calculations were carried out on the IBM System 370 Model 3033 computer at the Pennsylvania State University. Angular distributions of scattered light were calculated for granules (homogeneous spheres) with diameters of 200, 300, 400, 600, 1000 and 1400 nm. Sizes and N/C ratios of cells (coated spheres) calculated were the same as in Chapter 4. All calculations were carried out for an incident wavelength of 488 nm.

The index of refraction of the core and coat in the coated sphere cell model were the same as those used in Chapter 4. Two indices of refraction were chosen for the granules. An index of refraction of 1.392 was used to simulate lysosomal type inclusions (300, 600, 1000, and 1400 nm) which were assumed to have an index of refraction similar to that of the nucleus. An index of refraction of 1.459 was used to simulate granules which contain predominately protein, such as the granules of the pituitary. Protein crystals are known to contain 20% to 70% water by volume (12). This implies that protein crystals are 30% to 80% protein. The dry weight density of proteins is between 1.05 and 1.20 (12). The specific refractive increment, dn/dc, is nearly constant for all proteins and has a mean value of 0.0018 (12,84). Assuming a value of 60% protein and a dry weight density of 1.15 in a typical granule gives an index of refraction of 1.459.

EPICS V cell sorter modifications

Two modifications were made to the Coulter Electronics, Inc. (Hialeah, Florida) EPICS V cell sorter to enhance the measurement of scattered light in forward angular intervals. The standard forward angle detector normally integrates the scattered light pulse because of the self-integrating nature of the large surface photodiodes used for detection. A 1K ohm resistor was placed in parallel with the parallel 100K ohm resistor-500 picofarad capacitor pair in the feedback loop of the integrating forward angle light scatter pre-amplifier. This yielded an approximate peak pulse. In addition the forward angle light scatter amplifier was altered to increase the bandwidth or slew rate of the amplifier. The list of modifications is given in Appendix 1. It should be noted that the implementation of these modifications voids the warranty from Coulter

Electronics, Inc. on these modules.

Kidney cells

Primary human fetal kidney cells were obtained from Microbiological Associates, Walkersville, Md. Cells were grown in DMEM-F12 media containing 10% fetal calf serum, and 1%antibiotic- antimycotic. Powdered media were obtained from Gibco Laboratories, Grand Island, N.Y. Cells were maintained in a 5% CO2 wet incubator and were passed at a split ratio of 1:2 at confluence. Kidney cells were removed for cell sorting by trypsinization and were pippeted until a single cell suspension was obtained. Cells were sorted on the Coulter Electronics, Inc. EPICS V cell sorter with the 76 μm quartz tip based on the integrated 90° and peak forward angle scatter signals and collected into 15 ml sterile Petri dishes containing media. The cells were then allowed to attach and at 24 hours were examined by microscopy to determine the morphological types. The cells were then placed on production media developed in this laboratory (phosphate buffered saline containing high glycine, lactate dehydrolysate and human serum albumin) and allowed to grow 48 hours. At this time media samples were taken to be assayed for urokinase. Urokinase levels were measured by the fibrin plate assay of Marsh and Gaffney (54). The fibrin plates were xeroxed and the area of the lysis zones measured.

Results.

Angular dependance of scattering by cells and granules.

In Figure 2 the scattered light intensity versus scattering angle is plotted for a 12 μm sphere ("cell") with a 6 m core ("nucleus") and for 4 small homogeneous spheres ("granules") with an index of refraction of 1.392 using an incident wavelength of 488 nm. For scattering angles between 10 and 40 the scattered light intensity from a "granule" is about 10 -0.05 that of the light scattered from a "cell". At higher or lower scattering angles the "granule" and "cellular" scattered intensities differ by as much as a million-fold. It should be noted that the coincident minima in granule scatter occuring between 50°and 60° and between 115° and 135° is probably not due to a monotonic behavior of the scattered light intensity with granule size but rather occurs due to the even seperation between granule sizes chosen for calculation. When this even seperation is broken, as in the case of the 300nm "granule", other sizes would have their maxima and minima in these regions, respectively. Certainly the conclusion from this graph is that unlike the case for gold particle scattering the scattering angles greater than 60° may not neccessarily be the optimum interval in which to detect granulation or internal structure in cells. In Figure 3 is plotted the scattered light intensity versus scattering angle for four sizes of "granules" having an index of refraction of 1.392 and three sizes having an index of refraction of 1.459. For both values of index of refraction, the scattering patterns of "granules" with diameters less than 400 nm have very little structure at scattering angles less than 60° and, at most, have only one minimum over the entire range of scattering angles. The scattering intensities of "granules" of 400 nm or less varies over 1000 fold from 0° to 180° and over a million-fold for the larger "granules".

Effect of cell size and nuclear size on the detectablity of structure.

The effect of whole cell size and N/C ratio on the scattered light intensity from a single cell is of equal importance in investigating the effects of internal structure as it is on the detectability of immunogold stained cells. The large variations in both N/C ratio and whole cell size will also be expected in experiments that study granulation and internal structure. The effects of N/C ratio and cell size on the detection of granulation is illustrated in Figure 4. The scattered light intensity is plotted versus

scattering angle for "cells" of 15 μm (N/C=0.5) and 8 μm (N/C=0.5,0.75) diameter and for three sizes of "granules" with an index of refraction of 1.459. From the top two panels of this figure it can be seen that a change in whole "cell" size from 8 μm to 15 μm leads on the average to a five fold greater separation between "granules" and "cells" in the scattering angle range of 95° to 130°. A typical effect of changes in the N/C ratio is shown in the bottom two panels of Figure 4. When the nucleus of an 8 μm "cell" is increased from 4 to 6 μm there is a twenty fold reduction in the average separation between "granules" and "cells" in the 95 to 130 interval. This set of results illustrates that changes in either whole cell size or in the N/C ratio can lead to order of magnitude differences in the relative scattered light intensity of "cells" compared to "granules".

Optimum angular interval for detection of granulation

In order to systematically investigate whether or not there would be an angular interval optimum for the detection of granules, the scattered intensities in nine angular intervals vetween 0° and 178° were calculated. The results of these integrations for 8, 10, 12, and 15 m spheres with N/C ratios of 0.5 and 0.75 and for "granule" spheres of 300, 600, 1000, and 1400 nm with an index of refraction of 1.392 are presented in Table 2. The results for the same "cell" sizes and for "granules" of 200, 400, 600, and 1000 nm with an index of refraction of 1.459 are given in Table 3. As was pointed out in Chapter 4 it is important to note that at scattering angles greater than 70 changes in the N/C ratio can have up to a hundred fold effect on the scattered light intensity from a "cell". The N/C ratio has little effect at angles less than 60°, and the effect at higher angles oscillates with "cell" size, having little effect for "cell" diameters of 10 and 15 μm and a large effect at 8 and 12 μm. As the calculations showed in Chapter 4 these oscillations in N/C ratio can be shifted to different cell sizes by altering the incident wavelength of light.

The variation in the scattered intensity within any angular interval for "granules" from 300 to 1000 nm with n=1.392 is between 10X and 500X for the intervals studied. The largest variations occur at the smaller scattering angles. For example, in the 10°-20° region there is a 500 fold change in intensity and in the 70°-110° interval there is only a 7 fold change in intensity. A similar range in intensities is seen for 200-600 nm "granules" with an index of refraction of 1.459. The "cellular" scattered intensities vary over a similar range, but the largest differences tend to occur at the higher angles. None of the angular intervals tends to always give the maximum value of "granule" to "cellular" scattered intensities. Although not always providing the optimum detection the angular intervals between 25° and 110° (excepting 95° -115°) do not tend to include the worst case ratios ($\geq 10^4$) of "cell" to "granule" scattered intensity.

Four tables will serve to clarify the effects of scattering angle, cell size, N/C ratio, granule size and granule number. In Tables 4-7 the ratio of the scattered light intensity within a given angular interval of a "cell" compared to a "granule" is given. Tables 4 and 5 are for a "granule" index of refraction of 1.392 and diameters of 300 and 1000 nm and Tables 6 and 7 are for a "granule" index of refraction of 1.459 and diameters of 400 and 1000 nm. This ratio of intensities gives the number of "granules" that would be required to double the intensity of a "cell" containing "granules" over that of a "cell" which did not contain "granules". Examining the 1.392 index of refraction "granules" the 45 -60 angular interval requires the smallest number of 300 nm "granules" per "cell" when the results are averaged over all the cell sizes. When the larger "granule" size is examined then the region of the smallest

ratio is in the 10°-20° interval. At the even larger size of 1400 nm the results (data not shown) within the 10°-60° regions are very similar. For an N/C ratio of 0.75 and for the smaller "granules" the intervals of 25°-35°, 45°-60°, and 70°-110° would all be reasonable for the detection of granules. For an N/C ratio of 0.75 and the larger "granules" the region between 10° and 35° is optimum but the entire range from 10°-130° is acceptable (only exception is for a "cell" diameter of 15 μm and scattering angles of 45°-130°). For this lower index of refraction examination of the tables shows that less than 400-500 300 nm "granules" would alter the scattering intensity from a whole "cell" and that for 1000 nm "granules" less than 25-50 would be required. The calculations for the higher index of refraction "granules" show similar results. The optimum regions when averaging over all the "cell" sizes are the 25°-35° and the 10°-20° intervals for the 400 and 1000 nm diameter "granules", respectively. For an N/C ratio of 0.75 and a "granule" size of 400 nm the entire angular region from 25° to 160° would require less than 400 "granules" with only six exceptions to alter the scattered intensity from a "cell" (average=127). For a "granule" size of 1000 nm with only one exception less than 400 "granules" would be required to double the scattered intensity of a "cell" (average=71).

In conclusion, although no angular interval stands out as vastly superior to all others, the optimum regions occur for scattering angles of 10° to 60°. For the smaller "granules" the optimum interval is in the upper portion of this range and as the size of the "granules" increases the optimum interval moves to the lower end of this range. It should be noted that for the smaller "granule" sizes the 10°-20° interval is poor. This range of scattering angles also has the advantage that it is affected less by changes in the N/C ratio than regions at higher angles. In many instances larger scattering angles provide adequate, and in specific cases superior, detection of granulation. If the experimental system has a narrow range of cell sizes and a constant N/C ratio (preferably large) then the use of larger scattering angles could prove beneficial.

Kidney cell sorting

The relationship of these light scatter calculations to experimental data obtained with live cells was examined in cell sorting experiments with embryonic human kidney cells in which the different cell types were sorted on the basis of 70°-110° and 2.5°-19° scattered intensity and examined microscopicly to determine the different cell types. The sorted fractions were also assayed for urokinase production using the fibrin plate method. It was found, that even in this case of less distinct differences in structure, enrichments of cells differing in morphology and function could be made based on these measurements. Cell populations with increased 70°-110° scattered light intensity were found to produce higher levels of urokinase and large epithelial cell were found to be enriched in cell populations with high 70°-110° and 2.5 -19 scattered light intensities. In Figure 7 is shown a plot of the number of kidney cells (counted on the z-axis) versus their forward angle scattered light intensity (2.5 -19) and their integrated 90° scattered light intensity. The population consists of a single ridge of cells running at approximately 45° to either the forward angle or 90° scattered light axis with a slightly greater increase in 90° scattered light intensities at the high forward angle intensities. In Figure 8a and 8b contour plots of these same parameters are shown with the brighter shades corresponding to the higher cell counts and with sort windows labeled as in Figure 6. In Table 9 are presented the results of the microscopic identification of the different cell morphologies contained in each sorted fraction. The data are presented as percentages and the sort windows are labeled as before. Again the sorted fractions are listed in the

table in order of increasing 90° scattered light intensity. In progressing from sort window BL to AR there are nearly equal increases in both the forward angle and 90° scattered intensities and the percentage of small epithelial cells decreases from 95% to 72% while the percentage of large epithelial cells increased from 3% to 20%. The BR sort window had a slightly higher forward angle intensity and a much higher 90° scattered intensity than the AR window. Within this window the small epithelial cells decreased to 37% while the large epithelial cells increased to 57%. The scattering intensities defining this window would indicate that this enrichment was not solely due to size. If the cell types, fenestrated and domed, which exhibit more structure are combined, then we see a three fold enrichment in the high 90° scattered intensity fractions (AR and BR) over the low 90° scattered intensity fractions (AL and BL). Media samples taken from cultures established from each of the sorted fractions were assayed for urokinase production by the fibrin plate method. The samples from the sorted fractions BL, BR and AR produced areas of 227, 276 and 330 mm , respectively. This result indicated that as the 90 scattered intensity increased the urokinase production also increased.

The results of this experiment are not as easily compared with the theoretical calculations as in the case of the pituitary results (1). However, the increase in both forward angle and 90° scattered light intensities as the size of the cells increased is certainly in aggreement with the conclusions of references (2 and 4). In addition the phenotype of urokinase secretion into the media is an example of differentiated function and is probably accompanied by some internal structural changes. If this is true then the association of increased urokinase production with increased 90 scatterd light intensity would be consistent with the predictions of Chapter 5. In any case these results demonstrate that even when structural differences are not easily defined in terms of dense granulation, intensity measurements can still serve to seperate cells based on differentiated function.

Discussion

The theoretical calculations of this study indicate that although no angular interval is vastly superior for the detection of granulation and internal structure for all cell sizes, N/C ratios and granule sizes, the angular region from 10° to 60° is, in general, optimum. The prediction that the higher angular intervals in this region are optimum for the smaller granules and that the lower intervals are optimum for the larger granules could prove interesting experimentally. However, due to the dependance of the scattered light intensity on whole cell size as well as granulation within this region, the use of an independant measure of whole cell size (24,51) might need to be incorporated in order to fully utilize this property. Depending on N/C ratio and cell size in some cases sensitivity could be gained by making measurements at scattering angles greater than 90°. But due to the strong dependance of whole cell scattered intensity on N/C ratio at certain cell sizes within this anglular region, if these parameters are broadly distributed within the sample, any benefits gained for one cell size or N/C ratio would be lost for another.

The theoretical work in this study would suggest that improvements in the separation of the kidney cell populations could be achieved by the use of scattered light intensity measurements within other angular intervals. The calculations would suggest that an improvement could be realized by measuring in the 10° to 60° interval. By making measurements at several intervals within this range one could take advantage of the observation that the optimum shift for different granule sizes occurs at different intervals within this range. The maximum benefit from this might be achieved if an independent measure of cell size (24,51) were also used. Examination of Tables 4-7 would also indicate

that due to the large size of some of these cell types that the use of scattering angles greater than 90 in addition to 10 to 60 might aid in the seperation of the different cell populations. Unfortunately due to the difficulty of installing sensors in these angular intervals on commercial instruments, such as the EPICS V, these experiments could not be performed.

Practically, the results of these calculations suggest that in experimental situations an array of detectors would be useful. Although in general the detection of the scattered light intensity at several intervals within the 10 to 60 region would be sufficient, there are many examples where increased sensitivity could be acheived at other angles. The ability to measure at many different angular intervals would allow the experimenter to empirically select the optimum intervals for the varying conditions of cell size, N/C ratio, granule size and internal structure from sample to sample. The feasibility of making scattered light measurements at many different intervals in flow cytometry has been demonstrated (6,64,71,72). The implementation of simplified versions of these techniques in conjunction with independant measurements of cell size could potentially improve the usefulness of flow cytometry in the study of the internal structure of cells. The use of other incident wavelengths could also be helpful. The experiments carried out in this work served to demonstrate that the use of the scattered light intensity in the 70 to 110 interval could prove useful in separating cells based on internal structure, morphology and function. Whether or not the instrumet changes suggested by this work would experimentally lead to the anticipated enhancements will have to wait for further experimentation.

BIBLIOGRAPHY

6. Bartholdi M, Salzman GC, Hiebert RD, Kerker M: Differential light scattering photometer for rapid analysis of single particles in flow. Appl Opt 19:1573, 1980.

9. Benson NC, McDougal DC, Coffey DS: The use of multiparameter flow cytometry to assess tumor cell heterogeneity and grade prostate cancer. Prostate 5:27, 1984.

10. Bernik MB, Kwaan HC: Origin of fibrinolytic activity in cultures of the human kidney. J Lab Clin Med 70:650, 1967.

12. Blundell . : Protein Crystallography

13. Bohmer RM, King NJC: Flow cytometric analysis of immunogold cell surface label. Cytometry 5:543, 1984.

15. Bohren CF, Huffman DR: Absorption and scattering of light by small particles. John Wiley and Sons, New York, NY, 1983.

16. Brunsting A, Mullaney PF: Light scattering from coated spheres: model for biological cells. Appl Opt 11:675, 1972.

17. Brunsting A, Mullaney PF: Differential light scattering from spherical mammalian cells. Biophys J 14:439, 1974.

24. Fulwyler MJ, Glascock RB, Hiebert RD, Johnson MH: Device which separates minute particles according to electronically sensed volume. Rev Sci Instr 40:42, 1969.

28. Goolsby CL: Application of light-scattering theory to flow cytometry of stained cells. M.S. dissertation, Pennsylvania State University, University Park, Pa, 1984.

36. Jamieson AM, Walton AG, Schafer IA

37. Jensen RH: Chromomycin A3 as a fluorescent probe for flow cytometry of human gynecologic samples. J Histochem Cytochem 25:573, 1977.

39. Kaplow LS, Adams LR: Instrumental differentiation of suspended leukocytes stained for peroxidase by the benzidine dihydrochloride technique. J Histochem Cytochem 21:411, 1973.

40. Kaplow LS, Dauber H, Lerner E: Assessment of monocyte esterase activity by flow cytophotometry. J Histochem Cytochem 24:363, 1976.

50. Leary JF, Kotter MFD, Todd P: Laser flow cytophotometric immunoperoxidase detection of herpes simplex virus type 2 antigens in infected cultured human cells. J Histochem Cytochem 24:1249, 1976.

51. Leary JF, Todd P, Wood JCS, Jett JH: Laser flow cytometric light scatter and fluorescence pulse width and pulse rise-time of mammalian cells. J Histochem Cytochem 27:315, 1979.

52. Loken MR, Sweet RG, Herzenberg LA: Cell discrimination by multiangle light scattering. J Histochem Cytochem 24:284, 1976.

54. Marsh MA, Gaffney PJ: The rapid fibrin plate-a method for plasminogen activator assay. Thrombos Haemostas (Stutg) 38:545, 1977.

55. Mie G: Beitrage zur optik truber medien, speziell kolloidaler metallosungen. Ann Physik 25:377, 1908.

62. Nielsen O, Larsen JK, Christensen J, Lenmark A: Flow sorting of mouse pancreatic B cells by forward and orthogonal light scattering. Cytometry 3:177, 1982.

64. Price BJ, Hollman VH, Salzman GC: Light-scatter analysis of microalgae. correlation of scatter patterns from pure and mixed asynchronous cultures. Biophys J 22:29, 1978.

65. Rabinovitch A, Russell T, Shienvold F, Noel J, Files N, Patel V, Ingram M: Preparation of rat islet B-cell-enriched fractions by light-scatter flow cytometry. Diabetes 31:939, 1982.

71. Salzman GC, Crowell JM, Goad CA, Hansen KM, Hiebert RD, LaBauve PM, Martin JC, Ingram ML, Mullaney PF: A flow-system multiangle-light-scattering instrument for cell characterization. Clin Chem 21:1297, 1975.

72. Salzman GC, Crowell JM, Hansen KM, Ingram M, Mullaney PF: Gynecologic specimen analysis by multiangle light scattering in a flow system. J Histochem Cytochem 24:308, 1976.

73. Salzman GC, Crowell JM, Martin JC, Trujillo TT, Romero A, Mullaney PF, LaBauve PM: Cell classification by laser light scattering: identification and separation of unstained leukocytes. Acta Cytol 19:374, 1975.

75. Schafer IA, Jamieson AM, Petrelli M------:Multiangle light scattering flow photometry of cultured human fibroblasts. Comparison of normal cells with a mutant line containing cytoplasmic inclusions. J Histochem Cytochem

84. Visser JWM, Cram LS, Martin JC, ------: Sorting of a murine granulocytic progenitor cell by use of laser light scattering measurements. In Proceedings of the International Conference on Pulse Cytophotometry, 1977.

Table 2.
Integrated scattered light intensities in seven angular intervals for "granules" with diameters of 300, 600, 1000 and 1400 nm and an index of refraction of 1.392. The intensities for spheres with diameters of 8, 10, 12 and 15 μm and N/C ratios of 0.5 and 0.75 are also tabulated.

granule size (nm)	θ interval 10-20	25-35	45-60	70-110	95-115	115-130	130-160	
300	$.23\times10^{1}$	$.17\times10^{1}$	$.12\times10^{1}$	$.36\times10^{0}$	$.20\times10^{-1}$	$.28\times10^{-2}$	$.36\times10^{-1}$	
600	$.11\times10^{3}$	$.31\times10^{2}$	$.64\times10^{0}$	$.13\times10^{1}$	$.31\times10^{0}$	$.38\times10^{0}$	$.24\times10^{0}$	
1000	$.11\times10^{4}$	$.14\times10^{2}$	$.45\times10^{1}$	$.31\times10^{1}$	$.68\times10^{0}$	$.11\times10^{1}$	$.25\times10^{0}$	
1400	$.29\times10^{4}$	$.13\times10^{3}$	$.15\times10^{2}$	$.87\times10^{1}$	$.26\times10^{1}$	$.17\times10^{1}$	$.69\times10^{0}$	
cell size (μm)								N/C ratio
8	$.25\times10^{5}$	$.67\times10^{4}$	$.99\times10^{3}$	$.33\times10^{4}$	$.16\times10^{4}$	$.13\times10^{4}$	$.41\times10^{4}$	0.5
	$.55\times10^{5}$	$.26\times10^{4}$	$.54\times10^{3}$	$.16\times10^{3}$	$.43\times10^{2}$	$.26\times10^{2}$	$.17\times10^{2}$	0.75
10	$.69\times10^{5}$	$.28\times10^{4}$	$.95\times10^{3}$	$.22\times10^{3}$	$.51\times10^{2}$	$.22\times10^{2}$	$.36\times10^{2}$	0.5
	$.85\times10^{5}$	$.37\times10^{4}$	$.80\times10^{3}$	$.24\times10^{3}$	$.86\times10^{2}$	$.52\times10^{2}$	$.75\times10^{2}$	0.75
12	$.13\times10^{6}$	$.74\times10^{4}$	$.32\times10^{4}$	$.44\times10^{4}$	$.23\times10^{3}$	$.18\times10^{3}$	$.56\times10^{4}$	0.5
	$.12\times10^{6}$	$.50\times10^{5}$	$.17\times10^{4}$	$.63\times10^{5}$	$.28\times10^{4}$	$.17\times10^{4}$	$.78\times10^{3}$	0.75
15	$.25\times10^{6}$	$.10\times10^{5}$	$.32\times10^{4}$	$.10\times10^{4}$	$.83\times10^{4}$	$.83\times10^{4}$	$.15\times10^{5}$	0.5
	$.15\times10^{6}$	$.68\times10^{4}$	$.72\times10^{4}$	$.45\times10^{4}$	$.19\times10^{4}$	$.17\times10^{4}$	$.56\times10^{4}$	0.75

Table 3.
Integrated scattered light intensities in seven angular intervals for "granules" with diameters of 200, 400, 600 and 1000 nm and an index of refraction of 1.459. The intensities for spheres with diameters of 8, 10, 12 and 15 μm and N/C ratios of 0.5 and 0.75 are also tabulated.

granule size (nm)	θ interval 10-20	25-35	45-60	70-110	95-115	115-130	130-160	
200	$.10\times10^{1}_{2}$	$.90\times10^{0}_{2}$	$.97\times10^{0}_{2}$	$.11\times10^{1}_{1}$	$.36\times10^{0}_{1}$	$.16\times10^{0}_{0}$	$.19\times10^{0}_{0}$	
400	$.59\times10^{2}_{3}$	$.34\times10^{2}_{3}$	$.10\times10^{2}_{3}$	$.16\times10^{1}_{1}$	$.14\times10^{1}_{1}$	$.75\times10^{0}_{1}$	$.52\times10^{0}_{0}$	
600	$.52\times10^{3}_{4}$	$.14\times10^{3}_{2}$	$.45\times10^{3}_{2}$	$.65\times10^{1}_{2}$	$.26\times10^{1}_{1}$	$.20\times10^{1}_{1}$	$.70\times10^{0}_{1}$	
1000	$.49\times10^{4}$	$.90\times10^{2}$	$.25\times10^{2}$	$.20\times10^{2}$	$.66\times10^{1}$	$.49\times10^{1}$	$.43\times10^{1}$	
cell size (μm)								N/C ratio
8	$.25\times10^{5}$	$.67\times10^{4}$	$.99\times10^{3}$	$.33\times10^{4}_{3}$	$.16\times10^{4}_{2}$	$.13\times10^{4}_{2}$	$.41\times10^{4}_{2}$	0.5
	$.55\times10^{5}$	$.26\times10^{4}$	$.54\times10^{3}$	$.16\times10^{3}$	$.43\times10^{2}$	$.26\times10^{2}$	$.17\times10^{2}$	0.75
10	$.69\times10^{5}$	$.28\times10^{4}$	$.95\times10^{3}$	$.22\times10^{3}$	$.51\times10^{2}$	$.22\times10^{2}$	$.36\times10^{2}$	0.5
	$.85\times10^{6}$	$.37\times10^{4}$	$.80\times10^{3}$	$.24\times10^{3}$	$.86\times10^{2}$	$.52\times10^{2}$	$.75\times10^{2}$	0.75
12	$.13\times10^{6}$	$.74\times10^{4}$	$.32\times10^{4}$	$.44\times10^{4}_{3}$	$.23\times10^{4}_{3}$	$.18\times10^{4}_{3}$	$.56\times10^{4}_{3}$	0.5
	$.12\times10^{6}$	$.50\times10^{4}$	$.17\times10^{4}$	$.63\times10^{3}_{5}$	$.28\times10^{3}$	$.17\times10^{3}$	$.78\times10^{3}_{5}$	0.75
15	$.25\times10^{6}$	$.10\times10^{5}$	$.32\times10^{4}$	$.10\times10^{5}$	$.83\times10^{4}$	$.83\times10^{4}$	$.15\times10^{5}$	0.5
	$.15\times10^{6}$	$.68\times10^{4}$	$.72\times10^{4}$	$.45\times10^{4}$	$.19\times10^{4}$	$.17\times10^{4}$	$.56\times10^{4}$	0.75

Table 4.
The ratio of the integrated scattered light intensity from one coated sphere ("cell") divided by that from one 300 nm "granule" with an index of refraction of 1.392 in seven angular intervals. Spheres with diameters of 8, 10, 12 and 15 μm and N/C ratios of 0.5 and 0.75 are tabulated.

cell size (μm)	θ interval 10-20	25-35	45-60	70-110	95-115	115-130	130-160	N/C ratio
8	10870	3941	825	9167	80000	464286	113889	0.5
	23913	1529	450	444	2150	9286	472	0.75
10	30000	1647	792	611	2550	7857	1000	0.5
	36957	2177	667	667	4300	18572	2083	0.75
12	56522	4353	2667	12222	115000	642857	155556	0.5
	52174	2941	1417	1750	14000	60714	21667	0.75
15	108696	5882	2667	27778	415000	2964286	416667	0.5
	65217	4000	6000	12500	95000	607413	155556	0.75

Table 5.

The ratio of the integrated scattered light intensity from one coated sphere ("cell") divided by that from one 1000 nm "granule" with an index of refraction of 1.392 in seven angular intervals. Spheres with diameters of 8, 10, 12 and 15 μm and N/C ratios of 0.5 and 0.75 are tabulated.

cell size (μm)	θ interval 10-20	25-35	45-60	70-110	95-115	115-130	130-160	N/C ratio
8	23	479	220	1065	2353	1182	16400	0.5
	50	186	120	52	63	24	68	0.75
10	63	200	211	71	75	20	144	0.5
	77	264	178	77	127	47	300	0.75
12	118	529	711	1419	3382	1636	22400	0.5
	109	357	378	203	412	155	3120	0.75
15	227	714	711	3226	12206	7546	60000	0.5
	136	486	1600	1452	2794	1546	22400	0.75

Table 6.
The ratio of the integrated scattered light intensity from one coated sphere ("cell") divided by that from one 400 nm "granule" with an index of refraction of 1.459 in seven angular intervals. Spheres with diameters of 8, 10, 12 and 15 μm and N/C ratios of 0.5 and 0.75 are tabulated.

cell size (μm)	θ interval 10-20	25-35	45-60	70-110	95-115	115-130	130-160	N/C ratio
8	424	197	99	2063	1143	1733	7885	0.5
	932	77	54	100	31	35	33	0.75
10	1170	82	95	138	36	29	69	0.5
	1441	109	80	150	61	69	144	0.75
12	2203	218	320	2750	1643	2400	10769	0.5
	2034	147	170	394	200	227	1500	0.75
15	4237	294	320	6250	5929	11067	28846	0.5
	2542	200	720	2813	1357	2267	10769	0.75

Table 7.

The ratio of the integrated scattered light intensity from one coated sphere ("cell") divided by that from one 1000 nm "granule" with an index of refraction of 1.459 in seven angular intervals. Spheres with diameters of 8, 10, 12 and 15 μm and N/C ratios of 0.5 and 0.75 are tabulated.

cell size (μm)	θ interval 10-20	25-35	45-60	70-110	95-115	115-130	130-160	N/C ratio
8	5	74	40	165	242	265	954	0.5
	11	29	22	8	7	5	4	0.75
10	14	31	38	11	8	5	8	0.5
	17	41	32	12	13	11	17	0.75
12	27	82	128	220	349	367	1302	0.5
	25	56	68	32	42	35	181	0.75
15	51	111	128	500	1258	1694	3488	0.5
	31	76	288	225	288	347	1302	0.75

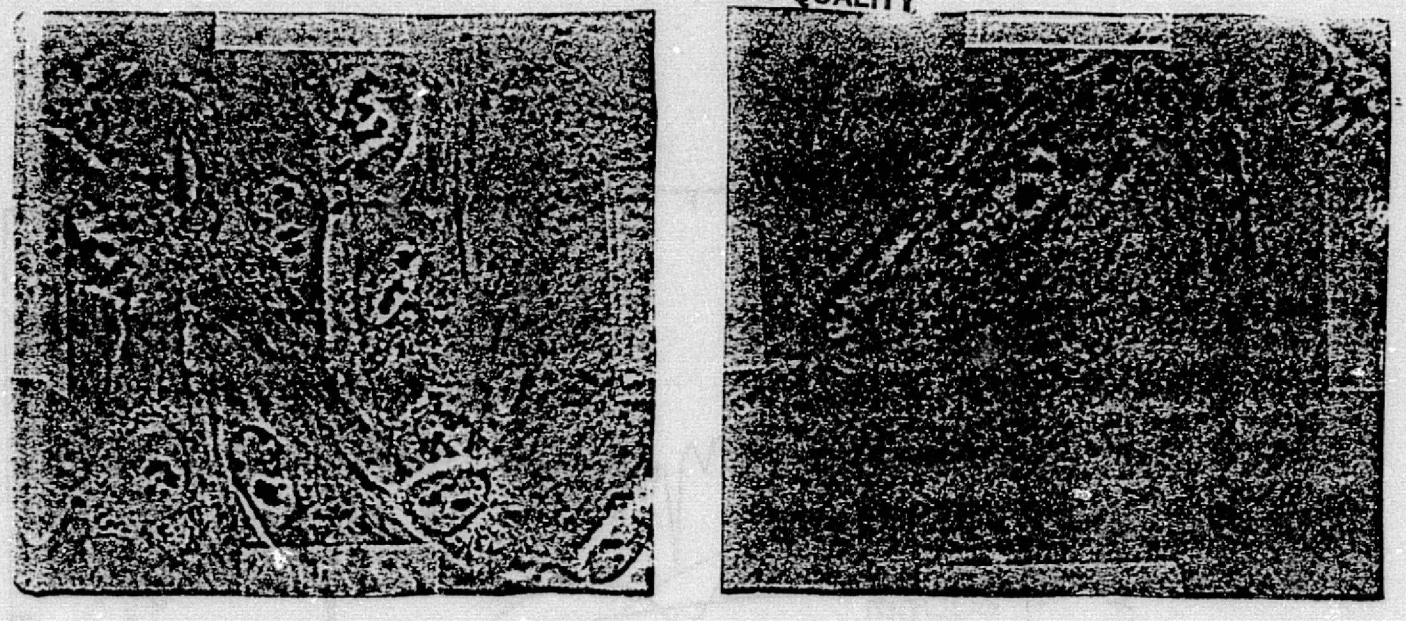

a b

FIG. 1. Photographs of the small epithelial (a), large epithelial (b), domed (c) and fenestrated (d) cells cultured from the human embryonic kidney.

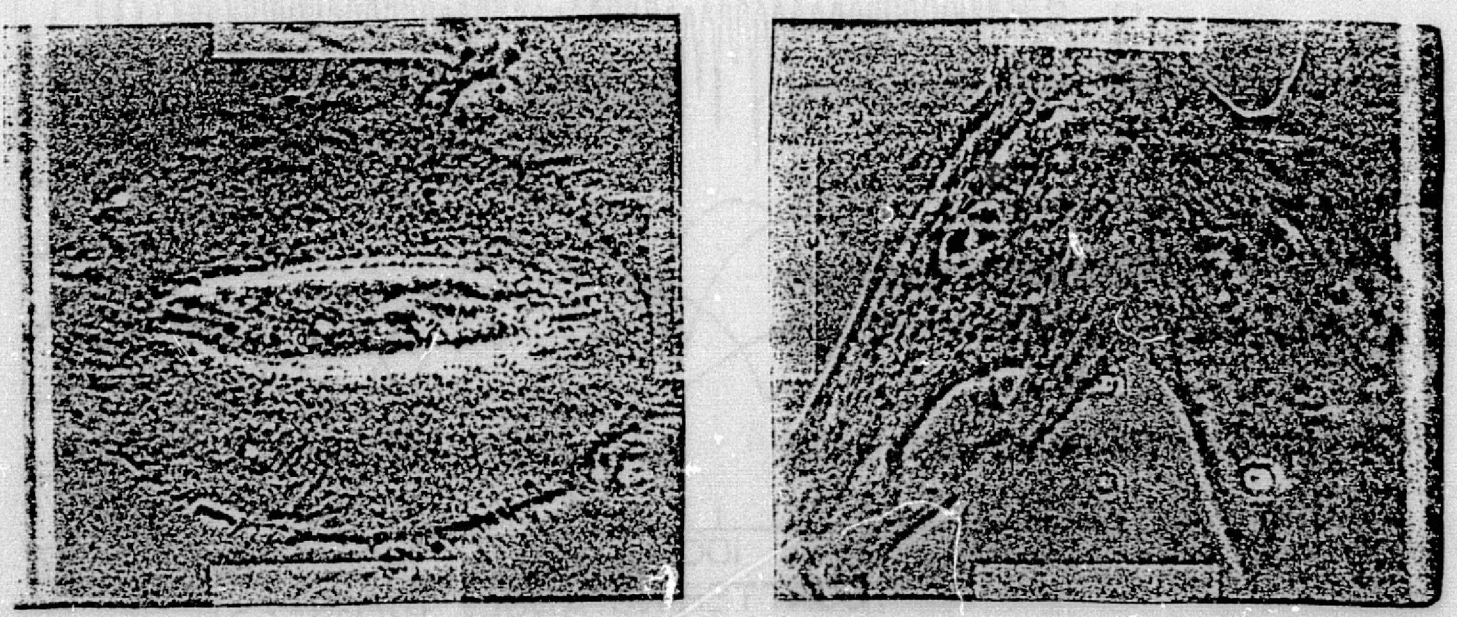

c d

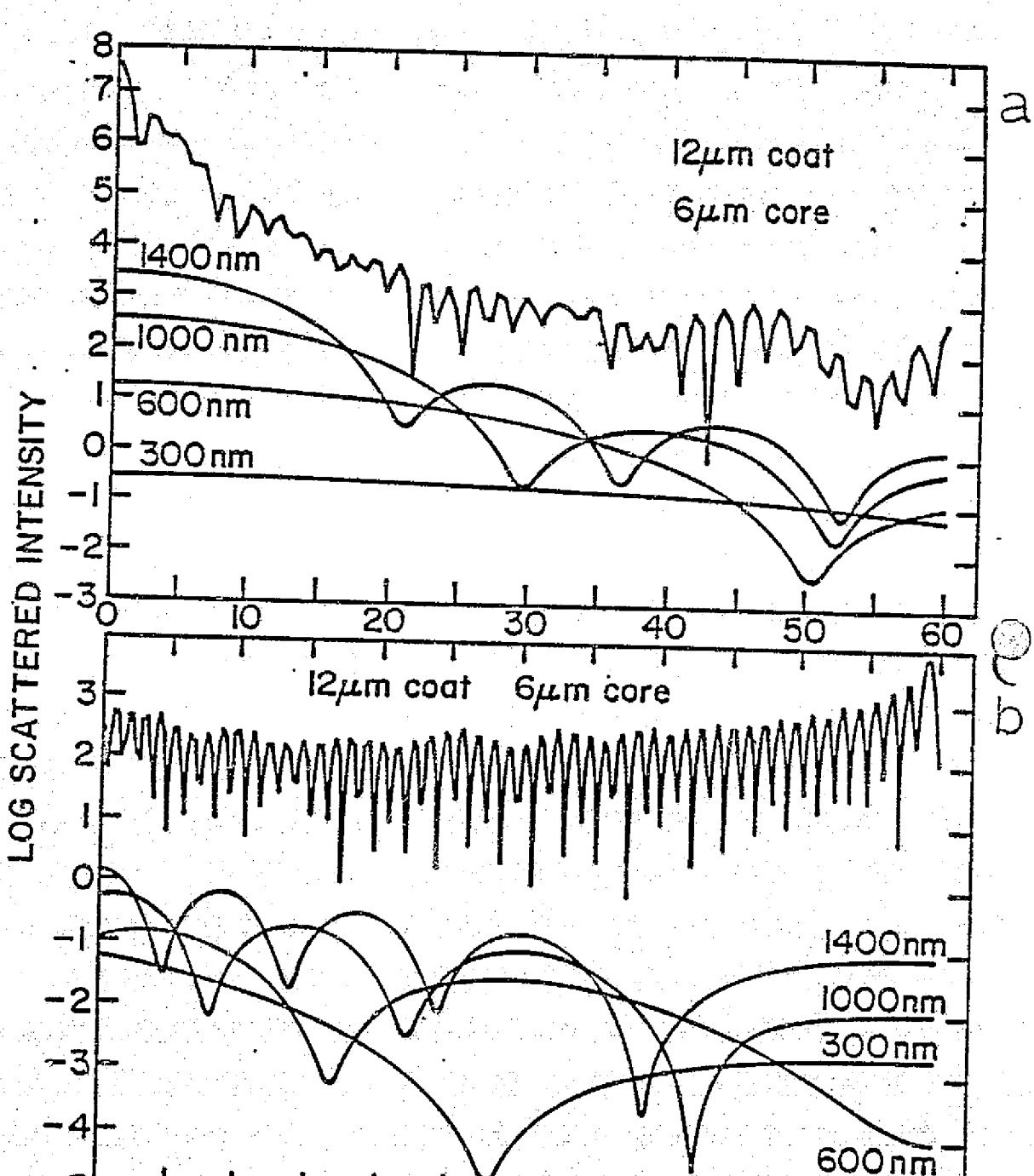

FIG. 2. Graph of the scattered light intensity versus scattering angle from 0°–50° and 60°–180° for a 12 μm sphere with a coat and a 6 μm core and two "granules" with diameters of 300, 600, 1200 and 1400 nm. The assumed index of refraction of the "granules" was 1.202.

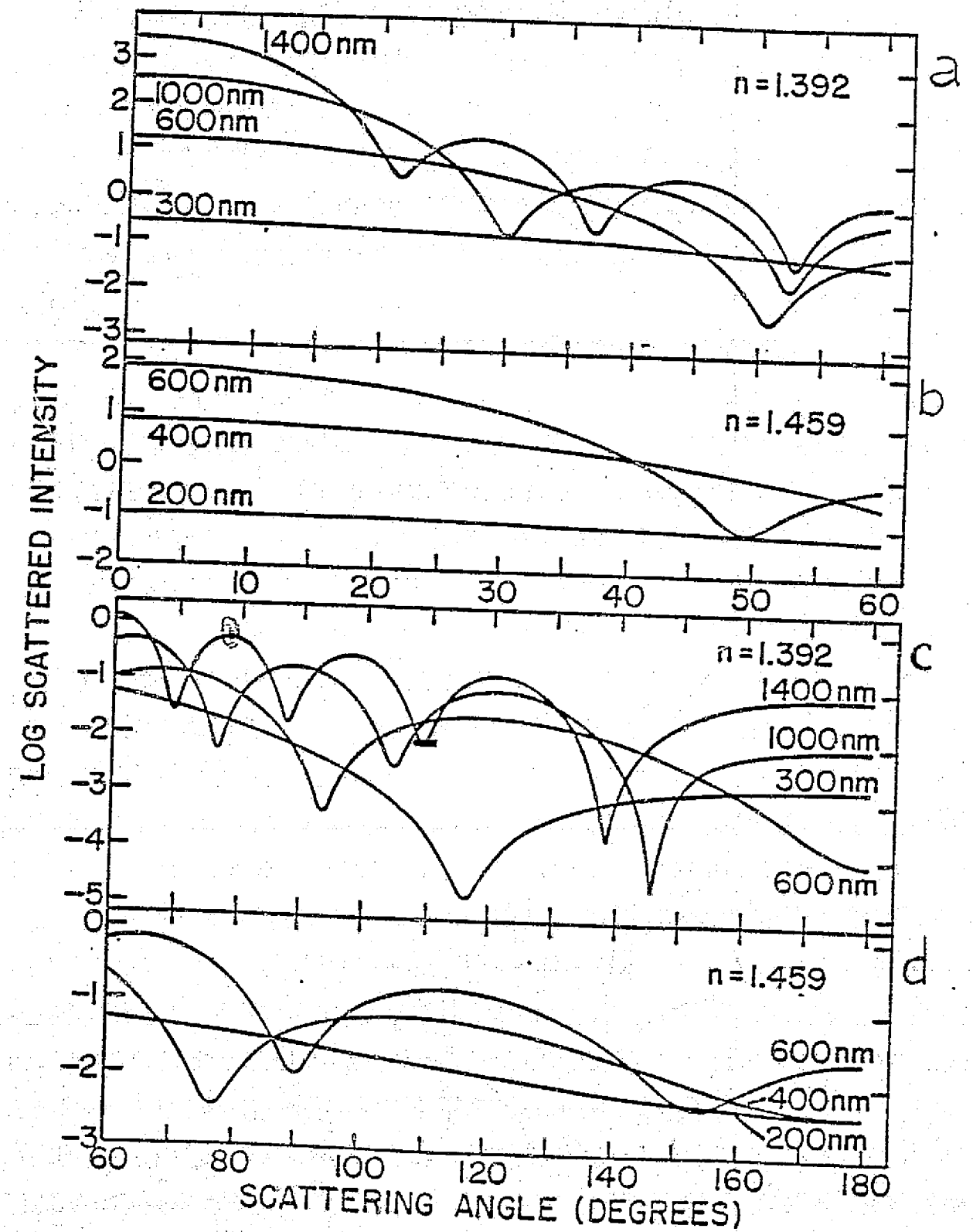

FIG. 3. Graph of the scattered light intensity versus scattering angle from 0°–60° and 60°–180° for "granules" with diameters of 300, 600, 1000 and 1400 nm and an index of refraction of 1.392 and for "granules" with diameters of 200, 400 and 600 nm and an index of refraction of 1.459.

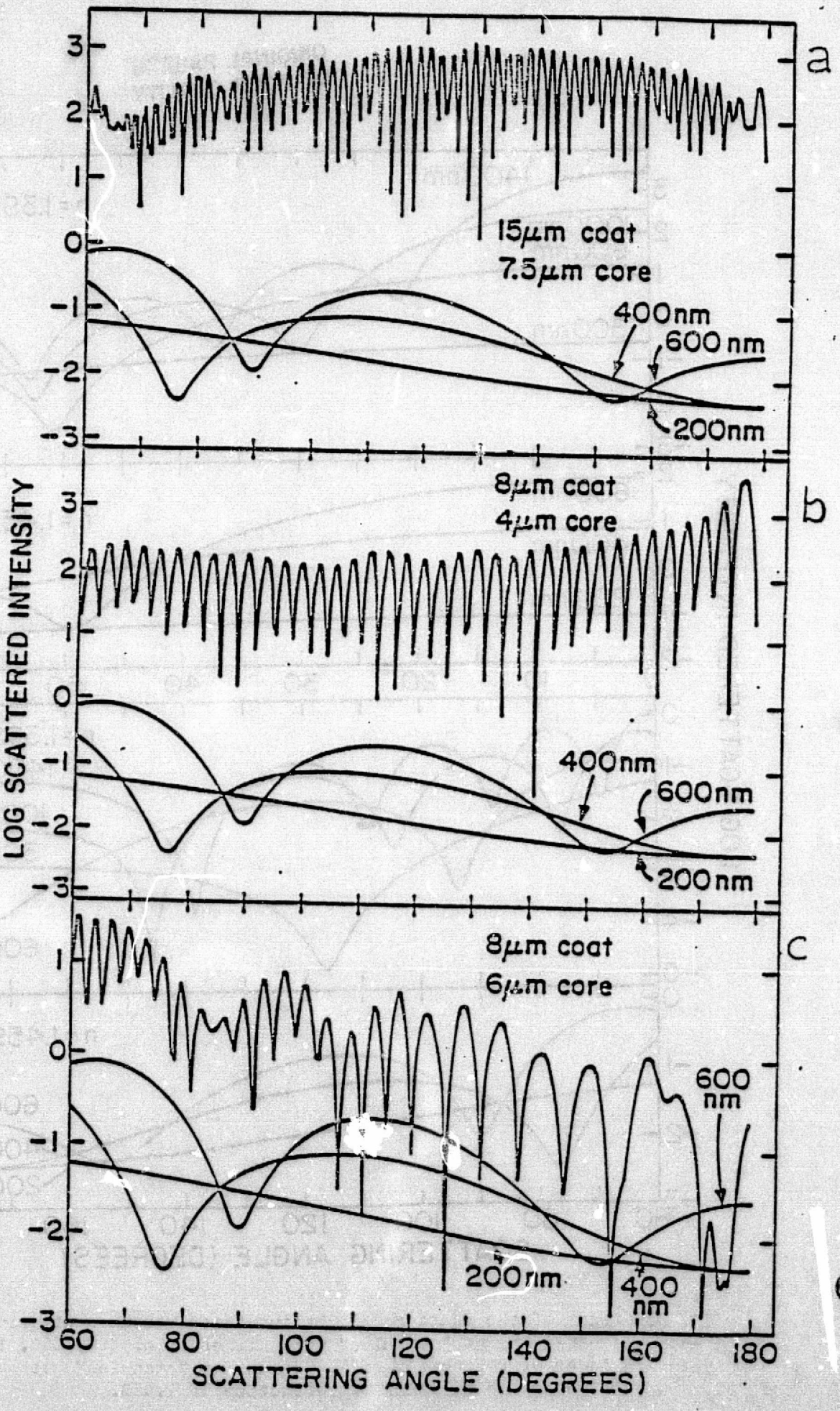

Graph of the scattered light intensity versus scattering angle [illegible] for a 15 μm sphere with a coat and a 7.5 μm core and a 8 μm sphere with a coat and 4 and 6 μm cores. Distributions for "granules" with [illegible] of 200, 400 and 600 nm and an index of refraction of 1.459 are also plotted.

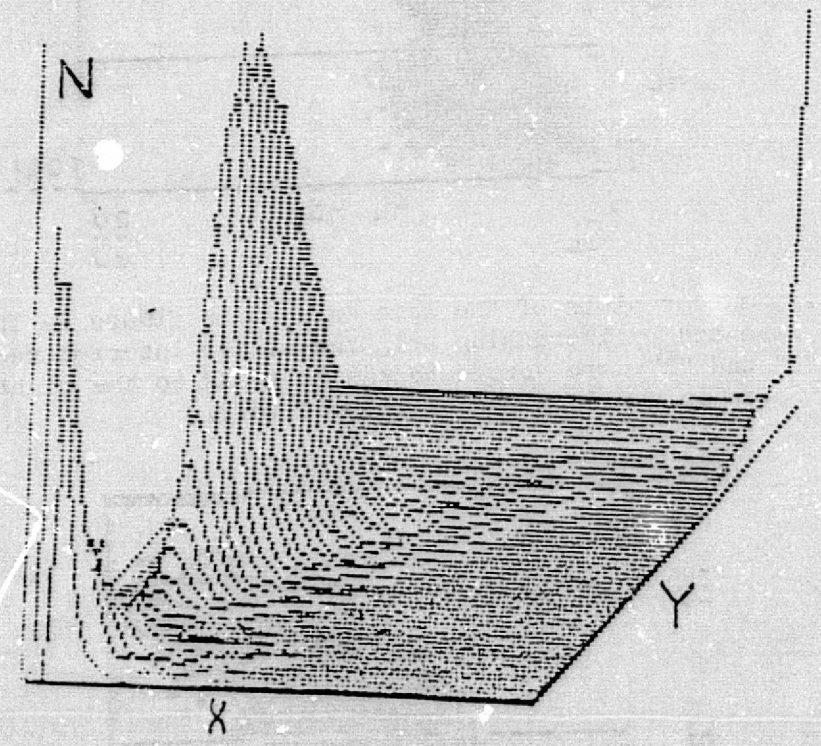

FIG. 7. Two-parameter distribution showing number of suspended kidney cells (vertical axis) as a function of both their scattered light intensity in the 70°-110° angular interval (integrated signal, x-axis) and the 2.5°-19° interval (y-axis).

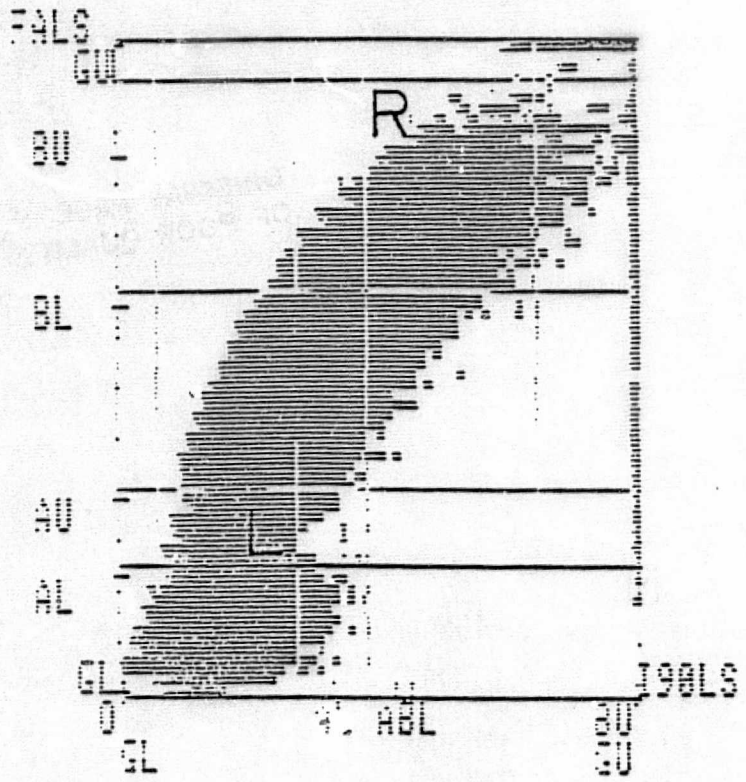

FIG. 8. Contour plots of the same data as in Figure 7. The number of cells is represented by increasing brightness. The interior rectangles containing "L" and "R" were sorted to the left and to the right, respectively. Sorts A and B are in panels a and b, respectively.

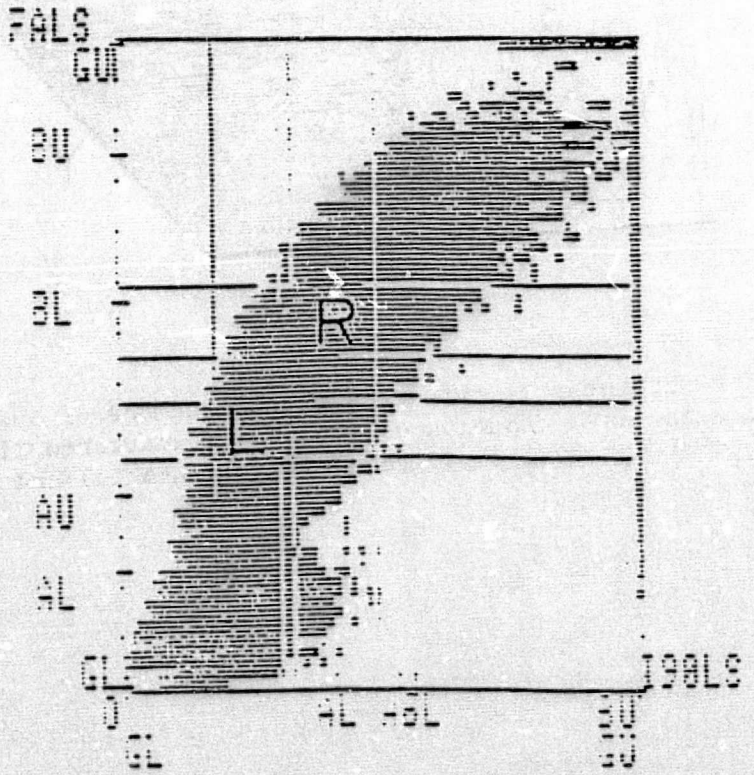

Chapter 31

Application of light scatter analysis to human embryonic kidney cell fractions separated on STS-8.

D25

FLOW CYTOMETRY OF HUMAN EMBRYONIC KIDNEY CELLS: A LIGHT SCATTERING APPROACH

M. Elaine Kunze[1], Charles Goolsby[1], Paul Todd[1], Dennis Morrison[2], and Marian Lewis[2]

[1]Althouse Laboratory, The Pennsylvania State University, University Park, PA 16802
[2]SD5/Bioprocessing Laboratory, L. B. Johnson Space Center, Houston, TX 77058

The mammalian kidney contains cells that transport water, convert vitamin D to active forms, synthesize hormones such as renin and erythropoietin, and produce enzymes such as urokinase, a plasminogen activator. Several of these functions are maintained by human embryonic kidney cells (HEK) cultivated in vitro. Biochemical study of these functions in their individual cell types in vitro requires purified populations of cells. Light-scattering activated cell sorting (LACS) was explored as a means of achieving such purifications. It was found that HEK cells at the first 1-5 passages in culture were heterogeneous with respect to 2-parameter light scattering intensity distributions, in which combined measurements included forward angle scattering (2.5-19°), 90° scattering, and time-of-flight size measurements. Size was measured at a resolution of 0.15 μm/channel in 256 channels using pulse-height independent pulse-width measurements. Two-parameter distributions combining these measurements were obtained for HEK cell subpopulations that had been purified by microgravity electrophoresis and subsequently propagated in culture. These distributions contained at least 3 subpopulations in all purified fractions, and results of experiments with prepurified cultured HEK cells indicated that subpopulations of living cells that were high in plasminogen-activator activity also contained the highest per cent of cells with high 90° light scatter intensity.

(Supported by National Aeronautics and Space Administration contract NAS 9-15584.)

INTRODUCTION

Cultured human kidney cells produce several products, such as renin, erythropoietin, vitamin D enzymes, urokinase (UK) and tissue plasminogen activator (TPA). This study focuses on flow cytometric analyses of fractions of cells obtained in an attempt to purify cells producing UK and TPA by microgravity electrophoresis. As there are four morphological subpopulations easily identified in cultures of human embryonic kidney cells (HEK) (domed, fenestrated, and large and small epithelioid cells) different types of cells should exhibit different light scatter properties. Electrophoretically separated kidney cells were therefore analysed on the EPICS V cell sorter to attempt to identify the various morphological types and to attempt to relate morphology to enzyme production.

MATERIALS AND METHODS

HEK cells obtained from MA Bioproducts were put into a single cell suspension using 0.05% trypsin and 0.37% EDTA in saline A and were analysed on the EPICS V cell sorter. Two-parameter 488nm light scatter distributions were obtained (forward angle light scatter and 90 deg integrated light scatter pulse) as well as 90-degree pulse-width "time-of-flight" for cell sizing. Two-parameter distributions combining these measurements were obtained for HEK cell subpopulations that had been purified by microgravity electrophoresis and subsequently propagated in culture.

HEK cells were purified by microgravity electrophoresis on space shuttle flight STS-8 (Barlow et al., 1985). Counts of viable cells were made on each sample. The cells were then plated for propagation in tissue culture. After allowing time for attachment and flattening, the medium was replaced with urokinase production medium (UKPM), and after several days the amount of urokinase per sample was determined. The resulting distribution of urokinase production among fractions, together with the number of viable cells in each fraction, is shown in Figure 3. Several fractions were further propagated, and the per cent of each morphological cell type was determined by phase contrast counting of 200 cells in each fraction.

RESULTS

The size measuring capability of the EPICS V sorter, which is a pulse height independent measure of pulse width using the unintegrated 90-degree light scatter signal (time of flight) was calibrated with different sizes of microspheres, and a resolution of 0.45 um/channel was obtained, as shown in Figure 1. Microscopic measurements of HEK cells were also performed using 9.5 um, 14.5 um and 20.5 um microspheres as standards. These results are shown in Figure 2, where it is seen that the majority of these passage-1 HEK cells are between 15 and 25 um in diameter.

The integrated 90-degree light scatter signal intensity reflects the internal structure of the cell, including granulation (Goolsby, Kunze and Todd, 1985), nuclear size (Brunsting and Mullaney, 1973), and shape (Latimer, 1978). Granular cells should scatter more light at 90-degrees than non-granular cells. Forward angle light scatter (2.5-19 degrees) is a measure of size and refractive index in live cells (Leary, Notter and Todd, 1978; Goolsby and Todd, 1985). Cells with a high refractive index have reduced forward angle light intensity.

Single cell suspensions of these fractions were analyzed on the EPICS V

cell sorter. Two-parameter distributions of integrated 90-degree light scatter vs time-of-flight, integrated 90-degree light scatter vs foward angle light scatter, and integrated 90-degree light scatter vs peak 90-degree light scatter were acquired. Two examples of these distributions are shown in Figure 4. Each distribution was divided into four regions (Figure 5), and the percentage of cells in each region was determined for each fraction (Figure 6).

A selected portion of these results, along with the uarokinase plus tissue plasminogen activator activity and the morphological observations are shown in the 3 graphs of Figure 7.

DISCUSSION

Results of these flow cytometric light scattering experiments with prepurified cultured human kidney cells indicate that subpopulations of living cells that were high in plasminogen activator activity also contained the highest percentage of cells with high 90-degree light scatter intensity.

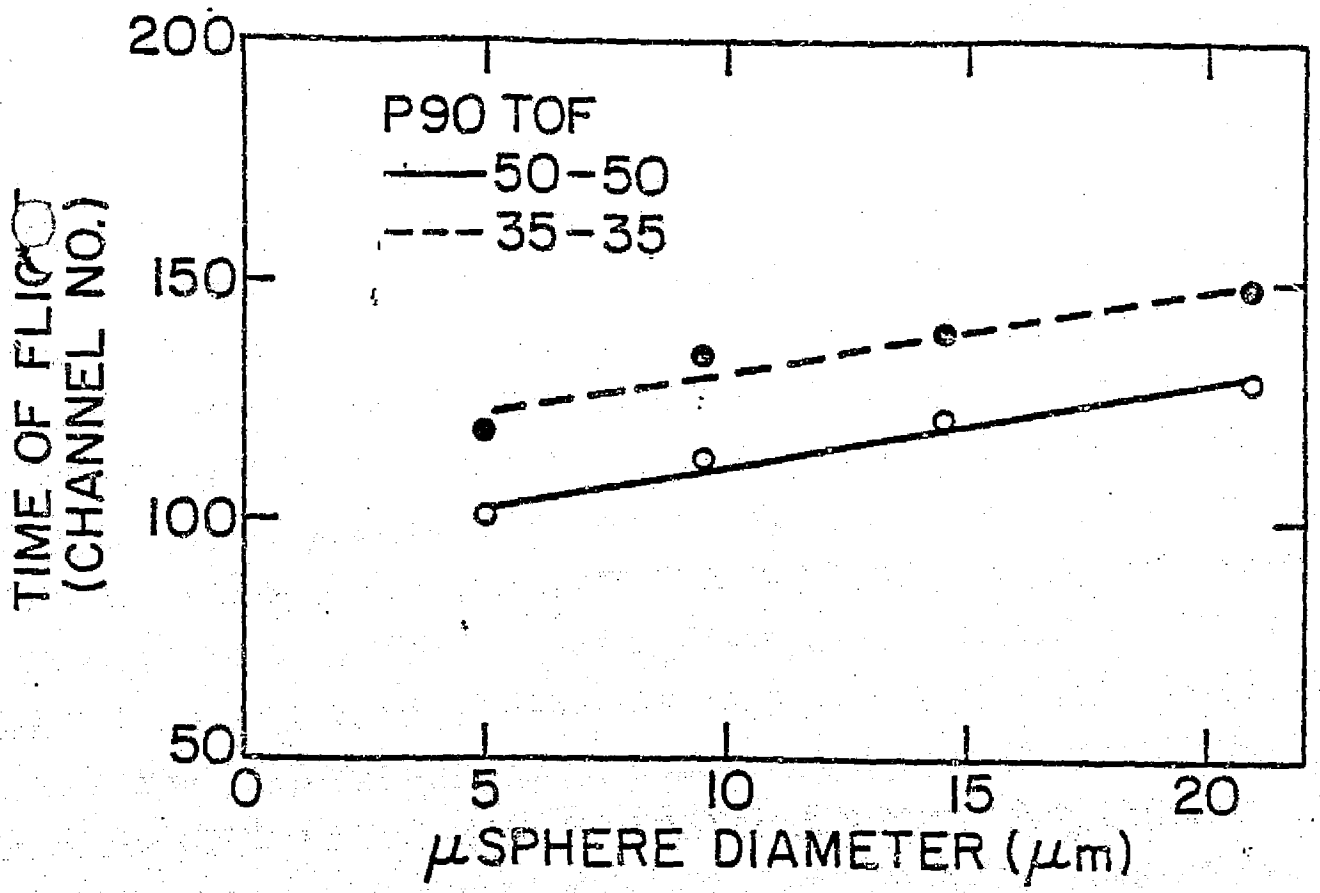

Figure 1. Calibration curve for pulse height independent time-of-flight sizing using 5, 10, 15, 20μm spheres. Pulse width measurements were made at 50% (solid line) and 35% (dashed line) of the peak height of the raw (unintegrated) 90-degree (70-110 degree) light scatter signal.

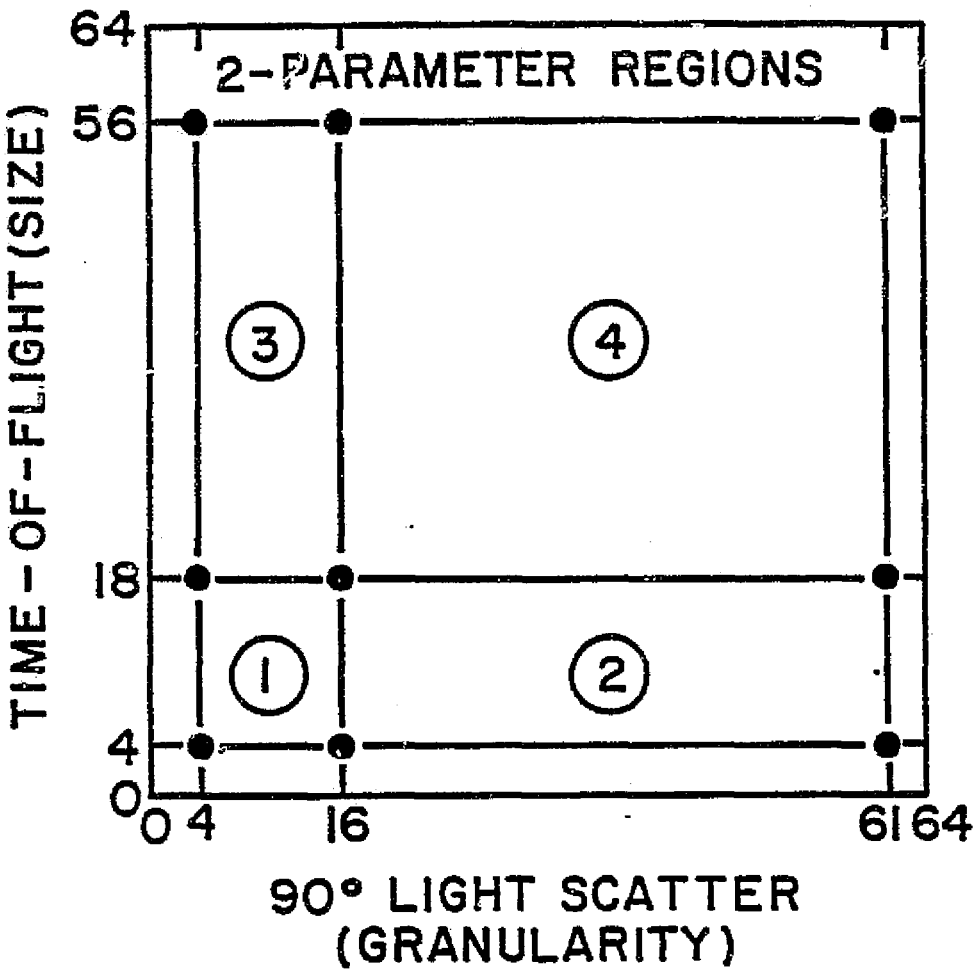

Figure 5. A diagram of the method of analysis of the histograms of the type shown in Figure 5. Each two-parameter histogram was divided into four regions, and the percentages of cells falling into each region was determined

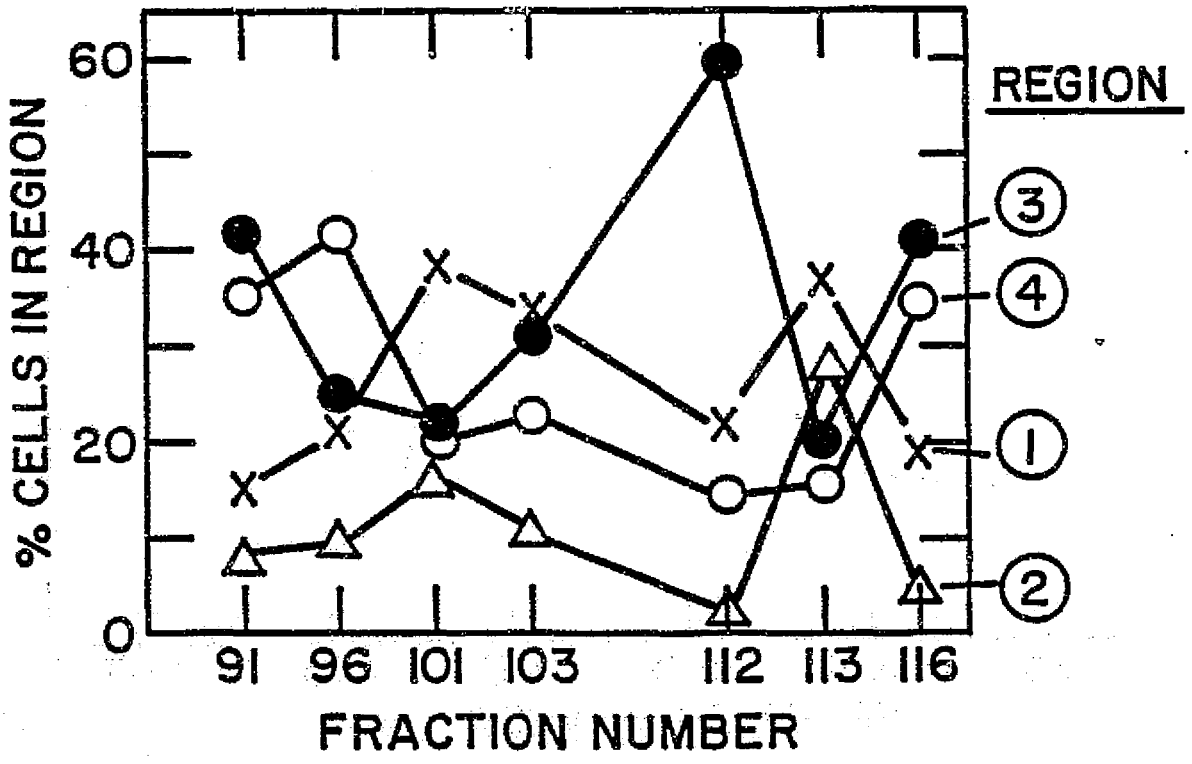

Figure 6. Percentages of cells falling into each of the 2-parameter regions displayed in Figure 5. Region 1 contained debris and was therefore eliminated from the further analysis.

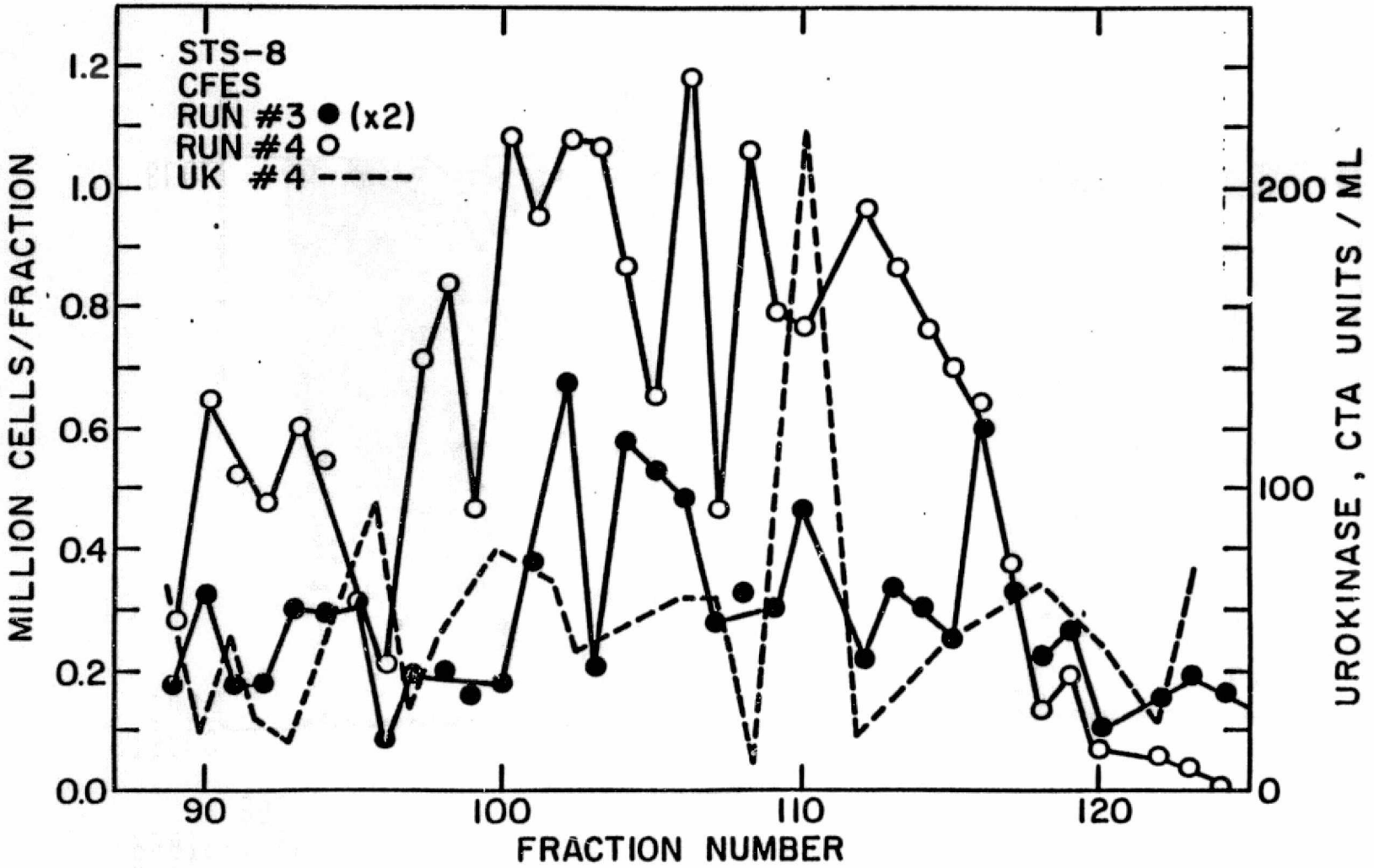

Figure 3. Post-flight analysis of HEK cells separated by continuous flow electrophoresis on Space Shuttle flight STS-8. The fraction number reflects the cell surface charge density of the cells; the higher the fraction the higher the surface charge density. Urokinase activity per fraction (dashed line) is given on the right ordinate, and viable cells per fraction for two separate separation experiments (closed and open circles) is given on the left ordinate.

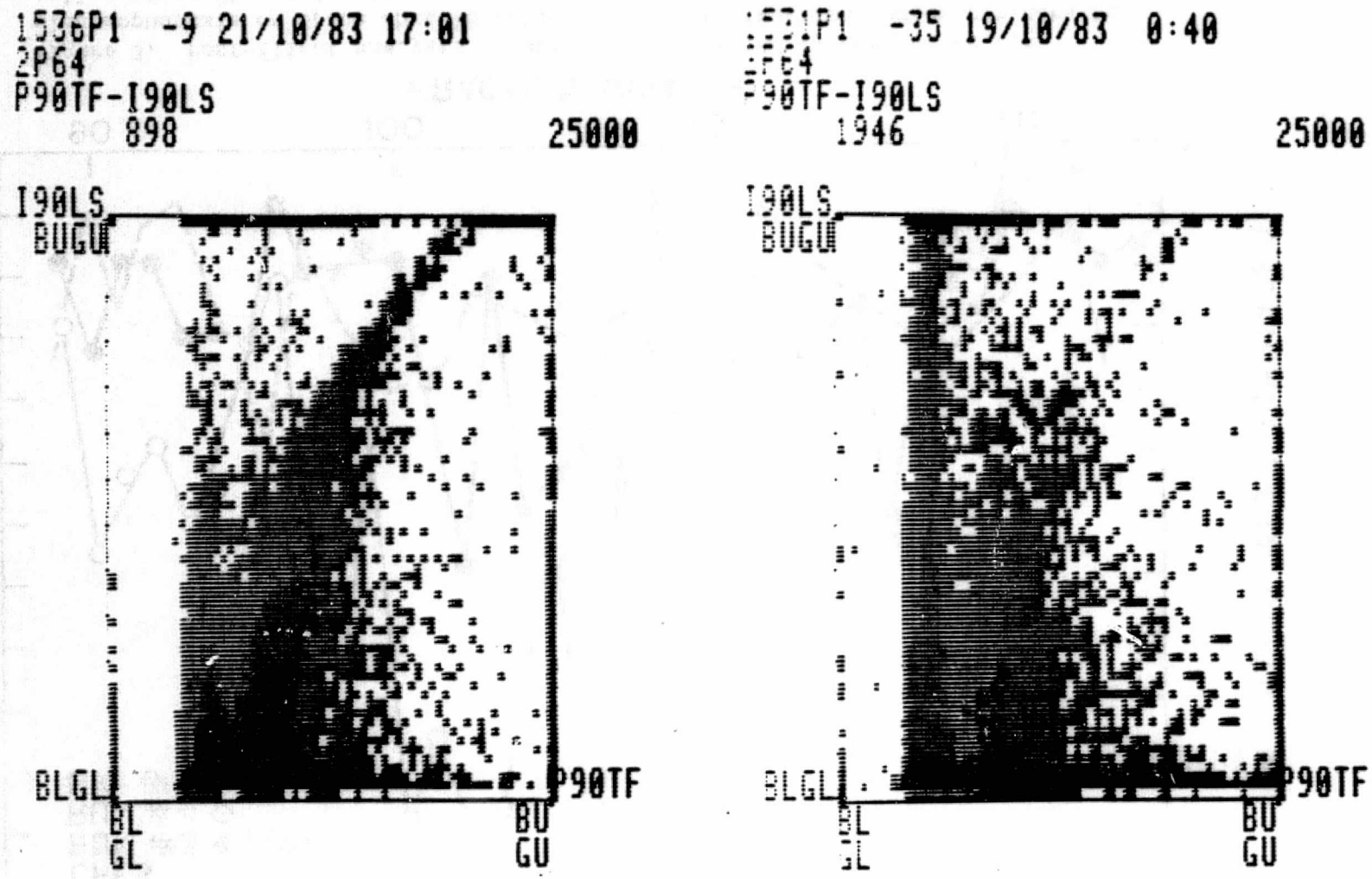

Figure 4. Two examples of raw histograms from the EPICS V cell sorter. Four two-parameter Light scatter distributions were obtained on each fraction available after the Shuttle flight. These are scattergrams of integrated 90-degree light scatter signals (ordinate) vs of time-of-flight cell diameter (abscissa) for two of the separated fraction from the STS-8 experiment.

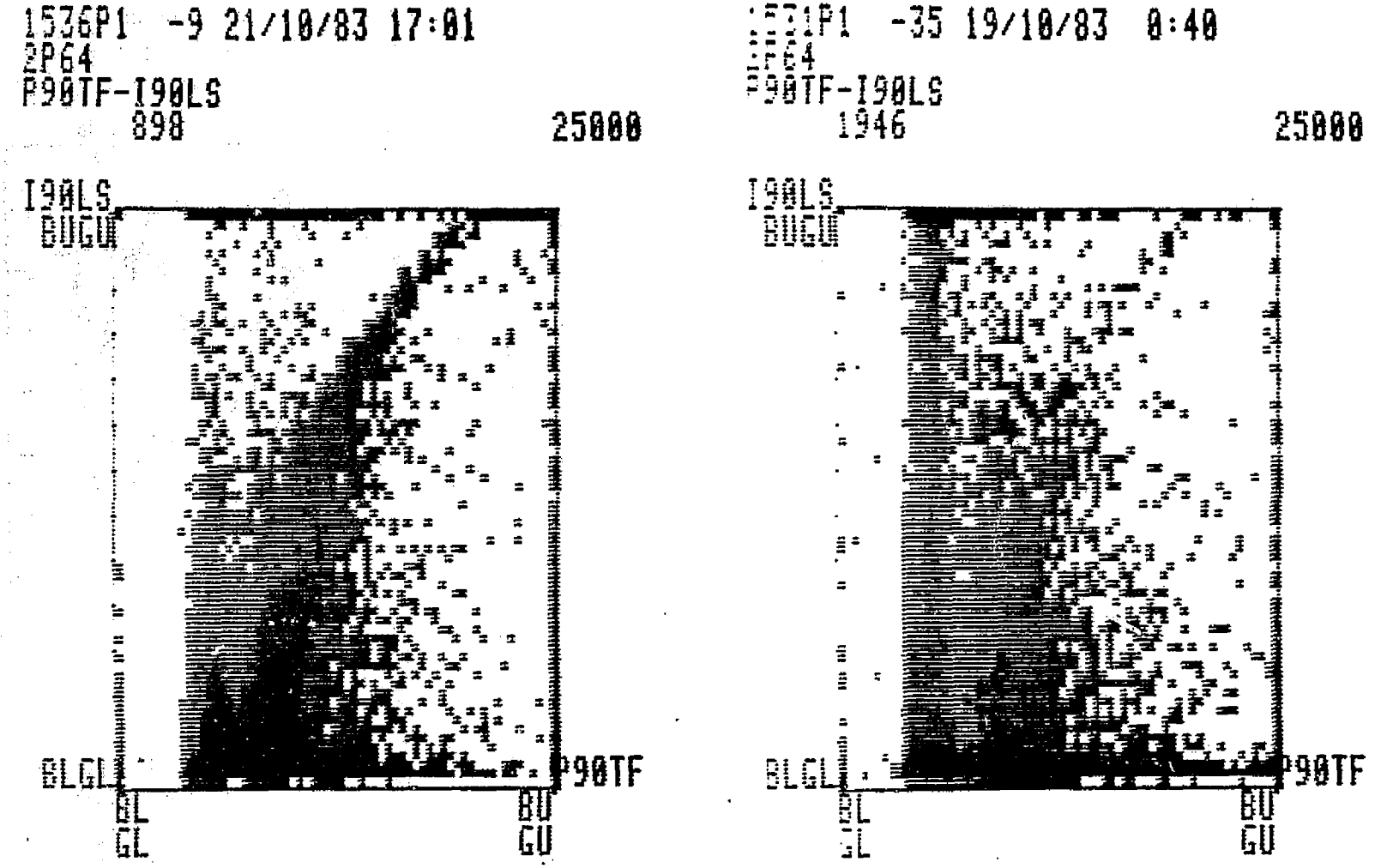

Figure 4. Two examples of raw histograms from the EPICS V cell sorter. Four two-parameter Light scatter distributions were obtained on each fraction available after the Shuttle flight. These are scattergrams of integrated 90-degree light scatter signals (ordinate) vs of time-of-flight cell diameter (abscissa) for two of the separated fraction from the STS-8 experiment.

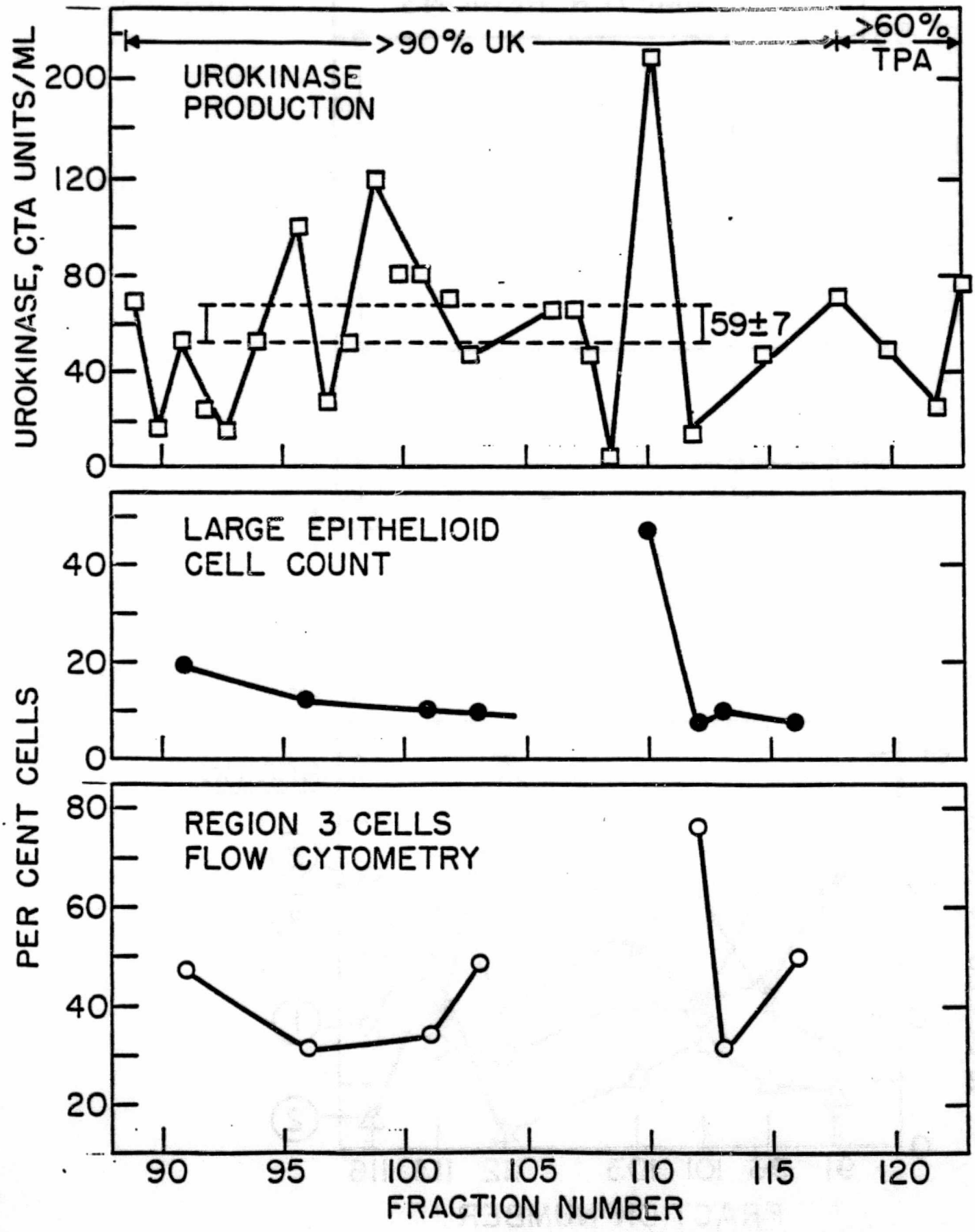

Figure 7. Comparison of three analyses of cells separated on Space Shuttle flight STS-8. Urokinase and TPA activity is given on the top graph. Percentage of large epithelioid cells determined microscopically from cells in tissue culture is given on the middle graph, and the percentage of cells in Region 3 determined by flow cytometry is given on the lower graph.

REFERENCES

Brunsting A, Mullaney PF: Light scattering from coated spheres: model for biological cells. Appl Opt 11:675, 1972.

Brunsting A, Mullaney PF: Differential light scattering from spherical mammalian cells. Biophys J 14:439, 1974.

Goolsby CL: Application of light-scattering theory to flow cytometry of stained cells. M.S. dissertation, Pennsylvania State University, University Park, Pa, 1984.

Hodkinson JR: Particle sizing by means of the forward scattering lobe. Appl Opt 5:839, 1966.

Jovin TM, Morris SJ, Striker G, Schultens HA, Digweed M, Arndt-Jovin DJ: Automatic sizing and separation of particles by ratios of light scattering intensities. J Histochem Cytochem 24:269, 1976.

Kerker M, Cooke DD Chew H, McNulty PJ: Light scattering by structured spheres. J Opt Soc Am 68:592, 1978.

Latimer P, Barber P: Scattering by ellipsoids of revolution. J Colloid Interface Sci 63:310, 1978.

Latimer P, Brunsting A, Pyle BE, Moore C: Effects of asphericity on single particle scattering. Appl Opt 17:3152, 1978.

Latimer P, Moore DM, Bryant FD: Changes in total light scattering and absorption caused by changes in particle conformation. J Theor Biol 21:348, 1968.

Leary JF: Laser light scattering detection and characterization of virally infected and transformed mammalian cells. Ph. D. Dissertation. Pennsylvania State University, University Park, Pa., 1977.

J. F. Leary, M. F D. Notter, and P. Todd. Laser flow cytophotometric immunoperoxidase detection of herpes simplex virus type 2 antigens in infected cultured human cells. J. Histochem. Cytochem. _24_, 1249-1257 (1976).

J. F. Leary and P. Todd. Laser Cytophotometric detection of variations in spatial distribution of concanvavalin-A cell surface receptors following viral infections. J. Histochem. Cytochem. _25_, 908-912 (1977).

J. F. Leary, P. Todd, J. C. S. Wood, and J. H. Jett. Laser flow cytophotometric light scatter and fluorescence pulse width and pulse rise-time sizing of mammalian cells. J. Histochem. Cytochem. _27_, 315-320 (1979).

Loken MR, Sweet RG, Herzenberg LA: Cell discrimination by multiangle light scattering. J Histochem Cytochem 24:284, 1976.

Marsh NA, Gaffney PJ: The rapid fibrin plate-a method for plasminogen activator assay. Thrombos Haemostas (Stutg) 38:545, 1977.
D. R. Morrison, G. H. Barlow, C. Cleveland, R. Grindeland, W. C, Hymer, M. E. Kunze, J. W. Lanham, M. L. Lewis, B. E. Sarnoff, P. Todd, and W. Wilfinger. Electrophoretic separation of kidney and pituitary cells on STS-8. Adv. Space

Res. (in press, 1984).

D. R. Morrison, M. L. Lewis, C. Cleveland, M. E. Kunze, J. W. Lanham, B. E. Sarnoff, and P. Todd. Properties of electrophoretic fractions of human embryonic kidney cells separated on Space Shuttle flight STS-8. Adv. Space Res. (in press, 1984).

Mullaney PF, Dean PN: Cell sizing: a small-angle light-scattering method for sizing particles of low relative refractive index. Appl Opt 8:2361, 1969.

Mullaney PF, Dean PN: The small angle light scattering of biological cells. Biophys J 10:764, 1970.

Mullaney PF, Van Dilla MA, Coulter JR, Dean PN: Cell sizing: a light scattering photometer for rapid volume determination. Rev Sci Instrum 40:1029, 1969.

Ritchie AW, Gray RA, Micklem HS: Right angle light scatter: a necessary parameter in flow cytofluorimetric analysis of human peripheral blood mononuclear cells. J Immuno Meth 64:109, 1983.

Salzman GC, Crowell JM, Hansen KM, Ingram M, Mullaney PF: Gynecologic specimen analysis by multiangle light scattering in a flow system. J Histochem Cytochem 24:308, 1976.

Salzman GC, Crowell JM, Martin JC, Trujillo TT, Romero A, Mullaney PF, LaBauve PM: Cell classification by laser light scattering: identification and separation of unstained leukocytes. Acta Cytol 19:374, 1975.

Salzman GC, Mullaney PF, Price BJ: Light-scattering approaches to cell characterization. In Flow Cytometry and Sorting, Melamed MR, Mullaney PF, Mendelson ML (eds.), John Wiley and Sons, 1979.

Schafer IA, Jamieson AM, Petrelli M------:Multiangle light scattering flow photometry of cultured human fibroblasts. Comparison of normal cells with a mutant line containing cytoplasmic inclusions. J Histochem Cytochem

Sharpless TK, Bartholdi M, Melamed MR: Size and refractive index dependence of simple forward angle scattering measurements in a flow system using sharply focused illumination. J Histochem. Cytochem 25:845, 1977.

P. Todd, W. C. Hymer, L. D. Plank, G. M. Marks, M. Hershey, V. Giranda, M. E. Kunze, and J. R. Mehrishi. Separation of functioning mammalian cells by density gradient electrophoresis. In _Electrophoresis '81_, Ed. R. C. Allen and P. Arnaud, W. DeGreuter Press, N. Y., 1981, pp. 871-882.

Chapter 32

Multiparameter cluster analysis for live cell sorting.

A CLUSTER ANALYSIS METHOD FOR IDENTIFICATION OF SUBPOPULATIONS OF CELLS IN FLOW CYTOMETRIC LIST-MODE ARRAYS

by Zhankui Li

ABSTRACT

Flow cytometric data often involve up to 6 or 7 measurements on each cell,and the data array usually recorded in "listmode", i.e. a set of 6 measurements on each cell. Usual method of displaying and analysing such data consists of a set of single-parameter histograms built by computer, combinations of single-parameter histograms of selected cell subpopulations, or two-parameters histograms. Owing to the two-dimensionality of graphic tradition, 6-parameter histograms are seldom displayed or analysed. Various methods of cluster analysis have been applied to multi-dimensional data array, including flow cytometric list-mode data. A specialized program was developed for this purpose using an heirarchical tree method for identifying and enumerating individual subpopulations, the method of principal components for a tow-dimensional display of 6-parameter data array,and a standard sorting algorithm for characterizing subpopulations. The program was tested against a published data set subjected to cluster analysis and experimental data sets from controlled flow cytometry experiments usung a Coulter Electronics EPICS V Cell Sorter. A version of the program in compiled BASIC is usable on a 16-bit microcomputer with the MS-DOS operating system. It is specialized for 6 parameters and up to 20,000 cells. Its two-dimensional display of Euclidean distances reveals clusters clearly, as does its 1-dimensional display. The identified subpopulations can ,in suitable experiments, be related to functional subpopulations of cells.

INTRODUCTION

The list-mode data aquisition method[2] introducted by cell-sorter manufactures[1] provides a very powerful tool available to cytologists, but the fulfillment of its promise has been limited mainly to display of raw or "gated" (selected on the basis of ranges of one or more para-

meter values) single-parameter histograms or tow-parameter histograms. The introduction of multi-angle differential light scattering into flow cytometry by Salzman and Mullaaney [3] prompted the development by Goad et al.[4] of cluster analysis algorithms to search for "peaks" in n-dimensional space, where n could be as high as 32. Other algorithm have been developed for the analysis of multiparameter data in general by various cluster analysis methods adapted to list-mode flow cytometry data [5], and cluster analysis algorithm have found uses in many fields of science [6].

The objetive of this research was the development of a cluster analysis algorithm which fulfilled the following requirements:

1. Ability to idantify clusters in an array of 6 variables and up to 20,000 objects.
2. Programmable on a desk-top microcomputer.
3. Capable of producing a visually interpretable tow-dimensional display
4. Capable of characterizing the clustered populations on the basis of their properties (up to 6 measurements).

MATHEMATICAL METHODS

There are tow major steps in cluster analysis that require suitable choice of mathematical methods: the search for clusters and the display of clusters. As soon as clusters are identified and displayed, the characterization of their corresponding populations in variables space is needed. This problem is a bookkeeping one.

1. Choosing a method for seeking clusters

In order to group cells into clusters,some measurement of similarity must be defined. Each cell must be compared with every other cell. The similarity between objects in a matrix can be measured in many mays,such as, distance, correlation, or covariance. Two different methods that can be used to identify clusters of objects were examined: the agglomeration method first finds centroids on the basis of the location in n-dimension

space of the two closest objects and then selects a range to enclose the objects in surrouding space in the specified region and by repeating this procedure all (except truly outlying) points can be included in several clusters[7];the method of heirachical trees succesively elimi-nates pairs of objects (or subcluster) on the basis of those with minimum Euclidean distance between them and merges them into clusters [8].

2. Choosing a method of displaying clusters

In order to display n-dimensional clusters in 1 or 2 dimensions on paper or a video screen, it is necessary to choice suitable proceture to project n-dimensions. Of several different methods available for doing this,two methods are convenient:the first one is the method of principal components which uses the covariance matrix of data set to identify a pair of axes,from which all points in n-dimensional space are minimally distance--a linear least-squares method of axes alignment [9]; the second one is nonlinear mapping display mathod which minimizes a mapping error function by first establishing a pair of axes with random orientation and minimizing the distances between data points with respect to diffe-rences between random points [10].

3. Nomenclature

Cluster analysis deal with objects , variables-cells and parameters respectively in flow cytometry (although "parameters" are realy varia-bles). In the dicussion that follows, the terms "parameters" and "varia-bles" will be used interchengeablelly. The data arrayed, as in a list-mode data set, as matrix of n variables by m objects, n parameters by m cells, with corresponding indices j=1 to n for parameters and i=1 to m for cells. Algorithm development (below) was based on an assumed typical situation with n=6 parameters and m=20,000 cells. The raw value of each parameter is xij, which normally corresponds to a channel number x value of the jth variable for the ith cell.

4. scaling of parameters

TO compress and to standardize the scale of parameters and to eliminate problems introduced by widely descrepant channel values among different parameters, a mean parameter value $\bar{x}i$ for every cell is calculated by averaging all 6 channel values,and a standard deviation si is calculated for every cell. This produces, instead of the raw matrix with elements xij, the STANDARDIZED matrix with elements zij:

$$zij = (xij - \bar{x}i)/si \qquad (1)$$

5. Calculation of the distance matrix

One measure of similarity between pairs of cells is their proximity in 6-parameters space. Using the standardized matrix, the STANDARD EUCLIDEAN DISTANCE dik between all pairs of cells can be calculated by Eq.(2)

$$dik = dki \text{ and } dik = \sqrt{\sum_{j}^{n} (zij - zkj)^2} \qquad (2)$$

These are elements of an M*M matrix, the standard Euclidean distance matrix D(I,K) with zero diagonal elements and with the off diagonal elements giving the distance between cell i and cell k in n-dimensional space:

$$D(I,K) = \begin{pmatrix} 0 & d12 & \cdots & dij & \cdots & d1m \\ & 0 & \cdots & d2j & \cdots & d2m \\ & & & \vdots & & \\ & & \cdots & dik & \cdots & \\ & & & \vdots & & \\ & & & & 0 & \cdots \\ & & & & & 0 \end{pmatrix}$$

6. The agglomeration method of cluster searching [7]

The distance matrix D(I,K) can be searched as a list, and the lowest-valued matrix element dpq identified. This value positions of the two cells p and q which are closest together, i.s., which have the smallest Euclidean distance between them:

$$dpq = \sqrt{\sum_{j}^{n} (zpj - zqj)^2} \qquad (4)$$

The point midway between them is taken as the first centroid in 6-dimensional space. A test sphere with the given radius is then "draw" in 6-dimensional space. All of the elements within the sphere are aggregated

surrounding the centroid in the distance matrix D(I,K). A new centroid can be then located outside the first sphere using the remaining elements of the distance matrix D(I,K) and another sphere is "draw". This process is repeated until all elements corresponding the cells are included (except outlying data points, if any).

Selecting centroids may be accomplished with the aid of a two-dimensional display using the method of principal components, described below. Also, a Euclidean distance histogram plot of all values of dik, numbers of dik vs. dik, is a useful visual aid for this purpose, we'll discuss this in the "RESULTS" section.

7. The hirrachical tree method of cluster searching [8]

As in agglomeration method, the tree method begins with the minimum distance matrix element dpq. A new distance matrix D'(I,K) is then established from the original one by omitting the qth row and pth row of the standardized data matrix Z(I,J) and by replacing the pth row and pth column with the average between the pth and qth row and all other rows of matrix Z(I,J).As this procedure is repeated, some elements in new Z'(I,J) matrix from which the new distance matrix D'(I,K) is calculated may be individual cells and some may be subclusters.This procedure is repeated M-1 times, until the cluster tree contains all objects in the original set. Criteria for assigning cells to clusters may be guided on the basis of the Euclidean distance histogram.

8. Euclidean distance histogram

If the Euclidean distance matrix element dik is small, cells i and k are very similar; if dik is very large they are very dissimilar. Thus one can expect a distribution of similarities.From a distribution of dik values,N(dik) vs.dik, a double guide to the application of the two above methods is provided; that is, values of dik small enough to belong to a cluster can be ascertained,and values of N(dik) large enough to indicate cluster can be chosen.Fig.7 is such an histogram, in which values of dik

ranged from 0.1 to about 5.0, so the array was divided into 50 classes with 0.1 class width.

9. Two dimensional display by the principal components method [9]

The principal components method is to project the 6 dimensions onto fewer axes which represent independent variables that give the structure of the original variables in an opimal way by using the covariance matrix to eliminate the redundant information in the correlation matrix. This is accomplished first by determining the mean channel zj for each parameter:

$$zj=1/m\times\sum_{i}^{m} zij \tag{5}$$

and the standard deviation s.j:

$$s.j=\sqrt{\sum_{i}^{m}(zij-\bar{z}j)^2/(m-1)} \tag{6}$$

and the correlation matrix R(L,J) can be defined as follows

$$R(L,J)=\begin{pmatrix} r11 & \cdots & r1j & \cdots & r1n \\ r21 & \cdots & r2j & \cdots & r2n \\ & & \vdots & & \\ \cdots & \cdots & rlj & \cdots & \cdots \\ & & \vdots & & \\ & & \vdots & & \\ rn1 & \cdots & rnj & \cdots & rnn \end{pmatrix}$$

where rlj=clj/(s.l s.j); clj is the element of the covariace matrix and

$$clj=1/(m-1)\times\sum_{i}^{m}(zil-z.l)\times(zij-z.j) \tag{7}$$

The principal component analysis is also called eigenvector analysis. The correlation matrix R can be considered as a linear transformation that transforms a vector $\vec{z}.j$ into a new vector $\vec{u}.j$ in such a way that the cells are represented by a new set of variables, each of which is a combination of the original variables. This transformation can be written as

$$\vec{U}=R\cdot\vec{Z} \tag{8}$$

when z satisfies Eq.(9)

$$R\cdot\vec{z}=\lambda\,\vec{z} \tag{9}$$

then Eq.(9) is called the eigen-equation of R. When $\vec{z}$ are eigenvectors, λ are eigenvalues which correspond the eigenvectors,and they satisfy

$$R \cdot \vec{v} = \lambda \vec{v} \qquad (10)$$

The λ's reflect the properties of the correlation matrix R , which contain the variations of original data and the eigenvector are the projections of original variables, so that $\vec{U}=v \cdot \vec{z}$, or

$$Uik=\sum_{j} vkj \times zij;\ k,j=1,2,.....,6;\ i=1,2,.....,m \qquad (11)$$

The U.k are called principal components, each of which is a linear conbination of the original values of the parametres, and the first two of which can be considered as axes, U.1, U.2. Finally, the 2-dimensional display is presented as a plot of UI1 vs UI2 as if they were orthogonal measurents on the Ith cell.

10. Two-dimensional data display by the method of nonlinear mapping[10]

To represent several dimensions data in two dimensions as faithfully as possible, a procedure has been developed to minimize the so-called mapping error E, a single-valued function given by the following relalowing relationship

$$E=1/\sum_{i<k}(dik*) \times \sum_{i<k} [(dik*-dik)^2/dik*] \qquad (12)$$

where dik* is the distance between the ith and kth cells in the 2-dimensional space.For each of the cells, the axes are chosen at random. Thus, the Y-position of the ith cell and these two variables will be respectively,

$$Y(I,J)=\begin{pmatrix} y11 & y12 \\ \vdots & \vdots \\ yi1 & yi2 \\ \vdots & \vdots \\ ym1 & ym2 \end{pmatrix} \qquad (13)$$

and the dik* is the Euclidean distance matrix element, and

$$dik*=\sqrt{\sum_{j} (yij-ykj)^2};\ i,k=1,2,.....,m. \qquad (14)$$

Now, the objective is to minimize the sum of squares of the differences between the Euclidean distances in the 6-dimensional and 2-dimensional representations. This is accomplished by substitution into equation (12) and reiterating with values of ypq for p=1 to m cells and q=1 to 2 dimensions:

$$ypq(m+1)=ypq(m)-(MF)\Delta pq(m) \quad (15)$$

where deltapq(m) may be determined from

$$\Delta pq(m)=[\partial E(m)/\partial ypq(m)]/[|\partial^2 E(m)/\partial ypq(m)^2|] \quad (16)$$

The (m) means the result of the mth iteration, and (MF) is determined empirically to be MF=0.3 or 0.4.

RESULTS

The program tested against the published data

The published data [11] is used to test our program. The results of clustering are shown in Fig.1,which is based on the principal component ttts method in 2-dimensional space.The 14 kinds of milk can be identified into 2,3, or 14 groups according to their fatty acids in it. The group number for the best configuration is given in Table 1. Several kinds of classi fications of objects are shown in Fig.1-1 to 1-5 ,respectively. In the Fig.1, the number is the sequence number of fatty acid, the asterisks represent the positions of the centroids which were calculated in the 10-dimensional space.In egneral, if the group construction of the data is distinct it is convenient to search the clusters within the distance matrix in n-dimensional space directly without repredicting the centroids from 2-dimensional display. On the contrary, the graphs of 2-dimensional display can be used to determine centroids,and, consequently, to accomplish clustering. For example, from Fig.1-4a, #6, #2, #10 and #5 can be tested as centroid respectively,then the members of the 4 clusters can be determined respectively and the properties of the clusters can be obtained The results of 4-group cluster is shown in Fig.1-4b.Usually,a display of data in 2-dimensional space is not the same as the calculation in n-dimensional space because principal components analysis may lead to a loss of information and biased representation.However,our procedure can obtain the

satisfactory coincidence with each other: the search for the centroids by calculation in n-dimensional space orientate in the centre positions of the membership of the cluster in 2-dimensional display, and the best 4-group cluster (see Table 1) is the same as the display (#2 and #10 are far from the others, e.s.,their properties are very different from those of the others, they should be a cluster individually, respectively.

Table 1. NUMERICAL ANALYSIS OF CLUSTERING FOR THE DATA [11]

	$\bar{r}$	$\bar{d}$	$\bar{r}/\bar{d}$
2	6.90	14.66	0.47
3	5.42	18.25	0.30
4	5.13	27.08	0.19 *
5	13.96	17.76	0.79

where $\bar{r}$ is the average between the members of clusters in 10-dimensional space, $\bar{d}$ is the average between the distances of centroids, the numbers of the first column is the number of the testing clusters. The asterisk represents the best confiqurition of these 14 objects.

Flow cytometry experiment

The 55 of 15,000 cells analyzed by flow cytometry were selected at random,and classified into several clusters,and the results were represented in Fig.2-1 to Fig.2-5.For the putative clusters,the centroids are expressed with asterisks.The properties of clusters are given in Table 2 The first column of Table 2 represents the number of the putative clusters in different clustering,the second gives number of the objects in the clusters.the last shows ratio of the average distance to the distance between the centroids,with which it is convenient to assay the clustering in conbination with the properties of the clusters. This shows that the

2-group cluster is the best confiqurition of these 55 cells.

Table 2. PROPERTIES OF CLUSTERS FOR 55 CELLS

	$\bar{r}$	$\bar{d}$	$\bar{r}/\bar{d}$	
2	11.36	5.99	1.90	*
3	19.75	6.81	2.90	
4	43.59	7.68	5.68	
5	31.95	8.45	-3.78	

where $\bar{r}$ is the average between the members of clusters in 6-dimensional space, the $\bar{d}$ is the average between the distances of centroids, the "*" is the best result of 55 cells.

For the 1360 of 20,000 cells, the relative frequency distributions of the first two principal components are shown in Fig.3-1 and Fig.3-2,respectively. It is clear that there are obvious constructions in them. It is best to conbine these two distrbutions to construct a so-called "address" matrix

$$A = \| a_{ij} \| \; ; \; i,j = 1,2,\ldots\ldots,P.$$

where p is the number of intervals wuich are selected by an operator based on the distributions. As mentioned in the MATHEMATICAL METHODS,P= 50. The elements aij concern aspects of the clusters being considered. The first is a subscript which indicates the address of the subregion that will be a component of the resultant region of cluster and the second is the number of the objects in it. They can be used to predict the number of each cluster (as below).

The purpose of this paper is not to discuss the results of the experiments. To illustrate the approach in matrix A, we expressed some of elements of A in the Table 3, which are representative and lie around the centroids, for 4-group cluster.

TABLE 3. NUMBER AND ORIENTATION OF CELLS IN THE MATRIX A

	1	2	3	4	5	6	7	8	9	10	11	12	13	14	15	.....	19	20	21	22	23	24	25	26	.....	50
1																					2					
2																						2	1	1		
3																							1			
4																				1	1		1	3	1	
5														1				1		1	3			1		
6										2				1					3	2	1		5	1	1	
7							1	1		1		2	1	2	1					-1		2				
8											3		2	1	3	2			1	1		4	1	1		
9										1	2	1	3	3	2	1				1		3	2	1	2	
10								1	3	4	5	2	3		3	2			1		2	4	2	1	2	
11								2	4	2	3	3	4	2		2			1	3	3	4	6	2	1	1
12									2	2	2	1	3	2	3	2			1	2	9	2	3	2	3	2
13								1	2	2	3	1	3	1	2	3	3			1	5	5	5	1		1
14								1		1		1	1		4	1		1		2	7	1	3	1	3	1
15																			2	1	2	5		2	1	2
16																				4	3	2	2			
17																			1		3		1	3	1	
18																				2	1	1	1	2	1	2
																					5	2	2		1	
:																										
:																										
24							1	1		1		1			1					1	6	2	4	1		
25							3	2	1	1		1	3	1	2	1			1	1	1	7	3	5	1	
26							1		1	3		1								1	6	7	1	1	1	
27								2							1	1			1	1		7	2	1		1
28							2	1	5	3	1	1		1	1				1		3	7	1		1
29								3	2	3			1	1		1					1	3	1	1	1
30								3	2	1	1	1	2	1	1	1				3	2	5			2
31									1	3	2	1		2	1	1						3	1	2		
32							1	2	2	4		1		1	1	1				1		3	1		2	
33										2			1	2	1	1			1	3		3	2	3	2	
34																										
:																										
:																										
50																										

In Table 3, each of numbers represents the quantity of the cells. The position occupied by the number depends on the properties of cells. In other words, the properties of cells determine not only the density of points in clusters, but the distance between the clusters. As a consequence, the properties of clusters can illustrate the extend of success of the experiment.

To test the cluster with A(I,J) in combination with the distributions

of Fig.3 and to evaluate the clustering,the numerical data are needed.For each of various putative clusters,the distribution of membership is considered as normal. The mean can be regarded as the centroid, the orientations of which can be pridicated on the address matrix, based on the relative frequency distributions of the first two principal components. If the objects are grouped into two clusters, the 19th interval of the first principal component can be considered as the boundary. The frequency distribution of the second can be considered as in equal probability proximately. As a result, the centroids are located at the A(9,20) and A(26,20) respectively. The distance between the centroids is 1.70. The width of clusters can be expressed by the average area which is occupied by each of objects in the cluster, or by the density of the objects in the cluster.Similarly, the centroids distributions between the centroids and densities can be calculated for the case of the 3-group cluster and the 4-group cluster. The results are shown in Table 4.

Table 4. comparision of different group cluster

		boundary (relative) x	y	centroids (x , y)	density (ρ)	average weighing ($\bar{\rho}$)	distance centroids ($\bar{d}$)	average of d's ($\bar{\bar{d}}$)	w ($\bar{\rho}\times\bar{d}$)
2	1	1,18	1,39	(9,20)	0.72	0.85	1.70	1.70	1.44
	2	19,41	1,39	(26,20)	0.94				
3	1	1,18	1,39	(9,20)	0.72	0.91	1.66	1.99	1.81
	2	19,26	1,19	(23,11)	1.01		2.29		
	3	19,41	1,39	(30,29)	0.93		2.03		
4	1	1,8	5,14	(7,12)	0.86	0.90	1.60 1.38	1.96	1.76
	2	19,26	1,19	(23,11)	1.01		2.86 1.94		
	3	1,18	5,39	(12,27)	0.77		1.93		
	4	19,41	1,39	(30,29)	0.93		1.91		

where the first column represents the quantity of the putative clusters,

the second the number of clusters. The numbers in the "boundary" and the centroids" two columns correspond the subscripts of matrix A(I,J). The last column represents the products of the average distance between the centroids and the weighing average of the density in the case of several grouping.It is clear that the bigger the W ,the higher the distinctness. W depends on the properties of the data, from which the best three-group cluster is obtained.The result is coincidence with flow cytometry.

Finally, the requirement in cluster analysis is capable of characterizing the clustered populations on the basis of their properties.Therefore,the application of clustering techniques to the field of flow cytometry can give us information on which cells behave in a similar manner and what parameters they possess in common. Several data are shown in Table 5.

TABLE 5. PARAMETERS OF CELLS

position	# of cells	parameters					
		UV/48	LPUV	LIUV	LP488	LI488	FALS
A(6,10)	565	77	146	88	74	28	130
	697	61	28	21	105	32	107
	1094	62	255	105	17	171	29
	1172	139	122	192	166	123	110
A(23,9)	384	138	128	177	107	95	162
	508	81	64	22	31	133	123
	857	150	126	5	0	6	159
	935	22	4	44	0	125	112
(30,23)	734	76	61	33	131	151	0
	755	106	91	24	141	148	33
	910	25	9	123	105	62	2
	1004	61	50	134	115	72	60

In Table 5, the first column represents position of cells in matrix

A(I,J),the second the numbers of cells, the last six columns the parameters of cells.

DICUSSION

Different methods of testing cluster [12] are used by different investigators. The width of clusters and the distance between the centroids are preferable. But, the parameters of clustering procedure are not always appropriate to evaluate the different clusters with different morphology in the parameters space, and to appreciate the differences of classification, from which the best group cluster can be obtained. We used the average distance between objects instead of the largest distance which is considered as the width of the cluster. For example, in identifying the fatty acid in milk, we found that the 4-group cluster is the best configuration of the objects and the #2 and #10 are considered as two individual subclusters.For the flow cytometry experiment,the data is in a list-mode,the result of clustering 55 cells which were selected at random is not the same as that of the 1360 cells': 2-group cluster is the best for the former and 3-group cluster for the latter because of statiistics.Though our method of testing clusters which is based on the relative frequency distribution of principal component requires as many objects as possible to accquire good statistical properties, it needs much smaller computer space and shorter computation time than that the distance matrix method, which asks for at least 2000k BN for 1000 cells.

We assume that points within clusters have GAUSSIAN distribution and the projections on these two principal components are normal.If the data have no substructure, the frequency distribution of projections will be single modal, as shown in Fig.3,Fig.4-1 and Fig.4-2. If the data have some substructures the distribution of the relative positions of the points in the pattern of points in the reduced space will be multigroup and the frequency distributions of the projections will be complex,usaully multimodal.The results are shown in Fig.5-1.Fig.5-2.Fig.6-1.Fig.6-2.which

ppear to be reasonable for the parameters of cells. According to the properties of the frequency distributions,the boundary and centroid of the cluster can be determined and the numerical criteria of clustering can be obtained, as shown in Table 4.

Fig.7 shows the frequency distribution of elements of the distance matrix D(I,K) in n-dimensional space, which is the same as those of the projections.This frequency distribution can be used to determine there is any substructure[12],and to group objects into clusters by measuring the χ^2 of the frequency distribution of the interpoint distance in putative cluster and that of the interpoint distance distributed at random in the cluster.In the results of former examples, the χ^2's are not given because there are not enough points in the cluster to obtain the satisfactory statistics.

REFERENCES

[1]

[2]

[3]

[4]

[5]

[6]

[7] D.L.MASSART ,L.KAUFMAN and D.COOMANS, An operational research model for pattern recognition. Analytica Chimica Acta,122(1980) 347-355

[8] J.ZUPAN, A new approach to binary tree-based heuristics. Analytica Chimica Acta, 122(1980) 337-346

[9] D. LUC MASSART, The interpretation of analytical chemical data by the use of cluster analysis. Chemical Analysis, vol.65(1983) 39-65

[10] JOHN W. SAMMON,JR. A nonlinear mapping for data structure analysis IEEE Transactions on computers,vol. c-18, no. 5, MAY (1969) 401-409

[11] Anne-Marie MASSART-LEEN and D.L. MASSART, The use of clustering techniques in the elucidation or confirmation of metabolic pathways , Biochem. J.(1981) 196,611-618

[12] MICHAEL A. GATES and ROGER I. C. HANSELL, On the distinctness of clusters. J.theor. Biol.(1983)101,263-273

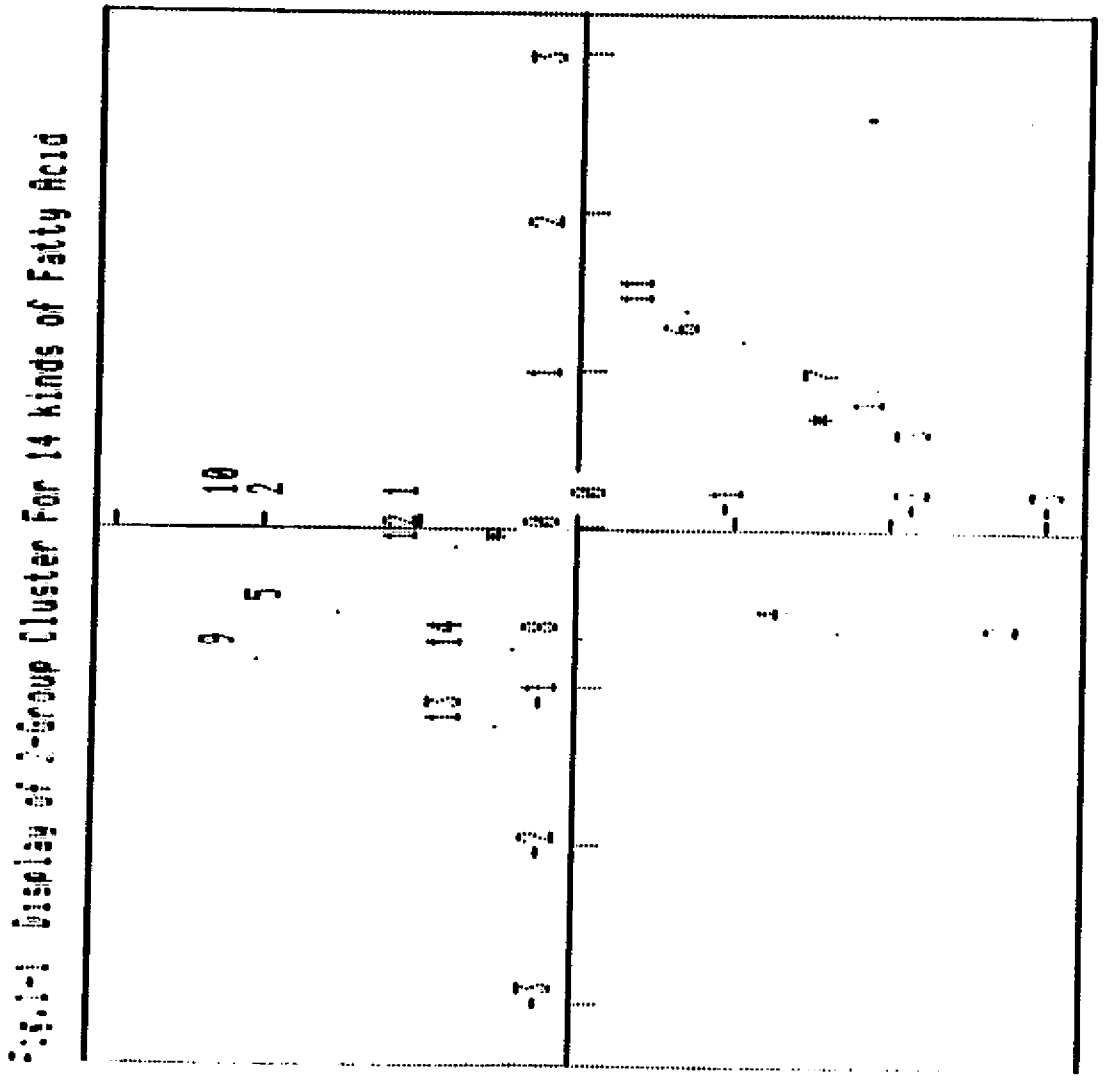
10
2
1
5
9
14
13
11

ORIGINAL PAGE IS
OF POOR QUALITY

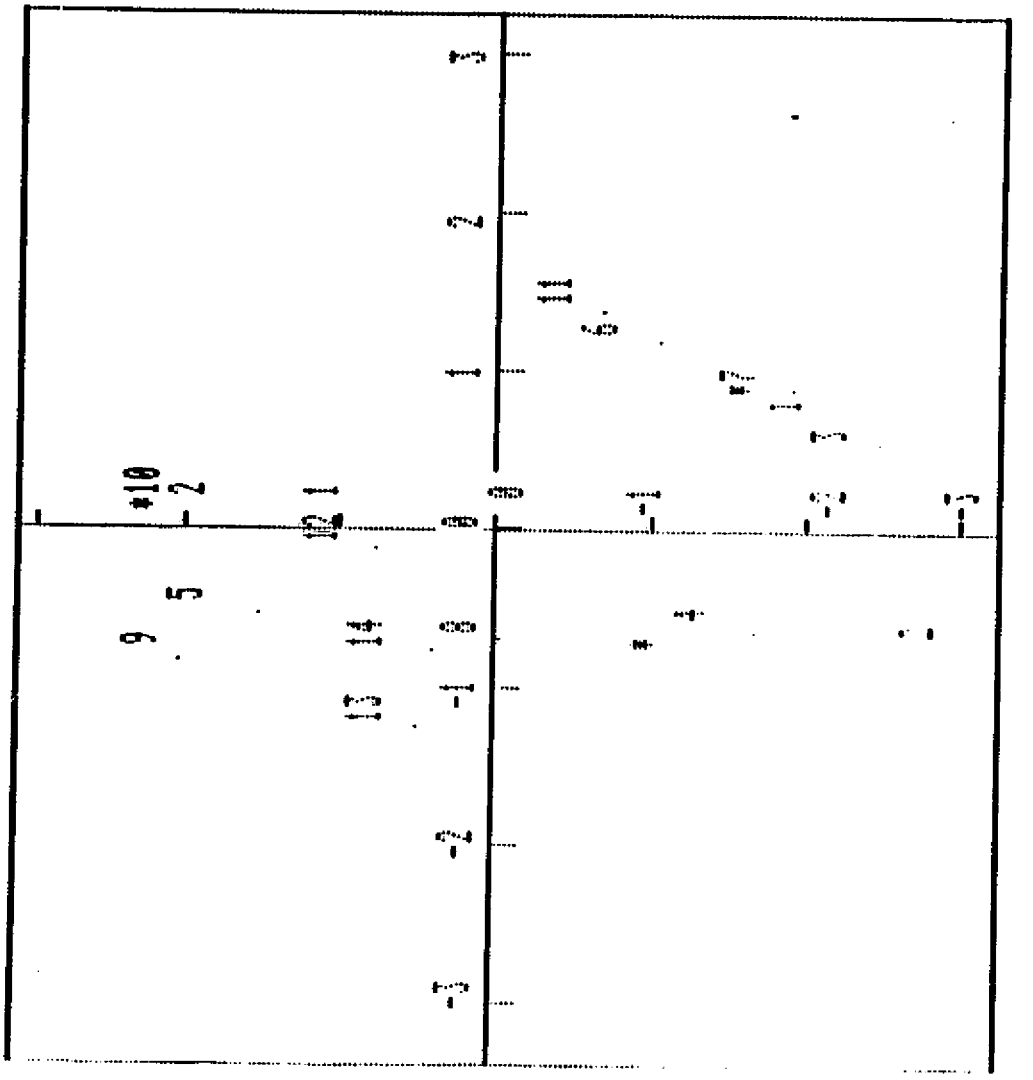

Fig. 1-2 Display of 3-Group Cluster For 14 Kinds of Fatty Acid

Fig.1-3 Display of 4-Group Cluster For 14 kinds of Fatty Acid

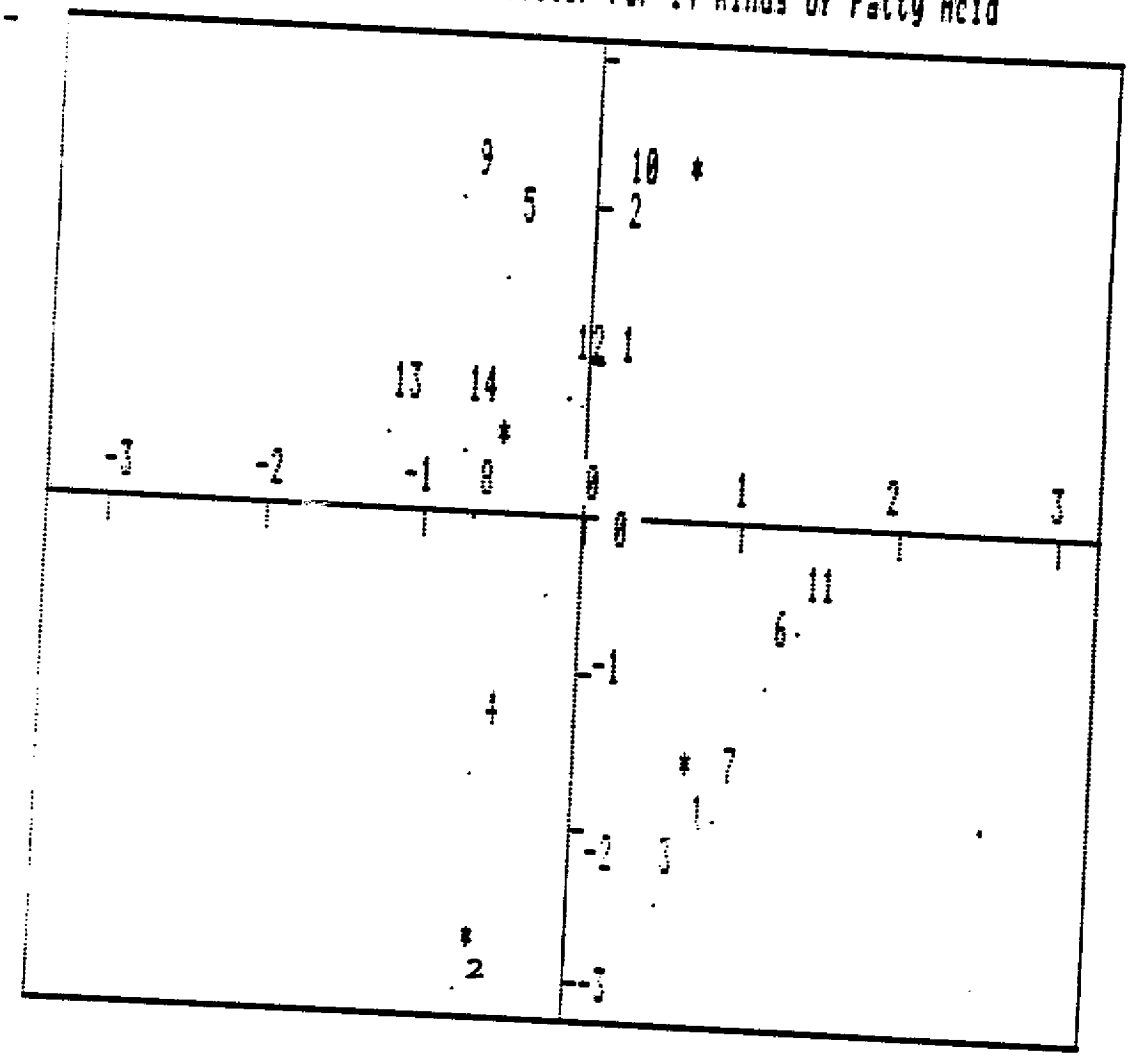

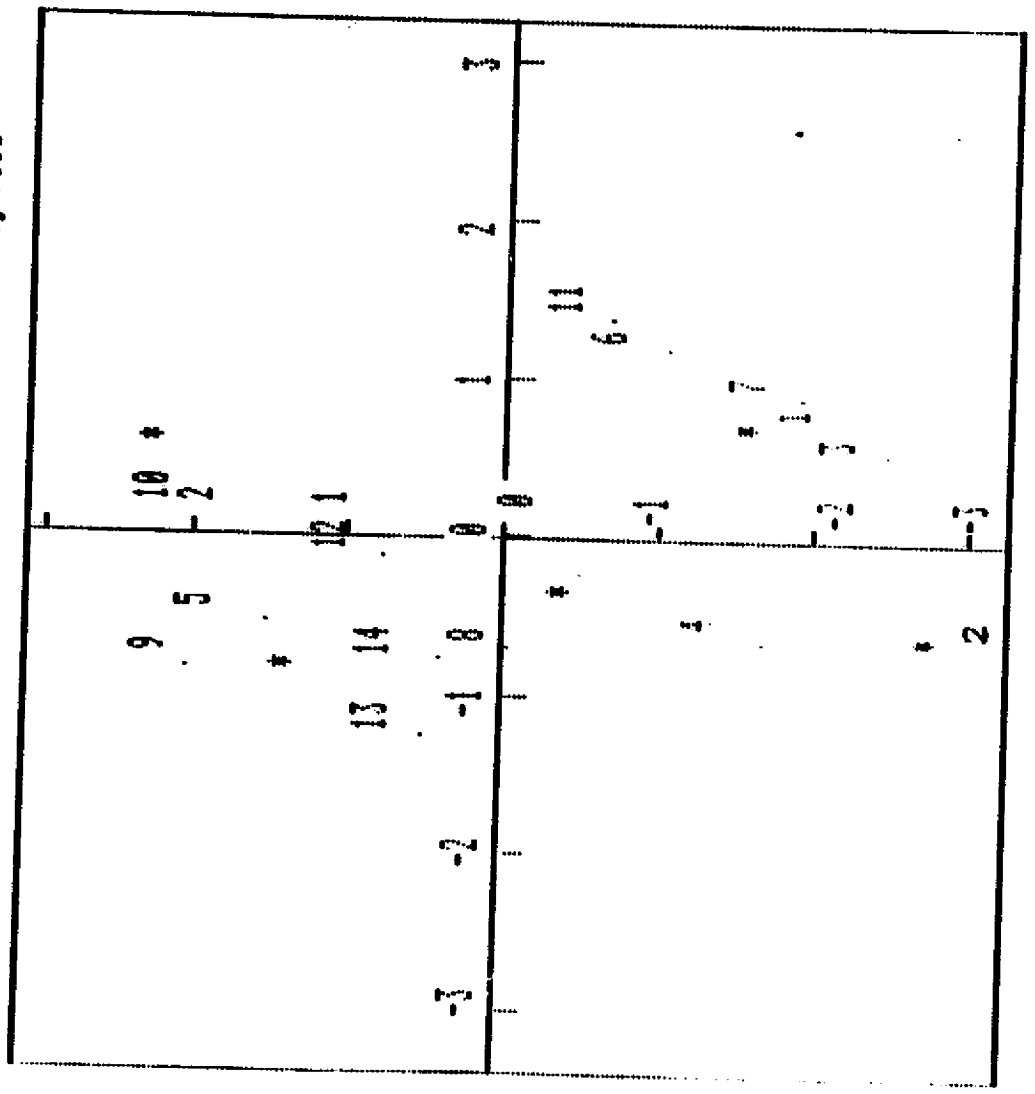

Fig.1-4 Display of 5-Group Cluster For 14 kinds of Fatty Acid

Fig.2-1 Display of 2-Group Cluster of 55 Cells For Flow Cytometry

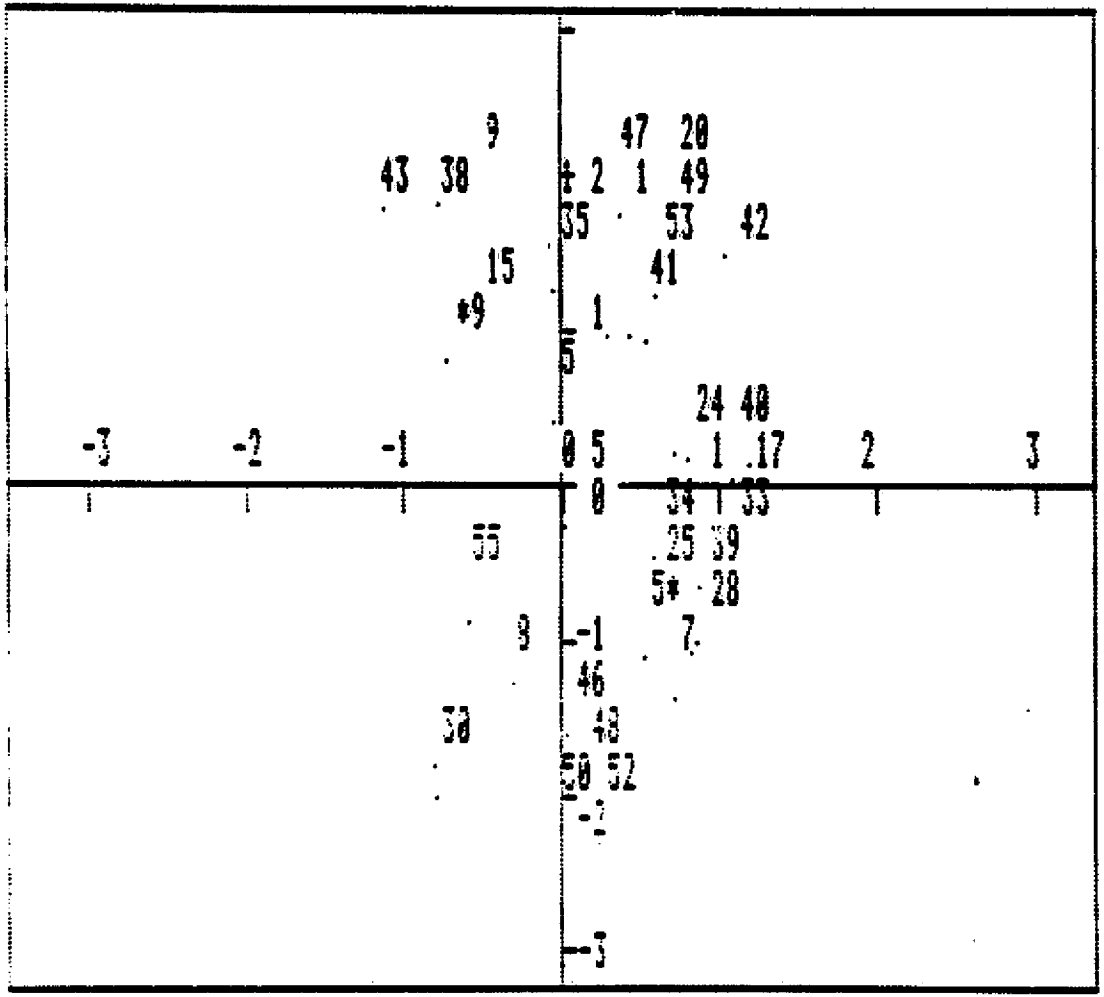

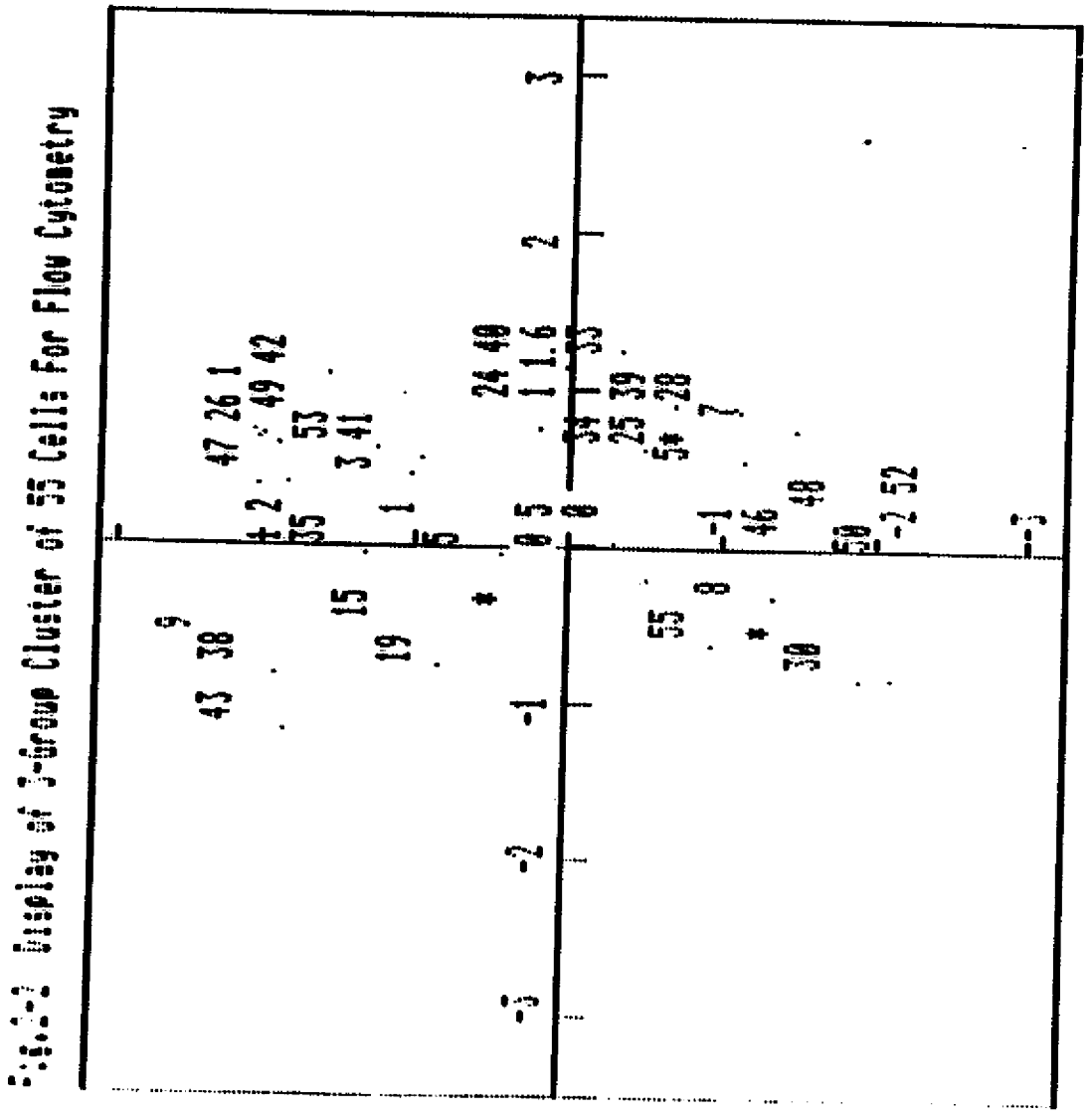

Fig.2-3 Display of 4-Group Cluster of Cells For Flow Cytometry

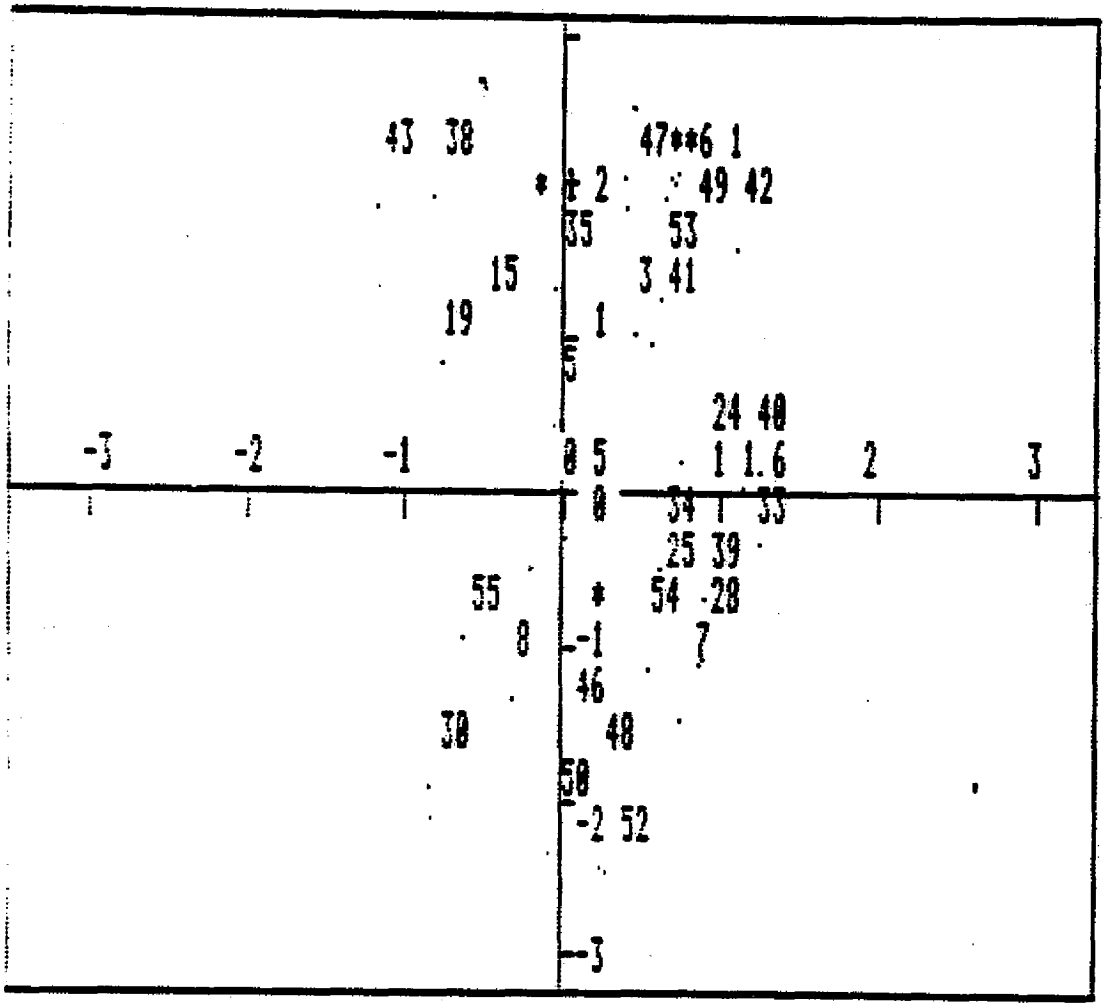

F:g.2-4 Display of 5-Group Cluster of 55 Cells For Flow Cytometry

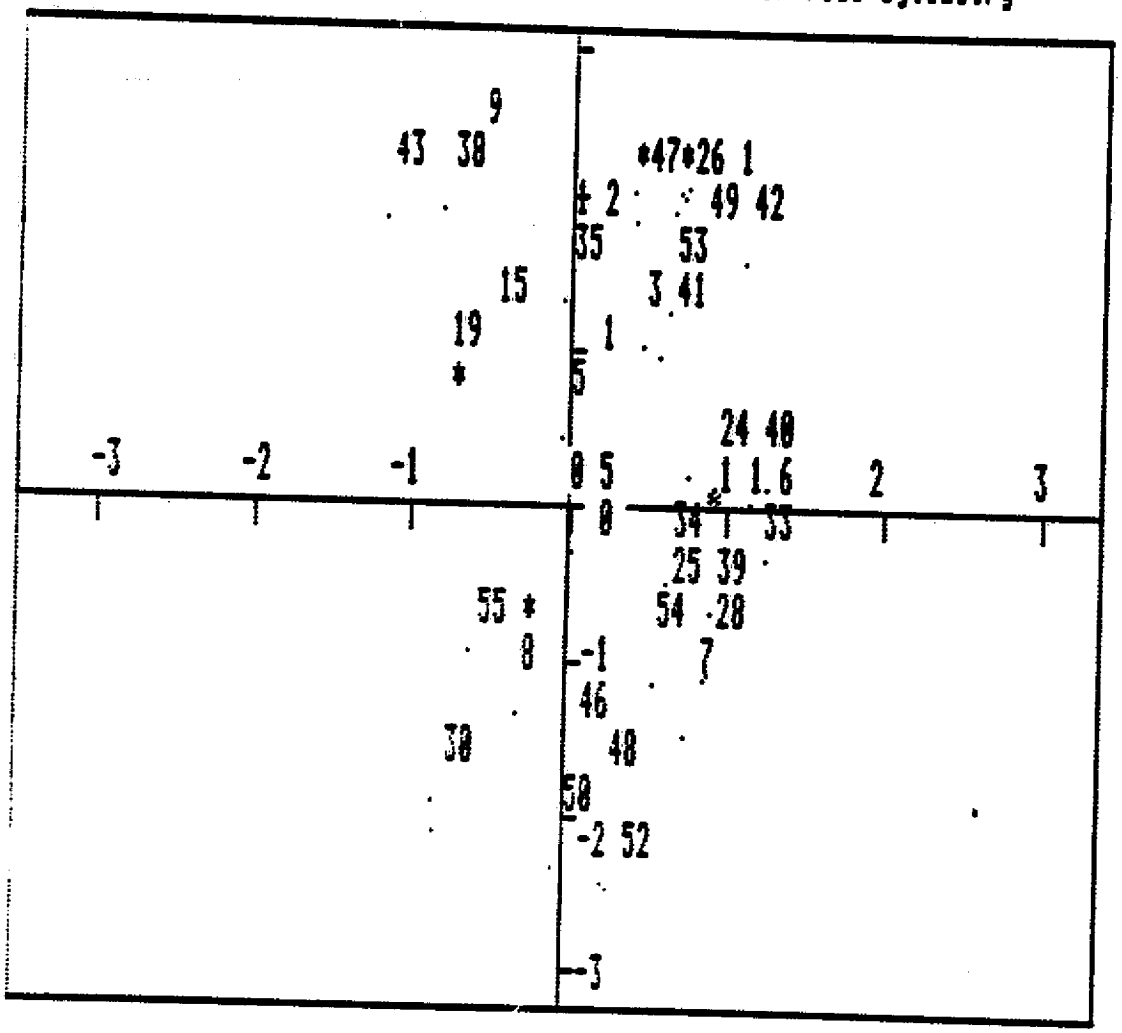

ORIGINAL PAGE IS
OF POOR QUALITY

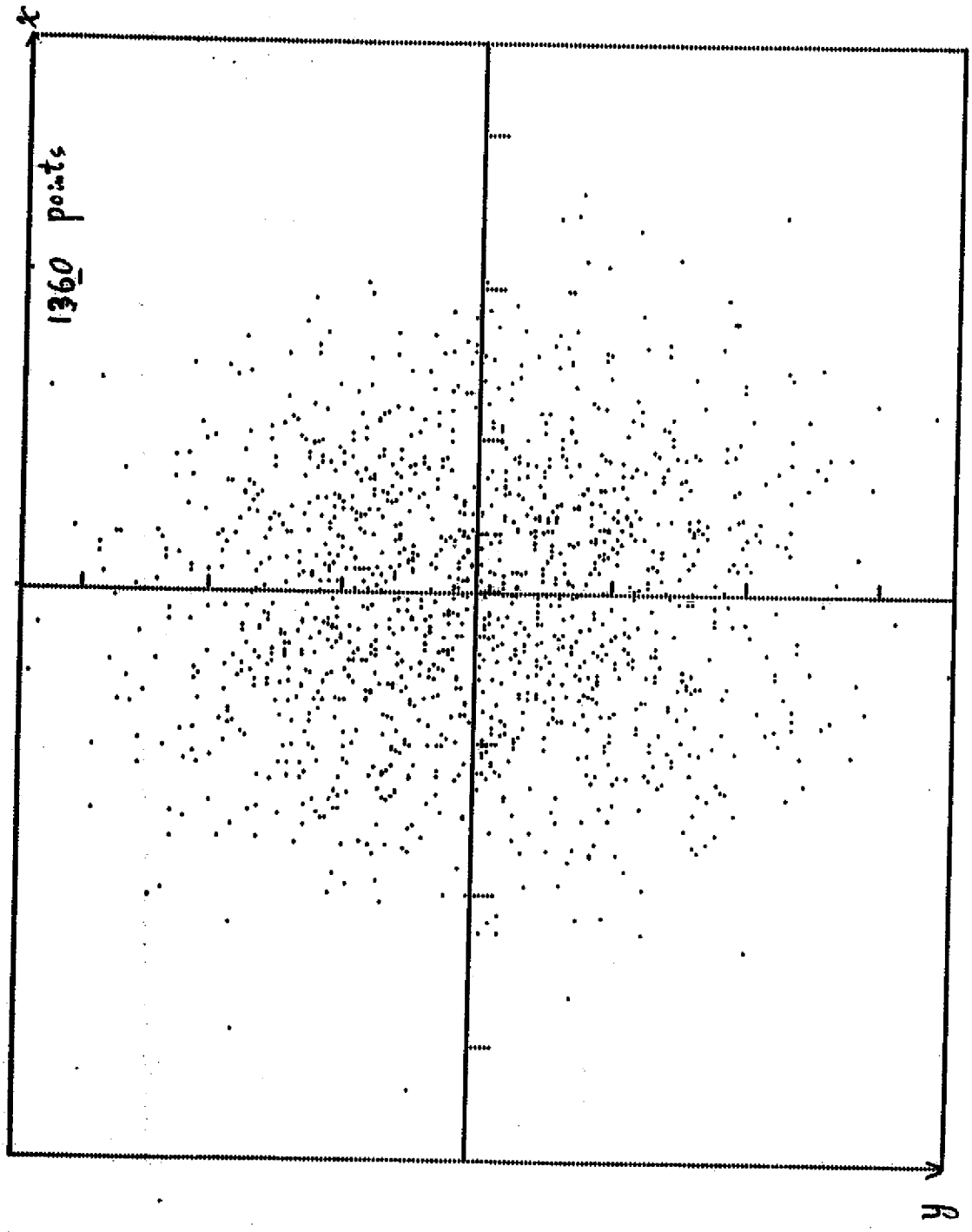

Fig. 3 Graph of a data set with Gauss distribution randomly

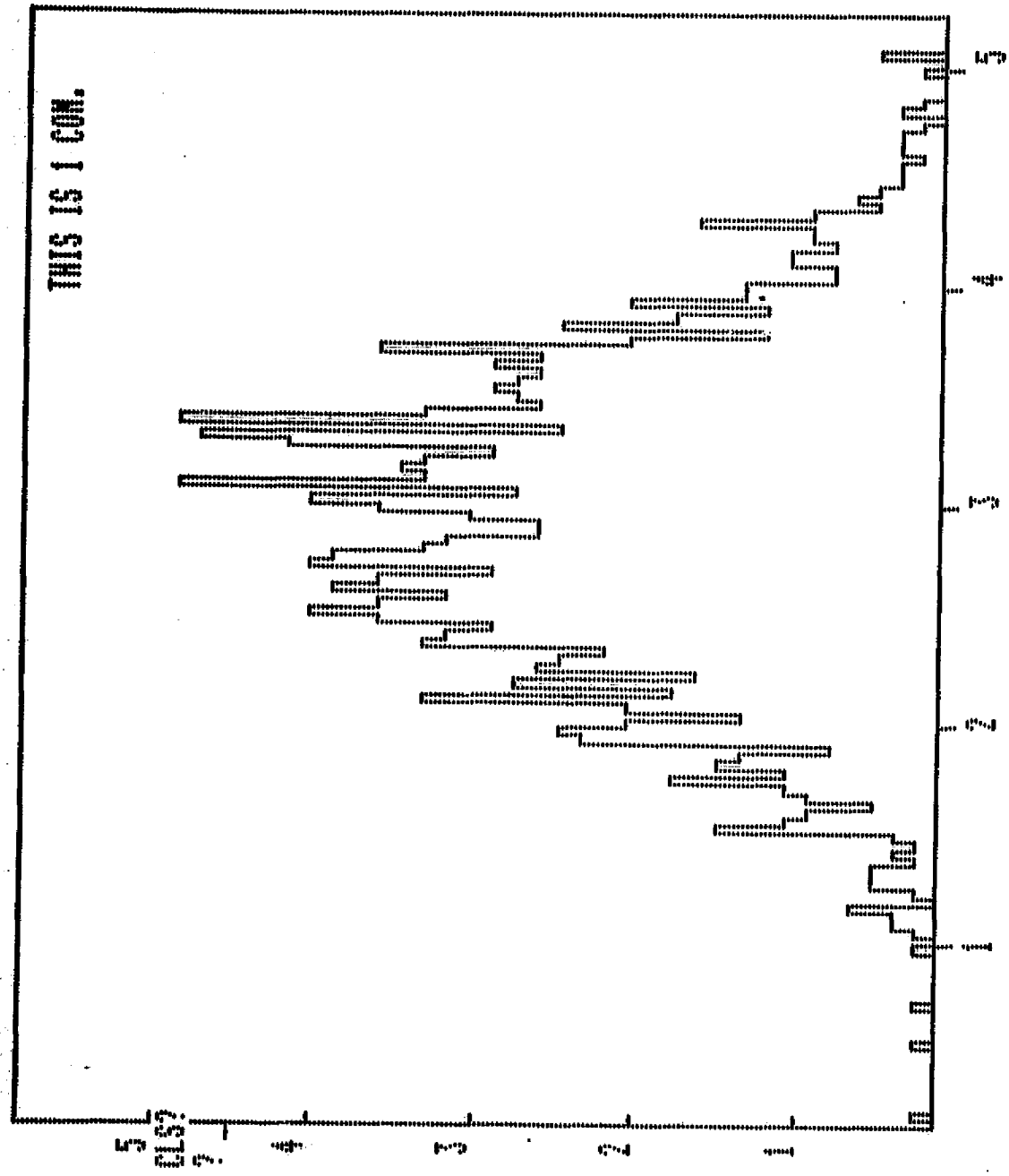

Fig. 4-1 Frequency distribution at random with Gaussian.

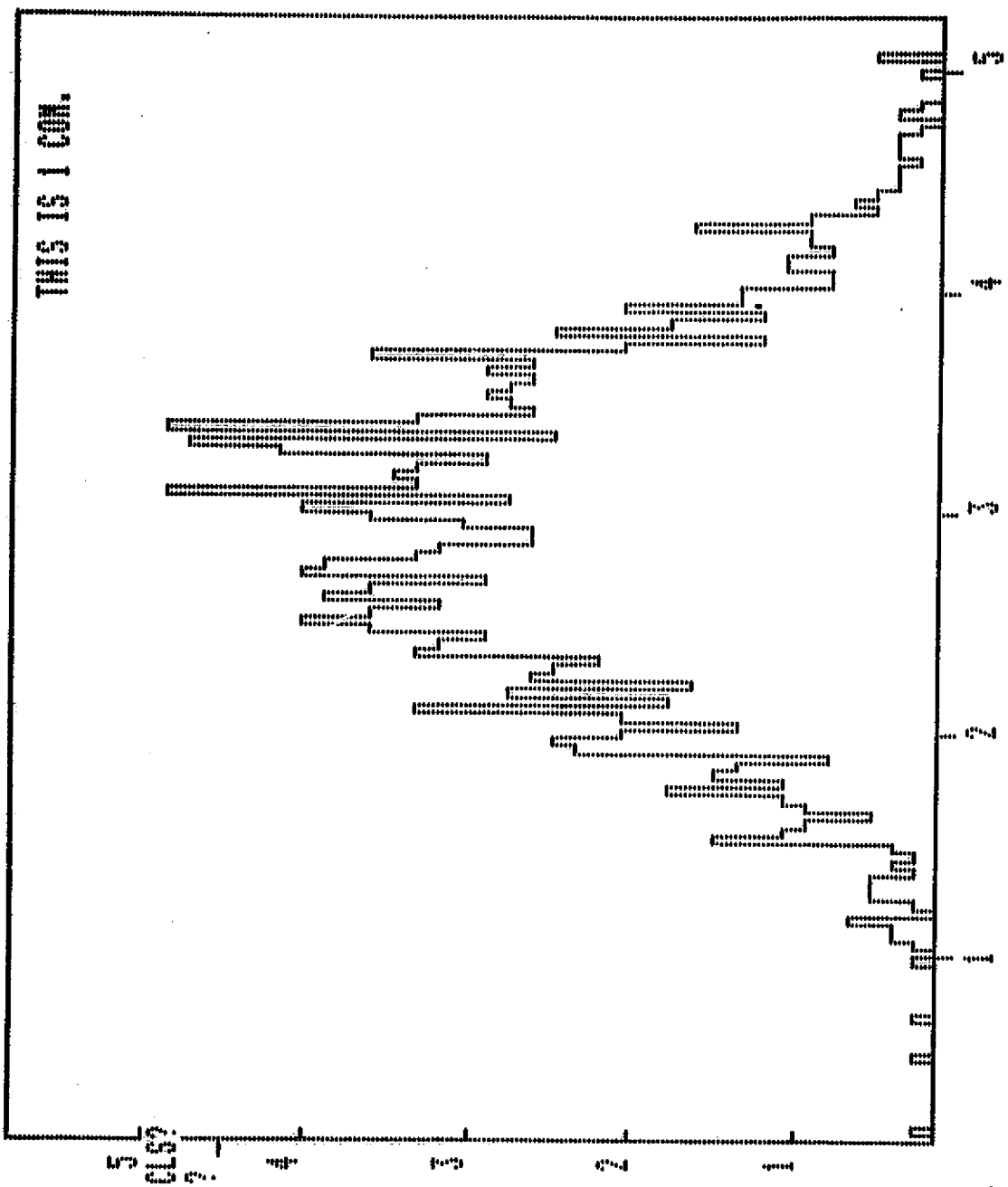

Fig 4-3 Frequency distribution at random with GAUSSIAN

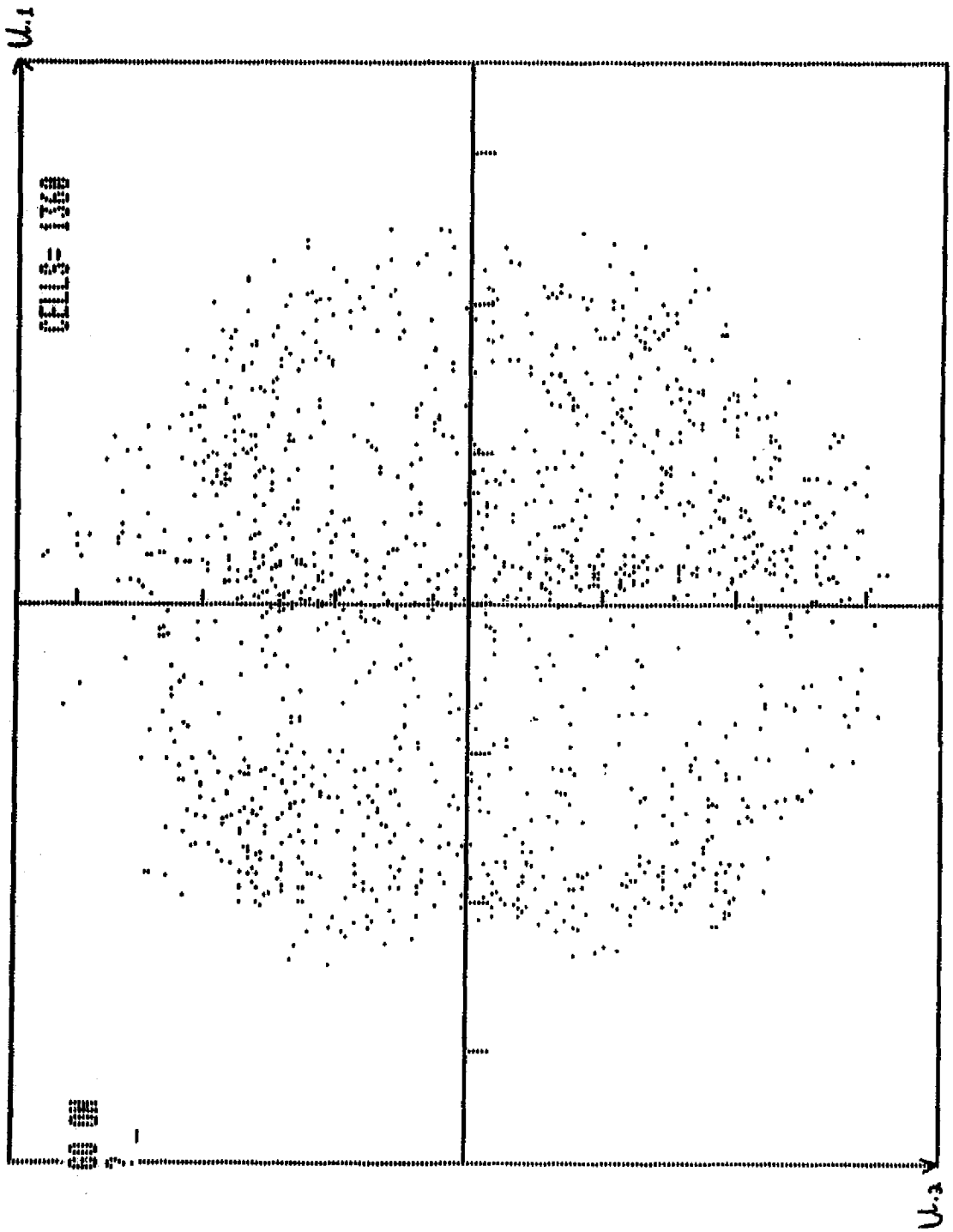

Fig. 8-1 Graph of a data set consisting of 1360 cells in two dimensional space.

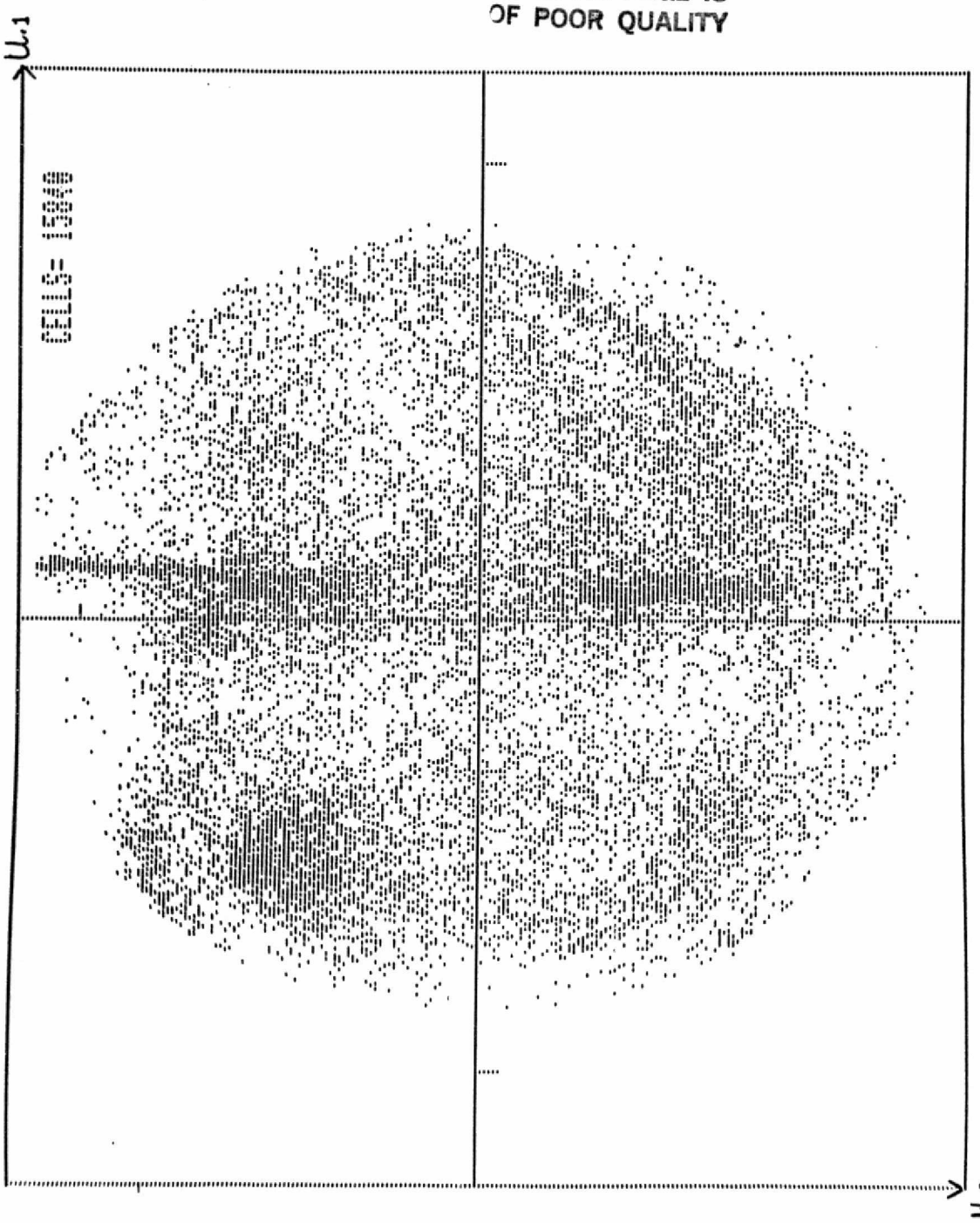

Fig. 5-2 Graph of a data set consisting of more than 15000 cells in two dimensional space (U_1 , U_2)

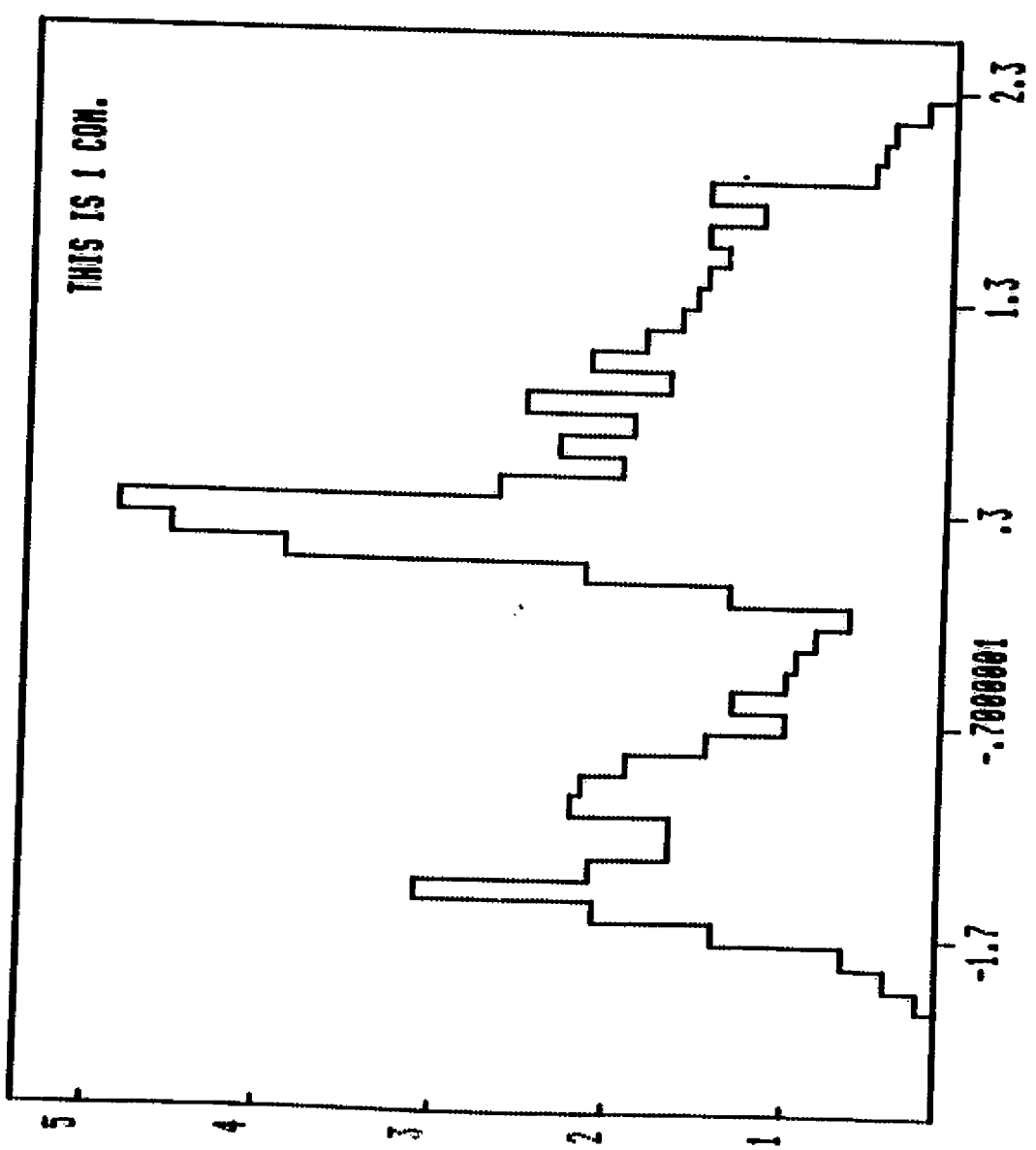

Fig.6-1 Frequency Distribution of The First Principal Component UK1

Fig.6-2 Frequency Distribution of The First Principal Component Uk2

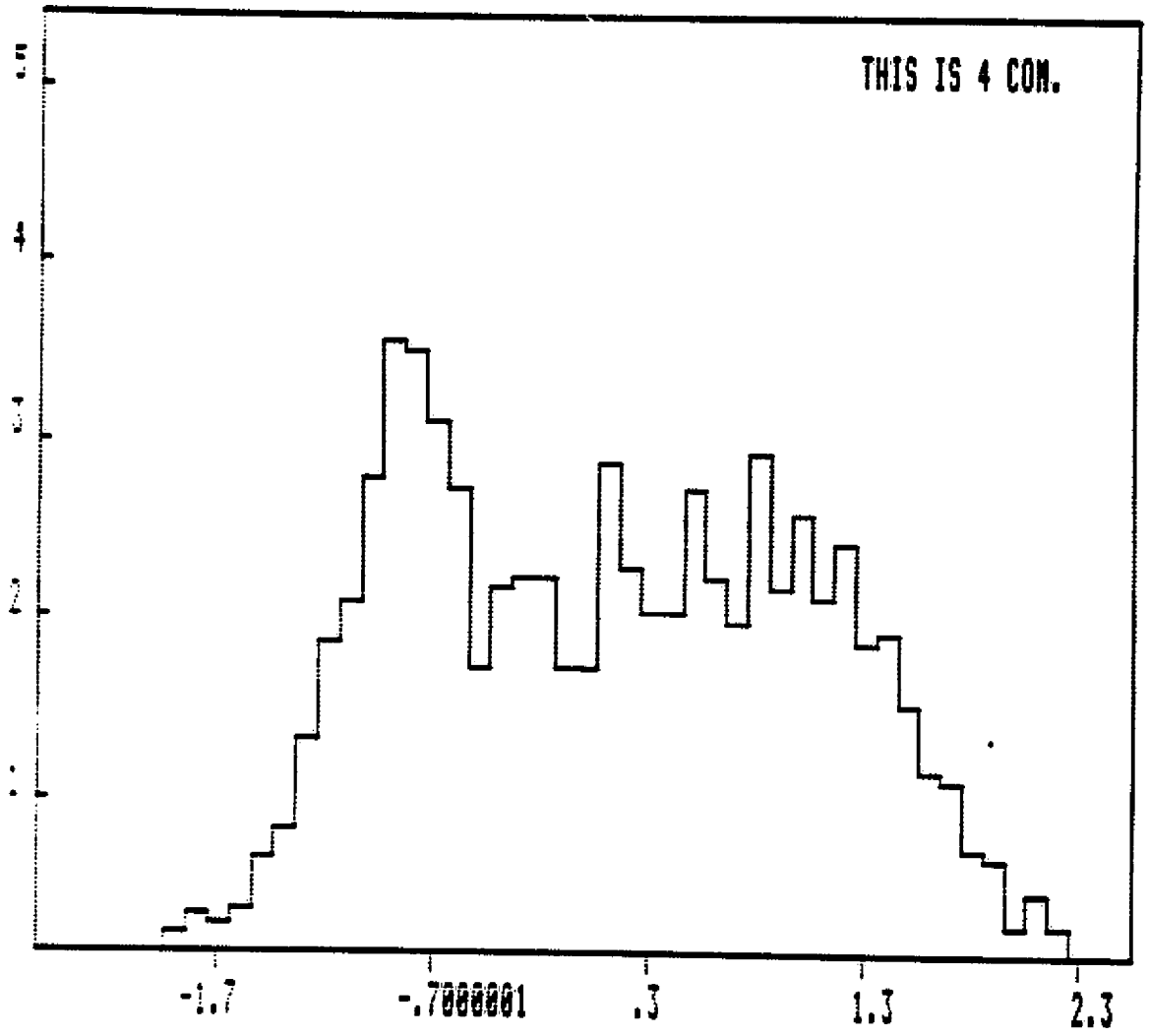

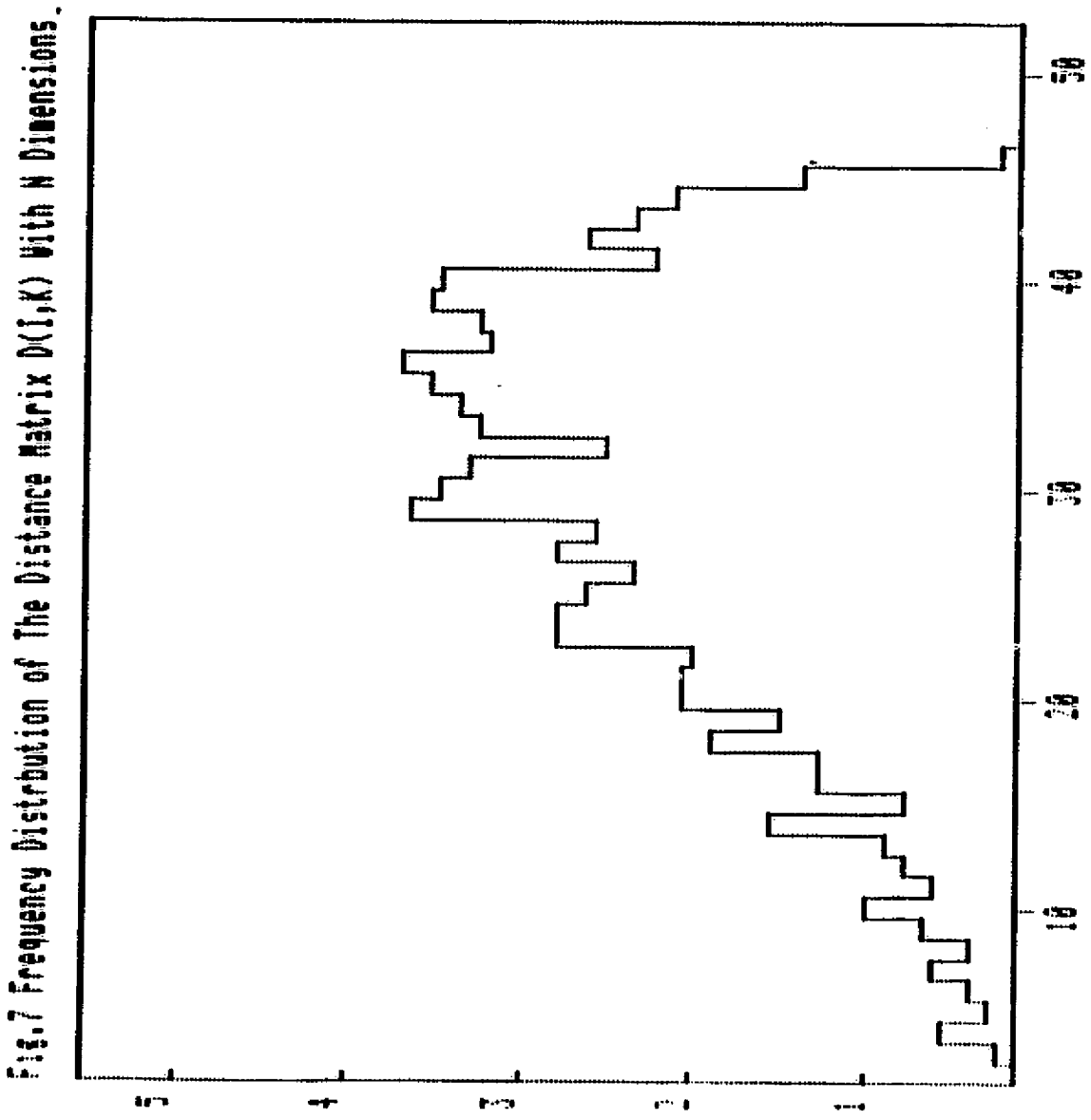

Fig.7 Frequency Distribution of The Distance Matrix D(I,K) With N Dimensions.

SPACE BIOPROCESSING AND RELATED REFERENCES

A6
P.-A. Albertsson. Partition of Cell Particles and Macromolecules. Wiley-Interscience, New York, 1971.
A9
R. E. Allen, G. H. Barlow, M. Bier, P. E. Bigazzi, R. J. Knox, F. J. Micale, G. V. F. Seaman, J. W. Vanderhoff, C. J. Van Oss, W. J. Patterson, F. E. Scott, P. H. Rhodes, B. H. Herren, and R. J. Harwell. Electrophoresis technology. In Apollo-Soyuz Test Project Summary Progress Report vol. 1, National Aeronautics and Space Administration Report NASA SP-412, Washington, 1977, pp. 307-334.
A11
R. E. Allen, P. H. Rhodes, R. S. Snyder, G. H. Barlow, M. Bier, P. E. Bigazzi, C. J. van Oss, R. J. Knox, G. V. F. Seaman, F. J. Micale, and J. W. Vanderhoff. Column electrophoresis on the Apollo-Soyuz Test Project. Sep. Purif. Meth. 6, 1-59 (1977).
B3
S. Bamberger, G. V. F. Seaman, J. A. Brown, and D. E. Brooks. The partition of sodium phosphate and sodium chloride in aqueousa dextran poly(ethylene glycol) two phase systems. J. Colloid. Interface Sci. in press, 1983.
B5
G. H. Barlow, S. L. Lazer, A. Rueter, and R. Allen. Electrophoretic separation of human kidney cells at zero gravity. In D. R. Morrison, Ed. Bioprocessing in Space, NASA TM X-58191, Lyndon B. Johnson Space Center, January 1977, pp. 125-142.
B10
P. H. Bartels, G. B. Olson, H. G. Bartels, D. E. Brooks, and G. V. F. Seaman. The automated analytical electrophoresis microscope. Cell Biophys. 3, 371-386 (1981).
B35
M. B. Bernick and H. C. Kwaan. Plasminogen activator activity in cultures from human tissues; an immunological and histochemical study. J. Clin. Invest. 48, 1740-1753 (1969).
B43
M. Bier. Bioprocessing: Prospects for space electrophoresis. In D. R. Morrison, Ed. Bioprocessing in Space, NASA TM X-58191, Lyndon B. Johnson Space Center, January 1977, pp. 117-124.
B45
M. Bier, J. O. N. Hinckley, and A. J. K. Smolka. Potential use of isotachophoresis in space. Protides of the Biol. Fluids Vol 22, H. Peeters, Ed., Pergamon Press Ltd., Oxford, 1975, pp. 673-678.
B48
M. Bier, N. B. Egan, R. A. Mosher, and G. E. Twitty. Isoelectric focusing in space. In Materials Processing in the Reduced Gravity of Space, Ed. G. E. Rindone, North-Holland, New York, 1982, pp. 261-268.
B49
M. Bier, D. A. Palusinski, R. A. Mosher, A. Graham, and D. A. Saville. A unified theory of electrophoretic processes. In Electrophoresis '84, Ed. , pp. 51-59 (1983).
B60
Boltz, R. C.,Jr., Todd, P., Streibel M. J., and Louie, M. K.: Preparative Biochem. 3, 383-401 (1973).
B62

R. C. Boltz, Jr., P. Todd, R. A. Gaines, R. P. Milito, J. J. Docherty, C. J. Thompson, M. F. D. Notter, L. S. Richardson, and R. Mortel. Cell electrophoresis research directed toward clinical cytodiagnosis. J. Histochem. Cytochem. 24, 16-23 (1976).
B64
R. C. Boltz, Jr., P. Todd, R. H. Hammerstedt, W. C. Hymer, C. J. Thompson, and J. J. Docherty. Initial studies on the separation of cells by density gradient isoelectric focusing. In: Cell Separation Methods (Ed. H. Bloemendal) Elsevier/North-Holland Biomedical Press, Amsterdam, 1977, pp. 145-155.
B66
R. C. Boltz, Jr., T. Y. Miller, P. Todd, and N. E. Kukulinsky. A citrate buffer system for isoelectric focusing and electrophoresis of living mammalian cells. In Electrophoresis '78 (Ed. N. Catsimpoolas) Elsevier/North-Holland Biomedical Press, Amsterdam, 1978, pp. 345-355.
B68
Boltz, R. C., Jr., and Todd, P.: In Electrokinetic Separation Methods (Eds. P. G. Righetti, C. J. van Oss, and J. Vanderhoff) Elsevier/North-Holland Biomedical Press, Amsterdam, 1978, pp. 229-250.
C43
A. Cogoli. Acta Astronaut. 8, 995 (1981).
C44
A. Cogoli, M. Valluchi-Morf, M. Muller, and W. Briegleb. Aviat. Space Environ. Med. 51, 29 (1980).
C45
A.Cogoli and A. Tschopp. Biotechnology in space laboratories. Adv. Biochem. Engin. 22. Space and Terrestrial Biotechnology. Ed. A. Riechter, Springer-Verlag NY, 1982. pp. 1-49.
C47
A. Cogoli, A.Tschopp, and P. Fuch-Bislin. Cell sensitivity to gravity. Science 225, 228-230 (1984).
Practically no stimulation of T-cell multiplication by conA in microgravity.
C50
C. L. Cooney. Bioreactors: design and operation. Science 219, 728-733 (1983).
C55
W. D. Corry, P. A. Bresnahan, and G. V. F. Seaman. Evaluation of density gradient separation methods. J. Biochem. Biophys. Meth. 7, 71-82 (1982).
D20
J. A. Deiber and D. A. Saville. Flow structure in continuous flow electrophoresis chambers. In Materials Processing in the Reduced Gravity Environment of Space Ed. G. E. Rindone, North-Holland, New York, 1982, pp. 217-224.
D30
L. Dintenfass and H. Jedrzejczyk. Morphology and kinetics of aggregration of red cells in 12.5 micrometer slits: A micro- and macro-photographic study. In Hemorheology and Diseases, Proc. 1st Europ. Conf. Hemorheol., Ed. J. F. Stoltz and P. Drouin, Doin, Paris, 1980.
D50
F. A. Dolbeare and R. E. Smith. Flow cytometric measurement of peptidases with use of 5-nitrosalicaldehyde and 4-methoxy-beta-naphthylamine derivatives. Clin. Chem. 23, 1485-1491 (1977).
D80
J. D. Dunning, B. J. Herren, R. W. Tipps, and R. S. Snyder. Fractionation of mineral species by electrophoresis. J. Geopphys. Res., in press (1984).
E10

Ecosystems International, Inc. Materials Processing in Space (MPS) (Jan 1984)
F20
D. Fisher. The separation of cells and organelles by partitioning in two-polymer aqueous phases. Biochem. J. 196, 1-10 (1981).
G11
R. A. Gaines. A Physical Evaluation of Density Gradient Cell Electrophoresis. Thesis. The Pennsylvania State University, University Park, Pennsylvania, 1981.
H9
J. S. Handler, F. M. Perkins, and J. P. Johnson. Studies of renal cell function using cell culture techniques. Am, J. Physiol. 238, F1-F9 (1980).
H13
K. Hannig. The application of free-flow electrophoresis to the separation of macromolecules and particles of biological importance. In Modern Separation Methods of Macromolecules and Particles. Ed. T. Gerritsen. Wiley Interscience NY, 1969. pp. 45-69.
H15
K. Hannig. New aspects in preparative and analytical continuous free-flow cell electrophoresis. Electrophoresis 3, 235-243 (1982).
H16
K. Hannig, H. Wirth, B. Meyer, and K. Zeiler. Theoretical and experimental investigations of the influence of mechanical and electrokinetic variables on the efficiency of the method. Hoppe-Szylers Z. Physiol. Chem. 356, 1209-1223 (1975).
H17
K. Hannig, H. Wirth, and E. Schoen. Electrophoresis experiment MA-014. In Apollo-Soyuz Test Project Summary Science Report, Vol. 1, NASA SP-412, Washington, 1977, pp. 335-352.
H20
D. H. Heard and G. V. F. Seaman. The influence of pH and ionic strength on the electrokinetic stability of the human erythrocyte membrane. J. Gen. Physiol. 43, 635 (1960).
H21
D. H. Heard and G. V. F. Seaman. The action of lower aldehydes on the human erythrocyte. Biochem. Biophys. Acta 53, 366-372 (1961).
H25
G.-G. Heidrich and M. E. Dew. Homogeneous cell populations from rabbit kidney cortex. J. Cell Biol. 74, 780-788 (1983).
H27
R. E. Hise and R. T. Jordan. Apparatus and method for microbial fermentation in a zero gravity environment. U. S. Patent No. 3,769,176, 1973 (Martin Marietta Corp.).
H30
Hjerten, S.: Free Zone Electrophoresis, Almqvist and Wiksells Boktr. AB, Uppsala, 1962.
H85
W. C. Hymer. Separation of Cells from the Rat Anterior Pituitary Gland. In Cell Separation: Methods and Selected Applications, Vol.3, pp. 163-194. Edited by T. G. Pretlow and T. Pretlow. Academic Press, NY (1983).
H87
W. C. Hymer, J. Harkness, R. Grindeland, E. Hibbard, M. Hatfield, M. Thorner, K. Kovacs, J. Parsons, A. Signorella, M. Angeline, C. Phelps, G. Mansur, A. Mastro, W. Taylor, M. Chu. Hollow Fiber Units: Their Application to the Study of Mammalian Cell Function in vivo and in vitro. In Regulation of Target Cell Responsiveness, Vol. 1, pp. 407-461. Edited by K.McKerns. Andivar Hansson, Plenum Publishing Corporation (1984).
J50

R. T. Jordan. Industrial microbiological application in zero-gravity. A vaccine satellite program (VACSAT). In Space Processing and Manufacturing, Marshall Space Flight Center, 1969, pp. 238-251.
J80
H. Juarez-Salinas, S. C. Engelhorn, W. L. Bigbee, M. A. Lowry, and L. H. Stanker. Ultrapurification of monoclonal antibodies by high-performance hydroxylapatite (HPHT) chromatography. BioTechniques 2, 164-169 (1984).
K20
C. R. Keese and I. Giaever. Cell growth on liquid microcarriers. Science 219, 1448-1449 (1983).
K60
J. I. Kreisberg, G. Sachs, T. G. Pretlow II, and R. A. McGuire. Separation of proximal tubule cells from suspensions of rat kidney cells by free-flow electrophoresis. J. Cell Physiol. 93, 169-172 (1977).
K91
M. Kunitz. A cell for the measurement of cataphoresis of ultra-microscopic particles. J. Gen Physiol. 6, 413-418 (1923).
K93
M. E. Kunze and P. Todd. Evaluation of Econazole as an antifungal agent in quantitative cell culture experiments. In Vitro 19, 175-178 (1983).
L18
J. Leighton, L. W. Estes, S. Mansukhani, and Z. Brada. A cell line derived from normal dog kidney (MDCK) exhibiting qualities of papillary adenocarcinoma and of renal tubular epithelium. Cancer 26, 1022-1028 (1970).
L17
J. Leighton, Z. Brada, L. W. Estes, and G. Justh. Secretory activity and oncogenicity of a cell line (MDCK) derived from canine kidney. Science 163, 472-473 (1969).
L29
J. A. Lever. Inducers of mammalian cell differentiation stimulate dome formation in a differentiated kidney epitheoial cell line (MDCK). Proc. Natl. Acad. Sci. U. S. A. 76, 1323-1327 (1979).
L30
S. Levine. A theory of electrophoresis of emulsion drops in aqueous two-phase polymer systems. In Materials Processing in the Reduced Gravity of Space, Ed. G. E. Rindone, North-Holland, New York, 1982, pp. - .
L50
W. Littke and C. John. Z. Flugwiss. Weltraumforsch. 6 (5), 325 (1982).
L52
W. Littke and C. John. Protein single crystal growth under microgravity. Science 225, 203-204 (1984).
25X crystal size beta-gal, 1000X lysozyme
L55
D. Livingston and M. Taub. Growth of functional proximal tubule cells from rabbit kidney in defined medium. Fed. Proc. 40, 1710 (1981).
M11
E. O. Major, S. Ehlke, and M. Lampert. Selection of somatic cell hybrids between BK virus transformed BHK-21 and human embryonic kidney cells to study viral gene expression. J. Virol Methods 1, 139-147 (1980).
M60
D. W. Mason. Biophys. J. 16, 407 (1976).
M70
R. H. T. Mattoni. Spaceflight effects and gamma radiaton interaction on growth and induction of lysogenic bacteria. BioScience 18, 602-608 (1968).
M80
T. H. Maugh II. First commercial product from space. Science 224, 264-265 (1984). 35 g 30-μm spheres worth $.5M.
M90

J. V. Mayeux. Influence of zero-g on single-cell systems and zero-g fermenter design concepts. In D. R. Morrison, Ed. Bioprocessing in Space, NASA TM X-58191, Lyndon B. Johnson Space Center, January 1977, pp. 181-190.
M32
A. A. McCracken and J. L. Brown. A filter immunoassay for detection of protein secreting cell colonies. Biotechniques 2, 82-87 (1984).
M35
L. R. McCreight. Electrophoresis for biological production. In D. R. Morrison, Ed. Bioprocessing in Space, NASA TM X-58191, Lyndon B. Johnson Space Center, January 1977, pp. 143-155.
M41
E. C. McKannan, A. C. Krupnick, R. N. Griffin, and L. R. McCreight. Electrohoretic separation in space--Apollo 14. National Aeronaoutics and Space Administration Report NASA TMX-64611 (1971).
M43
J. K. McGuire and R. S. Snyder In: Allen, R. C. and Arnaud, P. (Eds.), Electrophoresis '81, Walter de Gruyter, Berlin 1981; pp. 947-960.
M44
J. K. McGuire, T. Y. Miller, R. W. Tipps, R. S. Snyder, and P. G. Righetti. New experimental approaches to isoelectric fractionation of cells. J. Chromatog. 194, 323-333 (1980).
M51
J. N. Mehrishi. Molecular aaspects of the mammalian cell surface. Progr. Biophys. Molec. Biol. Vol. 25, 1-20 (1972).
M54
P. O'B. Montgomery, Jr., J. E. Cook, R. C. Reynolds, J. S. Paul, L. Hayflick, D. Stock, W. W. Shulz, S. Kinzey, R. G. Thirolf, T. Rogers, D. Campbell, and J. Murrell. The response of single human cells to zero-gravity. In Biomedical Results from Skylab, Ed. R. S. Johnston and L. F. Dietlein, NASA, Washington, 1977, pp. 221-234.
M55
P. O'B. Montgomery, Jr., In Vitro 14, 165 (1978).
M60
D. R. Morrison, Ed. Bioprocessing in Space, NASA TM X-58191, Lyndon B. Johnson Space Center, January 1977.
M61
D. R. Morrison and M. L. Lewis. Electrophoresis tests on STS-3 and ground control experiments: a basis for future biological sample selections. In 33rd International Astronautical Federation Congress, Paper No. 82-152 (1983).
M65
D. R. Morrison, G. H. Barlow, C. Cleveland, R. Grindeland, W. C, Hymer, H. E. Kunze, J. W. Lanham, M. L. Lewis, B. E. Sarnoff, P. Todd, and W. Wilfinger. Electrophoretic separation of kidney and pituitary cells on STS-8. Adv. Space Res. (in press, 1984).
M68
D. R. Morrison, M. L. Lewis, C. Cleveland, H. E. Kunze, J. W. Lanham, B. E. Sarnoff, and P. Todd. Properties of electrophoretic fractions of human embryonic kidney cells separated on Space Shuttle flight STS-8. Adv. Space Res. (in press, 1984).
M75
R. A. Mosher, O. A. Palusinski, and M. Bier. Theoretical studies in isoelectric focusing. In Materials Processing in the Reduced Gravity of Space, Ed. G. E. Rindone, North-Holland, New York, 1982, pp. 255-260.
M5

L. T. Napolitano. Marangoni convection in space microgravity enrionments. Science 225, 197-198 (1984).
N31
G. L. Nicholson. Cancer metastasis. Organ colonization and the cell-surface properties of malignant cells. Biochim. Biophys. Acta 695, 113-176 (1983). Review of cell surface role. Two-phase partition, EPM. Steps in met, the
N90
L. K. Nyiri. Some questions of space bioengineering. In D. R. Morrison, Ed. Bioprocessing in Space, NASA TM X-58191, Lyndon B. Johnson Space Center, January 1977, pp. 159-180.
N91
L. K. Nyiri and G. M. Toth. Joint application of biosynthesis and separation techniques under microgravity conditions. Annual Tutorial on Material Processing in Microgravity, Lehigh University, Bethlehem, Nov. 1976.
O50
S. K. Omenyi, R. S. Snyder, D. T. Absolom, A. W. Neumann, and C. J. van Oss. J. Effects of zero vander Waals and zero electrostatic forces on droplet sedimentation. Colloid Interface Sci. 81, 402-409 (1981).
P2
C. H. T. Pan., R. L. Gause, and A. F. Whitaker. Tribology experiment in zero gravity. Science 225, 202-203 (1984).
P3
W. J. Patterson, W. J., National Aeronautics and Space Administration Report, 1976, NASA TMX-73311 (1976).
P20
L. D. Plank, W. C. Hymer, M. E. Kunze, and P. Todd. Studies on preparative cell electrophoresis as a means of purifying growth-hormone producing cells of rat pituitary. J. Biochem. Biophys. Meth. 8, 273-289 (1983).
P40
E. C. Pollard. Theoretical considerations on living systems in the absence of mechanical stress. J. Theoret. Biol. 8, 113-123 (1965).
P50
T. G. Pretlow II and T. P. Pretlow. Cell electrophoresis. Int. Rev. Cytol. 61, 85-128 (1979).
P52
T. G. Pretlow II, E. E. Weir, and J. G. Zettergren. Problems connected with the separation of different kinds of cells. Int. Rev. Exp. Pathol. 14, 91-204 (1975).
R2
C. A. Rabito and D. A. Ausiello. Effect of cell-substratum interaction on hemicyst formation by MDCK cells. In Vitro 16, 461-468 (1980).
R3
F. D. Raymond and D. Fisher. Partition of rat erythrocytes in aqueous polymer two-phase systems. Biochim. Biophys. Acta 596, 445-450 (1980).
R10
P. H. Rhodes. high resolution continuous flow electrophroesis in the reduced gravity environment. In Electrophoresis '81, Ed. R. C. Allen and P. Arnaud, W. deGruyter, Berlin, 1981, pp. 919-932.
R12
P. H. Rhodes, and R. S. and Snyder. Materials Processing in the Reduced Gravity of Space, Ed. G. E. Rindone, North-Holland, New York, 1982, pp. 225-232.
R17
G. E. Rindone, Ed. Materials Processing in the reduced Gravity of Space, North Holland, New York, 1982.
S5
B. E. Sarnoff, M. E. Kunze, and P. Todd. Analysis of red blood cell electrophoresis experiments on Space Shuttle flight STS-3. In Proceedings of Conference on Manufacturing in Space, R. O'Neill, ed. : Adv. Astronaut. Sci. 53, 139-148 (1983).

J. Shen-Miller and C. Miller. Distribution and activation of the Golgi apparatus in geotropism. Plant Physiol. 49, 634-639 (1972).
S36
J. Shen-Miller and R. R. Hinchman. Gravity sensing in plants: A critique of the statolith theory. BioScience 24, 643-651 (1974).
S30
G. V. F. Seaman. Electrokinetic behavior of red cells. In: Surgenor, D. M. (Ed.) The Red Blood Cell, 2nd Ed., Academic Press, New York 1975, pp. 1135-1229.
S40
G. V. Sherbet. The Biophysical Characterisation of the Cell Surface. Academic Press, London, 1978.
S45
A. Signorella, and W. C. Hymer. Development of an Enzyme-linked Immunoadsorbent Assay for Rat Prolactin. Anal. Biochem. 136:372-381 (1984).
S50
R. S. Snyder. Electrophoresis demonstration on Apollo 16. National Aeronautics and Space Administration Report NASA TMX-64724 (1972).
S52
Snyder, R. S., Bier, M., Griffin, R. N., Johnson, A. J., Leidheiser, H., Micale, F. J., Ross, S., and van Oss, C. J. Free fluid particle electrophoresis on Apollo 16. Sep. Purif. Meth. 2, 258-282 (1973)
S54
Snyder, R. S., Rhodes, P. H., Herren, B. J., Miller, T. Y., Seaman, G. V. F., Todd, P., Kunze, M. E., and Sarnoff, B. E.: Electrophoresis (submitted 1984).
S70
A. Strickler and T. Sacks. Continuous free-film electrophoresis: The crescent phenomenon. Prep. Biochem. 3, 269-277 (1973).
T3
C. S. Tannenbaum, H. J. Guyda, and B. I. Posner. Insulin-like growth factors: A role in growth hormone negative feedback and body weight regulation via brain. Science 220. 77-79 (1983). Injected insulin like growth factors in rat brain; plasma GH decreased in 2 hr.
T7
M. Taub, L. Chuman, M. H., Saier, and G. H. Sato. The growth of a kidney epithelial cell line (MDCK) in hormone-supplemented serum-free media. Proc. Natl. Acad. Sci. U.S.A. 76, 3338-3342 (1979).
T11
G. R. Taylor. Space microbiology. Ann. Rev. Microbiol. 28, 121-137 (1974).
T12
G. R. Taylor. Cell Biology experiments conducted in space. BioScience 27, 102-108 (1977).
T13
G. R. Taylor. Survey of cell biology experiments in reduced gravity. In D. R. Morrison, Ed. Bioprocessing in Space, NASA TM X-58191, Lyndon B. Johnson Space Center, January 1977, pp. 77-101.
T14
G. R. Taylor and J. R. Dardano. Aviat. Space Environ. Med. 54 (Suppl 1), S55 (1983).
T30
C. J. Thompson, J. J. Docherty, R. C. Boltz, Jr., R. A. Gaines and P. Todd. Electrokinetic alterations of the surfaces of herpes simplex virus infected cells. J. Gen. Virol. 39, 449-462 (1978).
T35

W. Thorman and R. A. Mosher. Simulation of electrophoretic processes. Trans. Soc. Computer Simulation 1, in press (1984).
T58
P. Todd. Gravity and the cell: intracellular structures and stokes sedimentation. In D. R. Morrison, Ed. Bioprocessing in Space, NASA TM X-58191, Lyndon B. Johnson Space Center, January 1977, pp. 103-115.
T60
P. Todd, R. P. Milito, R. C. Boltz, Jr., and R. A. Gaines. Cell electrophoresis. In Flow Cytometery and Sorting (Eds. M. L. Melamed, M. M. Mendelsohn, and P. F. Mullaney) Wiley, New York, 1979, pp. 217-230.
T62
P. Todd, W. C. Hymer, L. D. Plank, G. M. Marks, M. Hershey, V. Giranda, M. E. Kunze, and J. M. Mehrishi. Separation of functioning mammalian cells by density gradient electrophoresis. In Electrophoresis '81, Ed. R. C. Allen and P. Arnaud, W. DeGreuter Press, N. Y., 1981, pp. 871-882.
T85
A. Tschopp and A. Cogoli. Experientia 39, 1323 (1983).
T90
A. Tulp, A. Timmerman, and M. G. Barnhoorn. In Electrophoresis '82 (1983).
T95
A. Tulp. Density gradient electrophoresis of mammalian cells. In Methods of Biochemical Analysis (1984).
V20
J. W. Vanderhoff, F. J. Micale, and P. H. Krummine. Continuous flow electrophoresis. In Electrokinetic Separation Methods, Ed. P. G. Righetti, C. J. van Oss, and J. W. Vanderhoff, Elsevier/North-Holland, Amsterdam, 1979, pp. 121-141.
V25
J. W. Vanderhoff, and C. J. van Oss. Electrophoretic separation of biological cells in microgravity.. In Electrokinetic Separation Methods, Ed. P. G. Righetti, C. J. van Oss, and J. W. Vanderhoff, Elsevier/North-Holland, Amsterdam, 1979, pp. 257-274.
V60
C. J. van Oss, C. K. Charny, D. R. Absolom and T. C. Flanagan. Detachment of cultured cells from microcarrier particles and other surfaces by repulsive van der Waals forces. BioTechniques 1, 194-197 (1983). Remove VERO cells from Cytodex3 w. 20% DMSO + 0.1% EDTA (ST=60 erg/cm2). 50-80% yield. CELL SURFACE
U20
K. M. Ulmer. Protein engineering. Science 219, 666-670 (1983).
V70
E. W. Voss, Jr. Prolonged weightlessness and humoral immunity. Science 225, 214-215 (1984).
No real effect noticable on IgG IgM IgE production
in Spacelab I participants
W20
H. Walter. Partion of cells in two-polymer phases: A surface affinity method for cell separation. In Methods of Cell Separation, Ed. N. Catsimpoolas, Vol. 1, pp. 307-354. Plenum, New York, 1977.
Z20
K. Zeiller and K. Hannig. Free-flow electrophoretic separation of lymphocytes. Evidence for specific organ distributions of lymphoid cells. Hoppe-Zeylers Z. Physiol. Chem. 352, 1162-1167 (1971).
Z40
N. N. Zhukov-Verekizhnikov et al. Results of microbiological and cytological investigations conducted during the flights of "Vostok" type vehicles. In Problems of Space Biology, Ed. O. Gazenko, USSR Acad. Sci., Moscow, 1965 (English translation NASA TT F-361).